**Milan ÁBEL**
**Ján VIŇÁŠ**
**Ľuboš KAŠČÁK**

Technical University of Košice, Slovakia

# INFLUENCE OF DEFORMATION ON A LIFETIME OF WELDING TIPS OF RESISTANCE SPOT ELECTRODES

*The contribution deals with the influence of welding electrode tips deformation on their lifetime. The influence of material properties, production technology and the intensity of welding electrodes load on their lifetime are presented. The electrode tips of the most used type of CUCr1Zr alloy of three basic standard shapes before and after the process of welding are evaluated. The process of welding is realized with low, middle and maximum welding parameters on programmable pneumatic spot welding machine VTS BPK 20. The influence of welding parameters on chosen material characteristics of welding tips is observed. Through the use of upsetting test, dependency of forming strength and deformation of material on used technology of welding tip production is observed.*

## INTRODUCTION

One of the most dynamic developing world industries at present time is automotive industry. Production of automobiles is continuously increasing and demands on quality are still higher. Various conventional and unconventional technologies of welding are used for joining of car-body sheets.

The most used method of car-body sheets welding is resistance spot welding. Despite of beginning to use special technologies of joining (laser welding, laser soldering, MIG welding and soldering, and also press joining and adhesive bonding), resistance spot welding still keeps the position of most widely used method of welding in automotive production.

Even though that it is conventional welding technology which is used practically for a long time, it is necessary to solve some problem tasks that successful resolution will lead to satisfaction of customers and automobile producers [1].

## METHODOLOGY OF EXPERIMENTATIONS AND APPLIED MATERIAL

Welding tips of shapes and dimensions presented at Figs 1, 2 and 3 were evaluated in experiments [2]. Electrodes were made from CuCr1Zr alloy, which physical and chemical properties are due to standard STN ISO 5182 presented in Table 1.

*Table 1. Physical and chemical properties of welding electrodes [3]*

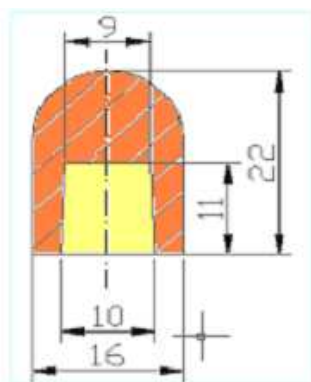| Alloy | Chemical composition %] | Production | Conductance [s.m$^1$.min] | Hardness [HV30] |
|-------|-------------------------|------------|---------------------------|-----------------|
| CuCr1Zr | Cu 98,12 – 99,47 | drawn $\geq 25$ | 43 | 130 |
| | Cr 0,5-1,4 | drawn $< 25$ | 43 | 140 |
| | Zr 0,02-0,2 | forged | 43 | 100 |

*Fig. 1. Hemispherical electrode*
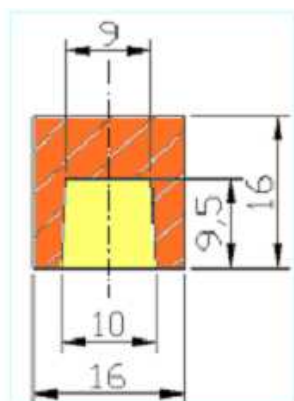


*Fig. 2. Conical electrode*



*Fig. 3. Cylindrical electrode*

## DESCRIPTION OF WELDING MATERIAL

Sheets of 2 mm thickness of C 45 EN 10083-2-91 material were welded by method of resistance spot welding. Chemical and mechanical properties of material stated by producer are shown in Table 2 and 3.

*Table 2. Chemical composition of C 45 EN 10083-2-91 material in ( % )*

| C | Mn | Si | Cr | Ni | Cu | P | S |
|---|----|----|----|----|----|---|---|
| 0,42÷0,50 | 0,5÷0,8 | 0,17÷0,37 | max 0,25 | max 0,30 | max 0,30 | max 0,04 | max 0,04 |

*Table 3. Mechanical properties of C 45 EN 10083-2-91 material*

| Yield stress Re [MPa] | Tensile strength Rm [MPa] | Tensibility A10 [%] | Hardness HB | Yield stress $Rp_{0,2}$ [MPa] |
|---|---|---|---|---|
| ≥ 335 | 540 - 690 | 18 | 225 | 390 – 470 |

### Welding parameters

Welding was realized by resistance spot welding machine BPK20 presented at Fig. 4 with using three different welding modes listed in Table 4.

### Measurement of microhardness

In accordance with ISO 6507-2 the microhardness of specimens was measured at device PMT 3 in two different dimensions (Table 6). Weighting of 200g was used.

**Upsetting test**

Forming strength is stress whereat material is permanently deformed. Dependence between this stress and effective deformation was defined by the upsetting test. Loading parameters are in Table 5.

The samples of CuCr1Zr alloy due to standard STN ISO 5182 were used for experiments. Dimensions of the samples are shown in Fig. 6.


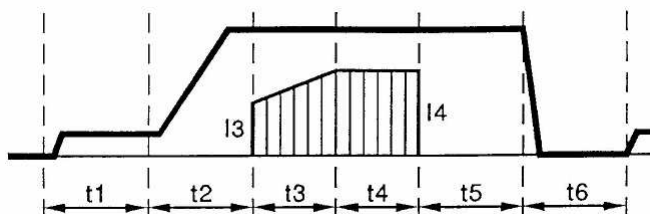


Fig. 5. Welding mode of spot welding machine
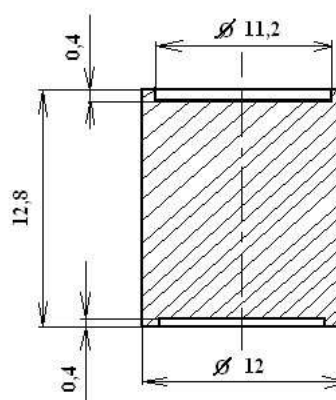


Fig. 6. Shape and dimensions of upsetting sample

Fig. 4.  Resistance spot welding machine BPK 20

Table 4.  Parameters of welding modes

| Welding Modes | Welding Time $(t_4)$ [time period] | Initial Current Value $(I_3)$ [kA] | Welding Current $(I_4)$ [kA] | Welding Force [kN] |
|---|---|---|---|---|
| 1. | 18 | 20 | 26 | 6,8 |
| 2. | 18 | 15 | 22 | 6,8 |
| 3. | 18 | 10 | 18 | 6,8 |

Table 5. Loading used in upsetting test

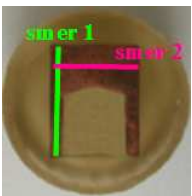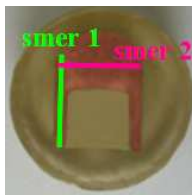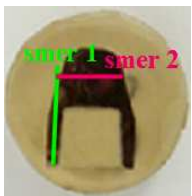| Measurement | 1. | 2. | 3. | 4. | 5. | 6. | 7. |
|---|---|---|---|---|---|---|---|
| Force F [N] | 20 | 40 | 60 | 85 | 99 | 119 | 140 |

**ANALYSIS OF ACHIEVED RESULTS**

Measured values in electrodes before welding in direction 1 show increasing trend of microhardness HV0,2 from top part of electrode to its contact surface. The lowest values of microhardness within the range of 143-147 HV0,2 were measured at cylindrical electrode.   Higher values was observed at hemispherical electrode, they vary from 149 to 152 HV0,2. The highest microhardness was found at conical electrode within the range from 150 to 153 HV0,2.

Measured values in direction 2 are lowest in middle part and value of microhardness rises towards the edges. As well as in direction 1, the lowest values of microhardness (145-147 HV0,2) were measured at cylindrical electrode. Values of microhardness at hemispherical electrode were within the range of 151-152 HV0,2 and at conical electrode were within the range of 151-153 HV0,2.

Low parameters of welding (I = 18 kA) didn't affect on material microhardness. Microhardness in direction 1 has increasing trend towards the contact surface at all types of electrodes. Cylindrical electrode has the lowest values of microhardness from 145 to 147, values from 148 to 151 HV0,2 were measured at hemispherical electrode and the highest microhardness from 149 – 152 HV0,2 was again determined at conical electrode.

*Table 6. Average values of microhardness HV 0,2 on tested specimens*

| | Cylindrical Tip | | Hemispherical Tip | | Conical Tip | |
|---|---|---|---|---|---|---|
| | Direction 1 | Direction 2 | Direction 1 | Direction 2 | Direction 1 | Direction 2 |
| Evaluation of microhardness before welding | | | | | | |
| 1. | 143 | 146 | 149 | 151 | 150 | 152 |
| 2. | 144 | 145 | 151 | 151 | 151 | 151 |
| 3. | 147 | 147 | 152 | 152 | 153 | 153 |
| Evaluation of microhardness after welding with low parameters | | | | | | |
| 1. | 145 | 147 | 148 | 151 | 149 | 151 |
| 2. | 145 | 146 | 150 | 149 | 151 | 151 |
| 3. | 147 | 147 | 151 | 151 | 152 | 152 |
| Evaluation of microhardness after welding with the middle parameters | | | | | | |
| 1. | 135 | 140 | 144 | 147 | 145 | 148 |
| 2. | 138 | 139 | 145 | 146 | 146 | 147 |
| 3. | 142 | 142 | 147 | 147 | 148 | 148 |
| Evaluation of microhardness after welding with the maximum parameters | | | | | | |
| 1. | 133 | 136 | 136 | 141 | 138 | 144 |
| 2. | 135 | 135 | 138 | 139 | 142 | 144 |
| 3. | 138 | 138 | 142 | 142 | 144 | 144 |

In direction 2 the lowest values were measured in the middle of electrode and in the marginal part of electrode. Microhardness of cylindrical electrode varies from 146 to 147 HV0,2, hemispherical electrode from 149 to 151 HV0,2 and conical electrode from 151 to 152 HV 0,2.

After welding process by using middle parameters (I = 22 kA), values of micro-hardness listed below were measured. In direction 1 the microhardness increased towards the contact surface. So microhardness of cylindrical electrode was 135-142 HV 0,2, hemispherical electrode 144-147 HV0,2 and conical electrode 145-148 HV0,2.

In direction 2 the range of microhardness was at cylindrical electrode from 139 to 142 HV0,2, at hemispherical electrodes from 146 to 147 HV 0,2 and at conical electrode from 147 to 148 HV0,2.

At all types of electrodes the microhardness decreased compared to the micro-hardness before and after welding process using low parameters.

Microhardness of electrodes after welding process using maximum parameters (I = 26 kA) was the lowest in both of direction.

In direction 1 the lowest values of microhardness were measured also at cylindrical electrode, and that is 133-138 HV0,2. The range of microhardness at hemispherical electrode was 136-142 HV0,2 and at conical electrode the microhardness was 138-144 HV0,2.

In direction 2 the microhardness in the edge part of electrode was higher then in the middle of electrode. It was the same for all types of electrodes. Their microhardness varied from 135 to 138 HV0,2 at cylindrical electrode, from 139 to 142 HV0,2 at hemispherical electrode and at conical electrode the microhardness was 144 HV0,2.

## Dependence of strain strength and real deformation

Measured results of upsetting tests are presented in Table 7.

*Table 7. Measured and calculated values after upsetting test [4]*

| Measurement | F [kN] | $h_i$ [mm] | $\Delta h$ [mm] | $d_i$ [mm] | $S_i$ [mm$^2$] | $k_p$ [MPa] | $\varphi$ | A [J] |
|---|---|---|---|---|---|---|---|---|
| 1. | 20 | 11,4 | 1,4 | 12,7 | 126,9 | 157,5 | 0,05 | 11,5 |
| 2. | 40 | 10,1 | 2,7 | 13,5 | 143,3 | 279,1 | 0,103 | 41,6 |
| 3. | 60 | 8,3 | 4,5 | 14,9 | 174,4 | 344 | 0,188 | 93,8 |
| 4. | 85 | 6,2 | 6,6 | 17,2 | 233,5 | 385,5 | 0,315 | 175,9 |
| 5. | 99 | 5,6 | 7,2 | 18,1 | 258,5 | 382,9 | 0,359 | 199,4 |
| 6. | 119 | 4,8 | 8 | 19,6 | 301,6 | 394,6 | 0,426 | 243,7 |
| 7. | 140 | 4,1 | 8,7 | 21,2 | 353,1 | 396,5 | 0,494 | 284,3 |

Upsetting test confirms theoretical assumes of material behavior during evaluation of mechanical characteristics by microhardness measurement.

## CONCLUSION

Based on the realized experimentation it is possible to observe that microhardness of all basic shapes of electrodes in all examined conditions mildly increased from top electrode towards its contact surface. In the middle part of electrode lower values of microhardness were measured in comparison with the edge parts, which was probably effected by water cooling process during the welding.

Low parameters of welding (I = 18 kA) don't have significant effect to the micro-hardness of tested material. Measured values of microhardness before welding and after welding varied minimally. Progressive increasing of welding current (I = 22 - 28 kA) caused the microhardness decreasing at all examined shape of electrodes. Lowest values of microhardness HV 0,2 were measured by using these electrodes in welding with maximum parameters.

Cylindrical electrode has the lowest values of microhardness during the whole experimentation. Following the hemispherical electrode the highest values of microhardness were measured at conical electrodes. It could be said that lifetime of welding tips is effected by shape of electrodes and mainly the technology of electrodes production. It is possible to expect that the conical one has the longest lifetime from all tested shapes, that is being verified in practice now.

Big influence on tips lifetime has also used technology of their production. It is possible to achieve strengthening of the material by forming – increase of hardness of the surface layers, which enables electrodes to be used for hardest modes of resistance spot welding. Strengthening of the surface layers is an alternative to increasing amount of alloying elements in material in order to achieve higher hardness with decreasing conductivity.

For each technology of electrodes production it would be also suitable to declare the rate of thermal processing and transfer of heat through the tool and joined material in the weld point and take consideration of heat and pressure influence on the change of welding electrodes lifetime.

Nowadays, methods of prolonging the lifetime of welding tips are continuously being researched, especially at dynamic developing automobile industry, where critical factors affected at welding tips lifetime are surface coatings of steel sheets, which create eutectics in the electrodes contact surface and cause electrical conductivity reduction.

## REFERENCES

1. Lipa M.: *Odporové zváranie*. 1. vyd.. Bratislava: Weldtech, 1995, 265 s.
2. Ábel M., Viňáš, J.: *Hodnotenie vplyvu zváracích parametrov na životnosť zváracích špičiek*. In: Acta Mechanica Slovaca. roč. 10, č. 4-a Povrchové inžinierstvo, Košice: Vienala, 2006, s. 7-12.
3. STN ISO 5182: *Zváranie. Materiály na odporové zváracie elektródy a pomocné zariadenia*
4. Ábel M., Evin E.: *Analýza vplyvu stupňa deformácie na životnosť zváracích elektród pre odporové zváranie*. In: Strojné inžinierstvo 2006 : Zborník príspevkov, Bratislava : STU, 2006. s. 514-520.

**Milan ÁBEL**
**Ján VIŇÁŠ**
**Ľuboš KAŠČÁK**
**Dagmar DRAGANOVSKÁ**

Technical University of Košice, Slovakia

# METALLOGRAFIC ANALYSIS OF ELECTRODE MATERIALS FOR RESISTANCE SPOT WELDING

*The contribution deals with metallographic analyses of welding tip materials and work-pieces used in their production. Microstructures of in practice most used alloys Cu for welding electrodes of resistance spot welding are evaluated. Alloys of CuCr1Zr, CuCoBe and CuBe2. Analyses of influence of alloying elements and production technology of the alloys on final properties of electrode materials are presented. The effort of producers is the maximum lifetime of welding tips on which many factors have influence during welding process. Used welding mode, material properties of the tips, technology of their production, sort and surface treatment of welded materials and so on.*

## INTRODUCTION

The most used method of car-body sheets welding is resistance spot welding. Even though it is conventional technology of welding which is used for a long time in practice, it is necessary to solve some problem tasks which successful resolution will lead to satisfaction of customers and automobile producers [1].

The biggest problem which the automobile welding centers deal with is limited lifetime of welding tips during the welding process of surface modified sheets. During the welding of these sheets, the lifetime of welding tips is multiple lower in comparison with black sheets. Their lifetime decreases rapidly due to adhesing the coatings with a low melting temperature on the contact surfaces of welding tips that cause beginning of the eutectics which have negative ifluence on transition resistance during the welding. That's why it is necessary to clean contact surface of tips periodically after specified welding cycle. Lifetime of welding tips is also considerably affected by material of which are made, pruduction technology, their shape, cooling intensity and the conclusive influence have used welding parameters.

The alloys with higher content of Cu for production of the welding tips are used, that guarantee high electrical conductivity. These alloys are used for tips production: CuAl, CuZr, CuCrZr, CuCoBe, CuCoNiBe, CuBe2, CuNiSi, CuNiSiCr, CuW and the others.

## ANALYSIS OF CURRENT CASE IN PRODUCTION OF MATERIALS FOR WELDING TIPS

Alloys of CuCr contain from 0,6% up to 1,2 %Cr. They are used for the reason of their high strength, corrosion resistance and electrical conductivity. These alloys could be hardened by ageing that means a change of properties which occur at high temperature due to chrome precipitation from solid solution. Strength of hardened CuCr alloy is almost double in comparison with pure copper (220MPa) and its conductivity is lower only about 15% than conductivity of Cu. These high-strength alloys keep their strength also at high temperatures (1000°C). CuCr alloy of is very good in cold forming. The alloy is used with advantage in production of electrodes for resistance spot welding, electrodes for seam welding, cable terminators, parts of braking systems and electrical and thermal conductor with higher strength [2]. Properties of CuCr alloys could be improved, except for Zr alloying, by arsenic alloying [3].

Hardening is in progress by increasing solubility of Cr in Cu with increasing temperature. While slow cooling process of CuCr alloy is in progress the structure is two-phase one including chrome and alfa-phase of copper. Excellent mechanical properties are achieved by rapid cooling of CuCr alloy from annealing temperatures, which causes Cr kept with Cu in the oversaturated solid solution. So there is a regular distribution of precipitates in the matrix during the ageing process. Rapid cooling doesn't allow the precipitation of Cr from solid solution so the final structure is composition only of alfa-phase of Cu. First pure Cu is solidifying, then the eutectic mixture alpha-phase of Cu and Cr. Eutectic mixture of alfa-phase Cu and Cr forms lamellar structure in the interdendritic areas [2].

To improve the splintery workability of CuCr alloy, alloying elements are added such as Se, Te and Pb. Mechanical properties could be modified by addition of Ti (up to 0,5%) and Be (up to 0,1%) [3].

CuCr alloys are used for their high strength and electric-thermal characteristics. By addition of small amount of alloying elements these alloys could be modified on the high-strength alloys or high-conductive alloys. For production of welding tips it is necessary to find compromise between the strength and conductivity which allow these alloys to be used also with hard modes of welding (high current – short time).

High-strength alloys consist of Be from 1,6% to 2% and approximately 0,5% of Co. In order to achieve high strength it is possible to increase Be content up to 2,7%. Alloys with high conductivity consist from 0,2 % to 0,7% of Be and higher content of Ni and Co.

These alloys are used for production of electronic connecting contacts, in electric devices as switches, inside the cases for magnetic switches, non-sparking applications, small sources, parts of injection forms for plastics and components of resistance welding. They are also suitable for production of casting by the reason of good leaking.

High strength of CuBe alloys is achieved by ageing hardening or precipitation hardening. Hardening is in the progress while precipitation of Be from oversaturated rigid solution of pure Cu. Precipitation is in progress during slow cooling of alloy, because decreasing temperature causes decreasing of solubility of Be in the alfa-phase of Cu. During the rapid cooling of alloys from annealing temperature Be remains inside of rigid solution of Cu [2]. Consequently inside the alloy precipitation comes in the

progress or hardening during the 1 hour in within temperature of 200 to 450ºC. Tempering causes separation of from the rigid solution.

During the first phase of precipitation, the homogeneous nucleuses of Guinier-Preston (G-P) areas occur. G-P areas are small precipitations inside the oversaturated solid solution of the alfa-phase of Cu. G-P zones don't have purely defined own crystalline structure and these zones contain of high concentration of Be atoms. Production of G-P zones is related to the changes of characteristics. In CuBe alloy increasing of strength occurs. During the ageing process, some coherent metastable gamma double primary precipitates occur in the G-P zones. Subsequently the primary gamma precipitates are separated. Strength of these alloys relates with the force of bonds which are in border of matrix and growing precipitation. Precipitation of balanced gamma phase decreases strength characteristics of the alloy by reduction of metastable primary gamma precipitates [4].

## METHODOLOGY OF EXPERIMENTS

Welding tips and workpieces dedicated to production of welding tips were evaluted in the experiments. Samples for observation were from bar material and were taken off by splintery process without thermal impact. Metallographical analysis of examined samples was realized on metallographical cuts with optical ligh microscope Olympus CX-31. Metallographical analysis was realized on Cu alloys which standard physical and chemical characteristics are presented in Table 1.

*Table 1. Standard physical and chemical characteristics of welding tips and workpieces [2]*

| Alloy Standard | Chemical composition | Hardness HB | Electrical conductivity | Sample shape |
|---|---|---|---|---|
| CuCr1Zr<br><br>DIN 2.1293 | Cr 0,8<br>Zr 0,08<br>Cu residue | 150 | 48 | Welding Tip |
| CuCoBe<br><br>ASTM-No. (UNS): C17500 | Co 2,4 – 2,7<br>Be 0,4 – 0,7<br>Ni max. 0,3<br>Fe max 0,1<br>Al max 0,1<br>Si max 0,2<br>Cu residue | 270 | 43 | Bar workpiece |
| CuBe2<br><br>DIN 2.1247 | Be =1,6 – 2<br>Ni + Co =0,4<br>Fe < 0,1<br>Cu residue | 350 | 14 | Welding Tip |

Observed workpieces and welding tips of standardized shapes and dimensions dedicated to resistance spot welding are mentioned at Figs 1, 2, 3.

*Fig. 1. Welding tips for metalographical analysis from CuCr1Zr material*



*Fig. 2. Bar workpiece for production of CuCoBe welding tips (ø 16mm x 300mm)*



*Fig. 3. Welding tips for metalographical analysis from CuBe2 material*

## RESULTS OF METALLOGRAPHIC ANALYSIS

At Fig. 4, there is the microstructure of CuCr1Zr alloy with typical rectangular double boundaries of grains of rigid solution of alfa-phase of Cu.

In the Cu matrix – see the Fig. 4 it is shown relatively massive Cu grains, separated on typical platy formation. For visualization of microstructure following etching was used: 1g of ammonium hydroxide $NH_4OH$ + 2g of ammonium persulphate $(NH_4)_2S_2O_8$ (2,4%) in 100ml of distilled water.

Microstructure of thermal treated CuCoBe alloy is at Fig. 5. Thermal treatment was realized by dissolving annealing at 940°C temperature and precipitation hardening at 480°C temperature during 3 hours. In this way maximum hardness which is required for production of welding electrodes could be achieved. At homogeneous fine-grained alfa-phase of Cu it is possible to observe the regularly situated inclusions of CoBe compounds inside the whole matrix.

For visualization of microstructure following etching was used: 1g of KCN, 100 ml of distilled water.
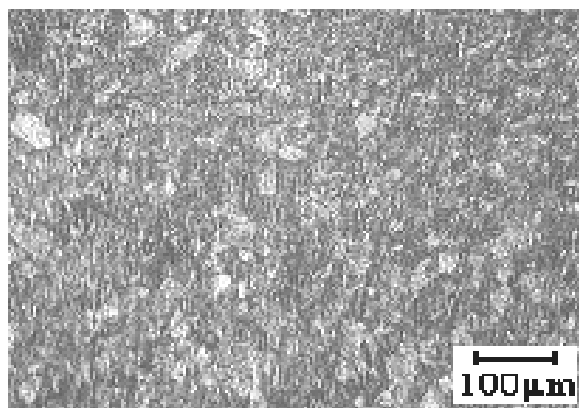
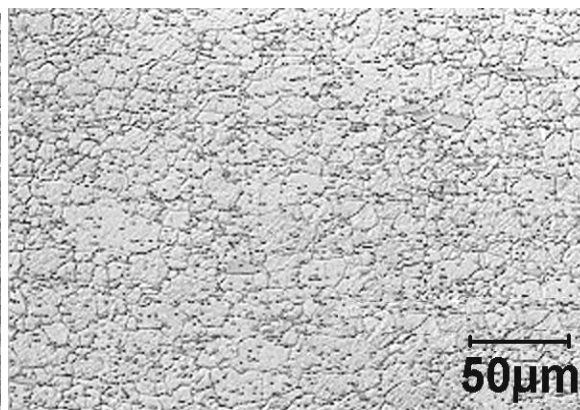*Fig. 4. Microstructure of CuCr1Zr alloy*          *Fig. 5. Microstructure of CuCoBe alloy*

At Fig. 6 there is microstructure of CuCoBe alloy hardened by dissolving anneal-ing at the temperature of 790°C and consequential rolling during the cooling. In this way, it is possible to increase hardness at about 35% in comparison with material without thermal treatment and forming.

Prolonged grains of alfa-phase and inclusions of CoBe could be observed in mi-crostructure. For visualization of microstructure following etching was used: 1g of ammonium hydroxide $NH_4OH$ + 2g of ammonium persulphate $(NH_4)_2S_2O_8$ (2,4%) in 100ml of distilled water.

CuBe2 alloy at Fig. 7 has typical dendritic structure of alfa Cu with Be phases. Berilids could be observed on buffed and unetch samples. Berilids appear during the solidification and they are typical with their elongated shape. Secondary berilids occur after solidification and they have lamellar structure.
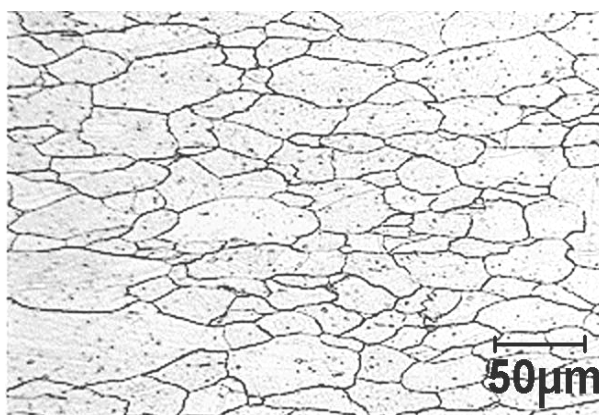


*Fig. 6. Microstructure of welding tip made by forming of CuCoBe*

Microstructure of the heat affected zone of the tip. Heat has a negative impact on the homogenity of structure and especially on the size of grains. Unhomogenity of the structure was caused by insufficient tip cooling.

For visualization of microstructure following etching was used: 1g of ammonium hydroxide $NH_4OH$ + 2g of ammonium persulphate $(NH_4)_2S_2O_8$ (2,4%) in 100ml of distilled water.
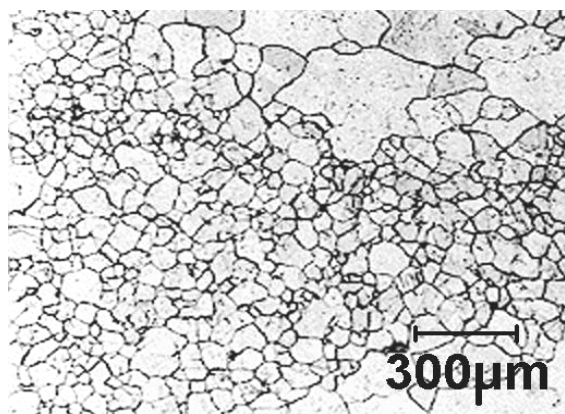
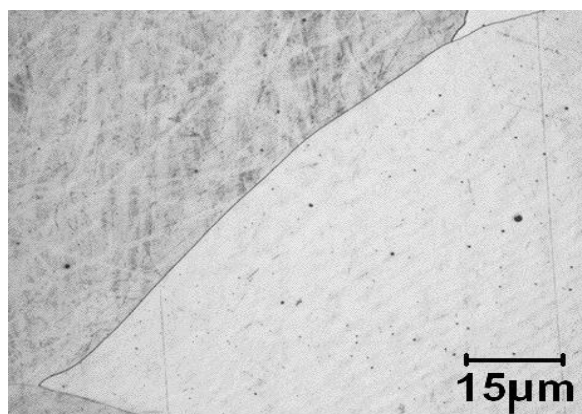Fig. 7. Microstructure of tip material after welding cycle      Fig. 8. Microstructure of CuBe2 alloy

At Fig. 8 it is microstructure of grain boundary of thermal unaffected material of CuBe2 tips, formed a precipitately hardened. It contains rectangular double boundaries of grains of alfa Cu with diffused elements of Ni, Co or Ni and Co with Be2.

For visualization of microstructure the following etching was used: 1g of ammonium hydroxide $NH_4OH$ + 2g of ammonium persulphate $(NH_4)_2S_2O_8$ (2,4%) in 100ml of distilled water.

## CONCLUSION

Development in the production of welding tips is constantly evolving. Alloys with high conductivity together with hardness are being observed. These enable their using in application of hard modes of resistance spot welding. One of the innovations is a special alloy dedicated to welding tips of AEG SVS Schweiss Technik company, namely „AEG Wirbalit NIB". It is alloy which electrical conductivity corresponds to the alloy CuCrZr, that is 48 MS/m and its hardness corresponds to the alloy CuCoBe, i.e. 270 HB [5].

Possibility of increasing the strength characteristics without the support of alloying elements comes only in limited range by choice of suitable technology of production where it is possible to use mainly the hardening effect of forming.

The way of increasing the lifetime of welding tips is the combination of alloying elements in the copper alloys, method of their production as well as geometric design.

## REFERENCES

1. Lipa M.: *Odporové zváranie. 1.* vyd.. Bratislava: Weldtech, 1995. 265 s.

2. Ábel M., Viňáš J.: *Hodnotenie vplyvu zváracích parametrov na životnosť zváracích špičiek.* In: *Acta Mechanica Slovaca.* roč. 10, č. 4-a Povrchové inžinierstvo, Košice: Vienala, 2006, s. 7-12.

3. Chvojka J.: *Neželezné kovy a jejich slitiny,* SNTL Praha,1971. s.240

4. STN ISO 5182: *Zváranie. Materiály na odporové zváracie elektródy a pomocné zariadenia*

5. Janota M.: *Procesy a riadenie odporového zvárania.* Bratislava: Výskumný ústav zváračský 1985. 120 s.

## Ali A. ASHRAF

College of Engineering in AlKharj, King Saud University, Saudi Arabia

# WEAR CHARACTERISTIC OF EXFOLIATED GRAPHITE NANO SHEETS/COPPER METAL MATRIX COMPOSITE

*Powder Metallurgy technique has been used to prepare composite samples made of exfoliated graphite nano sheets (EGNS) and graphite flakes (GF) of 1, 3 and 5 weight % with copper chips. Effect of both graphite and its size on morphological, mechanical, and tribological behavior of copper matrix composite has been investigated. Some unexpected characteristics have been identified due to the addition of graphite flakes and its exfoliated nano sizes with copper metal matrix. Nano-like grain boundary (NLGB) phenomenon has been reported. A decrease in hardness has been measured within the used weight fractions. Surprisingly, there was an increase in wear rates with an increase in wt% GF added to the copper matrix. In the case of EGNS, an increase in wear rate is reported for a weight fraction of 1%, which then decreases as more EGNS is added until it reaches approximately the same wear rate of pure Cu matrix at 5% EGNS. It is believed that the increase in wear at 1% EGNS is due to delamination domination theory. Measuring the counter part wear characteristics more deeply, evaluating the dispersion quantitatively, and explaining the delaminating theory of the EGNS/Cu metal matrix composites is recommended for future work.*

## 1. INTRODUCTION

Nanomaterials and especially carbon nanomaterials such as carbon nanotubes, flurens and exfoliated graphite nanosheets increasingly attract scientific and technological interest by virtue of their significant advantages over most existing materials [2, 5, and 8]. Also, lamellar structure and softness of solid lubricants of graphite makes it a very good candidate for wear and tribological applications [9].

Graphite can be intercalated by exposing it to appropriate atoms or molecules, known as the intercalating agent, which enter between the carbon layers of the graphite. The resulting material, known as a graphite intercalation compound (GIC), is composed of carbon layers and intercalated layers stacked on top of one another in a periodic fashion, for example –C-C-I-C-C-I-CC-I-C-C-, where C is a carbon layer and I is an intercalated layer. The number of carbon layers between each pair of intercalated layers is called the stage. GIC prepared from chemical oxide intercalation are mostly stage 1 to stage 5. Rapid heating of intercalated graphite flakes to a sufficiently high temperature causes exfoliation, a sudden increase in the dimension perpendicular to the carbon layers of the GIC. This forms vermicular graphite, also known as expanded graphite [3].

Exfoliated graphite has mainly been used as a raw material for making flexible graphite sheets which have a wide application for sealing because of their excellent properties, e.g. compressibility, resilience, thermal stability, corrosion resistance, etc.

Recently, experimental results have revealed that exfoliated graphite is also a good absorbent, especially for materials with large molecular size and weak polarity [4]. Exfoliated graphite nano sheets have been found in the literature as a nano platelet reinforcement material for electrospun PAN nano fiber composite [7].

Copper matrix composites are increasingly being used in a variety of components where high electrical and thermal conductivity, good corrosion and wear resistance were required, such as continuous casting mould, electrodes of resistance welding, and the nozzle of $CO_2$ gas shielded welding [9]. The incorporation of particulate reinforcements improves mechanical properties as well as wear resistance of the composites by acting as load-bearing components, while retaining considerably high conductivity [10].

An J-W, et al. [1] studied the tribological properties of hot pressed alumina-CNT composites and showed a decrease in the wear rate and friction coefficient for 2 and 4 CNT weight%. An increase in both wear rate and friction coefficient was found at 10 and 12 CNT weight% due to poor cohesion between the CNT and the alumina matrix as it was speculated in the paper. In another paper [5] 5, 10 and 20 weight% CNT has been added to carbon-carbon composite materials and the tribological behavior of these new materials showed a different behavior in the wear rate. As CNT weight% increases from 5 to 20 weight% a decrease in coefficient of friction has been reported, as well as increase in wear rate. Also, the effect of CNT distribution on the tribological behavior of Alumina-CNT composites has been studied recently by Lim D-S, et al. [6]. In this paper an increase in the wear loss for the hot pressed composites has been reported at 8 and 12 CNT weight% even it was more than the pure alumina sample's value. Also, the improvement in the tribological behavior was reported at 4 CNT weight%. Good and bad dispersion of the CNT in alumina matrix and its agglomeration during the composite sample's preparation have been used to explain these results.

## 2. EXPERIMENTAL WORK

### 2.1. Dispersion of GF and EGNS in Cu Chips

Graphite flakes with particle size of 75+ mesh (75% min) supplied by Fluka and Sigma-Aldrich, catalog number 332461, have been used to prepare exfoliated graphite nano sheets (EGNS) as follows: 120 grams of graphite flakes (GF) were added to a mixture of 532 ml of concentrated sulfuric acid and 133 ml of concentrated nitric acid. The reaction mixture was stirred continuously for 20 hours. The acid-treated GF was washed with distilled water until neutralized and then was dried at $100^{\circ}$ C to remove any remaining water. Every 5 grams of the dried particles were heat treated at $1050^{\circ}$ C for 30 seconds to obtain expanded graphite particles with a C dimension about 300 times that of the original C direction dimension. The expanded graphite here was loose and vermicular or wormlike. Its structure was similar to parallel boards which desultorily collapse and deform, resulting in many pores of different sizes as seen in Figure 1. One grams of the above expanded graphite was then immersed in a mixture of 260 ml alcohol and 140 ml distilled water in an ultrasonic bath. The dispersion was filtered and dried after 12 hours of sonication. The thickness of the graphite sheets in the exfoliated graphite ranged from 100 to 400 nm. The sonicated graphite worm (Fig. 1) was completely torn into sheets with thickness of 30-80 nm and a diameter of 5-20μm,

named exfoliated graphite nanosheets based on the preparation method has been used as reported in literature.
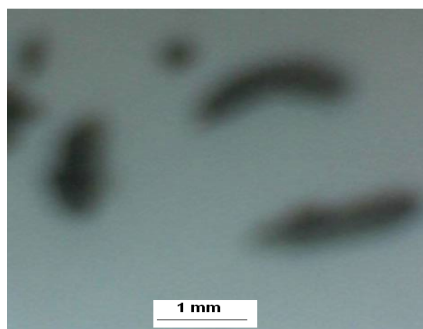


Expanded graphite before sonication
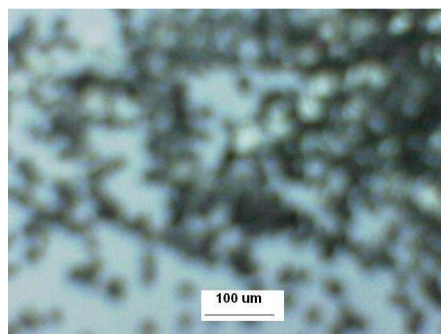


After 12 hours of sonication

*Fig. 1. Expanded (vermicular) graphite*

A mechanical mixer has been used with an average rotating speed for 30 minutes to distribute the GF in Cu chips. The distribution of the GF has been observed and found to be acceptable based on previous experiences. The mixing time was kept the same for all the GF weight fractions.

A volatile solvent with a boiling point of $155^{o}$ C was used to well disperse the EGNS in the Cu chips. After 30 minutes of stirring the mixture was heated to $200^{o}$ C to vaporize the solvent completely. The same procedure was followed for all EGNS weight fractions.



GF/Cu mixing technique



GF/Cu after 30 min of mixing



EGNS/Cu mixing technique



EGNS/Cu after 30 min stirring

*Fig. 2. Mechanically Dispersed GF and EGNS in Copper Chips*

Figure 2 shows photos of the used mixer and stirrer as well as the resultant mixture of both GF and EGNS in Cu chips. In this figure it can be noted that the color of

the EGNS is much darker (Graphite color) than GF for same fraction, which can be easily explained by the large difference in surface area for the same volume of GF and EGNS.

## 2.2. Sample Preparation

### 2.2.1. Cold Pressing and Sintering

A hydraulic press of 1000MPa maximum pressure was held for 30 minutes at 500 MPa to form the composite samples made of graphite flakes and nanosheets with copper chips. The press and mold used in the preparation of composite samples is shown in Fig. 3. The inner dimensions of the mold cavity were 120x60x12 mm and the sample's final dimensions were 90x60x12 mm.

Cold pressed samples were isolated and heat treated in a tube furnace filled with inner gas at $850^{o}$C for 3 hours.



*Fig. 3. Hydraulic press and steel mold*

## 2.3. Wear Test

A 10x10 mm cross sectional sample was used in all the wear tests. A live picture of the wear experiment with 10 N loads in a full contact mode between the sample and the rotating disc is shown in Figure 4. 2, 5 and 10 N loads have been used with each sample to study the effect of applied load on the wear behavior.
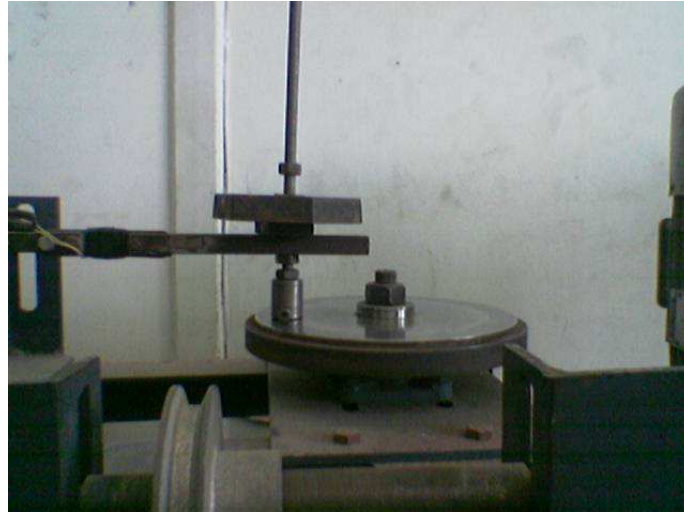
*Fig. 4. Close look to the pin on disc wear test rig*

## 3. RESULTS AND DISCUSSION

### 3.1. Morphology Results

An optical microscope with 500x magnification was used to view the morphology of the polished GF/Cu and EGNS/Cu samples at all weight fractions. A nano like grain boundary phenomenon has been observed clearly at 5wt% for the EGNS/Cu samples, forming contouring lines which might create a potential for an easy separation (Figure 5).
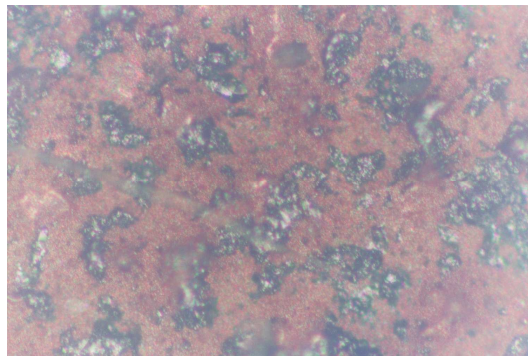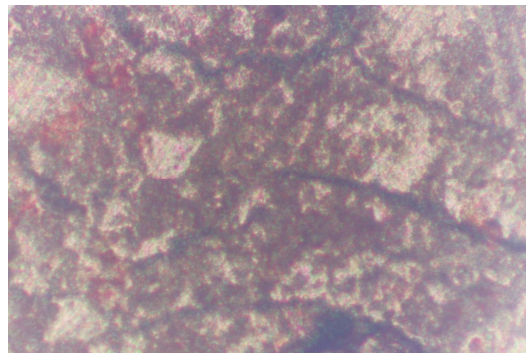


500x        5wt% GF/Cu        500x        5wt% EGNS/Cu

*Fig. 5. Nano likes grain boundaries phenomenon*

### 3.2. Hardness Results

An F scale Rockwell hardness test has been conducted for all the well-polished samples produced. Figure 6 shows the average measurement of five readings for each sample. As shown in Figure 6 the hardness values for both GF and its EGNS decrease as weight fraction increases, which may be attributed to the effect of the nano-like grain boundary phenomenon discovered for EGNS/Cu as well as agglomeration or lack of dispersion in case of GF/Cu.
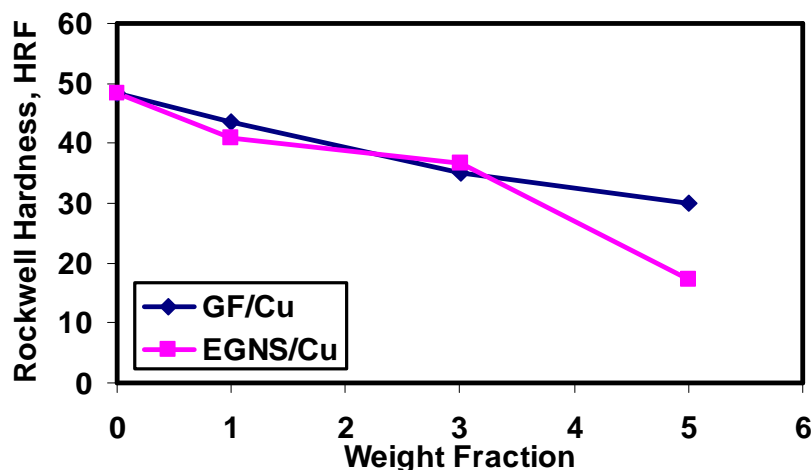
*Fig. 6. Effect of GF and EGNS on hardness values of Cu composites*

### 3.3. Wear Test Results

A delamination domination theory can be introduced here based on visual observation and measured wear values in both GF and EGNS to explain the results presented in Figures 7 and 8. In the case of GF (Figure 7), as weight fraction increases the GF acts as a separator, forming weak layers of graphite and allowing the delamination to dominate as it presents more. In case of EGNS (Figure 8), for the lower weight fraction most of the EGNS prefers to follow the grain boundary contours, forming a separation zone and leaving nothing in the Cu matrix to improve wear characteristics. These separation contours become more pronounced as the applied load increases, which are observed for 1wt% EGNS for 2N to 10N loads. As the EGNS weight fraction increases, a saturation of grain boundary contours with EGNS is established and other EGNS can be seen in Cu matrix areas aiding in the improvement of wear characteristics, as well as balancing the separation. Based on delamination domination theory, wear mechanics eventually fall to the original values, especially at low applied loads.
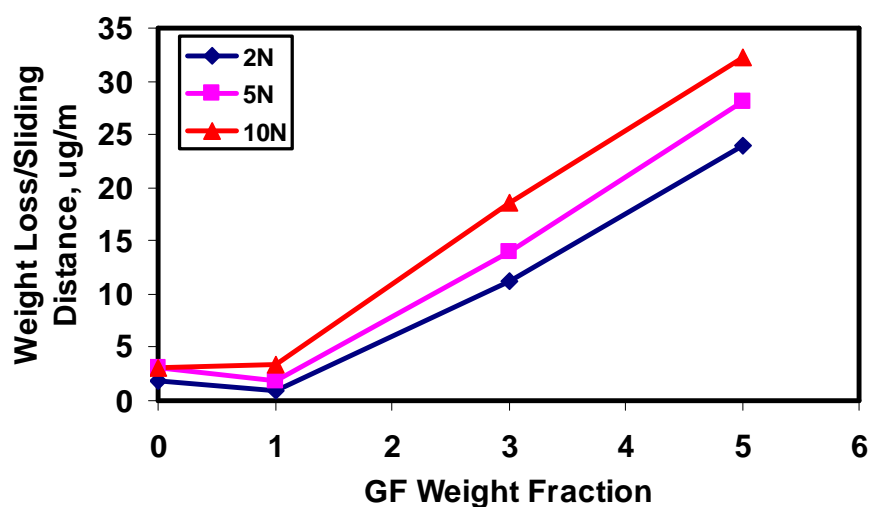


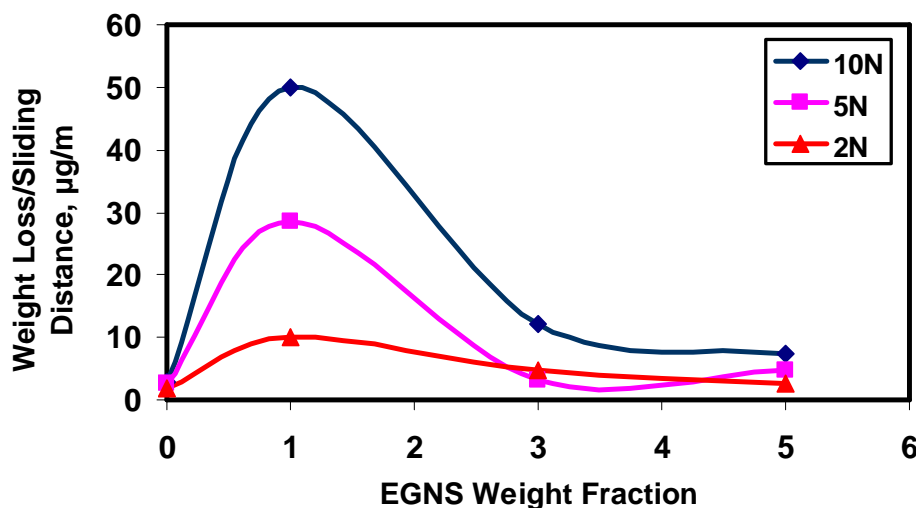*Fig. 7. Effect of GF on wear characteristics of GF/Cu composites*

*Fig. 8. Effect of EGNS on wear characteristics of EGNS/Cu composites*

## 4. CONCLUSIONS

Nano like grain boundary phenomenon has been reported at all weight fractions. Also, delamination domination theory has been observed at low EGNS weight fractions and found to be most affected in wear rate at higher applied loads. A measurement of wear counterpart, methods to improve the dispersion of nano particles (such as using a high power sonicators), experimentation on other matrix materials (such as ceramics and polymers), and a morphological study of nano like grain boundary phenomenon are essential, in order for EGNS to be used in practical and useful industrial applications.

## REFERENCES

1. An J-W, You D-H, Lim D-S, Tribological properties of hot-pressed alumina-CNT composites, Wear, 2003;255:677-681.

2. Chen W.X., Tu J.P., Wang L.Y., Gan H.Y., Xu Z.D., Zhang X.B.: *Tribological application of carbon nanotubes in a metal-based composite coating and composites*. Carbon, 2003;41:215-222.

3. Chen G., Wu D., Weng W., Wu C.: *Exfoliation of graphite flake and its nanocomposites*. Carbon, 2003;41:619-621.

4. Kang F., Zheng Y-P., Wang H-N., Nishi Y., Inagaki M.: *Effect of preparation conditions on the characteristics of exfoliated graphite*. Carbon, 2002;40:1575:1581.

5. Lim D.S., AN J.W. Lee H.J.: *Effect of carbon nanotube addition on the tribological behavior of carbon/carbon composites*. Wear, 2002; 252:512-517.

6. Lim D-S., You D-H., Choi H-J., Lim S-H., Jang H.: *Effect of CNT distribution on tribological behavior of aluminum-CNT composites*. Wear, 2005;259:539-544.

7. Mack J., Viculis L., Ali A.A., Luoh R., Yang G., Hahn T., Ko F., Kaner R.: *Graphite Nanoplatelet Reinforcement of Electrospun Polyacrylonitrile Nanofibers*. Advanced Materials, 2005; 17:77-80.

8. Zhou S.M., Zhang X.B., Ding Z.P., Min C.Y., Xu G.L., Zhu WM.: *Fabrication and tribological properties of carbon nanotubes reinforced Al composites prepared by pressureless infiltration technique*. Composite A, 2006; Article in press:1-6.

9. Zhan Y., Zhang G.: *The role of graphite particles in the high-temperature wear of copper hybrid composites against steel*. Materials and Design, 2006;27:79-84.

10. Zhan Y., Zhang G.: *The effect of interfacial modifying on the mechanical and wear properties of SiCp/Cu composites*. Materials Letters, 2003;57:4583-4591.

## Velina BOZDOUGANOVA

University of Rousse, Bulgaria

# A QUADRILATERAL HYBRID-STRESS MACRO-ELEMENT WITH INCOMPATIBLE INTERNAL DISPLACEMENTS

*A quadrilateral macro-element, containing two-triangle elements, is developed by the hybrid-stress method with incompatible internal quadratic displacements. Stress approximation satisfies the energy compatibility condition. The element stiffness matrix is determined by the Hellinger-Reissner principle. Several test problems are used to compare displacement and stress solution accuracy of the proposed macro-element with published in the literature solutions.*

## INTRODUCTION

Macro-elements consisting of a limited number of basic elements allow achieving high accuracy with fewer degrees of freedom. A quadrilateral macro-element, containing two-triangle elements, is commonly applied. A hybrid stress quadrilateral macro-element with two triangular sub-domains is proposed in [9]. Compatible linear displacements are used on its two triangular sub-domains, and a 5-parameter incomplete linear stress mode is suggested. The present article investigates a similar macro-element with incompatible internal displacements and stress modes, obtained through energy compatibility condition, for the purpose of solving elasticity problems. The hybrid stress method is used to construct the proposed macro-element.

The purpose of this research is to derive the stiffness matrix and to compare the properties of different macro-elements.

In this article the suggested in [1] hybrid macro-element MH with incompatible internal displacements is modified. The difference in the new macro-element MHI is that prescribed boundary displacements are used for finding stress modes through energy compatibility condition.

## HYBRID-STRESS MACRO-ELEMENT WITH INCOMPATIBLE INTERNAL DISPLACEMENTS AND ENERGY COMPATIBILITY CONDITION

For a triangular 3-node finite element with 6 degrees of freedom based on the Hellinger-Reissner principle constant stresses are received as a result of the solution independently of the stress functions power (constant stresses of the element correspond to constant strains). To obtain an effective macro-element, consisting of two triangles, the displacement function character should conform to the stress function in advance.

Therefore, additional higher power incompatible internal displacements are introduced [4, 5, 7, and 8]. In this article, a similar approach is used for the hybrid macro-element.

The internal displacements are introduced for each of the two triangular elements composing the macro element using the approximation

$$u_e = u_q + u_p = N_q^e \, q_e + N_p^e \, p_e = N^e \, r_e, \quad e = 1, 2. \tag{1}$$

The following quantities are used in this formula:

$u_q$ are compatible element displacements, expressed in terms of an element nodal displacements vector

$$q_e = [u_1 \, v_1 \, u_2 \, v_2 \, u_3 \, v_3]^{\mathrm{T}};$$

$u_p$ are incompatible element displacements, expressed in terms of constant parameters vector

$$p_e = [p_1 \, p_2 \, p_3 \, p_4 \, p_5 \, p_6]^{\mathrm{T}};$$

$r_e = [\, q_e^T \ p_e^T \,]^T$ is a generalized coordinates vector;

$$N_q^e = \begin{bmatrix} L_1 & 0 & L_2 & 0 & L_3 & 0 \\ 0 & L_1 & 0 & L_2 & 0 & L_3 \end{bmatrix} \text{ is a shape functions matrix in area coordinates}$$

$L_i \, (i = 1, 2, 3)$ [11] and

$$N_p^e = \begin{bmatrix} L_1^* & 0 & L_2^* & 0 & L_3^* & 0 \\ 0 & L_1^* & 0 & L_2^* & 0 & L_3^* \end{bmatrix} \text{ is an incompatible displacements matrix}$$

where the following functions are used: $L_1^*=L_1L_2$, $L_2^*=L_2L_3$, $L_3^*=L_3L_1$. These functions are hierarchical (they have zero values in the element nodes) and are quadratic area functions.

The stresses are approximated in advance in the form

$$\sigma_e = P_e \, \beta_e, \tag{2}$$

where

$$P_e = [P_1 \, P_2], \, P_1 = I, \, P_2 = [L_1{}^*I \, L_2{}^*I].$$

Here I is the 3x3 identity matrix and $\beta_e = [\beta_1 \, \beta_2 \, \beta_3 \, \ldots \, \beta_9]^{\mathrm{T}}$ are stress parameters to be determined. The parameters number is consistent with the necessary stiffness matrix rank condition [3] and with an invariance requirement [6].

Hellinger-Reissner principle is used to derive the hybrid macro-element stiffness matrix [2]. In this principle the displacements are chosen in the element interior and it is not necessary for the stress functions to be in equilibrium. This ensures more flexi-

bility in the choice of the variables approximation. For each of the two composing tri-angular elements, when the terms corresponding to applied loads are neglected, the Hellinger-Reissner functional has the following form:

$$\Pi_{HR}^e(u,\sigma) = \int_{V_e} (-\frac{1}{2}\sigma_e^T E^{-1}\sigma_e + \sigma_e^T D u_e)dV - \int_{S_u} (u_e - \bar{u})^T n^T \sigma_e \, dS \,, \qquad (3)$$

where $E^{-1}$ is the elastic compliance matrix, $D$ – the differential operator relating displacements and strains, $n^T\sigma_e$ – the element boundary tractions, $n$ – the outward normal matrix of the element boundary, $V_e$ – the volume of the element, $S_u$ – the boundary of the element with prescribed displacements, and $\bar{u}$ – the compatible boundary displacements.

Recognizing that $u_p$ is an incompatible displacements vector and $u_p = u_e - \bar{u}$ on the boundary, the last integral in (3) can be written as

$$\int_{S_u} (u_e - \bar{u})^T n^T \sigma_e \, dS = \int_{S_u} u_p n^T \sigma_e \, dS$$

and according to the idea in [10], this integral can be annulated, i.e. it can fulfill the energy compatibility condition

$$\int_{S_u} u_p n^T \sigma_e \, dS = 0 \,. \qquad (4)$$

This means that the introduced incompatible displacements modify the stresses (2), chosen in advance. Satisfying (4), we get the formula

$$M\beta_e = [M_1 \ M_2] \, [ \, \beta_e^* \ \bar{\beta}_e \, ]^T = 0,$$

from which

$$\bar{\beta}_e = -M_2^{-1}M_1\beta_e^* \,.$$

Therefore the modified stresses are obtained in the form of

$$\sigma_e^* = P^*\beta_e^* = (P_1 - P_2 M_2^{-1}M_1)\beta_e^* \,. \qquad (5)$$

The volume integral in (3) can be transformed by the Gauss-Ostrogradsky formula

$$\int_V (Du)^T \sigma dV = \int_{S_u} u^T n^T \sigma \, dS - \int_V u^T D^T \sigma dV$$

and by implementing the energy compatibility condition (4), the Hellinger-Reissner principle obtains the form

$$\Pi^e_{HR}(u,\sigma) = \int_{V_e} (-\frac{1}{2}\sigma^T_e E^{-1}\sigma_e + \sigma^T_e Du_q)dV .$$ (6)

By substituting the modified stresses (5) and the displacements (1) in (6) we get

$$\Pi^e_{HR} = -\frac{1}{2}\beta^{*T}_e H_e \beta^*_e + \beta^{*T}_e G_e q_e,$$ (7)

where

$$H_e = \int_{V_e} (P^*_e)^T E^{-1} P^*_e dV , \; G_e = \int_{V_e} (P^*_e)^T DN^e_q dV .$$

The parameters $\beta^*_e$ can be expressed in terms of nodal displacements $q_e$ after varying the equation (7), i.e.

$$\beta^*_e = H^{-1}_e G_e q_e.$$

They are substituted in (7) and the stiffness matrix of each triangular element is obtained in the form

$$K_e = G^T_e H^{-1}_e G_e .$$

The macro-element stiffness matrix is received by assembling the two element matrices.

Calculation of the stresses can be done using (5) for each triangle and averaging the stress values in common nodes of the macro-element.

**EXPERIMENTAL RESULTS**

The suggested hybrid macro-element MHI in this article is compared with the similar macro-elements MH [1] and HQM [9] using the stiffness matrix eigenvalues and standard test problems.

The stiffness matrix eigenvalues of the macro-elements shown in Figure 1 are determined in test 1.
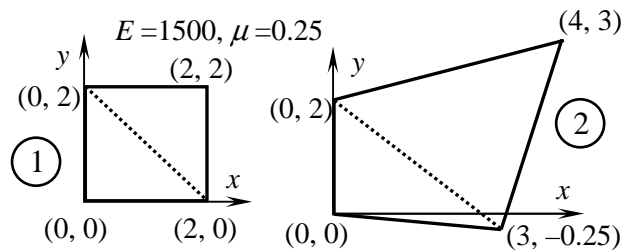


*Figure 1. Macro-elements whose stiffness matrix eigenvalues are calculated*

As it is seen from Table 1, the stiffness matrices have the expected rank ($\lambda_1=\lambda_2=\lambda_3=0$) and have no spurious modes. The stiffness matrix eigenvalues for macro-element HQM are the largest and the eigenvalues of MHI are in the narrowest interval.

*Table 1. Stiffness matrix eigenvalues*

| elements | $\lambda_4$ | $\lambda_5$ | $\lambda_6$ | $\lambda_7$ | $\lambda_8$ |
|---|---|---|---|---|---|
| macro-element 1 | | | | | |
| MHI | 250 | 500 | 500 | 500 | 853,6 |
| MH | 146,5 | 500 | 500 | 500 | 853,6 |
| HQM | 500 | 500 | 1200 | 1200 | 2000 |
| macro-element 2 | | | | | |
| MHI | 233,5 | 264,6 | 534,5 | 614,3 | 939,4 |
| MH | 83,8 | 225,6 | 553,5 | 666 | 1050 |
| HQM | 298 | 649 | 983 | 1344 | 2541 |

A beam under bending (a) and shear (b) is investigated in test 2 (Figure 2). The finite element mesh of the beam consists of only two macro-elements. Vertical displacements sensitivity of the points A and B by mesh distortion is estimated using the distortion parameter *e*.
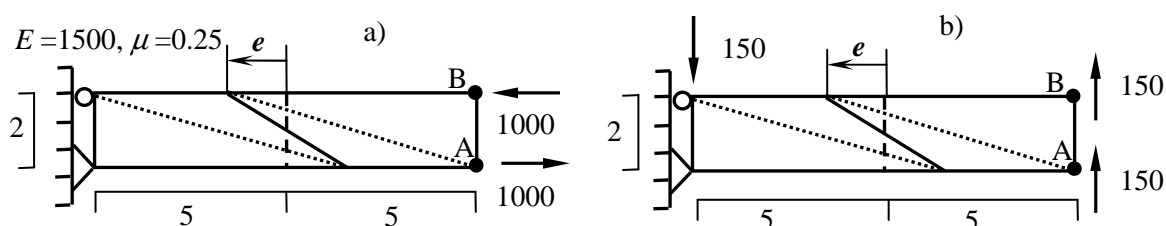


*Figure 2. Cantilever beam for mesh distortion test*

Note that only the macro-elements MHI and MH are insensitive to mesh distortion and have referential displacements ($v_A = v_B = 100$) when the beam is under bending (Table 2a). The macro-element HQM gives the referential displacement value only at $e = 0$, but its accuracy decreases with mesh distortion. In the case of shear (Table 2b), data for the macro-element HQM are missing in [9]. The results for the macro-element MHI are more accurate than the ones for MH.

*Table 2. Cantilever beam for mesh distortion test*

| (a) | elements | $e = 0$ | $e = 1$ | $e = 2$ | $e = 3$ | $e = 4$ | referential |
|---|---|---|---|---|---|---|---|
| | MHI | 100 / 100 | 100 / 100 | 100 / 100 | 100 / 100 | 100 / 100 | |
| $v_A$/ $v_B$ | MH | 100 / 100 | 100 / 100 | 100 / 100 | 100 / 100 | 100 / 100 | 100 |
| | HQM | 100 / 100 | 68,1 / 63,4 | 65,1 / 56,5 | 71,4 / 57,5 | 78 / 57,9 | |
| (b) | elements | $e = 0$ | $e = 1$ | $e = 2$ | $e = 3$ | $e = 4$ | |
| | MHI | 119/119 | 116,5/116,4 | 116/116 | 131/131 | 169/169 | |
| $v_A$/ $v_B$ | MH | 138,2/138 | 119,9/119,6 | 115,7/115,3 | 129/128,5 | 166/165 | 102,6 |

Test 3 is Poisson's ratio locking-free test at plane strain pure bending (Figure 3). The stress at point B and the vertical displacement at point A are investigated when

Poisson's ratio $\mu$ is close to the critical value 0.5 (near the incompressible limit) where the standard 4-node compatible displacement quadrilateral and the constant strain triangle both yield poor results.
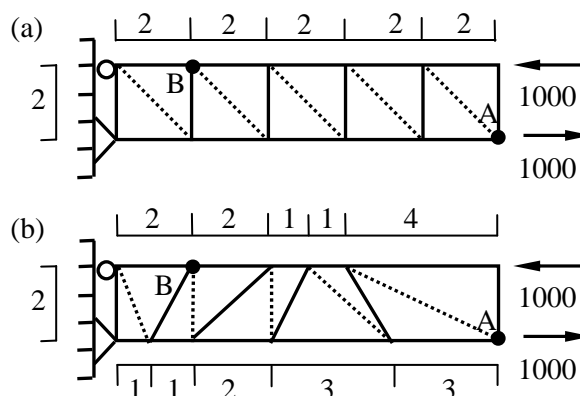


*Figure 3. The plane strain pure bending test*

It is seen from Table 3 that the macro-elements MHI and MH are insensitive when $\mu$ approaches 0.5 and both the stresses and the displacements have the referential values. The macro-element HQM exhibits weak sensitivity and gives values close to the referential ones in the case of an irregular mesh (b).

*Table 3. Results for Poisson's ratio locking-free test*

| | elements | $\mu$ =0,25 | 0,49 | 0,499 | 0,4999 |
|---|---|---|---|---|---|
| $\sigma_{xB}$ | | (a) – regular mesh | | | |
| | MHI, MH | -3000 | -3000 | -3000 | -3000 |
| | HQM | -3000 | -3000 | -3000 | -3000 |
| | | (b) – irregular mesh | | | |
| | MHI, MH | -3000 | -3000 | -3000 | -3000 |
| | HQM | -2999,6 | -2999,6 | -2999,6 | -2999,6 |
| | referential | -3000 | -3000 | -3000 | -3000 |
| $v_A$ | | (a) – regular mesh | | | |
| | MHI, MH | 93,75 | 75,99 | 75,1 | 75,0 |
| | HQM | 93,8 | 76,0 | 75,1 | 75,0 |
| | | (b) – irregular mesh | | | |
| | MHI, MH | 93,75 | 75,99 | 75,1 | 75,0 |
| | HQM | 90,6 | 74,5 | 73,6 | 73,6 |
| | referential | 93,75 | 75,99 | 75,1 | 75,0 |

The next frequently used test problem is MacNeal's test (test 4). The investigated object is the straight slender cantilever beam (Figure 4). The beam has dimensions 6 x 0.2 x 0.1 and is loaded with unit forces at the free end, in case 1 – under bending, in case 2 – under shear. Three types of meshes are used for beam discretization: mesh (a) – regular shape elements (rectangles), (b) – parallelogram shape elements, and (c) – trapezoidal shape elements. The vertical displacement at upper right vertex of the beam is determined in the case when the elastic modules are $E = 10^7$, $\mu = 0.3$.
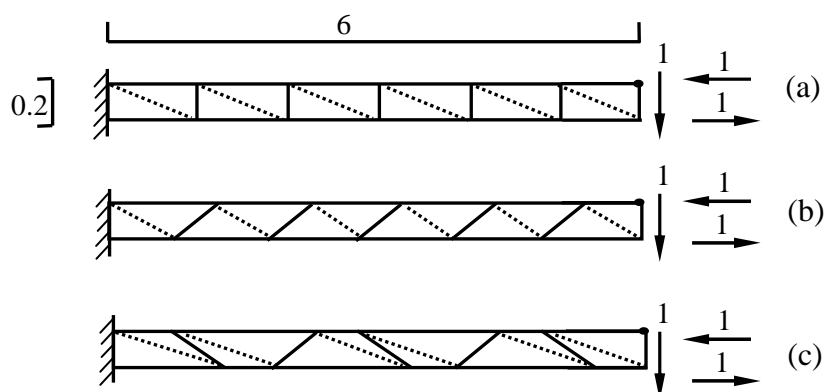
*Figure 4. MacNeal's test*

Typical elements used in the different meshes in MacNeal's test are shown in Figure 5.
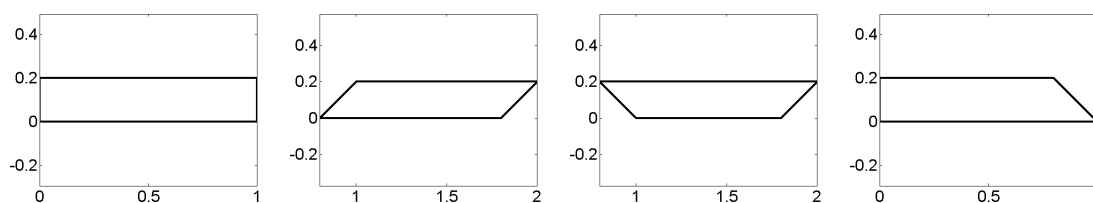


*Figure 5. MacNeal's test elements*

The obtained results are given in Table 4 and only the macro-elements MHI and MH are investigated, because there are no data in [9] for the macro-element HQM. Under bending, both macro-elements have the referential value for all the meshes. In the case of shear, the more accurate results are for the macro-element MHI.

*Table 4. MacNeal's test (vertical displacement)*

| | elements | mesh a | mesh b | mesh c | referential |
|---|---|---|---|---|---|
| load M (bending) | MHI | -0,0054 | -0,0054 | -0,0054 | -0,0054 |
| | MH | -0,0054 | -0,0054 | -0,0054 | |
| | elements | mesh a | mesh b | mesh c | referential |
| load p (shear) | MHI | -0,1097 | -0,1094 | -0,1097 | -0,1073 |
| | MH | -0,1119 | -0,1149 | -0,1116 | |

A disadvantage of the suggested macro-element MHI though is that it does not pass the patch test because the constant stress modes are connected with the linear ones.

## CONCLUSIONS

The main conclusions of this study can be summarized as follows:

1. The comparison of the stiffness matrices eigenvalues shows that "the stiffest" macro-element is HQM. The spectrum of MHI stiffness matrix is the narrowest.

2. Under pure bending and distorted mesh of a membrane, the displacements determined by the macro-elements MHI and MH are insensitive in contrast to the macro-element HQM. Under shear load, the macro-element MHI gives displacements nearer to the referential value.

3. The macro-elements MHI and MH give accurate results under pure bending for both regular and irregular meshes.

4. The proposed macro-element MHI in this article gives better results under shear than MH.

5. It is expedient to use the macro-elements MHI and MH in plane elasticity problems when non- rectangular elements are used in the finite element mesh.

6. For plane strain problems at the nearly incompressible limit, the macro-elements MHI and MH can successfully be used.

## REFERENCES

*1.* Bozdouganova V., Todorov M.: *Investigation of quadrilateral macro-elements obtained by hybrid-stress and modified-force methods*. Mechanics of machines, 68, 179-183, Varna, 2007 (in Bulgarian).

2. Pian T. H., Chen D. P.: *Alternative ways for formulation of hybrid stress elements*. Int. J. Numer. Methods Eng., 18, 1679-1684, 1982.

3. Pian T. H., Chen D. P.: *On the suppression of zero energy deformation modes*. Int. J. Numer. Methods Eng., 19, 1741-1752, 1983.

4. Pian T. H., Sumihara K.: *Rational approach for assumed stress finite elements*. Int. J. Numer. Methods Eng., 20, 1685-1695, 1984.

5. Pian T. H.: *Some notes on the early history of hybrid stress finite element method*. Int. J. Numer. Methods Eng., 47, 419-425, 2000.

6. Spilker R. L., Maskeri S. M., Kania E.: *Plane isoparametric hybrid-stress elements: invariance and optimal sampling*. Int. J. Numer. Methods Eng., 17, 1469-1496, 1981.

7. Wilson E. L., Taylor R. L., Doherty W. P., Ghaboussi J.:. *Incompatible displacement models*. Numerical and Computer Methods in Structural Mechanics, Fenves SJ et al. (eds). Academic Press: New York, 41-57, 1973.

8. Wu C. C., Cheung V.: *On optimization approaches of hybrid stress elements*. Finite Elements Anal. Des., 21, 111-128, 1995.

9. Xiao-Ping Xie. *An accurate hybrid macro-element with linear displacements*. Commun. Numer. Methods Eng., 21, 1-12, 2005.

10. Xie Xiaoping, Tianxiao Zhou. *Optimization of stress modes by energy compatibility for 4-node hybrid quadrilaterals*. Int. J. Numer. Methods Eng., 59, 293-313, 2004.

11. Zienkiewicz O. C., Morgan K.: *Finite elements and approximation*. Moscow, Mir, 1986 (in Russian).

**Marino BRČIĆ**
**Marko ČANAĐIJA**
**Josip BRNIĆ**

Department of Engineering Mechanics, Faculty of Engineering, University of Rijeka, Croatia

# STRUCTURAL MODEL OF A CARBON NANOTUBE

*In this paper a theory about single and multi walled carbon nanotubes and a suitable way for modeling them using finite element method is presented. Precisely, in order to model a carbon nanotube, first we have to describe and find a linkage between molecular mechanics system and structural mechanics system and then use those results and demonstrate them on example. A brief theory concerning MWNT is given, as well as a theory of modeling a connecting interface between layers, as a result of van der Waals interactions. Different loading conditions are used for example of single and multi walled carbon nanotubes under specific load. Results are compared with results given by the other authors.*

## 1. INTRODUCTION

In the past twenty years nanotechnology and nano oriented materials, especially carbon nanotubes, have aroused a major interest among engineers and scientists, owing to works of Iijima [8] and Tersoff [9]. Carbon nanotubes have unique and remarking mechanical and electrical properties, such as high stiffness, strength and the ability to recover from elastic buckling. Results for Young's and shear moduli of carbon nanotubes obtained by experiments and theoretical considerations, around 1 TPa for Young's and 0.5 TPa for shear modulus, give us a reason to further research carbon nanotubes. One of the most interesting applications of carbon nanotubes is in nanocomposite materials. In order to fully explore its potential for application in composite materials, knowledge about elastic properties and behaviour of carbon nanotubes is necessary. Production of these materials and composites are performed on microscopic, nanometer scale, with aim to obtain macroscopic usage. Their extremely small size presents significant challenge to researches, so computer modeling is one of the logical solutions.

Experimental results show that tensile strength of carbon nanotubes is below 65 GPa [2], while theoretical considerations give tensile strength of carbon nanotube up from 100 GPa [4] to extraordinary 300 GPa. The main issue in computer modeling of carbon nanotubes is representing a molecular mechanics structure of carbon nanotubes to reasonable structural model, which can substitute carbon nanotube in further research and examination.

### NANOTECHNOLOGY AND CARBON NANOTUBES

A carbon nanotube can be observed as a large molecule consisting of carbon atoms, forming a hexagonal mesh. Also, it may be regarded as a one atom thick sheet of graphite rolled into a tube, with high aspect ratio, up to ten thousand. Such cylinder

can be observed as a fundamental structural unit and is called a single walled carbon nanotube (SWNT). Using that fundamental structural unit we can form a multi walled carbon nanotube (MWNT). Each carbon atom in a SWNT has three nearest neighbor atoms, and they are bonded by covalent bonds, which have characteristic properties, such as bond length and bond angle. MWNTs are in fact concentrically nested SWNTs, with distance between two layers, or walls, of 0.34 nm. Atoms on different layers of MWNT, are not connected by covalent bonds and only interaction between them is through van der Waals forces. Van der Waals forces are rather weak compared to covalent bonds.

A SWNT is characterized in terms of diameter and chiral angle $\theta$, or with chirality of a tube. Chirality affects nanotube's metallic or semiconductor behaviour, as there are three basic pattern type of SWNT, in addition to being classified as single or multi walled nanotube: zig-zag, with chiral angle $\theta = 0°$, armchair with chiral angle $\theta = 30°$ and basic chiral nanotube with chiral angle in range from $0° < \theta < 30°$ [3]. Since the layers of MWNT are structurally independent of one another, the chirality of the layers may be different. The distance between neighboring layers is assumed to be 0.34 nm, that is, the same as the spacing between adjacent graphene sheets in graphite.

## 3.  STRUCTURAL MECHANICS NANOTUBE MODEL

### 3.1.  Finite element model of carbon nanotube

A carbon nanotube is a frame like structure, with characteristic bond length and bond angle. Thus, when a nanotube is subjected to external load the displacements of atoms are constrained by these bonds, and total deformation of the nanotube is the result of bond interactions. Therefore, a substitution of these bonds with isotropic beam elements and instead of carbon nanotube can be made, to form a frame like structure consisting from nodes and elements. In order to do so, a linkage must be found between molecular mechanics and structural mechanics. That linkage can be described using the force field, which is generated between carbon atoms, generated by electron – nucleus and nucleus – nucleus interactions. That force field can be expressed in the form of steric potential energy:

$$U = \sum U_r + \sum U_\theta + \sum U_\phi + \sum U_{vdw} \tag{1}$$

where $U_r$ denotes energy associated to bond stretch interaction, $U_\theta$ a bond angle bending, $U_\phi$ torsion, dihedral and out of plane and $U_{vdw}$ a nonbonded van der Waals interaction (forces). Terms for individual energy are given:

$$U_r = \frac{1}{2} k_r \left( r - r_0 \right)^2 = \frac{1}{2} k_r \left( \Delta r \right)^2 \tag{2}$$

$$U_\theta = \frac{1}{2} k_\theta \left( \theta - \theta_0 \right)^2 = \frac{1}{2} k_\theta \left( \Delta \theta \right)^2 \tag{3}$$

$$U_\phi = \frac{1}{2} k_\phi \left( \Delta \phi \right)^2 \tag{4}$$

where $r$ and $\theta$ refer to distance and bond angle after deformation, $r_0$ and $\theta_0$ refer to undeformed distance and bond angle, while terms $\Delta r$, $\Delta\theta$ and $\Delta\phi$ correspond to change in bond length, bond angle and angle change of bond twisting. Constants $k_r$ represents bond stretching force constant, $k_\theta$ bond angle bending force constant and $k_\phi$ torsional resistance of the chemical bond.

We can substitute these bonds with isotropic beam elements and so instead of carbon nanotube, we have a frame like structure. The beam elements have length $L$, cross sectional area $A$ and moment of inertia $I$. If we now subject these beams to three types of load (axial, torsional and bending), but not at the same time, because in terms (2), (3) and (4) is given potential energy for individual interaction in molecular mechanics so we have to consider energies in structural mechanics also under individual forces, we obtain the following:

- the strain energy of uniform beam of length $L$ subjected to axial force $N$:

$$U_A = \frac{1}{2}\int_0^L \frac{N^2}{EA}\,dL = \frac{1}{2}\frac{N^2 L}{EA} = \frac{1}{2}\frac{EA}{L}(\Delta L)^2 \tag{5}$$

- the strain energy of a uniform beam under pure bending moment $M$ :

$$U_M = \frac{1}{2}\int_0^L \frac{M^2}{EI}\,dL = \frac{2EI}{L}\alpha^2 = \frac{1}{2}\frac{EI}{L}(2\alpha)^2 \tag{6}$$

- the strain energy of a uniform beam under pure torsional moment $T$:

$$U_T = \frac{1}{2}\int_0^L \frac{T^2}{GJ}\,dL = \frac{1}{2}\frac{T^2 L}{GJ} = \frac{1}{2}\frac{GJ}{L}(\Delta\beta)^2 \tag{7}$$

In equations (5), (6) and (7), $\Delta L$ denotes axial deformation, $\alpha$ denotes the rotational angle, or bend angle, and $\Delta\beta$ is relative rotation between the ends of the beam, or twist angle.

Equations (2) – (4) and equations (5) – (7) represent the same quantities, only in different systems, molecular and structural. To establish a link between those two systems, assuming that $\Delta L$ is equivalent to $\Delta r$, $\alpha$ equivalent to $\Delta\theta$ and $\Delta\beta$ equivalent to $\Delta\phi$, we can identify them and thus obtain direct relationship between the molecular mechanics parameters, $k_r$, $k_\theta, k_\phi$ and structural mechanics parameters, the tensile stiffness ($EA$), cross sectional bending stiffness ($EI$) and torsional rigidity ($GJ$) as follows:

$$\frac{EA}{L} = k_r\,, \quad \frac{EI}{L} = k_\theta\,, \quad \frac{GJ}{L} = k_\phi \tag{8}$$

The parameters in terms (8) are sufficient for modelling a single walled carbon nanotube as a frame like structure with beam elements.

## 3.2. Van der Waals forces

Atoms on different layers of MWNT, are not connected by covalent bonds. Only interaction between them is through van der Waals forces, which can be either an at-

traction force or a repulsion force. The attraction will appear when atoms approach each other within a certain distance, while repulsion will occur when the distance between atoms becomes less then the sum of their contact radii. Since van der Waals interactions are non bonded, in comparison with covalent bonds between atoms, van der Waals interactions are very weak. Consequently, they are not going to be introduced in this paper. It is of special interest to see influence of these interactions on Young's and shear moduli. Introduction of such bonds leads towards substantial increase in computational costs, so dropping out these from the model can be beneficiary.

Using the general Lennard – Jones "6–12" potential, given in term (9), a van der Waals interaction can be modelled.

$$U(r) = 4\varepsilon \left[ \left( \frac{\sigma}{r} \right)^{12} - \left( \frac{\sigma}{r} \right)^6 \right] \tag{9}$$

In above term, $r$ represents distance between interacting atoms, $\varepsilon$ and $\sigma$ are the Lennard – Jones parameters, and for carbon atoms their amount is $\varepsilon = 3.86 \cdot 10^{-13}$ Nnm, $\sigma = 0.34$ nm. Deriving upper term in regards to distance between interacting atoms, an expression for van der Waals force is obtained:

$$F(r) = -\frac{\mathrm{d}U(r)}{\mathrm{d}r} = 24 \frac{\varepsilon}{\sigma} \left[ 2 \left( \frac{\sigma}{r} \right)^{13} - \left( \frac{\sigma}{r} \right)^7 \right] \tag{10}$$

In MWNT, an atom situated in one layer can form an interacting pair with several atoms from neighbour layer as long as the distance between the pair of atoms is less then 2.5 $\sigma$ (0.85 nm). So, the conclusion is that the van der Waals force between two atoms is highly nonlinear.

## 4. DETERMINATION OF CARBON NANOTUBE MODULI

### 4.1. Modeling of covalent bonds

Modeling of carbon nanotube can be divided in two steps. In the first step, substitution of covalent bonds with beam elements is made. Next in order is calculation of beam element properties, such as cross section area of beam element, moments of inertia and torsional constant using molecular mechanics parameters $k_r$, $k_\theta$ and $k_\phi$ which are deducted from (8). Young's modulus, can be arbitrary selected as 1 nN/nm$^2$, $v$ is Poisson's number, is selected to be 0,3 what gives shear modulus $G = 0,384 \, nN/nm^2$, $A$ is cross section area of beam element. The shape of beam element is circular bar, with length 0,143 nm.

Constant values are taken from previous works [1] and experience with graphite sheets and their amount is $k_r = 651,72 \, \text{nN/mm}, k_\theta = 0,875 \, \text{nNnm/rad}^2, k_\phi = 0,2779 \, \text{nNnm/rad}^2$. Using these values, structural mechanics parameters of beam element are calculated from above equations. Thus, cross sectional area of beam element that models covalent bond is $A = 92,544 \, \text{nm}^2$, moments of inertia are $I_1 = I_2 = 0,1243 \, \text{nm}^4$ and torsional constant is $J = 0,10277 \, \text{nm}^4$.

## 4.2. Frame – like structure model of SWNT

With such model of covalent bond at hand, second step in modeling of carbon nanotube is modeling a carbon nanotube with frame-like structure (Fig. 1). Initially, the carbon nanotube is loaded with axial force and Young's modulus, shear modulus and Poisson's number are obtained. Moduli obtained in that way will serve as a verification tool since they will be compared with experimental data provided by other authors.
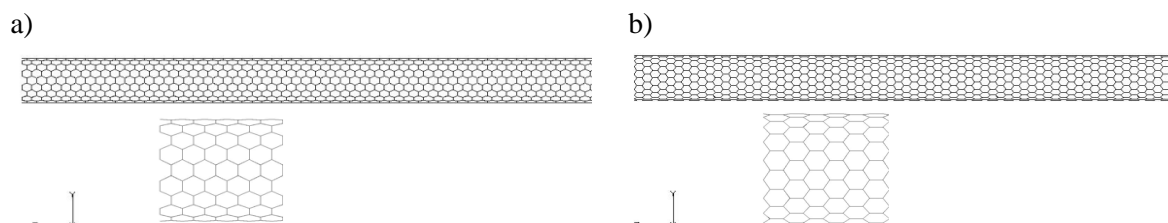
a)                                                    b)



*Fig. 1. SWNT frame like structure model; a) armchair pattern and detail, b) zig – zag pattern and detail*

A single walled carbon nanotube with both patterns, armchair and zig – zag, were subjected to axial load. Nanotubes were constrained to form a cantilever beam and were loaded at their free end with axial force of 5 nN. In table 1. are given some geometric and mesh properties for two differenet types of nanotube patterns, while they have some different geometric properties due to different formation of hexagonal cells.

*Table 1. Geometric properties of SWNT patterns*

| Pattern / Value: | Armchair | Zig – zag |
|---|---|---|
| Initial length, $L$ [nm]: | 17,22 | 17,283 |
| Diameter, average, $D_{avg}$ [nm]: | 1,352 | 1,404 |
| Thickness, $t$ [nm]: | 0,34 | 0,34 |
| Area, $A$ [nm$^2$]: | 1,445 | 1,5 |

With cross section area $A$ calculated from $A = D_{avg} \cdot \pi \cdot t$, trial axial force and elongation of nanotube obtained from FE model, using following equation:

$$E = \frac{F \cdot L}{A \cdot \Delta L},$$ (11)

Young's modulus for both patterns of SWNT is obtained. Results are given in table 2.

*Table 2. SWNT load results*

| Pattern / Value: | Armchair | Zig – zag |
|---|---|---|
| Trial axial force, $F$ [nN]: | 5 | 5 |
| Elongation, $\Delta L$ [nm]: | 0,05739 | 0,055 |
| Calculated Young's modulus, $E$ [TPa]: | 1,038 | 1,047 |

At the free end of axially loaded nanotube diameter reduction $\Delta D$ is calculated. Using those displacements and with expressions for longitudinal and lateral deformation,

a shear modulus of SWNT can be obtained. Expressions for deformation are used to obtain Poisson's number, *v*:

$$G = \frac{E}{2(1+v)}, \quad v = \frac{\varepsilon_p}{\varepsilon_z}, \quad \varepsilon_z = \frac{\Delta L}{L}, \quad \varepsilon_p = \frac{\Delta D}{D_{avg}}. \tag{12}$$



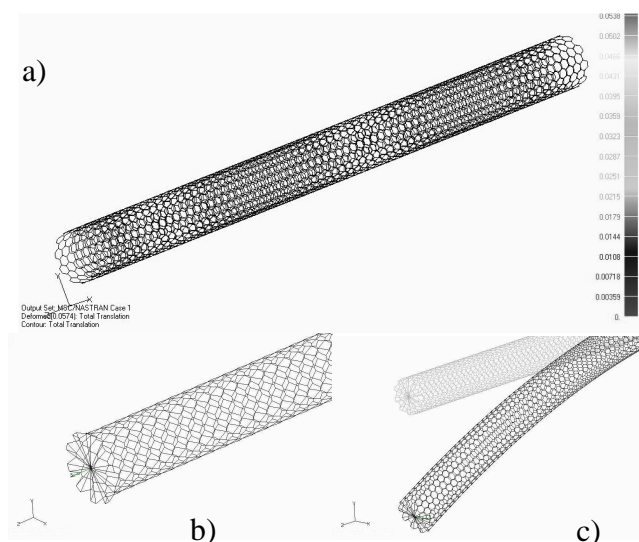Fig. 2. SWNT armchair, a) axially loaded, b) torsion, c) bending

*Table 3. Calculated results for shear modulus*

| Pattern / Value: | Armchair | Zig – zag |
|---|---|---|
| Lateral deformation, $\varepsilon_p$: | 0,000793 | 0,000377 |
| Longitudinal deformation, $\varepsilon_z$: | 0,00332 | 0,00318 |
| Poisson's number, $v$: | 0,238 | 0,12 |
| Shear modulus, $G$ [TPa]: | 0,4196 | 0,467 |

When compared to results given by Kalamkarov et al. (2006.) [3], for single walled carbon nanotube, with specified diameter, deviations are very small. Concerning Young's modulus, for armchair and zig – zag nanotube with diameters from 1,35 to 1,4 nm, they give *E* in range from 1,01 to 1,04 TPa, and our results are in that range. For shear modulus, armchair nanotube has something smaller modulus then zig – zag nanotube, which is also the case with our results. They give range of *G* from 0,4 to 0,45 TPa for nanotubes between 1,35 to 1,4 nm diameter, and as shown in upper table, for armchair nanotube we obtained shear modulus of 0,4196 TPa, and for zig – zag nanotube, which is said to be slightly greater then armchair, is 0,467 TPa.

## 4.3. Frame – like structure model of MWNT

With the knowledge from FEM modelling of SWNT, a model of multi walled carbon nanotube with two layers – Double Walled Carbon Nanotube (DWNT) is straightforward (Fig. 3). Using that model, through different loads, Young's and shear moduli of a DWNT will be determined.

Values used for modelling covalent bonds between atoms with beam elements are same as for modelling a SWNT. Our DWNT consist of two armchair SWNT, of which

inner tube was (10,10) armchair SWNT, whilst outer tube was (15,15) armchair SWNT. Interlayer spacing is 0.34 nm. Some geometry characteristics are given in lower tables.

*Table 4. Inner nanotube geometric properties*      *Table 5. Outer nanotube geometric properties*

| Inner SWNT | |
|---|---|
| Type: | Armchair |
| Chirality: | 10, 10 |
| Avg. diameter: | 1.4 nm |
| Length: | 17.22 nm |

| Outer SWNT | |
|---|---|
| Type: | Armchair |
| Chirality: | 15, 15 |
| Avg. diameter: | 2.08 nm |
| Length: | 17.22 nm |
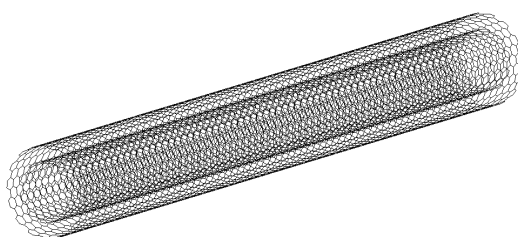


*Fig. 3. FEM model of DWNT*

To obtain Young's modulus, nanotubes were connected with rigid element, i.e. top nodes of each nanotube were connected with central positioned master node, constrained to form a cantilever beam, and axially loaded at their free end with force of 5 nN. Young's modulus is calculated from eq. (11). *A* is cross sectional area of DWNT, which is calculated as:

$$A = \frac{\pi}{4}\left[ \left(d_o + 0.34\right)^2 - \left(d_i - 0.34\right)^2 \right] . \tag{13}$$

In term (13) $d_o$ represents outer tube diameter and $d_i$ inner tube diameter. Using terms (11), (13) and with elongation obtained through axial load, $\Delta L = 0.0223053$ nm, result for Young's modulus of DWNT, is $E = 1.04$ TPa. Comparing this to results given by Li and Chou (2002.) [10], where they obtain Young's modulus of two layer armchair MWNT, with same diameters, $E = 1.05 \pm 0.05$ TPa, results are in the same range.

In order to determine shear modulus, a DWNT must be subjected to a torsional load, i.e. a DWNT will be constrained in the same manner as in axial loading, forming a cantilever beam and loaded with torsional moment $M = 5$ nNnm. The shear modulus $G$ is calculated using following term:

$$G = \frac{M \cdot L}{\varphi \cdot I_P} , \tag{14}$$

where $M$ is applied moment, torque, $L$ length of DWNT, $\varphi$ represents the torsional angle at the end of the tube and $I_p$ is the polar moment of inertia, which is calculated as follows:

$$I_p = \frac{\pi}{32}\left[\left(d_o + 0.34\right)^4 - \left(d_i - 0.34\right)^4\right] \tag{15}$$

The torsional angle obtained through tosional load, $\varphi = 0.063455$ rad, and using it in terms (14) and (15), shear modulus is obtained, for DWNT $G = 0.418$ TPa. According to Li and Chou (2002.) [10], average shear modulus for two layer MWNT is about 0.4 TPa and is lower than of an SWNT. If those two shear modulus compared and in further comparison with shear modulus of a SWNT modelled in this paper (G = 0.419 TPa), conclusion can be made that all results are satisfying.

## 5. CONCLUSIONS

Structural mechanics models of a single walled and multi layered carbon nanotube, using finite element method, were presented in this paper. The results of modelling, expressed through Young's and shear moduli, were compared with the results from other authors. Next step in CNT research, is incorporation or, better said, further investigation of influence of van der Waals interactions on MWNT properties, i.e. finding a proper and correct way of modelling of a such non bonded interactions. Using those findings, behaviour of a MWNT in different conditions and with different parameters can be explored. These can be, for example, influence of a diameter and a number of layers on a MWNT properties, temperature influence etc. The main goal of these CNT researches is finding a right way to incorporate a SWNT and a MWNT model in composite material, using a multiscale modelling for analyzing nanocomposite materials.

## REFERENCES

1. Chunyu Li, Tsu–Wei Chou: *A structural mechanics approach for the analysis of carbon nanotubes*. International Journal of Solids and Structures, vol. 40, 2003, pp. 2487-2499.
2. Chunyu Li, Tsu–Wei Chou: *Modeling of elastic buckling of carbon nanotubes by molecular structural mechanics approach.* Mechanics of Materials, vol. 36, 2004, pp. 1047-1055.
3. Kalamkarov A.L., Georgiades A.V., Rokkam S.K., Veedu V.P., Ghasemi-Nejhad M.N.: *Analytical and numerical techniques to predict carbon nanotubes properties*. International Journal of Solids and Structures, vol. 43, 2006, pp. 6832-6854.
4. Odegard G.M., Gates T.S., Nicholson L.M., Wise K.E.: *Equivalent-continuum modelling of nanostructured materials*. Composites Science and Technology, vol. 62, pp. 1869-1880.
5. Fu Yiming, Xu Xiaoxian: *Analysis of material mechanical properties for single-walled carbon nanotubes*. Acta Mechanica Solida Sinica, vol. 18, 2005, pp. 46-51.
6. Rappe A.K., Casewit, C.J., Colwell, K.S., et al.: *A full periodic-table force-field for molecular mechanics and molecular dynamics simulations*. Journal of American Chemical Society, vol. 114, 1992, pp. 10024 – 10035.
7. Scientific American, Volume 295, Number 5, 2007, pp. 58-65.
8. Iijima S.: *Helical microtubes of graphitic carbon*. Nature 354, 1991, pp. 56-58.
9. Tersoff J.: *Energies of fullerenes*. Phys. Rev. B, 1992, vol. 46, pp. 46
10. Li C., Chou T.W.: *Elastic moduli of multi-walled carbon nanotubes and the effect of van der Waals forces.* Composites Science and Technology, vol. 63, 2003, pp. 1517-1524.
11. Batra R.C., Sears A.: *Continuum models of multi-walled carbon nanotubes*. International Journal of Solids and Structures, Vol. 44, (2007), pp. 7577-7596.

**Janette BREZINOVÁ**
**Anna GUZANOVÁ**

Faculty of Mechanical Engineering, Technical university of Košice, Slovakia

# THE THERMAL BALANCE OF MECHANICAL SHOT PEENING PROCESS

*The paper deals with the temperature influence of substrate during shot peening with using of contact measure method by thermocouples. Identical results like in process of shot peening are possible to achieve by application of high-speed cold forming processes. Relative mass of energy absorbed by deformated material is reduced with increasing deformation degree. Heating measure depends on deformation condition, speed and degree of deformation.*

## INTRODUCTION

Technology of shot peening belongs to the part of mechanical treatment of substrate surface. Its tool – shot brings some qualitative changes in surface layers by impact on substrate besides it created a characteristic surface morphology [1]. From the point of view of shot peening effect on basic material is shot peening understood as a process of plastic deformation of surface respectively as a process of elasticity – plastic deformation of metal in its whole volume. The total energy of shot peening will be consumed on own plastic deformation accompanied by hardening of basic material, thermal effect, structural changes and change of mechanical and technological properties. The secondary effects of shot peening process are as follows: residual stresses and change of surface character.

Shot peening is characterized by high velocity of the tool, large plastic deformation and short time of process duration. Shot peening method will absorb a past of energy consumed on plastic deformation, the other part will be convert on warm development. The thermal influence of substrate by shot peening also as the circumstances by plastic deformation depends on deformation conditions [2, 3]. The strength of material surface layers goes down with temperature increased. Because the activity of atoms decreases with risen temperature, it is possible that by diffusion controlled processes will substantially influence the behaviour and feature of material surface layers by elevated temperatures [4, 5].

Submitted contribution deals with thermal influence of substrate by shot peening using contact measuring method by thermocouples.

## MATERIALS AND METHODS

Shot peening was performed on pneumatic peening equipment type TJVP-320, with operating pressure 0,5 MPa by using cylindering nozzle with inside diameter φ 9 mm. Distance of nozzle from surface samples was 250 mm. Mono-dispersing steel shot S 280 dz = 0,85 was used. Angle of shot impact to worked substrate was 90°. Specimen φ 30x3 mm were made from material 11375.10 and placed in wooden panel, which secured the minimal thermal affection of samples. Circular form of samples was chosen for purpose to uniform heat removal into the sample. Impacting shot stream was directed to the middle of samples, Fig. 1.
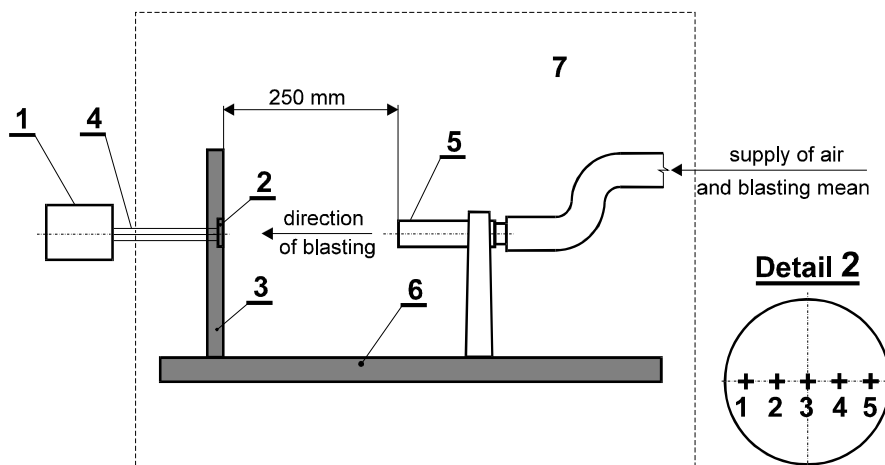


*Fig. 1. Scheme of substrate thermal balance measurement: 1-measure equipment, 2 – sample, 3 – wooden panel, 4 – thermocouples, 5 – jet, 6 – stand, 7 – peening box*

Measuring of thermal effect of the shot peened substrate was realized by thermo-couple of NiCr-Ni type, diameter 1 mm. Thermocouple have a minimal thermal persistence they measure the temperature almost immediately. Used thermocouples consisted of metal tube, in which was rammed isolation material and fixation rider of thermocouple. Measurement accuracy in extent 100-400°C was ±0,3°C. Correction was realised by calculations after measurement. Scanning and record of measured temperatures was realised by means of measuring data logger Therm 5500. Scanning interval was 2 s. Cut of thermocouple is illustrated in Fig. 2.
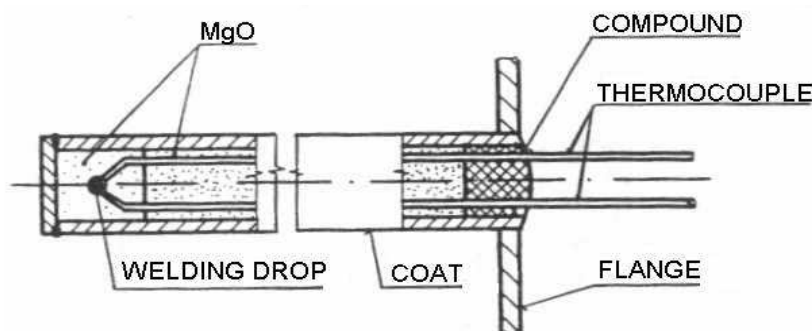


*Fig. 2. Cut of thermocouple*

   The thermocouples were placed in a specimen in depth 1,5 mm and 0,5 mm under surface substrate. Five pieces of thermocouples were used by each measurement by distance 5 mm each, Fig. 1, Detail 2.

## RESULTS AND DISCUSSION

   Pneumatic shot peening is characterised by free airflow from jet. Peening medium forms the tracks after impact on surface. Their form and density depends on shot peening parameters. Distributions of impact density of granulate influences the distribution of thermal fields on specimen. The surface of peening substrate is continually cooled by air supplied from the jet during pneumatic peening as well as by heat removal into substrate and shot medium material.

   Fig.3 shows time dependence of temperature changes in individual place. Start phase of shot peening process was about 0,32 min. The courses present three characteristic areas, which belong to temperature changes. The first area is characterised by temperature, which rise to maximum value. The second one is characterised by moderate fall of temperature of samples and material features. The third one is characterised by gradually temperature compensation towards room temperature. This area corresponds to the ending of the shot peening process. Maximum temperature was 144,4°C in the depth 0,5 mm under surface of samples after 1 min of shot peening. Measurement was obtained by thermocouple No. 4.
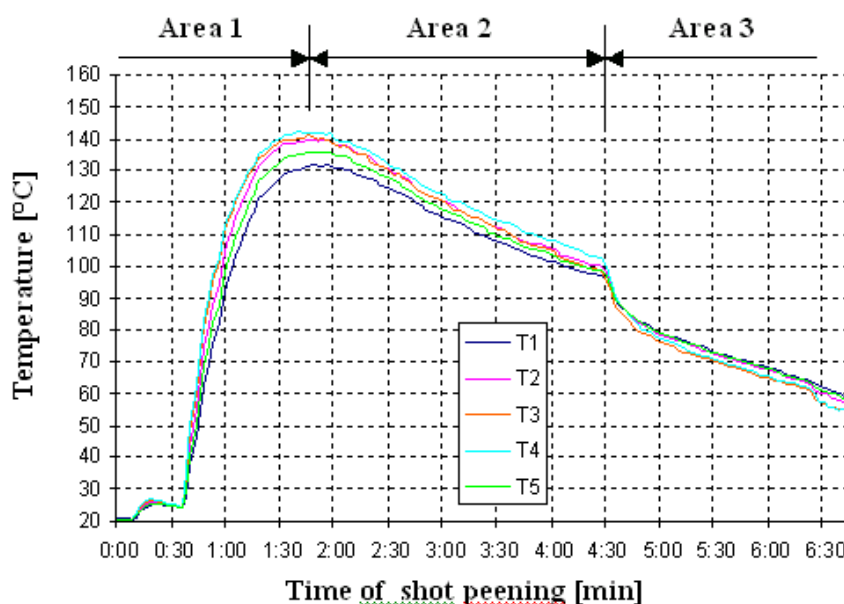


*Fig. 3. Changes of temperature during shot peening process*

   Fig. 4 shows the distribution of temperature in sample level. The lowest temperatures were measured in sample borders. They are caused by the boundary conditions of warm. The highest temperature was measured in the middle of sample (thermocouple 2,3 and 4). The temperature pushing towards the thermocouple 4 can be caused by conditions of medium flow from the jet. The warm transfer is occurred mainly by conduction in this case.
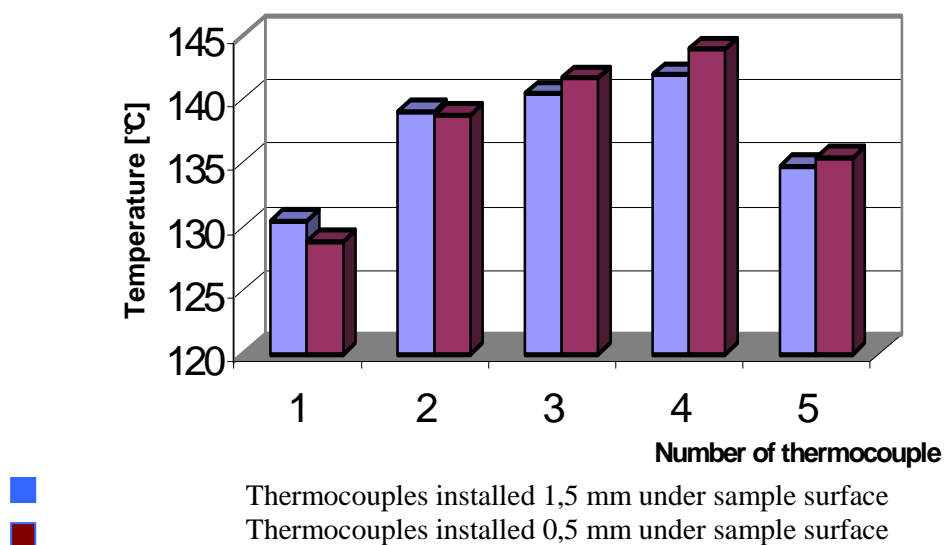
*Fig. 4. Distribution of temperature in sample level*

**CONCLUSION**

By using of knowledge about cold forming processes at high velocities it is possible to reach partly identical results by shot peening. The temperature value of peened material surface increases with growth of peening time towards a certain value. The warm transfer in the investigated material is mostly realised by conduction. The relative quantity of energy absorbed by deformed material decreases according to increased deformation degree. Shot peening conditions, peening time, size of peened surface and impact density of shot influences the temperature level.

**REFERENCES**

1. Kniewald D.: *Nové poznatky pri výrobe matovaných plechov*. Kandidátska dizertačná práca. Košice, VŠT SjF, 1971.

2. Takáč K.: *Vplyv režimu tryskania na životnosť tryskacích prostriedkov*. Kandidátska dizertačná práca. Košice, VŠT SjF, 1969.

3. Pollák L.: *Vplyv deformácie povrchu na dynamické vlastnosti tenkých plechov*. Kandidátska dizertačná práca. Košice, VŠT SjF, 1967.

4. Zrník et. al.: *Vybrané kapitoly z fyzikálnej metalurgie*. Degradačné procesy. TU HF, Košice, 2000.

5. Hasegawa N. et. al.: *The temperature change on surface of workpiece during peening*. ICSP 7, Wasaw, Poland 1999.

**Janette BREZINOVÁ**
**Anna GUZANOVÁ**

Faculty of Mechanical Engineering, Technical university of Košice, Slovakia

# POSSIBILITY OF MECHANICAL DEPOSITION OF PROTECTIVE Zn COATINGS

*This paper presents actual investigation results of experiment that was oriented to the verification of the possibility of applying zinc on steel surface by blasting technology using zinc-coated cut wire. Suitable method for zinc layers deposition and evaluation of their corrosion resistance was determined. Accelerated laboratory tests with presence of $SO_2$ and long term working tests in atmospheric conditions was used. Creation of incoherent zinc coatings was established on the bases of metallographic and spectral analysis. Process of cold zinc by blasting is able to use as temporary anticorrosion protection of steel surface.*

## INTRODUCTION

The surface treatment, in most causes, requires the surface pre-treatment of basic material. Increased claims on production quality require higher cleanness and quality of surface for the final surface treatment. Almost all the materials succumb to destroying in contact with the surrounding environment. It is caused by heterogeneous chemical and electrochemical reactions taking place between material surface und surrounding aggressive environment. The corrosion can be defined as chemical depreciation of material. The various technical and other consequences to be considered by study of corrosion [1].

One of the widely used mechanical pre-treatment of surface for applying as functional as protective paints is blasting technology. Blasting is a kind of mechanical treatment of base surface where a blasting medium (further BM) as a tool of blasting involves the qualitative changes in the surface layers of substrate in which originates the characteristic surface morphology [2]. The blasted surface has a high surface activity. In real conditions decreases its activity very quickly at chemical adsorption of atmospheric gases and oxidation [3].

Activity of blasted surfaces influences the character of deformation of subsurface layer. Sub-surface layer influenced by plastic deformation after blasting has a higher energetic level in comparison with non-influenced metal. Under influence of deformation increases the quantity of failures in crystal grating, increases dislocation density

what increases the ability of metal to react with surrounding environment. The deformation helps to ion-atom of metal to overcome the metal binding and gives it's a possibility to retire from the grate i.e. it decreases the ion output work. In consequence of this reality electrode potential of metal decrease. According to the further information the deformation influences the adsorption ability, which is higher on the active places of metal surface. The strengthened oxygen adsorption moves the initial potential of anode dissolution and passivity potential [4, 5, 6]. Therefore it is to say that surface of blasted parts is in very active state. It is a reason for temporary protection against corrosion so pre-treated surface for the following coating. There are several possibilities of temporary metal protection e.g. passivation of electron stream on metal surface between anodic and cathodic area; creation of physical hydrophobic layer which hinders to direct contact of moisture with metal surface and so enters between metal and electrolyte, at regulation of pH value of electrolyte e.t.c. [7].

Zinc coating is one of the metal coatings used to corrosion prevention. Its higher corrosion protection in water and anodic character to the steel gives reason to zinc utilization. In primary stage zinc predominantly acts as a sacrificed metal and protect cathode the uncovered places of steel. More negative potential of zinc against the iron and majority of other metals enables its use as protector in cathode protection system. Its resistance in atmospheric conditions is much higher as by other metals. It causes the different mechanism of corrosion stimulators, which come in contact with metal surface. Besides the base material is protected electrochemical on place of zinc coating failure [8, 9, 10].

Zinc coatings have been applied by different technologies: electro galvanizing and zinc-dipping. Mechanical deposition of zinc layer belongs for the present among less investigates technologies. The works [11, 12] were dedicated to the research of possibility of zinc coating deposition by blasting technology. The submitted paper deals with evaluation of surface activity of zinc-coated surface and its protective effects in conditions of atmospheric corrosion

## EXPERIMENTAL METHODS

On the basic of present research results [4] the experiments were aimed on verification of the possibility of applying zinc on steel surface by grit blasting, the proposal of the suitable method of obtained zinc coatings evaluation and determination their corrosion resistance. Low carbon hot-rolled steel sheet 11 375.11 of 3 mm thickness with not pre-treated scaled surface has been used as base material. Tested specimen size were 150 x 100 x 3 mm. There was used for zinc coatings deposition monodisperse blasting medium - zinc-coated cut wire of grain size $d_z = 1,12$ mm.

The blasting was realized at mechanical laboratory blasting wheel Di – 2.

Parameters of blasting:

1  distance of specimens from the blasting wheel L = 200 mm
2  cut wire velocity  $v_{TP} = 78,1$ m.s$^{-1}$
3  impact angle  $\alpha = 30°, 45°, 75°$.

The surface roughness after blasting was evaluated on surface analyser Surftest SJ – 301. Average value of Ra = 16 μm. The surface of specimens was blasted by such quantity of BM, which is necessary for full surface coverage $q_{nR}$ and by multiplied quantities for comparison. Destructive gravimetric method according to STN 03 8156

was applied for determination of average thickness of coating deposited on steel surface. The weight of zinc coatings was determined as weight difference of examined specimens before and after dissolving of coating in the solution [5]. The average thickness of coating was calculated by an equation:

$$s = \frac{(m_1 - m_2).10^4}{A.\gamma}$$

(1)

where   $m_1$ – specimen weight before dissolving of coating [g], $m_2$ - specimen weight after dissolving of coating [g], A  - surface area of specimen with zinc coating [cm$^2$], $\gamma$  - specific mass of zinc [g.cm$^{-3}$].

The calculations have not considered the actual size of surface and uniform distribution of zinc coating. Blasted surface images for study of zinc coating creation has been taken by scanning electron microscope (SEM) Hitachi  S – 450 and presence of zinc on surface of samples was also confirmed by energy-disperse records with help of analyser LINK AN 10000.

The activity of surface after blasting with zinc coated BM was evaluated on the basis of electrode potential changes. Tested specimens were exposed in interior and the activity of specimen couple was measured as follows: immediate after blasting, after 2, 6, 24 and 48 hours. Activity value was established as arithmetical average of specimen couple.  Potential measurements were made against saturated calomel electrode. The apparatus arrangement is showed in Fig.1. Specimen couple (3,4) was measured simultaneously by two circuits and they were switched by switch (8). Bridge (6) has realized the conductible contact both of electrolyte and specimens. Apparatus for measuring of potential (7) has owned the inner resistance of $10^4$ Ohms. The level of electrolyte was held out 100 mm over the surface samples because the depth of plunge has significant influence on course of corrosion process at corrosion with oxygen depolarisation. The electrolyte was distilled water.



1 - STOJAN
2 - MERACÍ ROZTOK
3,4 - VZORKY
5 - ELEKTRÓDA
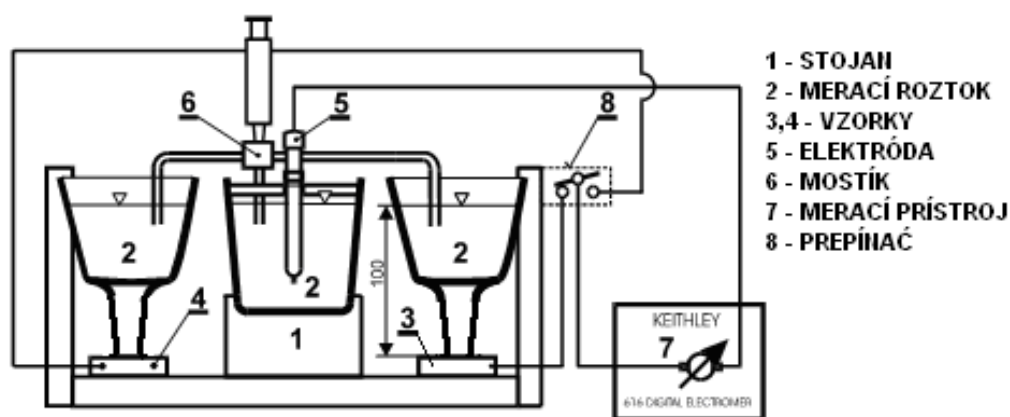6 - MOSTÍK
7 - MERACÍ PRÍSTROJ
8 - PREPÍNAĆ

*Fig.1 Scheme of equipment for electrode potential measurement: 1 – stand 2 - measuring solution 3, 4 – samples 5 – electrode 6 – joining bridge, 7 – measuring apparatus 8 - switch*

Single-layer of S 2000 paint was applied on the surface blasting with zinc-coated cut wire. Average thickness of coat was 52,5 μm. Applying of coat on the samples has

been performed immediate after blasting and after 2, 6, 24 and 48 hours according to activity measurement of blasting surface.

For determination of applied zinc interlayer influence has been evaluated the coat adhesion to the base by destructive test according to STN EN 24624 with help of glue ChS EPOXY 1200, which was used as adhesive between test roll and paint. Adhesion was expressed at strength acting vertically to base material surface which is needed to overcome for the tear coat from the base.

Specimens with applied coat were exposed to accelerated corrosion test under present of $SO_2$ and water vapour condensation according to STN ISO 6988. Exposure time was 28 days. Evaluation of coating appearance was realized according to STN 03 8103. Coating surface has been observed by free eye with the describing of corrosion manifestation presence, by light microscope observation and by photographic documentation was taken by digital camera.

## EXPERIMENT RESULTS

### Mechanism of Zn coatings creation

Evaluation of blasted surfaces by SEM has shown the origin of discontinuous zinc coat on the steel base, Fig.2. Energy-disperse records of surfaces, Fig.3, also confirmed the presence of zinc on surface of samples.
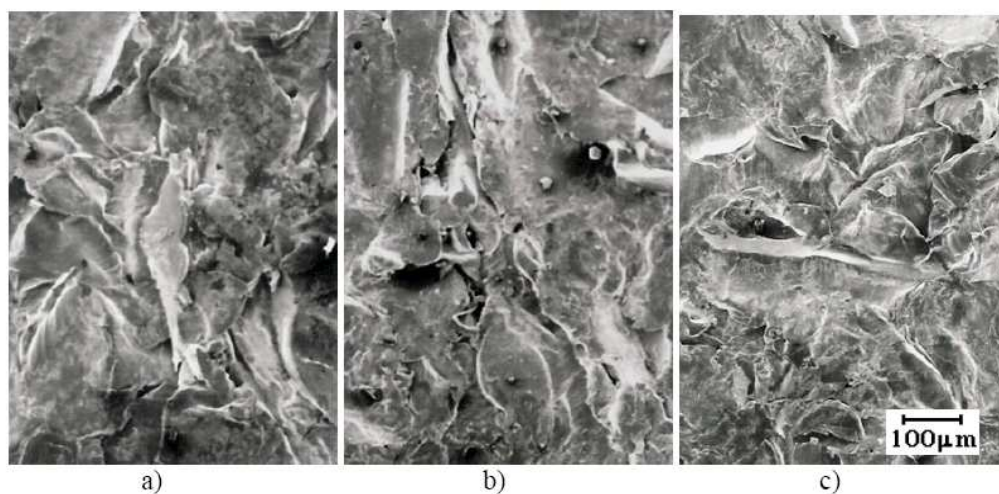


*Fig. 2. Appearance of surface after blasting with zinc-coated cit wire at various impact angles: a) 30°, b) 45°, c) 75°*

Discontinuous distribution of zinc coat may cause the rub of accidental oriented grains of zinc-coated cut wire after the fall on steel surface because zinc coat has occurred on the roll circumference of cut wire only. Repeated fall of BM grains may destroy already the created coat respectively to push back it into the material and hereby cause total coat discontinuity.

It is possible that the transposition of material surface layer cause the origin of cracks and hacks in dependence on the impact angle used. The higher mean thickness of zinc coat has been found out by impact angle of 75°. Coat thickness increased in dependence from the mass of BM necessary quantity, Tab.1.
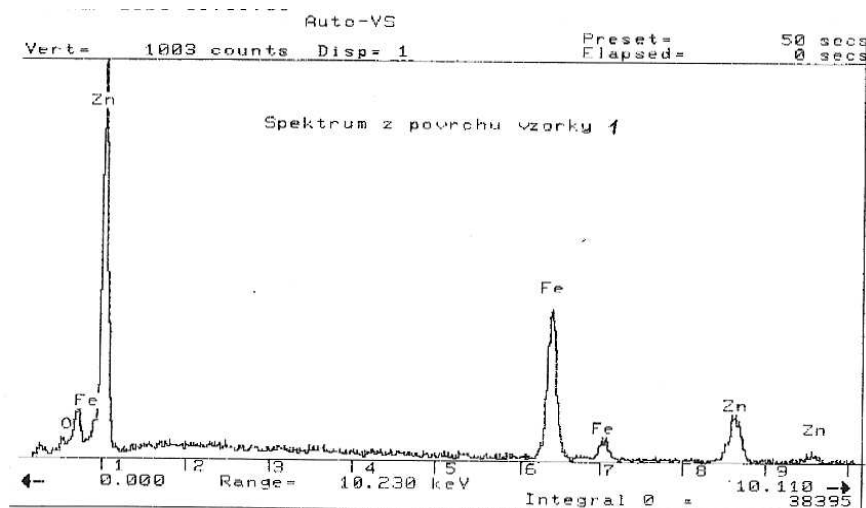
*Fig. 3. Energy-disperse record of surface after blasting with zinc-coated BM*

*Tab. 1. Average thickness of zinc coatings applied by blasting*

| – | Thickness of zinc coatings [μm] blasted by | | |
|---|---|---|---|
| | necessary quantity $q_{nR}$ | double necessary quantity $2xq_{nR}$ | triple necessary quantity $3xq_{nR}$ |
| 30° | 0,9493 | 1,6329 | 1,7183 |
| 45° | 1,4715 | 1,7943 | 2,2215 |
| 75° | 1,6519 | 2,2879 | 2,867 |

## Evaluation of surface activity

Results of electrode potentials measuring by reference calomel electrode are shown in Fig. 4. Electrode potential measured in dependence on samples exposure time in atmosphere shows that the highest values of potential were found immediately after blasting. Increase in exposure time causes decrease of surface activity.
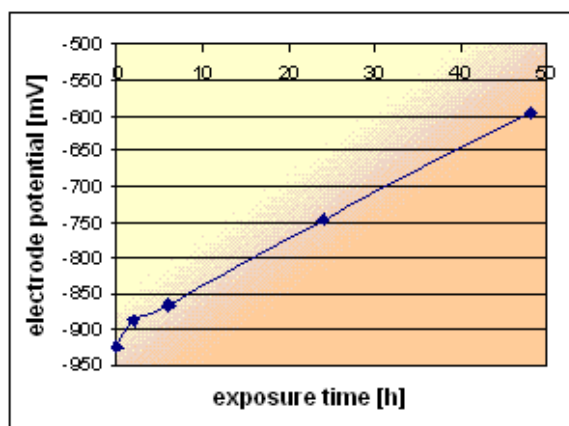


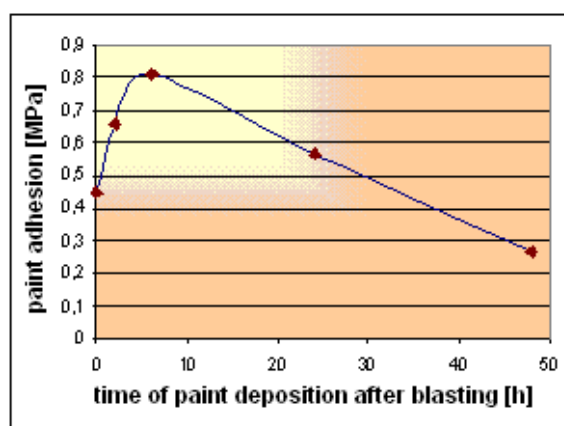*Fig. 4. Course of electrode potential changes in dependence on exposure time of specimens*

*Fig. 5. Adhesion changes in dependence on time from painting application*

**Evaluation of paint adhesion**

Adhesion of paint was evaluated in dependence on time from blasting with zinc-coated BM to paint application. Measured values of adhesion, Fig.5, not correspond with ones of surface activity in whole extent. The reason of this anomalism may be presence of ZnO under applied coat what has been not confirmed yet.

**Corrosion resistance of zinc coat**

Corrosion test in condensation chamber was realized in according to STN ISO 6988. Tested specimens have been exposed to the influence of water vapour under presence of $SO_2$. It was evaluated the influence of applied zinc-coating by blasting on corrosion resistance of upper paint. Corrosive effects after the first day of exposure has been observed on those specimens, which was covered with paint 48 hours after blasting. By these specimens series of has occurred the mild presence of pitting. On the third day of exposure has been found a corrosion of zinc on the sample surfaces under of ZnO, Fig.6. The longer time from surface blasting to applying of paint the greater extend of so-called white rust was occurred.



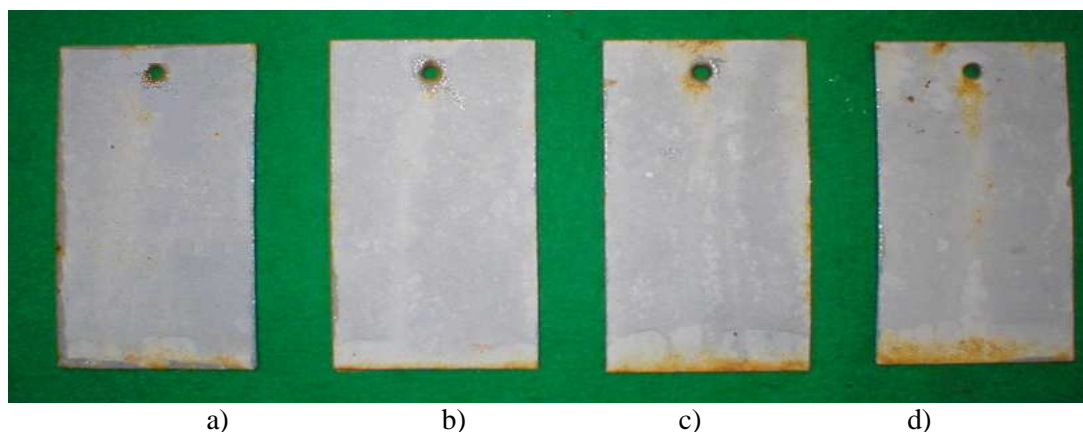a)                    b)                    c)                    d)

*Fig. 6. Appearance of painted samples after exposure in corrosive environment: a) immediately after blasting, b) after 2 h, c) after 6 h, d) after 24 h*

**CONCLUSIONS**

Realized results of experiments shows that it is possible to create zinc coating by blasting technology with zinc-coated BM on the surface of steel substrate. Applying of zinc coatings by blasting takes place simultaneously with process of scale removing, surface roughening and surface hardening. Destructive gravimetric method used for determination of zinc coat thickness shows suitable. Impact angle of BM also influences the thickness of zinc-coats created by blasting technology. The largest thickness of zinc coatings was reached at impact angle of 75°.

Submitted paper presents the first experimental results of surface activity evaluation created by blasting with zinc-coated BM. Increase in exposure time causes decrease in surface activity by influence of chemical reactions between the surface and surrounding atmosphere. The method of electrode potential measurement against saturated calomel electrode shows suitable when is considered oxygen depolarisation. On the basis of experimental results we can say that adhesion of paint depends on time be-

tween blasting and the following paint applying. Zinc interlayer has influenced the features the whole paint system as adhesion as its anticorrosion protection.

The aim of experiment was to determine the function of zinc interlayer on adhesion of applied paint and anticorrosion protection the created paint system. The reached results have confirmed that zinc coating applied by blasting may be used as temporary protection of surface and simultaneously as surface pre-treatment with possibility of following surface treatment of material. With regard to price of blasting media will be the economic consideration of the suitability the given technology for temporary surface treatment of metal surfaces as the object of further work.

This work was done within the scientific project VEGA No.1/0144/2008.

## REFERENCES

1. Palček P., Hadzima B., Bokůvka O., Chalupová M., Nový F.: *Corrosion resistance of magnesium and its alloys*. Komunikácie, 3, 2003, s.21.

2. Kniewald D., Brezinová J.: *Zmeny akosti kovového povrchu po tryskaní*. In: 35th International Conference on Coatings Technology, ČR, Pardubice 2004, s.489-496, ISBN 80-7194-660-5.

3. Kováč J. et all.: *Hodnotenie aktivity otryskaných povrchov na základe merania ich elektródových potenciálov*. In: Koroze a ochrana materiálu, 2002, roč.45, č.5, s.103-107, ISSN-1335-1532.

4. Kocich J., Tuleja S.: *Korózia a ochrana kovov*. VŠT v Košiciach, SjF, ALFA  Bratislava, 1983, 119s.

**5.** Kováč J., Brezinová J., Kniewald D.: *Vplyv zmeny režimu tryskania na aktivitu otryskaného povrchu*. Acta Metallurgica Slovaca 2/2001, roč.7, s.177-183, ISSN 1335-1532.

6. Skočovský P. et all.: *Náuka o materiáli pre odbory strojnícke*. Žilinská univerzita v Žiline, 2001, s.167-171, ISBN 80-7100-831-1.

7. Zerust Worldwide Corrosion Prevention. www.fatrani.cz

8. Hadzima B., Palček P., Chalupová M.: *The development of the magnesium alloys structure at artificial ageing*. Acta Metallurgica Slovaca, Vol.10, special issue 1/2004, 2004.

9. Brezinová J.: *Štúdium zákonitostí procesu tryskania z aspektu degradačných javov*. Doktorandská dizertačná práca, SjF TU Košice, 2002.

10. Hadzima B., Palček P., Demitrovová I.: *Environment influence to electrochemical characteristics of AZ31 and AZ80 magnesium alloys*. In.: Proc of 21st Danubia Adria symposium on Experimental Methods in Solid Mechanics. Eds.: Jecić S., Semenski D.. Croatian Society of Mechanics, Zagreb 2004, p.154

11. Kniewald D., Brezinová J.: *Study of process cold zinc by blasting*. CO-MAT-TECH 2003, Trnava, 2003, s.485-488, ISBN 80-227-1413-5.

12. Brezinová J.: *Dočasná ochrana studeným zinkovaním*. Povrchové inžinierstvo 2003. Acta Mechanica Slovaca, 4-A/2003, roč.7. s.29-32, ISSN 1335-2393.

**Mahmoud CHIZARI**
**Bin WANG**
**Mel BARRETT**

School of Engineering, University of Aberdeen, United Kingdom

# INTRODUCING A FAILURE CRITERIA
# FOR A LIVING CELL DURING MICROINJECTION

*This paper presents finite element modelling of the deformation of a detached living cell subjected to microinjection and through the simulation, an investigation of the material properties of the cell components. The model is verified using images of the deformed cell as well as the measured penetration forces in the tests reported in open literature. It is hoped that the modelling in this context will help to quantitatively evaluate the mechanical properties of the cells, and in particular, the failure strain of the cell cortex when penetration occurs.*

## INTRODUCTION

Though microinjection has been widely used, little is known about the response of cells and the consequence of penetration of the cell cortex. Under normal physiological conditions, cells are continuously subjected to mechanical forces that deform the cells and directly or indirectly influence cellular functioning. Biological effects of mechanical forces include signal transduction, gene expression, growth, differentiation, and survival [1, 2]. Although necessary for cellular functioning, excessive deformation results in cell damage or death, such as seen in pressure ulcers [3,4], during freezing of cells [5], and in bioreactors [6]. Depending on the magnitude, direction and distribution of these mechanical stimuli, cells can respond in a variety of ways. The mechanical compression of cells is known to modulate proteoglycan synthesis [7]. Furthermore, the tensile stretching of cell substrate can alter both cell motility and orientation [8]. As such, the understanding of how cells mechanically respond to physical loads is an important first step to further investigate how the transmission and distribution of these mechanical signals are eventually converted to biological and chemical responses in the cell [9].

The modelling of a living cell as a viscose fluid surrounding an elastic membrane have been widely used in the literature [10-17]. But the lack of reliable data on the individual subcellular rheology and its contraction with other parts, is a big issue for an accurate analysis. The effect of stresses and/or strains may be reflected in changes of the cell cortex, such as thinning and possibly bursting under a high aspiration pressure. In this case a strategy for the current study is to develop mechanical models that can

predict the distribution of stresses and strains at the cell level using the continuum mechanics, and to relate that to the subcellular components. The ultimate challenge will be to determine accurately a threshold for stress and strain in order to create a failure criterion for cortex rupture.

The aim of the present study is to create a numerical simulation based on a rather simple model of living cells during microinjection process. The mechanical property of the individual parts of cell is quantitatively evaluated corresponding to the measured data and images. This is followed by simulations of two different cells subjected to penetration and aspiration using the proposed finite element model. The results are then compared with the available experimental data obtained from open literature.

## NUMERICAL ANALYSIS

### Finite element explicit modelling

The commercial finite element solver, ABAQUS/Explicit [18] was used to investigate the mechanics of a cell subjected to penetration by a rigid object. The numerical code uses an explicit dynamic finite element formulation to simulate the deforming process of the cell cortex and cell interior. The cell was modelled using the equations of state (EOS) embedded in the finite element code. The EOS defines the material's volumetric strength and determines the pressure as a function of density and specific energy (the internal energy per unit mass). It is available as Mie-Grüneisen equations of state (thus providing the linear Hugoniot form) and assumes an adiabatic condition [19].

### Geometry and structural elements

In order to describe the mechanical behaviour of a cell, the complex structure of the cell was simplified to a model consisting of the cell cortex and cell interior. The remaining cell organelles was neglected and assumed that they do not contribute much to the mechanical behaviour of the cell. Both two and three-dimensional numerical models of a cell were used in this paper. A two-dimensional model of an originally undeformed circular shape were built with a thin outer layer of cortex and an interior, Fig. 1(a). The cortex was bounded the cell interior which is assumed to be composed of a watery material. Both cortex and cell interior are assumed to be homogeneous and isotropic. The whole cell is assumed to be recovered upon withdrawal of the needle [20]. The components were built with a finite element mesh to model the cell cortex and the cell interior. The boundary of the mesh where was initially in contact with the micropipette glass was fixed. A tied interaction with a small slippage was defined between the cell interior and cortex. The contact between these two materials assumed to be frictionless. The velocity field at the interface between the cortical layer and the internal core was assumed to be linear and continuous. A needle, which was defined as a rigid body, was applying a uniaxial loading force to the outer layer of the cortex towards the cell centre. Fig. 1(b,c) shows the deformation of the cell by an injecting needle.

The cell interior and cortex were modelled using a large number of elements, with six degrees of freedom per node to enable it to carry out large deformation. The cell is modelled by a three-dimensional solid element C3D4 element type which is a 4-node

linear tetrahedron, with reduced integration and hourglass control. The needle and micropipette were modelled by R3D4 element which is a 4-node 3D bilinear rigid quadrilateral element type [18].
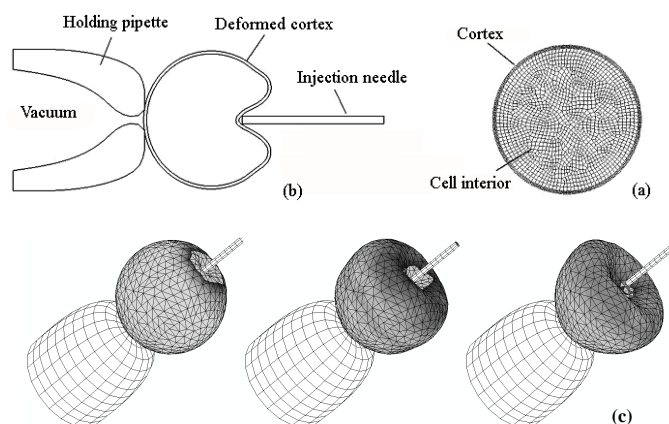


*Fig. 1. A model of a cell (a); and the simulated cell deformation under the microinjection (b); and 3D model of microinjection of a cell (c)*

## Material properties

Material properties which determine the relationship between the loading force, stresses and strains have to be derived specifically form the cell and its components. While the mechanical properties of the individual organelles of a cell are difficult to specify, the model employed in the current investigation allows at least a partial determination of the simplified material properties of the cell interior and cortex. The paper assumes that the properties of the cell interior are similar to those of pure water, as reported by Saul [21]. The data they obtained corresponds well to that for pure water at ambient pressure.

*In addition to the above-mentioned assumptions, the speed of sound for the cell interior, which is an input to derive the equation of state embedded in the program to analyse the fluid part of the model, was assumed to be that of water (in the range of 1435 m/s to 1500 m/s depending on salinity, etc.).*

*The cortex was modelled as a linear elastic material. Some of the input data were estimated then modified during the simulation to obtain verification from reported experimental data from open literature.*

## Mechanical analysis

Due to the definition of the cell model, the cortex is considered to be a thin layer and it is assumed that the inner cytoplasm provides a hydrostatic pressure on the cortex. Throughout modelling, the following was assumed.
- The cortex encapsulates a liquid (i.e., cytoplasm) that exerts a uniform hydrostatic pressure on the cortex.
- The interior liquid loss may occur during microinjection process, but it was not considered in the study.
- The cell is free of initial cortex stress or residual stress.

The needle exerts a force on the cortex, creating a dimple with semicircular curved surfaces before puncturing of the cortex. Fig. 2 shows the result of numerical model-

ling in comparison to the corresponding stages of the experimental images of microinjection of a cell. The result implies that the numerical simulation well mimics the experimental procedure.
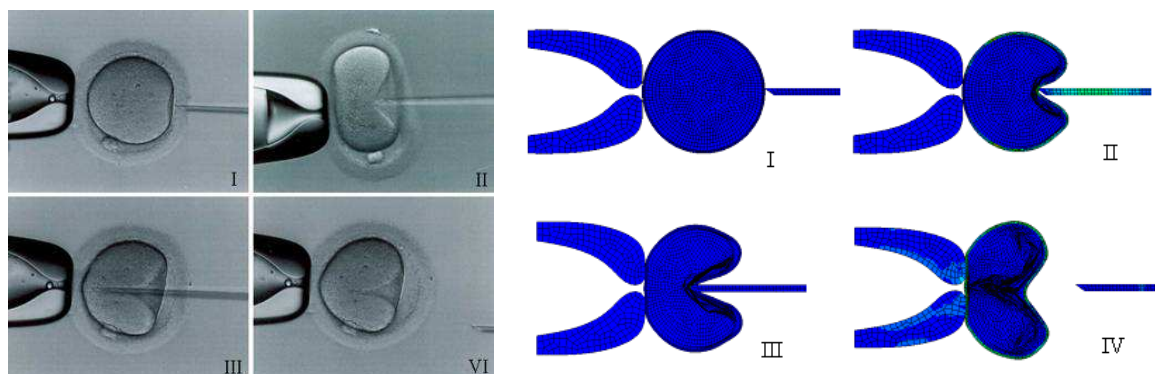


*Fig. 2. Four experimental stages of the microinjection persidure of a living cell and result of numerical modelling in comparison to the corresponding stages of the experimental work.*

The Mises stress as a representative value of the stress tensor is used to give a concise analysis of the load on the cell. Although the concept of the Mises stress was originally developed to predict the yielding of metals, it shows to be suitable for the prediction of cell failure [22].

The finite element code computes values of element-based variables at the element centroid by extrapolation. Figs 3(a,b) show the simulated history of the pressure and Mises stress at the centroid of the element (see Fig. 3(c)) in the cortex area, which is in contact with the corners of the flat frontal needle head.
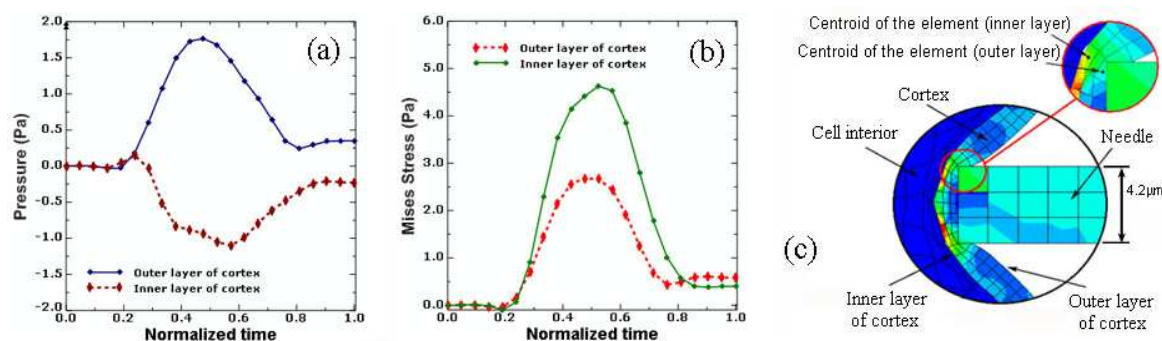


*Fig. 3. History of (a) pressure, (b) Mises stress from the simulation of the cortex in the area in contact with the corner of the needle tip. The latter is modelled having a rectangular profile with a flat frontal surface (c)*

The pressure and stress reach their maximum values just prior to the puncture, then drop to a nominal value and remain largely constant after the puncture. In order to determine the puncture load of the cell, the program requires a criterion for failure in the cortex.  Fracture strain in the cortex may be taken as a suitable criterion. However its value is unknown and it is not clear how this can be directly measured from an experiment. For the analysis presented here, the simulated value of strain in the cortex at the needle-contacted area was recorded as the failure strain when the simulated force in the needle equals that determined from the experiment at the moment penetration

occurs (i.e. when a sharp drop of the penetration force was observed in the experiment). Note that the calculated force applied to the needle is a combined reaction from the deformation of both the cortex and cell interior, reflecting the physical process in the experiment.

In following to gain a confidence in the credibility of numerical simulation, study cases with two different types of cell, i.e. malaria-infected red blood cell and mouse ooytes, were carried out using the numerical method described earlier.

## COMPARISON BETWEEN NUMERICAL AND EXPERIMENTAL RESULTS

### Study 1: micropipette aspiration of a malaria infected cell

In the micropipette aspiration experiment, the critical excess suction pressure is defined as that which results in a static hemispherical projection of the cell body forming inside the pipette. An excess pressure beyond this threshold will cause the cell to flow into the pipette continuously. Zhou et al. [23] examined the progression of the disease state of a similarly malaria infected red blood cell from the early ring form stage to the late schizont stage using the micropipette aspiration technique. At the schizont stage, the infected red blood cell is found to exhibit a viscoelastic behaviour which is in contrast to the mechanical behaviour demonstrated by the healthy and early stage infected red blood cell. This is due to the multiplication of the parasites within the cell as well as gross internal structural and molecular changes that the cell has undergone.

A 3D finite element modelling was performed to simulate the micropipette aspiration. Three stages of aspiration and deformation of the cell into the pipette are shown in Fig. 4 in form of axisymetric and 3D models.

Lim et al. [7] reported an experimental data on a malaria-infected red blood cell the shizont stage. The data was available in a form of displacement versus pressure curve. We have mimiced the experiment to produce a similar curve using the created numerical model. Fig 5 shows the comparison of both numerical and experimental results. There is a reasonable agreement between the two curves, thus providing some confidence in the current approach of the modelling.
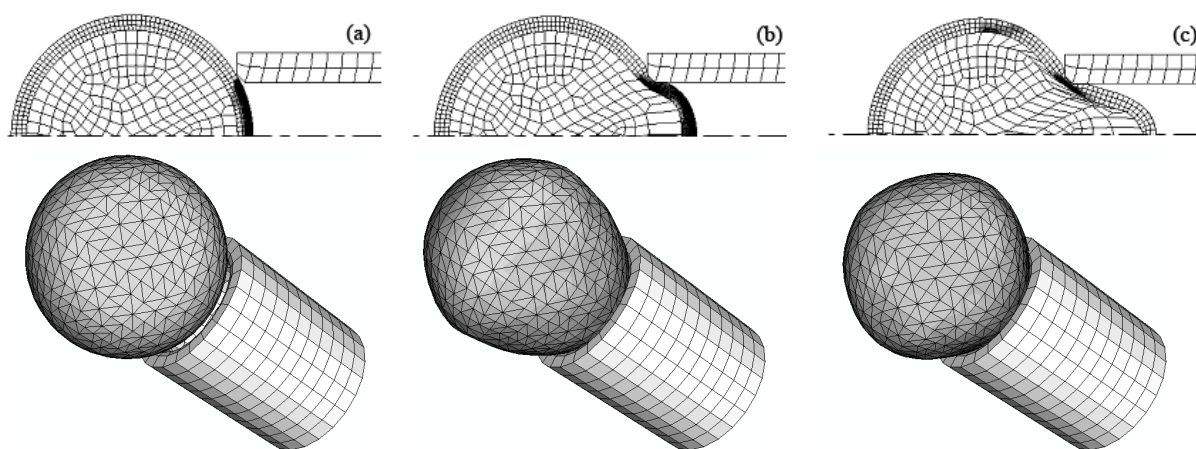


*Fig. 4. Axisymetric (top row) and 3D (bottom row) finite element stages of micropipette aspiration of a malaria infected red blood cell*
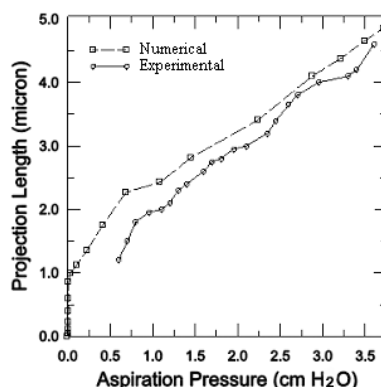
*Fig. 5. Projection length - aspiration pressure relationship from numerical and experimental [7] results of micropipette aspiration on a malaria infected red blood cell at the shizont stage*

The shear modulus of 3.1 µN/m and poison ratio of 0.15 was adopted for the cortex in the model. The density of the cell interior and cortex were assumed to be 1350 kg/m$^3$ and 1380 kg/m$^3$, respectively.

### Study 2: microinjection of a mouse ooyte

A numerical model was created to evaluate the microinjection of a mouse ooyte cell and compare the result with the experimental data reported by Sun et al. [23]. The mechanical property of the cell was obtained from an interpretation of the experimental data. A shear modulus of 3.0 µN/m and poison ratio of 0.10 was assumed for the cortex. The density of the cell interior was assumed to be 1326 kg/m$^3$ and the cortex density to be 1347 kg/m$^3$.

Figs. 6(a,b) show the experimental stages of the needle penetration and cell deformation during the microinjection process. The results from the numerical model are shown in Fig. 6 (c, d). There is a close agreement between the results. Figs. 6(b) and (d) show qualitative agreement in the deformed profiles of the cell recorded in the experiment and the simulation for the final stage of injection.
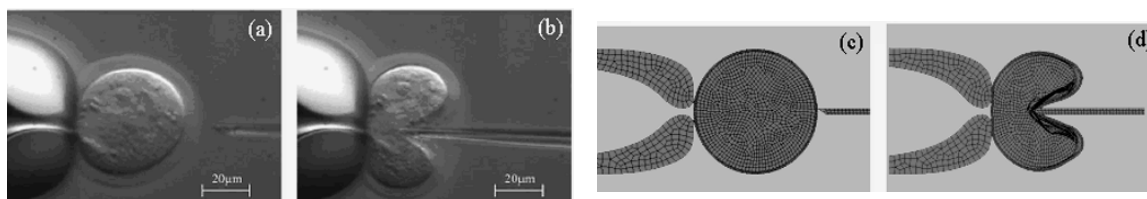


*Fig. 6. Experimental stages of microinjection of a mouse oocyte cell (a,b); and the corresponding numerical stages which mimic the experiment (c,d)*

Sun et al's [23] data also provides measured needle force with the deformation of the cell. This is plotted in Fig. 7(a) along with the simulated results for comparison. The non-linear trend of the forces obtained from the simulation and the experiment are similar, although the simulated force remains higher than the measured value in the early stage of penetration. The two curves converge and intersect at a later stage. Overall there is a reasonably good agreement between the simulation and the experiment, particularly close to the penetration. The dished vertical line in the figure shows

the point of sudden drop of the loading force as recorded in the experiment, indicating the penetration of the cell. This is used as the cutting-off point in the simulation. The calculated strain at this point is regarded as the failure strain in the cortex which allows the penetration to occur. Thus the failure strain can be determined numerically.

The experimental data shows that when the cell deformation (or the needle tip displacement) reaches 45 micron, the cell's cortex is punctured. And the puncturing force is approximately 7.5 micro-Newton. The resistance force from the cortex, which acts on the needle, then drops suddenly almost to zero. The deformation value at this point is then used as the threshold to find the simulated strain in the cortex area in contact with the needle tip.

The simulations also provide data on strains as a function of displacement in the cortex, as shown in Figs. 7(b). It shows the history of strain in the inner and outer layers of the cortex, from which it can be seen that the strain in the outer layer is 0.42 at the puncture threshold. It is reasonable to assume that this is the failure strain with the fracture starting at the outer layer then propagating through the thickness of the cortex. Following penetration, the needle proceeds further into the cell interior with little resistance only from frictions of the pieced cortex and that of the cell's internal liquid. The results therefore suggest a strain vale of 0.42 as a criterion for fracture failure of mouse ooyte cortex.
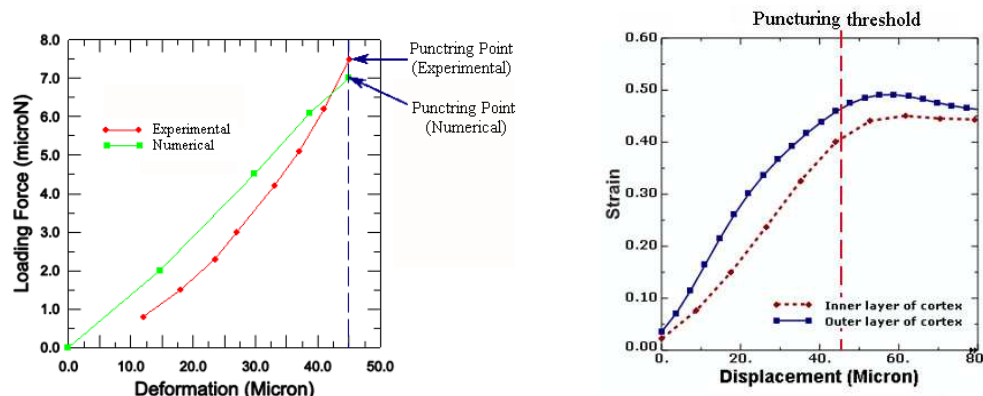


*Fig. 7. Comparison of the force-deformation curves which gives the fracture strain of the ooyte cell cortex (a); Strain curve and determined puncturing threshold in the microinjection of the cortex (b)*

## DISCUSSION

Although this study has adopted a simple approach to studying the mechanical property of a living cell, it has provided a means to investigate how seemingly unrelated data can be integrated, and hence provided a good starting point for work towards a better understanding of cell mechanics.

Our simple approach has moved a step forward towards creating a numerical model of cells at the continuum level to allow more accurate description of the structural and dynamic complexity of the cell. In general, as we work towards developing more accurate models for cell mechanics, appropriate structural model for the various subcellular regions and components need to be considered.

The numerical result obtained in this study compared reasonably well with the experimental data for two types of cell reported in the literature. To improve the simula-

tion, more comprehensive experimental data for cells are required, which will subsequently enable the construction and modification of more accurate models to be achieved, thus, making the numerical results to match better with experimental observations.

The study uses strain parameter to define a failure mechanism for the cell cortex. The strain was determined from the reaction force applied to the cell. Obviously the force applies to the combined cortex and cell interior. Further investigation requires defining the force applied to each cortex and cell interior during the microinjection process.

The Mises stress and shear strain were used in this study to compare the mechanical and biological behaviour of a cell. The results suggest that these may be a valid approach to predict failure in the cell but it requires further study.

As the current study assumed the needle head to be of a cylindrical shape and have a nominal diameter (actual dimensions of needles used in cited experiments being unknown), the effect of needle shapes and sizes may require further investigation.

## CONCLUSIONS

Numerical modelling of microinjection and micropipette aspiration of a living cell offer a tool to predict mechanical properties of the cell and thus assist in the reduction of experimental tests and assists in the further development and operating procedures for microinjection and micropipette techniques.

The technique described herein provides a useful approach to investigate the mechanical behaviour of cells. However, for the described cells, the penetration strain as a failure property of a cell has been quantified numerically and is suggested as a criterion for quantifying the failure (puncturing) of the cortex. The assumptions and simplifications used in the model appear to be justified by good agreement with experimental results.

## REFERENCES

1. Chen, C.S., Ingber, D.E.: *Tensegrity and mechanoregulation: from skeleton to cytoskeleton*. Osteoarthritis and Cartilage 7 (1), 81–94, 1999.
2. Watson, P.A.: *Function follows form-generation of intracellular signals by cell deformation*. FASEB Journal 5, 2013–2019, 1991.
3. Bouten, C.V.C., Knight, M.M., Lee, D.A., Bader, D.L.: *Compressive deformation and damage of muscle cell subpopulations in a model system*. Annals of Biomedical Engineering 29, 153–163, 2001.
4. Bouten, C.V., Oomens, C.W., Baaijens, F.P., Bader, D.L.: *The etiology of pressure ulcers: skin deep or muscle bound?* Archives of Physical Medicine and Rehabilitation 84, 616–619, 2003.
5. Takamatsu, H., Kumagae, N.: *Survival of biological cells deformed in a narrow gap*. Journal of Biomechanical Engineering 124, 780–783, 2002.
6. Zhang, Z., Ferenczi, M.A., Lush, A.C., Thomas, C.R. *A novel micromanipulation technique for measuring the bursting strength of single mammalian cells*. Applied Microbiology and Biotechnology 36, 208–210, 1991.
7. Lim, C.T. Zhou, E.H., Quek, S.T.: *Mechanical models for living cells – A review*. Journal of Biomechanics, 39, 195–216, 2006.

8.  Liu, S.C., Derick, L.H., Duquette, M.A., Palek, J.: *Separation of the lipid bilayer from the cortex skeleton during discocyteechinocyte transformation of human erythrocyte ghosts*. European Journal of Cell Biology, 49, 358–365, 1989.

9.  Peetersa, E.A.G., Oomensa, C.W.J., Boutena, C.V.C., Baderb, D.L., Baaijensa, F.P.T.: *Mechanical and failure properties of single attached cells under compression*. Journal of Biomechanics, 38, 1685–1693, 2005.

10. Alcaraz, J., Buscemi, L., Grabulosa, M., Trepat, X., Fabry, B., Farre´, R., Navajas, D.: *Microrheology of Human Lung Epithelial Cells Measured by Atomic Force Microscopy*. Biophysical Journal Volume 84, 2071–2079, 2003.

11. Balland, M., Richert A., and Gallet, F.: *The dissipative contribution of myosin II in the cytoskeleton dynamics of myoblasts*. Eur. Biophys. J. Biophys. Lett., 34 (3): 255-261, 2005.

12. Desprat, N., Richert, A., Simeon, J., Asnacios, A.: *Creep Function of a Single Living Cell*. Biophysical Journal Volume 88, 2224–2233, 2005.

13. Fabry B., Maksym G.N., Butler J.P., Glogauer M., Navajas D., Fredberg J.J..: *Scaling the microrheology of living cells*. Phys Rev Lett, 87:148102, 2001.

14. Lau, A. W. C., Hoffman, B. D., Davies, A., Crocker, J. C., and Lubensky1, T. C.: *Microrheology, Stress Fluctuations, and Active Behavior of Living Cells*. Phys. Rev. Lett, 2003.

15. Lenormand G., Millet E., Fabry B., Butler J.P., Fredberg J.J.: *Linearity and time-scale invariance of the creep function in living cells*. Journal of the Royal Society (London): Interface, 1:91-97, 2004.

16. Dahl K.N., Engler A.J., Pajerowski J.D., Discher D.E.: *Power-law rheology of isolated nuclei with deformation mapping of nuclear sub-structures*. Biophys J., 89, 2855-286, 2005.

17. Yanai M., Butler J. P.,  Suzuki T., Sasaki H., Higuchi H.: *Regional rheological differences in locomoting neutrophils*. Am J Physiol Cell Physiol 287: C603-C611, 2004.

18. ABAQUS Analysis User's Manual, Version 6.4, HKS Inc., Providence, Rhode Island, 2005.

19. Bennett B. I.: *On obtaining the zero-temperature equation of state from shock data*. Los Alamos National Laboratory, Los Alamos, New Mexico, 87544, 1984.

20. Hartmann C., Mathmann K., Delgado A.: *Mechanical stresses in cellular structures under high hydrostatic pressure*. Innovative Food Science and Emerging Technologies, 2005.

21. Saul A., Wagner W.: *A fundamental equation for water covering the range from the melting line to 1273K at pressures up to 25000 MPa*. Journal of Physical and Chemical Reference Data 18, 1537–1564, 1989.

22. Smith A.E., Moxham K.E., Middelberg A.P.J.: *Wall material properties of yeast cells*. Part II. Analysis. Chemical Engineering Science 55, 2043–2053, 2000.

23. Zhou E. H., Lim C. T., Tan K. S. W., Quek S. T., Lee A., Liau B.: *Investigating the progression of disease state of malaria-infected red blood cells using micropipette aspiration*. 2nd World Congress for Chinese Biomedical Engineers, Beijing, China, 2004.

24. Sun Y., Wan K., Roberts K.P., Bischof J.C., Nelson B.J.: *Mechanical Property Characterization of Mouse Zona Pellucida*. IEEE Transactions on Nanobioscience, 2, 279-286, 2003.

## Krassimir DOTCHEV

The Manufacturing Engineering Centre (MEC), Cardiff University, United Kingdom

# RAPID MANUFACTURING OF CASTFORM PATTERNS FOR INVESTMENT CASTING

*Laser Sintering (LS) is a layer manufacturing technique and currently it is extensively used to produce concept models, functional parts, and also patterns for investment casting (IC). CastForm$^{TM}$ Polystyrene (CF) is a powdered material used for fabrication of IC patterns employing the LS process. The use of the CF material is one of the fastest and most cost effective Rapid Manufacturing (RM) routes to produce small quantity wax-like patterns for shell or flask IC. The manufacture of CF casting patterns constitutes two stages. The first is the building of a "green" part and second is its infiltration with wax. The accuracy of the patterns, and ultimately the final accuracy of the metal castings, is determined by the CF material properties and the applied process parameters. The factors affecting the accuracy of the CF patterns are investigated in this paper. In addition, different ways to improve the process accuracy are discussed. An analysis of advantages and limitations of this RM technique for IC patterns fabrication is provided.*

## INTRODUCTION

Rapid Manufacturing (RM) is a term used to name a group of additive fabrication technologies that have evolved from Rapid Prototyping (RP) and it gained a wide acceptance in the last 5 years [1, 2]. It should be noted that RM refers only to rapid production of end use parts or finished goods directly from virtual 3D CAD data. The rapid production of tooling which can be directly used to manufacture end-use parts can be also considered as part of RM. The application of RM in Investment Casting (IC) can reduce dramatically the lead-time and cost. Currently there are several RM techniques available for fabrication of IC patterns such as: selective laser sintering (SLS) or laser sintering (LS) with CastForm$^{TM}$ (CF) Polystyrene material [3, 4] and PrimeCast 100 [5], Stereolithography (SLA) Quick Cast$^{TM}$ process [6, 7], Thermojet MJM wax process [3], Envisiontec Perfactory [8] for micro castings, etc.

LS with CF is one of the fastest and most cost effective RM techniques to produce a small quantity of wax-like patterns for shell or flask IC in the dimensional range of 50mm to 500mm. CF is the commercial name of a polystyrene powder introduced by the DTM Corp. in 1999 [9]. Currently, it is available from 3D Systems Corp., which acquired DTM Corp. in 2001, to be used only on their SLS machines type "Sinterstation 2500", "SLS Vanguard" and "Sinterstation HiQ" [3]. The properties of CF patterns are similar to conventional wax patterns and therefore can be processed applying

standard foundry practices. Another advantage of this RM route is that geometries with complex and hollow internal structures can be easily produced. This is because the LS process does not require support structures like the SLA.

The technical capabilities of different RP technologies suitable for fabrication of patterns for investment casting were investigated by many research groups [7, 10, 11, 12 and 13]. In other RP studies the focus was on overall part quality and processing accuracy in the X-Y plane and few if any analysed systematically the dimensional accuracy of the LS process and CF patterns in particular [14, 15].

Unlike other LS applications the RM of CF patterns involves two stages: 1) LS of a "green" part, and 2) its infiltration with wax. During the first stage the "green" part shrinks along X, Y and Z directions. Based on our experiments, the pattern shrinks further at the wax infiltration stage. In this paper, the LS process capabilities to fabricate accurate CF patterns and the factors affecting their final accuracy are investigated and analysed.

## FACTORS AFFECTING THE PATTERN QUALITY

### Process description

Fig. 1 depicts the steps in fabricating CF patterns. The first four steps are common for all LS applications. The input data, an STL or a slice file, is loaded into the machine software to prepare a build. During the LS process a "green" part is fabricated out of CF powder. The $CO_2$ laser controlled by the scanning system draws each slice (or layer) of the part sequentially and applies a sufficient amount of energy to fuse the powder particles together. The LS is a "change of phase" process where the powdered material is transformed from a solid to a liquid and then back to a solid again. During the interaction the specific volume decreases resulting in material shrinkage. Because of this "green" parts are dimensionally smaller then the input geometry. Then, the "green" parts are cleaned from the material un-sintered powder and further infiltrated with liquefied casting wax. The wax seals all surfaces and makes the part fully dense and suitable for casting. After cooling down to room temperature the final material tensile strength is sufficient for the patterns to withstand handling and further processing. However, the strength is much smaller during wax infiltration. The "green" part is in its weakest state at 79-80°C while being infiltrated with wax. The part weight could trigger material creep and thus result in deformation and breakage. If the infiltration time is very long then some tall parts or unsupported features could deform and collapse.

### LS process parameters

All RP processes are machine / process specific and therefore their capabilities should be considered in the context of a specific machine type and fabrication process. In the case of LS, the mechanical inaccuracy of the re-coating system, feed cartridges and part pistons, the temperature control, the laser and scanning system accuracy, and also powder properties result in systematic and random errors. The main LS process parameters that affect the part quality can be grouped under the following categories: 1) <u>laser / scanning parameters</u>: fill laser power, scan spacing, scanning strategy

("sorted fill enable / disable"), scanning direction ("X only" or "X and Y cross fill scan"), and outline laser power; 2) <u>thermal parameters</u>: part bed temperature, powder feed temperature, and part cylinde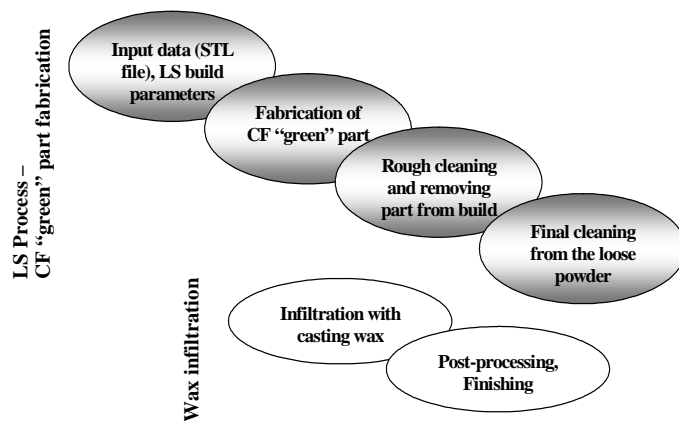r temperature. These parameters have an effect on the total amount of energy delivered to the part bed and thus will have a direct impact on the process accuracy. For example:



*Fig. 1. CastForm process - laser sintering and wax infiltration*

- If the laser scanning energy is higher then the effective laser beam spot size would be larger. This would lead to an increase of external dimensions and a reduction of internal dimensions in the X-Y plane. In addition, "green" parts would have higher density and strength that would reduce the risk of breakage:

- If the part bed temperature is maintained too high and thus the total energy delivered is high, the whole part bed would be sintered and it would be impossible to separate the parts;

- On the contrary, if the sintering energy is not sufficient then the "green" parts would be weak and some features could break. Thus, the risk of part distortions and breakages increases during the following wax infiltration stage.

   Due to the thermal nature of the LS process, significant errors are introduced by the machine during its heating up and cooling down. Normally, the "green" parts start to cool down while being built which leads to in-build shrinkage. This continues after the end of the build until the parts cool down to room temperature which introduces a post-build shrinkage. In addition, the uneven temperature distribution and heat dissipation in the build chamber causes non-linear shrinkage rates across the part bed. Thus, parts positioned in the middle of the part bed would cool down and shrink slower than those along its periphery. At the same time the part bed piston moves down with constant increments, i.e. layer thickness, and each new layer of fresh powder compensates to a larger extent the Z shrinkage of the previous layers. As a result of this, parts placed in the middle of the part bed experience less in-build shrinkage and continue to shrink after the end of the process. In contrast, parts placed around the periphery of the part bed have more in-build and less post-build shrinkage. This phenomenon is the main cause of the observed non-linear shrinkage in the vertical or Z direction and will be investigated in the next sections. The influence of these factors together with the different geometry of the built parts makes it even more difficult to predict the Z shrinkage and thus to compute exactly the Z scaling factor.

## Wax infiltration

   The "green" parts are placed onto a dipping tray and preheated up to 79-80°C in atemperature controlled oven. Then, the tray is immersed into a vat with molten wax. The time for preheating and infiltration depends on part height, volume, and wall thickness. If it is longer than required the parts may deform and collapse. The reason

for this is that polystyrene has a low melting temperature and like all polymers has visco-elastic behaviour. The set temperature in the oven during wax infiltration (79-80°C) is close to the glass transition temperature of 89°C for this material. Thus the weight of the "green" parts together with the additional weight of the molten wax could trigger a material creep. Our experience showed that this lead to higher shrinkage along the Z axis in comparison with that along X and Y. This phenomenon is not described or explained in the CF process literature in spite of the fact that it has a significant effect on patterns' dimensional accuracy. After the wax infiltration the patterns contain about 40% polystyrene and 60% wax in weight. This proportion could vary depending on the specific LS processing parameters such as part bed temperature, laser power, scan spacing, and wax infiltration time. Due to the surface tension of the liquefied wax, during the cooling down, this stage introduces further shrinkage.

## EXPERIMENTAL RESULTS

### Test parts

The combined effect of all factors on the final process accuracy was analysed using two test parts, a "pyramid" (X and Y) and a "staircase" (Z) shown in Fig. 2. The test parts were built several times on DTM Sinterstation 2500CI applying: fill laser-power 13W, part bed temperature 82°C, left/right feed cartridges temperature 48°C, scan spacing 0.15 mm, outline laser power nil, wax infiltration oven temperature 79-80°C, preheating time 10 min. and infiltration time 10 min. In order to analyze the impact of the two main processing stages on the final accuracy all parts were measured twice: at the "green" stage after the LS process and then after the wax infiltration.
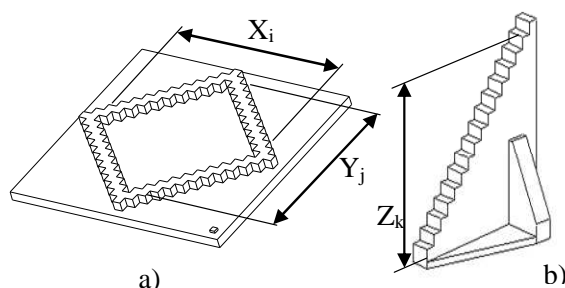
### X and Y directions

The results of measurements shown in Figs 3 and 4 represent the error of the actual dimensions of the three test parts in X (X1, X2,
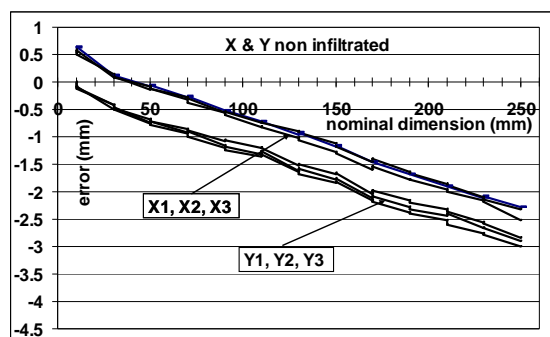


*Fig. 2. The test parts: a) "pyramid"; b) "staircase"*



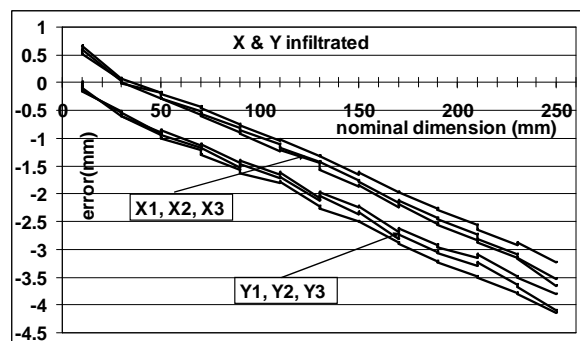*Fig. 3. The error in X and Y directions at "green" stage*

*Fig. 4. The error in X and Y directions after wax infiltration*

X3 data sets) and Y (Y1, Y2, Y3 data sets) directions against their nominal values before and after the wax infiltration stage.
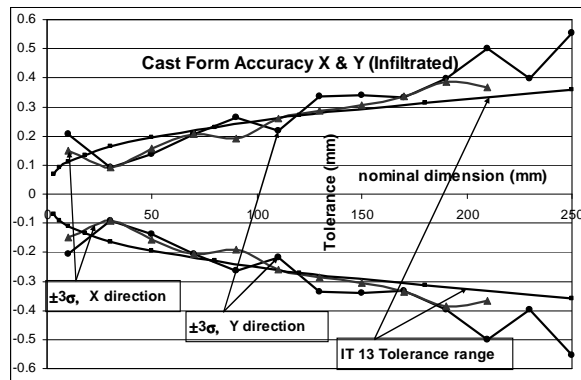
Fig. 5. *Process capability in X and Y directions after wax infiltration*

Each data set contains systematic and random errors. The systematic error depends mainly on the material shrinkage, applied laser power, part-bed temperature and on the quality of the carried out laser calibration. The errors for each data set at "green" stage and after infiltration show a linear dependence with the nominal dimensions. To a large extent these errors could be compensated by applying constant scaling factors. Using the experimental data the average shrinkages $\alpha_x$, $\alpha_y$ and scaling factors $S_x$, $S_y$ in X and Y directions respectively were calculated (Table 1).

In order to estimate the CF process capability in X and Y the standard deviations, $6\sigma$, are calculated and shown in Fig. 5. Comparing these results against the standard IT tables [16], the closest accuracy class achievable in X and Y directions is IT13. This could be used as a guideline for assigning process tolerances to CF patterns for IC.

Table 1. *The shrinkage and scaling factors in X and Y directions*

|  | "Green" part | Infiltration only | After infiltration |
|---|---|---|---|
| Scaling factor $S_x$ | 1.0119 | 1.0044 | 1.0163 |
| Scaling factor $S_y$ | 1.0115 | 1.0043 | 1.0159 |
| Shrinkage $\alpha_x$ | 0.0117 | 0.0044 | 0.0161 |
| Shrinkage $\alpha_y$ | 0.0114 | 0.0043 | 0.0157 |

### Z direction

All "staircase" test parts were fabricated simultaneously in one build. All parts were positioned at the same height in the building chamber but at different X-Y locations in the part bed. Fig. 6 depicts the error (deviation) of the actual dimensions in Z direction from their nominal values at the "green" stage. Fig. 7 shows the total error after the wax infiltration. It could be seen in these figures that the part shrinkage has a clear non-linear character. The shrinkage depends not only on parts' nominal dimensions in Z but also on their location in the X-Y plane. Parts b2 and m2 positioned in the middle of the part bed exhibit a higher than that of the parts positioned along its periphery, b1, b3 and m1.
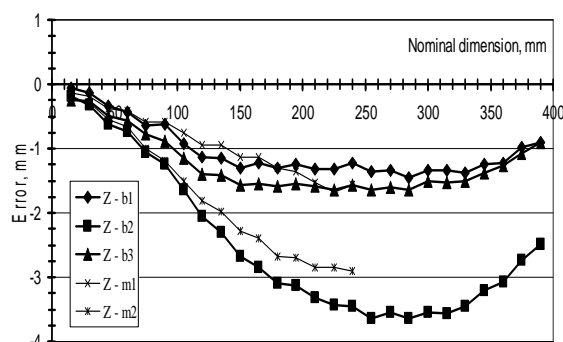


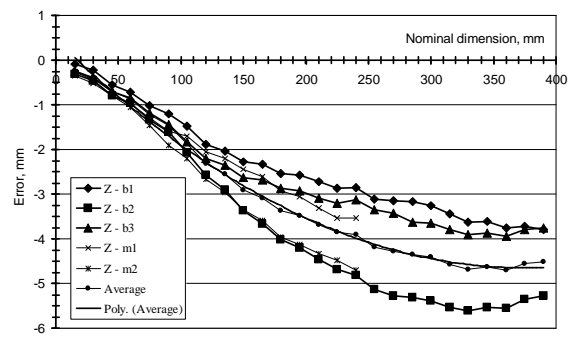Fig. 6. *The error in Z direction at "green" stage*



Fig. 7. *The error in Z direction after the wax infiltration*

In order to estimate the process accuracy in Z direction the data from the five sets were re-grouped into two sets taking into account the part positions. The first set contains the data of the parts placed around the periphery and the second one those placed in the middle of the build. Fig. 8 provides an indication about the process capabilities after the wax infiltration stage assuming a normal distribution. Comparing these results against the IT tables [16] it could be judged that the achievable accuracy in Z direction is IT14 for parts placed in the middle of the part bed and IT15 for those around the periphery.

Usually in the RP business the delivery time and cost have the highest priority and often there is no time to build the parts twice for a more precise process calibration. In that case, a non-linear functi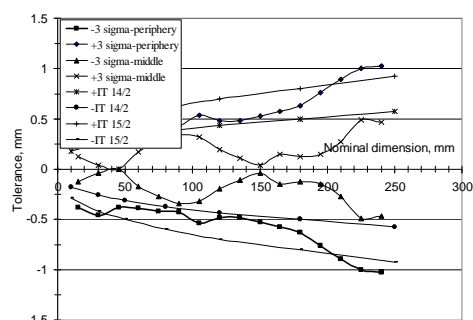on depending only on the Z height can be applied to scale the parts. This function is calculated from the average shrinkage taken from Fig. 7.

It takes into account the nominal Z height but not the X-Y part placement. Thus, the final dimensional accuracy would be worse especially for very tall parts.

Because of the varying part geometry and build arrangements it is practically impossible to predict precisely the non-linear shrinkage that would result in each particular case. This systematic error cannot be estimated accurately and thus cannot be compensated off-line. In order to achieve good accuracy in RM of CF patterns, the only option is to fabricate each part at least twice. The first time the part is built without applying any scaling factors in order to calculate its shrinkage and Z scaling function that depend on the part Z height and X-Y placement. Then, the build is repeated by applying the scaling factors that are specific for that part.



Fig. 8. CF process accuracy in Z direction after wax infiltration

Also, in order to maintain minimum error in Z, the smallest part size should be oriented along the machine vertical Z axis. This will also minimise the build time.

## CASE STUDY

In this project a heat exchanger (Pratt & Whitney PW6000 engine) was manufactured using CF patterns and Sinterstation 2500CI LS machine (Fig. 9). The 3D CAD assembly included three cast aluminium parts. These complex castings incorporated multiple ports, manifolds with complex internal structure, and flanges (Fig. 9b). The largest component was 650 mm long and 350 mm in diameter(Fig. 9c). In order to fit it into the machine building chamber it had to be split in 2 components (Fig. 9a) which were CF made separately and then joined together. A number of sets were build and cast until the design was finalised. The dimensional accuracy was within IT13 tolerance band and only in Z direction some of the longest dimensions (above 300mm) were within IT14. Machining allowances were added to the model in order to compensate for these inaccuracies which a standard practice in any casting application. The time to make 1 off the largest pattern in CF using LS was: LS building time - 45h, cleaning – 4h, infiltration – 4h, joining and quality control – 2h. The main benefits of employing the LS CF process in this case were: very fast, no need for complex and

expensive tooling, many design improvements were performed between the builds and testing in a short time, no need to freeze the design. As a result the LS process with CF was approved as a production method for the fabrication of the required casting patterns for this demanding aerospace application.
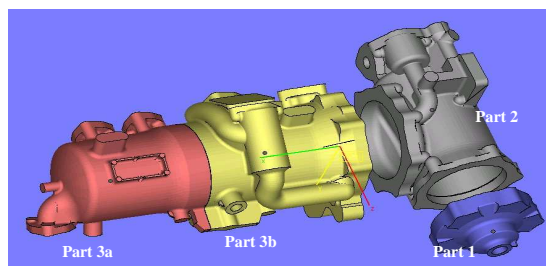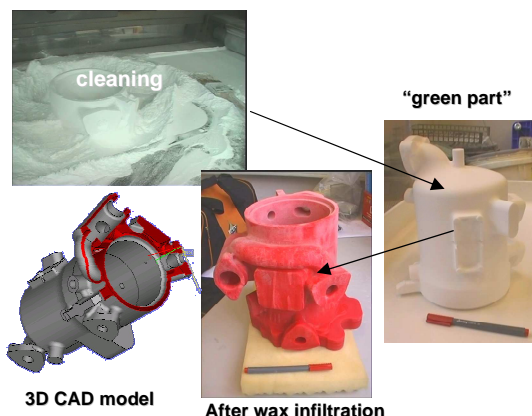


Fig. 9a. The 3D CAD model



Fig. 9b. The CF process



Fig. 9c. CF "green" and infiltrated parts



Fig. 9d. Final assembled castinds

## CONCLUSIONS

The LS process with CF material is an efficient RM route for producing patterns for IC. Some of its key advantages are: fast and cost efficient compared to other RP techniques; it has a capability to fabricate complex parts with internal cavities; foundry processing of the CF patterns as normal wax patterns without any changes in the conventional IC practices; short burnout cycles; low ash content; and a low pattern expansion during the shell firing.

At the same time, the process has some disadvantages and limitations as discussed in this paper, which should be taken into account when selecting it for RM of IC patterns. In particular, the wax infiltration increases the manufacturing time and introduces further dimensional errors and higher risk. The dimensional error, due to linear shrinkage in X and Y directions, could be compensated by applying a set of constant scaling factors. The achievable pattern accuracy in these directions is the best and can be maintained within IT13 tolerance range. The part shrinkage along the Z-axis is non-linear and could be compensated more accurately only by introducing a non-linear scaling function. It depends on the LS machine type and calibration, part geometry, and mostly on the X-Y part location and orientation within the LS machine building

envelope. The error in Z increases with the nominal and is within IT14 – IT15 tolerance range.

The final CF pattern quality is very much dependant on the LS process and wax infiltration parameters and therefore finding their optimum settings is essential for the successful implementation of RM. In general, LS CF patterns are a cost effective alternative when a small number of parts, up to 10, are required and the cost of a mould tool for wax patterns or the time to make it is prohibitive.

## REFERENCES

1. Wohlers Report 2007, State of the Industry, Annual Worldwide Progress Report: *An in-depth worldwide progress report on the Rapid Prototyping, tooling, and manufacturing*, Wohlers Associates Inc., 2007, ISBN 0-9754429-3-7.

2. Hopkinson N., Hague R.J.H., Dickens, P.M.: *Rapid Manufacturing: An Industrial Revolution for the Digital Age*. John Wiley&Sons Ltd., 2006, ISBN 13-978-0-470-016113-8.

3. 3D Systems Web page, 2008: *3D Systems – Valencia*. CA – Headquarters, 26081 Avenue Hall, Valencia, California, USA, http://www.3dsystems.com .

4. DTM Corporation: *SLS – Selective laser sintering*. 2001, DTM Corporation, 1611 Headway Circle, Building 2, Austin, Texas 78754.

5. EOS Web page, 2008: *EOS GmbH – Electro Optical Systems*. Headquarters – Munich, Robert-Stirling-Ring 1, D-82152, Kreilling / Munich, Germany, http://www.eosint.com .

6. Dickens P.M., Stangroom R., Greul M., Holmer B., Hon. K.K.B., Hovtun R., Neumann. R., Noeken S., Wimpenny D.: *Conversion of RP models to investment castings*. Rapid Prototyping Journal, 1995, Volume 1, Number 4, p. 4-11.

7. Cheah C.M., Chua C.K., Lee C.W., Feng C., Totong K.: *Rapid Prototyping and Tooling Techniques: A Review of Applications for Rapid Investment Casting*. International Journal of Advanced Manufacturing Technology, United Kingdom, Vol 25, No 3-4, pp 308-320, February 2005.

8. Envisiontec Web page, 2008: *Perfactory Standart RP System*, http://www.envisiontec.de

9. DTM Corporation: *The Synterstation systems*. Guide to materials: CastForm PS, April 1999.

10. Lee C.W., Chua C.K., Cheah C.M., Tan L.H. and Feng C., "Rapid Investment Casting: Direct and Indirect Approaches via Fused Deposition Modeling", International Journal of Advanced Manufacturing Technology, United Kingdom, Vol 23, No 1-2, pp 93-101, January 2004.

11. Chua C.K., Feng C., Lee C.W., Ang G.C.: *Rapid Investment Casting: Direct & Indirect Approaches via Model Maker II*. International Journal of Advanced Manufacturing Technology, United Kingdom, Vol 25, pp 26-32, January 2005.

12. Dotchev K., Soe S.: *Rapid manufacturing of patterns for investment casting: improvement of quality and success rate*. Rapid Prototyping Journal, 2006, Volume 12, Issue 3, pp. 156-164.

13. DTM Corporation: *SLS$^{\circledR}$ Selective laser sintering technology for investment*. DTM white paper, 1999.

14. Shen J., Steinberger J, Gopfert J, Gerner R., Daiber F., Manetsberger K., Fetstl S.: *Inhomogenous shrinkage of polymer materials in Selective Laser Sintering*. Solid Freeform Fabrication Symposium Proceedings, 2000, Austin, USA, pp. 298-305.

15. Ippolito R., Luliano L., Gatto A.: *Benchmarking of rapid prototyping techniques in terms of dimentional accuracy and surface finish*. CIRP Annals, 1995, 44(1), pp. 157-160.

16. BS EN 20286-1:1993: *ISO system of limits and fits*, 1993.

**Mariana DOTCHEVA**
**Huw MILLWARD**

University of Wales Institute Cardiff (UWIC), Cardiff, United Kingdom

# OPTIMISATION OF UP- AND DOWN-MILLING PROCESSES FOR A CORNER FEATURE

*This paper presents the specifics of the two types of end-milling, up- and down-milling, in the context of process planning of a finishing operation for machining complex pocket features. An optimisation mechanism is used for a pocket type of end-milling operation with the aim of comparing the results from up- and down-milling when the same process constraints have been applied. Two sets of cutting conditions have been generated and analysed for each type of end-milling. The first cutting condition has constant parameters for the entire tool path, derived from the worst case of cutting, representing the usual process planning approach. The second set of cutting conditions represents the optimised process. The predicted results were verified through experiments. The optimised, measured cutting parameters, when machining the critical corner, accurately demonstrate the important changes in magnitude and direction of the radial cutting-tool deviation and surface error.*

## INTRODUCTION

Despite tremendous developments in CAM software, cutting-tool technology and machine-tool technology, end-milling results still depend to a large extent on the knowledge inherent within manufacturing staff [1, 2]. End-milling machining is a complex process in terms of process planning due to intricate geometry, the evolution of new materials and high-precision requirements of the final product. Consequently, the full potential of the machine tool system is under utilised in many cases. Commercial CAM products develop the CNC programmes mainly from the mathematical point of view and usually the feed rate and spindle speed are constant for a given tool path, derived from the worst-case cutting condition.

The available commercial CAD/CAM systems also fail to take into account the mechanical aspects of the milling process. The mechanical parameters such as cutting forces and cutting-tool deviation are important for an evaluation of process capabilities and machining results. The finishing-milling process requires high levels of reliability for the cutting process in order to obtain good contour accuracy and surface finish.

The other issue in finishing pocket milling is determining which type of end-milling should be used: up-milling or down-milling. Traditional workshop practice recommends down-milling for finishing profiling. Some researchers also consider down-milling as a better method for finishing [3]. However, some researchers [4]

show that the accuracy of a surface cut by up-milling is much better than the accuracy of the same surface machined by down-milling and that the $F_Y$ force in down-milling is generally larger then the same force in up-milling as the difference varies between 4% and 50%.

This paper shows that the type of milling affects the process efficiency and process accuracy and it presents the specifics of up- and down-milling in the context of optimisation of an end-milling machining process of a pocket-type part feature. A comparison of two end-milling operations is presented when up- and down-milling are applied.

## SPECIFICS OF UP- AND DOWN-MILLING

In general, up- and down-milling differ in the method of creating the chip thickness. In peripheral cutting, down-milling starts with the largest chip thickness in one cutter rotation and finishes with zero chip thickness. In up-milling the cutting starts with zero chip thickness and ends with the largest chip thickness. To create these two different types of end-milling the rotation of the cutting tool has to be in opposite directions.

### Cutting force model

The specifics of the chip-thickness creation process in up- and down-milling reflect the direction and the magnitude of the cutting forces. The mechanistic force model has been considered as the most appropriate for cutting force analysis in this study. The mechanistic force model directly represents the effect of the variation of the chip thickness on the cutting forces, and then on the part accuracy.

In most end-milling applications a helical fluted cutter is employed, and the chip thickness varies not only with cutter rotation but also along the Z-axis. Therefore the end-milling process can be simulated by discrete increments of the cutter: angle by angle ($\varphi(i)$), flute by flute (k), and finally dividing the end mill into elemental axial dicks slice by slice (a(j)). The total instantaneous X, Y and Z force components at the cutter rotation angle $\theta(i,k,j)$ are the sum of the forces acting on the simultaniously engaged flutes and disk elements in cutting:

$$\begin{Bmatrix} F_X(\theta) \\ F_Y(\theta) \\ F_Z(\theta) \end{Bmatrix} = \sum_{k=1}^{N_f} \sum_{j=1}^{N_z} \xi_F(\theta(i,k,j)) \begin{Bmatrix} F_x(i,k,j) \\ F_y(i,k,j) \\ F_z(i,k,j) \end{Bmatrix} \tag{1}$$

where $\xi_F(\theta(i,k,j))$ is an index to indicate that tooth (insert) i is in the cut at angular position $\theta(i,k,j)$:

$\xi_F = 1$ if $\tau_{en} < \theta(i,k,j) < \tau_{ex}$

$\xi_F = 0$   otherwise

The force equations (1) describe the instantaneous cutting forces in up- and down-milling when they are defined in the same coordinate system, as it is shown in Fig. 1.

The $F_Y$ cutting force that causes the radial cutter deviation, in down-milling is generally larger than the equivalent force in up-milling. Although both forces have the same direction, the difference is that the $F_Y$ force in up-milling is towards the machined surface and could cause overcut. In down-milling, the $F_Y$ force is directed away from the machined surface and could create undercut. Knowledge of the specifics of the two milling types included in the modelling process helps in making effective decisions during the process planning.
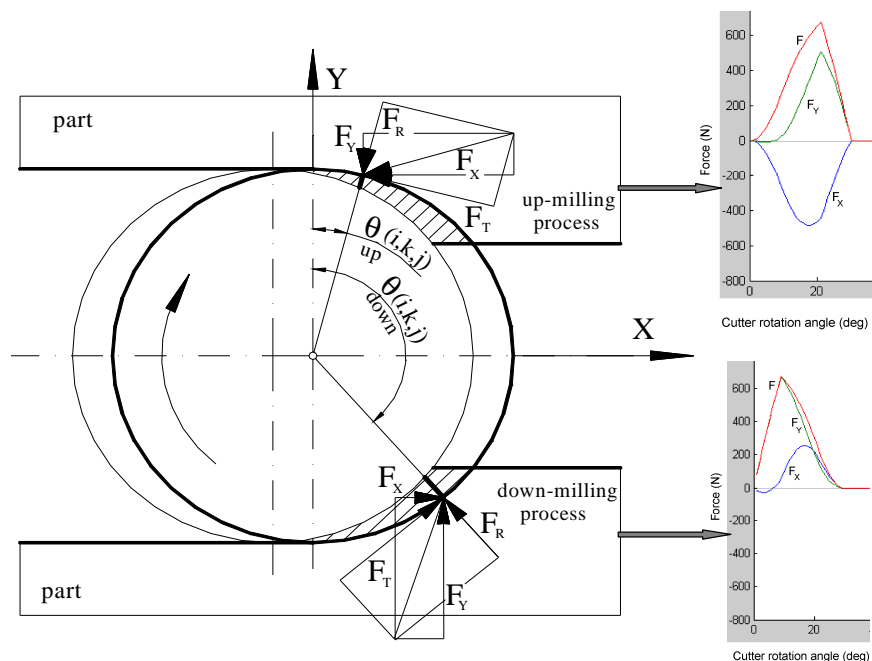


*Fig. 1. The cutting forces in up-milling and in down-milling*

## Cutting tool deflection estimation

To asses the accuracy of the planned milling operations a model of the deflected cutting tool is required. This study employs a static model, which considers the end mill as a cantilever, to calculate the deviation of the cutting tool. The model does not take into consideration the deflection of the machine tool, cutting tool holder and test part's deformation; it is assumed that these deflections are minor in comparison to the cutting tool deflection. The cutting tool is simplified as a two-step cylindrical cantilever beam. The general case of dual-mode deflection of a cutting tool has been addressed in [5, 6].

## Generation of the machined surface

During the cutting process the surface topography is created by the coordinated movements between the cutting tool and the work-piece. In this study a cylindrical cutting tool with helical flutes was used for the process modelling and optimisation, and for the test trials. When a helical cutting tool is employed in an end-milling operation several elemental axial disks take part in cutting. Only one of them generates the machined surface topography at a certain moment. The elemental disk that forms the machined surface is the disk a(j) that crosses the surface formation line at a certain rotational angle $\theta(i,k,j)$, as shown in Fig. 2.

Although only the deviation of the cutting tool at the crossing point between the helical cutting edge and the surface formation line defines the surface error, the other elemental disks that are simultaneously engaged also contribute to the error. In this surface generation mechanism the specifics of the chip formation and cutting forces magnitude and direction in up- and down-milling play a significant role. Fig. 2 b) presents the $F_Y$ cutting forces in down-milling process, induced by each elemental disk when they are engaged in cutting. This is an example of end-milling operation when the radial depth of cutting is 0.5mm and the axial depth of cutting is 9mm. As a result of the helical cutting edges, each elemental disk starts cutting at a displaced position. The resultant deflection of the cutting tool during the down-milling process is shown in Fig. 2 c).
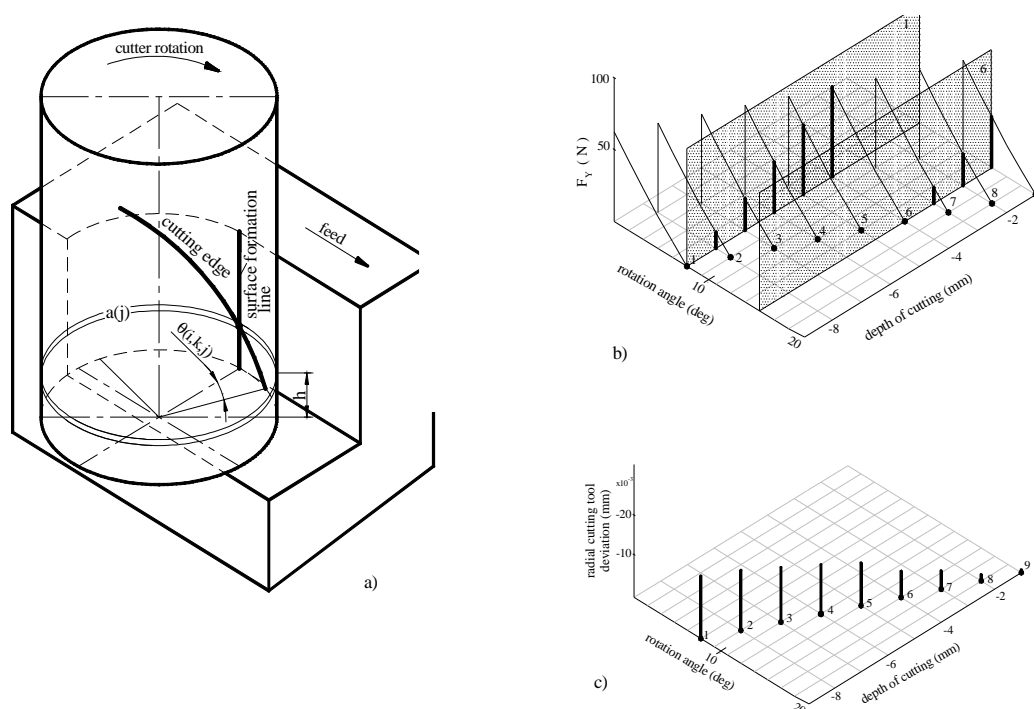


*Fig. 2. The process of surface generation in end-milling operation*

In up-milling, the elemental disks cross the formation line at the start of their cutting during one cutter rotation. In the presented end-milling operation in Fig. 2, when up-milling is applied, the largest cutter deflection occurs at the mid-section of the axial depth of cutting, because the number of the engaged elemental disks is greater than the number when disks one and two are crossing the formation line. The deflection at the mid-points is larger than the deflection at the last two points despite, the fact that the instantaneous $F_Y(i,k,j)$ cutting forces in points eight and nine are larger, because the crossing points eight and nine are closer to the clamped end of the cutting tool.

The real trajectory of the cutting tooth is trochoidal. Up- and down-milling do not use the same part of the trochoidal tooth path during the cutting because of the different rotational directions of the cutter. In down-milling, the height of the feeding marks is larger than the height of the marks in up-milling obtained with the same feed rate. Therefore the surface roughness in down-milling is expected to be larger compared to up-milling. The larger cutting force $F_Y$ and higher surface roughness in down-milling make it theoretically less efficient than up-milling under the same cutting conditions.

## THE OPTIMISATION PROCESS FOR END-MILLING

The optimisation process used in this work is based on an 'in tolerance' optimisation strategy developed for finishing end-milling operations [6]. This strategy adopts a model-based method [7] for optimisation and control of the cutting process. This is an off-line technique that adjusts the controlled parameter to the maximum allowed limit, before the actual cutting, based on the predicted data from the process model. The feed rate is the controlled parameter in the optimisation process and the required surface tolerance and the surface roughness are the constraints. For the general case, it is assumed that the cutting tool, machine tool and machining process are determined, and the dimensional accuracy and surface roughness are specified. As the cutting-tool deviation reflects the action of the cutting forces and is the dominant parameter in the machining error estimation, it takes the major role in the optimisation process. The optimised end-milling processes are judged in terms of a combination of surface accuracy, surface roughness and machining (finishing) time.

The optimisation process has been applied to a pocket-type test piece presented in Fig. 3. The roughing radius was set at 25mm and the finished inside-corner radius at 16mm. The difference between the radius of the roughing cutter and the radius of the finished corner creates a cutting geometry with variable chip thickness. The test piece was designed to incorporate two identical surfaces cut with different cutting conditions. The first cutting condition was derived from the worst-case of cutting along the whole tool path. The second cutting condition was obtained after applying the optimisation strategy to the same contour with variable geometry.

The allowable deviation of the cutting tool under the cutting forces was set to be $\delta_{lim}=\pm0.03$mm. This accuracy constrain was applied to both types of end-milling: up- and down-milling. The cutting tool and work-piece data used in the experimental work is presented in Fig. 3.
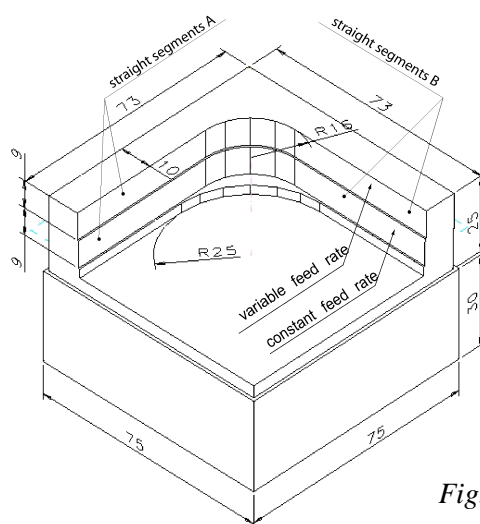
| Cutting tool: | 16 mm HSS 3 fluted with 30° helix angle |
|---|---|
| Cutting tool rake angle: | 7° |
| Cutter overall length: | 77 mm |
| Cutter effective length: | 50 mm |
| Flute length: | 30 mm |
| Cutting-tool material: | High Speed Steel (HSS) |
| Modulus of elasticity: | 200 GN/m$^2$ for HSS (Ashby and Jones 1996) |
| Test-piece material: | Aluminium alloy 6082 |
| Cutting-force coefficients: | $K_T = 1292(t_c)^{-0.1657}$ $K_R = 0.4477(t_c)^{-0.01307}$ |
| Machine tool: | Mikron HSM 400 |

*Fig. 3. The geometry of the test piece and the experimental data for the cutting processes*

There are two key steps within the optimisation process, when planning an end-milling operation for machining a pocket-type surface. In the first phase, the mechanistic force model is applied to the work piece geometry in order to predict the corner cutting forces and the deviation of the cutting tool at several cutter positions. All cutting forces are based on a constant feed rate ($f_{con}$), derived from the worst-case milling

condition, whereby the peak chip thickness for a given tool path generates the maximum tool loading.

The second phase of modelling uses the data from phase one to modify the feed rate with the aim of generating optimised cutting conditions, taking into consideration the allowable deviation of the cutting tool $\delta_{lim.}$ The feed rate adjustment mechanism is applied to the whole tool path. The final optimised feed-rate data has to satisfy a surface roughness constraint too. Fig. 4 shows the results from the optimisation process when up- and down-milling is used.



a) up-milling
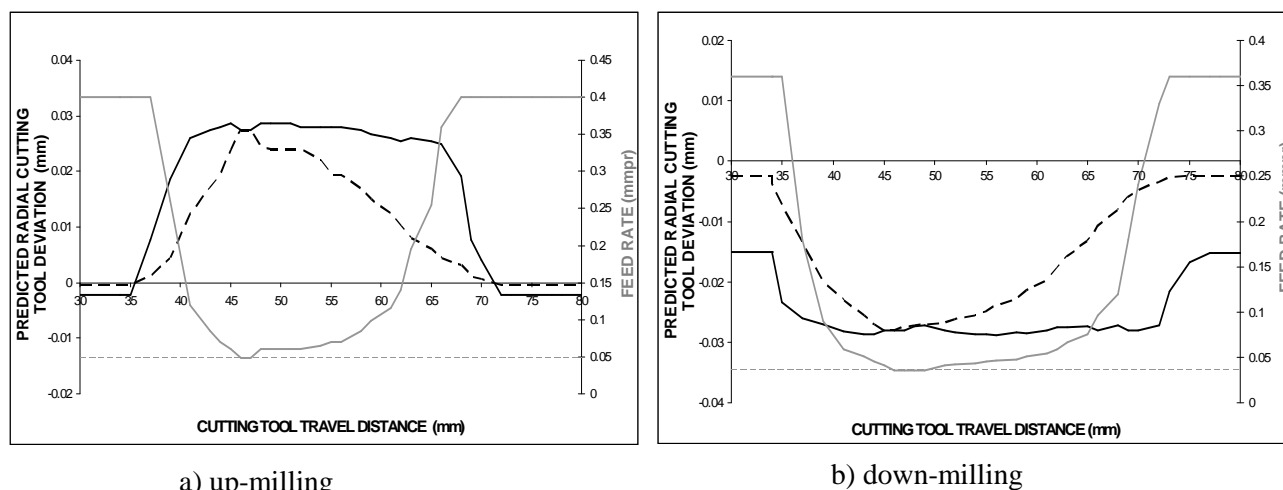
b) down-milling

*Fig. 4. Constant and variable cutting conditions in up- and down milling. The predicted radial deviation is in black, and the constant-feed-rate condition is shown with a dashed line. The feed rates are illustrated in grey, and the line used for the constant feed rate is dashed*

The cutting conditions and the predicted results for the cutter deviation for the two types of milling shown in Fig. 4 a) and Fig. 4 b) are clearly different. Generally, the radial force $F_Y$ in down-milling has larger values compared to the up-milling radial force when the same geometry is cut with the same cutting condition. Therefore, the optimisation process of up-milling generates higher levels of the feed rate than the same process applied to down-milling. The constant feed rate for up-milling is f = 0.048mmpr, whilst for down-milling it is f = 0.036mmpr. The variable feed rate, which is a result of the optimisation process, is larger in up-milling than the variable feed rate in down-milling for the whole cutting process. The higher feed rate determines shorter machining time, which means that the up-milling optimised process is expected to be more efficient than the optimised down-milling, whilst maintaining the same surface accuracy and surface roughness.

## RESULTS AND DISCUSSION

After generating the new feed-rate data for up- and down-milling, two test pieces were machined applying the new cutting conditions. The geometry of the part is the same as shown in Fig. 3. The measured surface error for up- and down-milling with constant and variable feed rate is presented in Fig. 5.

As predicted, cutting the straight parts of the tool path is more stable, with small variations in surface error. In the transient parts, and especially at the corner, the surface error varies noticeably. The surface error resulting from the variable feed-rate ap-

plication is larger in the straight segments compared to the error for the corresponding surface machined with constant feed rate. But at the corner, the peak surface error obtained from the constant feed-rate cutting is larger than the equivalent error of the surface machined with variable feed-rate conditions. Taking into consideration the larger values of the variable feed rate compared to the constant feed rate it can be concluded that the optimised cutting conditions satisfy the design requirements and create a more efficient milling process.



a) up-milling                                          b) down-milling
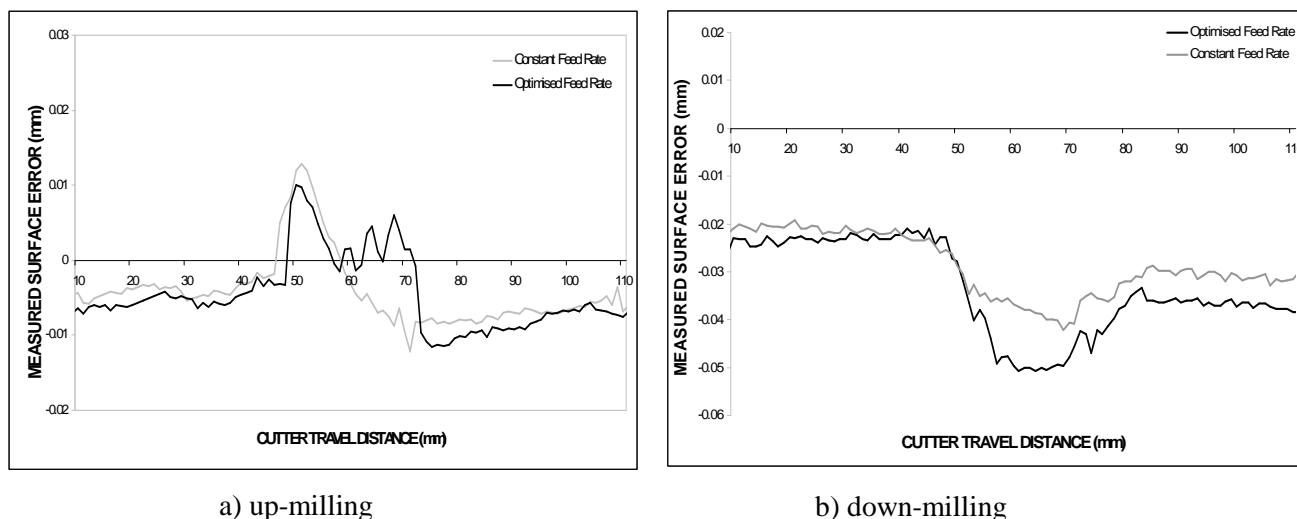
*Fig. 5.  The measured surface error in straight and corner segments of the controlled surfaces with up-milling*

The results from the test pieces cut with up- and down-milling are summarised in Table 1. Up-milling demonstrates better results than down-milling in terms of process efficiency, surface accuracy and surface roughness. The experiments displayed good agreement between the predicted data and the machining results. The maximum surface error in down-milling is significant due to the specifics of this type of milling. Besides the fact that the radial cutting force in down-milling is larger than the same force in up-milling, in down-milling the $F_Y$ force is directed out of the machined surface and there is nothing to resist the cutter deviation. In up-milling when the radial force becomes larger its direction is towards the machined surface, which resists deflection. The surface roughness results do not exceed the required surface roughness $R_a=0.80\mu m$, and also establish up-milling as the better method for finishing milling. The constant feed-rate condition creates lower roughness than the surface roughness of the strips cut with optimised feed-rate conditions. In both types of milling the operations cut with optimised feed-rate are more efficient than the operations with constant feed rate. For up-milling, the machining time of the optimised tool path is 78% shorter than the machining time of the operation with constant feed rate. In down-milling the machining time of the optimised operation is 74% of the machining time with constant feed-rate cutting. The considerable difference between the machining time of the operations with variable and constant feed-rate comes from the geometry of the finishing operation. This geometry was deliberately designed to create extreme cutting conditions. The experimental results confirm the predicted trend. Comparing the finishing machining times, up-milling is 46 % more efficient than down-milling.

**CONCLUSIONS**

This paper presents the specifics of the two types of end-milling, up- and down-milling, in the context of process planning of a finishing operation for machining complex pocket features. Two different cutting conditions of each type of end-milling have been simulated and experimentally verified. The advantage of the variable cutting conditions over the constant cutting conditions is significant in both up- and down-milling processes as presented in Table 1.

*Table 1. Summary of key machining measurements*

|  | Up-milling | | Down-milling | |
|---|---|---|---|---|
|  | Constant Feed Rate | Optimised Feed Rate | Constant Feed Rate | Optimised Feed Rate |
| Maximum Measured Surface Error (mm) | 0.0129 | 0.0115 | 0.0421 | 0.0506 |
| Measured Surface Roughness $R_a$ (µm) | 0.0680 | 0.2620 | 0.1950 | 0.2530 |
| Finishing Time (±1 s) (s) | 55.0 | 12.0 | 97.0 | 25.0 |

The results show that the finishing machining time can be reduced in both machining with constant and with variable feed rate by applying up-milling. The measured surface error and surface roughness have lower values in the work-piece machined with up-milling than in the test piece cut with down-milling. The predicted and experimental results confirm the importance of the type of end-milling engaged in finishing cutting when complex pocket type surfaces are machined. The corner cutting was demonstrated as a critical case of finishing cutting, which needs special analysis and planning, regarding the surface error and the type of end-milling used for its machining.

**REFERENCES**

1. D'Souza R.: *Selecting an optimal Tool Sequence for 2.5 Pocket Machining while Considering Tool Holder Collisions.* Journal of Intelligent Manufacturing, 17(3), 2006, 363-372.

2. Li Z.Z., Zheng M., Zheng L.; Wu Z.J., Liu D.C.: *A solid model-based milling process simulation and optimization system integrated with CAD/CAM.* Journal of Materials Processing Technology, 138, 2003, 513-517.

3. Landon Y., Segonds P., Lascoumes P., Lagarrigue P.: *Tool positioning error characterisation in milling.* Int. Journal of Machine Tools and Manufacture, 2004, 44, 457-464.

4. Lee S.K., Ko S.L.: *Improvement of the accuracy in the machining of a deep shoulder cut by end milling.* Journal of Materials Processing Technology, 2001, 111, 244-249.

5. *Xu A.P., Qu Y.X., Zhang D.W., Huang T.:* Simulation and experimental investigation of the end milling process considering the cutter flexibility. *International Journal of Machine Tools and Manufacture, 2003, 43, 283-292.*

6. *Dotcheva M., Millward, H.:* The application of tolerance analysis to the theoretical and experimental evaluation of a CNC corner-milling operation. *Journal of Materials Processing Technology, 2005, 170, 284-297.*

7. *Childs T.H.C., Maekawa K., Obikawa T., Yamane, Y.:* Metal Machining-Theory and Application. *London: Arnold, 2000.*

**Mariana DOTCHEVA**
**Daniel THOMAS**
**Huw MILLWARD**

University of Wales Institute Cardiff, United Kingdom

# DESIGN AND RAPID MANUFACTURE OF SELECTED CELLULAR TYPE STRUCTURES

*The work presented in this paper aims to explore the enhancements that the Selective Laser Melting technology can bring to the design, manufacture, and performance of cellular type structures. Cellular type structures possess valuable characteristics such as low density, high strength, good energy absorption, good thermal and acoustic properties. These advantageous characteristics make them industry desirable but the difficulties of producing them limit their applications. The capabilities of some metal cellular structures as fundamental elements for creating new internal material configurations for injection moulding tools has been evaluated. The preliminary investigation highlights the requirements and the feasibility of such structures for the purpose of injection moulding tooling. Lattice cellular structures appear to be mechanically competitive alternatives to prismatic honeycombs structures. It has been illustrated that lattice core of injection moulding can be capable of supporting significant structural and process loads while also could facilitating cross flow heat exchange.*

## INTRODUCTION

Cellular metal structures have been used in different industrial applications such as light constructions, heat exchangers, reconstructive surgery, chemical, automotive and aerospace industries. They possess valuable characteristics such as low density, high strength, good energy absorption, good thermal and acoustic properties [1, 2]. These advantageous characteristics of the cellular structures make them desirable but the difficulties of producing them limit their applications. The new layer-additive technologies such as Direct Metal Additive Manufacturing technologies, Electron Beam Melting, Direct Metal Laser Sintering, and Selective Laser Melting (SLM), enable manufacturing free-form solid parts using laser technology and layers of metal powder. SLM gives the opportunity to produce complex parts from engineering materials (stainless steel, tool steel, titanium alloy, cobalt-chromium) in a short lead time, directly from 3D CAD data. This gives the designers freedom to use the cellular materials where they are needed creating better product functionality without sacrificing their mechanical quality. Using the SLM technology as a manufacturing process for producing injection moulding tools or inserts has been shown to be beneficial in three areas:
　　(1)　　　the freedom of the part's geometry that SLM provides [3, 4];

(2)        the reduction of the production cycle time [5, 6, 7];

(3)        the ability to build conformal cooling channels along with the 3D geometry of the tools [8, 9].

Creating a conformal cooling system is restricted by the geometry of the injection moulding tools and inserts. In tools or tool areas where it is not possible to design conformal cooling channels, the cooling process depends mainly on the thermal conductivity of the mould's material. Alternative material or design solutions are needed to help in these cases for making the moulding process more efficient and accurate. The weakness of all laser-based freeform manufacturing processes is the huge consumption of time for building large solid parts, since only considerably small quantities of material can be processed per unit time. This can be improved significantly by employing the ability of the SLM technology to build cellular structures. SLM can create specific internal cellular structures simultaneously when producing moulding tools with complex external design and conformal cooling channels. A cellular type interior will reduce the production cycle and can contribute to the thermal management of the moulding process. The cooling portion of an injection moulding time can represent up to 75 % of the total cycle time. This number shows how important any reduction of the cooling time is. Better cooling also contributes to the quality improvement of the plastic parts. With SLM built skin/core structure, material is only used where the designer requires it in order to correspond to the load.

This paper presents the design and SLM manufacturing of selected cellular structures that are considered suitable as a core material for injection moulding tools. 3D CAD modeling and FEA are used for preliminary design evaluation and engineering analysis.

## CELLULAR STRUCTURES FOR INJECTION MOULDING TOOLS

Solid cellular materials are classified as stochastic and ordered [1]. Stochastic materials, such as solid foams can have excellent heat- and sound- insulation properties and possess the ability to absorb a lot of energy. Ordered cellular materials, such as honeycombs and truss structures have great mechanical properties. They are widely used to enable the design of light structures, for creating unidirectional fluid flows, for absorbing the energy of impacts, to facilitate thermal transport across faces. The advantages of ordered cellular structures that make them desirable in injection moulding tools are their strength-to-mass ratio, and their high surface-to-mass ratio that defines their excellent heat transfer characteristics [2, 10]. The ordered cellular structures provide consistent mechanical parameters of the part and can be implemented in moulding tool design.

Truss structures or as they are also called lattice structures were analysed in this research. They appear to be mechanically competitive alternatives to prismatic honeycombs. It has been foreseen that these lattice structures could be of particular interest for injection moulding design because of their fully open interior structure which could assists multifunctional applications. The lattice core of injection moulding tools can be capable to supporting significant structural loads while also facilitating cross flow heat exchange

## Cellular structures design analysis

The design of cellular core structure for injection moulding tools have to combine the material mechanical properties and the functional requirements. This approach integrates design requirements and manufacturing capabilities. The chosen cellular structures have to correspond to three groups of requirements:

1. Geometry:
   - Cellular architecture;
   - Low relative density;
2. Mechanical properties:
   - Adequate strength;
   - Maximum displacement of the pressure contact surfaces;
3. SLM Manufacturability:
   - Cellular elements not inclined at less than 45º [from PDR experience];
   - Diameter of the strut more than 0.1mm [11];
   - To avoid hanging flat surfaces that required support.

The geometry requirements have been defined from the general characteristics of cellular materials and from the desire to introduce the cellular structure as a thermal management element during the moulding process. The mechanical requirements are derived from the moulding process and from the quality requirements towards the tooling. The SLM limitations are derived from the capabilities of this layer-additive technology.

Rehme and Emmelmann [11] investigated the manufacturability and scaling laws for mechanical properties of periodic lattice structures. The layer-additive manufacturing process used in this work is SLM. Eight different unit cell types are presented that can be produced by SLM technology. Following the results reported in [11] we selected two designs that demonstrate the best compression stress results and that are SLM feasible. These two designs shown in Fig. 2 a) and b), posses low relative density, they response well to compressive load and they do not have struts that are orientated at an angle less than 45º with respect to the build plane. Lattice truss structures have several of these flow directions and very high specific surface area for contact with a coolant flow. As a result, they can provide efficient heat removal which is valuable for the injection moulding process. The two structures are named as follow: a) wall centred truss structure, b) half-wall centred truss structure.
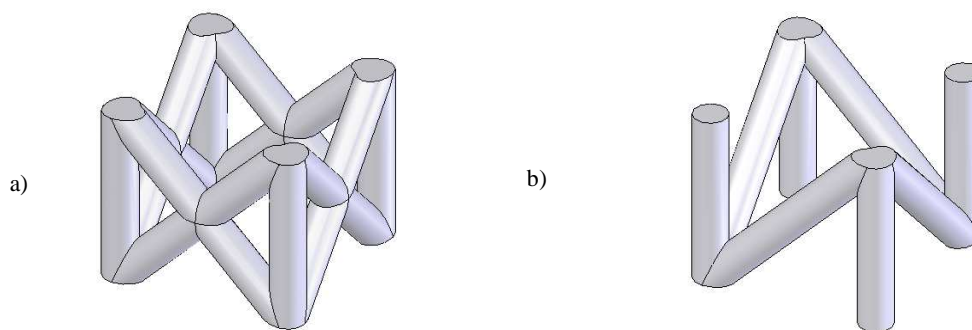


a)                     b)

*Fig. 1. The selected cellular units*

**Sample design**

There were two recommendations to the preliminary design that has been generated for all four selected cellular structures. Firstly, the strut diameter has been defined as 2mm [11]. The second design recommendation concerns the width of the cellular units. In order to coordinate the width of the cells with the maximum diameter of a cylindrical surface that SLM can produce without support, it has been accepted that the cell size has to be smaller than 7 mm. The second recommendation has been introduced such that the cellular structure can accommodate additional design elements that do not require support for SLM production. Any additional support will significantly reduce the fluid flow trough the cellular structure.

Commercial CAD software was used for constructing the samples. The cellular structures were created by patterning a unit sell and the generated models can be combined with other models. The sample models are cubic shape featuring 3 cells in each direction as illustrated in Fig. 2 a). The overall sample dimensions are 23x23x23 mm. As the modelled cellular materials will be used as internal structures in injection moulding tools, a skin element has been introduced to each cellular sample as it is shown in Fig. 2. b). In order to investigate the influence of the depth of the skin on the mechanical behaviour of the skin-cellular structures several samples were modelled with skin depth of 2 mm, 3 mm, 4 mm, 5 mm and 6 mm. The cellular samples have same overall element cell dimensions, but different relative density.
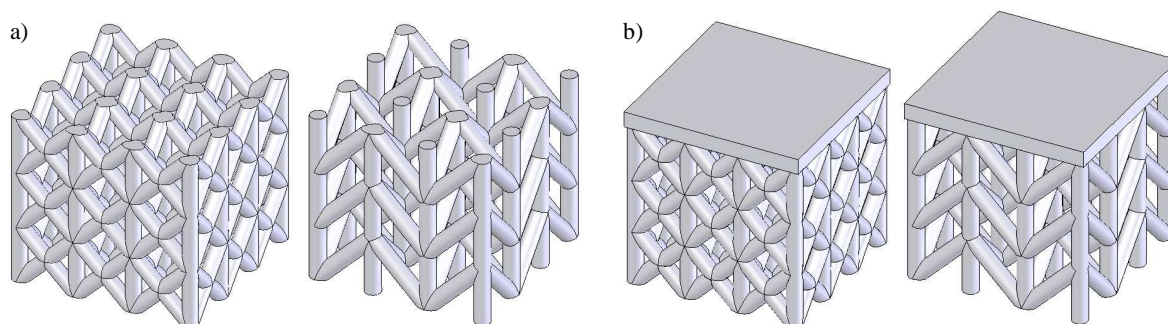


*Fig. 2.  Models of wall centred samples without and with skin*

To produce the sample shown in Fig. 3 a) and to avoid the introduction of support structure for the flat overhanging feature, the part has to be positioned upside-down (Fig. 3 b)) and the build will start with the skin. The major problem with this orientation is the significant shrinkage that the first layers experience. To eliminate the inaccurate portion of the skin element of the part, additional layers have to be added and later removed mechanically by a cutting operation. This solution will make the whole production process longer and less efficient. If it is decided to build the skinned truss part starting with the cellular structure a support will be required for the flat horizontal features as it is illustrated in Fig. 3 c). This conventional support Fig. 3 d) will reduce the flow rate of the cooling fluid and will subside the functionality of the lattice structure as an active and important element of the thermal management of the moulding process.
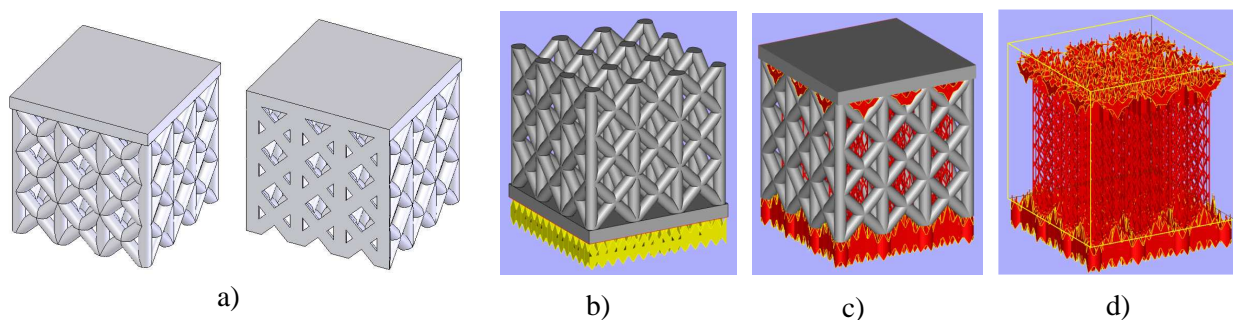
*Fig. 3. The skinned truss part with conventional support*

The other answer of the overhanging feature problem that has been experimented within this study is to introduce additional design elements into the part structure that will be able to support the horizontal surfaces without the need of the conventional supporting elements. One of the initial design requirements is the cell size to be smaller than 7 mm in order to accommodate the maximum diameter of a cylindrical surface that SLM can produce without support. Fig. 4 shows the design of the test samples created by using wall centred truss structure with additional designed supporting features and the required support for SLM production.
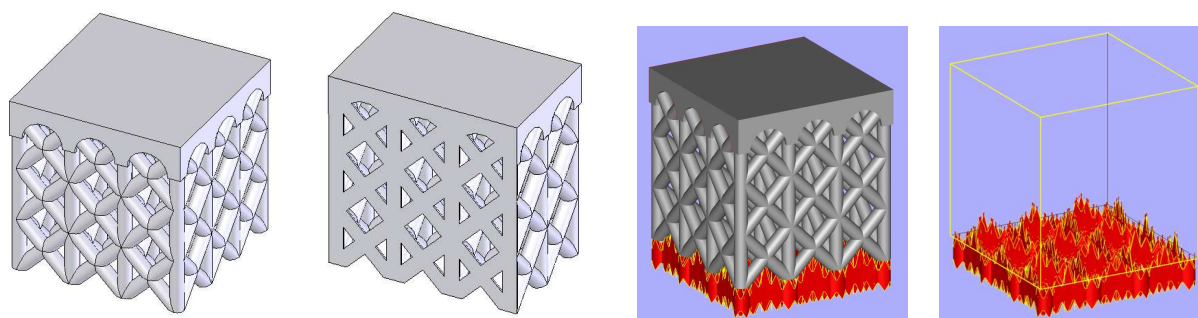


*Fig. 4. Wall centred truss structure parts with additional support elements for the flat horizontal features and the simple support system*

## MECHANICAL SIMULATION AND RESULTS

After structure modelling, the second step for introduction of cellular materials in injection moulding applications requires mechanical analysis of the capabilities of the structure to satisfy injection moulding process demands. FEA is used for the structure analysis. The created cellular structures were analysed on compressive loading similar to the loading in injection moulding tools.

The average peak pressure that the contact surfaces experience is accepted in this study as 3.5 MPa. We applied a uniform pressure on the top surfaces of the samples. The samples are fixed in all 6 degrees of freedom. The material is Stainless Steel 316L with Modulus of Elasticity E = 193 GPa, and yield strength 170 MPa. For computational efficiency, due to the symmetry, only one-quarter of the samples need to be modelled. Samples with 2mm, 3mm, 4mm, 5mm and 6mm horizontal skin have been analysed and the results for the maximum stress and displacement are presented in Fig. 5 with respect to the skin depth.
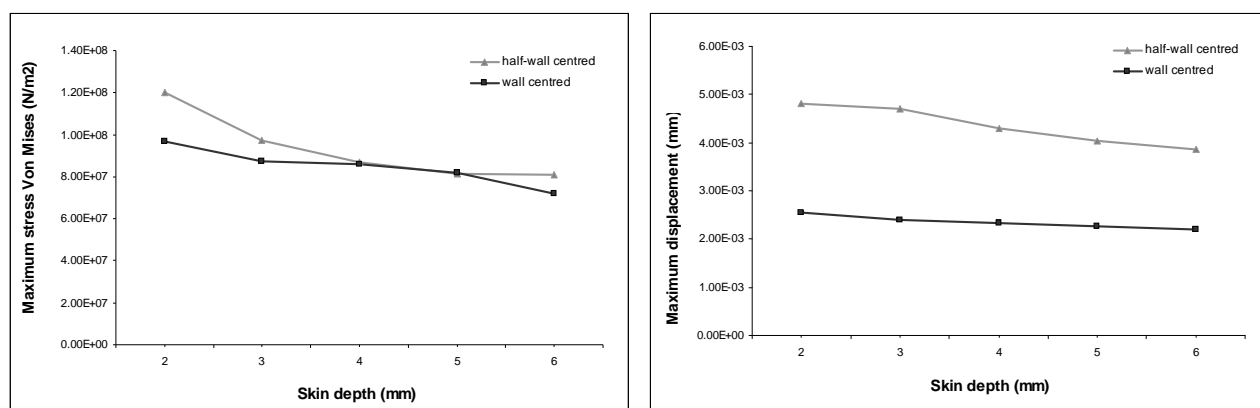
*Fig. 5. Maximum stress and maximum displacement of the four structures with skin with respect to the skin depth*

The stress and displacements levels of the cellular structures with skin (Fig. 5) are higher compared to the same parameters when the structures are without skin shown in Table 1. The maximum stress and the maximum displacement reduce as the depth of the skin of the parts increases. It has been noticed that after 4 mm skin depth the stress and displacement for each structure change a little. The FEA simulation with thicker skin up to 10mm was conducted and the trend is maintained. Taking this fact into consideration it could be concluded that there would not be a significant advantage for the mechanical characteristics of a part with cellular internal structure that has skin thicker than 4 mm. This fact is important for SLM produced parts, because the smaller quantity of solid part's areas means shorter machining time, less material, less energy.

*Table 1. Comparison of the truss structures with and without skin and with supporting features*

| | | Half wall-centered cells | Wall-centered cell | Wall-centered cell with support |
|---|---|---|---|---|
| Maximum stress (von Mises stress N/m$^3$) | | $9.384 \times 10^6$ | $1.207 \times 10^7$ | |
| | With 2 mm skin | $1.199 \times 10^8$ | $1.116 \times 10^8$ | $8.689 \times 10^7$ |
| Maximum displacement (mm) | | $4.460 \times 10^{-4}$ | $3.907 \times 10^{-4}$ | |
| | With 2 mm skin | $5.258 \times 10^{-3}$ | $3.255 \times 10^{-3}$ | $2.934 \times 10^{-3}$ |
| Relative density | | 0.2938 | 0.3070 | 0.3776 |

The presented structures are uniform and capable of supporting the pressure that is experienced during the moulding process. They create repeatable and predictable parts characteristics. At the same time the density of the cellular material can contribute to the better cooling of the moulding. Some design optimisation approaches [12]-[13] create variable topology of the cellular structures in order to put material only in these positions where it is required from the load. This approach is efficient when the cellular structure is used only to correspond to certain loading. In our case the idea to use

the cellular structures as an active element of the cooling phase of the injection moulding process requires that the cellular structure creates uniform coolant flow. If the density of the cellular material is variable it will create more material resistance in some areas and will slow the fluid flow.

To validate the manufacturability of the modelled truss structures all presented designs were produced by SLM and shown in Fig. 6 a), b), and c). Fig. 6 c) illustrates the better geometry that the design with created support elements provides: the edges are sharper, the dimensions are more accurate, and the skin feature is flat and horizontal. As it is highlighted in Table 1 the relative density of the supported design is a little higher than the relative density of the conventional part design with horizontal skin feature. But the design with arched supporting features provides less stress and less displacement which is advantage for its functionality.



a)

b)                                      c)
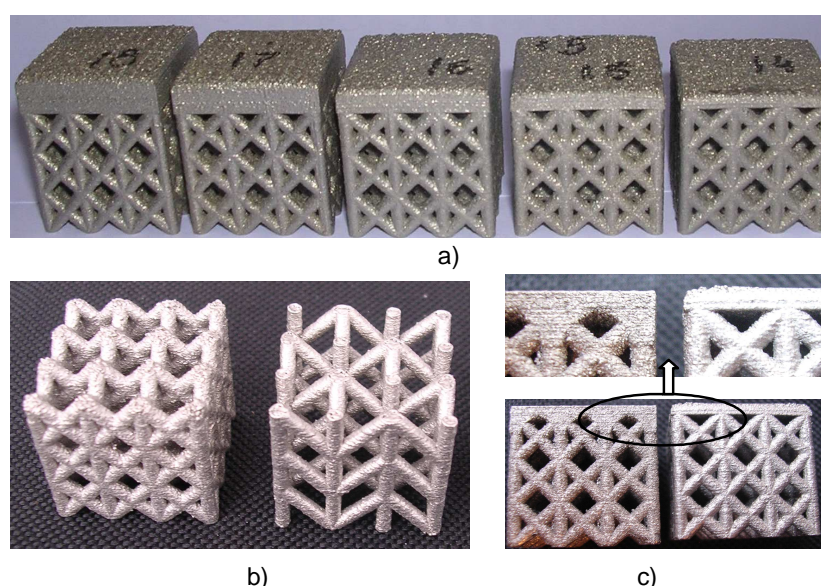
*Fig. 6. SLM built test parts*

## CONCLUSION

The idea of applying the cellular material in injection moulding tools is motivated by the capabilities of SLM technology for fast building of 3D complex geometry and by the desire to improve the functionality of the moulding tools. Due to the limitations of the traditional manufacturing processes, the geometry and the applications of the cellular structures are restricted.

This study investigated selected cellular structures which are SLM manufacturable and satisfy the design requirements. The preliminary investigation highlights the feasibility of such cellular structures for the purpose of injection moulding tooling. Lattice cellular structures appear to be mechanically competitive alternatives to prismatic honeycombs structures. It has been illustrated that lattice core of injection moulding can be capable of supporting significant structural and process loads while also could facilitating cross flow heat exchange. Next steps of this research will be physical testing, thermal simulation and thermal physical testing [14].

The combination of structural strength with the potential for better thermal conductivity of the cellular core structure and the ability of SLM technology to build complex

3D shapes makes the proposed approach very desirable for injection moulding tooling. Future work will investigate the thermal characteristics of the cellular lattice structures and their application in injection moulding tools.

## REFERENCES

1. Gibson L.J., Ashby M.F.: *Cellular solids: Structure and properties*. 2nd edition, Cambridge University Press, 1997.

2. Haydn N. C., Wadley G.: *Multifunctional periodic cellular metals*. Philosophical Transactions of the Royal Sosiety A, 364, 2006, 31-68.

3. Regenfuss P., Hartwig L., Klötzer S., Ebert R., Brabant Th., Petsch T., Exner, H.: *Industrial free-form generation of micro tools by laser micro sintering*. Rapid Prototyping Journal, 11/1, 2005, pp. 18-25.

4. Santos E. C., Shiomi M. Osakada K., Laoui, T.: *Rapid manufacturing of metal components by laser forming*. Int. J.  Mach. Tools & Manufact., Vol. 46, 2006, pp. 1459-1468.

5. Rehme O., Emmelmann C.: *Rapid manufacturing of lattice structures with SLM*. Proceedings of SPIE, Vol. 6107, February, 2006.

6. Mognol P., Rivette M., Jegou L., Lesprier, T.: *A first approach to choose between HSM, EDM and DMLS processes in hybrid rapid tooling*. Rapid Prototyping Journal, 13/1, 2006, pp. 7-16.

7. Rännar L-E., Glad A., Gustafson C-G.: *Efficient cooling with tool inserts manufactured by electron beam melting*. Rapid Prototyping Journal, 13/3, 2007, pp. 128-135.

8. Levy G. N., Schindel, R.: *Overview of layer manufacturing technologies, opportunities, options and applications for rapid tooling*. Proc. IMechE, Part B: Journal of Engineering Manufacture, Vol. 216 (12), 2002, pp. 1621-1634.

9. Norwood A.J., Dickens P.M., Soar R.C., Harris R., Gibbons G., Hancel, H.: *Analysis of Cooling Channels Performance*. Int. J.  Computer Integrated Manufacturing, 17(8), 2004, pp.669-678.

10. Liu C. Z., Sachlos E., Wahl D.A., Han Z. W., Czernuszka J. T.: *On the manufacturability of scaffold mould using a 3D printing technology*. Rapid Prototyping Journal, 13/3, 2007, 163-174.

11. Rehme O., Emmelmann, C.: *Cellular Design for Laser Freeform Fabrication*. Proceedings of the Forth International WLT-Conference on Lasers in Manufacturing 2007, Munich, June 2007.

12. Watts D.M., Hague R. J.: *Exploting the design freedom of RM*. Solid Freeform Fabrication Proceedings, Solid, Freeform Fabrication Symposium, Atlanta, Texas, August, 2006, pp. 656-667.

13. Wang H. V., Williams C., Rosen D.W.: *Design synthesis of adaptive mesoscopic cellular structures with unit truss approach and particle swarm optimisation algorithm*. Solid Freeform Fabrication Proceedings, Solid Freeform Fabrication Symposium, Atlanta, Texas, August, 2006, pp. 433-455.

14. Tsopanos S., Sutcliffe C.J., Owen I.: *The manufacture of micro cross-flow heat exchangers by selective laser melting*. Proceedings of Fifth International Conference on Enchanced, Compact and Ultra-Compact Heat Exchangers, NJ, USA, September, 2005, pp. 410-417.

**Kazimiera DUDEK**

Rzeszów University of Technology, Poland

# THE DECORATIVE PROPERTIES OF BURNISHED SURFACE LAYERS

*In this paper was presented a decorative properties of burnished surface layers. It was emphasized that except the most important functional properties, such as: increase fatigue strength, corrosion resistance or abrasion resistance the burnished surface layers receive the meaningful decorative properties. As the result of the one burnishing operation are realized aims: both increase mechanical properties and esthetic.*

## INTRODUCTION

The surface layer created as a result of using different burnishing methods have most of all technical function because of the high requirements it needs to face, such as: increase machine elements durability and tool life working under friction and fatigue loads conditions (often with corrosive influence of a surrounding environment). In mechanical engineering burnishing is used mainly to decrease the roughness and improve the hardness of the surface layer. Burnishing is also used, but not so often, to improve the precision of work or for decoration, nevertheless this kind of plastic working ensures the meaningful esthetical stocks, what confirmed experimental work, dozens years ago and now.

Between the sixties and seventies U. G. Schnejder worked out a oscillatory method of burnishing and simultaneously initiated a new direction of burnishing development. He defined burnishing as decorative working, which has been, with success, applied in series production, substituting engraving, polishing and even painting and decorative – protective surface coating [12]. Simultaneously, have been noticed that among a lot of effects of burnishing such as: increase of fatigue strength and abrasion resistant, also effects such as: increase of reflect light ability of surface and also decorative values can be used with success in industry.

## OSCILLATORY BURNISHING

The oscillatory burnishing consists in plastic forming, on work surface, continuous groove by hard element, for example ball which performs an oscillatory motion along workpiece, under definite pressure and relocating with a feed (Fig. 1). It makes the surface of regular roughness receiving possible.
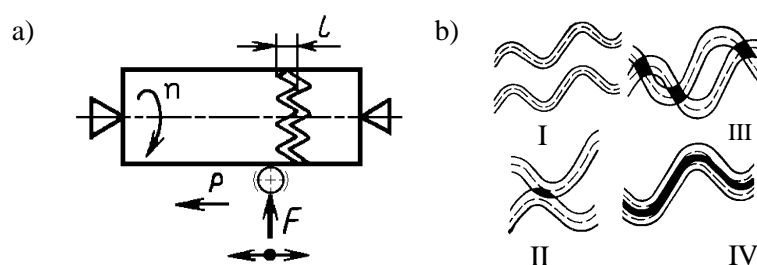
*Fig.. 1. The diagram of shaft oscillatory burnishing: a) the kinematics and characteristic quantities of working system: F – pressure force of ball, l – amplitude of ball oscillation, p – feed [1]; b) various kinds of grooves on work surface [6]*

This method has enabled the embossing on workpiece surface various micro – grooves systems about sinusoidal shape (Fig. 2). Their number and system on work surface can be effectively change with the aid of kinematic parameters of processing, namely: oscillation frequency of burnishing element, rotational speed of workpiece, feed of burnishing, amplitude of ball oscillation [9]. Adequately selection of these technological parameters enables part or whole of work surface covering, by after processing traces. Simultaneously, it makes possible the obtainment a high – homogeneity of mickro – unevenness, in respect of their shape, size and spacing.
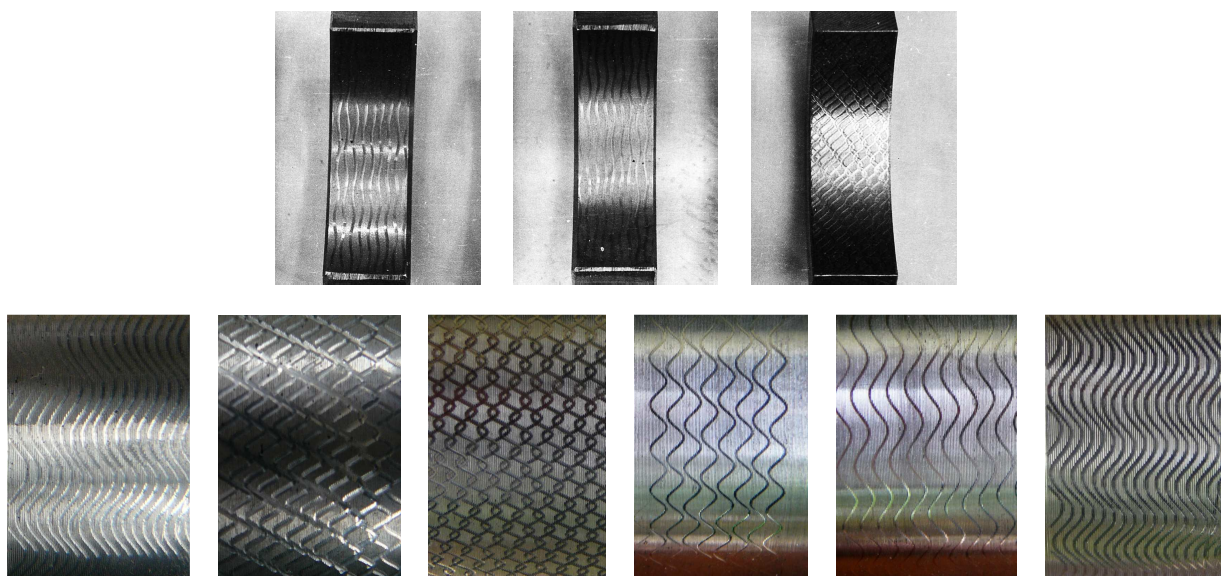


*Fig. 2. Various kinds of micro – grooves after oscillatory burnishing*

The regular micro – channels on work surface, received after oscillatory burnishing created, most of all, the natural containers of the lubricant. In this manner pay attention to fact, that surface with regular profile, so – called relief, can be distinguished by resistance of abrasive wear resistance and seizing of machine components [1, 9, 12]. The suitable surface geometry causes that surface layer enable to accumulate the lubricating medium (oil) and also accumulate the wear product. Surface with regular reliefs is characterized by smaller of wear for friction spot, but in each particular case, for a particular friction pair (kinematic pair) it is necessary to experimentally verify an optimal surface state (relief parameters). Abrasive wear of oscillatory burnishing surface mainly depends on relative surface of cavities on work surface which the opti-

mum value depends upon, for example, kind of friction pair and kinematics of her motion. The research realized of sleeve of engine cylinder, flat way and blade of compressor which have been oscillatory burnished, showed that abrasive wear of oscillatory burnished surface equals from 28% to 43% [7]. Moreover, roughness surface, plastically formed as result of oscillatory burnishing, increase the seizing resistance even about 300% [7], as compared with ground surface. It is result from the fact that effective counteraction of seizing consist in, among other things, suitable preparation of surface layer, so as to prevention the missing of oil film continuity. It is possible as result of forming the surface about large bearing surface with simultaneous producing the cavities being the containers of lubricative substance [11].

Reliefs received as result of oscillatory burnishing on work surfaces, except the ability to accumulate the lubricating medium assured also the significant aesthetical value. The variety of forms, sizes and distribution of micro – grooves caused that burnishing started to apply on a large scale for decorative purpose, replacing labour – consuming polishing [12].

Application of burnishing, especially oscillatory burnishing enabled the obtention, on work surface, roughness about high spacing of irregularities and rounding radius. Both that shape of unevenness and their glossy surface reduced dispersion of incident of this surface luminous rays, as compared with ground surface or polished (in case of grinding and polishing the work surface possessed sharp and law spacing of irregularities). This property is used to polishing, for example, different kind of metal mirrors in optical quantum generators and reflectors (executed of aluminium alloys) [8, 9, 12], because for reflectors is required the large light reflection coefficient. The oscillatory burnishing was applied also instead of polishing and engraving of metallic fancy goods, among other things: lighters, pens and ball pens (which were produced in high – series) and also instead of polishing in technology of aluminium ware (for example: pots, kettles and the like) and artistic products. In electrical industry the oscillatory burnishing was applied to finishing of projector mirrors clerical heater (Fig. 3).
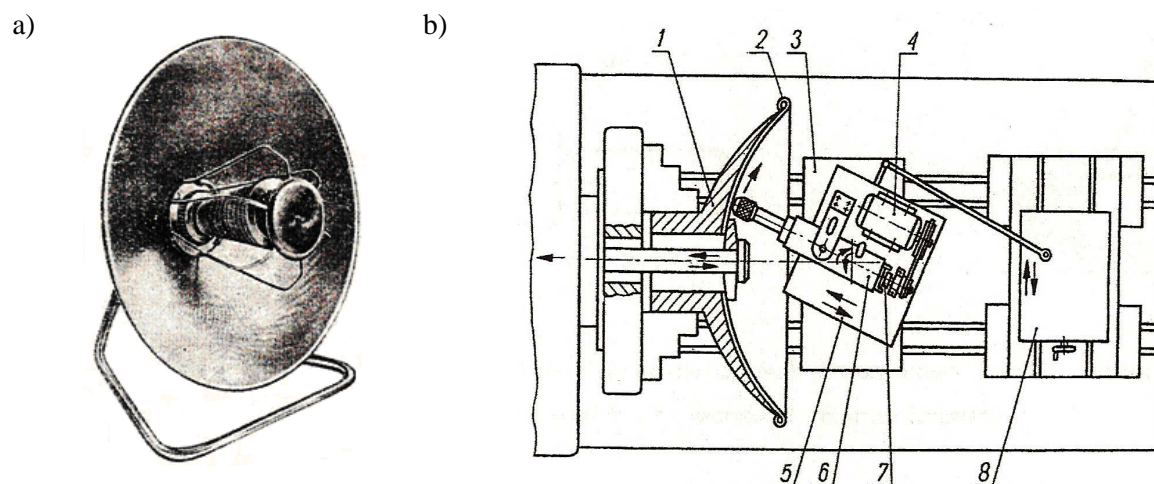


*Fig. 3. The example of oscillatory burnishing application as decorative working: a) a mirror canopy of electrical heater [8], b) head structure enabling oscillatory burnishing of concave surface: 1 – the chuck clumping workpiece, 2 – workpiece, 3 – base of head, 4 – belt transmission motor, 5 – rotational plate, 6 – head spindle, 7 – gyral eccentric element, 8 – cross slide of turning lathe [5]*

The oscillatory burnishing of reflector (pressed of sheet aluminium) made possible the elimination pretreatment of machine cutting and abrasive polishing, moreover this kind of working increased the esthetics of products.

Basic decorative criterion of surface layers is their appearance. Moreover, the important factors which have been taken into consideration during evaluation of appearance are: colour, luster, smoothness, hiding power and also resistance to tarnish. In esthetic respect the surface layer of oscillatory burnished elements could be shaped in a optional manner. Degree of coverage the machined surface by micro – channels was greater when frequency and amplitude of oscillatory motion and also pressure force and diameter of ball were greater. Whereas, this degree was smaller when rotational speed of workpiece and feed of burnishing were larger [9].

Therefore, the aim of oscillatory burnishing can be production the application oil grooves on co – operating surfaces (under friction conditions), for example of: pins, bearings, ways, cylinders and pistons, so as to raise their seizing resistance and abrasive wear resistance. Moreover, the aim of oscillatory burnishing can be also production the various patterns (reliefs) on burnished surfaces, for example of: aluminium ware, ball – pens, lighters and another metallic fancy goods.

The experimental work realized in Department of Manufacturing Process and Production Organization of Rzeszow University of Technology confirm that burnished surface layers (among other things: percussive and slide burnished surface layers) are characterized simultaneously by advantageous tribological properties and meaningful decorative properties.

## PERCUSSIVE BURNISHING

The method of burnishing which make the formation of regularly disposed cavities on work surface possible (not continuous grooves) are percussive burnishing. This is a kind of dynamic method of burnishing which enable the procurance various and repeatable systems of after – working traces (so – called lubricative pockets), in a form of cavities about specified size and arrangement and shape imitating the shape of burnishing tool tip.

The classification of arrangements of lubricative pockets received on percussive burnished surfaces is presented in [3]. Kinematics of percussive burnishing makes the optimization of cavities structure possible. It can be able to distinguish the following traces: not abutting (Fig. 4a), abutting (Fig. 4b), overlapping (Fig. 4c) and also reticular structures (Fig. 4d).
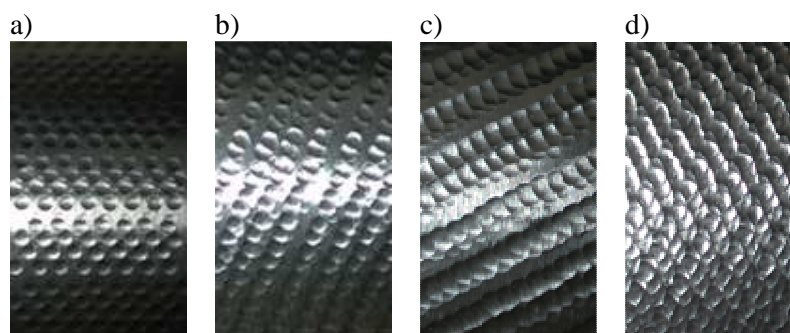


*Fig. 4. Various arrangements of lubricative pockets about spherical shape, after percussive burnishing*

The percussive burnishing is one of concentrated dynamic method of burnishing and is characterized by perpendicular method of tool impact in workpiece and possibility of accurate of space in which impact will occur.

Most of all, the cavities received on percussive burnished surface layers create both the natural lubricative pockets which accumulate lubricative substance and containers of impurities and wear products. Meanwhile the received surface is characterized by meaningful regularity and cause possibility of her accommodation to exploational requirements.

Except the spherical shape of cavities (presented in Fig. 5a), the percussive burnishing make embossing drop – shaped cavities possible (using the beater about different end), for example: shorter drop – shaped cavities (Fig. 5b), longer drop – shaped cavities (Fig. 5c).
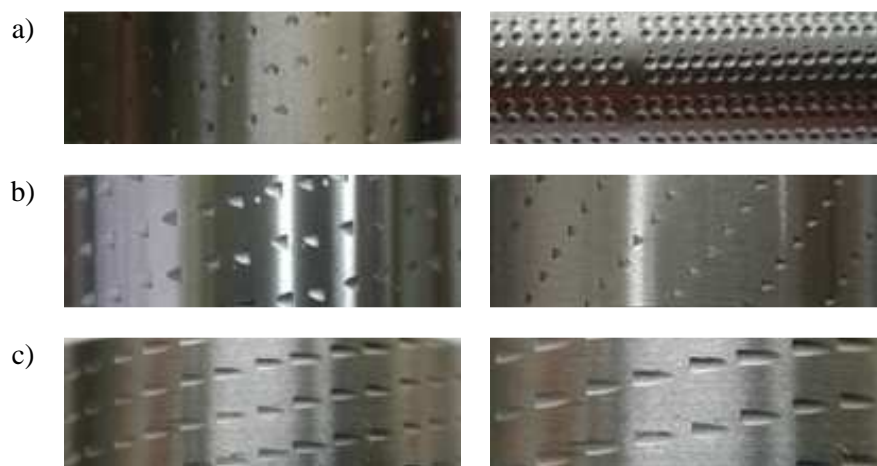


*Fig. 5. The examples of various cavities on percussive burnished surfaces*

Percussive burnishing enables accurately to plan the traces arrangements after impacts on work surface. With the aid of adequate selection of working parameters it is possible to regulation, over a wide range, among other things: size of traces after impacts and their reciprocal position. This kind of burnishing enable the betterment of fatigue strength and wear resistance and seizure resistance [2,10]. Kinematics of percussive burnishing makes the optimization of cavities arrangement possible (for the various frictional pairs) [2].

At present, the general engineering development and appearance of new solution (which can considerably rationalize processing) favour the different burnishing methods development. The computer programs turn out a great facilitation. They make the obtainment an answer, in what manner the proper selection of kinematic processing parameters have an effect on work surface topography. Computer programs enabling the process control (before processing) permissive to get the specified geometry of surface layer (among other things: number, size, shape and cavities system). They also enabling to count the degree of coverage of surface by impact traces (at specified size of cavities).

The example computer program, to simulation of percussive burnishing, (which window is presented in fig. 6), enable to generate the graph which illustrate distribution of traces on the work surface.
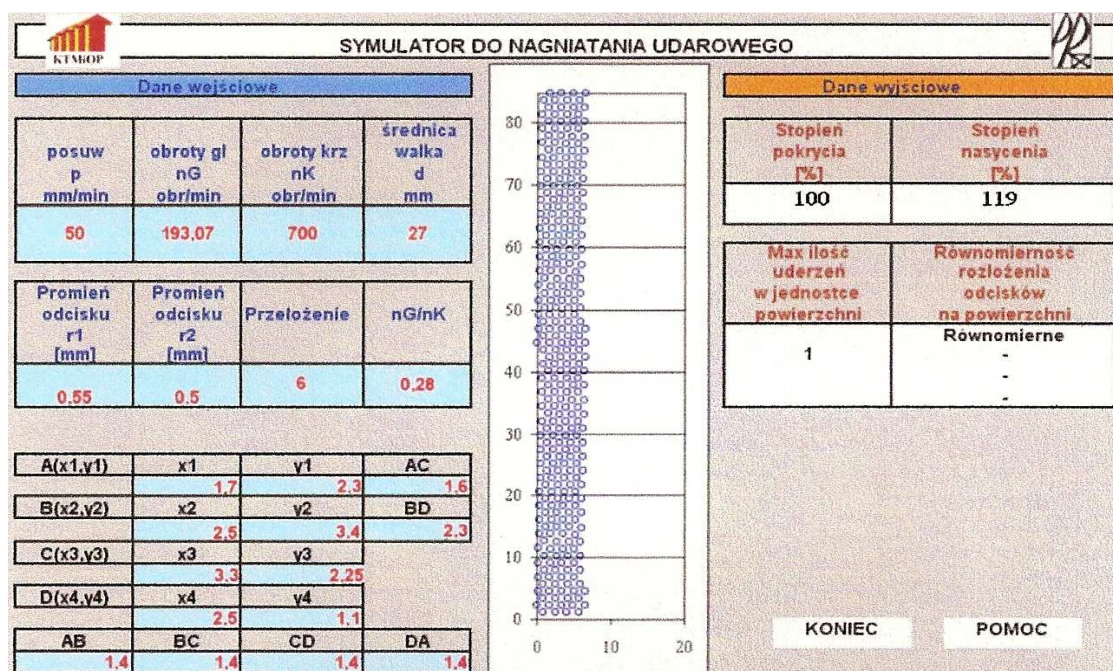
*Fig. 6. The view of computer window to simulation of percussive burnishing [10]*

So, depending on specifications for the burnished surface layer we can easily, without lead of arduous tests and measurements but through computer simulation), choose the processing parameters which permit to obtain the required effects of surface covering by structural changes.

## SLIDE BURNISHING

It's worth to devote one's attention to static method of burnishing, namely slide burnishing. During processing (realized on machining station, which general view is represented in fig. 7), the end of tool is displaces on the work surface and simultaneously clamped to it with the force causing the plastic deformation and planishing of surface roughness. Hence, the possibility of obtainment of considerable improvement of surface roughness is the most characteristic feature of this kind of burnishing [4].

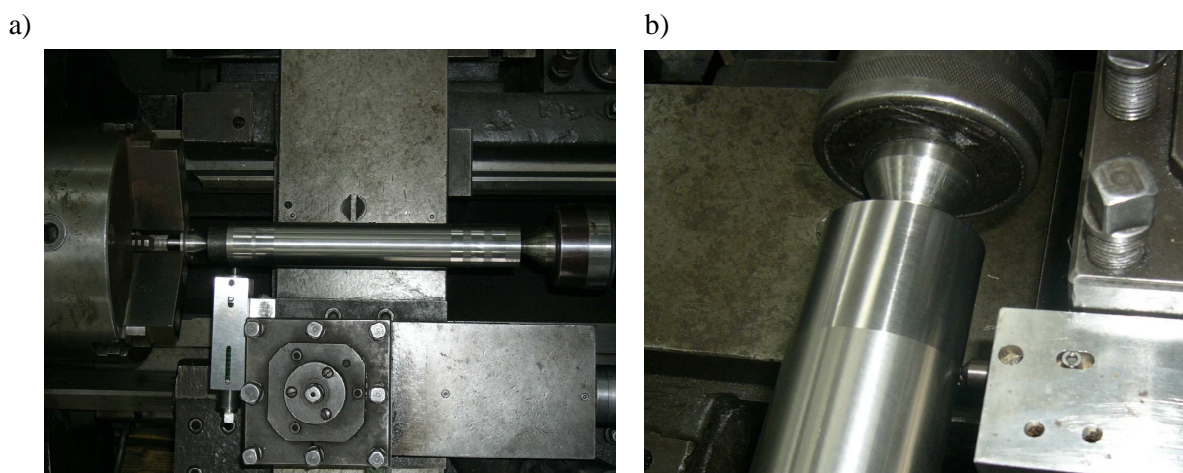a)                                                  b)



*Fig. 7. Slide burnishing of shaft: a) the photography of slide burnishing machine, b) a comparison of surface reflectiveness; at the top – slide burnished surface, at the bottom – ground surface*

With point of view of decorativeness, slide burnished surface layers are characterized by the very good reflectiveness. It is possible thanks to large spacing of irregularities and flat tops. Ground surfaces and polished surfaces have not such properties. The surfaces after grinding and polishing have sharp unevenness, which occur at small intervals.

Therefore, the described method can be applied in order to aesthetical appearance assurance of surfaces of usable objects.

Making an estimation of burnished surface layers we make an appraisal of their appearance. It might be say that the decorativeness is useful properties it which misjudgment has a objective character because features, such as: colour, luster or smoothness we can value subjectively and visual.

## CONCLUSIONS

The aim of this study is show that the different burnishing methods assure a meaningful decorative effects and that burnishing technology can be, with success, applied as consolidate – smoothness and also decorative – protective processing.

Micro – grooves or cavities, received as a result of oscillatory or percussive burnishing during the work of frictional pair, are kind of micro – containers which accumulate a lubricant and products of abrasive wear and also another impurities. But the same traces on burnishing surface can also provide a meaningful decorative values. They can be a reason of using this burnishing technology in order to increase esthetics of metallic products. At that time, burnishing become a kind of processing, in which consequence we can be done a decorative useful metallic objects.

Using burnishing method it places a special and primary emphasis on possibility of getting the advantageous useful characteristics which provide the most suitable state of surface layers (for specified work conditions of definite elements). Received decorative effects perform a not large function. Often, they are secondary- or third – rate aim of working. Whereas, it's worth to say that possibility of formation of, for example: surface about meaningful esthetic values, smooth surface which is characterized by the high reflectiveness or surface covered by the traces of plastic deformation, covering surface as o whole or creating the regular micro – reliefs, in concrete cases can be become the main aim.

## REFERENCES

1. Chworostuchin L. A., Szuszkin S.W., Kowalew A. P., Iszmakow R. A.: *Powyszenie nesuszczej sposobnosti detalej maszin powerchnostnym uproczneniem.* Maszinostrojenie, Moskwa 1988.

2. Gałda L., Koszela W., Pawlus P.: *Modyfikowanie właściwości tribologicznych przez wykonywanie kieszeni smarowych na współpracujących powierzchniach.* Tribologia, nr 3, 2006, s. 47-61.

3. Gałda L., Stadnicka D.: *Możliwość kształtowania regularnej mikrogeometrii czopów łożysk ślizgowych w procesie obróbki nagniataniem udarowym.* Tribologia, nr 3, 2004, s. 111-119.

4. Korzyński M.: *Nagniatanie ślizgowe.* Wydawnictwa Naukowo – Techniczne, Warszawa 2007.

5. Koszela W.: *Nagniatanie impulsowe powierzchni walcowych pracujących w warunkach tarcia.* Praca doktorska, Rzeszów 2003.

6. Odincow L. G.: *Finaisznaja obrabotka detalei almaznym wygłaziwaniem i wibrowygłaziwaniem.* Maszinostrojenie, Moskwa 1981.

7. Przybylski W., Hochschulz R.: *Technologia wytwarzania mikrorowków na powierzchni tarcia łożysk ślizgowych przez nagniatanie oscylacyjne*. Tribologia, nr 5, 1999, s. 625-638.

8. Przybylski W.: *Obróbka nagniataniem. Technologia i oprzyrządowanie*. WNT, Warszawa 1979.

9. Przybylski W.: *Technologia obróbki nagniataniem*. Wydawnictwo Naukowo-Techniczne, Warszawa 1987.

10. Stadnicka D.: *Wpływ nagniatania udarowego na właściwości warstwy wierzchniej stali*. Rozprawa doktorska. Politechnika Rzeszowska, Rzeszów 2004.

11. Szczerek M., Tuszyński W.: *Badania tribologiczne. Zacieranie.* Wydawnictwo i Zakład Poligrafii Instytutu Technologii Eksploatacji, Radom 2000.

12. Sznejder U. G.: *Obrazowanie reguljarnych mikrorelefov na detalach i ich eksplatacjonnyje svojstva*. Maszinostrojenie, Leningrad 1972.

**Andrzej DZIERWA**
**Paweł PAWLUS**

Rzeszow University of Technology, Poland

# SELECTED PROPERTIES OF CHROMIUM COATING ELEMENTS AFTER SHOT PEENING

*The paper presents results of the experimental investigations concerning chosen properties of chromium coating in relation to specimens made from 41Cr4 steel (coating thickness about 25 $\mu m$) and finished by shot peening. It has been found that shot peening of chromium coating can improve level of fatigue strength and slightly increase its microhardness.*

## INTRODUCTION

Chromium electroplating is widely used to obtain high levels of hardness, wear and corrosion resistance and a low coefficient of friction, for applications in the aerospace, automotive and petrochemical fields [1-3].

An important characteristic of chromium electroplating is the high tensile residual internal stresses, which increases as thickness increases and are relieved by local microcracking during electroplating [4, 5]. Hard chromium electroplating is used in landing gear components as: shock absorber, hydraulic cylinders and shafts. High tensile residual stresses and microcracks density contained in the electroplated chromium coating reduce fatigue strength of a component [6]. An efficient way of removal or considerable decrease in this negative influence on usage properties of the layers is application of burnishing process. With the appropriate selection of the layer material and burnishing conditions, increase in surface wear resistance can be repeated [7]. Among the burnishing methods used for layer processing the following are used most frequently: shot peening, micro ball peening and pneumatic ball peening, roller, ball burnishing and slide burnishing (slide planishing, slide diamond burnishing). The combination of electrolytic processing and burnishing may appear to be more efficient way of surface usage properties improvement than individual application of each of them [8].

Shot peening is a cold working process applied to the surface of metal parts to increase their fatigue resistance, fretting fatigue, stress corrosion cracking, corrosion fatigue and various other tensile stress related metal failures. Shot peening, by bombarding the surface with millions of tiny spheres of steel, glass or ceramic, totally covers the surface with indentations, creating an even layer of compressive stresses.

From the literature review [10, 11] we found that shot peening could be applied for elements from steel of great hardness. Therefore one can believe that processing of chromium coatings (of high hardness) would be efficient, too.

The aim of the investigation was determination of the effect input parameters on microhardness and fatigue strength of chromium coatings as the results of peening.

## MATERIAL AND METHODS

The studies were conducted on steel 41Cr4 of hardness 36±2 HRC. The base pre-treatment included turning and grounding (Ra = 0.63 µm). The finishing treatment of the coating (of 25 µm thickness) was shot peening in 16 different variants as:

- ✓ Variant 1      – balls=s110, p=0.3 [MPa], l=100 [mm], t=3 [min],
- ✓ Variant 2      – balls=s110, p=0.3 [MPa], l=100 [mm], t=6 [min],
- ✓ Variant 3      – balls=s110, p=0.3 [MPa], l=200 [mm], t=3 [min],
- ✓ Variant 4      – balls=s110, p=0.3 [MPa], l=200 [mm], t=6 [min],
- ✓ Variant 5      – balls=s110, p=0.9 [MPa], l=100 [mm], t=3 [min],
- ✓ Variant 6      – balls=s110, p=0.9 [MPa], l=100 [mm], t=6 [min],
- ✓ Variant 7      – balls=s110, p=0.9 [MPa], l=200 [mm], t=3 [min],
- ✓ Variant 8      – balls=s110, p=0.9 [MPa], l=200 [mm], t=6 [min],
- ✓ Variant 9      – balls=s230, p=0.3 [MPa], l=100 [mm], t=3 [min],
- ✓ Variant 10     – balls=s230, p=0.3 [MPa], l=100 [mm], t=6 [min],
- ✓ Variant 11     – balls=s230, p=0.3 [MPa], l=200 [mm], t=3 [min],
- ✓ Variant  12    – balls=s230, p=0.3 [MPa], l=200 [mm], t=6 [min],
- ✓ Variant 13     – balls=s230, p=0.9 [MPa], l=100 [mm], t=3 [min],
- ✓ Variant 14     – balls=s230, p=0.9 [MPa], l=100 [mm], t=6 [min],
- ✓ Variant 15     – balls=s230, p=0.9 [MPa], l=200 [mm], t=3 [min],
- ✓ Variant 16     – balls=s230, p=0.9 [MPa], l=200 [mm], t=6 [min].

where: s110, s230 – type of balls: s110 = Ø 0,3 mm; s230 = Ø 0,6 mm.

Chromium plating was done in universal bath under following conditions: temperature 50 – 55°C, cathode current density 40 – 45 A/dm$^2$ and current efficiency 15%.

The hasten pendular bending fatigue tests were carried out using an electro-dynamic vibrator with resonance frequency of the samples adopting the boundary number of cycles of $2 \cdot 10^6$. The used technique, that consisted in cutting samples out of special shaped cylinders, was described in [9] in details. The fatigue strength was calculated using stepped method on the basis of results of experiments on 16-sampled batches. The microhardness measurements were performed using a Vickers Diamond Microhardness Tester (type: Brivisor KL2+), with a 0.1 kG load and a loading time of 15 s. Parameters of microhardness is specified by the equations:

$$S_u = \frac{H_m - H_p}{H_p} \cdot 100 \ \% \tag{1}$$

$$H_s = H_r \pm \frac{C_{wu}}{h_u} \tag{2}$$

$$C_{wu} = \int_{h_1}^{h_u} [H(h) - H_r]\, dh \tag{3}$$

where: $S_u$ – degree hardening, $H_m$ – maximum microhardness of chromium coating after shot peening, $H_p$ – medium microhardness of chromium coating, $H_s$ – average microhardness of surface layer, $h_u$ – effective case depth, $H_r$ – microhardness of core,

The performed calculate of coefficients of linear correlation between microhardness parameters of surface layer too.

## RESULTS AND DISCUSSION

The fatigue experiments results are shown in Tab. 1. From the fatigue examination we found that the higher fatigue strength we achieved in variants IV, IX, X, III. (Zgw above 400 MPa). The other variants of chromium coating treatment was found less beneficial. The most unbeneficial was variant XIV (Zgw = 307, 28 MPa).

The performed microhardness tests showed that unpeened coating samples had maximum microhardness on the level 665 [HV]. The shot peening process increased this value to 713 [HV] in the case of sample with following input parameters: balls diameter 0.58 [mm], spraying pressure 0.9 [MPa], distance between nozzles and peened elements 100 [mm] and time of treatment 6 [min] (the maximum value of coefficients $H_s$ and $S_u$ were also then obtained).

The average microhardness of surface layer $H_s$ increased a the result of shot peening from the value 539.7 [HV] to the range 563.6 - 582.3 [HV]. The value of the degree hardening $S_u$ and indicator of hardening $C_{wu}$ surface layer after the shot peening process were in ranges, appropriately: 7.2-12.3 % and 7.52 - 8.78 [MPa mm].

*Tab. 1. The results of the fatigue strength and microhardness experiments*

| Variant of treatment | $Z_{gw}$ [MPa] | $\Delta Z_{gw}$ [%] | $H_m$ [HV] | $H_s$ [HV] | $S_u$ [%] | $C_{wu}$ [MPa•mm] |
|---|---|---|---|---|---|---|
| 1 | 398.43 | 32.36 | 690 | 572.5 | 8.7 | <u>7.52</u> |
| 2 | 398.43 | 32.36 | 701 | 580.2 | 10.4 | 8.34 |
| 3 | 401.57 | 33.41 | 689 | <u>563.6</u> | 8.5 | 7.95 |
| 4 | 411 | 36.54 | <u>681</u> | 580.5 | <u>7.2</u> | 8.57 |
| 5 | 395.28 | 31.32 | 690 | 574.3 | 8.7 | 8.26 |
| 6 | 392.14 | 30.28 | 704 | 580.2 | 10.9 | 8.74 |
| 7 | 385.86 | 28.19 | 690 | 578.1 | 8.7 | 7.77 |
| 8 | 395.28 | 31.32 | 701 | 582.2 | 10.4 | <u>8.78</u> |
| 9 | 404.71 | 34.45 | 697 | 574.1 | 9.8 | 8.38 |
| 10 | 401.57 | 33.41 | 697 | 576.7 | 9.8 | 8.27 |
| 11 | 376.43 | 25.06 | 699 | 577.3 | 10.1 | 8.32 |
| 12 | 367 | 21.93 | 698 | 574.9 | 9.9 | 8.23 |
| 13 | 345 | 14.62 | 702 | 573.8 | 10.5 | 8.23 |
| 14 | 307.29 | 2.09 | <u>713</u> | <u>582.3</u> | <u>12.3</u> | 8.37 |
| 15 | 357.57 | 18.74 | 701 | 577.7 | 10.4 | 8.4 |
| 16 | 334 | 10.96 | 704 | 578.6 | 10.9 | 8.36 |

*Tab. 2. Coefficients of linear correlation among microhardness parameters of surface layer*

| Parameter | $H_m$ | $H_s$ | $S_u$ | $C_{wu}$ |
|---|---|---|---|---|
| $H_m$ | 1 | 0.434 | 0.99 | 0.396 |
| $H_s$ | – | 1 | 0.433 | 0.601 |
| $S_u$ | – | – | 1 | 0,391 |
| $C_{wu}$ | – | – | – | 1 |

Table 2 present the results of the linear correlation between parameters characterizing the microhardness of surface layer. This analysis showed that the parameters were statistically independent except coefficients $H_m$ i $S_u$.

## CONLUSIONS

The results indicate that shot peening can increase microhardness of chromium coating elements. The greatest values of microhardness parameters were achieved for following parameters: $d_k = 0.58$ mm, p = 0.9 MPa, l = 100 mm, t = 6 min.

The results of the realized fatigue tests showed the distinctly advantageous effect of shot peening on the improvement of fatigue strength of chromium coating elements. The greatest value was obtained for following parameters: $d_k$=0.28 mm, p = 0.3 MPa, l = 200 mm, t = 6 min.

On the basis of testing presented in this paper we can see that the same input machining parameters cause the greatest microhardness parameters and the smallest fatigue strength value (variant XIV).

Performed investigations of chromium coating shot peening process have revealed the possibility of the shot peening process realization without fear of cracks, scalings or other defects. The conclusion of the investigations is the necessity of the further studies in this topic.

## REFERENCES

1. Bodger B. E., Mcgrann R. T. R., Somerville D. A.: *The Evaluation of Tungsten Carbide Thermal Spray Coatings as Replacements for Electrodeposited Chrome Plating on Aircraft Landing Gear.* Plating and Surface Finishing 1997 vol. 84.

2. Eckersley J. S.: *Shot Peening Process Controls Ensure Repeatable Results.* The Shot Peener, Vol 15/Issue 2, Summer 2001.

3. Jones A. R.: *Microcracks in hard chromium electrodeposits.* Plating and Surface Finishing 1989, vol. 76.

4. Dulpernell G., Lowenheim F. A.: *Mod Electroplating,* 1968.

5. Nascimento M. P., Voorwald H. J. C., Souza R. C., Pigatin W. L.: *Evaluation of an electroless nickel interlayer on the fatigue & corrosion strength of chromium-plated AISI 4340 steel.* Plating and Surface Finishing 2001, vol. 80.

6. Nascimento M. P., Souza R. C., Miguel I. M., Pigatin W. L., Voorwald H. J. C.: *Effects of tungsten carbide thermal spray coating by HP/HVOF and hard chromium electroplating on AISI 4340 high strength steel.* Surface and Coating Technology 2001, vol 138.

7. Korzynski M.: *Nagniatanie powlok chromowych.* Oficyna Wydawnicza Politechniki Rzeszowskiej, Rzeszow 1994.

8. Dzierwa A.: *The investigation of chosen properties of chromium coatings after pneumatic ball peening.* The 17th International DAAAM Symposium - Intelligent Manufacturing & Automation: Focus on Mechatronics & Robotics, Vienna 2006.

9. Lunarski J.: *Porównawcza ocena własności zmęczeniowych w badaniach technologicznych.* Technika Lotnicza i Astronautyczna, 1981, vol. 3.

10. Watanabe Y., Hattori K., Handa M., Hasegawa N., Takaji K., Ikeda M., Duchazeaubeneix J. M.: *Effect of ultrasonic shot Peening on fatigue strength of high strength steel.* Conf. Proc.: ICSP-8, Garmisch-Partenkirchen 2002 r.

11. Kopsov I.E.: *The influence of hammer peening on fatigue in high-strength steel.* International Journal of Fatigue, Vol. 13, 1991 r.

**Miroslav GOMBÁR**
**Sergej HLOCH***

University of Prešov, Slovak Republic

*Technical University of Košice with a seat in Prešov, Slovak Republic

# ANODIC OXIDATION FACTORS  ANALYSIS SIGNIFICANCE

*The paper deals with mathematical modeling of dependence between anodic oxidation factors in sulfuric acid and thickness of created layer $Al_2O_3$. By means of full factorial design were studied four independent variables the amount of sulfuric acid, aluminum, time and voltage. Results show the anodic oxidation factors significance and their effect to the layer thickness. It is the first step towards to the optimization of the eloxal process.*

## INTRODUCTION

Anodizing is a commonly used method for surface treatment of aluminum. This is due to a number of properties offered by this technique. Depending on the process conditions the following properties can be obtained: corrosion resistance, decorative surfaces, surfaces in almost any color on the palette, except white, hard and wear resistant surfaces, electrical and thermal insulation, the surface can be used as a base for organic finishing and for plating, the anodizing technique is expected to have an increasing advantage over many [1].

## RELATED AND PREVIOUS WORKS

Technologic process of anodic oxidation in real objects is in the most of cases very dynamic and stochastic process. Analytic process identification seems to be no effective and of low practical use. By its application, it is not possible to achieve the completed model of the process – the influence of certain parameters are neglected (fig. 1), in some of the factors there are not known the exact values, they are variable in time and most often, the intuition is applied to determine them. Their complicacy incomplete knowledge functioning mechanisms and large amount factors entering to the process complicate of mathematical model fitting by theoretical and analytical methods.

Vice versa a mathematic-statistical method allows fitting of statistical models even from relative large amount input data. The figure 1 shows influence of the operation time on thickness layer [2, 5]. The anodic oxidation of process factors optimization has been accelerated because of the need for improvements of process quality. Moreover, the process features change drastically with eloxal process factors entering the anodic

oxidation process. For such classic experimental design (fig. 1), some routine is needed and it is not effective from the time point of view. On the other hand, the mathematical statistical methods the statistic model designs outsourcing from the great amount of independent variables [3, 4].
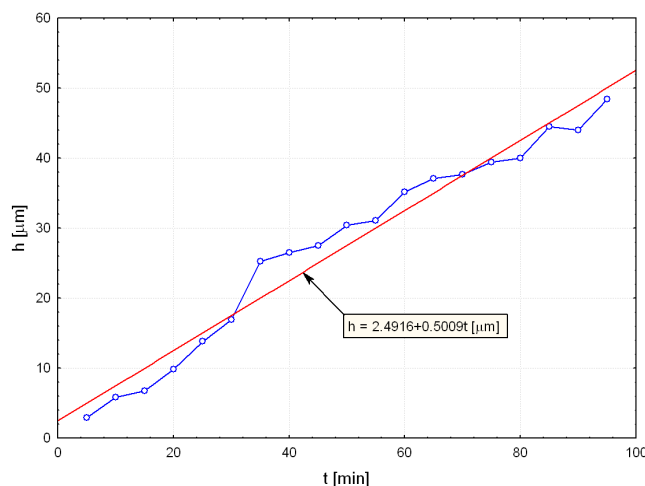


*Figure 1. Influence of the operational time t [min] at the anodic oxidation process on thickness layer h [μm]*

## EXPERIMENTAL PROCEDURE AND ANALYSIS

In order to investigate the influence of anodic oxidation process factors on layer thickness full factorial design for four independent variables has been designed. Full factorial analysis was used to obtain the combination of values that can optimize the response, which allows one to design a minimal number of experimental runs. Four factors submitted for the analysis in the factorial design of each constituent at levels [–1; +1] are listed in the table 1.

*Table 1. Experimental set up*

| Factors | | Factor level | |
|---|---|---|---|
| Var. | Terminology and dimension | -1 | +1 |
| $x_1$ | Sulfuric acid $H_2SO_4$ [l] | 0.15 | 0.25 |
| $x_2$ | Aluminium Al [g.l$^{-1}$] | 4.5 | 7.5 |
| $x_3$ | Time $t$ [min] | 7 | 13 |
| $x_4$ | Voltage $U$ [V] | 9 | 15 |

A tank with dimension $210 \times 130 \times 100$ mm has been used with volume of electrolyte of 2.2 l. Experiment was realized at constant temperature of 21 °C, that had been controlled by laboratory thermometer. Samples that have been eloxed was connected to anode and aluminum plates were connected on pole of adjustability unidirectional voltage. The experiments were carried out based on the analysis using Statistica 7.0 and Matlab to estimate the responses of the thickness layer h [μm]. A digital thickness gauge MINITEST 400 has been used to calculate the thickness layer with 0.02 μm precision of measurement. The measurement procedure consisted of measure variable dependent h with replicates of 5-times yielding total of 80 measurements.

## RESULST AND DISCUSSION

The quantitative description of the conditions effects on thickness layer $h$ [μm] was performed. Response surface methodology is an empirical modeling technique used to evaluate the relationship between a set of controllable experimental factors – independent variables and observed results – dependent variable thickness layer $h$ [μm]. The experiment results were analyzed using the analysis of variance. The regression coefficients and equations obtained after analysis of variance gives the level of significance of variable parameters tested according to Student's t-test. Obtained regression coefficients that show no statistical significance has been reject from the further evaluation. All terms regarding of their significance are included in the following equation (1):

$$h = \frac{10^{62,330}.x_1^{90,484}.x_3^{57,798.\log x_4}.x_1^{85,949.\log x_3.\log x_4}}{x_3^{67,738}.x_4^{52,159}.x_1^{98,745.\log x_3 + 78,193.\log x_4}} \tag{1}$$

These results can be further interpreted in the Pareto Chart, which graphically displays the magnitudes of the effects from the results obtained. Fig. 2a graphically displays the influence magnitudes of the effects, which are sorted from largest to smallest, from obtained results.
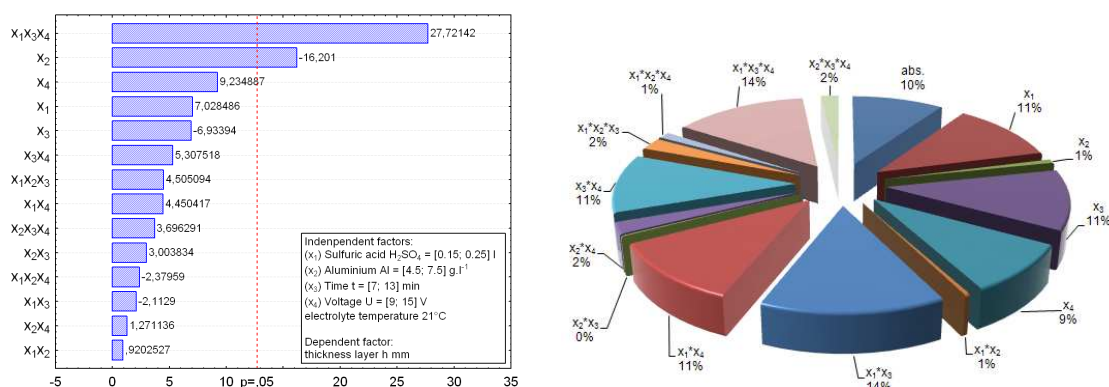


*Figure 2. a) significance of evaluated factors and their interactions that affects the layer thickness h [μm], b) percent expression of the significance of evaluated factors and their interactions that affects the layer thickness h [μm]*

From the Pareto chart is evident that the significant influence that affect the thickness layer have the interaction $x_1 x_3 x_4$ (sulfuric acid, operation time and the voltage) and the main effect $x_2$ – the amount of the aluminum. With the raising of the sulphuric acid amount the conditioned value of studied dependent variable – the thickness layer. The figure 4 shows the significance of the factors and their interactions that affects the layer thickness h [μm]. As can be seen the most important factor affecting the thickness layer from controllable factors is the interaction - $x_1 x_3 x_4$ (29%). The second most important factor is the amount of the aluminum in the electrolyte that significance in percent proportion is 19 %.

According to (Fig. 3) as the amount of the sulfuric acid and the voltage will be rising in the electrolyte, the thickness of the layer will be raising. The reverse trend has

the influence of the aluminum amount in the electrolyte, at which as the amount of the aluminum in electrolyte will be higher the thickness of the deposited layer will decrease.
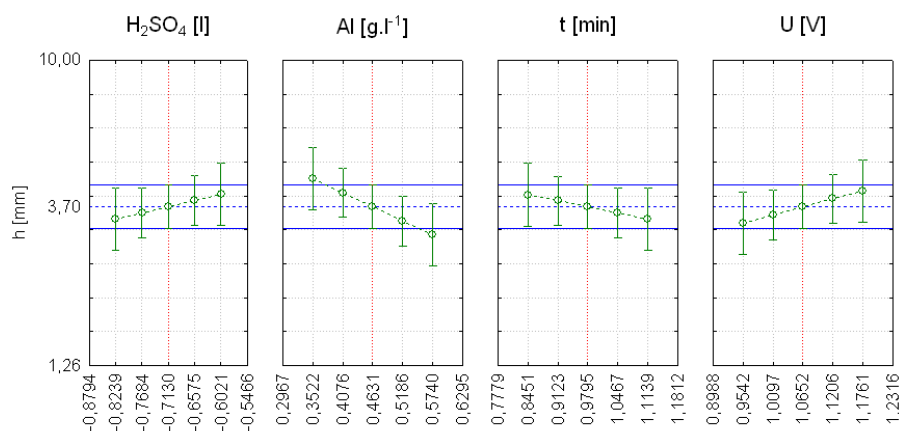


*Figure 3. Plots of the main effect of the factors at the eloxal process on thickness layer*

## CONCLUSIONS

Technological process of anodic oxidation of aluminum and its alloys from the point of view of created layer pursuant of realized experiment is mainly affected by interaction of the amount of sulphuric acid and the operation time and by the voltage. With the raising of the sulphuric acid amount the conditioned value of studied dependent variable – the thickness layer. On the contrary with the raising of the aluminum amount in electrolyte the value of the thickness layer decreases. Thickness layer decreasing on operation time can be explained by process of creation and properties of anodic layer, which is none conducted. In the anodic oxidation process of aluminum, is necessary to pay attention to identify the state of the electrolyte, mainly the aluminum amount and the amount of the overall and free sulphuric acid. Relative high influence on thickness created layer has the electrolyte temperature that was constant at the experiment. The total rate evaluated factors and further neglected factors that affect the anodic oxidation process, by means of statistical analysis represent 54%. In further research it will be necessary to study those factors, which affect the created layer.

## REFERENCES

1. Montgomery, D. C.: *Light Metals Finishing Process Manual*, AESF. 1990.
2. Wernick S., Pinner R., Sheasby P. G.: *The Surface Treatment and Finishing of Aluminium and its alloys*. 5th edition. 1987.
3. Kreibich V.: *Theory and technology of surface treatment*. ES ČVUT Praha, 1999.
4. Mohyla M.: *Metal surface treatments technologies*. VŠB Ostrava, 1995.
5. Bekes J., Andonov I.: *Analysis and synthesis of the engineering processes and objects*. 1.edition., Bratislava: Alfa, pp. 376.

**Grzegorz GORCZYCA**

# EFFECTIVE PROJECT MANAGEMENT

*Projects taken in live give us opportunity to develop our business, experience, the constrains we are struggling keep us on track in achieving the goal. The road to success do not need to be hard and painful, base on solid fundament of business philosophy can be more effective. In effective chain of project management, the weakest link are people and wrong interpretation of business philosophy by them.*

## BUSINESS PHILOSOPHY ROLE

The most fundamental concept in the field of project management is the idea of the project itself. The project according to Project Management Institute and PMI Guide to the Project Management Body of Knowledge or PMBOK is "a temporary endeavor undertaken to crate a unique product, service, or result" [1].Starting the project the most important think is too base him on solid fundament of philosophy. However, which is the best and can cover all area of business organization? There is one simple way to answer on that question-only that philosophy stays and is used daily which gives the best results and is the most effective. Live verify everything, the best example of that is Six Sigma which start in Motorola and cared company to success, the same think with holding General Electric and Textron. Six Sigma is deeply understanding the potential clients needs, decide using facts, data, statistic analyze in improving and create business processes. Fortune magazine creates every year the list of hundred the best companies in the world- lucking answer for question, way the financial company results are that good. The answer for that question is in human nature. Human evaluate, measure everything and calculate in value for them most suitable way- in amount of money, they reject systems, which are not profitable, effective like for example quality systems like Reengineering, Total Quality Management etc. 2008 "Fortune" magazine in Aerospace and Defense category give the first place Textron for the Most Admired Company, the last year jump from  seven place is one of the biggest achievement in that business sector. For that multi industrial company that success is a grate achievement and effect of implementation Textron Six Sigma system for whole company. To explain way using Six Sigma give so much we need go beck to 1947 and W. Edward Deming trip to Japan were he expertise quality control technique. Deming train hundreds of engineers, managers, and scholars in statistic process control (SPC) and concept of quality. Deming's message to Japanese chief executive was: improving quality will reduce expenses while increasing productivity and market share [2]. Deming start fallow the best way in biasness the way voice of the customer, Japanese automotive market demand was different then in US. Market was based on small quantity, good quality of the product and low price. The resold of that trim we can see until now looking on company like Toyota, Suzuki, Honda, Sony, Panasonic etc. Success of Japanese company change US engineers of thinking about quality, Ford

Motor Comp. was one of the first corporations to seek help from Deming. Since 1979 to 1982, Ford had incurred 43 billion in losses after Deming start helping company.

"The prevailing style of management must undergo transformation. A system cannot understand itself. The transformation requires a view from outside. The aim of this chapter is to provide an outside view-a lens-that I call a system of profound knowledge. It provides a map of theory by which to understand the organizations that we work in.

"The first step is transformation of the individual. This transformation is discontinuous. It comes from understanding of the system of profound knowledge. The individual, transformed, will perceive new meaning to his life, to events, to numbers, to interactions between people.

"Once the individual understands the system of profound knowledge, he will apply its principles in every kind of relationship with other people. He will have a basis for judgment of his own decisions and for transformation of the organizations that he belongs to. The individual, once transformed, will:

- Set an example.
- Be a good listener, but will not compromise.
- Continually teach other people; and
- Help people to pull away from their current practices and beliefs and move into the new philosophy without a feeling of guilt about the past" [3].

## PROJECT LIFE CYCLE

Project are usually divided into phases. Collectively, these phases make up the project live cycle. Industries, governments agenesis, and business enterprise have their own terminologies for explaining the project live cycle. Defense acquisition project will go through the steps of determination of mission need, concept exploration and definition, demonstration and validation, engineering and manufacturing development, production and development. In generic way life cycle is divided on next four phases.

- Initiation.
- Planning.
- Implementation.
- Closeout.

The key aspect of project management are the triple constrains, scope-cost-time (Fig. 1). Each constrain is critical and related to the other two, changing one almost inevitably change one or both of them.
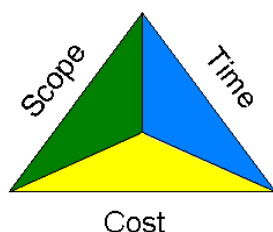
Scope is the work or requirements, which need to be accomplished to delivered a project. The Work Breakdown Structure is essentially the scope statement reduced to individual pieces of work. To build the WBS the team leaded by project manager need to have full understanding purpose of the project. They need to under-



*Fig. 1. The key aspect of project management*

stand voice of customer, which is the basic key to achieve the project success. Understanding the customer give the team on the beginning of the project had better view

what resources they need and if time they have is sufficient. Statistic give us tool for analyze and eliminate potential treat for the project like FMEA. The biggest treat for project are people, to much exaggeration guide in direction where project do not need to go. Developing objectives have big influence on other two constrains-time can be expended and leads to thread of project accomplishing because the budget of the project is not prepared for new tasks and cost related. To WBS can take multiply form, and each format has it own advantages. The two most common form WBS are indented and graphic. Transfer WBS to Network Diagram shows chronological work packages brake down into activities relationship between scheduled actions. Network Diagram work packages divide project into small steps, graphic form show set of activities in visible form. If we have A, B, C, D, E, F, G.

*Table 1. Network Diagram work packages*

| Activity | Predecessors | Duration in workdays |
|----------|--------------|----------------------|
| A | project start | 1 |
| B | A | 3 |
| C | A | 1 |
| D | A | 2 |
| E | C and D | 3 |
| F | B and E | 1 |
| G | F | 1 |

The fooling network diagram represents set of activates in graphic format is presented in Fig. 2.
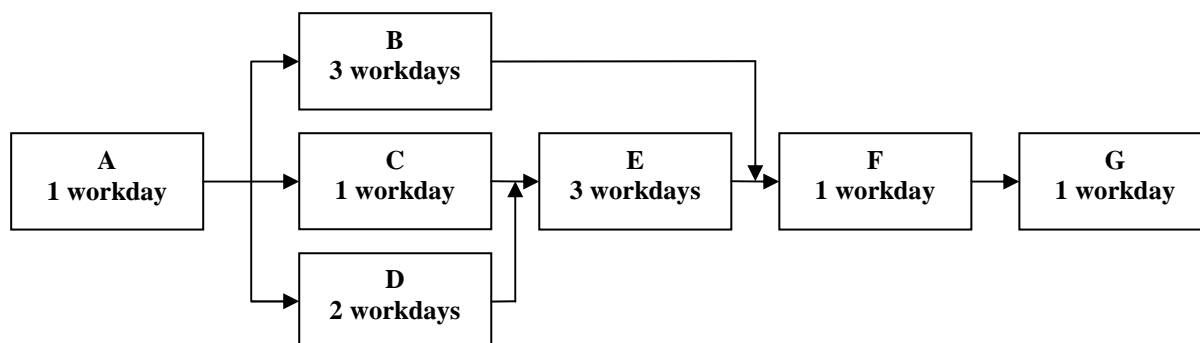


*Fig. 2. The fooling network diagram represents set of activates*

The critical path for that project is A, D, E, F, G and can be easy recognize like the zero value for time float.

Effective project management is strictly related with proper work breakdown structure, work packages split project for smaller portion, which can be easier to manage and control by smaller team. Project managing is elastic process and cannot be stick to hard boundaries, with the time project is evolving not only because of developing work progress, but also because of new buissnes enviroment, which force to go further and be more successful.

Backing to Six Sigma (SS) philosophy base on Deming PDCA cycle or Shewhart cycle named after Waltera Shewhart Deming master (Plan-Do-Check-Action), market force on company has to be more competitive and eliminate waste being six sigma ef-

fective. Start analyze depending on what area of Six Sigma we are, for example Textron.
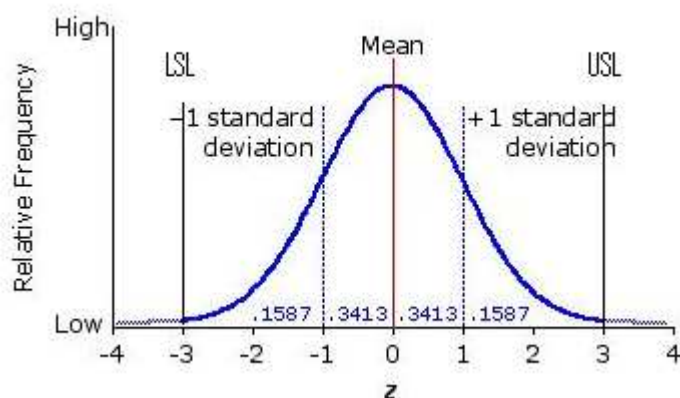
Company spread SS for DFSS (Designee For Six Sigma ) for new process/ projects or for calicle broken to grow and innovate, DIMAIC (Define Analyze Measure Analyze Control) for improving existing processes to reduce variability and Lean Manufacturing to eliminate the waste. To measure effectiveness of the process in Six Sigma is use DPMO (Defect per Million Opportunities) and after that DPMO calculated in sigma's where six sigma is 3,4 DPMO. Elimination cause of defects have directly impact for process effectiveness (e.g. work package ) part of every project. To keep second constrain on track (Time) the Gantt chart is use to monitor progress of project and status according to planed schedule.

Status of the process capability (project part) in visible way is shown on Gauss chart (Fig. 3).

To successfully finish the project, all phases (Initiation, Planning, Implementation, Closeout) need to be base on solid fundament of business philosophy and key aspect of project management (triple constrains) related with team and people management in organization.

## MANAGER ROLE

To accomplish project effectively in each process need to be eliminated the weakest link in the chain. People have the biggest influence on project life cycle, project manager is the most important person, which coordinate and take responsibility for progress. Manager is a knowledgably person, which covers all aspect of project, most of the time project team are divided on small teams responsible for parts of work. Leader keep them of right direction of work, the biggest threat for teams is fanaticism of them self and colleagues. Way- even the best business philosophy can by destroyed because of misunderstanding or bad interpretation of theory. Manager roll is to lead team to achievable project goals. Six Sigma opens new door in managing, system cover all aspects of managing in organization from idea to real action, service or product using statistic tools known from decades. People accept not complicated systems ,which can be easy visual, helps them in work, make it easer and more effective. Live evaluate managing system very hard and Six Sigma past that exam. After improvement Japans economy Deming was welcome in US with slide difference, Japan take years to understand how important quality is, Americans take that decades.

## REFERENCES

1. PMBOK Guide.

2. *Deming's 1950 Lecture to Japanese Management*. Translation by Teruhide Haga.

3. 3. Deming, Edwards W.: *The New Economist for Industry, Government, Education. Second edition*, 1993.

**Ivan G. GRABAR**
**E.G. OPANASYUK**
**E.V. ZABASHTA**
**Dima B. BEGERSKIY**


Zhitomir State Technological University, Ukraine

# MATHEMATICAL MODEL OF MOTION
# OF PNEUMONIC TYRE ON DRY SOIL

*Mathematical model of motion of pneumonic tyre on dry soil, which takes into account the change of radius and rigidity of tyre is proposed. Experimental data of dependence of static radius of a tyre from tangent force are presented.*

Essential contribution into the development of theory of motor vehicle wheel propeller, improvement of criterion of their operation process was made by such scientists as: Kosharniy M. F., Bezborodova G. B., Ageikin Y. S., Smirnov G. A. [1, 2, 3, 4, 5], etc.

However, in spite of increase of information volumes about the mechanics of interaction of the wheel propeller with hard base surfaces and deformed ground, the main factors of its rolling, energy expenses on the formation of the clutch power are the focus of attention of many investigators.

While determining the clutch coefficient and the coefficient of resistance to rolling, investigators proceed from different theoretical prereguisites, that does not allow to estimate the correctness of the well-known workings. Experimental data are reccived with the help of different methods at unequal ground conditions. Furthermore, design formulas are just only for fixed processes of interaction of propeller with ground and do not reflect the real couplings and vibrations in "transmission – wheel propeller – ground" system.

In many works the fact, that the power of friction in contact of a wheel with the ground depends only on characteristics of the ground, is marked. At the same time in works [8, 9], devoted to the ground mechanics, it is said that the properties of grounds can be changed greatly under the influence on the mass of ground vibration. Figure 1 shows the dependence of vibroviscosity of sand from vibrational accelerations. It is clear from the diagram that vibroviscosity coefficient which is very big for immovable sand mass, greatly reduces under the influence of vibrations on it and achieves the values which are equal to viscosity of some liquids.
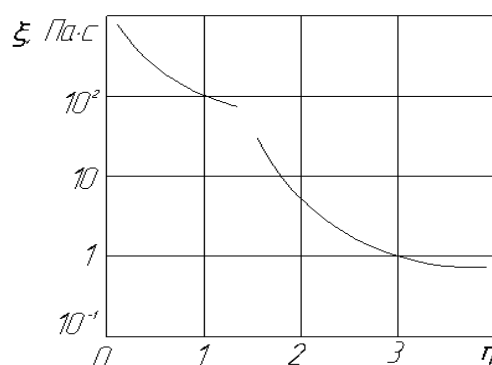
*Fig. 1. Dependence of coefficient of sand vibroviscosity from vibrational accelerations*

Such behaviour of sand under the influence of vibration, as well as the onset of oscillations in contact of a tyre with the ground, is not taken into account by formulas for determination of the main parameters of interaction of a wheel with the ground. Furthermore, the formulas do not take into account the changes of elastic properties of pneumonic tyre at joint action of radial and tangent load [11, 12] on it.

That is why mathematical model of interaction of a wheel with the ground is proposed. The model takes into account not only the properties of the ground but also the properties of a pneumonic tyre. Fig. 2 shows design scheme of interaction of a wheel with the ground.
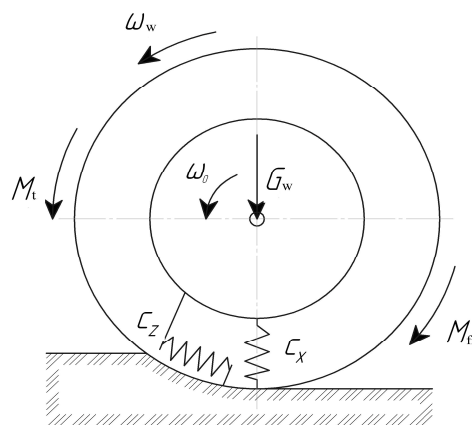


*Fig. 2. Design scheme of interaction of a wheel with the ground*

Movement of a wheel can be divided into two alternated phases:
   1) sediment phase, of which the following conditions are just;

$$0 \leq t \leq t_1$$

$$M_{el} \leq M_{fr}$$

$$0 \leq M_{fr} \leq M_{st} ,$$

$$\omega_0 = const$$

$$\varphi(t) = 0$$

   2) jump phase:

$$t_1 \leq t \leq t_2$$

$$M_{el} \geq M_{fr}$$

$$M_{st} \leq M_{fr} \leq M_{sl} ,$$

$$\omega_0 = const$$

$$\varphi(t) \neq 0$$

where $M_{el}$ – moment of elasticity force; $\grave{I}_{fr}$ – moment of friction force; $\grave{I}_{st}$ – moment of static friction force; $\omega_0$ – angular velocity of wheel axis; $\varphi(t)$ – angular shift of external part of the tyre; $M_{sl}$ – moment of sliding friction force; $M_t$ - twisting moment; $G_w$ - vertical load.

Let's consider the second phase of wheel movement in detail. Differential equation of movement at the given conditions will be the following:

$$I \ddot{\varphi}_w = M_t - M_{fr} . \tag{1}$$

The torque moment can be assumed through traction force on the wheel and its dynamic radius:

$$M_t = P_p r_d .$$

With due regard for tangent stiffness of a tyre traction force can be assumed as:

$$P_p = c_x (\dot{\varphi}_0 t - \varphi_w) .$$

In this case the moment of friction force on the wheel will be equal to:

$$M_{fr} = F_{fr} r_d .$$

The equation 1 will be:

$$I \ddot{\varphi}_w = c_x r_d (\dot{\varphi}_0 t - \varphi_w) - F_{fr} r , \tag{2}$$

or:

$$I \ddot{\varphi}_w + c_x r \varphi_w = c_x r \dot{\varphi}_0 t - F_{fr} r . \tag{3}$$

The received inhomogeneous linear differential equation is easily solved with the help of standard methods [10]. Having done all necessary transformations we'll get the total solution of the equation 3:

$$\varphi(t) = C_1 \cos \omega t + C_2 \sin \omega t + \dot{\varphi}_0 t - \frac{F_{fr}}{c_x},$$

(4)

$$\dot{\varphi}(t) = -C_1 \omega \sin \omega t + C_2 \omega \cos \omega t + \dot{\varphi}_0$$

where $C_1, C_2$ – constants of integration, $\omega = \sqrt{\dfrac{\tilde{n}_x r}{I}}$

To find particular solutions we take the initial statement: at $t_0 = 0$, the turning angle and the angular velocity of the external part of the tyre are equal to zero:

$$\varphi(t_0) = 0$$

$$\dot{\varphi}(t_0) = 0$$

Substituting the given statements into equations 4, we get:

$$C_1 = -\frac{\Delta F_{fr}}{c_x}.$$

$$C_2 = \frac{\dot{\varphi}_0}{\omega}.$$

The final solution of the equation of wheel movement will be the following:

$$\varphi(t) = -\frac{\Delta F_{fr}}{c_x} \cos \omega(t) - \frac{\dot{\varphi}_0}{\omega} \sin \omega(t) + \dot{\varphi}_0 t - \frac{\Delta F_{fr}}{c_x},$$

(5)

where $\Delta F_{fr} = F_{st} - F_{sl}$ .

Friction force can be shown as a product of normal reaction of base surface and friction coefficient:

$$F_{fr} = Rf .$$

In this case normal reaction of base surface can be defined as:

$$R = G_w + m_w g .$$

Or with due regard for redial stiffness of a tyre:

$$R = c_z \Delta r .$$

So, the difference between the static friction force and sliding force can be defined from equality:

$$\Delta F_{fr} = c_z \Delta r (f_{st} - f_{sl}).$$

Then, the equation 5 can be written in the following way:

$$\varphi(t) = \frac{c_z}{c_x} \Delta r (f_{st} - f_{sl}) \cos(\omega t) - \frac{\dot{\varphi}_0}{\omega} \sin(\omega t) + \dot{\varphi}_0 t - \frac{c_z}{c_x} \Delta r (f_{st} - f_{sl}). \tag{6}$$
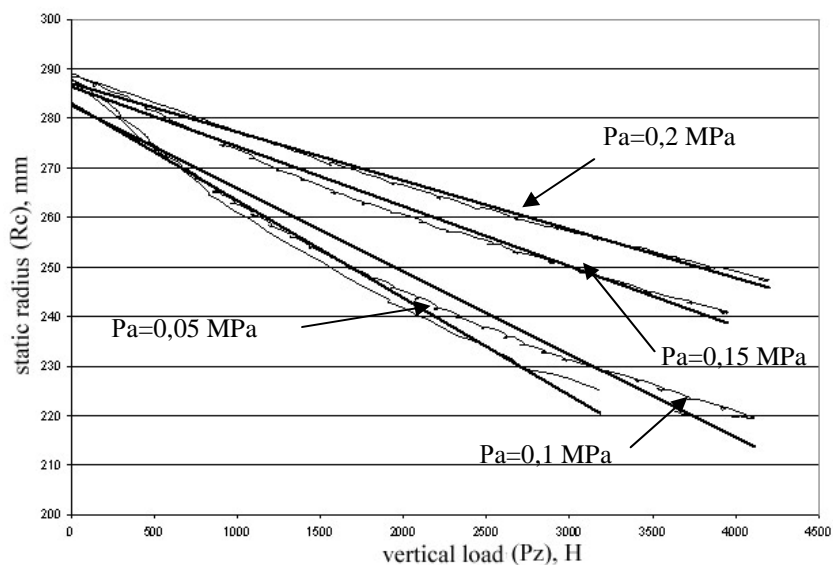


*Fig. 3. Dependence of tyre radius „Pirelli"  175/70 R 13  from vertical load at different values of air pressure in the tyre*
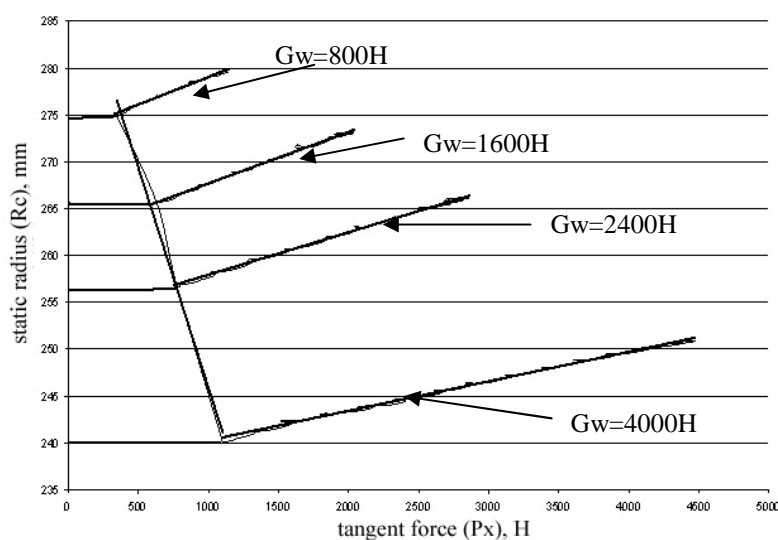


*Fig. 4. Dependence of tyre radius „Pirelli"  175/70 R 13  from tangent load at different values of vertical load on tyre*

It should be noted that the tyre radius is a variable quantity, which depends not only from the quantity of vertical load and radial stiffness of a tyre, but also from its tangent stiffness and a moment on a wheel. That is $r = f(c_x; c_z; G_k)$. Radial stiffness of a tyre depends on air pressure in a tyre and stiffness of tyre frame, and tangent stiffness of a tyre – from its tangent deformation (twist angel): $c_z = f(P_a)$, $c_x = f(\varphi_t)$. Fig. 3, 4 show graphs of tyre radius changes from vertical and tangent loads and air pressure in the tyre:

As it was shown in the article [12] static tyre radius can be defined by empirical dependence:

$$
\begin{cases}
0 \le P_x \le 0{,}2064 G_w + 195{,}9 \\
R_{\tilde{n}} = -\dfrac{1}{\tilde{N}_z} G_w + R_0 \\
P_x \ge 0{,}2064 G_w + 195{,}9 \\
R_{\tilde{n}} = \dfrac{1}{C_x} P_x - \dfrac{1}{\tilde{N}_z} G_w + R_0
\end{cases}
, \tag{7}
$$

where $R_c$ - static tyre radius; $R_0$ - free tyre radius; $P_z$ - radial load; $P_x$ - tangent load; $c_z$ - radial tyre stiffness; $c_x$ - tangent tyre stiffness.

Fig. 5 shows dependence of radial tyre stiffness ИД – 195 and Я – 288 from twisting deformation
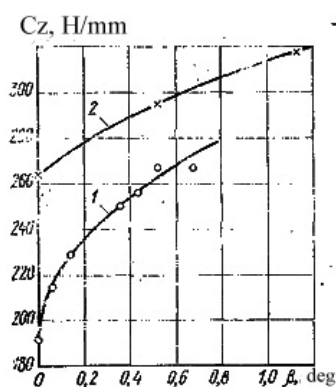


*Fig. 5. Dependence of radial stiffness of tyre ИД – 195 (1), Я – 288 (2) from twisting deformation [11]*

Fig. 6 shows dependence of tangent elasticity of a tyre ИД – 195 from twisting angle at different vertical load.

It is clear from formula 6, that angular shift of external part of a tyre relative to the wheel axis depends on relationship of its radial and tangent stiffness.

Fig. 7 shows graphic dependence of angular shift of external part of a tyre relative to the wheel axis, from time at constant angular velocity of a wheel axis and at different values of relationship of its tangent and radial stiffness, received by equation 6 with due regard for tyre radius changes tangent and vertical loads and air pressure in the tyre, according equation 7.
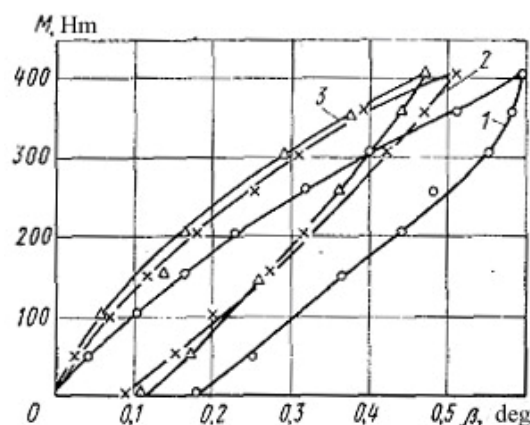
*Fig. 6. dependence of elasticity moment of a tyre ИД – 195 from twist angle at different vertical load: 1 – 2,9 kN; 2 – 3,9 kN; 3 – 4,9 kN [11]*
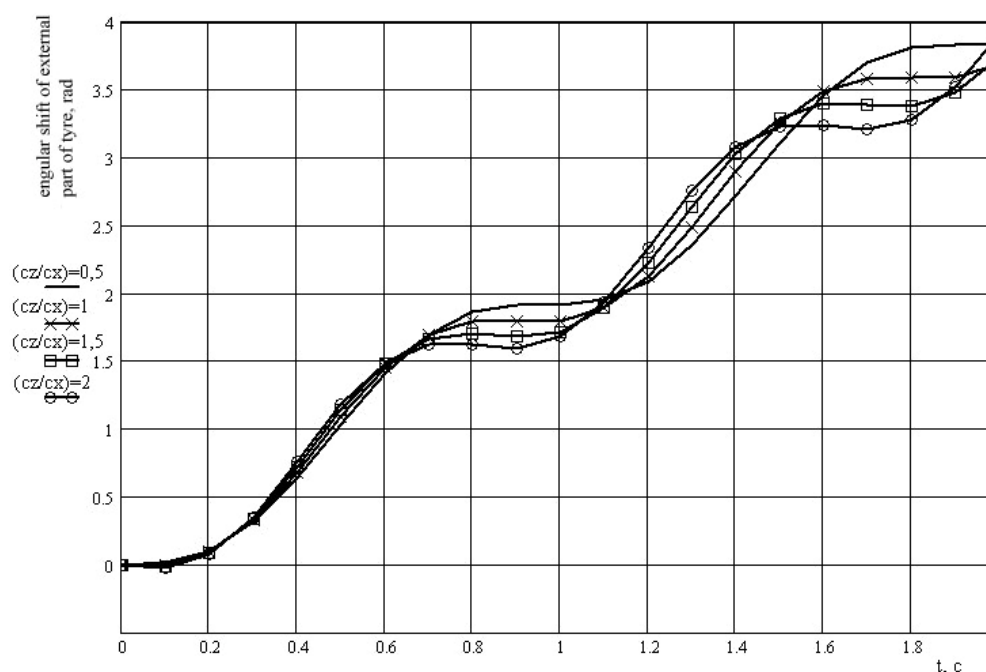


*Fig. 7. Dependence of angular shift of external part of tyre relative to the wheel axis, from time*

## CONCLUSION

1. Mathematical model, which describes the process of interaction of a single wheel with the ground (not taking into account vertical vibrations caused by cushion masses) is created.
2. Dependences of elastic properties of pneumonic tyre from vertical and tangent loads at their simultaneous operation, air pressure in the tyre, are considered.
3. The considered model allows to take into account the ground properties and their changes, and also the change of tyre elastic properties while researching the process of interaction of a wheel with deforming base surface.

## REFERENCES

1. Кошарный Н.Ф.: *Технико-эксплуатоционные свойства автомобилей высокой проходимости*. К., Вища школа, 1981, 208 с.

2. Безбородова Г.Б., Галушко В.Г.: *Моделирование движения автомобиля.* Киев: Вища школа, 1978, 163 с.

3. Агейкин Я.С.: *Вездеходные колесные и комбинированные движетели*. М.: Машиностроение, 1972, 184 с.

4. Смирнов Г.А.: *Основы теории многоприводных колесных машин: Уч. пособие*. М.: Тип. МВТУ им. Н.Э.Баумана, 1977, 73 с.

5. Чудаков Е.А.: *Избранные труды*. Т. 2. М.: Изд-во АН СССР, 1961, 343 с.

6. Сирота В.И.: *Исследование процесса буксования автомобильных шин*. Автореф. дис. канд. техн. наук. Киев, 1973, 25с.

7. Говорущенко Н.Я., Туренко А.Н.: *Системотехника транспорта (на примере автомобильного транспорта)*. Изд. 2-е перераб. и доп. Харьков: РИО ХГАДТУ, 1999, 468 с.

8. Цейтлин М.Г., Верстов В.В., Азбель Г.Г.: *Вибрационная техника в свайных и бурових работах*. Л.: Стройиздат, Ленингр. отд-ние, 1987, 262 с.

9. Фролов И.К.: *Вибрация – друг или враг?* М.: Наука. Сер. Наука и технический прогресс. 1949, 144 с.

10. Фильчаков П.Ф.: *Справочник по высшей математике*. К.: Наукова думка, 1972, 743 с.

11. Енаев А.А., Глазырин Ю.М., Шалдыкин В.П., Яценко Н.Н.: *Упругость и демпфирование шин при совместном радиальном и тангенциальном нагружении*. Автомобильная промышленность №7, 1982, с. 17 – 19.

12. Грабар І.Г., Опанасюк Є.Г., Бєгєрський Д.Б.: *Дослідження пружних властивостей пневматичної шини*. Вісник ЖДТУ, 2008, №  (44) / Технічні науки, с. 26 – 33.

**Attila HERDITZKY**
**Maria KICKOVA**

# LIFE CYCLE INCREASING OF MECHANICAL COMPONENTS USING THERMAL COATINGS WITH RECASTS

*This article concerned with proposition of friction and deterioration of functional components surfaces in adhesive deterioration area and contact endurance. It's centered for possibilities how to decrease deterioration and extend a life cycle of component choosing appropriate material, component surface adjustment, or abrasion-resistant coatings painting with expressively better properties against basic material.*

## INTRODUCTION

Heating coating represent perspective technology providing functional effective coating using at many industrial branches. This flexible, high-quality and economic technologies allows optimally adjust components surface properties to operation conditions, what leads to life cycle extension, reliability increasing and components safety.

In experiment we used alloy powder based on nickel, which are often used as powders for paint coatings with recasts. For layers making at functional surfaces, it has advantages, at first, low fusion point, good adhesive to base, surface smoothness, choice of coatings combination at various hardness and ability to get very thin layers. It's produced in wide line with various hardness.

## MATERIAL AND TREATMENT

Tested was coating given by firing spraying with follow-up recasting of powder from Výskumný ústav zváračsky (Research Welding Institute) with working mark - NP 22 P 1155 in gradation  45 μm + 5μm . Powder material up-welding was realized using equipment SUPER EUTALOY JET at VUZ (RWI) PI   Bratislava. Base material was bar material sized  d = 55, L = 150  from 11 532 steel material (Pict. 1).

Testing disc samples was produced by TU – SjF Košice, electro erosion cutting at required size, Pict. 1, surface grinded with roughness Ra= 0,2 μm.  Chemical composition of spraying powder is in Table 1.
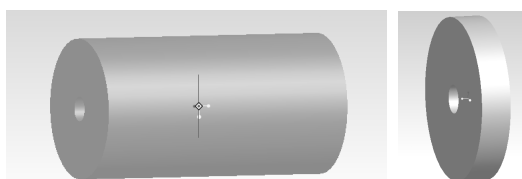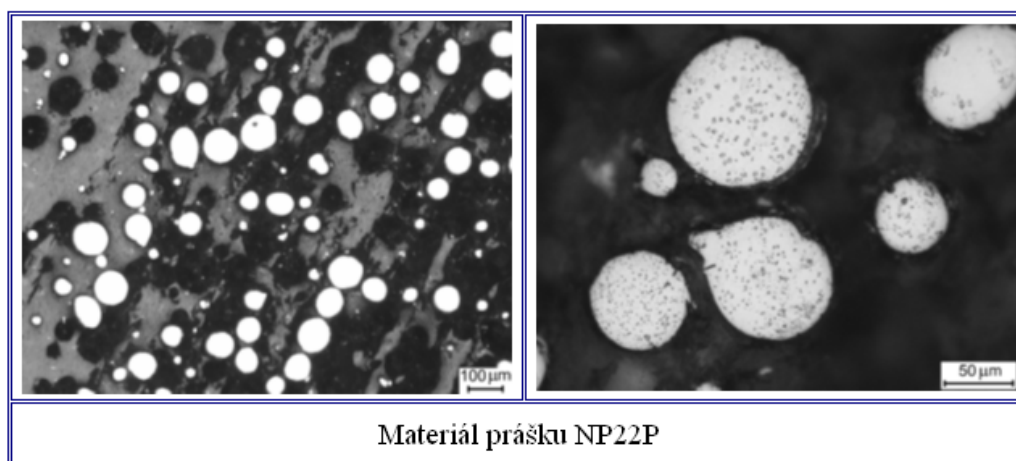


*Pict. 1. Tested sample*

*Table 1. Chemical composition of metallic powder*

| Chemical composition of metallic powder NP 22 P 11 55 | | | | | | | | | | | | | | | |
|---|---|---|---|---|---|---|---|---|---|---|---|---|---|---|---|
| C [%] | Si [%] | Mn [%] | P [%] | S [%] | Cr [%] | Mo [%] | Fe [%] | V [%] | W [%] | Cu [%] | Al [%] | Co [%] | Ti [%] | B [%] | Ni [%] |
| 0,21 | 3,52 | 0,07 | 0,06 | 0,012 | 8,85 | 1,3 | 2,63 | 0,01 | 0,02 | 0,73 | 0,004 | 0,02 | 0,01 | 1,48 | 81,08 |

Grains shape of this powder material is documented in Pict. 2. Powder grains NP22P for flame spraying has regular globular pattern.



Materiál prášku NP22P

*Pict. 2. Detailed powder grains*

Coating properties and follow-up functionality are almost resulting of interaction between surface coating, composition and powder morphology.

Prepared samples was tested in adhesive deterioration conditions for F [N] load at range of 270N, 770N and 1170N on testing equipment AMSLER, where tested sample is pressed to verge of standard rotating disc [companion part made of 14220 steel material HV 823].

Pressure is providing by pressing the spring and value of load power is generated to PC. During test it can constantly be measured friction moment conclude by pressing power, friction factor a diameter of companion part. Its size in time is recorded to PC. Friction pair is shown in Pict. 3.
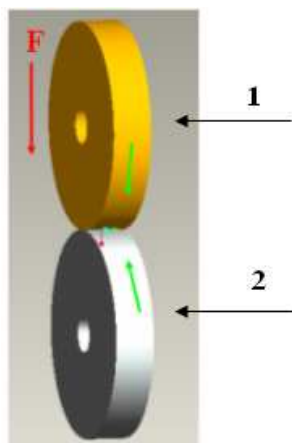


*Pict. 3. The friction pair*

**EXPERIMENTAL RESULTS AND DISCUSSION**

**Coating quality** past deterioration was judged using optical microscopy method on metallographic scratch patter structure. In the Pict. 4 are shown crossing scratch patterns of NP22P spraying with steady structure contained scattered poruses.

Hard structural components are steady spitted in nickel matrix. Coating is a good quality. Poruses can relate to insufficient grease removal surface as before coating application.
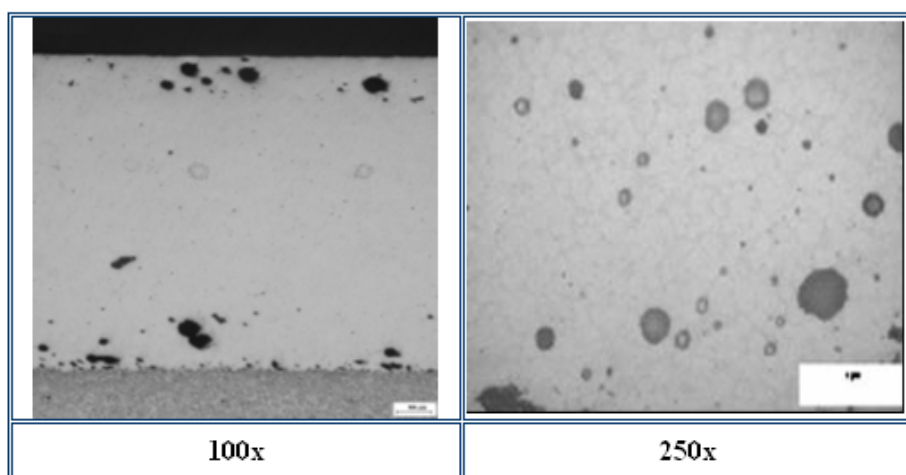


*Pict. 4. Crossing scratch of NP22P coating   /100 and 250 x/*

In the Pict. 5 is NP22P coating structure with existing poruses in layer. Phase interface layer (foundation in document photos is without existing oxides, passing from foundation to layer is continual).
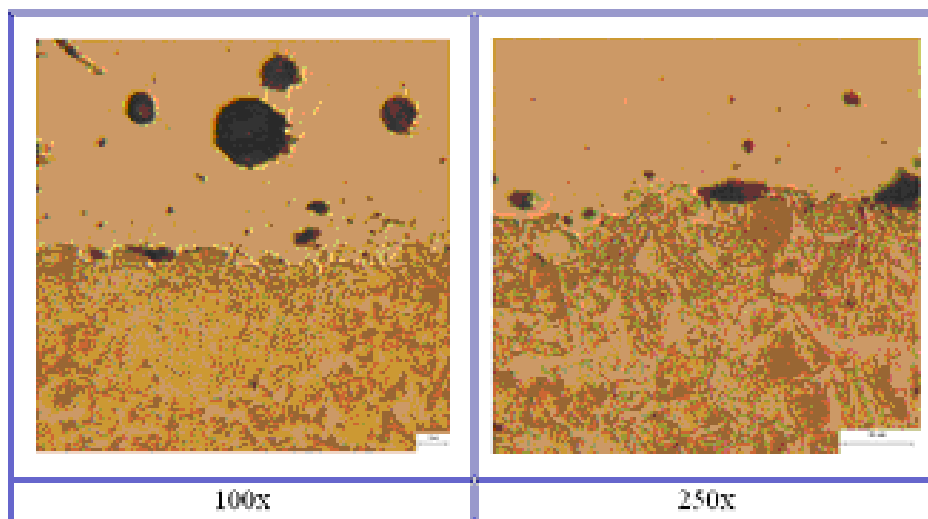


*Pict. 5. Foundation layer*

After recasting, the structure is steady with hard phase splitter in Ni matrix. Micro hardness value HV30 = 429 to 467 describes existing chrome carbides. Weldment has homogeny structure. Microstructure of coatings contains poruses and cavities, which can create the initiation of fractures and micro cracks (Pict. 6) [34].
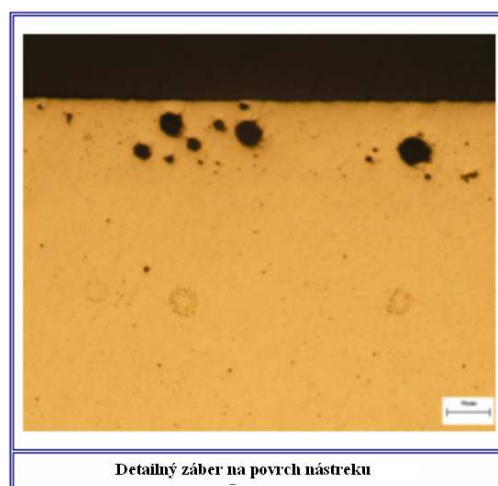
*Pict. 6. Detailed picture of spraying surface*

**Deterioration rating** was done based on weight loss. Because of this reason, we measured the weight of companion parts before and after deterioration. Results are shown in Table 2.

*Table 2. The weight of companion parts before and after deterioration*

| Sample | F[N] | $M_o$[g] | $M_1$[g] | Weight differences |
|--------|------|----------|----------|--------------------|
| N2P | 270 | 108.8164 | 108.8027 | 0.0137 |
| N1P | 770 | 109.1634 | 109.0858 | 0.0776 |
| N3P | 1170 | 108.7817 | 108.5837 | 0.1980 |

Impact of load size on weight lost was rated for required tests mode. Along was executed analyze of structure morphological changes and also triboparts studying. In Pict. 7 are shown graphical dependencies of weight lost on load at F = 270, 770 and 1170 N. Samples were tested for 24 HRS at 152 RPM. Friction track for tested samples is 33 914 m
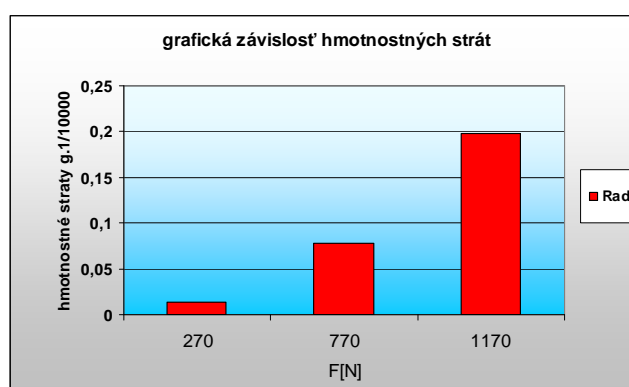


*Pict. 7. Graphical dependencies of weight lost*

As shown of Graph, samples on tests resist the deterioration very well at load of 270 – 770 N. At 1170N load, deterioration was 14 times great then at the first test on 270 N loads.

**Morphological changes analyze** of surfaces and triboparts studying was executed by stereo microscope, snapshots are shown in the Pict. 8. Firing spraying layers properties are strongly depending on spraying parameters.

On tested samples was observed, recorded and rated basic properties of coatings, as is look, relation of coating, fusion with base and so on.



N2P pri záťaži F=270N
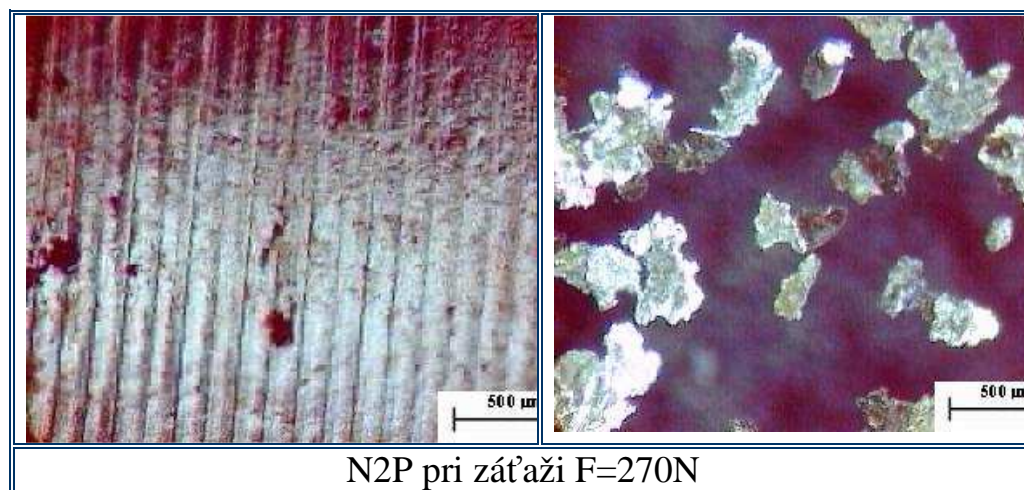
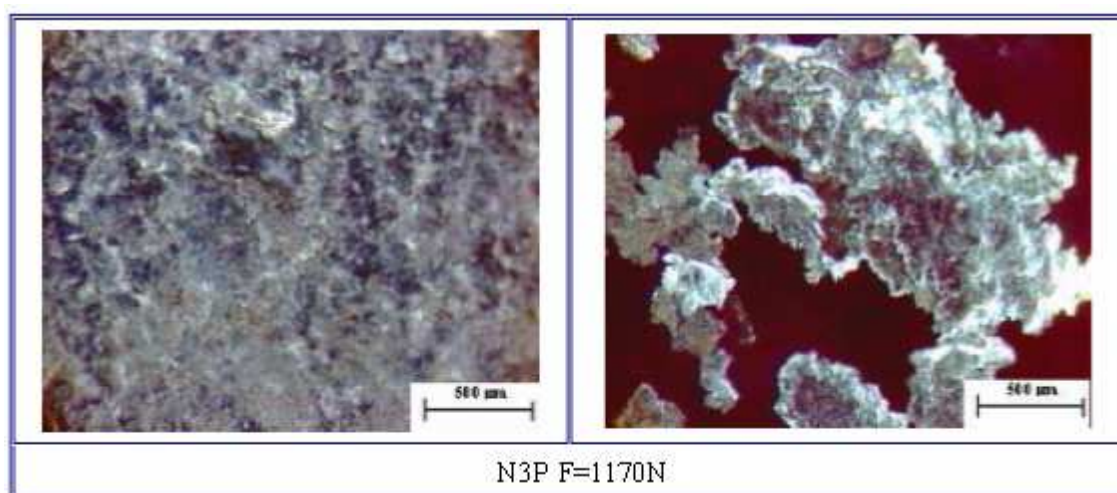*Pict. 8. Snapshot of surface and flakes while loaded of F = 270N*

At testing mode with F = 270 N load, coating shows very good resist against adhesive deterioration. Sample surface is smooth without any special roughness changes, and surface topography contains marks after grinding samples preparation. Abrasion parts seem like soft flakes, Pict. 9, and are same sized.



N1P F= 770N
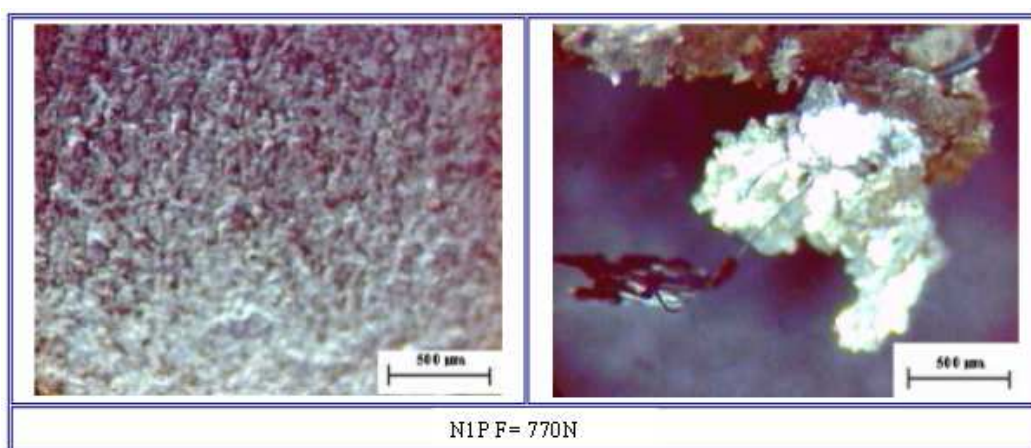
*Pict. 9. Snapshot of surface and splinter while loaded of F = 770N*

Snapshot of surface after 24 HRS test of F = 770 N load, shows soft and uniform surface roughage without any special defects. Products of deterioration have flakes character. While this load, coating still good resisted to adhesive deterioration and did not degrade. Pict. 10.

While F = 1170 N of load, surface topography is joined with intensive impact of abrasive parts in contact zone and impact to degradation of spray surface. Products of deterioration has very similar plate shape, but it's rolled up and has rugged surface, what can related to higher pressure in contact zone.

*Pict. 10. Snapshot of surface and splinter while loaded of F = 770N*

## CONCLUSIONS

Functional coating NP22P, made by spraying on the base material, is with base material joined homogeneously. Finished coating is compact, relation with base is good. Results of laboratory tests of thermal coatings NP22P deterioration are in suit with abrasive resistance tests, made on Falex tester. Consequent on tests, which surface pressure above 500 MPa for status coatings, is almost high in tested grinding system in dry grinding condition.

Thermal flame sprays NP22P based on nickel has generally good abrasive resistance – adhesive deterioration, which is increasing together with growing hardness of coatings and are using in the case, where is not possible to make safe greasing and where a greasing is disallowed. Considering the practical and economical aspects, application of these coatings is very important.

## REFERENCES

1. Smetana Š., Jančo V.: *Žiarové nástreky ako spôsoby tvorby povrchových vrstiev v oblasti strojárstva*. In: Kvalita v zváraní. Tatranaská Štrba 2006, pp.152 -158.

2. *Dielčia správa COST 532-M8*, 2005 pp.20

3. Zdravecká E., Żórawski W., Chomjaková I.: *Selected tribological properties of thermally sprayed HVOF coatings and the visualization of surfaces changes*. In: Acta Mechanica Slovaca. PROTECH-MA, roč. 8, Košice, 2-B/2004, s. 477-484, ISSN 1335 – 2393

4. Matejka D., Benko B.: *Plazmové striekanie kovových a keramických práškov*. Alfa, Bratislava 1988

**Sergej HLOCH**
**Jan VALÍČEK***
**Katarína MONKOVÁ**

Technical university of Košice with a seat in Prešov, Slovak Republic
*Institute of physics, VŠB TU – Ostrava, Czech Republic

# EXPERIMENTAL ANALYSIS OF AISI 304 SURFACE IRREGULARITIES CREATED BY ABRASIVE WATERJET BY MEANS OF 3D OPTICAL MEASUREMENT

*The paper deals with experimental analysis of AISI surface irregularities created by abrasive waterjet by means of 3D optical measurement. The surface irregularities has been evaluated by static quality characteristics the arithmetic average height Ra, root mean square roughness Rq and peak to valley height Rz that has been obtained from 24 measurement traces. The surface irregularities have been measured by means of contactless optical method, namely by using an optical commercial profilometer MicroProf (FRT). The main emphasis is put on the analysis of results for defining the process of creation of a new surface generated by the stream of abrasive waterjet, including its geometric parameters and mechanisms of cutting tool-material interaction.*

## INTRODUCTION

At present, more than 50,000 constructional materials are known. This number tends to increase rapidly. Most new materials are "man made" and designed by material scientists to obtain specified properties. Manufacturers are being confronted with the need to adapt existing technologies or to develop new technologies for the specific behaviour of these new materials 16. Because of its characteristics, abrasive waterjet (AWJ) fits this trend extremely well. The flexibility and cool cutting characteristics of AWJ makes it an effective tool for machining new materials such as composites and sandwiched materials that present special machining problems where the materials with special properties are used.  One of these materials is stainless steel. The aim of this study is to experimentally investigate the surface irregularities created by abrasive waterjet by means of 3D optical measurement.

## RELATED AND PREVIOUS WORKS

Surface irregularities in the form of striations and roughness have been ongoing problems associated with (AWJ) cutting of engineering materials. The causes of these surface defects that put multifaceted limitations on the wider use of the AWJ technology in industry have been the subject of a large number of investigations [1-3]. A

number of mechanisms that are thought to cause these observed striations and rough-ness on the cut-wall surfaces have been proposed by various authors who conducted studies in this area [4, 5]. In AWJ machining, the workpiece material is removed by the action of high-speed water mixed with abrasive particles. A high-speed waterjet transfers kinetic energy to the abrasive particles and the mixture impinges on to the workpiece [6, 7, 10, 11]. The material removal rate is dependent on the abrasive attack and mechanical properties of target metal. The AWJ machining process is defined by a number of parameters, which in turn govern the material removal rate and the devel-opment of the characteristics of the surface. A considerable effort was made in under-standing the influence of the system operational process parameters such as waterjet pressure, abrasive flow rate, standoff distance, number of passes on depth of cut, angle of cutting, and traverse speed [5, 11, 13]. The results of the studies showed that the AWJ machining is significantly affected by the variation of process parameters. How-ever, the degree of influence of parameters depends on the magnitude of parametric variation and machine ability of the material (Fig. 1). Traverse speed of the jet has a strong influence on the surface finish of the workpiece and material removal rate [15, 16].
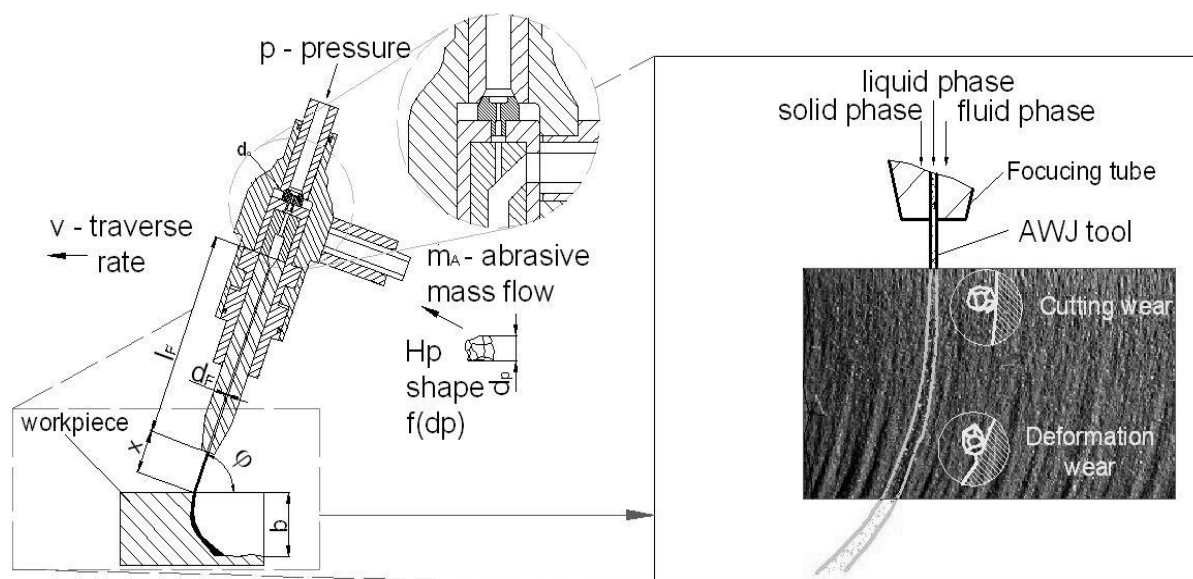


*Fig. 1. Cause of the surface irregularities at abrasive waterjet cutting.  p – pressure [MPa], $d_0$ – dia-mond orifice diameter [mm], $m_A$ – abrasive mass flow rate [g.min$^{-1}$], $d_p$ – abrasive particle diameter [mm], $H_p$ – abrasive hardness, $d_f$ – focusing tube diameter [mm], v – traverse speed [mm.min$^{-1}$], z – standoff [mm], φ – angle attack [°], δ – angle deviation [°], $Y_{ret}$ – retardation of cutting front, Ra, Rq, Rz – surface profile parameters [μm]*

According to Ojmertz [15] has shown that low traverse speeds result in an irregular surface morphology and significantly increased material removal rates but despite this, lower surface roughness values are observed. Fowler et al. [15] have shown that low jet traverse speed not only results in high material removal rates, but also in high sur-face waviness. But according to published research papers, there is necessary to take into account more factors together or hydro-mechanical cutting process depends on a large number of process factors such as water pressure, orifice diameter, standoff dis-tance, abrasive and material feed rate etc. [16].

## EXPERIMENTAL PROCEDURE

A two dimensional abrasive waterjet machine Wating, was used in this work with following specification: work table x-axis 2000 mm, y-axis 3000 mm. The high-pressure intensifier pump was used the Ingersoll-Rand Streamline model with maximum pressure 380 MPa. As a cutting an Autoline cutting head from Ingersoll-Rand head has been used. Standoff distance z = 3 mm. Variable factors have been pressure p = 200 - 350 MPa, orifice diameter $d_o$ = 0.25 mm, abrasive mass flow rate $m_A$ = 300 - 500 g.min$^{-1}$, focusing tube diameter $d_f$ = 1 – 1,2 mm, and traverse speed v = 70 – 120 mm.min$^{-1}$. Specimens have been made from following material AISI 304. Cut surfaces of the square samples were prepared according to design of experiments. The properties of each sample are: the length of 20 mm, the width of 20 mm, and the height of 8 mm. The Barton Garnet was used as abrasive materials with MESH 80. From each abrasive material 10 samples were cut to be analysed. The surface quality of each side of the samples was measured by an optical method using an optical commercial profilometer MicroProf (FRT). From 24 depth traces have been obtained the surface profile parameters Ra, Rq and Rz (Fig.2)
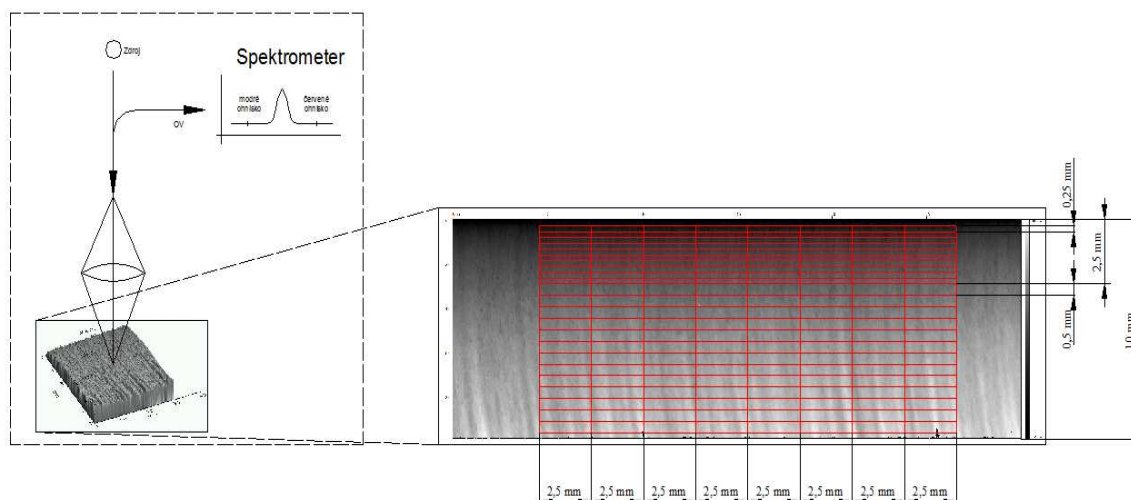


*Fig. 2. Depth traces, where have been obtained the surface profile parameters Ra, Rq and Rz*

## RESULST AND DISCUSSION

On the contrary, results obtained by an optical profilometer MicroProf (FRT) show that more detailed information on the initiation zone can be provided. From the mechanical point of view, this entry region is of importance to the subsequent clarification of a mechanism of material removal and the explanation of AWJ-material interaction in this initiation zone (Fig. 3a,b). From the practical point of view, it is then necessary to talk on impacts on the quality of output control of products machined. In our opinion, in the mechanism of origin of newly generated surface topography, the initiation zone cannot be ignored. This is the first contact with a disintegration tool, which is here a high-energy jet of the mixture of water, air and abrasive. In terms of description of AWJ spread and degradation, it is possible to observe some phenomena (Figs. 3a,b) i.e. the initiation zone with a steep increase in Ra, Rq and Rz values. Then, after exceeding the modulus of elasticity and overcoming the total resistance of material in the initiation zone, there is a sharp drop in Ra, Rq and Rz values.
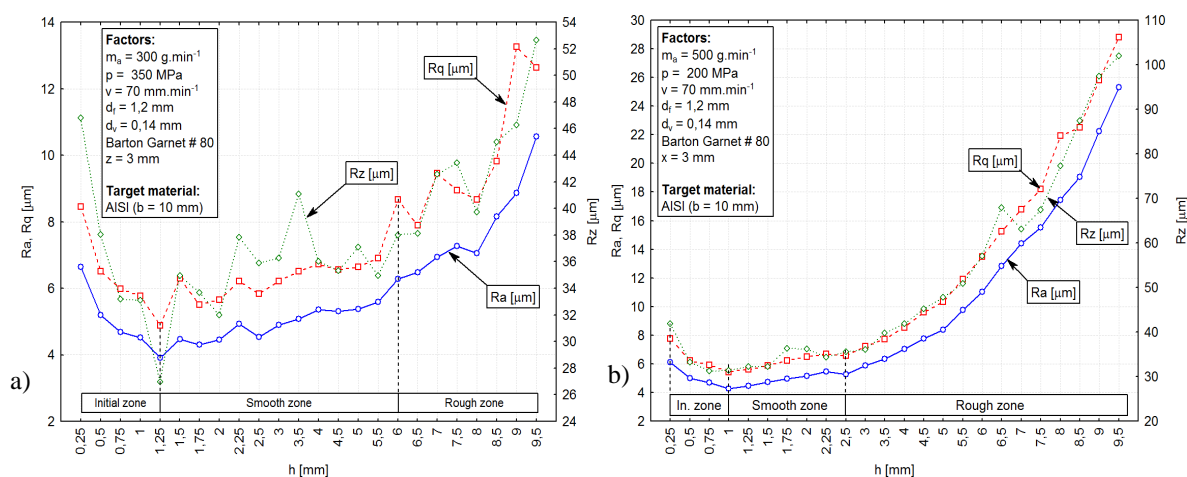
*Fig. 3. Experimental plot of surface of profile parameters Ra, Rq and Rz, related to depth obtained from 24 measured traces from surfaces created by AWJ different experimental condition*

This phenomenon is related to the fact that a removed material from the sidewalls entered the jet when passing through the entry part of material; an abrupt oversaturation took place and also a contrast division of jet structure into the inner core and the external envelope with a high concentration of abrasive grains lagging behind the inner core. In the external envelope, the kinetic component of hydraulic energy transforms quickly to the potential one similarly to the case of hydraulic water shock. By the potential energy excess, a deeper groove having, however, a rather smooth trace will be formed, to which the optical device will respond by a decrease due to a low Ra, Rq and Rz value. The initiation zone is characterised by losses of energy of the jet due to collaring the material, overcoming the elastic limit of material and energy stabilisation of hydraulic and hydrodynamic conditions of the cut, further the zone with a high proportion of strain energy in the creation of so-called smooth and transition zones and a zone with a lower proportion, or shortage of strain energy, which corresponds to the deformation zone. What is a specific of surfaces generated by means of AWJ is the fact that they are rough. Thus they may be regarded as surfaces produced by various classical technologies, such as collaring into the material in the initiation zone, grinding (high-energy area-zone) and machining in the medium part of the cut, across the area of rather rough turning, planning and rough dressing at the end of the cut.

**CONCLUSIONS**

The main task of the paper was to bring the detailed knowledge about the interaction of abrasive waterjet with cutting material. In order to describe the basic geometrical properties of topography of surfaces produced by the AWJ technology, an optical commercial profilometer MicroProf (FRT) has been used. On the basis of optical measurements the values of Ra, Rq and Rz roughness in relation to the depth of cut h, have been evaluated. It has been proved the existence of initial zone. Further the surface profile parameter will be statistically and analytically processed for optimising the technology, improving the quality of output control and studying the mechanism of disintegration interaction between the high-speed abrasive waterjet and the material machined.

## REFERENCES

1. Bátora B., Vasilko K.: *Machined surfaces: technological heredity, functionality*. Trenčín, 2000, pp. 183.

2. Cebalo R., Stoić A.: *Optimisation of the roughness of the ground surface by diamond roller dressing*. Tehnički vjesnik 3, 4, 2003, pp. 3-8.

3. Fabianová J.: *Význam skúmania vplyvu rezných parametrov pri rezaní vodným lúčom*. In: Výrobné inžinierstvo. roč. 6, č. 2, 2007, s. 53-55. ISSN 1335-7972.

4. Gombár M.: *Statistical model of surface roughness*. In: Electrotechnics in practise. 2006, vol. 16, no. 11-12, pp. 26-28.

5. Hloch S., Gombár M., Fabian S., Straka L.: *Factor analysis of abrasive waterjet process factors influencing the cast aluminum surface roughness*. In: Manufacturing Science  and Technology. Malaysia, 2006, pp. 145–149.

6. Kozak D., Vojvodica J., Gubeljak N., Semenski D.: *Factors influencing the yielding constraint by cracked welded components*. Program and book of abstracts of 12th Conference on Materials and Technology / Jenko, Monika, editor(s). Ljubljana: Institut za kovinske materiale in tehnologije, 2004. Pp. 79-79

7. Kušnerová M., Hlaváč L. M.: *Self vibrating chambers with continuous passage of liquid*. Sborník vědeckých prací VŠB - TUO. Řada strojní č. 1/2006, roč. LII. VŠB-TUO, Ostrava, 2006, s. 127- 134. ISSN 1210-0471.

8. Ohlídal M., Páleníková K.: *Možnosti optického profilometru MicroProf FRT při 3D hodnocení kvality povrchu*. Jemná mechanika a optika, Vol.49, (2004), No.9, pp.251-255, ISSN 0447-6411

9. Páleníková K., Ohlídal M.: *Potentialities of optical profilometer MicroProf FRT for surface quality measurement*. 14 th Slovak-Czech Polish Conference on Wave and Quantum Aspects of Contemporary Optics, pp.59451O-1-59456, ISBN 0-8194-5951-8, (2005), SPIE - The international-Society for Optical Engineering.

10. Stoić A., Lucić M., Kopač J.: *Evaluation of the Stability During Hard Turning*. Strojniški vestnik 52, 11, 2006, pp. 723-737.

11. Stoic A., Samardzic I., Klaric S.: *Cutting errors in abrasive water jet cutting*. CIM 2007 Computer Integrated Manufacturing and High Speed Machining / Aberle, Eberhard ; Udiljak, Toma ; Ciglar, Damir, editor(s). Zagreb : Croatian Association of Production Engineering, 2007. pp. 333-338

12. Valíček J., Držík M., Ohlídal M., Mádr V., Hlaváč L., M.: *Optical method for surface analyses and their utilization for abrasive liquid jet automation*. In: Proc. of the 2001 WJTA American Waterjet Conference, M. Hashish (ed.), WJTA, Minneapolis, Minnesota, pp. 1–11, 2001.

13. Valíček J., Hloch S.: *Surface topography optical identification generated by abrasive waterjet*. In: Fine Mechanics and Optics. vol. 51, no. 11-12, 2006, pp. 320-322.

14. Vasilko K., Lipták J., Kozáková D., Modrák V.: *New materials and technologies of their machining*. Alfa, 1990, pp-365.

15. Hascalik A., Caydas U., Gurun H.: *Effect of traverse speed on abrasive waterjet machining of Ti–6Al–4V alloy*. In. Materials & Design, Volume 28, Issue 6, 2007, pp. 1953-1957.

16. Kulekci, K., M. *Processes and apparatus developments in industrial waterjet applications*. International Journal of Machine Tools & Manufacture 42 (2002) 1297–1306.

**Andrey V. ILCHENKO**
**Elena V. ZABASHTA**
**Vladimir A. LOMAKIN**

Zhitomir State Technological University, Ukraine

# CHANGE OF THE MOMENT OF INERTIA OF V-TYPE CRANK-CONNECTING ROD MECHANISM OF INTERNAL COMBUSTION ENGINE

*Mathematical model of change of equivalent moment of inertia of V-type crank-connecting rod mechanism of piston internal combustion engines from the angle of swing of crankshaft is proposed. All wide-spread schemes of V-type crank-connecting rod mechanisms are analyzed, and adequacy of the given models in КОМПАС-3D V8 system is checked.*

## ANALYSIS OF THE PROCESS OF CHANGE OF EQUIVALENT MOMENT OF INERTIA OF V-TYPE CRANK-CONNECTING ROD MECHANISM OF PISTON INTERNAL COMBUSTION ENGINE. RAISING THE TASK OF RESEARCH

It is common when designing internal combustion engines (ICE) to consider the equivalent moment of inertia (EMI) of crank-connecting rod mechanism (C-CRM) to be constant [1-5]. It is known, that while increasing the mass and dimensions of C-CRM elements the EMI will also increase. This also influences the torque of ICE. It is necessary to measure the torque of ICE, and this is done with the help of different techniques.

Mathematical model of the process of change of EMI of C-CRM for monocylinder and multicylinder piston ICE was considered in robots [6-9]. Dependence of EMI of central C-CRM of monocylinder ICE, which has one crank of $R$ radius without counterweights, and also connecting rod and piston group, from its mass-geometric parameters (MGP) (ie: density mass of connecting rod $m_{ш}$, density mass of piston group $m_{n}$, density mass of one crank $m_{к}$, ratio of crank radius to the connecting rod length $\lambda$, relative distance from axis of piston pin to the centre of mass (CM) of connecting rod $x$, relative distance from crankshaft axis to the centre of mass of connecting rod without counterweights $k$, length of connecting rod $L$, piston diameter $D_n$, crank radius $R$, central moment of inertia (CMI) of connecting rod $I_{ш}$, CMI of crank $I_к$ and CMI of piston group $I_n$) was determined, $kg \cdot m^2$:

$$I = A\cos^2\varphi + B\cos\varphi + C + I_{ш} + I_{n} + I_{к}, \qquad (1)$$

where   $A = 1{,}58 D_n{}^2 R^2 \left( m_n + m_w (1 - 2\frac{x_L}{L}) \right)$,      $B = 1{,}57 D_n{}^2 R \left( L(m_n + m_w) - m_w x_L \right)$,

$$C = 0{,}79 D_n{}^2 \left( \begin{array}{l} L^2(m_n + m_w) - R^2(m_n + m_w - 2\frac{x_L}{L} - k^2 m_\kappa) \\ + m_w x_L (x_L - 2L) \end{array} \right).$$

To make analysis and comparison of different C-CRM more convenient it was proposed in [6] to estimate the change of EMI of C-CRM for the period, using coefficient of change of EMI of C-CRM of ICE:

$$\delta_I = \frac{I_{\max} - I_{\min}}{I_{cp}}, \tag{2}$$

where $I_{\max}$ – maximum EMI of C-CRM, $kg \bullet m^2$; $I_{\min}$ – minimum EMI of C-CRM, $kg \bullet m^2$; $I_{cp}$ – medium EMI of C-CRM for the period of its change, $kg \bullet m^2$.

In [7] was proposed approach for choice MGP C-CRM ICE, which provides the minimum of coefficient of change of EMI of C-CRM of ICE

In work [8] the change of EMI of C-CRM of most wide-spread in-line piston ICE was considered. It was also proposed to estimate the period of its change according to formula:

$$T = \frac{360°}{k} \tag{3}$$

where $k$ – the quantity of noncoinciding half-planes, which are formed by the axis of rotation of crankshaft and by any point which is on the axis of crankpin, pcs.

It was determined that coefficient of change of equivalent EMI of C-CRM for in-line piston engines takes the following meanings (for taken MGP [9]): one- and two-cylinder C-CRM of ICE with the angle between cranks 360° – $\delta_I$ =0,958, four- and two-cylinder C-CRM of ICE with the angle between cranks 180° – $\delta_I$ =0,138, five-cylinder C-CRM of ICE – $\delta_I$ =5,31•10$^{-5}$, six-cylinder – $\delta_I$ =0,01, eight-cylinder – $\delta_I$ =0. Adequacy of mathematical model (1) of the four-cylinder in-line ICE with the help of КОМПАС-3D V8 system was checked. It was determined that maximum relative error of mathematical model [9] relatively to data of КОМПАС-3D V8 system for a revolution of crankshaft constitutes 1,02 %, and a coefficient of change of EMI of C-CRM with a flywheel $\delta_I$ =0,075.

Since inconstancy of EMI for a revolution of crankshaft influences torque of ICE, the task of the given research is the determination of quantities and periods of change of EMI of C-CRM of V-type ICE relatively the axis of crankshaft depending on turning angle.

**SUMMARY OF THE BASIC MATERIAL**

Different schemes of C-CRM of multi-cylinder piston ICE [1, 2] are known, that is: single-row, V-type, opposite, W-type, H-type, triangular, star-type etc. [11].

In order to use mathematical model (1) to schemes of V-type ICE, it is necessary to find the sum of EMI of C-CRM of each cylinder depending on turning angle of crankshaft.

To find EMI of V-type ICE use the scheme (figure. 1), which is analyzed as two in-line C-CRM with included angle of cylinders $\gamma$.
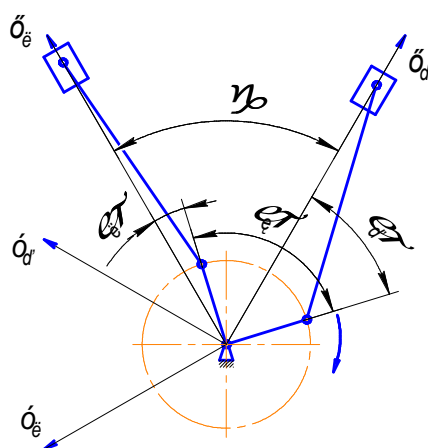


*Fig. 1. The scheme of determination of EMI of C-CRM of V-type ICE*

It is clear from figure 1, that to find the total EMI of all cylinders it is necessary to know relation between turning angles of cranks of the right and left rows of cylinders,

$$\varphi_{\pi} = \gamma + \varphi_{\pi} - \varphi_{\kappa}, \tag{4}$$

where $\varphi_{\pi}$ - turning angle of cranks of left row cylinders at turning of right row cranks to $\varphi_{\pi}$, °; $\varphi_{\kappa}$ - angle between cranks, °; $\gamma$ - included angle of cylinders, °.

In order to compare different schemes of V-type C-CRM with the help of coefficient of change of EMI of C-CRM of ICE $\delta_I$, let's take analogous MGP of C-CRM of ICE [9].

The initial turning angle of crankshaft is angle $\varphi_{\pi} = 0°$, when the piston of the first cylinder is in top dead centre.

*Four-cylinder V-type engine with the angle 90° between the rows of cylinders and angle 90° between cranks* [1, 2]. Taking into account (4) the law of change of EMI will be the sum of laws of change of EMI of C-CRM of cranks of cylinders 1, 4 and EMI of C-CRM of cranks of cylinders 2, 3, shifted to 180° (fig. 2), *kg·m²:*

$$I = 4\left(A\cos^2\varphi + C + I_{uu} + I_n + I_{\kappa}\right) \tag{5}$$

In this case coefficient of change of EMI of C-CRM of ICE $\delta_I$:

$$\delta_I = \cfrac{A}{\cfrac{\sum\limits_{i=0}^{j}\left(A\cos^2\varphi_i\right)}{j} + C + I_{uu} + I_n + I_{\kappa}} \tag{6}$$

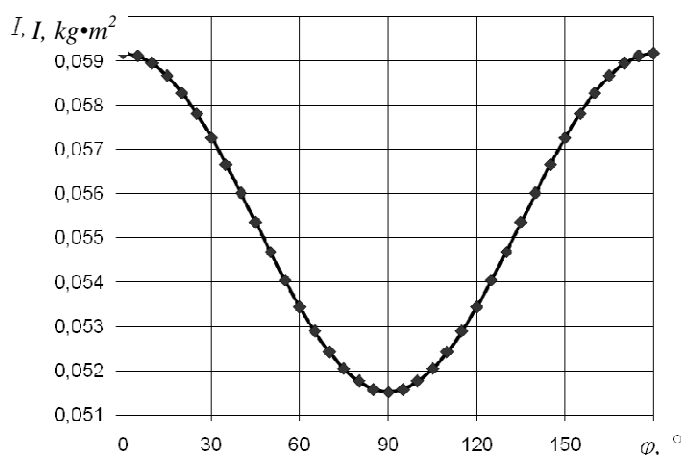where *j* – quantity of meanings of turning angle of crankshaft for the period of change.

*Fig. 2. Change of EMI of C-CRM of V-type four-cylinders ICE (included angle of cylinders -90° angle between the cranks-90°)*

For values of MGP of C-CRM of ICE [3] without flywheel the coefficient of change of EMI of C-CRM four-cylinder V-type ICE constitutes $\delta_I = 0,138$.

It is clear from fig. 2 that the law of change of EMI and coefficient of change of EMI of C-CRM of ICE $\delta_I$ for four-cylinder V-type C-CRM of ICE coincides with the law and quantity of coefficient of change of EMI of C-CRM of ICE and the period of change for in-line four-cylinder ICE with the angle 180° between the cranks [9].

*Six-cylinder V-type engine with the angle 90° between the rows of cylinders and the angle 120° between the cranks* [1, 2]. For it the law of change of EMI is the sum of laws of change of EMI of cranks of the right row of the fifth cylinder, the forth cylinder shifted to -120°, the sixth cylinder shifted to +120°, and the left row of the second cylinder shifted to -30°, the first cylinder shifted to -150°, and the third cylinder shifted to +90°. After transformation, taking into account (4),the total EMI, *kg·m²:*

$$I = 3\left(A + 2\left(C + I_{\phi} + I_{i} + I_{\hat{e}}\right)\right), \tag{7}$$

Analysis shows that in this case EMI is constant, coefficient of change of EMI of C-CRM of ICE is $\delta_I = 0$. But according to [7], coefficient of change of EMI of C-CRM of ICE is $\delta_I = 0,0071$. The period of change of EMI, which is 120°.

*Six-cylinder V-type engine with an angle 60° between the rows of cylinders and the angle 60° between the cranks* [1, 2]. For C-CRM of such ICE the law of change of EMI is the sum of cranks EMI of the right row the 4-th cylinder, the 6-th cylinder shifted to +120°, 5-th cylinder shifted to -120°, and the left row of the 1-st cylinder, the 2-nd cylinder shifted to -120° and 3-d cylinder shifted to +120°. The total EMI of the given C-CRM is calculated as in the previous case according to (7).

According to [7] the period of change of EMI is 120° and so, the coefficient of change of EMI of C-CRM of ICE is $\delta_I = 0,01$.

*Eight-cylinder V-type engine with the angle 90° between the cylinder rows and the angle 90° between the cranks* [1, 2]. The law of change of EMI is the sum of laws of change of cranks EMI of the right row of the 6-th cylinder, the 5-th cylinder shifted to -90°, 8-th cylinder shifted to +90°, 7-th cylinder shifted to +180°, and the left row of the 1-st cylinder, the 2-nd cylinder shifted to +90°, the 4-th cylinder shifted to +180°

and the 3-d cylinder shifted to -90°. The total EMI for the given C-CRM will be, k$g \cdot m^2$:

$$I = 4\left(A + 2\left(C + I_{\emptyset} + I_{ï} + I_{ê}\right)\right), \tag{8}$$

For the given scheme of C-CRM EMI is constant, the coefficient of change of EMI of C-CRM of ICE is $\delta_I = 0$.

*Twelve-cylinder V-type engine with the angle 60° between the cylinder rows and the angle 120°* between the cranks (table. 1). In this case the law of change of EMI is the sum of laws of change of cranks EMI of the right row of the 9-th and 10-th cylinders, the 7-th and the 12-th cylinders shifted to -120°, 8-th and the 11-th cylinders shifted to +120°, and the left row of the 1-st and 6-th cylinders shifted to -60°, 3-d and the 4-th cylinders shifted to +60°, 2-d and the 5-th cylinders shifted to -180°. After mathematical transformation the total EMI, $kg \cdot m^2$:

$$I = 6\left(A + 2\left(C + I_{\emptyset} + I_{ï} + I_{ê}\right)\right) \tag{9}$$

In this case EMI is also constant, the coefficient of change of EMI of C-CRM of ICE is $\delta_I = 0$.
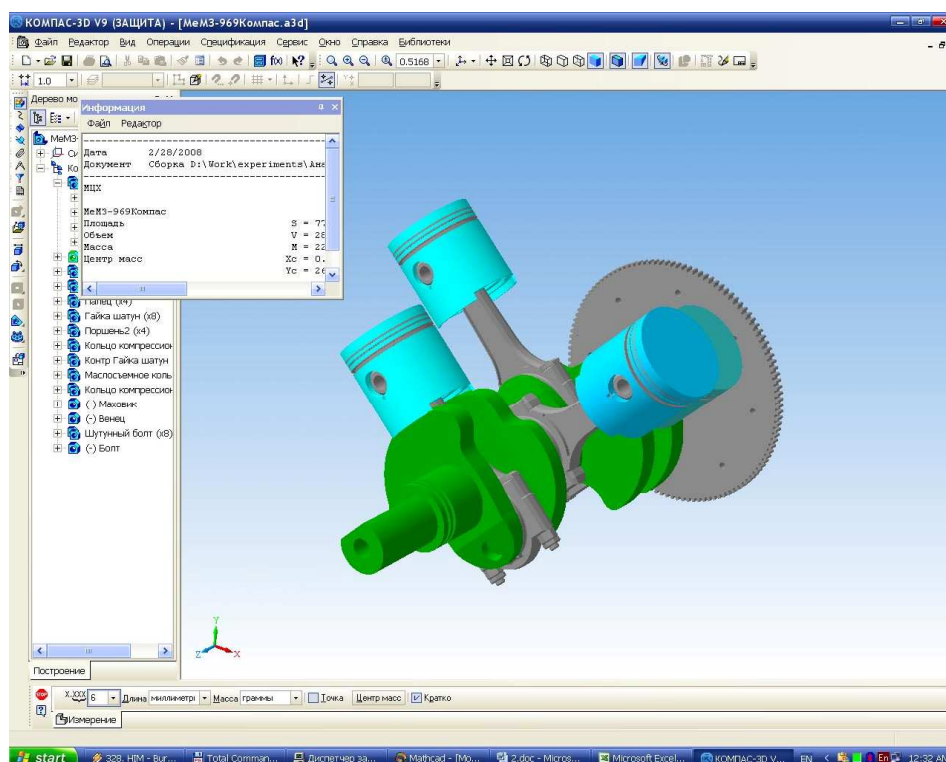


*Fig. 3. The research of EMI of C-CRM of MeM3-969A from the turning angle of crankshaft in the КОМПАС-3D V8 system*

For checking of mathematical model (5) of EMI change of multicylinder V-type piston ICE the three-dimensional computer model of C-CRM of 4-cylinder ICE MeM3-969A in the system КОМПАС-3D V8 [12] (fig. 3) with parameters , which the
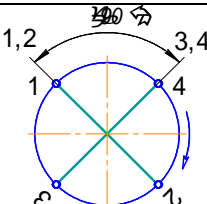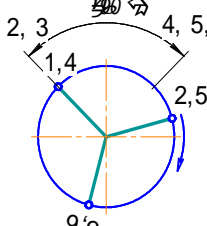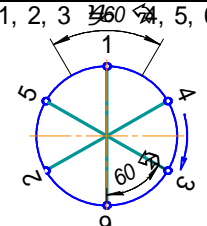
plant-producer specifies was created. The crank radius is *R=33 mm*, specific mass of connecting rod is $m_{uu}$= *154,747 kg/m²*, specific mass of piston is $m_n$=*111,724 kg/m²*, relation of the crank radius to the connecting rod length is *λ=0,232*, relative distance from the axis of finger to centre of mass of the connecting rod is *x=0,787*, relative distance from the axis of crankshaft to its centre of mass is *k=0,059*, the piston diameter is $D_n$=*76 mm*, moment of inertia relatively to the axis, which goes through centre of mass of the connecting rod is $I_{uu}$=*2,4·10⁻³ kg·m²*, moment of inertia of the piston group is $I_n$=*4,61·10⁻⁴ кg·m²* and moment of inertia of the crankshaft with the flywheel is $I_к$=*0,036 kg·m²*.

Having analyzed the data of computer experiment and developed mathematical model (5), taking into account that centre of mass of the piston group lies *8,62 mm* higher then the axis of a piston finger, it was considered that the maximum relative error of EMI change at turning angle of a crankshaft is 1,23%, and a coefficient of change of EMI of the given C-CRM is $\delta_I$ =0,061.
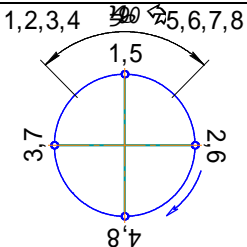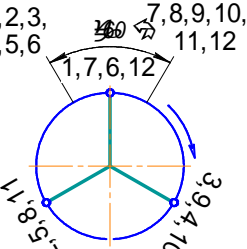
It is clear from fig.1 and (7, 8), that the period of EMI change of V-type C-CRM of ICE can be defined with the help of (3), using it relative to one row of cylinders as for in-line ICE.

The results of the research are shown in Table 1.

*Table 1. The EMI change of C-CRM of V-type ICE*

| The quantity of cylinders | The scheme of cranks arrangement | The formula for definition of the period of EMI change, °. | The period of change of EMI, °. | The formula for the definition of coefficient of EMI change | The size of EMI of C-CRM, $\delta_I$ |
|---|---|---|---|---|---|
| 4 |  | $T = \dfrac{360^\circ}{2}$ | 180 | $\delta_I = \dfrac{A}{\dfrac{\sum\limits_{i=0}^{j}\left(A\cos^2\varphi_i\right)}{j} + C + I_{uu} + I_n + I_к}$ | 0,138 |
| 6 |  | $T = \dfrac{360^\circ}{3}$ | 120 | – | 0,0071 |
| 6 |  | $T = \dfrac{360^\circ}{3}$ | 120 | – | 0,01 |

*Continuation of Table 1.*

| | | | | | |
|---|---|---|---|---|---|
| 8 | 1,2,3,4 ... 5,6,7,8 / 1,5 / 3,7 / 2,6 / 8,4 | – | – | – | 0 |
| 12 | 1,2,3,4,5,6 ... 7,8,9,10,11,12 / 1,7,6,12 / 2,5,8,11 / 3,9,4,10 | – | – | – | 0 |

Note: values $\delta_I$ are calculated for the following MGP of C-CRM (not taking into account the flywheel): radius of the crank is $R = 40$ mm, specific mass of connecting rod is $m_{ш} = 176,1$ kg/m$^2$, specific mass of piston is $m_n = 111$ kg/m$^2$, specific mass of one crank of the crankshaft without counterweights is $m_к = 184,1$ kg/m$^2$, the relation of the crank radius to the connecting rod length is $\lambda = 0,286$, the relative distance from the axis of the piston finger to centre of mass of the connecting rod is $x = 0,75$, the relative distance from the axis of crankshaft to centre of mass of the crank without counterweights is $k = 0,59$, the piston diameter is $D_n = 70$ mm, moment of inertia relatively to the axis, which goes through its centre of mass of the connecting rod is $I_{ш} = 2,75 \cdot 10^{-3}$ kg·m$^2$, moment of inertia of the piston group is $I_n = 2,55 \cdot 10^{-4}$ кg·m$^2$ and moment of inertia of the crank without counterweights is $I_к = I_к = 4,39 \cdot 10^{-4}$ kg·m$^2$.

## CONCLUSIONS

1. All wide spread schemes of V-type crank-connecting rod mechanisms of internal combustion engines from the point of view of change of equivalent moment of inertia of crank-connecting rod mechanism are analyzed. It is considered that to determine the engine torque it is necessary to take into account the inconstancy of moment of inertia of the given engines from the turning angle of the crankshaft, which is actual for the internal combustion engines with V-type crank-connecting rod mechanisms and the quantity of cylinders up to 4 inclusive.

2. It is determined that the coefficient of change of equivalent moment of inertia of crank-connecting rod mechanism for V-type piston engines (at accepted mass-geometric parameters) changes: Four-cylinder with the angle 90° between the rows of cylinders and the angle 90° between   cranks – $\delta_I$ =0,138, six-cylinder with the angle 90° between the rows of cylinders and the angle 120° between the cranks – $\delta_I$ =0,0071, six-cylinder with the angle 60° between the rows of cylinders and the angle 60° between the cranks – $\delta_I$ =0,01, eight-cylinder engine with the angle 90° between the cylinder rows and the angle 90° between the cranks, twelve-cylinder engine with the angle 60° between the cylinder rows and the angle 120° between the cranks – $\delta_I$ =0.

3. Adequacy of the developed mathematical model of determination of moment of inertia after the example of V-type engine МеМЗ-969А with the help of КОМПАС-3D V8 system was checked. It was considered that the maximum relative error of equivalent moment of inertia change at turning angle of a crankshaft is 1,23%, and a coefficient of change of equivalent moment of inertia of the given crank-connecting row $- \delta_I$ =0,061.

4. It was determined, that the offered formula for defining the period of change equivalent moment of inertia of in-line crank-connecting rod mechanisms can be used also for V-type, substituting the meaning of quantity of noncoinciding half-planes, which are formed by the axis of rotation of the crankshaft and any point of the crankshaft crankpin, which is on the axis, only for one row of cylinders.

## REFERENCES

1. Абрамчук Ф.І., Гутаревич Ю.Ф., Долганов К.Є., Тимченко І.І.: *Автомобільні двигуни*: Підручник. 3-тє видання. К.: Арістей, 2007, 476 с.

2. Колчин А.И., Демидов В.П.: *Расчет автомобильных и тракторных двигателей*: Учеб. Пособие для вузов. – 2-е изд., перераб. и доп. М.: Высшая школа, 1980. – 400 с., ил.

3. Вырубов Д.Н., Ефимов С.И., Иващенко Н.А. и др.; Под ред. Орлина А.С., Круглова М.Г.: *Двигатели внутреннего сгорания: Конструирование и рассчет на прочность поршневых и комбинированных двигателей*. Учебник для студентов втузов, обучающихся по специальности «Двигатели внутреннего сгорания» – 4-е изд.,перераб. и доп.–М.: Машиностроение, 1984.–384с., ил.

4. Байков Б.П. и др.: *Дизели. Справочник*. Л.: Машиностроение, 1964, 600 с.

5. Зейнетдинов Р.А., Дьяков И.Ф., Ярыгин С.В.: Проектирование автотракторных двигателей. Учебное пособие Ульяновск: УлГТУ. 2004, 168 с.

6. Грабар І.Г., Ільченко А.В., Ломакін В.О.: *Вплив масово-геометричних параметрів кривошипно-шатунного механізма на крутний момент двигуна внутрішнього згоряння*. Вісн. Східноукр. держ. ун-ту. №6(112), 2007, с. 52-56.

7. Грабар І.Г., Ільченко А.В., Ломакін В.О.: *Моделювання процесу зміни положення центра мас кривошипно-шатунного механізма двигуна внутрішнього згоряння*. Вісник ЖДТУ № ІІІ (42), 2007, с.17-23.

8. Грабар І.г., Ільченко А.В., Ломакін В.О.: *Математичне моделювання процесу зміни момента інерції кривошипно-шатунного механізма двигуна внутрішнього згоряння*. Вісник ЖДТУ №ІV (43), 2007, с. 15-25.

9. Ільченко А.В., Ломакін В.О.: *Зміна моменту інерції кривошипно-шатунного механізму рядних двигунів внутрішнього згоряння*. "Восточно-Европейский журнал передовых технологий" №1/5 (31) 2008, с.16-21.

10. Ільченко А.В., Ломакін В.О.: *Зміна моменту інерції дезаксіального кривошипно-шатунного механізму поршневого двигуна внутрішнього згоряння*. Вісник ЖДТУ №І (44), 2008, с. 34-38.

11. ГОСТ 23550-79 *Двигатели внутреннего сгорания поршневые*. Обозначение и нумерация цилиндров.

12. КОМПАС-3D V8. *Руководство пользователя*. Т.3. ЗАО АСКОН, 2005.–316 с.

**Milenko JOKIC**
**Marko CANADIJA**

University of Rijeka, Croatia

# PHYSICAL AND NUMERICAL MODEL OF THERMOMECHANICAL BEHAVIOR OF COOKING VESSEL

*The paper presents elements of balance laws of continuum mechanics necessary for proper modelling of cooking vessel. The problem at hand must deal with multiphysical behaviour that involves both thermal and mechanical model. Coupled nature of the problem is solved by the separation of problem into two sequential steps. First step is the thermal step that gives temperature distribution throughout the cooking vessel. Upon calculation of temperature field, stresses are calculated. The mechanical phase involves calculation of permanent strains. Upon definition of physical model, constitutive model is briefly presented. The proposed procedure is verified on the one geometry of a cooking vessel.*

## INTRODUCTION

Almost old as mankind, cooking vessels are indispensable part of our lives. So, one could expect that their design is perfected through the centuries that passed. But, this is far from true; in every household there is or was some cooking vessel that is deformed due to various reasons. Development of cooking vessels is mainly based on experience and empirical techniques. A little effort has been done to provide a proper thermomechanical model of a cooking vessel.

This can be attributed to the rather complex issues that must be addressed in the appropriate thermomechanical model. Such problems can be rather computationally intensive, see [1] for example. Problem must solve for temperature distribution that is used a starting point of mechanical calculations. Thermal part of the problem must also provide suitable boundary conditions. On the other hand, mechanical part will involve material nonlinearity - plastic deformations.

This paper starts with the presentation of basic laws of continuum mechanics. These are starting point for the model at hand. Since the problem is of coupled nature and involves both thermal and mechanical modelling, familiarity with these laws is crucial. After brief introduction to continuum mechanics laws, discussion about materials used in cookware follows. Finally, a case study presents the model into details. Behaviour of a cooking pan made of thin stainless steel is analysed by the finite element model. At the end, some conclusions are drawn.

## ELEMENTS OF CONTINUUM MECHANICS

Temperature distribution is the most significant loading if cooking vessels are concerned. Therefore, before mechanical quantities are calculated, temperature field must be obtained. As a starting point, we use the first law of thermodynamics or balance of energy equation in the most general form [4]:

$$\rho_0 \dot{E} + \mathrm{DIV}\, \mathbf{Q} = \frac{1}{2}\mathbf{S}:\dot{\mathbf{C}} + \rho_0 R \tag{1}$$

In the above equation $E$ is internal energy per unit mass, $\rho_0$ is reference mass density, $\mathbf{Q}(\mathbf{X},t)$ is heat flux vector, $\mathbf{S}$ is second Piola-Kirchhoff stress tensor, $\mathbf{C}$ is right Cauchy-Green strain tensor, DIV is divergence operator with respect to the reference configuration and $R(\mathbf{X},t)$ is heat input per unit mass. Helmholtz free energy is defined as:

$$\Psi = E - N\theta \tag{2}$$

where $N$ is entropy and $\theta$ temperature. Without going into deeper analysis, we just briefly state that this equation can be rephrased into the following form:

$$\rho_0 \theta \dot{N} = -\rho_0 \theta \partial_\theta \left[ -D_{mech} + \rho_0 \dot{\theta}\partial_\theta \Psi + \frac{1}{2}\mathbf{S}:\dot{\mathbf{C}} \right] \tag{3}$$

where $D_{mech}$ is mechanical dissipation. Briefly speaking, this term describes heat release during plastic deformation. Breakage of crystalline bonds during plastic strains is the source of heat. In most cases, 85-95 % of the plastic power is transformed into heat; the remaining part remains frozen in the crystal lattice.

Some other standard terms can be introduced, namely

$$c = \theta \partial_{\theta\theta}^2 \Psi \tag{3}$$

specific heat at constant strain, while

$$H = -\theta \partial_\theta \left[ \frac{1}{2}\mathbf{S}:\dot{\mathbf{C}} - D_{mech} \right] \tag{4}$$

term is known as elastic structural heating. This term describes phenomenon widely used in thermodynamics of gases – drop in pressure of gas is accompanied by the decrease of the gas temperature; also if the pressure in some gas in increasing, temperature rises too. The same effect is present in solids. However, when solids are concerned, this term is frequently neglected. Particularly, in the case of steels, stress variation of the order 1 MPa leads toward variation in temperature of 1 mK.

After some additional manipulation the temperature evolution equation is obtained:

$$\rho_0 R - \text{DIV } \mathbf{Q} = \rho_0 c \dot{\theta} + \rho_0 H - D_{mech} \tag{5}$$

In the cooking vessel analysis, elastic structural heating can be neglected. Also, mechanical dissipation due to plastic deformation is also very small compared to the other heat inputs in this problem. Therefore, we obtain the final form of the temperature evolution equation:

$$\rho_0 R - \text{DIV } \mathbf{Q} = \rho_0 c \dot{\theta} . \tag{6}$$

Above equation is augmented with the suitable boundary conditions, like convection and radiation to the environment:

$$\mathbf{Q}^S = h\left(\theta^e - \theta^S\right) + \kappa\left(\theta^r - \theta^S\right) \tag{7}$$

where first term corresponds to convection and second term to the heat exchange by radiation. $\theta^e$ is given temperature of the environment, $\theta^S$ temperature of surface, $\theta^r$ given temperature of external radiative source, $h$ is convection coefficient and $\kappa$ is radiative coefficient.

Mechanical part of the problem is governed by the balance of momentum:

$$\rho_0 \dot{\mathbf{V}} = \text{DIV } \mathbf{P} + \rho_0 \mathbf{B} \tag{8}$$

Here $\mathbf{P}(\mathbf{X},t)$ is the first Piola-Kirchhoff stress tensor, $\mathbf{B}(\mathbf{X},t)$ are body forces with respect to unit mass and $\mathbf{V}$ is velocity. It is not purpose of the paper at hand to go further into details of continuum mechanics. We will just briefly note that evolution equations for plastic flow are obtained from the principle of maximum of plastic dissipation.

## CONSTITUTIVE MODEL

Constitutive model for thermal part of the problem is based on the standard Fourier's law of heat conduction. Heat input is represented by the electrical cooking plate, while heat is released into the environment through convection and radiation. Stationary heat flow is considered.

Mechanical model involves temperature dependency of elastic modulus and flow properties. Plastic model is based on the von Mises yield criterion and mixed hardening rule. Since both change with temperature increase, such behaviour is also incorporated into the model at hand.

## MODELLING OF HEAT SOURCE

Modern cookware assumes energy input from three possible sources: heat released during burning of gas, through the use of electric resistivity or by microwave radiation. Heat does not flow uniformly through the bottom of cooking vessel. In the case of burning of gas, flow of heat can be represented by circularly distributed hot spots - flames. This situation is rather complex to model. Significantly simpler is the situation with heat released due to electrical resistivity. Source of heat is a spiral placed into a

heating plate. This case also does not produce uniform heating field, since there are areas on the heating plate where spiral is not present and consequently heat flow is lower. However, if the steady state heat transfer is concerned, due to high heat conductivity of metals, it is reasonable to assume that heat flow is uniform through the heating plate with satisfactory accuracy.

## MATERIALS USED IN COOKING VESSELS

Materials used in cooking vessels have to solve several issues. As explained earlier, heat inflow is often non-uniform. Situation can be alleviated with materials that are good heat conductors, like metals for example. Of further interest is heat capacity of metals. Higher heat capacity means longer time to heat up cooking vessels; therefore metals with low heat capacity are preferred for cookware.

Most often used metals for cookware production are stainless steel, cast iron, copper, aluminium and carbon steel. All of them have some specific advantages and drawbacks. From these, copper have the highest coefficient of heat conductivity and lowest heat capacity, making it an ideal selection. However, on the other side, it is very soft material, easily scratched and can be associated with health problems. Copper is also rather expensive metal, so its applications in cooking vessels are limited.

Aluminium also posses advantageous thermal conductivity and low cost compared to the copper. Although aluminium has highest specific heat capacity of all mentioned metals, due to its low mass, cooking vessels can accumulate very small amount of heat. Therefore, aluminium cooking vessels frequently involve thick structures in order to reach reasonable heat capacity. However, combinations with stainless steel can also lead to high costs. Aluminium can be also associated with health issues.

Cast iron is inexpensive material, but should be enamelled. Due to manufacturing limitations, it is produced thick, what combined with high density and high specific heat capacity leads to very high heat capacity of vessel. This results in uniform heating, but longer heating and cooling time. Carbon steel is also low-cost material and is produced in thin sheets. Unfavourable thermal behaviour leads to non-uniform temperature distribution.

Stainless steel is very popular selection today. Although his thermal properties are rather poor (lowest heat conductivity and high heat capacity), it is reasonably priced. It can be combined with aluminium and copper what significantly improve its thermal properties. Resistance to corrosion and reactivity are very high, it is easy to clean and aesthetic appearance is very favourable.

## CASE STUDY

Case study involves analysis of cooking pan made of thin sheet of stainless steel EN 1.4462. Thickness of pan is 2 mm, diameter of the bottom is 18 cm. Behaviour of cooking pan is investigated in the most critical situation – dry pan, without any ingredients. Steady-state heat transfer was considered. For the thermal part of analysis, following material parameters are selected: heat conduction coefficient is $\lambda = 15\,\text{W/mK}$, heat flux at the bottom side of pan $q = 47157\,\text{W/mK}$ (this should model heat input through the electrical heating element of 1200 W), heat convection coefficient $\alpha = 90\,\text{W/m}^2\text{K}$ for the elements at the pan's bottom and for the rest ele-

ments $\alpha = 28 \, \text{W/m}^2\text{K}$. Emissivity coefficient for all elements was taken as $\varepsilon = 0,1$. Initial and environmental temperature were 20 $^{\text{o}}$C. Contact with cooking plate is assumed to be ideal.

Problem was numerically solved by the finite element method. Standard 3D isoparametric finite elements were used. From the mechanical point of view, problem was separated into two steps. First step solve for tempeature, whereas second one gives displacements and stresses.

Analysis was carried out for the stationary heat flow and obtained temperature distribution is given in Fig. 1.Maximal temperature is obtained at the centre of the pan, while minimal temperature was obtained at the edge of the pan. It may be concluded that obtained temperature is distributed as expected.
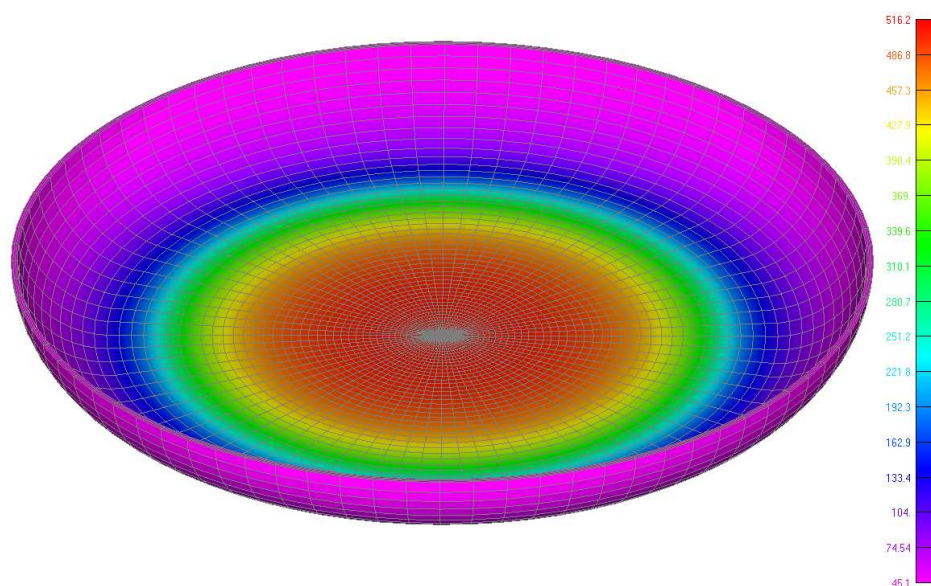


*Fig. 1. Temperature distribution in $^{o}$C; upper side of cooking pan*

Obtained temperature distribution was used as a loading for the mechanical phase. Pan was loaded by the 10 consequent heating/cooling temperature cycles. Development of permanent deformation was monitored.

Materials properties for stainless steel EN 1.4462 at elevated temperature were taken from [2]. In particular, Young modulus is:

$$E(T) = 227\left(1 - \frac{T-22}{900}\right), \quad [\text{GPa}]$$

Poisson's ratio $\nu = 0,3$, temperature expansion coefficient $\alpha = 130 \cdot 10^{-7} \, 1/^{\text{o}}\text{C}$. Used stress-strain curves at different temperatures are presented in Fig. 2.

Obtained results in the mechanical phase are presented in Figs. 3-6. Deformation plot indicates forming of the convex bottom, so-called "belly". Such deformation is clearly unwanted in the cookware. Deformation tends to increase with number of cycles. However, it is expected that after certain number of cycles deformation with start to converge to certain shape. It should be noted that assumption of ideal contact be-

tween pan's bottom and cooking plate brings some errors in the analysis. In the case of cooking plate, development of the convex bottom will lower heat input in the subsequent cycles and therefore lower the amount of permanent deformation. If the source of heat is burning of the gas, then heat input will remain approximately the same in subsequent cycles.
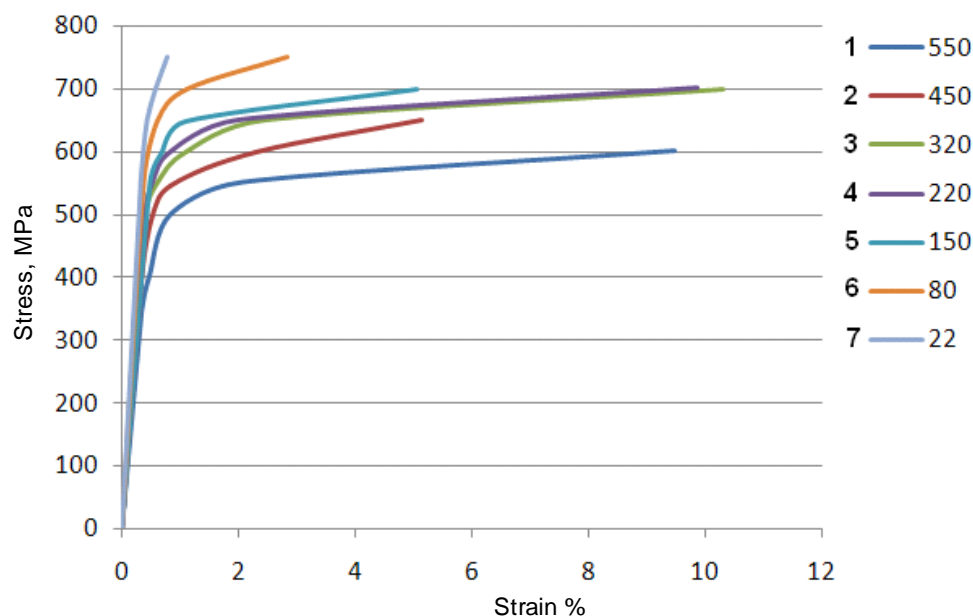


*Fig. 2. Stress-strain curves for EN 1.4462 at different temperatures [XXXXx]*
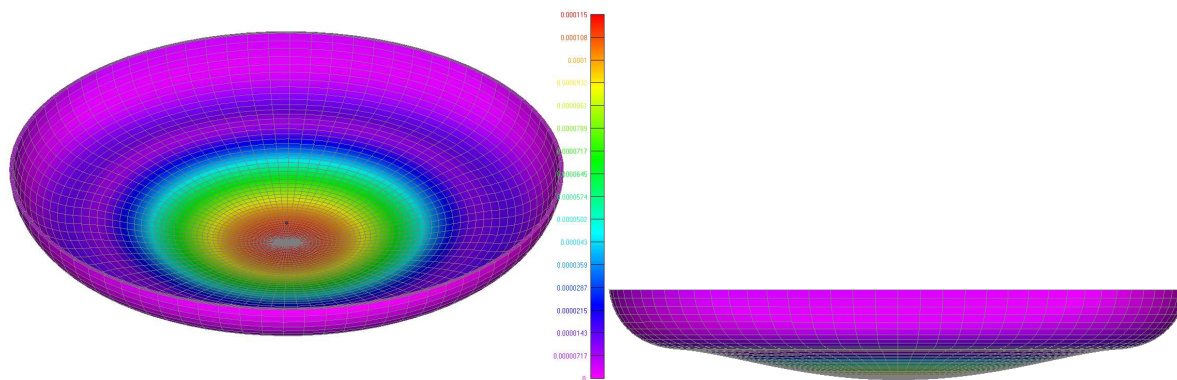


*Fig. 3. Deformed shape of cooking pan after 10 heating – cooling cycles*

Regarding residual stresses, Fig. 5-6, they tend to appear at the edge connecting bottom and the side of cooking pan. Maximal value after 10 cycles is about 130 MPa. Small zone of residual stresses also appear at the centre of the pan. Principal source of plastic strains are large temperature gradients in the region.

It should be noted that this case study involved pan with a thin bottom. Thicker bottom should alleviate the problem. Further reduction of plastic strain should be achieved if the normal cooking application is considered – meaning with thermal model if food is used.
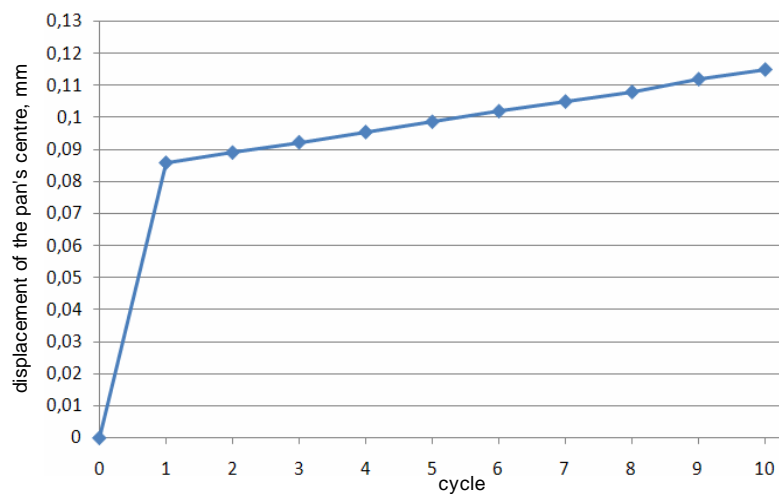
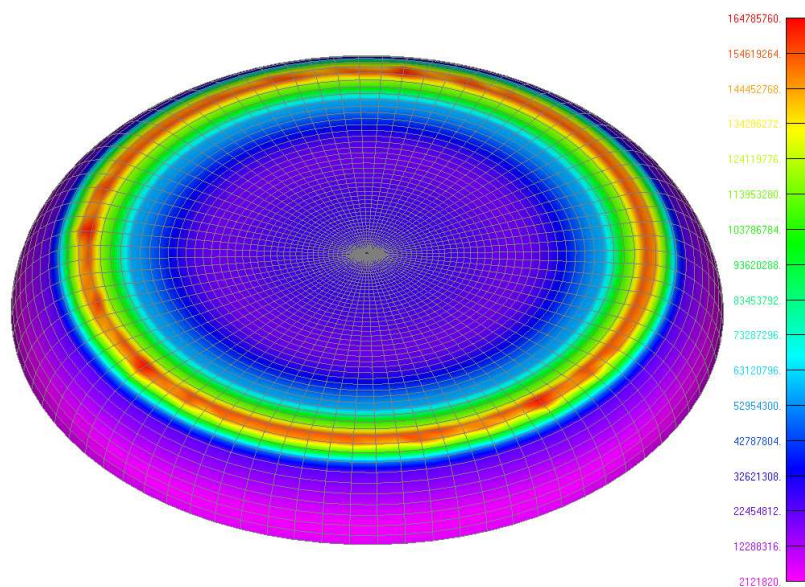*Fig. 4. Vertical displacement of the pan's centre vs. cycles*



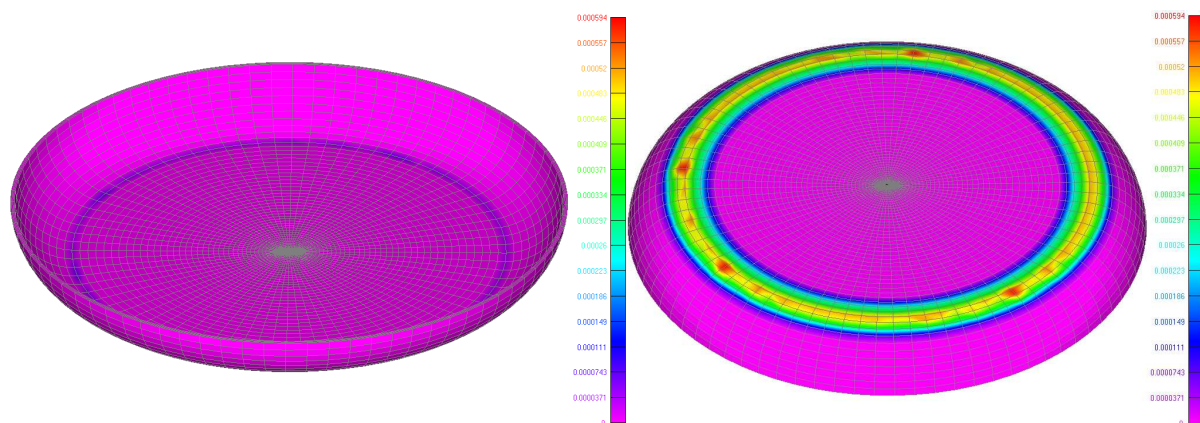*Fig. 5. Residual stress in cooking pan after 10 cycles, lower side of pan*



*Fig. 6. Equivalent plastic strain after 10 cycles*

**CONCLUSIONS**

Paper presented a model for simulation of thermomechanical behaviour of cooking vessel. Although cooking vessels are in used for centuries, a little effort has been undertaken to develop such model. Paper presented a brief overview of continuum mechanics balance laws upon which the model is based. Such laws are basis for discretization by the finite elements. Besides physical complexity of the problem at hand, boundary conditions are also of special importance. This is especially true for thermal phase where as a heating source electric cooking plate was considered. Implementation of gas combustion as a heat source brings up some further complications which were not subject of this paper. Beside this, further improvements of the model can be directed to include adequate food model and nonstationary heat transfer that occurs during rapid immersion into water, for example.

Presented case study clearly demonstrated that model behaves as expected. Therefore, it can be applied for simulation of thermomechanical behaviour of other cookware.

**REFERENCES**

1. Canadija, M., Brnic, J.: *Associative coupled thermoplasticity at finite strain with temperature-dependent material parameters*. International Journal of Plasticity, vol. 20, pp. 1851-1874, 2004.

2. Chen, J., Young, B.: *Stress-strain curves for stainless steel at elevated temperatures*. Engineering Structures, vol. 28, pp. 229-239, 2006.

3. Kondjoyan, A., Bussière, P.-H , Verrier, F.: *Preliminary Modelling of Heat and Mass transfer During Grilling and Roasting of Meat*. Proceedings of the COMSOL Users Conference, Paris, 2006.

4. Malvern, L.E.: *Introduction to the Mechanics of a Continuous Medium*. Prentice Hall, Englewood Cliffs, 1969.

**Michail KARSHAKOV**
**Nely GEORGIEVA\***

Rousse University „Angel Kanchev", Bulgaria
\*Technical College – Yambol, Bulgaria

# DYNAMICS OF THE MOBILE TWO-SKIVING BLOCK IN THE HOLE'S CUTTING

*Because of the mistakes in the technological system, in the hole cutting by the mobile two-skiving block is given a fluctuation in the depth of cutting, respectively in the action forces. In the present work are established the dependence between forcese, operating over the mobile block through cutting and mutually disposition of the block and cutting hole in the plane of the measure's formation YOZ.*

## INTRODUCTION

Holes' processing with high requirements of dimensions and shape precision is one of the constantly live problems in the up-to-day machine building.

In machining deep holes the practical application have skiving tools with two blades, which are opposite located in one common block with possibility for free movement in a plane perpendicular of the machine turning axis [2, 3, 6]. By neglecting friction forces in guides, the mobile two-skiving block will be in ceaseless dynamical equilibrium with radial direction. This describes by the equality of the two opposite operating radial cutting forces [1, 5]. In real circumstances a perfect equilibrium is not realizable because of the resistance of the friction forces against the radial movement of the mobile block and the deflections of the symmetry axis' machining hole toward the machine turning axis, as well as of the block location toward its two axes, a result of mistakes of the location of the detail and tool, and of the tool processing. As a result of these deflections this is a variation of the magnitude, direction and proportion of the active (cutting forces) and reactive (friction forces) forces, which are caused movements of the block in a radial and tangential direction [4, 6].

The aim of the present work is to determine the power load of the mobile two-skiving block in the hole's cutting depending on the reciprocal location of the block and the machining hole in the plane YOZ in which the dimensions are created.

## EXPOSE

When deep holes are machined by the skiving rod and mobile two-skiving block it is an ideal case in which the symmetry axes of the block (C) and detail's hole (O₃) coincide with the machine turning axis (O) (Fig. 1). In this case the forces, which cave in the skiving rod, are absent or slight.

In the reasons, which are mentioned in the introduction, the symmetry axis of the cross-section of the hole in each moment from the axis feed of the tool doesn't coincide with the machine turning axis. Let us assume that shape deviations of the hole in this section is are slight and the turning frequency of the detail is a small it is obviously that through one full turning of the detail round the axis $O$ of the machine the hole's axis of the detail $O_3$ will describe a circle with a radius, equal of the transitory deviation e between the two axes (Fig. 1).
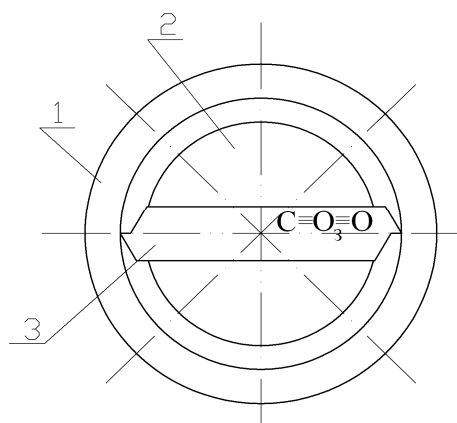


*Fig. 1. Scheme of the hole's mashing with a mobile two-skiving block: 1-detail; 2-skiving rod; 3- skiving block*

In Fig. 2 it is presented the one of the three possible cases, in which the centre of the block symmetry C coincide with the turning axis of the machine O. Through one full revolution of the detail it can describe geometrical all possible locations of the hole section of the detail toward to two-skiving block. On the figure are presented the four borderline cases through axes Y and Z by the admission that the block with dimension $L_H = AB$ is immovable toward the skiving rod and elastic deformations are zero. It is not difficult to determine that the position 1 is identical with 3, and the position 2 - with 4.
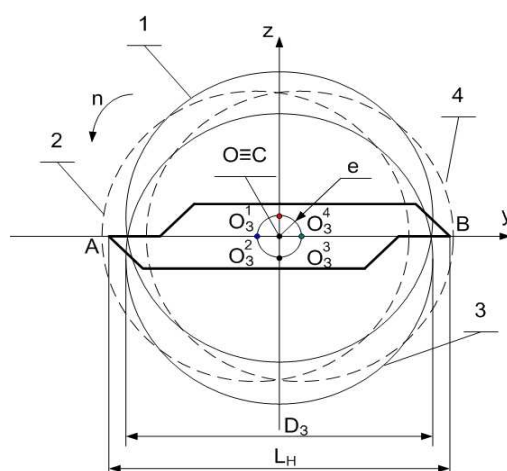


*Fig. 2. Borderline positions of the detail's hole with an immovable two-cutting block*

In these circumstances there will be fluctuations of the cutting depth respectively of the cutting forces which will be depend from the size of the work adjusting dimension of the block $L_H$ and of the deflection e. And fluctuations will be bigger in tangential direction Oz, than in radial direction Oy.

If the Fig.2 is considered with mobile cutting block, the striving for balancing of the radial cutting forces $F_{YA}$ and $F_{YB}$ will lead to its periodic movement toward the positions 2 and 4 of the detail's hole so that the centre $C$ to coincide with $O_3^2$ and $O_3^4$. The movement is realized under action of the force $\Delta F_Y = \left| F'_{YA} - F'_{YB} \right|$ and it continues until it is performed the circumstance $\Delta F_Y > F_{TP.}$, where $F_{TP.}$ is the friction force between the guides and the block (Fig. 3). When $\Delta F_Y \leq F_{TP.}$, the block stays immovable toward the skiving rod.

The turning of the detail's hole from the position 2 to 3 or from 4 to 1 leads to increase of the cutting depths, which reflects over the power loading and the circumstance of the block equilibrium.

For determination of the power dependences, which are results from the non-coincidence of the axes there is made geometrical analysis of the forces (Fig.3), which are acted over the mobile block, for the position 3 form the Fig.2. Besides the already indicated restrictions it is accepted that the two cutting parts have same geometry and wear intensity and their apexes lie in a plane, perpendicular toward turning axis of the machine. It is accepted that the cutting depths of the two cutting parts are the same and the changes of their geometry are slight.

From Fig. 3 it is obviously that as a result of the deflection e of the axis $O$ toward the symmetry axis $O_3^3$ of the detail's hole the cutting depth $t$ increases with $\Delta t$. Moreover there increase the cutting forces and it sets up a diameter $D = L_H + 2\Delta t$. In addition the radial cutting forces $F_{YA}$ and $F_{YB}$ arouse the origine of cross forces $F_A^H$ and $F_B^H$, which going in direction, opposite to the deflection e.
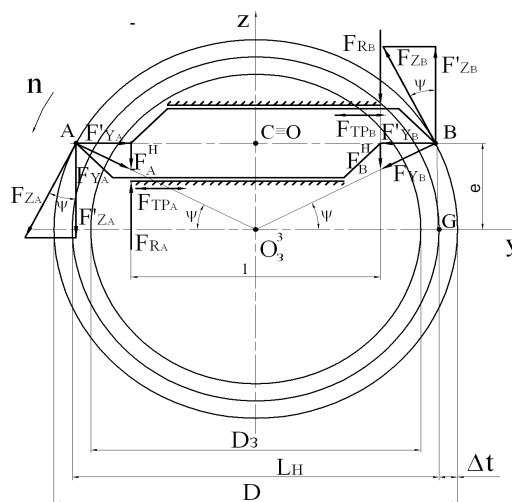


*Fig. 3. Scheme of the power loading of the mobile block through deflection toward the turning axis in tangential direction*

The increased cutting forces can calculate by the known empirical dependences [7] if we determine the increased cutting depth: $t_A = t_B = \dfrac{D - D_3}{2}$ , where $D$ is the transitory diameter of the machined hole.

From the geometrical drawing in Fig.3 it has

$$t_A = t_B = t + \Delta t = \frac{L_H - D_3}{2} + \Delta t ,$$
(1)

and

$$\Delta t = O_3^3 B - \frac{L_H}{2} .$$
(2)

From the right-angle triangle $O_3^3 GB$

$$O_3^3 B = \sqrt{O_3^3 G^2 + BG^2} = \sqrt{\left(\frac{L_H}{2}\right)^2 + e^2} ,$$
(3)

and

$$\Delta t = \frac{L_H}{2}\left(\sqrt{1 + \left(\frac{2e}{L_H}\right)^2} - 1\right) .$$
(4)

After substitution of (4) in (1) and transformation

$$t_A = t_B = \frac{L_H}{2}\sqrt{1 + \left(\frac{2e}{L_H}\right)^2} - \frac{D_3}{2} .$$
(5)

With known cutting forces we can write that

$$F_A^H = F_{YA} \sin \psi , \quad F_B^H = F_{YB} \sin \psi ,$$
(6)

where from $\Delta O_3^3 GB$ , $\psi = arctg \dfrac{2e}{L_H}$ .

As the position 3 from Fig.2 is a moment from the uniform turning movement of the detail in the indicated direction, then from this position forward the conventional equality between the cutting forces will upset. The detail's hole will move to position 4 and the block – to the cutting part $B$ under action of the force $\Delta F_Y$ . Moreover the cutting depth decreases and reaches to minimum value $\dfrac{L_H - D_3}{2}$ when the detail's hole holds a position 4.

Through the full turning cycle of the detail round the axis $O$ the cutting forces periodically change its magnitude and in this way they bring influence over the friction forces, which are opposite again the movement of the block in direction $O_Y$. With the described construction of the guides that are the forces $F_{TP.A}$ and $F_{TP.B}$ (Fig.3), which are caused from the tangential cutting forces $F_{ZA}$ and $F_{ZB}$, as well as the friction force $F_{TP.X}$, which is caused from non-marked of the figures axes cutting forces $F_{XA}$ and $F_{XB}$.

The total resistance force from the friction between the block and the guides will be

$$F_{TP} = F_{TP.A} + F_{TP.B} + F_{TP.X},$$
(7)

The friction forces can be received through the dependences:

$$F_{TP.A} = F_{RA}.\mu; \ F_{TP.B} = F_{RB}.\mu;$$

$$F_{TP.X} = (F_{XA} + F_{XB}).\mu,$$
(8)

where $\mu$ is the coefficient of the friction between the block and its guides.

For the determination of $F_{RA}$ and $F_{RB}$ - the couple forces, which are balanced the moment of the action of the tangential cutting forces and the cross forces we use the circumstances for equilibrium of the forces through the axis $O_Z$ and of the moments toward the axis $O$.

$$\left[(F'_{ZA} + F^H_A) + (F'_{ZB} - F^H_B)\right]\frac{L_H}{2} - \frac{l}{2}(F_{RA} + F_{RB}) = 0$$

$$F'_{ZA} + F^H_A - F_{RA} + F^H_B + F_{RB} - F'_{ZB} = 0$$
(9)

where l is the length of the guides.

According to the proposition for equilibrium of the cutting forces and Fig.3

$$F'_{ZA} = F'_{ZB} = F_Z \cos\psi; \ F'_{YA} = F'_{YB} = F_Y \cos\psi;$$

$$F^H_A = F^H_B = F_Y \sin\psi$$
(10)

As a result of calculating of the system (9) and according to (10) and (6) we receive

$$F_{RA} = \frac{L_H}{l} F_Z \cos\psi + F_Y \sin\psi; \; F_{RB} = \frac{L_H}{l} F_Z \cos\psi - F_Y \sin\psi$$

$$\text{(11)}$$

After substitution of (11) and (8) in (7) and rendering the account that $F_{XA} = F_{XB} = F_X$ the expression for determination of the total friction force gets the form

$$F_{TP.} = 2\mu \left( \frac{L_H}{l} F_Z \cos\psi + F_X \right)$$

$$\text{(12)}$$

**CONCLUSIONS**

Through machining with mobile two-skiving block the non-coincided of the turning axis of the machine and the symmetry axes of the of the hole cross-section and the tool leads to periodical variation of the cutting depths respectively the cutting forces. Their maximum values are got when the fluctuation between the axes is in a plane, which is perpendicular to the direction of the radial movement of the block. The arising in this plane cross forces have one-way action and cause curving skiving rod's load. It is proved that they don't exert influence on the total friction force between the block and the guides. The sensitiveness of the block to the difference between the radial cutting forces depends on the fluctuation e by its reflection on the magnitude of the cutting forces $F_Z$ and $F_X$.

With these results can expect that the non-coincided of the mentioned axes will lead to appearance mistake about shape of cross section, which expressed by increase of the diameter of the machined surface in direction $O_Z$. In the case $O \equiv C$ the increase will be symmetrically in the two directions. In the rest cases it is expected non-coincided with more strong marked of the diameter in the direction of the centre C moving toward the axis O.

**REFERENCES**

1. Костадинов В.С., Костадинов С.В.: *Относно размерообразуването при комбинирано обработване с плаващ режещ блок*. Механика на машините, бр. 48, Варна, 2003.

2. Костадинов В.С., Костадинов С., Димитрова Г.: *Комбиниран инструмент за ППД*. Механика на машините", бр.48, Варна, 2003.

3. Костадинов В.С.: *Комбинированный инструмент для обработки отверстий путем ППД*. Mechanině Technologija XXX, Kaunas, 2002.

4. Костадинов В.С.: *Кинематический анализ комбинированного инструмента для поверхностного пластического деформирования вращающимся режущим блоком*. MECHANIKA-2002, KAUNAS, 2002.

5. Кършаков М.К, Георгиева Н.А., Петров П.П.: *Изследване поведението на подвижни двуножови блокове при разстъргване на отвори*. Русе, Научна конференция AMTECH 2005, том 44, серия 2, стр. 452-457.

6. Кирсанов С.В. и др.: *Инструменты для обработки точных отверстий* М., Машиностроение, 2003.

7. Малов А.Н. и др. *Справочник технолога машиностроителя*. Том 2, М; Машиностроение, 1972.

**Michail КARSHAKOV**

Rousse University „Angel Kanchev", Bulgaria

# PARAMETERS OF THE CUTTING LAYERS WHITH TURNING BY ROUN CUTTING INSERTS

*Abstract: In this paper the motives of round cutting insert's using with machining of tubular surfaces by cutting are explained. Here works out dependences which present the relation between the area, physical and technological parameters of the cutting layer depending on the inserts' nose radius. Restrictive circumstances are showed in and they fix the mode of the cutting layer's section.*

## INTRODUCTION

The using of round cutting inserts for cutting of cylindrical surfaces find comparatively diffusion in the machine building practice. One of the main reasons about this is a result of the circumstance, that through increase the cutting depth and the insert's radius it grows vastly the width of the cutting layers (the length of the cutting edge's active part). This leads to great cutting forces and vibrations' rise in the technological system, which make worse the machining conditions and the quality of the receiving surfaces. In the other side through increase of the radius decrease the values of the rake and relief cutting edges. This leads to various effects. Through decrease of cutting edge angle $\kappa_r$ the thickness of the separated chip a decrease too and their width b increase. With decrease of cutting edge angle $\kappa_r$ the thickness of the separated chip a decrease too and their width b increase. With decrease of end cutting edge angle $\kappa_r'$ decrease the height of the non-cutting of areas, i.e. the geometrical and from that the true roughness of the machining surface. These effects are especially optimum for deep apertures' boring, where the main problem is surmounting the low performance of the process. Its successful decision requires increase of the feed. In this way the big nose radius of the insert ensures receiving of as thin wide chip, which is convenient for a reliable transportation out off the cutting area by the cooling fluid, as a comparatively small roughness, which is suitable for a next finishing machining or for final processing according the technical requirements. The chose of a suitable nose radius of the round cutting insert for the concrete machining circumstances requires recognition of its influence over physical parameters of the cutting layer [1,4,7], from which depend the specific cutting force respectively the cutting forces of the three machine's axis.

The size of the physical parameters depends from the elements of the cutting regime, too – cutting depth t and feed S, which are known as technological dimensions of the cutting layer. In this case the physical parameters give better notion for the form of the cutting layer and the occurrence in the cutting area. Here the relation between the physical parameters and technological dimensions is more complicated and the degree of their reciprocal dependence is influenced from nose radius of the round cutting insert [5,6].

There exist theoretical investigations [1,2,3,5], which in one or other degree disclose the indicated relations but in the most cases there are only partial results. There the section of the cutting layer is considered as formed by cutting edge with rectilinear and curvilinear cutting elements or the theoretical investigations are missing of sufficient thoroughness and precision.

**EXPOSE**

The main prerequisites in the present investigation are the following:
- The cutting edge of the insert, which go in a contact with the detail's material, are the part of a circumference;
- The conditional apex of the cutting part lies in the horizontal plane, which is contained the mandrel's axis;
- The cutting edge inclination is 0°;
- The elastic deformations of the cutting and machining surfaces are ignored.

With these circumstances the turning passes by cutting of a layer, which has comparatively complicated in the cross-section shape. According to the accepted definitions in the cutting theory, this layer is described with the following dimensions: thickness a, width b and area f, which are called parameters of the cutting layer. The occurrences that accompany chip's separation are in the direct dependence as from the values of this parameters as and from the section's shape of the cutting layer. In the Fig.1 it is showed with the outline *ABCD*, which is got from the moving *S* of the cutting insert with radius *R* and centre $O_1$, in the direction of the feed, till the position with centre *O* in the frame of reference xOy. Moreover, the cutting contour of the insert is divided from the conditional apex *B* to two sections – cutting edge (the arc *AB*) and end cutting edge (the arc *BC*).
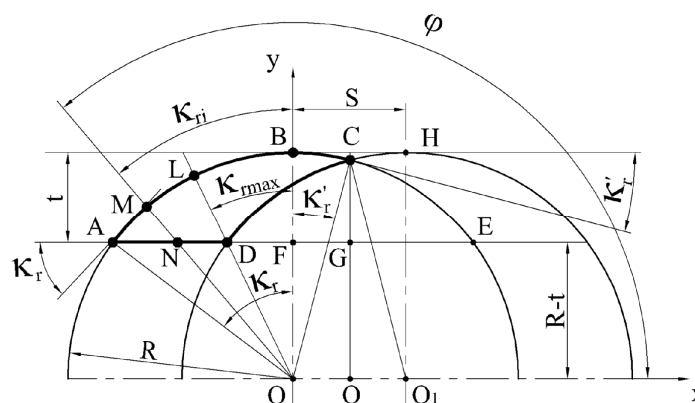


*Fig. 1. Section of the cutting layer with round cutting inserts*

The thickness of the cutting layer is measuring like a distance between the intersection's points of the radius with centre point $O$ and the contour $ABCD$. Its current size $a_i=MN$ is changed from 0 in the points $A$ and $C$ till $a_{max}$ in the point $D$. The sizes of the cutting edge angles are variable, too.

The current sizes of the cutting edge angles $\kappa_{ri}$ and the end cutting edge angles $\kappa'_{ri}$ grow up from zero at the apex $B$, duly to $\kappa_r$ and $\kappa'_r$ at the point $A$ and $C$. These maximum angles are in the direct relation from the elements of the cutting regime and the nose radius of the insert. They are received by simple calculations and are accepted as geometrical parameters, which describe the cutting conditions.

By the right-angled triangle $AFO$ (Fig.1) it cants to determine, that $\angle AOF = \kappa_r$, and

$$\kappa_r^o = \arccos \frac{FO}{AO} = \arccos \frac{R-t}{R} \tag{1}$$

In the same place $\angle BOC = \angle OCQ = \kappa'_r$ and from the right-angled triangle $OQC$ $\angle OQC = \kappa'_r = \arcsin \frac{OQ}{OC}$. From drawing it is obviously that $OQ = \frac{OO_1}{2} = \frac{S}{2}$, a $OC = R$.

Moreover here receives

$$\kappa_r^{'o} = \arcsin \frac{S}{2R} \tag{2}$$

The knowing of the cutting edge angles $\kappa_r^o$ and $\kappa_r^{'o}$ enables to determine the width of the cutting layer, which is a sum from the arcs

$$\overset{\frown}{AB} = R\kappa_r = \frac{\pi R}{180}\kappa_r^o \tag{3}$$

and

$$\overset{\frown}{BC} = R\kappa'_r = \frac{\pi R}{180}\kappa_r^{'o} \tag{4}$$

where $\kappa_r$ and $\kappa'_r$ are in radians.
When

$$b_0 = \overset{\frown}{AB} + \overset{\frown}{BC} = \frac{\pi R}{180}\left(\kappa_r^o + \kappa_r^{'o}\right) \tag{5}$$

where $b_0$ is the width of the cutting layer in $\lambda_s = 0°$.

The variable mettle of the width of the cutting layer imposes this parameter to be presented with its average value $a_{av}$ . The complicated shape of the cutting layer's section is a reason for its determination to use the dependence

$$a_{av} = \frac{f}{b_0} \tag{6}$$

where    $f = f_{ABCD}$  is the area of the cutting layer's section.

According to Fig.1, for determination of the area $f$ , it can express by areas with the following  symbols: $f_{ABE} = f_1$; $f_{CEG} = f_{CDG} = f_2$; $f_{BCGF} = f_3$; $f_{OFGQ} = f_4$; $f_{OBCQ} = f_5$.

Moreover it is obviously that

$$f = f_1 - 2f_2 \tag{7}$$

and

$$f_2 = \frac{f_1}{2} - f_3 \tag{8}$$

After substitution of (8) in (7) it is receiving

$$f = 2f_3 \tag{9}$$

The area $f_3$ with some approximation can calculate from the formula

$$f_3 = BF.FG = t\frac{S}{2} \tag{10}$$

and, under what after substitution of (10) in (9) the quested area is

$$f = t.S \tag{11}$$

The final formula is analogous with this, from which is calculated the areas with rectilinear cutting edges and it can use for practical designation, but without recognizing the influence of the nose radius over the section's shape and measurement of the cutting layer. From this reason the formula gives lightly inflated values.

If the formula (11) and formula (5) are substituted in the formula (6) for the thickness of the cutting layer is got the following approximate dependence

$$a_{av} = \frac{180° t \, S}{\pi R \left( \kappa_r^o + \kappa_r^{'o} \right)} \tag{12}$$

For an exact determination of the cutting layer's area, the area $f_3$ can be got by dependence

$$f_3 = f_5 - f_4 \tag{13}$$

According to Fig.1

$$f_4 = \frac{S}{2}(R - t) \tag{14}$$

The area $f_5$ is got by integrating the equation of the circumference with centre point $O$ in the frame of reference xOy. Under this the determination of the integral has the form [4]

$$f_5 = \int_0^{\frac{S}{2}} \sqrt{R^2 - x^2} \, dx = \frac{x}{2}\sqrt{R^2 - x^2} + \frac{R^2}{2}\arcsin\frac{x}{R}\bigg|_o^{\frac{S}{2}} \tag{15}$$

After substitution of the limits

$$f_5 = \frac{S}{4}\sqrt{R^2 - \frac{S^2}{4}} + \frac{R^2}{2}\arcsin\frac{S}{2R} \tag{16}$$

If the formula (2) is substituted in (16) and takes into consideration the fact that in the determination of the integral the angles must be in radians it is received

$$f_5 = \frac{S}{4}\sqrt{R^2 - \frac{S^2}{4}} + \frac{\pi R^2}{360}\kappa_r^{'o} \tag{17}$$

Dependences (14) and (17) are substituted in (13), and from there in a dependence (9) and as takes no account of the expression $\frac{S^2}{4}$, the formula of the cutting layer's area takes on the appearance of

$$f = \frac{\pi R^2}{180}\kappa_r^{'o} - S.(0{,}5R - t) \tag{18}$$

On the bases of formulas (18) and (5), which are substituted in (6), the average thickness of the cutting layer is

$$a_{cp} = \frac{R\kappa_r^{'o} - \dfrac{180S}{\pi R}(0{,}5R - t)}{\kappa_r^{o} + \kappa_r^{'o}} \tag{19}$$

The expressions (18) and (19) allow exact calculate of the indicated parameters of the cutting layer and research of their bearing depending on the complex influence of the insert's nose radius and the elements of the cutting regime.

From Fig.1 follow that the maximum thickness of the cutting layer $a_{max}$ can specify from the formula

$$a_{max} = LD = R - OD \tag{20}$$

From the right-angled triangle $OFD$

$$OD = \sqrt{(R-t)^2 + DF^2} \tag{21}$$

For determination of the segment $DF$ it is necessary to find abscise of point $D$ in the frame of reference xOy. For the aim it is calculated the system, which is compound from the equation of the circumference with centre point $O_1$ and the equation of the straight line $AF$. The system has the form

$$\left| \begin{array}{l} (x-S)^2 - y^2 = R^2 \\ y = R - t \end{array} \right. \tag{22}$$

The roots of this quadratic equation are

$$x_{1,2} = S \pm \sqrt{t(2R-t)} \tag{23}$$

It is obviously that the demanded abscise of point $D$ is the segment

$$DF = S - \sqrt{t(2R-t)} \tag{24}$$

After consecutive substitution of (24) in (21) and in (20) and transformation, the formula for determination of $a_{max}$ takes on the appearance of

$$a_{max} = R - \sqrt{R^2 + S^2 - 2S\sqrt{t(2R-t)}} \tag{25}$$

The thickness of the cutting layer $a_i$ in unspecified point from cutting edge $AC$ can find [5] as difference between the insert's nose radius and radius-vector r, which in polar coordinates of the frame of reference xOy determines the position of the contour $ADC$ and its a continuation cross the edge $AC$. Moreover the orthogonal co-ordinates of these points are

$$x = r.\cos\varphi \quad \text{и} \quad y = r.\sin\varphi \tag{26}$$

where $\varphi$ is the angle, which is located between the plus direction of the polar axis Ox and the radius-vector $r$.

For determination of r in the part *AD* from indicated contour we use the equation of straight line

$$y = R - t \tag{27}$$

from which, after substitution of y in the formula (26), we receive

$$r = \frac{R - t}{\sin \varphi} \tag{28}$$

According to the exhibited approach

$$a_i = OM - ON = R - r \tag{29}$$

through this, after substitution of (28) in (29)

$$a_i = R - \frac{R - t}{\sin \varphi} \tag{30}$$

If the angle parameter $\varphi$ express the cutting edge angle

$$\varphi = 90 + \kappa_{ri}^{\circ} \tag{31}$$

the formula for determination of the current thickness of the cutting layer in the section *AL* of the cutting edge takes on the appearance of

$$a_i = R - \frac{R - t}{\cos \kappa_{ri}^{\circ}} \tag{32}$$

where $\kappa_{r\,max}^{\circ} < \kappa_{ri}^{\circ} < \kappa_{r}^{\circ}$ .

For the determination of $\kappa_{r\,max}^{\circ}$ we can use the right-angled triangle *OFD*, from where

$$\kappa_{r\,max}^{\circ} = arctg \frac{DF}{OF} \ . \tag{33}$$

From Fig.1 $OF = R - t$, and $DF$ is define from formula (24),after it is substituted in (33), but before this it multiplies with -1, to ensure positive size of the segment.

Moreover the formula for determination of the cutting edge angle corresponding $a_{max}$ takes on the appearance of

$$\kappa_{r\,max} = arctg \frac{\sqrt{t(2R - t)} - S}{R - t} \tag{34}$$

For determination of the radius-vector r in the section $DC$ we use the equation of the circle with centre point $O_1$ in the frame of reference xOy:

$$(x - S)^2 + y^2 = R^2 \tag{35}$$

from where after substitution of (26) in (35) and solving the final quadratic equation we receive

$$r = S\cos\varphi + \sqrt{R^2 - S^2 \sin^2\varphi} \tag{36}$$

When, according to (29) and (36), the determination of $a_i$ in the section $LC$ of the cutting edge can define through the dependence

$$a_i = R - S.\cos\varphi - \sqrt{R^2 - S^2 \sin^2\varphi} \tag{37}$$

Similarly, in this case the final formula for the current size of the cutting layer's thickness is received after substitution of the angle parameter $\varphi$ in formula (37), but for the particular segments of the cutting edge it expresses through different cutting edge angles:

- For the segment $LB$ from the cutting edge angle $\varphi$ is took from (31), with which

$$a_i = R + S.\sin\kappa_{ri}^{\circ} - \sqrt{R^2 - S^2 \cos^2 \kappa_{ri}^{\circ}} \tag{38}$$

where $0 < \kappa_{ri}^{\circ} < \kappa_{r}^{\circ}$;

- For the segment $BC$ from the end cutting edge angle $\varphi = 90 - \kappa_{ri}^{'\circ}$, with which

$$a_i = R - S.\sin\kappa_{ri}^{'\circ} - \sqrt{R^2 - S^2 \cos^2 \kappa_{ri}^{'\circ}} \tag{39}$$

where $0 < \kappa_{ri}^{'\circ} < \kappa_{r}^{'\circ}$

It is obviously e, that with $\kappa_{ri}^{\circ} = \kappa_{ri}^{'\circ} = 0$ from last both dependence we receive a thickness of the cutting layer $BP$ at the conditional apex $B$

$$a_B = R - \sqrt{R^2 - S^2} \tag{40}$$

Besides, formula (38) takes one more opportunity for determination of $a_{\max}$, if in it's the current value of the cutting edge angle is substituted with this one from formula (34).

Up to here, the presented dependence for determination of the cutting layer's dimensions are worked out with the premise that the angle $\lambda_S = 0°$. With round cutting inserts its change is implementing by inclining in the axis plane, at that the cutting and

end cutting parts of the cutting edge take on same values $\lambda_S \neq 0^\circ$ – Fig.2. This affects to thickness of the cutting layer through the dependence
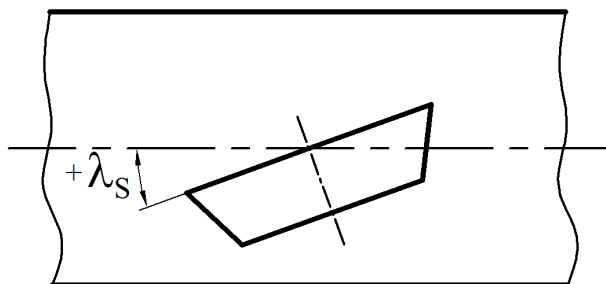


*Fig. 2. Situation of the round cutting insert with cutting edge inclination $\lambda_S \neq 0^\circ$*

$$b = \frac{b_0}{\cos \lambda_S} \tag{41}$$

at this according to formula (6)

$$a_{cp} = \frac{f \cos \lambda_S}{b_0} \tag{42}$$

In this case, after substitution of (5) and (18) in (42)

$$a_{cp} = \frac{R.\kappa_r^{'\circ} \cos \lambda_S - \dfrac{180S}{\pi R}(0,5-t)\cos \lambda_S}{\kappa_r^{\circ} + \kappa_r^{'\circ}} \tag{43}$$

## CONCLUSIONS

Turning with round cutting inserts is described with complicated section shape of the cutting layer. Important precondition for a correct choice of the regime parameters and nose radius of the inserts is the knowing the physical volumes and especially the thickness of the cutting layer.

Here are deduced dependences which allow with precision to determine the parameters of the cutting layer and in particular its thickness for each point of the cutting edge. This is allows to analyze the possibility for chips separation along the all its active part.

Here are analyzed the circumstances for the rise of normal and opposite section shapes of the cutting layer and are determined the limits of their existence in dependence on feeding as a factor from which depend the productivity of the machining.

On the basis of the receiving dependences it is necessary to accomplish theoretical and experimental researches, which to lead to practical applicable results. These results must allow prognostication of the technical and economic parameters by the turning with round cutting inserts.

## REFERENCES

1. Бобров В.Ф.: *Основы теории резания металлов*. Москва, Машиностроение, 1975.

2. Григоров В.И., Сакакушев Б.Б, Костадинов С.В.: *Анализ на модулната структура при схемните варианти за комбинирано обработване на гладки валове, чрез плаващ блок*. Научни трудове на РУ ”А.Кънчев”, Русе, т. XXXXI, 2004.

3. Григоров В.И., Костадинов С.В., Сакакушев Б.Б.: *Анализ на връзките между структурните елементи за комбинирано обработване на гладки валове, чрез плаващ блок*. Научни трудове на РУ ”А. Кънчев”, Русе, т. XXXXI, 2004.

4. Исаев А.И.: *Процес обработвания поверхностного слоя при обработка металлов резанием*. М., Машгиз, 1950.

5. Kostadinov V.S.: *Peculiarities in dimension formation in combined processing through plastic surface deformation*. Journal of Materials Science and Technology, Vol. 10, 2002, No 2.

6. Kostadinov V.S., Kostadinov S.V.: *Kinematic Analysis of a Self-Centering Tool for the Surface Plastic Flow*. MECHANIKA-2007, Technologija, Kaunas, 2007.

7. Filonenko C.H.: *Metal cutting*. Kiev, Technica, 1975,

**Ľuboš KAŠČÁK**
**Emil SPIŠÁK**

Technical University of Košice, Slovak Republic

# EVALUATIONS OF PROPERTIES OF CLINCHING AND RESISTANCE SPOT WELDING

*The paper deals with evaluation of properties of joints made by clinching and resistance spot welding. Clinching method is a relatively new technique of material joining which is beginning to find its place in the automotive industry as an alternative to resistance spot welding, especially in joining materials of different thicknesses and qualities and with various surface treatments. The advantages and disadvantages of clinching and the possibilities of its usage in the automotive industry are described in the paper. Deep drawn steel sheets of various thicknesses, qualities and various surface treatments produced for the automotive industry by U.S.Steel Ltd. were used for the experiments. Samples with single clinch joints, double clinch joints and samples with single resistance spot welded joints were prepared, whereby various combinations of thicknesses and qualities of joined materials were used. The influence of the sheet's position in clinching of materials of various thickness considering the active parts of the tool i.e. punch and die was observed. Consequently the carrying capacities of clinch joints and spot welded joints were evaluated and compared.*

## INTRODUCTION

Material joining technologies influenced by development of automotive industry in recent years have experienced new tendencies in developing new joining techniques and modifications of existing joining techniques. Trends of material saving and energy saving are applied in car body production. Car production with lower weight and consequently with lower fuel consumption is following ecological demands of emission reduction in the environment. Due to the demands there is a new need of joining of materials of various thickness and quality (well-known project UltraLight Steel Auto Body – ULSAB), coated or uncoated and also ferrous and non-ferrous materials [2]. Their application in automotive industry opens the new possibilities for the designers in optimal using of properties of various sorts of sheets which can be combined to the one unit and possibilities of influence of strength, toughness or corrosion resistance in various parts of pressed material. The cheapest sheets can be situated in the common parts of pressing, quality sheets can be situated in the critical places of deformation and high-strength sheets can be used in the exposed places due to demands of construction [3].

The above mentioned demands lead to the need of further research in the area of material joining with the accent mainly on carrying capacity of joints, their lifetime, eventually corrosion resistance.

One of the joining methods used in automotive industry is clinching. This method should be used as an alternative to resistance spot welding, especially in joining of galvanized sheets and in the situation where classical welding cannot be used.

The contribution deals with evaluation of joints made by clinching and resistance spot welding.

## MATERIAL AND EXPERIMENT

For particular joining methods deep-drawn steel sheets EN FePO4, EN FePO3, EN FePO2 and galvanized steel sheet EN FePO5G of U.S.Steel Košice Ltd. production were used. Their mechanical properties and chemical composition given by the producer are shown in table 1 and table 2. Thicknesses of used sheets were $a_0 = 0,62$; 0,7; 0,76; 0,8; 0,9 and 0,98 mm. Average thickness of zinc coating of EN FePO5G was 22 µm.

*Table 1. Basic mechanical properties of used steels*

| Material | $Rp_{0,2}$ max. | Rm | $A_{80}$ min. |
|---|---|---|---|
| *EN FePO4* | 180 | 270 – 330 | 40 |
| *EN FePO3* | 200 | 270 – 350 | 38 |
| *EN FePO2* | 240 | 270 – 370 | 34 |
| Material | Re | Rm | $A_{80}$ min. |
| *EN FePO5G* | 140 - 260 | 270 - 380 | 30 |

*Table 2. Chemical composition of used steel sheets*

| Material (thickness) | C [%] | Mn [%] | Si [%] | P [%] | S [%] | Al [%] | Ti [%] | V [%] | Nb [%] |
|---|---|---|---|---|---|---|---|---|---|
| *EN FePO4 (0,62 mm)* | 0,05 | 0,27 | 0,01 | 0,013 | 0,014 | 0,039 | | | |
| *EN FePO4 (0,7 mm)* | 0,05 | 0,20 | 0,01 | 0,01 | 0,015 | 0,040 | | | |
| *EN FePO4 (0,80 mm)* | 0,04 | 0,162 | 0,06 | 0,008 | 0,0065 | 0,043 | | | |
| *EN FePO4 (0,90 mm)* | 0,04 | 0,18 | 0,06 | 0,008 | 0,006 | 0,043 | | | |
| *EN FePO3 (0,7 mm)* | 0,03 | 0,2 | 0,006 | 0,008 | 0,008 | 0,043 | | | |
| *EN FePO3 (0,8 mm)* | 0,03 | 0,15 | 0,006 | 0,008 | 0,008 | 0,042 | | | |
| *EN FePO3 (0,9mm)* | 0,04 | 0,3 | 0,005 | 0,008 | 0,01 | 0,042 | | | |
| *EN FePO3 (1,00 mm)* | 0,083 | 0,332 | 0,005 | 0,009 | 0,0126 | 0,043 | | | |
| *EN FePO2 (0,76 mm)* | 0,037 | 0,13 | 0,005 | 0,012 | 0,0086 | 0,045 | | | |
| *EN FePO5G (0,98 mm)* | 0,07 | 1,54 | 0,4 | 0,01 | 0,0032 | 0,052 | 0,013 | 0,07 | 0,051 |

Following combinations of steel sheets for both methods of joining were used:
EN FePO3 ($a_0 = 0,90$ mm)   and   EN FePO3 ($a_0 = 0,70$ mm) - sample **A**
EN FePO4 ($a_0 = 0,90$ mm)   and   EN FePO4 ($a_0 = 0,62$ mm) - sample **B**
EN FePO3 ($a_0 = 0,80$ mm)   and   EN FePO2 ($a_0 = 0,76$ mm) - sample **C**
EN FePO4 ($a_0 = 0,70$ mm)   and   EN FePO4 ($a_0 = 0,80$ mm) - sample **D**
EN FePO5G ($a_0 = 0,98$ mm) and   EN FePO3 ($a_0 = 0,80$ mm) - sample **E**
EN FePO5G ($a_0 = 0,98$ mm) and   EN FePO4 ($a_0 = 0,62$ mm) - sample **F**

The samples of 40 x 90 mm dimensions with the length of lapping 30 mm were used for the experiments. Five samples were prepared for every combination of sheets. Surfaces of samples were cleaned with acetone before resistance spot welding, but before clinching no surfaces cleaning was necessary.

Clinching was performed on the tension machine ZD 40 of Werkotoffrufmaschinen Leipzig company with the loading range of 40 kN. The force needed for joining was in the range of 14 – 19 kN in dependence on quality and thicknesses of joined materials. The force for blankholder was 8 kN. Three types of samples were made by clinching: samples with single clinch joint, samples with double clinch joints and samples with single clinch joint in combination of sheets B and F, where orientation of joined material was being changed considering to punch and die.

For resistance spot welding, spot welding machine BP 10.27 of BEZ Bratislava and welding electrodes of CuCr material with diameter of working surface $d_e = 5$ mm were used.

The following welding parameters for resistance spot welding were chosen:

1. For combination of samples consisting of uncoated sheets:

   Compressive force: $Fz = 2,0$ kN

   Welding time:        $t = 8$ periods (1 period = 0,02 seconds)

   Welding current:    $I = 8$ kA

2. For combination of samples consisting of uncoated and coated sheets:

   Compressive force: $Fz = 2,2$ kN or 2,0 kN (for F samples)

   Welding time:        $t = 9$ periods or 8 periods (for F samples)

   Welding current:    $I = 9$ kA

Carrying capacities of joints made by resistance spot welding and clinching were compared due to standard STN 05 1122 – Tensile test of spot welded joints. This test was used for discovering the maximal carrying capacities of spot welds and clinch joints in tensile stress. After tensile test, variation coefficient $v_k$, which represents regularity of ripping of welding nugget was observed. The test was carried out on the testing machine for determination of strength of metals TIRAtest 2300 made by VEB TIW Rauenstein in loading speed 8 mm / min.

**RESULTS AND DISCUSSION**

In resistance spot welding, two types of joints were observed: fusion welded joint and cold welded joint (Fig.1 a,b). Diameters of nuggets of fusion welded joints did not fall under the minimal allowed limit $4.\sqrt{a_0}$, where $a_0$ is thickness of the sheet. The variation coefficient $v_k$ did not exceed the maximal allowed limit 7%. Cold welded joints were observed in samples C and D. Lower carrying capacities of these samples were measured too.

Concerning the clinch joints, various values of carrying capacities of B and F samples with single clinch joint were measured. In these samples, the position of materials towards the punch and die was altered (table 3). The samples where the thinner of the two joined sheets was on the side of the die carried higher carrying capacity in comparison with the samples, where thinner sheet was on the side of the punch (Fig.1 c,d). It was caused by unequal thinning of sheets in the critical area of clinch joint (Fig. 2).

*Table 3. Percentage comparison of carrying capacities (\* thinner sheet on the die side)*

| Average values of carrying capacities | | | | | | |
|---|---|---|---|---|---|---|
| Type of joint | samples A | samples B | samples C | samples D | samples E | samples F |
| Spot weld | 3225,54 | 2903,56 | 3267,28 | 2954,62 | 4100,02 | 3303,62 |
| Single clinch joint | 894,1 | 772,3 | 983,4 | 885,7 | 998,2 | 554,8 |
| Single clinch joint* | ------ | 1277,22 | ------ | ------ | ------ | 1334,70 |
| Double clinch joint | 2097,4 | 2453,26 | 2131,00 | 2239,50 | 2728,10 | 2698,30 |
| Percentage carrying capacity of single clinch joint to spot weld | 27,72% | 43,99% | 30,10% | 29,98% | 24,35% | 40,40% |
| Percentage carrying capacity of double clinch joints to spot weld | 65,02% | 84,49% | 65,22% | 75,80% | 66,54% | 81,70% |
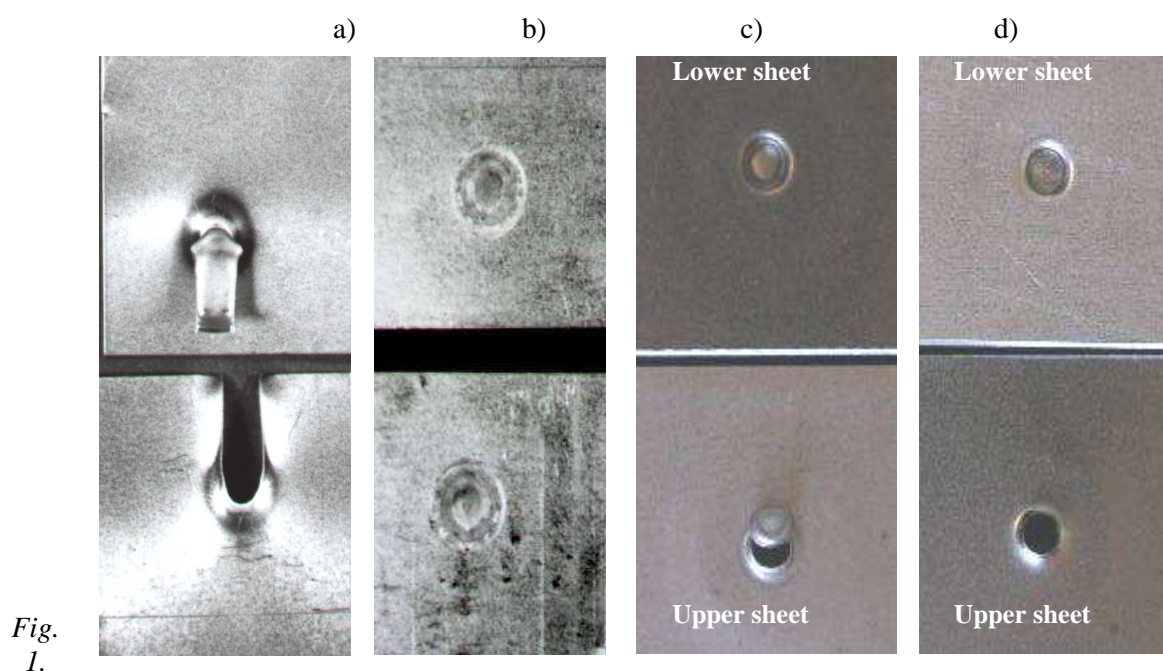


*Fig. 1.*
*Samples after tensile test: a) fusion spot welded joint, b) diffusive spot welded joint, c) press joint - thinner sheet on the die side (0,62mm), d) press joint - thicker sheet on the die side (0,98mm)*
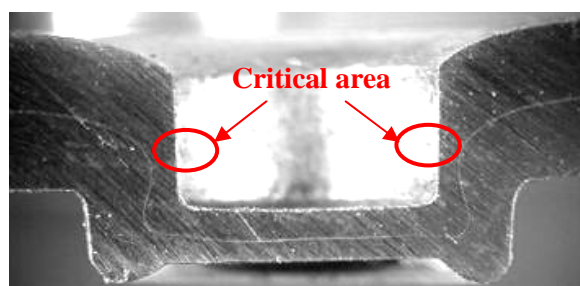


*Fig. 2. Critical area in press joint*

As shown on Fig.3, the highest carrying capacities were measured in spot welded samples with the exception of cold joints (samples C and D on Fig.4), where carrying capacities were lower than carrying capacities of samples with double clinch joints.

Concerning F samples, carrying capacities of spot welds in two cases were approximately on the same level. The single clinch joint achieved about 33% of carrying capacity of the spot weld and double clinch joint achieved about 73% of carrying capacity of the spot weld.
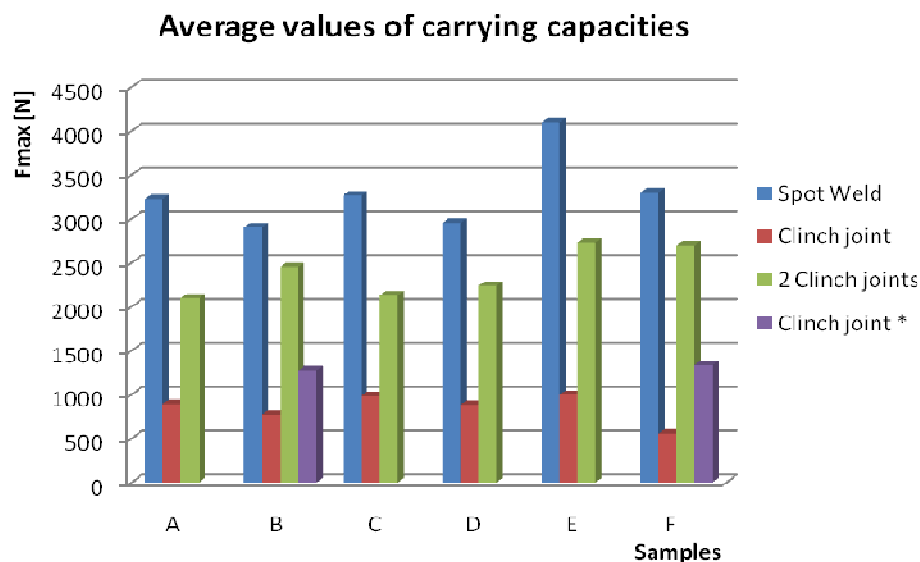


*Fig. 3. Average values of carrying capacities (*clinch joint with the thinner sheet on the die side)*
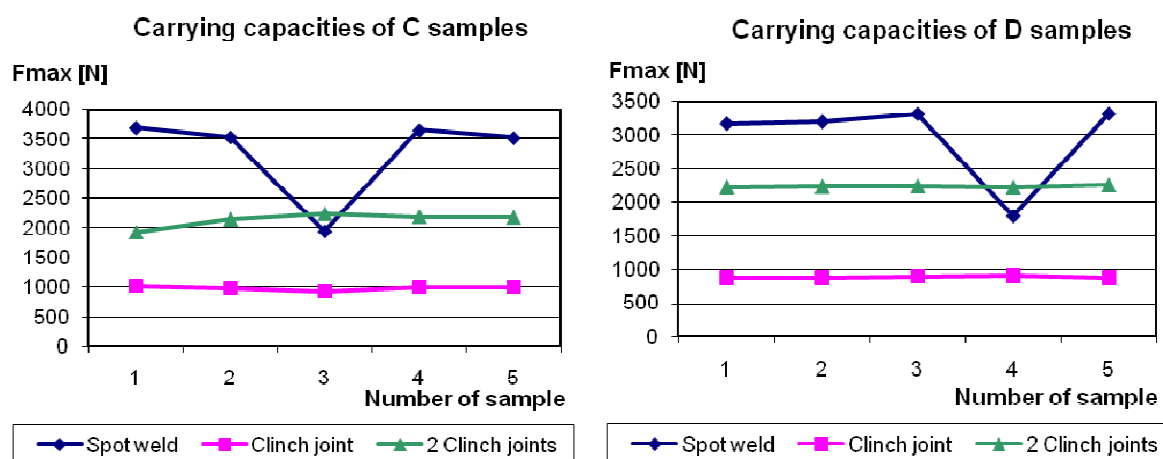


*Fig. 4. Carrying capacities of C and D samples*

## CONCLUSIONS

The highest carrying capacities were measured in the samples with resistance spot welds, followed by samples with double clinch joints. The lowest carrying capacities were measured in the samples with a single clinch joint. However, in the samples with cold welded joints, carrying capacities were lower in comparison to the samples with double clinch joints.

When clinching materials of various thicknesses, it is better to put joined materials so that thinner of the joined materials is on the die side and thicker one is on the punch side. In the case of opposite orientation the carrying capacity is reduced by 40% (sample B) or 59% (sample F).

In terms of carrying capacities of the joints, resistance spot welding method is better; however, it should be taken into consideration that in clinching there is no need for surface cleaning, no cold joints occur, and clinching is an energy saving method in comparison to resistance spot welding. The energy costs of clinching amount to as little as 10% of the energy costs of resistance spot welding.

## REFERENCES

1. Spišák E., Kaščák Ľ.: *Porovnanie únosnosti spojov vytvorených tlakovým spájaním a bodovým odporovým zváraním*. FORMING 2004, Vysoké Tatry – Štrbské Pleso, 2004, s. 256 – 261.
2. Kaščák Ľ., Spišák E.: *Tlakové spájanie oceľových plechov pre automobilový priemysel*. PRO-TECH-MA 2005, Progressive Technologies and Materials, Rzeszów – Bezmiechowa 2005, s. 76 - 81.
3. Spišák E., Kaščák Ľ.: *Spájanie oceľových plechov v automobilovom priemysle*. In: MAT/TECH automobilového priemyslu 2005. s.97 – 102.

**Michail KHEIFETZ**
**Sergey KOUKHTA**
**Gennady PREMENT**
**Sergey KLIMENKO\***

Polotsk State University, Belarus
*Institute of Super Firm Materials it. V. Bakul, National Academy of Sciences of Ukraine

# CHOICE OF DESIGN DECISIONS DURING MODELLING TRANSFER OF PARAMETERS OF QUALITY OF DETAILS OF MACHINES

*It is shown, that computer support of life cycle of products with use of CALS-technologies demands development of through mathematical models of inheritance of a complex of parameters of quality of products. At the automated designing intensive methods of processing of details of machines it is offered to use domination of properties of relations of technological decisions. On a basis synergetic the approach models of loss of serviceability of units of friction are considered.*

## INTRODUCTION

When in mathematical modelling, engineering and technological design, manufacturing and running of complex technical systems, the portability of decisions is based on principles of transfer of properties in life cycle of products. Application of synergistic concept makes it possible to generate a mathematical model of technological and operational inheritance of quality indexes, which describes various modes of behavior when in manufacturing and applying of technical systems.

Definition and estimation of changes in technological and operational processes of quality indexes of machines with a glance their mutual influence are complicated with multiply connected character of interactions of forming properties of products. To develop a mathematical apparatus of transfer of quality indexes at technological and operational inheritance it is necessary to decrease dimension of description problem of property transformation [1] in a correct way.

Replacement of set of the objects, cooperating with a product, by one object − the technological or operational environment at identity of results of such a replacement − favours the correct decrease of dimension of description problem of property transformation. Definition of manifold characteristics allows, if disposing of cooperation results with a product, to find out rational level quality indexes and to carry out the directed formation of the technological and operational environment. These manifolds should favorable development of useful properties and suppression of development of the properties, which lower quality of products, by means of use of technological and operational barriers [2].

As a result, the method of processing is understood as a set of energy and information processes directed on change of a form, sizes, quality of a surface and physical and chemical properties of a constructional material [1, 2].

# 1. ALGORITHM OF CHOICE OF TECHNOLOGICAL SOLUTIONS

For the purpose of formalization of conditions of the purposeful creation of new methods of treatment, each aggregate of homogeneous elements of the system is described as some set of technological solutions (TS). Such approach [2, 3] allows presenting any method of treatment as a cortege, each component of which is an element of the TS set.

Let us suppose that any two elements of the treatment method possess even only one common property. Then there is a link between the two on the community of properties. The gives an opportunity to organize the choice of TS according to the equivalence and preference [3]. The equivalence permits to choose heterogeneous solutions, which, according to the aggregate of their properties, must correspond to each other. The preference allows to choose solutions but out of the number of the homogeneous ones that possess the best values of the essential properties.

Such an approach makes it possible to formalize conditions of TS choice according to a certain level of the established selection criterion and enables to choose a solution according to several criteria corresponding to various TS properties.

**1.1 The analysis of relation properties.** Making TS in the systems of the automatized projecting is traditionally based on the analysis of the equivalence (x≡y) and the preference (non-strict x≤ y or strict x<y) of the solutions, which are inserted in the knowledge base. This presupposes the use of properties [4]:
1)      reflexivity (x≡x, x≤x – true; x<x - false);
2)      symmetry (x≡y⇒y≡x true; x≤y and y≤x⇒x=y - anti-symmetrical; x<y and y<x⇒ mutual exclusion - non- symmetrical);
3)       transitivity (x≡y and y≡z⇒x≡z, x≤y and y≤z⇒ x≤z, x<y and y<z⇒x<z – true).

In the result, using the property of transitivity, the most preferable of all the previous solutions is compared with a new offered or chosen out of the knowledge base on the basis of properties of quality indexes.

However, in the general case different non-equivalent TS are the most preferable for different quality parameters from the whole complex of properties. In this it is necessary to use the dominating TS (x<<y), characterized by the following properties :
1)      anti-reflexivity (x<<x - false);
2)      non-symmetry (x<<y and y<<x ⇒ mutual exclusion);
3)      non-transitivity (x<<z does not go out of x<<y).

**1.2. Synergetic approach.** To determine the parameter prevalence, when there is no transitivity or symmetry, it is rational to apply a synergetic concept that uses a mode of analog random quantity, which is such a parameter value, when the density of its distribution has a maximum [5].

Distributions of random variables on which background modes are shown, are described by laws [6]:
1)   even $f(x) = 1 / (\mu_1 - \mu_0)$ at $\mu_0 \leq x\, \mu_1$;
2)   exponential $f(x) = (1 / \mu)\, exp\, (-x / \mu)$ at $\mu > 0,\, x > 0$;

3)   normal $f(x) = (1 / (\sigma \sqrt{2\pi})) \exp(-(x - \mu)^2 / (2\sigma^2))$, at $\sigma > 0$, $-\infty < \mu < \infty$, $-\infty < x < \infty$ or other, where $\mu$ – mathematical expectation; $\mu_0$ and $\mu_1$ – imitations; $\sigma^2$ – a dispersion of random variables $x$.

To judge on the degree of correlation of statistical data to the law of distribution allows the ratio of Romanovsky:

$$R = (\lambda_p^2 - k) / \sqrt{2k}$$

where $\lambda_p^2$ – Pirson's criterion; $k$ - number of degrees of freedom, i.e. quantity of groups in the investigated line, designed ($\mu$, $\sigma$, etc.) and used at calculation of theoretical distribution of statistical characteristics.

Statistical analysis of production characteristics in the frames of wide nomenclature of the technologies tools and equipment applied permits to limit the subsequent growth of the nomenclature of objects and processes. Choosing a quantity of imitations for objects and processes it is rational to consider interdependence of inconsistent requirements on reliability and flexibility of manufacturing system. As a result, the reliability- stability and flexibility-adaptability relations can serve as a criterion for accepting of TS about rational structure of manufacturing system.

**1.3. Self-organizing systems.** In self-organizing systems reliability and adaptability can be governed by changing the number of subsystems [7]. Each subsystem $i$ has outlets: $q_1$ – strictly determined and $q_2$ – fluctuating with dissipated characteristics.

Full outlet of a subsystem as a first approximation with a glance on additivity of material and information flows is $q^{(i)} = q_1^{(i)} + q_2^{(i)}$.

Considering, that in conditions of manufacturing $q^{(i)}$ is an independent random variable, the full size of an output is the following: $Q = \sum_{i=1}^{n} q^{(i)}$.

The full output, according to the limiting central theorem, grows in proportion to the number of subsystems $n$ while the size of dispersion grows only as $\sqrt{n}$. These estimations are based on the analysis of linear dependence, in truth a feedback coupling, inherent in manufacturing systems, results in even more significant suppression of parameter dispersion [7].

Thus, in computer-aided design the acceptance of technological solutions on perfection of manufacturing systems are to be carried out on a basis of synergetic analysis of technological and operational processes and objects [8].

## 2. THERMODYNAMIC MODEL OF PROCESSES OF PROCESSING

According to the synergetic conception of the steady mode adjusted to the dominating unsteady mode and can be excluded. This leads to the abrupt reduction of the number of the controlled parameters - degrees of freedom. The remaining unsteady mode can be the parameters of sequence, which define TS [7].

**2.1. The equations of unstable processes.** The equations in the process of such reduction of parameters group up into several universal classes of the following type [7]:

$$\frac{\partial}{\partial \tau}\vec{U}* = \vec{G}\left(\vec{U}*, \nabla \vec{U}*\right) + D\nabla^2 \vec{U}* + \vec{F}(\tau),$$

where $\vec{U}*$ – controlled parameter; $\tau$ – current time; $G$ - nonlinear function of $\vec{U}*$ and probably of a gradient $\vec{U}*$; $D$ – a coefficient, describing diffusion when its value is valid, or describing distribution of waves, at imaginary value; $\vec{F}$ – fluctuating forces caused by interaction with an environment and by the dissipation within the system.

The equations of such type are similar to the describing elements of phase transitions of the first and the second type, which are defined by the criteria of transfer.

**2.2. Phase transitions.** According to the synergetic conception phase transitions take place in the result of self-organization [7], the process of which is described by three degrees of freedom, which correspond to the parameter of sequence (S), the field conjugated to it (C), and governing parameter (G) [8].
It is possible to use the only degree of the freedom-parameter of sequence - for describing only the quasi-static phase transformation. In the systems considerably moved away from the state of thermodynamic balance, each of the pointed degrees of freedom obtains its own value [7]. Therefore, besides the process of relaxation to the balanced state during the time - $\tau^p$ - with the participation of two degrees of freedom, an auto-oscillatory condition can be realized. If three degrees of freedom participate, transition to the chaotic state is possible [8]. As a result, the overall state of the technologic system is characterized by several conditions;
1)     relaxational - realized when the time of relaxation of the sequence parameter much surpasses the times of relaxation of other degrees of freedom ($\tau_S^p \gg \tau_G^p$ and $\tau_S^p \gg \tau_C^p$);
2)     auto-oscillation - requires commensurability of the typical times of changing in the sequence parameter and in the governing parameter, or in conjugated field ($\tau_S^p \gtrsim \tau_G^p$ or $\tau_S^p \gtrsim \tau_C^p$);
3)     stochastic - characterized by a strange attractor and is possible through the commensurability of all the three degrees of freedom $\left(\tau_G^p \gtrsim \tau_S^p \gtrsim \tau_C^p\right)$;
4)     remembering - defined by the 'frozen' disorder at the transition point from the disorderly state and is realized when the relaxation time of the sequence parameter turns out to be much less than other times ($\tau_S^p \ll \tau_G^p$ and $\tau_S^p \ll \tau_C^p$).

Thus, at modelling of technological and operational inheritance, the decrease of dimension of a description task of transfer of quality indexes up to three degrees of freedom of environment is possible during processing and wear process of a product. Modelling of transfer processes on a basis of synergetic approach allows to take into account stability of formation of quality indexes and to consider mechanisms of management of stability of technological and operational processes using feedback [1].

## 3. THE ANALYSIS OF PROCESSES OF WEAR PROCESS OF SURFACES

At the analysis wear process of machine details and their interfaces it is expedient to consider a vector [9]:

$$\varphi\,(X,\,t) = [\,\xi_{u_1}\,(X,\,t),\,\ldots,\xi_{u_i}\,(X,\,t),\,\ldots,\,\xi_{u_n}\,(X,\,t)],$$

where $\xi_{u_i}\,(X,\,t)$ – speed of wear process of detail $i$ (interface) at the moment of time $t$ while loading influence $X$ on a unit of a machine.

Then it is accepted, that the wear process possesses a consequence, if the module and a direction of vector $\varphi\,(X,\,t)$ at the moment of time $t$ depends not only on the module and a direction of a vector $X$ at present time, but also on the module and a direction of a vector $X$ at the moment of time $\tau < t$, and also on the size of deterioration $U$ of rubbed surfaces for a period $[0,\,t]$ (here $U$ – a n-dimensional vector: $U = (u_1,\,\ldots,\,u_i,\,\ldots,\,u_n)$; at which $u_i$ - size of deterioration of detail $i$) [9]:

$$u_i\,(t) = \int\limits_{0}^{t} \xi_{u_i}\,(\tau)\,d\tau\,.$$

It is typical for wear process without consequence that the module and the direction of vector $\varphi(X,\,t)$ at the moment of time $t$ depend on the module and a direction of a vector $X$ only at present.

Depending on time $\tau_p$, when the loss of the serviceability, connected to background of operation of a product, is kept, there are two kinds of consequences: the first and second sort. The consequence of the first sort is characterized by the changes during loss of serviceability of the products caused by background of loading influence $X$, remains during all service life of product $\tau_o$, i.e. $\tau_p \geq \tau_o$. If $\tau_p < \tau_o$, it is a process with «fading memory» or a consequence of the second sort.

Dependences of intensity of wear process of units of friction of machines on operation time $t$ differ from each other with a kind of connections between managing parameter – loading influence $X$ and the wear process connected to it by intensity $J$.

The choice of ordering parameter $H$ in each concrete case depends on research problems (definition of durability, comparison of wear resistance, an estimation of dynamic properties of system in view of wear process of its elements, etc.). It is possible, that for the same detail, but for various parameters, process of loss of serviceability can have or not have consequence at constant intensity of wear process $J$ of rubbed surfaces. It is caused by a kind of connection (linear or nonlinear) between the ordering parameter $H$ on which the estimation of a resource of serviceability of a researched product and by saved up deterioration $U$ [1].

Let's consider various connections between external influences and parameters of system $_{fH}$, and also between characteristics of process of loss of serviceability $g_H$.

**3.1. Model of loss of serviceability process of frictional units without consequence.** In a case when connected to ordering parameter $H$ intensity of wear process $J$ depends only on size of loading influence $X$:

$$\begin{cases} J\,(t) = f_H\,\big(X\,(t)\big); \\ H\,(t) = g_H\,\big(X\,(t),U\,(t),t\big). \end{cases}$$

If process of wear process is considered as continuous stochastic process [18] it is possible to receive a condition of wear process without consequence. Under constant conditions of friction the increment of deterioration $U(\varDelta t) = U(t + \varDelta t) - U(t)$ does not depend on time (process with independent increments), hence, speed of wear process $\xi_u = dU/d\tau$ is stationary during time $\tau$ [9]. Therefore such a wear process is described by a mode with storing: $(\tau_{\Pi}^{\text{p}} \ll \tau_{\text{y}}^{\text{p}} \text{ и } \tau_{\Pi}^{\text{p}} \ll \tau_{\text{C}}^{\text{p}})$.

However processes of loss of serviceability of details during the periods extra earnings and catastrophic destruction of superficial layers cannot be described with the help of the resulted equations as intensity of wear process $J$ during these periods is not a constant, and depends on sizes of saved up deterioration $U$ of rubbed surfaces.

**3.2. Models of loss of serviceability processes of frictional units with the consequence of the first sort** In cases when intensity of wear process $J$ depends both on size of loading influence $X$ and on size of saved up deterioration $U$, by the considered moment of time $t$:

$$\begin{cases} J(t) = f_H\big(X(t), U(t), t\big); \\ H(t) = g_H\big(X(t), U(t), t\big). \end{cases}$$

And at the account of a feedback of loading influence $X^*$ with deterioration $U$:

$$\begin{cases} J(t) = f_H\big(X^*(t), U(t), t\big); \\ H(t) = g_H\big(X^*(t), U(t), t\big); \\ X^*(t) = q_H\big(X(t), U(t), t\big). \end{cases}$$

Changes during time $\tau$ of intensity of wear process $J$ of rubbed interfaces at constant loading influence on an input of technical system $X$ can be caused by two groups of reasons [9]:

- not taking into account a feedback of loading $X$ with deterioration $U$, such as distinction of physic and mechanical properties of a material on depth of a superficial layer of the product, caused by manufacturing techniques; the ageing of lubricants resulting in their deterioration of frictional properties, to change of a thermal operating mode of interface, and in some cases and to change of kinds of wear process of rubbed surfaces; increase while in service concentration of abrasive particles, products of deterioration, etc.;

- taking into account changes of dependence $q_{\text{и}}$ loading influence $X^*$ on a detail of unit of friction as a result of deterioration of interface $U$ which are connected to increase in backlashes in rubbed interfaces; with transformation of macrogeometry of surfaces of friction at wear process and короблении details; with change of contact rigidity of mobile joints, etc.

Considered processes of loss of serviceability with последействием the first sort concern to processes with strong correlation which have certain connection between sizes of parameter about $H_i(\varDelta t)$ and $H_{i+1}(\varDelta t)$ even at rather big $\tau = t_{i+1} - t_i$. Here $H_i(\varDelta t) = H(t_i + \varDelta t) - H(t_i)$; $H_{i+1}(\varDelta t) = H(t_{i+1} + \varDelta t) - H(t_{i+1})$, $t_i < t_{i+1}$.

Thereof processes of loss of the serviceability, caused by the first and second groups of the reasons, are characterized self-oscillatory ($\tau_{\Pi}^{\text{p}} \gtrless \tau_{\text{y}}^{\text{p}}$ or $\tau_{\Pi}^{\text{p}} \gtrless \tau_{\text{C}}^{\text{p}}$) and stochastic $\left( \tau_{\text{y}}^{\text{p}} \gtrless \tau_{\Pi}^{\text{p}} \gtrless \tau_{\text{C}}^{\text{p}} \right)$ by modes with two and three degrees of freedom of technical system.

**3.3. The model of loss of serviceability process of frictional units with consequence of the second sort.** Consequence of the second sort is shown at change of loading influence as special transitional in wear process of rubbed surfaces [9]. In a transition period [$t_0$, $t_1$] intensity of wear process $J$ differs from those values which it accepted at the previous level of loading influence $X_{i-l}$, and from the value corresponding to new level $X_i$:

$$J(t) = \begin{cases} f_H\left(X_i, X_{i-1}, ..., X_{i-n}, t\right), t_0 \le t \le t_1; \\ f_H\left(X_i, t\right), t > t_1. \end{cases}$$

Occurrence of transition periods speaks the several reasons [9]: an operational heredity of the materials deformable during friction of superficial layers of details; change diagram specific pressure in a zone of contact of details at transition from one level of loading influence on another and connected to it «secondary aging» rubbed surfaces; gradual restoration of conformity between size of loading influence and distribution of greasing and products of deterioration on rubbed surfaces.

Proceeding from representations about the nature of the phenomena последействия the second sort it is possible to conclude, that from a position вероятностного the analysis processes of wear process in transition periods [$t_0$, $t_1$] are characterized by strong correlation connection between increments of deterioration $U_i$ ($\Delta t$) and $U_{i+1}(\Delta t)$ [9].

In this connection they should be considered as релаксационные ($\tau_{\Pi}^{\text{p}} > \tau_{\text{y}}^{\text{p}}$ and $\tau_{\Pi}^{\text{p}} \gg \tau_{\text{C}}^{\text{p}}$) with the characteristic period [$t_0$, $t_1$].

Thus, downturn of dimension of a task of the description of transfer of properties of products in technological and operational processes is made by allocation of parameters of the order and definition of modes of a condition of system. After that on each of modes it is expedient to consider interrelations of the basic parameters of quality of a product with the determining parameter of the order and a condition of their steady formation.

**3.4. Parameters of quality of surfaces of products.** Parameters of quality of products of the mechanical engineering, being the basic, share on two categories [1]: what are characterized by the hereditary phenomena connected to properties of materials of products concern to the first; to the second - connected to geometrical parameters of their surfaces.

Parameters of both categories in multicoherent technological and operational environments mutually influence against each other. Geometrical parameters of products, such as their configurations and the sizes can influence the voltage distributed in a material of a basis and superficial layers. And, on the contrary, the voltage formed during technological operations and stages of operation, can lead eventually to to changes of geometrical parameters of precision details. It testifies to mutual connection and conditionality of the phenomena accompanying technological and operational processes.

Inheritance of the basic parameters of quality is the most full is opened by consideration of sequence of processes with synergetic of positions of joint action of technology factors at mutual influence of parameters. Initial parameters of quality of details of the machine at various scale levels change while in service [1].

Exception is made with residual voltage and structure of the basic material which can be kept before full destruction of rubbed surfaces of details. In most cases already during the period extra earnings the roughness and structure of a superficial relief essentially varies, the sinuosity and structure of superficial layers of a detail change at the established wear process, and the geometrical form of a surface of friction remains within the limits of the admitted values accepted at manufacturing, practically up to the end of service of unit of friction if the estimation of its serviceability is made on parameters of accuracy.

## CONCLUSION

As a result of the analysis of processes of wear process of surfaces and loss of serviceability of units of friction, studying of features of management by processes of processing the expediency of application synergetic the approach to technical systems is shown. On a basis synergetic the approach the mathematical model of technological and operational inheritance of parameters of quality in life cycle of products of the mechanical engineering, describing various modes of behaviour is generated by manufacture and application of technical systems. Mathematical modelling and algorithmization of decision-making, by definition of a kind of the equations have shown, that the system analysis at the automated designing methods of processing, besides equivalence and preference, should be based on domination of properties of relations of design decisions.

## REFERENCES

1. Vasilyev A., Dalsckiy A., Klimencko S. et al.: *Technological Basis of Machine Quality Control.* Moscow: Mechanical Engineering, 2003, 256 p.

2. Ryzhov A., Averchenckov V.: *Technological Process Optimization of Machine Working*. Kiyiv: Navukovaia dumka, 1989, 192 p.

3. Golodenko B., Smolencev V.: *Object-Orientated Forming Organization of New Methods of Combined Processing*. Mechanical Engineering Herald., 4, 1994, pp. 25 – 28.

4. Korshunov Yu.: *Mathematical Basis of Cybernetics*. Moscow: Energoatomizdat, 1987, 496 p.

5. Aberling V.: *Pattern Formation at Irreversible Processes.* Moscow: Mir, 1979, 279 p.

6. Sigorsckiy V.: *Mathematical Apparatus of an Engineer*. Kiyiv: Technology, 1977, 768 p.

7. Haken G.: *Synergetics*. Moscow: Mir, 1980, 404 p.

8. Olemsckiy A., Koplyk I.: *Theory of Spatio-temporal evolution of Nonequilibrium Thermodynamic System*. Physical Sciences Progress, 10, 1995, v. 165, pp. 1105 – 1144.

9. Scorynin Yu.: *Accelerated Wearing Tests of Machine's Details and Equipment*. Minsk: Science and Technology, 1972, 159 p.

**Katarzyna KORZYNSKA**

Rzeszow University of Technology, Poland

# A METHOD OF EVALUATING ENVIRONMENTAL ASPECTS IN THE ISO 14001 ENVIRONMENTAL MANAGEMENT SYSTEMS

*The article suggests a way of evaluating environmental aspect importance in the Environmental Management Systems which comply with the ISO 14001 standard. An appraisal is required by the ISO 1401 modal standard, which means the necessity of evaluating environmental aspects in order to point out the significant ones. However, the standard does not say how to do it. This arises some problems for the organisations implementing the ISO 14001 requirements and this article can help to solve them.*

## INTRODUCTION

The Environmental Management Systems which are in accordance with the ISO 14001 standard are actually not as popular as ISO 9001 systems, but their popularity is growing steadily. Most organisations that have already implemented ISO 9001 systems aim at creating Integrated Management Systems and then, most often, to achieve this, they cannot ignore Environmental Management Systems. In Europe there are two groups of available models of environmental systems: those based on the ISO 14001 standard and the others whose basis is the Decree of the European Council of 19th March, 2001 EMAS. Since EMAC, including the ISO 14001 norm requirements, is a sort of extension of the norms, the organizations tend to implement the ISO 140001 based systems more often. For instance, in Poland, eight organizations are registered in the EMAS system, whereas about 15000 organizations are holders of the ISO 14001 standard. As the Environmental Management system based on the latter standard is becoming so natural a way of management developement in organizations, it is worthwhile joining in the discussion about the issues of its implementation. Quite a number of instructions, courses, postgraduate studies or other forms of education are focused on how to implement ISO 14001 based systems, and, first of all, on how to solve the implementation related problems. One of them is the evaluation of environmental aspects. It is just this problem that the article is on.

## ENVIRONMENTAL ASPECTS

The ISO 14001 standard, point 3.6, defines the environmental aspect as an element of an organization's activities or its products and services which can interact with the environment. A significant environmental aspect is the one which has or may have a marked effect on the environment. [1]

While trying to meet the point 4.3.1 requirements, those who want to effect the implementation face the problem of introducing and maintaining the procedure of:

1) identifying environmental aspects

2) determining those environmental aspects which have or may have an important effect(s) on the  environment (i.e. finding significant environmental aspects).

In the first case, the ISO 1400 standard itself gives hints where and how such aspects may  be searched for. Namely, it recommends that enviromental aspects be identified  considering their input and output data related to activities, products and services.

Although there is no one approach to the identification of environmental aspects, we stand a good chance of pinpointing them all if we consider:

a) emissions into the air,

b) discharges into the water,

c) dumping into the soil,

d) consumption of raw materials and natural resources,

e) consumption of energy,

f) emitted energy, e. g. heat, radiation, vibrations,

g) waste and by-products,

h) physical characteristics, e. g. size, shape, colour, look [1].

Some problem, in the case of environmental aspects, arises when an organization, being in the possession of a list of the identified enviromental aspects, makes an attempt at meeting the other requirement, i. e. selecting the significant ones. Here, three procedures may be possible:

1) choice of the simplest method – e. g. the employee (or a team of experts) that is the most experienced at environmental protection makes arbitrary decisions to select significant aspects. The model is not recommendable because of its subjectivity and low degree of evaluation precision.

2) choice of the method that is used the most frequently – e. g. the score method consisting in assigning the previously decided criterium values to particular aspects, e. g. within the 1-5 bracket, which is followed by adding (or multiplying) criterion values for a given aspect. In the last resort, the sum (product) of the points obtained determines the validity of the criteria – significant aspects are those with the highest sum (product). The model, though more correct than the previous one, may turn out to be unsufficiently precise in some cases as it does not make allowance for the importance of the criteria considered.

3) choice of a method fitting a particular organization – most often the model is based on the score method modified to fit the organization. The model is the most recommendable, but it takes fuller involvment in the evaluation process at its initial stage.

 It is a difficult decision to choose the third model with regard to the fact that people responsible for the implementation do not often have either enough knowledge or, most importantly, lack experience in implementing such systems. However, it seems worthwhile setting oneself the task, then describing it within the required procedure in order to successfully apply it later on. Such a method will first of all point out the really essential aspects in a more adequate, objective and mathematical way. Based on such significant, priority aspects it will be possible to create the appropriate Environmental Policy – foundations and the most comprehensive summary of the system real-

ized, since the ISO 14001 standard requires that significant environmental aspects should be taken into consideration while founding, implementing and maintaining a system of environmental protection.

## EVALUATION OF ENVIRONMENTAL ASPECTS

The proposed evaluation of selected environmental aspects takes into account the following, often practically applied criteria:

1) time of affecting the environment ( duration of the environmental effect, repair time of possible damage and whether the effect of the aspect is of cumulative nature),

2) extent of the effect of the aspects, extent of the effect compared to the quantities allowed by law and licences),

3) effect on the environment (whether the aspect causes noise, odour or landscape degradation, which might be undesirable for the company's neighbourhood and badly affect its image),

4) environmental risk (a possible occurance of exceptionally great threat to the environment) and

5) possible occurrance of environmental damage (can the damage related to environmental risk be significant).

Of course, the criteria presented are of a model nature. Under other, concrete conditions they may be replaced by more relevant ones. The criteria of the assessment of the identified environmental aspects together with a five- step marking scale are shown in Table 1.

In accordance with the popular practice the five- step grading of the criterion evaluation was adopted and the 1-5 scale was applied.

*Table 1. Criteria of identified environmental aspect evaluation*

| Criterion | Basis for aspect assessment | Evaluation | | | | |
|:---:|:---:|:---:|:---:|:---:|:---:|:---:|
| | | definitely not | rather not | moderately/ indifferently | rather yes | definitely yes |
| 1 | Environmental effect duration | 1 | 2 | 3 | 4 | 5 |
| 2 | Legal requirements | 1 | 2 | 3 | 4 | 5 |
| 3 | Effect on the environment | 1 | 2 | 3 | 4 | 5 |
| 4 | Environmental risk | 1 | 2 | 3 | 4 | 5 |
| 5 | Environmental damage | 1 | 2 | 3 | 4 | 5 |

Since criterion significance appraisal is an element of a precise environmental aspect evaluation, the criteria shown in Table1 were assigned (here purely hypothetically) the significances presented in Table 2.

*Table 2. Criterion significances from Table 1*

| Criterion | Basis for aspect evaluation | Criterion significance |
|---|---|---|
| 1 | Environmental effect duration | 2.0 |
| 2 | Legal requirements | 3.0 |
| 3 | Effect on the environment | 1.0 |
| 4 | Environmental risk | 1.5 |
| 5 | Environmental damage | 2.5 |

The evaluation of the aspect could be expressed as follows:

$$EA = (2 \cdot C_1) \cdot (3 \cdot C_2) \cdot (1 \cdot C_3) \cdot (1,5 \cdot C_4) \cdot (2,5 \cdot C_5)$$

where: $EA$ – value of the assessed environmental aspect, $C_i$ – evaluated criterion

The next step would be assigning the identified and evaluated aspects to one of the three groups:

I – significant aspects – aspects related to very negative effects on the environment, reflected in the Programme, Environmental Aims and Tasks accepted by an organoization.

II – moderate aspects – aspects which require monitoring, without a direct negative effect on the environment.

III – negligible aspects – aspects of slightly negative effect on the environment.

The criteria that may be used to classify environmental aspects are shown in Table 3.

*Table 3. Criteria to classify environmentak aspects*

| Group | Group classification | Aspect evaluation (*EA* according to formula 1) |
|---|---|---|
| I | Significant | above 2000 pts |
| II | Moderate | above 1000 pts up to 2000 pts |
| III | Negligible | up to 1000 pts |

It is obvious that the values listed in Table 3 should be selected after the aspect evaluation has been made. The selection should be carried out in such a way so the presented methodology may point out at most a few significant aspects (best 2-4) an organization's priority activities will focus on in the nearest future. Lack or too great a number of significant aspects will render the effective functioning of an environmental management system impossible.

An example of how to use an evaluation of environmental aspects together with importance criteria is shown in Table 4. The traditional (product) method of calculating the "aspect value" is in the frame and that suggested in this article is on the right.

It is obvious that the doubts that may arise with regard to the assumed values classifying particular aspects into one of the three groups are partially justified, but they should not discourage us from applying importance – based methods of calculating the value of environmental aspects because their evaluation with traditional methods (i. e. without grading criteria with respect to their significance) follows the same procedure.

*Table 4. An example of the application of a chosen "traditional" method of environmental aspect evaluation and that described in the article*

| No | Identified aspect | Criterion | | | | | Evaluation AxBxCxDxE | Comments | Evaluation | Comments |
|---|---|---|---|---|---|---|---|---|---|---|
| | | A | B | C | D | E | | | | |
| 1 | Air | 2 | 1 | 4 | 1 | 1 | 8 | negligible | 180 | negligible |
| 2 | Water | 4 | 2 | 3 | 1 | 4 | 96 | moderate | 2160 | significant |
| 3 | Electric Energy | 4 | 5 | 1 | 2 | 2 | 80 | moderate | 1800 | moderate |
| 4 | Thermal Energy | 4 | 4 | 1 | 2 | 4 | 128 | significant | 2880 | significant |
| 5 | Lubricants | 4 | 1 | 4 | 2 | 2 | 64 | moderate | 1440 | moderate |
| 6 | Paint | 4 | 1 | 3 | 1 | 2 | 24 | negligible | 540 | negligible |
| 7 | Solvents | 4 | 1 | 3 | 4 | 2 | 96 | moderate | 2160 | significant |
| 8 | Batteries | 2 | 2 | 1 | 2 | 2 | 16 | negligible | 360 | negligible |
| 9 | Cleansers | 1 | 1 | 1 | 1 | 1 | 1 | negligible | 22,5 | negligible |
| 10 | Steel | 1 | 1 | 1 | 1 | 1 | 1 | negligible | 22,5 | negligible |

## CONCLUSIONS

The implementation of environmental management systems involves the necessity to meet the ISO 14001 standard requirements. One of them is the identification and evaluation of environmental aspects. The above mentioned standard does not specify how an aspect evaluation should be carried out. Hence, there are a few approaches in practice. Actually, each of them is up to the standard requirements. Generally, the procedure boils down to the choice of some aspect evaluation criteria and assigning them values, most often those from the 1-5 bracket for each identified aspect. The values of the criteria for the given aspect are often multiplied and the quotient determines whether the aspect is significant, moderate or negligible. Such an approach gives rise to the question: Are all the criteria really equally important for every organization? Most answers are, unfortunately, in the negative. That is just the reason why the article proposes a methodology of environmental aspect evaluation which takes into account the significance of the criteria. This is only a suggestion and not a finished algorithm. In a specific organization attention must be paid to the selection of the criteria and next to their significance interrelations. A later choice of the significant ones based on the results obtained is no problem if the principle of pointing out some priority aspects is

followed. A possible incovenience of the suggested solution may be the necessity of making not so much painstaking as a little bit too much time consuming calculations. However, in the JT area it is a minor problem since it only takes using a Microsoft Exel sheet as a register of environmental aspects and entering the appropriate formulas. An unquestionable benefit from the presented approach to the environmental aspect evaluation is a possibility of a precise selection of significant aspects which will be a foundation of an Environmental Management System complying with the ISO 14001 standard.

**REFERENCES**

1) PN-EN ISO 14001: *Systems of Environmental Management. Requirements and implementation guidelines.* PKN, Warsaw, May 2005.

**Vasil KOSTADINOV**
**Michail К. КARSHAKOV**

Rousse University „Angel Kanchev", Bulgaria

# PROCESSING OF THE GROOVES THROUGH SURFACE PLASTIC DEFORMATION

*The processing of the grooves for a putting gaskets in the hydraulic holes is embarrassed because the high requirements for their precision and roughness. In this case like a method for finish processing it is suitable using surface plastic deformation. This method ensures as the quality of the machining surface as higher productivity.*

## INTRODUCTION

The processing of the grooves for a putting gaskets in the hydraulic holes is embarrassed because the high requirements for their precision and roughness.

The using of the grinding like a method for machining of the groove cylindrical surface leads to the necessity of special shaping of the grinder and made more expensive the technological process. The execution of this operation is embarrassed or impossible through machining of cast iron, non-ferrous metals and other.

In this case the using of the surface plastic deformation (SPD) like a method for finish processing is suitable. SPD as the quality of the machining surface and its exploitation features as higher productivity [1, 2].

There are known one-roll tools for SPD which have a simple construction but their application is limited because some failings [3, 5]:
- over the technological system machine - appliance – tool – detail (MATD) there are applied one-way deformation force, which creates deformation circumstances in  MATD. In its turn this is a cause for appearance of processing mistakes [3, 4];
- availability compulsory  two movements (axis and radial) through start and end work of the tool.
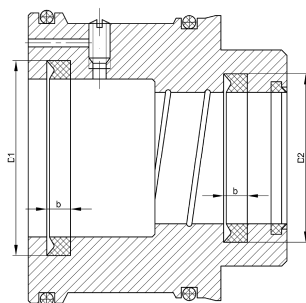


*Fig. 1. Detail set*

In the production program of a company "Hydraulic Elements and Systems" – Yambol there are details from type „Obturator" (Fig. 1). To the grooves of this type details laid down requirements of precision and roughness.

## EXPERIMENTAL DETAILS

The suggested tool is designed for grooves machining of details from GS20. These grooves are intended for putting rubber packs, which must ensure hermetical with wide range fluid pressures. It follows that comparatively high requirements for the roughness of the cylindrical surface of the groove, which are impossibly to be reach by using of the extant technological process - double turning, this can't ensure the demanded roughness from plan Ra = 1,25μm.

For removing mention shortcomings of the one-roll tools for SPD it is developed a tool which is shown on Fig. 2 in start position. It is two-rolls, without separator, with hard action, adjusted and it has following main parts: body 4, in which are assembled the carriers 23, with fitted in deformation rolls 20, by the stems pivots 22 and the insertions 21, bearing cotter 13, pegs 15 and 18, thrust bearing 19, cup 1, stop 2, nuts 7 and 9, stopper 5, washer 6, springs 17 and 25, insertions 10 and 12, screw special 24, cup 14, tail-end 16, screws 3, 8 and 11.

This tool hasn't mentioned disadvantages and it can use with a different machines. Through its design the following requirements are took account of: possibilities for exploration as in horizontal as and vertical position; technological of the design; possibilities for hand applying of the deformation force; possibilities works like immovable and turning tool.

The reciprocal corner location of the body 4 and the cup 14 toward the bearing cotter (it is cut through because the peg 18) is fixed with the cylindrical pegs 18 and 15. The carriers look like prismatic devices with possibility for radial moving in corresponding guides of the body 4 and they are constantly pressed to the bearing cotter 13 through springs 25 and the special screws 24. They support the cylindrical deformation rolls 20, which bear over the bronze insertions 21, they are immovable toward pivots 22. The distance between the detail joint to the groove is adjusted by the nut 7, which with the thrust bearing 19 determines the axis location of the stopper 5. The work adjusting dimension of the tool (the radial position of the rolls) is determined from the position of a nut 9, which is fixed with a screw. For protecting from contamination there are ensure the cup 1 and insertions 10 and 12.

The two-roll tool works in the following sequence.

In a non-work position under the action of the spring 17, the cup 14 and the bearing cotter 13 hold right end position toward the body 4, and the carriers 23 are located over most narrow part of the cotter. It is realized a turning moving of the spindle and through axis feed the tool is free get in the cylindrical hole of the detail. In the moment when the joint of the stopper 5 touches the detail joint the stopper 5 stops its turning because the availability of the thrust bearing 19 and the deformation rolls are locates opposite the groove, which has to machining. With continuous feed moving the bearing cotter is moved toward the body 4 while the cup 14, bending the spring 17, reaches to the nut 9. Besides the rolls are moved radially till to adjusting dimension of the tool and they are pressed to the bottom of the groove and in this way the rolls machine the groove. The deformation forces are got mainly on account of the elastic deformations, which are due to the difference of the groove diameter and adjusting dimension (tightness).

The going out of the tool is made in opposite turn, as under the action of the springs 17 and 25, the bearing cotter 13 is moved and the rolls 20 are took into the body 4. In this way it is accomplished the machining on the vertical position with the work on the scheme „immovable detail – turning tool", through the tool settle down with its tail end 16 into the machine spindle.

When it is worked in a horizontal position the scheme is „movable detail – immovable tool". Through this scheme the detail is made only the turning movement and the tool only axis feeding movement.

The groove parameters are: diameters $D_1 = 70$ mm and $D_2 = 60$ mm; a width $b = 10$ mm. The dimensions limits are respectively $T_{D_1} = T_{D_2} = 0,190$ mm and $T_b = 0,2$ mm.

For checking the technological possibilities of the tool and determination of the work regime with the tool is held the appropriate experiment. 30 pieces patterns put to the examination. They are received from the factory-producer with cut through grooves. Because of this that the groove dimensions don't allow directly controlled of the machining precision and roughness, the patterns are separated in two groups by 15 pieces. The patterns of the one of the groups are made additional cut through and in this way it is ensured free access to the cylindrical surface of the groove.

For controlling the mention parameters are used two measurement devices – universal length-measures and profilometer – profilograph TALYSURF-6.

In this way it is accomplished the measuring of the receiving in the factory-producer roughness respectively $Ra = 2,2 \div 3,4$ μm and fringing field of the diameter $\omega_D = 0,153$ mm.



*Fig. 2. Two-roll tool for groove machining*

The patterns from the second group are machined through SPD with the help of a vertical drilling machine BK-32. The adjusting dimension is ensured through hand

pressing with the flywheel of the drilling machine, of the putted into the spindle tool toward to the detail joint. As lubricant is used a combination from engine oils M10D, LT-2T and naphtha in proportion 1:1:5. It is feed through the cooling system of the drilling machine and at the same time helps as for taking out the chipa as for lubrication of the deformation rolls and the machining surface. The measuring of the machining surfaces after cut through of the patterns shows that the fringing field of the diameter $\omega_D$ don't change materially and it has a value $\omega_D = 0,142$ mm. The roughness is decreased to Ra = 0,64÷0,85 μm depending on the magnitude of the adjusting dimension (tightness) and numbers of passages (numbers turning of the tool m).

It is determined that the minimum roughness is received with maximum tightness C = 0,16 mm) and numbers turning m = 5. The increasing of the numbers turning m over five don't influence materially on the roughness.

With advisable regime: tightness C = 0,1 – 0,16 mm, numbers turning of the tool m = 5 and frequency of turning n = 180 min$^{-1}$, the single time for machining is 0,2 min.

The hydraulic tests, which are took over the product with build-in details and machining with the described tool, are get very good results in relation of the hermetically of the  observed compounds.

## CONCLUSIONS

From the accomplished experimental examination it can do following conclusions:
- the accomplished technological  research proves the working capacity of the creating tool.
- the roughness measuring on the parameter Ra is decreased  approximately 1,5 parts in comparison with the  advisable at the plan.
- the dispersing of the roughness parameter Ra after SPD is due to as the fluctuation of the deformation force (because of the sizable limit of the diameter) and the hard action of the tool as the dispersion of the initial roughness.

## REFERENCES

1. Георгиева Н.А., Кършаков М.К., Стефанов Г.Д.: *Самоустановяване на разстъргващ блок с праволинейни режещи ръбове*. Научно-приложна конференция с международно участие, Ямбол, 2003.

2. Григоров В.И., Кършаков М.К, Костадинов С.В.: П.П.Петров. *Плаващ блок със значими еластични свойства и два срещуположни, осово разместени режещи елемента*. Научни трудове на РУ ”А.Кънчев”, Русе, т. XXXXV, с.2, 2006, с. 40 - 42.

3. Костадинов В.С., Кършаков М.К.: *Повишаване качеството на вътрешни цилиндрични повърхнини обработени чрез повърхностно пластично деформиране*. Девети младежки симпозиум, Пловдив, 1977.

4. Стефанов Г.Д.: *Изследване износването на шийките на коляновите валове на двигатели*. Селскостопанска техника, №5, 1998.

5. Григоров В.И., Костадинов С.В.: *Особености на схемните варианти за комбинирано обработване на гладки валове, обусловени от разположението на изпълнителните елементи в деформиращ или режещо-деформиращ плаващ блок*. Научни трудове на РУ ”А.Кънчев”, Русе, т. XXXXI, 2004.

## Vasil KOSTADINOV

Rousse University „Angel Kanchev", Bulgaria

# COMBINED TOOLS FOR SURFACE PLASTIC DEFORMATION WITH RADIAL FEED

*Like a method for a finishing processing, the surface plastic deformation improves the exploitation characteristics of the machining surfaces and increases their qualities. Moreover – it achieves sizable decrease of the machining times in comparison with the other finishing methods. The using of combined tools creates circumstances for simultaneously processing with the prior machining, which leads to augmentation of the machining productivity.*

## INTRODUCTION

As a method for the finishing processing the using of the surface plastic deformation (SPD) increases the machining surface quality and improves their expiation characteristics. Moreover it achieves sizable decrease of the machining times in comparison with the other finishing methods [1, 4].

The combining of the prior and finishing machining, (cutting and SPD) leads to using of the combined tools for SPD. They create circumstances for augmentation of the machining productivity of the finishing processing through preservation of the method SPD.

There are known combined tools, compounded from cutting (CM) and deformation (DM) modulus. The deformation module looks like a tool for surface plastic deformation with axis feeding of the deformation elements [1, 2]. Despite comparatively its wild application there are presences of some failings, which is due to the machining scheme and kind of the deformation module [3, 5]:

-  the combined of the two process lead to considerable difficulties through determination of optimum, for each of them, regime elements when they machining simultaneously with realization of the finishing и processing.

## EXPERIMENTAL DETAILS

The combined tool, which satisfies mentioned above circumstances, is shown on Fig. 1. It consists of cutting and deformation modulus, each of them is formed according to the circumstances of the combined machining.
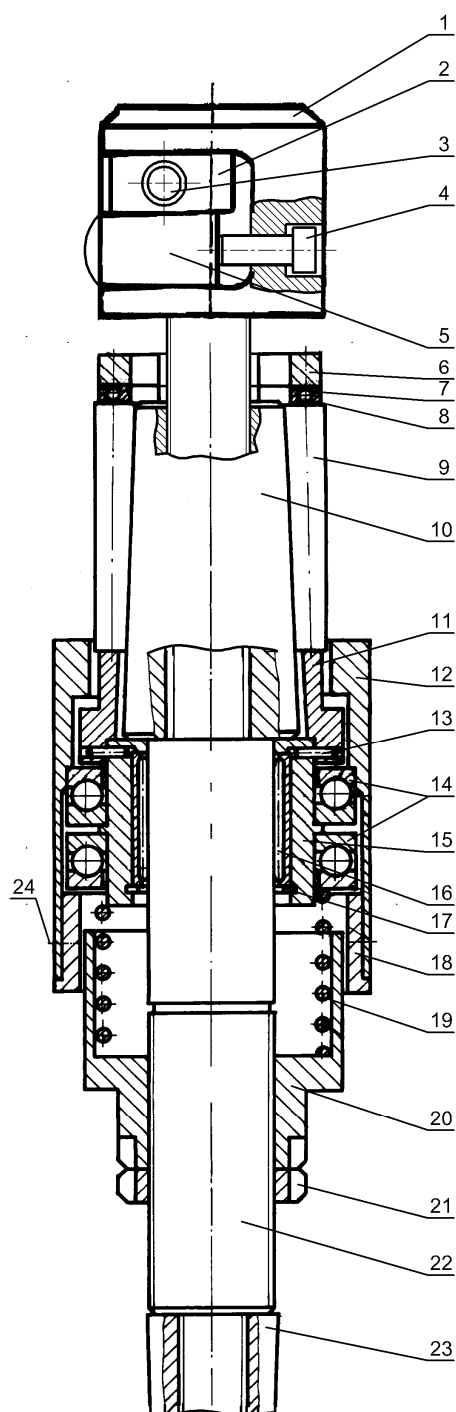
*Fig. 1. Tool for combined machining with radial feed*

For ensuring productivity of the cutting process and as envisage kind of the machining materials, into the deformation module 1 there are used carbide cutting insert 5 with big nose radius. The insert is laid in special socket, machined in the cutting module 1. Its fixture is made through a pressed cotter 3 and the screw 2. The dimension adjusting is made through a screw 4, after the vacation of the cotter 3 and unwinds of a screw 2. After the dimension adjusting of the necessary position its invariability establishes through the screw 2 and the pressed cotter 3. The cutting module is assembled toward the deformation module through thread.

The deformation module looks like a tool for SPD with radial feeding of the deformation elements. These elements are long conical rolls with a length longer than the length of the machining hole.

The deformation module consists of: conical deformation rolls 9, laid in the slots of the separator 11, fulcrum cap 12 fixed through screws, thrust bearings 14, spring 19, adjusting nut 20 and back nut 21, located over the bearing shaft 22, quil bearings 16, laid in a bush 15, which by the pins 13 is made as a whole with a separator 11, bearing cone 10, cap 6, balls 7, separator 8 for balls 7.

On the free end of the bearing shaft 22 there is step, toward which through thread is assembled tail-end with necessary joint dimensions for the relevant machine.

The tool shown in Fig. 1 is on non-work situation. The dimension of the deformation module (the diameter of the described circumference around the rolls) is smaller than the finish diameter of the machining hole.

Advantage of the suggested combined tool is that it can work as in horizontal as and in vertical position. Furthermore it will be with turning or immovable bearing shaft (respectively cutting module). In all these cases the cutting module is adjusted on dimension in advance through the help of an appliance. If need be it does precise adjustment through the screw 4.

When it works over the machines from the group of the lathes the detail does the main turning movement and the tool – axis feeding.

The tool action is the following:

Through entering into beforehand turned hole, the tool works like ordinary skiving rod for finishing cutting. This allows the choosing of optimum cutting regime. It is realized through bigger feed, because of the using of a carbide cutting insert with big nose radius. The continuing feeding leads to movement of the bearing shaft 22 toward the separator 11 and this cause of the spring 19 when the joint end of the fulcrum cap 12 reaches to the joint end of the detail. The bearing cone 10 push out the deformation conical rolls 9 in radial between the conical surface of the bearing shaft 22 and the detail, it creates a possibility for relative turning of the separator toward the bearing shaft 22 and the rolls do planetary movement as in this way machining the surface simultaneously through the all length. The process SPD takes ordinarily 2 – 3 full revolution of the separator, which is too small in comparison with the single time for accomplishment of the transition.

The deformation process continues till the full flexion of the spring 19 and touching of the adjusting nut 20 the joint surface of the axis bearing 14. What dimension will receive after proceeding depend as from the dimension of the prior machining as from the adjusting dimension for SPD. It is achieved through moving of the adjusting nut 20, which limits the motion of the bearing shaft 22 and increases or decreases the tightness (the tightness is an element of the machining regime by SPD).

When the machining is stopped, the tool is returned on rapid traverse and under action of the spring 19 the separator 11 with the deformation rolls 9 are in a starting position for a new proceeding. When it works over the drill machines the combined tool does as a main movement as and feeding movement.

For determination the technologic possibilities of the tool it is accomplished an experimental examination with cast-iron details, received from factory-producer with in advance drilled holes. The machined hole has a diameter Ø60H7.

The preliminary cutting and the combined machining are realized on the turning lathe C11MB. The tool is located into a device which is assembled over the cross lathe carriage.

With the cutting module it is used P10 (T15K6) with nose radius R = 18 mm and geometry $\alpha_o = 8°$, $\varkappa = 8°$, $\lambda_s = 0°$.

It is used the following regime of cutting: speed V = 126 m/min; feed f = 1,25÷1,5mm/tr and depth a = 0,2÷0,3 mm.

Because of the tool for SPD is with hard action, the deformation force is due to the negative difference between its work diameter (the diameter of the described circumference around the rolls) and the hole diameter. The tightness fluctuation is due to the dispersing of the dimension of the prior machining. The revolution number of the separator (m) is chooses according to effectiveness of the rate frequency the deformation act applying.

As deformation rolls are used conical deformation rolls with a length l = 90mm, large diameter to the joint surface of the rolls d = 0,98 mm and angle in the vertex of the rolls $\alpha_p = 3°4'$.

It is used the following regime of SPD: tightness 0,05÷0,08 mm; frequency of turning 1000min$^{-1}$ and numbers turning of the separator m = 3.

As lubricant is used a combination from engine oils M10D, LT-2T and naphtha in proportion 1:1:5. It is feed through the cooling system of the turning lathe and at the same time helps as for taking out the chips as for lubrication of the deformation rolls and the machining surface.

Through described circumstances a consignment from 50 details are machined. They are cut consecutively with the same adjusting dimension of the tool and after control of the roughness and the diameter it is done SPD and after that it is controlled again the mentioned quality characteristics.

The measuring of the precision of the hole diameter is done with indicating calipers and the control of the roughness by the parameter - with profilometer – profilograph „TALYSURF-6".

## CONCLUSIONS

The measuring results are done statistical through the help of PC and program „BBSTAT". There are got the following numerical characteristics:

|  | cutting | SPD |
| --- | --- | --- |
| - spread, $R$ | 0,059 | 0,0578 |
| - average arithmetic, $\overline{X}$ | 0,031 | 0,0256 |
| - mean square deviation, $S[X]$ | 0,013 | 0,011 |
| - dispersion, $S^2[X]$ | 1,44 | 1,26 |
| - asymmetry, $\chi_1[X]$ | -0,17 | -0,795 |
| - excess, $\chi_2[X]$ | -323,33 | -270,08 |

In keeping with got numerical characteristics by the Pirson criteria it is proved normal or logarithmic-normal distribution.

It is obvious that after SPD the dispersing field is narrowed approximately 1,2 times. The roughness is improved from Ra=3,8÷5μm to Ra = 0,5 ÷ 0,6μm, this can't ensure with till now the applied reaming

## REFERENCES

1. Григоров В.И., Кършаков М.К., Костадинов С.В.: *Особености на схемните варианти за комбинирано обработване на гладки валове, обусловени от разположението на режещи елементи с праволинейни режещи ръбове в плаващия блок*. Научни трудове на РУ "А.Кънчев", Русе, т. XXXXI, 2004, с. 139 - 146.

2. Костадинов В.С.: *Относно крайщния ефект при инструменти за ППД работещи с радиално подаване*. Н.тр. ВТУ, Русе, 1986.

3. Кършаков М.К., Георгиева Н.А., Костадинов С.В.: *Инструмент за комбинирано обработване на отвори*. "Механика на машините", ТУ-Варна, кн. 6, 2005, с. 86-89.

4. Кършаков М.К., Григоров В.И.: *Моделиране разпространението на пластичните деформация при обработване с ППД с инструменти с еднократно или периодично радиално подаване*. сп. Машиностроене, 1993.

5. Стефанов Г.Д., Кършаков М.К.: *Определяне на микроструктурата и микротвърдостта на образци от цилиндрови втулки с различна довършваща обработка*. Сборник доклади от ЮНС'99, НИММЕСС-София, т.7, сер.1, 1999.

**Valerii KYRYLOVYCH**
**Oleksandr PIDTYCHENKO***

Institute of Business and Advanced Technologies, Ukraine
*Zhytomyr State Technological University, Ukraine

# AUTOMATED TECHNOLOGICAL EQUIPMENT LAYOUT IN INDUSTRIAL ROBOTS' WORKING AREA HAVING COMPLICATED SHAPE

*The conception and methods of computer-aided solution of flexible manufacturing cells technological equipment layout relative to industrial robot (IR) with optimization by a set of accepted criteria are presented. The software realization of this task for IR having working area (WA) of complicated shape is presented. The idea of surface analytical description of IR WA having complicated shape and interactive editor for its computer-aided forming are presented.*

## 1. INTRODUCTION

One of the directions of machine-building and instrument-making automation based on robotic technologies usage is Flexible Manufacturing Systems (FMS) introduction. At other side, designing FMS and their components is the complicated, multi-variant and laborious task that demands the taking into account a substantial quantity of technical and economical demands, criteria and limitations [1, 2, 9]. At the same time the especial significance lies in that the hierarchical makeup of FMS, containing flexible manufacturing modules and flexible manufacturing cells (FMC) in various combinations, and the presence of the set of technological, transport, geometrical, energy and other ties between components determine the FMS as the complicated technical systems [9]. All of this points to the advisability and urgency of the computer-aided design means development of the FMS and their components, that allows to decrease the designing laboriousness significantly and at the same time to increase the quality of assumed decisions.

While designing new flexible mechanoprocessing productions and robotization of the existing productions, one of the important tasks is the technological equipment (TE) layout within FMC serviced by industrial robots (IR) [1, 2, 8]. At the same time layout optimization can be fulfilled on such parameters as: total distance between TE units or IR manipulation trajectory reference points; IR cycle manipulation trajectory length considering TE servicing sequence; productivity indices; IR working cycle total

power inputs indices; square occupied by FMC etc [1, 9]. This task feature is the <u>necessity of taking into account</u> the sets of technical and technological demands for TE operation, <u>geometrical limitations</u> for some or all TE units layout, and also <u>technical and technological ties</u> between individual equipment units while TE place definition (i.e. at layout realization). For the last ones belong, for example, workpiece processing technological route (WPTR) and accepted strategy of TE servicing that determines IR movements makeup (IR actions sequence at TE transport servicing) and cycle trajectory [4]. At that time, just as while solving many other applied tasks of layout (for example "close packing" tasks type), the efficiency of the obtained solution depends on the sequence of the objects (TE units at this case) are placed. All of that determines the task of TE layout as <u>discrete optimization task on permutations with limitations presence</u> [7, 9, 10].

Thus, the <u>aim</u> of this work is the presentation of the proposed conceptual approach, methods and software realization of computer-aided FMC TE layout with taking into account the set of criteria, factors and limitations, that reflect problem domain features.

## 2. THE PROBLEM STATE AND LAST PUBLICATIONS ANALYSIS

In the most of literature sources about mechanoassembly and mechanoprocessing FMS [2, 8, 13] the conceptions of FMS and their components are given, reviews of structures, schemes and descriptions of their functioning are given also, but the attention to the problems of designing, especially computer-aided, is not given enough.

In some literature on problems of mechanoprocessing FMS and FMC designing and work organization [1, 7, 9] the important place is given to the problem of TE layout relative to IR, that fulfills TE transport servicing – the moving of object of production (workpiece) between TE units: taking from input storage or previous mechanoprocessing position, moving to the next TE according to WPTR, setting the workpiece for the next operation fulfillment and further taking it for moving to the next processing position or into output storage.

In particular the contents and task statement of designing robotic technological complexes (RTC) are covered in [1], and in contents of this task the place is shown and the task statement is formulated for equipment layout plan building (further it's named <u>TE planning</u>). Taking into account that RTC are similar for FMC structure units of FMS, further only FMC are spoken about, considering that all regarding to RTC is right for FMC. In [1] the <u>TE arrangement variants</u> (linear, polar; with common or separate inputs/outputs; one/two line etc) are considered, the organization of transport-accumulating system of FMS, able to cooperate with FMC servicing IR, is discussed. Two types of FMC basic arrangements are presented. They determine <u>two possible TE layout criteria</u> concerning IR cycle trajectory: the arrangement with <u>minimal quantity of positioning points</u> (MQPT) on every IR degree of freedom – for IR with cycle control systems, and the arrangement with <u>minimal movement trajectory length</u> (MMTL), that is determined as minimum of the sum of distances between adjacent IR trajectory movement reference points: IR gripping device (GD) entrance/exit points to/from TE work area (WA) relatively to adjacent TE, and also end points of workpiece set/taking moves in TE. The question of presence of several IR in FMC and TE orientation variants regard to trajectory of IR movement between adjacent TE units, i.e. trajectory of inter-aggregate movement (IAM), is considered. The sequences, schemes and algo-

rithms of FMC designing and TE layout in FMC with one IR are proposed. At that time it is mentioned about <u>layout sequence influence on result indices</u>, particularly on IR trajectory length. Generally to the task of FMC planning such stages are included: TE layout sequence choice, TE orientation regard to IR choice, building of IR trajectory parts near every TE unit, linear or polar plan designing, assembling the FMC with separate parts, each of that contains one TE. It's also marked that <u>geometrical agreement of TE units</u> and IR includes two demands: compatibility of GD moves with set/taking direction in TE and the absence of IR collisions with TE. However the question of <u>IR accessibility of necessary trajectory point in TE is not covered</u>, i.e. the task of ensuring of TE hit to IR WA, that is enough urgent question if the IR WA is not rectangular in vertical profile (normal to movements between TE). Further let name such WA as <u>complicated shape WA</u>. For such WA <u>TE placing height and depth</u> (distance from IR IAM to TE in horizontal plane) <u>are interrelated</u>. The variation of one of these values can determine different summary length of IR trajectory parts on height and to TE depth.

In [7] the question of TE layout in FMC in general is covered, also two variants of this task classification at the mathematical point of view are given: as <u>linear or quadratic task on assignment</u>. Although a number of comments and recommendations to this task are given, the methods of its solution are not covered.

In [9] the question of TE layout is covered on the FMS workshop layout level, at that time the tasks of TE transport servicing are also covered not on IR level, but on the level of FMS workshop transport system interaction with individual production divisions. So the question of TE layout regard to IR inside certain division is not covered. However a number of allied tasks are considered that mathematically are <u>combinatorial tasks of discrete optimization</u>. In [9] the task of TE layout is put to the tasks of FMS organization-technical structures synthesis tasks that in general include building arrangements structures, TE layouts and organization of transport servicing. A number of criteria and limitations at the solution of given tasks are marked.

The tasks of TE layout automation are considered in a number of works [3, 6, 10, 11, 12]. Particularly in [10] among others the tasks of optimal layout of robotic divisions (similar to FMC) inside workshop FMS on the minimum of transport movements' criterion are solved. The task is classified as discrete optimization one on permutations. In the works [3, 6, 11, 12] the task of computer-aided TE layout regard to IR having either Cartesian rectangular or polar coordinate system (CS) in horizontal plane is solved, i.e. in any case the vertical profile of IR WA is either a rectangular or a ring.

Thus, <u>the task of computer-aided TE layout regard to IR</u> having <u>complicated shape WA</u>, for example, portal-type IR with horizontal axis of cylindrical or angular CS (the profile is limited by the curves of second degree), spherical CS etc, <u>is urgent</u>. At the same time it is necessary for definite layout sequence to place TE as close as possible, and also to get minimal possible sum of moves length on height and in horizontal towards TE. It's advisable <u>to search the optimal TE layout sequence</u>, but not on minimum of IR cycle trajectory length, but <u>on final productivity indices</u>. For this, in previous works [4, 5] the FMC model for the tasks of TE layout, servicing organization and simulation (for the aim of determining productivity indices of FMC variants being synthesized) was presented.

## 3. THE CONCEPTION OF TE LAYOUT AND ITS COMPUTER-AIDED REALIZATION

The solution of TE layout task (Fig. 1) supposes determining the position and orientation of every equipment unit in regard to IR that are servicing them, and also coordinated of IR manipulation trajectory reference points coordinates inside equipment units WA and near them (points of entrance into WA start and WA exit end). At the same time <u>manipulation trajectory</u> is first approximation of the way, gone by every workpiece from the entrance to FMC in state of slug till exit from FMC in state of processed part and is the union of IR GD movement parts inside TE WA (local and regional IR moves), entrance and exit in/out of TE WA parts (regional moves) and IR inter-aggregate movements (global moves). In contents the <u>layout task</u> lays in determinating the FMC arrangement scheme (i.e. determined set of geometrical places for TE units and their orientation), TE layout sequence (variant of correspondence of TE units to reserved places for them), coordinates of TE characteristic (tying) points in IR CS and coordinates of IR manipulation trajectory reference points.
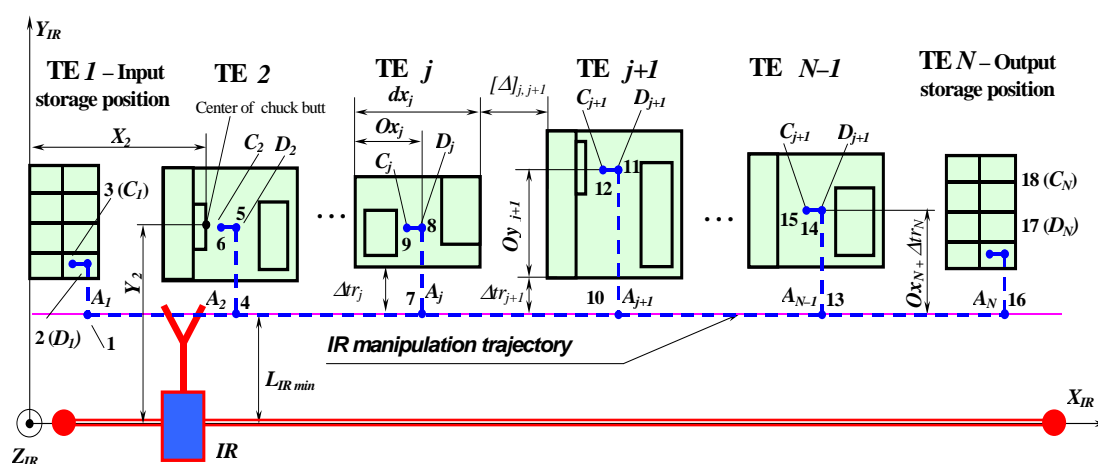


*Fig.1. Conception of TE layout*

The <u>FMC arrangements scheme</u> is determined by the IR WA form and its kinematics, particularly by the possibilities of geometrical realization of TE servicing when its layout in individual IR WA points. TE arrangement scheme defines the demands to relative mutual TE layout and TE units' orientation regards to IR. Different <u>TE layout sequence</u> by coordinate X near IR (variant of assignment of every TE unit on reserved places) determines different length of IR IAM trajectory parts, different length of the total cycle IR GD movement trajectory (considering the sequence of TE servicing by IR), and that's why influences on FMC work cycle duration. This is resulting from different geometrical sizes of individual TE units and different demands to minimal distances between adjacent equipment units. The <u>existence of TE layout sequence</u> when either the minimum of IR movement trajectory length in work cycle, or minimum of work cycle duration, or energy costs minimum etc are reached, creates the research area for optimal layout sequence.

At the Fig. 1 are marked: points $A_j$ – IR IAM trajectory on the start of the entrance to TE WA; $D_j$ – points of the end of the entrance to TE WA and the ones of start of the setting move; $C_j$ – points of the end of workpiece setting move. It is evident that three

coordinates describe every point: $A_j (Ax_j; Ay_j; Az_j)$. The positions of TE units are defined by the coordinates of chuck butt center (CBC) point in the IR CS  (X, Y, Z). It's worth to mark that while TE placing it's necessary to ensure minimal needed spaces between different TE units (in Fig. 1 – $[\Delta]_{j, j+1}$), and also between TE units and IR GD movement trajectory $\Delta tr_j$ (in consideration of making possible to service TE technically and absence of the risk of IR GD collisions with the equipment during movements). Coordinates X of the points are interrelated. If it's defined the previous TE coordinates, then the IR trajectory reference points and the next TE coordinates are defined:

$$Cx_j = X_j + P; \quad Dx_j = Cx_j + W; \quad Ax_j = Dx_j; \quad X_{j+1} = X_j + (dx_j - Ox_j) + \Delta_{j,j+1} + Ox_{j+1},$$

where P – distance between workpiece point of gripping by IR GD to its left butt-end; W – space between workpiece left butt-end and TE chuck butt before setting the workpiece; $dx_j$ – the TE length by X; $Ox$ – distance from the left end of TE to the center of its chuck butt.

The determination of Y and Z coordinates are much more complicated and depends on IR WA vertical profile shape. For analytic description of WA of any shape the next statements are adopted: WA surfaces, near and far relatively to OZ axes along Y axes, are described separately (the first is named "near face", the second – "far face"), the faces are approximated either by planes or by cycle cylinders; if the description of the faces by the vertical line is ambiguous then all the WA is separated along Z axes into layers (zones), inside ones both near and far faces are described unambiguously. It's necessary to mark that there is only one near face and only one far face allowed to be at some horizontal plane.

The realization of geometrical layout on coordinates Y and Z, i.e. determination of TE geometrical coordinates relatively to IR by the height and in horizontal plane from IR towards TE, inseparably linked with the demands for manipulation trajectory, that, as was said above, come to two criteria – MMTL (see Fig. 1) and MQPT of IR GD. At the proposed work the MMTL is realized that supposes for IR WA of complicated shape the preliminary finding on accepted height of placement $Az$ the Y-coordinate of IAM trajectory pass, that is determined by the coordinate of the edge of crossing the IR WA near face on the height $Az$ by horizontal plane. From the coordinate $Ay$ it is necessary to indent the minimal allowed distance $\Delta tr_j$ and to add the distance by Y from the point of TE CBC towards front edge of the TE. If the got coordinate TE $Y_j$ comes out of WA far face, then the equipment must be moved up or down till hit to WA if such is possible. If there is such TE unit that cannot be put into WA at any start height $Az$ it means that this equipment cannot be placed.

It's adopted that vertical profile of IR WA doesn't vary along X axes. In such case the tasks of placement by coordinates X and Y-Z can be fully separated, because they are not interrelated geometrically and there are different optimization criteria used at them. So it is possible to make optimal placement of TE units in Y-Z plane by criterion of minimal total distance between IR movement trajectory reference points, and optimal placement by X (on the set of layout orders) according to criteria of best productivity indices.

## 4. COMPUTER-AIDED PREPARATION OF SOURCE DATA

Because the computer-aided TE layout supposes the presence of analytical description of IR WA surfaces (near and far faces), so the means of <u>computer-aided forming surfaces equations</u> are necessary, that is realized in the designed visual IR WA editor (Fig. 2) in limits of proposed software product. The surfaces are described in general case by algebraic equations of second degree including variables Y and Z.
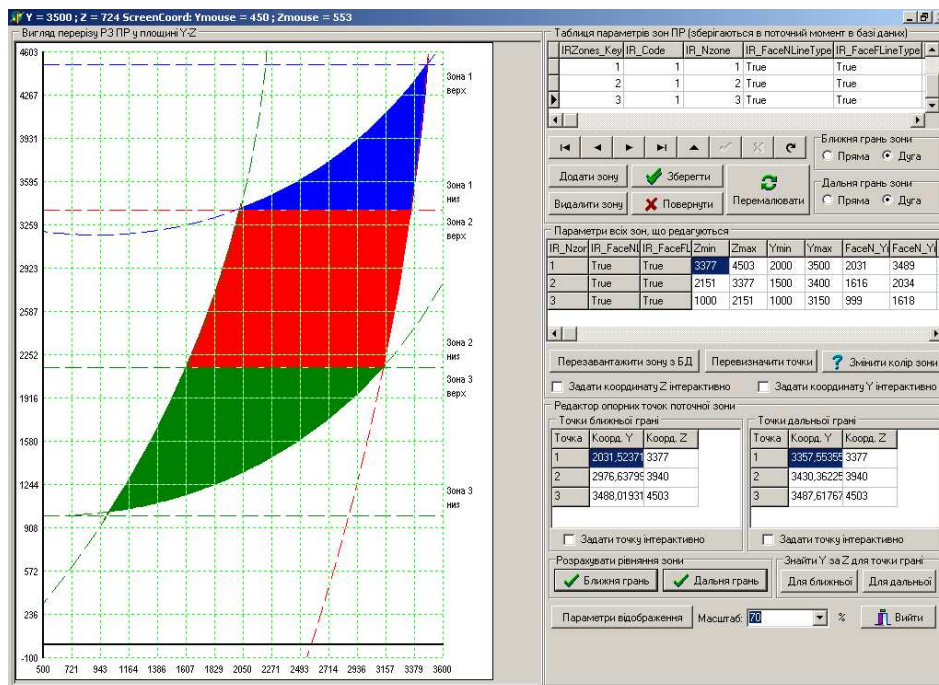


*Fig.2. Visual editor of IR WA*

The editor allows to create/delete zones, set interactively (by computer mouse or by number entering) the limits of zones at the height Z and depth Y, then specifying reference points of straight lines (two ones) or arcs (three) of the profile, to form the face equations automatically and to save them in IR database (DB). The editor allows creating, editing and viewing at various scales the IR WA profiles practically of any shape. The profile of IR WA can be drawn filled with colors or not. When running editor the proposed reference points of faces are calculated according to zones' equations and can be edited. The changes, made while editing can be saved in DB or canceled. For the polar CS the polar angle can be interpreted in a similar manner as coordinate X.

## 5. THE SOFTWARE REALIZATION OF TE LAYOUT

The work with software starts with forming the composition of TE in FMC (from the primary and auxiliary TE DB), forming orders of TE units' succession along X axes (all possible *n!* orders can be formed for *n* TE units, also any orders can be added or deleted) and the choice of IR from the corresponding DB (Fig. 3). The DB files used by the software are: IR DB, IR WA description DB, primary and auxiliary TE DB, TE orders DB, and DB where results of layout are saved (DB with placement by Y-Z and DB with placement by X according to TE orders).

*Fig.3. Screen forms for setting source data*

The layout is fulfilled after pressing the buttons "Place TE" or "Look over all orders". At the last case the layout task is solved for all formed layout orders. As a result we have the DB with TE coordinates for all proposed heights *Az* of IR IAM, the chosen variant that has minimal sum of the moves by Y and Z, and also the results of placement by X axes for the best variant of placement by Y-Z (Fig. 4). When some TE has too high CBC point then all other TE and IR are lifted for necessary height.



*Fig.4. Screen forms with results of layout*

## 6. RESUME

At this moment the software allows to fulfill the TE optimal layout for linear arrangement. For the polar arrangement the determination of polar angle calculation procedure is necessary. Early developed methods and algorithmic basis of forming service routes and simulation [4, 5], that are also implemented in the developed software product, allow to fulfill FMC work simulation and determinate productivity indices for the aim of choice the satisfactory or the best TE layout variants.

## REFERENCES

1. Бурдаков С. Ф. и др.: *Проектирование манипуляторов ПР и роботизированных комплексов.* С.Ф. Бурдаков, В.А. Дьяченко, А.Н. Тимофеев. – М.: Высш. Шк., 1986, 264 с.

2. Довбня Н. М., Кондратьев А.Н., Юревич Е.И.: *Роботизированные технологические комплексы в ГПС*. Л.: Машиностроение. Ленингр. отд-ние , 1990, 303 с.

3. Івахненков Ю. В., Кирилович В. А. , Сачук І. В.: *Автоматизоване формування траєкторії переміщення схвата агрегатно-модульних промислових роботів за мінімумом точок позиціонування*. Вісник ЖІТІ. Технічні науки. Спеціальний випуск, 2002, с. 85–92.

4. Кирилович В., Пидтыченко А.: *Имитационное моделирование для определения производительности гибких производственных систем*. Systemy informacyjne w ksztalceniu tehnicznym. Red. Antoni Świć. Lublin: Wydawnictwa Uczelniane Politechniki Lubelskiej, 2005, s. 51–56.

5. Кирилович В.А., Підтиченко О.В.: *Склад математичної моделі гнучких виробничих комірок для задачі автоматизованого планування обладнання*. Оптимизация производственных процессов. №9, Севастополь, СевНТУ, 2006, с. 46–53.

6. Кирилович В. А., Сачук І. В.: *Геометричний аспект траєкторних задач роботизованих механоскладальних технологій*. Збірник наукових праць Кіровоградського державного технологічного університету. Техніка в сільськогосподарському виробництві, галузеве машинобудування, автоматизація. Вип.12. Кіровоград: КДТУ, 2003, с. 210–214.

7. Козловский В.А.: *Организационные и экономические вопросы построения производственных систем*. Л.: Изд-во Ленингр. ун-та, 1981, 216 с.

8. Козырев Ю. Г., Кудинов А. А., Булатов В. Э. и др.: *Роботизированные производственные комплексы*. Под ред. Ю. Г. Козырева, А. А. Кудинова. М.: Машиностроение, 1987, 270 с.

9. Лищинский Л.Ю.: *Структурный и параметрический синтез гибких производственных систем*. М.: Машиностроение, 1990, 312 с.

10. Романов В.А.: *Математическое и программное обеспечение задач выбора и размещения оборудования на участке машиностроительного производства*. Дис. ... канд. физ.-мат. наук: 05.13.11. Институт прикладной математики им. М.В. Келдыша. М., 1986, 133 с.

11. Сачук І.В.: *Автоматизований вибір агрегатно-модульних промислових роботів для ГВС*. Дис. ... к.т.н.: 05.13.20 / НТУУ "КПІ". К., 2005, – 227 с.

12. Ivahnenkov Y., Kyrylovych V., Sachuk I.: *Computer-aided determination of geometrical compatibility of aggregate-modular industrial robots and production machinery*. Zeszty Naykowe Politechniki Rzeszowskiej. № 196. Mechanika, z.59. Materialy III Miedzynarodowej Konferencji Naukowo-Technicznej, Modulowe Technologie i Konstrukcje w Budowie Maszyn. MTK 2002, Poland, Rzeszow, 2002, s. 173–183.

13. Keramas James G.: *Robot technology fundamentals*. New York, Delmar Publishers, 1999, 408 p.

**Kirill L. LEVINE**
**Jude O. IROH**

University of Cincinnati, USA

# INFLUENCE OF POLYPYRROLE ON CURING OF POLY (AMIC ACID)

*Polyimides are widely used in industry because of their excellent resistance to heat and very good mechanical properties. Electrically conductive polyimide composites are under focus of the research for application in electronics, aircraft and automobile industry. To prepare electrically conductive polyimides we used conjugated polymer: polypyrrole. The presence of conjugated double bonds in the composite resulted in intermolecular complexes with charge transfer. The presence of polypyrrole also affected an imidization temperature: the temperature of poly(amic acid) conversion to polyimide. In this paper imidization of poly(amic acid) was investigated by Fourier transform infrared spectroscopy, and differential scanning calorimetry. Morphological changes in polypyrrole/polyimide composite were studied by scanning electron microscopy. Results were explained by conformational changes in poly(amic acid) under the influence of polypyrrole.*

## INTRODUCTION

Polyimides (PIs) attract a lot of attention nowadays because of excellent perspectives of their application in nanotechnology. PI's with non linear optic chromophore groups find application in optical data storage [1], PIs with dopants, such as azo-dye, are suggested for holographic recording [2]. PIs have shown to enhance quantum dot luminescence properties [3]. Their composites with intrinsically conducting polymers (ICPs), such as polypyrrole (PPy), show considerably high electrical conductivity [4]. Composites of PIs and ICPs, obtained electrochemically, show the interpenetration of the components of the composite on molecular level. From the electrochemical behavior of the PPy/PI composite follows the appearance of charge transfer complexes between ICP and its matrix that allowed to discuss "doping" of PPy by PI, resulting in interesting impedance behavior as a function of applied potential [5]. Besides, PIs possess excellent thermal stability, very good chemical resistance, and excellent mechanical properties [6, 7]. High applied significance of the PPy/PI composite generated interest to the influence of PPy on PI processing parameters.

PIs processing involves so-called imidization, (Fig. 1), conversion of poly(amic acid) (PAAc) to PI by either chemical or thermal treatment.

Reduced activation energy results in lower temperatures of imidization and affects morphology of the resulting composite.
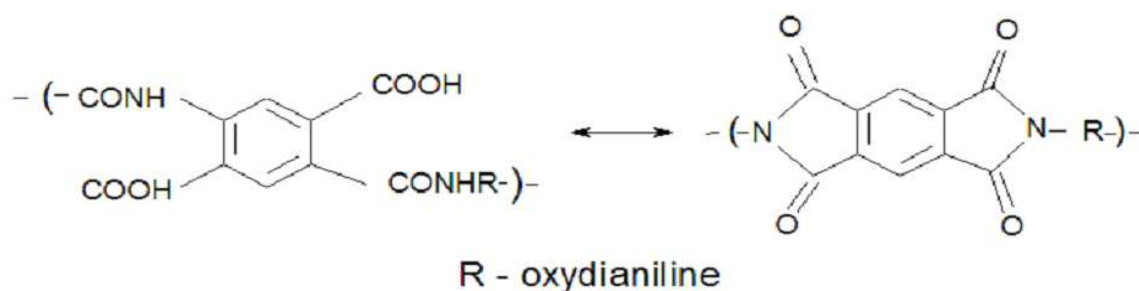
*Figure 1. Schematic representation of imidization*

Reducing the temperature and duration of imidization, the cost of manufacturing can be decreased. For these purposes low temperature curing agents were suggested [8]. In this paper we characterize the influence of PPy on activation energy of conversion of imidization by differential scanning calorimetry (DSC) and Fourier transformed infrared spectroscopy (FTIR).

## EXPERIMENTAL

*Chemicals*
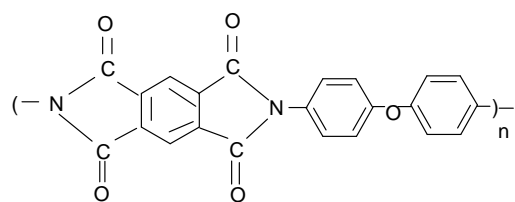


Pyrromellitic Dianhydride 4,4`-oxydianiline

PAAc of Pyromellitic Dianhydride 4,4` - oxydianiline was obtained from Dupont Chemical Company as a 13.8% solution in n-methyl-2pyrrolidone. All other chemicals were purchased from Aldrich Chemical Company and used as received without further purification.

*Apparatus*

Potentiostat-Galvanostat Princeton 273A was used for the electrochemical deposition. The reaction was monitored by Princeton Applied Research Electrochemistry Software version 250.

FTIR was carried out by Perkin-Elmer FTIR spectrometer. All the spectra were taken at a resolution of 4 cm$^{-1}$ from 4000 cm$^{-1}$ to 400 cm$^{-1}$ at a 50 scans for each sample in dry nitrogen atmosphere.

Scanning electron microscopy (SEM) was carried out by Hitachi S-4000 scanning electron microscope. SEM microphotographs were recorded on gold sputtered samples.

DSC was performed by 2010 DSC TA Instruments calorimetr. Analytical Instruments software was used for data acquisition and analysis. Samples for DSC were sealed in aluminum pans and equilibrated at 25°C for 10 min before each scan.

*Samples preparation*

**Preparation of the PPy/PI composite**

*PI coating*

PAAc additionally diluted with dimethylacetamide (DMAc) to 15% Vol (balance stock solution ) was subsequently cast and dried on the surface of stainless steel (SS)

working electrode. The solid contents of PAAc was chosen to form coatings of 20 - 25 μm thickness. Samples were air-dried at 50°C and imidized either thermally or chemically after the completion of drying. A schematic representation of imidization is shown in Fig. 1. Chemical imidization was performed by immersing PAAc coated electrodes into a mixture containing pyridine, acetic anhydride, triethylamine (TEA) and benzene in molar percent (N) composition: N-20/N/N+20/1.5N at room temperature [9]. In this mixture, pyridine performed an oxidizing function, acetic anhydride accepted proton. TEA suppressed isoimide formation to avoid brittleness of the film. Imidization was interrupted by taking samples out of mixture and placing them to benzene. Imidization was FTIR controlled. The desirable percent of imidization was achieved by interrupting the reaction at different time.

*PPy deposition*

Electrodeposition of PPy was carried out galvanostatically in a solution containing 0.01 M Py and 0.1 M $KPF_6$ in acetonitrile (AN). A single-compartment electrochemical cell was used for the deposition. It was comprised of the SS working electrode coated with PI film and the SS counter electrode. Saturated Calomel Electrode (SCE)[1] was used as the reference electrode. Current density of 1 mA/cm$^2$ was applied until the desired amount of charge passed. After the electrodeposition films were rinsed in AN for 10 min and air dried.

*Composite preparation*

To obtain the PPy/PI composite PPy was electrochemically deposited on bare stainless steel (SS) surface followed by cast and dry deposition of PAAc top coating. Samples were subsequently imidized thermally no later than 24 hours after the completion of PAAc drying. Thermal imidization was carried out by air heating to 350°C for 4 hours.

*Characterization*

Percent of imidization ($\alpha$) was determined from FTIR data as:

$$\alpha = \frac{[\dfrac{I_{1780}}{I_{1015}}]_{x\%}}{[\dfrac{I_{1780}}{I_{1015}}]_{100\%}}$$

Where:

$I_{(1780)}/I_{(1015)}$ - ratio of the intensity of imide peak to the intensity of standard peak, with subscript *x* related to studied sample, with subscript *100%* related to a sample where imidization was assumed to be completed. Hydrogen in the phenyl ring peak (1015 cm$^{-1}$) was chosen as a standard.

An activation energy of imidization was determined from the shift of DSC peaks made at different scan rates, as described for example in [10, 11] on the basis of the

---

[1] All the potentials were applied vs. SCE.

assumption that the thermal treatment during DSC experiment causes imidization. Although applied heating rate was rather fast (10 °/s or higher), imidization created well-resolved peaks on a thermogram. Heat flow (dH/dt) is proportional to the reaction rate, $d\alpha/dt$ [12]. The relationship between the rate of imidization $d\alpha/dt$ and the reaction rate constant $k$ that is given by the equation:

$$\frac{d\alpha}{dt} = kf(\alpha)$$

*(1)*

Coefficient $k$ is assumed to be in Arrhenius form:

$$k = k_0 e^{-\frac{E}{k_b T}}$$

(2)

where: $k_0$ - reaction factor, $E$ - activation energy, T- absolute temperature, $K_b$ - Boltsman constant, $f(\alpha)$ - functional form of $\alpha$ that depends on the reaction mechanism and for the 1st order reaction can be taken as (1-$\alpha$) [11].

By integrating Eq. 1 we obtain:

$ln(1 - \alpha) = kt$ (3)

By interrupting thermal imidization at different time coefficient k can be determined from the dependence of FTIR determined $\alpha$ vs. time of thermal imidization.

## RESULTS AND DISCUSSION

The morphology of the composite films depended on the time of PPy deposition and the time of chemical imidization.  Pure PI possessed smooth and uniform structure (Fig. 2). The structure depended on imidization time. It roughened at 100 s of PPy deposition in both cases of 1 h (80 %) and 4 h (nearly 100 %) imidization (Fig. 3) and 3(a)). The structure also depended on the time of PPy deposition proportional to the PPy amount. The increased time of PPy deposition caused an increased roughness of the surface (Fig. 3) and 4b).

FTIR spectra of PAAc with 20 % conversion without PPy and after different time of PPy deposition are shown in (Fig. 5). The PPy absorption bands in the PPy/PI spectra are mostly screened by the stronger PI vibrations. However, PI spectra attain some changes due to PPy. Spectra show that:

1) presence of PPy forced the appearance of imide peak at 1780 cm$^{-1}$.
2) PAAc shoulder at 1550 – 1580 cm$^{-1}$ disappears.
3) Intensity of central peak at 500 cm$^{-1}$ – 620 cm$^{-1}$ triplet increases significantly.

 (1) and (2) of the above indicated that the presence of PPy affected conversion to PI, shifting PAAc $\leftrightarrow$ PI equilibrium to the side of PI, (3) indicated interaction.
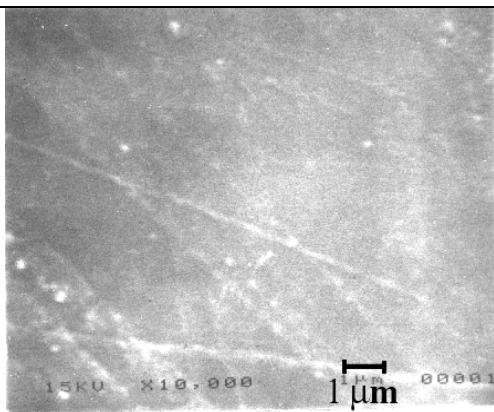
*Figure 2. SEM image of 100 % chemically imidized PI film*
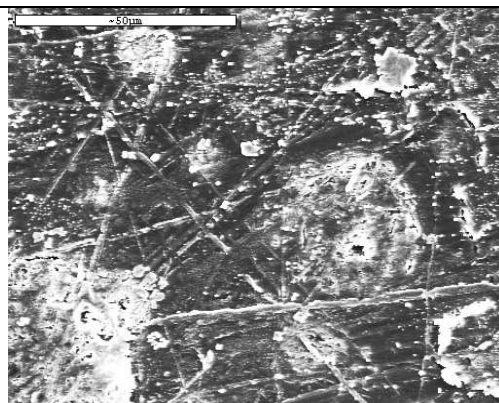


*Figure 3. SEM image of the PPy/PI composite [PPy deposition 100 s, chemical imidization 1 h]*

a)



b)
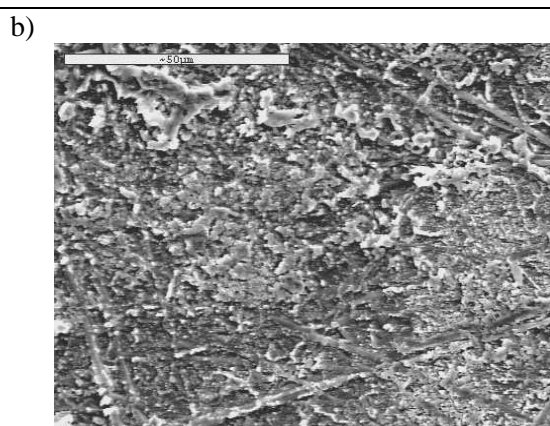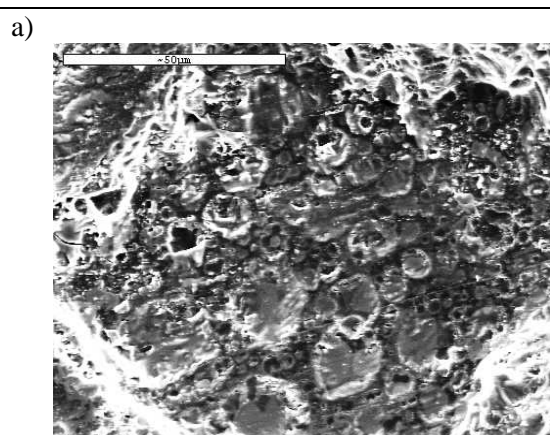


*Figure 4.  SEM image of the PPy/PI composite: a) PPy deposition 500 s, chemical imidization 1 h, b) PPy deposition 500 s, chemical imidization 24 h*

In Figure 5 wavelength shift for two different peaks is plotted as a function of an electric charge passes through unit area during PPy deposition. A wavenumber shift was observed for the absorption of C=C and C=O functional groups of PI molecule in the presence of PPy, (Table 1). The shift to shorter wavenumber (3520-3490 cm$^{-1}$) (Fig. 6), was possibly related to intermolecular hydrogen bonding between PPy and PI moieties. This effect was related to the polarization of $\pi$ electrons because of their high mobility along a polymer chain. In the case of hydrogen bonding, the whole molecular system gains resonance energy, which results in lengthening of the original double bonds [13].

Table 1. FTIR wavenumber shift observed in the PPy/PI composite at different amounts of PPy

| PPy amount, mg/cm$^2$ | Band, cm$^{-1}$ [14] | | | | |
|---|---|---|---|---|---|
| | $\beta$ CH=CH | $\nu$ C=0 in aromatic | $\nu$ C=0 | $\nu$ C=0 | $\nu$ C-N |
| 0 | 1350 | 1748 | 1712 | 1653 | 1088 |
| 3.6 | 1349 | 1748 | 1712 | 1653 | 1088 |
| 7.2 | 1354 | 1742 | 1718 | 1660 | 1093 |
| 11 | 1357 | 1743 | 1720 | 1667 | 1094 |
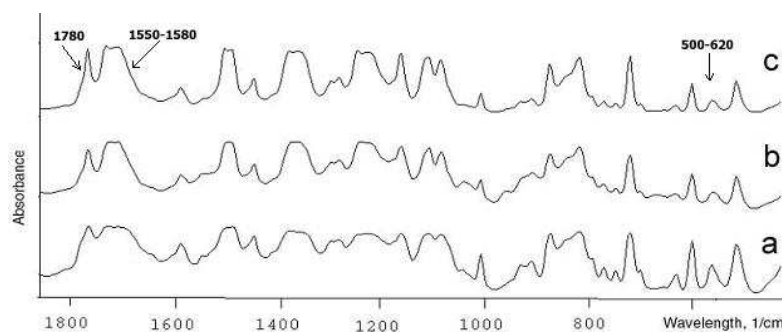
*Figure 5. FTIR spectra of the PPy/PI composite at different times of PPy deposition at 1 mA/cm$^2$ current density. PAAc with imidization 20% was taken as a matrix: (a) without PPy, (b) PPy deposition 60 s,  (c) PPy deposition 180 s*
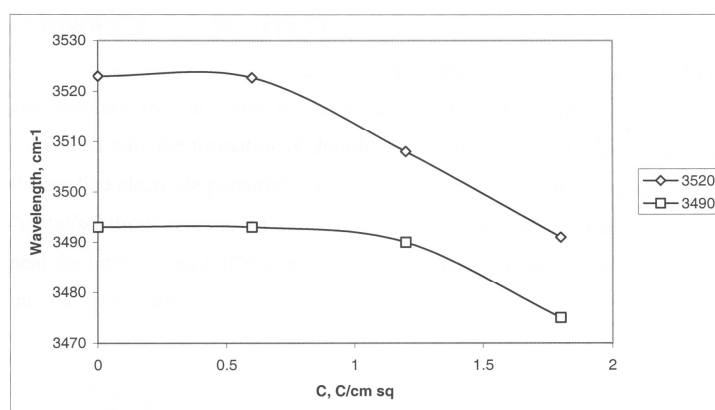


*Figure 6. FTIR wavelength shift as a function of unit charge for peaks 3520 cm$^{-1}$ and 3490 cm$^{-1}$*

Imidization activation energy was determined by different independent techniques: DSC and FTIR.

PAAc to PI conversion is an exothermic reaction. The DSC thermogram for imidization in Figure 7 showed two distinct peaks at around 100ºC and 180ºC. The 100ºC peak was possibly related to the evaporation of solvent while the 180ºC peak was due to imidization. The second scan showed the disappearance of both of these peaks proving that both solvent evaporation and imidization were completed during the forward temperature sweep. At the presence of PPy the imidization peak shifted to lower temperatures (156ºC at the same heating rate), suggesting that in the presence of PPy imidization  started at lower temperatures (Fig. 8).

Imidization activation energy was DSC determined for electrochemically obtained and chemically imidized samples with the amount of PPy varied from 0 to 60 %[2]. It was found to depend linearly on the amount of Py as:

$$E_{im} = E_0 – k\,m \tag{4}$$

where: $E_{im}$ – imidization activation energy, kJ/mol, $E_0$ – activation energy without PPy, kJ/mol, $m$ – amount of PPy, %, $k$ – coefficient, kJ.

Based on FTIR obtained experimental data coefficients in Eq. 4 were determined as 72.8 kJ/mol for the activation energy and 0.77 kJ for $k$.

---

[2] here and further in the text mass percentage was used.
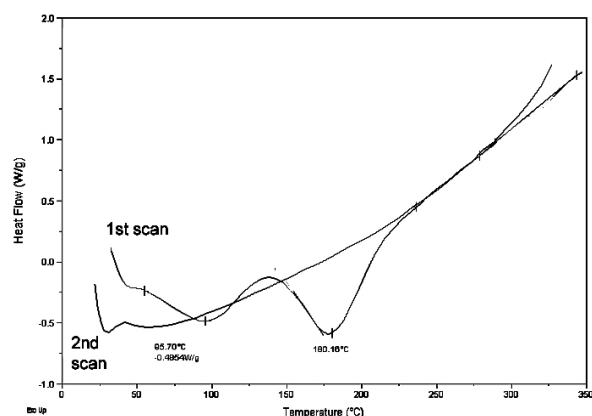
Figure 7. Differential Scanning Calorimetry plot
of PAAc film. Heating rate 30 °/min
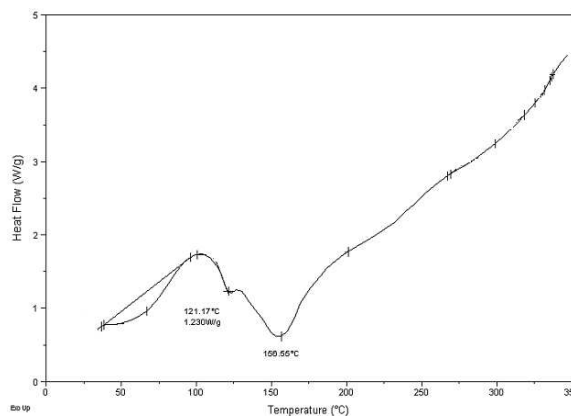
Figure 8. Differential Scanning Calorimetry
plot of the PPy/PI composite, Heating rate
30 °C/min

Same coefficients were FTIR determined on samples obtained electrochemically and imidized thermally. Amount of PPy in this case varied from 0 to 6 %. $E_0$ was found to be equal to 60.8 kJ/mol and $k$ was 0.72 kJ that was relatively close to DSC values. Therefore, PPy promoted the imidization irrespectively to samples preparation method.

## DISCUSSION

Kinetic nonequivalence of amic acid moieties during imidization could be the result of
1) hydrogen bonding between carboxyl and amide groups [15, 16],
2) rotational isomerism of amic acid groups [19]
3) influence of adjacent groups [20] and
4) variation of molecular mobility [21-24].
Imidization likely occurs from para PAAc molecules [25]. PPy acts as a catalyst to imidization, possibly because it can perform as a dopant for PI [4], therefore redistributing electron density along PI backbone in a way that an activation energy for imidization reaction decreases.

The activation energy of imidization ($E_{IM}$) measured experimentally in this paper and by others [11] is (60 – 75) kJ/mol. The presence of PPy lowers PAAc → PI transition (imidization) by 25-30 kJ/mol that was shown by DSC measurements.

## CONCLUSIONS

In the PPy/PI nanocomposite, PPy significantly lowered the temperature of PAAc imidization by lowering down the activation energy of PAAc conversion to PI. As a result of PPy addition, morphological properties of the composite also changed. Obtained results suggest using PPy as a low temperature-curing additive for PAAc, and open an avenue to creating new type of electrically conducting composites based on polyimide, where conjugated double-bonded structure of PPy is superimposed with delocalized π electron polyimide system, resulting in new amazing electrical and mechanical properties.

## REFERENCES

1. Saadeh H., Yu D., Wang L. M., Yu L. P.: *Highly stable, functionalized polyimides for second order nonlinear optics*. J. Mater. Chem., 9, 1999, 1865–1873.

2. Sek D., Schab-Balcerzak E., Solyga M., Miniewicz A.:  Synth. Met., 127, 2002, 89-93.

3. Levine K., Iroh J., Kosel P.: *Synthesis and properties of the nanocomposite of zinc oxide and poly(amic acid)*. Applied Surface Science, 230, 2004, 224-33.

4. Levine K., Iroh, J.: *Electrochemical behavior of the composite of polyimide and polypyrrol*. Journal of the Materials Chemistry, 11, 2001, 2248-2252.

5. Levine K., Iroh J.: *Resistance of the Polypyrrole/Polyimide composite by electrochemical impedance spectroscopy*. Journal of Porous Materials, 11, 2004, 87-95.

6. Bessonov M.I., Zubkov V.A. (editors): *Polyamic acids and polyimides: synthesis, transformations, and structure*. CRC Press, 1993.

7. *Sazanov Yu.N.: Applied sigificance of polyimides. Russian Journl of Applied Chemistry, 74, 2001, 1253.*

8. Polotskaya G.A., Kostereva T.A., Elyashevich G.K.: *Separation and Purification Technology*. 14 1998, 13–18.

9. Koton M.M., Kudryavtsev V.V, Zubkov V.A., Yakimansky A.V., Meleshko T.K., Bogorad N.N.: Vysokomol. Soedin. A, 26, 1984,  2584.

10. Jordan K., Iroh J.O.: Polymer Engineering and Science, 36,1996, 2550.

11. Kissinger H.: J. Anal. Chem., 21, 1957, 1702.

12. Barton J.: Adv. Polym. Sci., 72 (1985) 111.

13. Bellamy L.J.: *The Infra-Red Spectra of Complex Molecules*. London, 1958.

14. Szymanski H.A. (editor): *Infrared Band Handbook*, New York, 1966.

15. Sergenkova S.V., Shablygin M.V., Kravchenko T.V., Opritz Z.G., Kudryavtzev G.I.: *The investigation of the peculiar features of cyclodehydration of benzamic acid systems*. Vysokomol. Soedin. A, 20, 1978, 1137.

16. Novikova S.V., Shablygin M.V., Sorokin V.E., Oprirz Z.G.: *The effect of non-organic acids on the cyclodehydration of polyamic acids*. Khim. Volokna, 21, 3, 1979.

17. Milevskaya I.S., Lukashev N.V., Eliashevich A.M.: *The conformational study of imidization*. Vysokomol. Soedin. A, 21, 1979, 1302.

18. Kardash I.E., Lavrov S.V. et al.: Vysokomol. Soedin. B, 23, 1981, 395.

19. Nechaev P.P, et al.: Izv. Akad. Nauk USSR Ser. Khim., 8, 1977, 1750.

20. Dobrodumov A.V., Gotlib Yu.Ya.: Vysokomol. Soedin. A, 24, 1982, 561.

21. Pravednikov A.N., et al.: Vysokomol. Soedin. A, 15, 1973, 349.

22. Kolesnikov G.S., et al.: Vysokomol. Soedin. A,  2, 1970, 317.

23. Krongauz E.S.: *New aspects of poly cyclization*. Usp. Khim., 42 (1973) 1854.

24. Semyonova L.S., et al.: Vysokomol. Soedin. A, 20 (1978) 802.

25. Backlagina Yu. G., Milevskaya I.S.: Polyamic Acids and Pilyimides, 210, in [6].

**Katarína MONKOVÁ**
**Jan VALÍČEK\***
**Sergej HLOCH**

Technical university of Košice with a seat in Prešov, Slovak Republic
*Institute of physics, VŠB TU – Ostrava, Czech Republic

# THE SUGGESTION OF NEW MANUFACTURING TECHNOLOGY FOR HAND-MADE SCREW BLADE FOR WIND-POWER PLANT

*The contribution deals by the suggestion of new manufacturing technology for hand-made screw blade for wind-power plant with complicated topology that exists without the drawing documentation. To obtain the dimensions of such undefined real part is often very difficult, especially, if the accuracy requirement is great. The automation of the manufacturing of hand-made prototypes is one of the main goals in present days what is enabled by the quick development of information technology and by the sequential application of computer aid into all areas of the production.*

## INTRODUCTION

The automation of the manufacturing by means of NC program creation and the complex manufacturing with the utilization of CNC machines is needful for the every plant that wants to be a success with its products on the market today. The generating of CL data as the output of CAM software enables to create NC program for selected control system very simply by postprocessor. The manufacturing of new part by means of CNC machine is very quickly and simple today. [4] The basis for computer CL data is 3D model that enables:

➢ The visualisation of the object.
➢ The optimization of its structural solution before the production, its quick modification (the dimensions editing), eventually the quick suggestion of the similar objects inside the group technology.
➢ The utilisation of the object in the assembly allows detecting the conflicts with other components not only in static, but in kinematics state, too, so in marginal constrains of the motion.
➢ The defining of the couples, loadings, materials and other 3D model properties enables to execute the various types of analysis (structural, thermal, dynamic…) on the object and so predicts the object behaviour in real conditions. [2]
➢ It is possible to simulate the machining process by means of the created 3D models and so to find out the collisions between the tool and the piece.
➢ One of the major advantages of 3D model is the possibility to generate CL data and with the utilization of postprocessor to make the NC program for the selected control system in very short time.

> ➢ Very simple preparation of the negative shape of 3D geometry for the skillets manufacturing and other.

The example of hand-made prototype is the screw blade for wind-power plant. (Fig.1)

It was made by the hand lamination in to the split form the epoxy resin and glass cloth. The long-time practices of the producer show the reliability and stability of the screw blade, but the manufacturing of this part with complicated shape was very time consuming and toilsome what decreases the production costs.
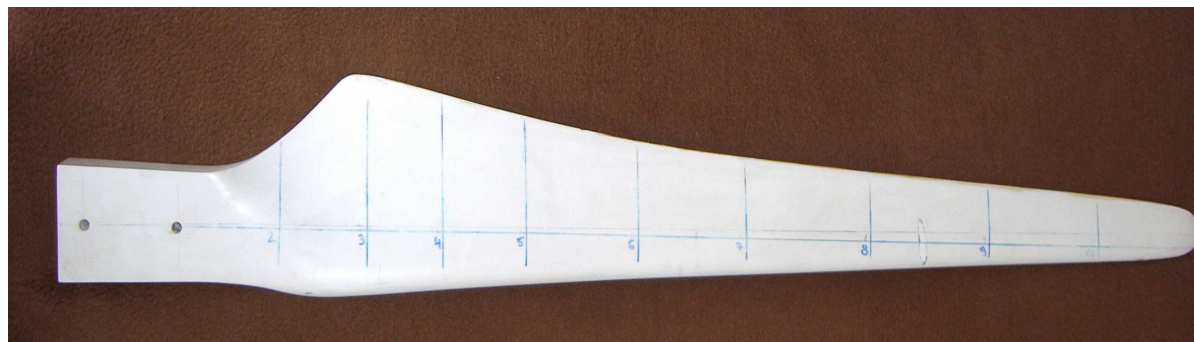


*Fig. 1. The hand-made screw blade for wind-power plant*

## THE DIGITIZING OF PROTOTYPE

To obtain the digital data from real existed part is very difficult, especially if the part topology of part is complicated. It can be done by various devices; one of them is 3D scanner.

3D scanners are devices which enable the conversion of real three dimensional objects to the digital versions. The principles of most of them is based on the object shape scanning in the discrete points, what means that the digitizing object is represented in the space as the so called "points cloud". According to the used technology of the scanning the scanners can be divided on contact and non-contact. The most common scanners are optical, mechanical or magnetically-resonant. [1] The choosing of the scanner type is depended on the precision requests between real and digitized model. The precision at the machining part is request rather high. Other important factors that affect the scanner choosing are the time of scanning and the size of the scanned object. The most quick are the laser scanners.

At the process of scanning it is necessary to solve several problems, such as for example:

> ➢ The reflex and shiny face of real part causes that laser beam reflects back and the surface can not be scanned. In this case it is needed to tarnish the part for example by spraying, not however by black colour, because that laser beam absorbs.
> ➢ The material, from which the physical model is made, should not be from transparent material (such as for example glass).
> ➢ The combination of concave and convex surfaces on one part caused that laser beam is not able to recover the shape as one whole entity. The solution of this problem is repeated scan of the object in various positions and with various settings. Consequently are partial surfaces merged and the unnecessary parts deleted. The combination of planar and rotating scan

> modes provides the possibility to scan already objects with difficult shapes.
>
> ➢ The size respectively the weight of scanned object in respect to technical parameters of scanner. This shortcoming it is possible to eliminate by the cutting of the object on minimum parts with the suitable dimensions. It is important to keep the alignment of the sections and so to preserve coincident position of individual parts of prototype in direction of vertical axis „z".

In this case the problem was too big dimensions of screw blade for the scanner LPX 250 with the Dr. PICZA software that is on the Faculty of manufacturing technology with a seat in Prešov of Technical University in Košice. It can be needed to cut the real part on 4 parts, to scan individual parts, to process the digital data in PIXFORM software and consequently it was necessary to import the data into CAD/CAM system. On the Fig. 2 is shown one scanned part of the screw blade for wind-power plant and on the Fig. 3 is imported data of whole prototype to the CAD/CAM system Pro/Engineer.
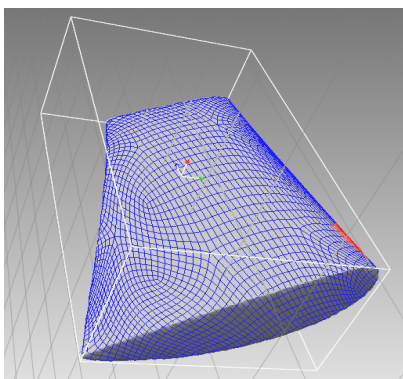


*Fig. 2. One scanned part of the screw blade for wind-power plant*
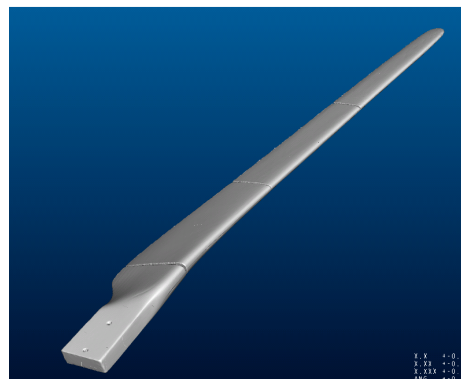
*Fig. 3. The imported data of whole prototype to the CAD/CAM system Pro/Engineer*

At the creating of 3D model was used various tools and techniques that the CAD/CAM system Pro/Engineer offers, such as the work with the curves and surfaces or quilts. The first was created the solid model of the screw blade, but it was used in praxis as shall. The modelled shell part is shown on the Fig. 4.

The obtained digital data of the prototype enable to suggest various kinds of production of the model.
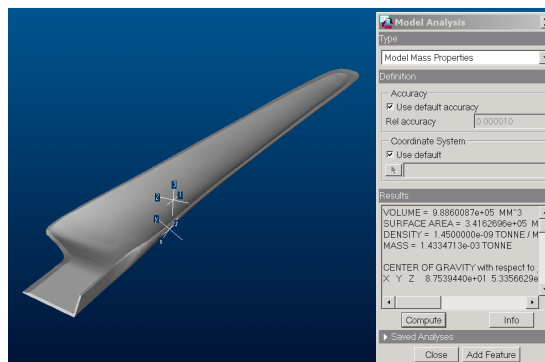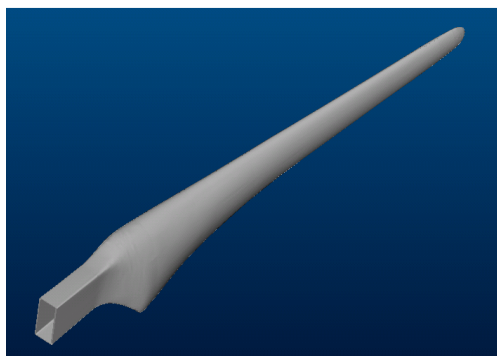


*Fig. 4. Created 3D model as the shell*

**THE SUGGESTION OF NEW MANUFACTURING TECHNOLOGY**

It was suggested the pressure die casting technology for the manufacturing of screw blade for wind-power plant and so it was needed to generate the negative shape geometry (Fig.5). On the basis of this geometry can be generated CL data by CAM module of Pro/Engineer system for the form within the choosing technology [3].
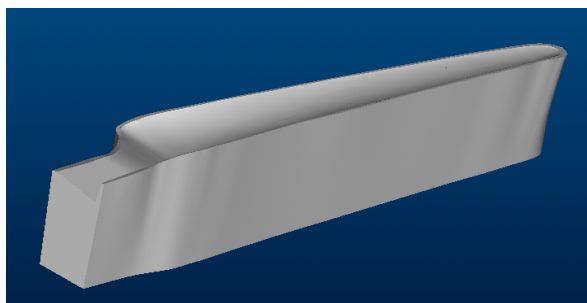


*Fig. 5. One part of negative geometry for the form designing*

The CAD/CAM system Pro/Engineer enables to simulate the manufacturing process of the form and so to detect eventual mistakes and collisions [7].
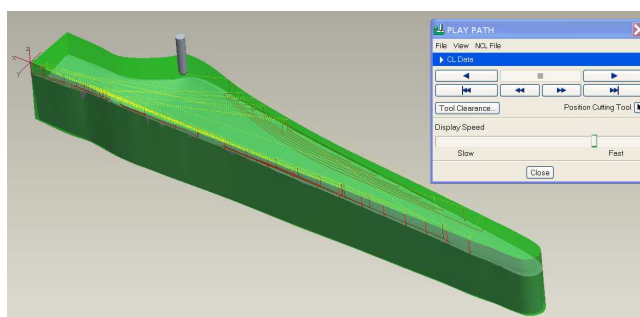


*Fig. 6. The simulation of the form manufacturing on the basis CL data*

At the suggestion of new technology (the pressure die casting technology) that would substitute handling production it was emanated from two alternative solutions of the screw blade section.

1. The first section would be created from 4 parts connected into one unit (Fig 6). Inside parts have great influence on the good bending strength properties, but the air in cavity can adversely affects of the screw blend operation, because the centrifugal force at the rotation has tendency to divide the part on two halves.
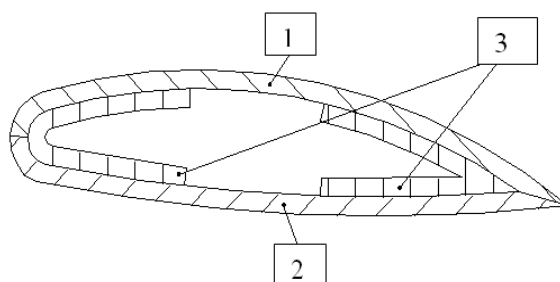


*Fig. 6. Alternative number 1 – four parts of the section: 1- top part of screw blend, 2 – bottom part of screw blend, 3 – backing of screw blend*

2. The second alternative is the possibility to cast the screw blade from one corpus with the using of functional core, Fig. 7. As the functional core it is possible to use the indurated polystyrene that improves the strength properties and also it absorbs a fraction of vibrations.
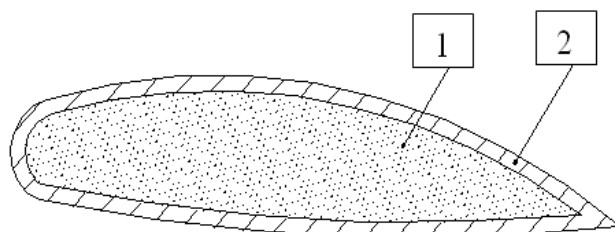


*Fig.7. Second alternative of the screw blend section: 1 – polystyrene core, 2 – shell of screw blend*

The polystyrene core is embedded into the cavity of form at the manufacturing and under the pressure it is infused to form the necessary mass of liquid plastic that creates the external shell. So it is made the final product with good strength properties in short time.

As the material at the hand manufacturing was used the epoxy resin, type M105 TC, which has the following strength properties:

> ➢ Limit of bending strength        90 MPa,     ISO 178
> ➢ Limit of tension strength        55 MPa,     ISO 527
> ➢ Setting time        60 min

The glass cloth improves the strength properties of resin.

For the pressure die casting technologies it was suggested the material with the next strength properties. The conditions satisfy the material Melanin that is used for die pressings for technical purposes. The strength properties of the Melanin are:

> ➢ Limit of bending strength        90 Mpa
> ➢ Limit of tension strength        65 MPa
> ➢ Density        1450 kg/m3

## CONCLUSIONS

Manufacturers must often process the existing products and prototypes by reverse manner to improve them or to substitute the actual manufacturing technology. For the manufacturing automation it is often needed to obtain the digital data that describes the shape and topology of prototype. But reverse engineering can be complicated and requires the digitizing of real part by means of various devices. One of them can be scanners. The processing of the object data involves the scanning of objects, perhaps in multiple part orientations, to get raw point-cloud or polygonal data. Technicians there scan existing parts with a 3D Alliance scanner and use the software to create accurate parametric CAD models. The company uses the models to fabricate replacement parts within strict tolerances and to improve designs to boost performance. Also, the firm ensures components get manufactured based on design intent by redesigning parts from scanned data. [5]

The suggested technology enables to produce the screw blade for wind-power plant in sufficient repeated accuracy and quantity, whereby the labour productivity and

quality increase (the substitution of hand work by machine), the manufacturing time decreases and at the same time the production costs are reduced.

## REFERENCES

1. Dúbravčík M.: *Prostriedky digitalizácie.* In: Transfer inovácií 8/2005, 2005, str. 52-54, ISBN 80-8073-461-5.

2. Hatala M., Čep R.: *Výběr vhodného řezného materiálu.* In: Sborník vědeckých prací Vysoké školy báňské - Technické univerzity Ostrava. Ostrava : VŠB-TU, 2006. vol. 52, no. 1 (2006), p. 23-28. ISSN 1210-0471.

3. Kratochvíl J.: *Zvyšování jakosti soustružení s využitím CAD/CAM Esprit.* In.: WORKSHOP Fakulty strojní 2005. Ostrava: VŠB - TU Ostrava, 2005, s. 60 + sborník na CD. ISBN 80-248-0750-5.

4. Dalton G.: *Reverse engineering using laser metrology.* Sensor Review, 18, no 2, pp 92-96, 1998

5. Monka P., Zajac J.: *Vplyv technologických parametrov obrábania a geometrických charakteristík rezného klina na charakteristiky drsnosti povrchu.* In: Acta Mechanica Slovaca. roč. 10, č. 4-a povrchové inžinierstvo 2006, ISSN 1335-2393.

6. Lee W.B., Cheng C.F., Li J.G.: *Applications of virtual manufacturing in materials processing.* Journal of Material Processing Technology, 113, pp 416-423, 2001

7. Weyrich M., Drews P.: *An interactive environment for virtual manufacturing*: *the virtual workbench*, Computers in Industry, 38, pp 5-15, 1999

## Irena NOWOTYŃSKA

Rzeszów University of Technology, Poland

# THE USE OF NUMERICAL IMAGE ANALYSIS FOR DETERMINE OF STRAIN DISTRIBUTION IN LAYERED COMPOSITES DURING EXTRUSION

*The possibility of application of numerical image analysis for determine of strain distribution in layered composites in the extrusion process was presented. Commercially available an ASAME (Automated Strain Analysis and Measurement Environment) program has been used. Basing on experimental study of layered composite extruded through different dies and use of the grid distortion method, strain distribution using ASAME program was presented.*

## INTRODUCTION

Progress in the production of metallic composites by extrusion depends on suitable designing of such types of material and its plastic deformation. Various approximate experimental and theoretical methods are used to estimate distribution of strain and stress in plastic deformation zone. Methods based on surface formulas, deserve special attention among many experimental methods. These methods consists of formulas plotted at the surface of analyzed component. Image analysis is used within the range of digital image processing methods. This method enables digital recording of strained sample surface during of after the process [1-4]. Among many experimental methods using image analysis during strain defining process, the most common method is grid analysis method and image analysis method using Fourier transformation. Grid method consists of two stages: first consists of defined grid nodes, second consists of calculations based on obtained measurement data. Using CCD cameras and scanners it is possible to record image during or after the test. Modeling processes of plastic processing, including extrusion process using incremental method of grid analysis permanently plotted at the surface of deformed material is based on theoretical analysis of experimental tests results and definition of kinematics and static at the plasticization area in select process stage. Research consists of measurement of deformed mesh in order to determine node displacement quantity. Coordinates measured for each strain stage enables defining components of displacement increment gradient for each node.

The possibility of application of numerical image analysis for determine of strain distribution in layered composites in the extrusion process using commercially program was presented.

## EXPERIMENTAL PROCEDURE

The experimental part of the study was carried out on a specially equipment, which allowed to apply direct extrusion process (Fig. 1). A set of flat die and convex die leading to the extrusion ratio $\lambda=3$ were used in forward extrusion without lubrication (Fig. 2). The composite billets consisting of the following model materials: hard lead (PbSb3)- as a core and soft lead (99.98%Pb) – as a sleeve have been used for testing. The composite billets have been prepared in concentric layout: core with circular section – sleeve in hard core-soft sleeve with volume ratio of the core $V_{core}/V_{composite} = 0.31$. Basic parameters of performed extrusion tests are presented in Table 1.
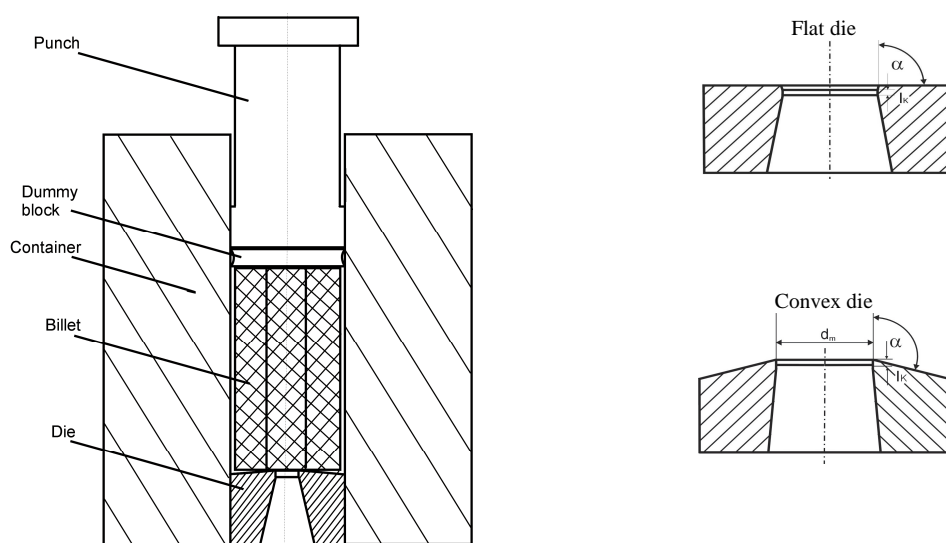


*Fig. 2. The dies used in the extrusion process - the scheme of longitudinal section of the die, $l_k$ –bearing length, $\alpha$ -die angle, $d_m$ – die orifice diameter*

*Table 1. Process parameters used in experimental work*

| Parameter | Unit | Value |
|---|---|---|
| Temperature of extrusion | $^{o}C$ | 20 |
| Die angle, $\alpha$ | degree | 90; 100 |
| Billet diameter | mm | 36 |
| Billet height | mm | 72 |
| Extrusion ratio $\lambda$ | - | *3* |
| Extrusion speed (ram speed) | mm/s | *1* |

Determination of strain distribution in layered composites during extrusion based on the grid deformation method (Fig. 3). Before extrusion each layer of the composite rods was firstly, split into two equal halves and square grids of 1.5x1.5 mm were inscribed onto the longitudinal symmetrical plane of the split half. Then two halves were fitted together and put into the container to implement the experiments of the extrusion of composite rods. In all cases, the process was stopped after 50% of the initial billet length was extruded.
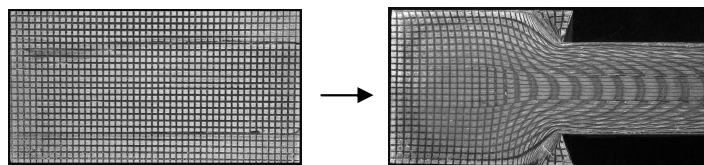
*Fig. 3. Samples for experimental extrusion with use of the grid distortion method method*

In the second part of the study commercially available an ASAME (Automated Strain Analysis and Measurement Environment) program with automated measuring position equipment with CCD camera to determine strain distribution during composite sample extrusion process has been used. Design such device with marked shift directions of particular elements is presented in Figure 4.
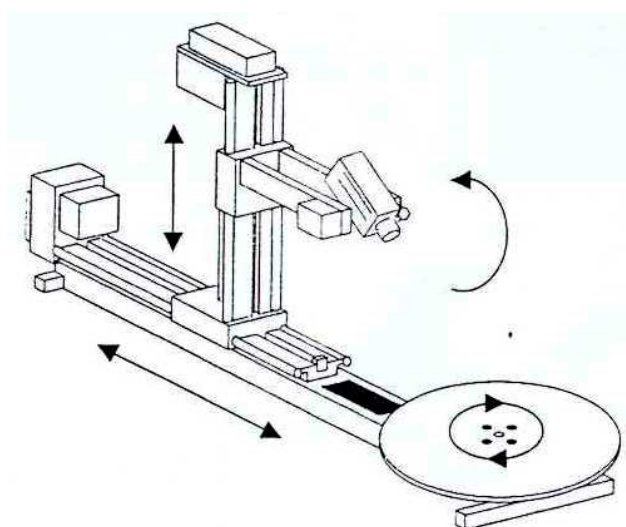


*Fig. 4. CCD camera with mechanism to recording of sample image [3]*

## RESULTS AND DISCUSSION

Grid distortion in the cross-section of the billet during extrusion of composite material has been presented in Figure 5.
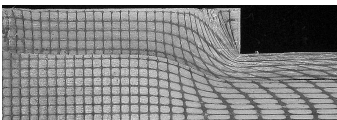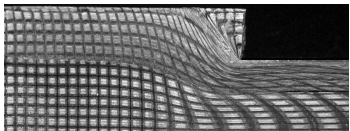
| Angle of the die | hard lead (core)- soft lead (sleeve) |
|---|---|
| | $V_{core}/V_{composite} = 0.31$ |
| Flat die $\alpha = 90^{\circ}$ |  |
| *Convex die* $\alpha = 95^{\circ}$ |  |

*Fig. 5. Grid distortion on the longitudinal section of the billet during extrusion through flat and convex dies*

Basing on the grid deformation, commercially available an ASAME (Automated Strain Analysis and Measurement Environment) program has been used in order to determine strain distribution during composite sample extrusion process. To calculate the true thickness strain and true effective strains from the true major and true minor strains, the following equations are used (Fig. 6):

$$\varepsilon_{thickness} = -\varepsilon_{major} - \varepsilon_{min\,or} \tag{1}$$

$$\varepsilon_{effective} = \frac{2}{\sqrt{3}} \sqrt{\varepsilon_{major}^2 + \varepsilon_{min\,or}^2 + \varepsilon_{major}\varepsilon_{min\,or}} \tag{2}$$

$$\varepsilon_{min\,or} = \ln\sqrt{1 + 2E_{min}} = \frac{1}{2}\ln(1 + 2E_{min}) \tag{3}$$

$$\varepsilon_{major} = \ln\sqrt{1 + 2E_{max}} = \frac{1}{2}\ln(1 + 2E_{max}), \tag{4}$$

where

$$E_{min} = E_{average} - r$$

$$E_{max} = E_{average} + r$$

$$E_{average} = \frac{E_{11} + E_{22}}{2}$$

$$r = \frac{1}{2}\sqrt{(E_{11} - E_{22})^2 + (2E_{12})^2}$$
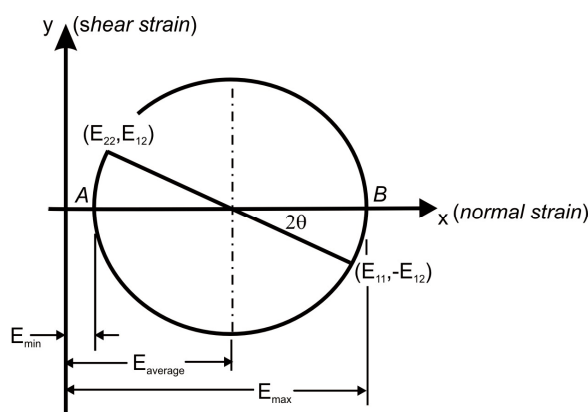


*Fig. 6. Mohr's Circle*

Strain distribution in composite sample extruded through different dies received with using ASAME program is presented in Figures 7 and 8.

FLAT DIE

a)



b)



c)



d)
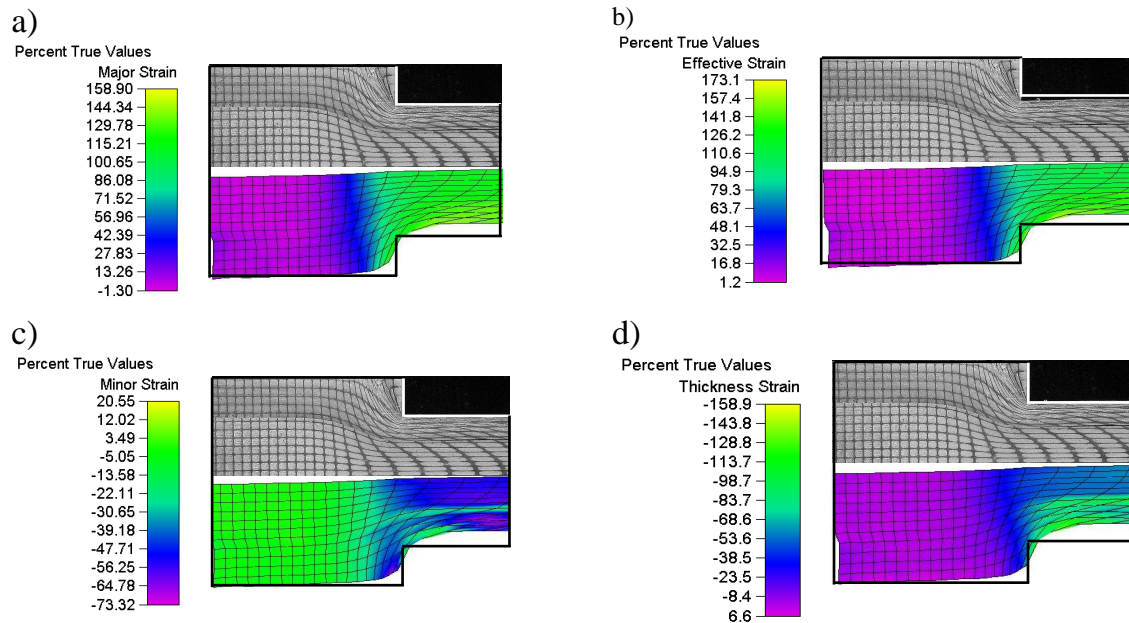


*Fig. 7. Strain distribution in composite sample extruded through convex die ($\alpha = 90^o$), hard core-soft sleeve type system, $\lambda = 3$, $V_{core}/V_{composite} = 0.31$: a) major strain, b) effective strain c) minor strain, d) thickness strain*

CONVEX DIE

a)



b)



c)



d)
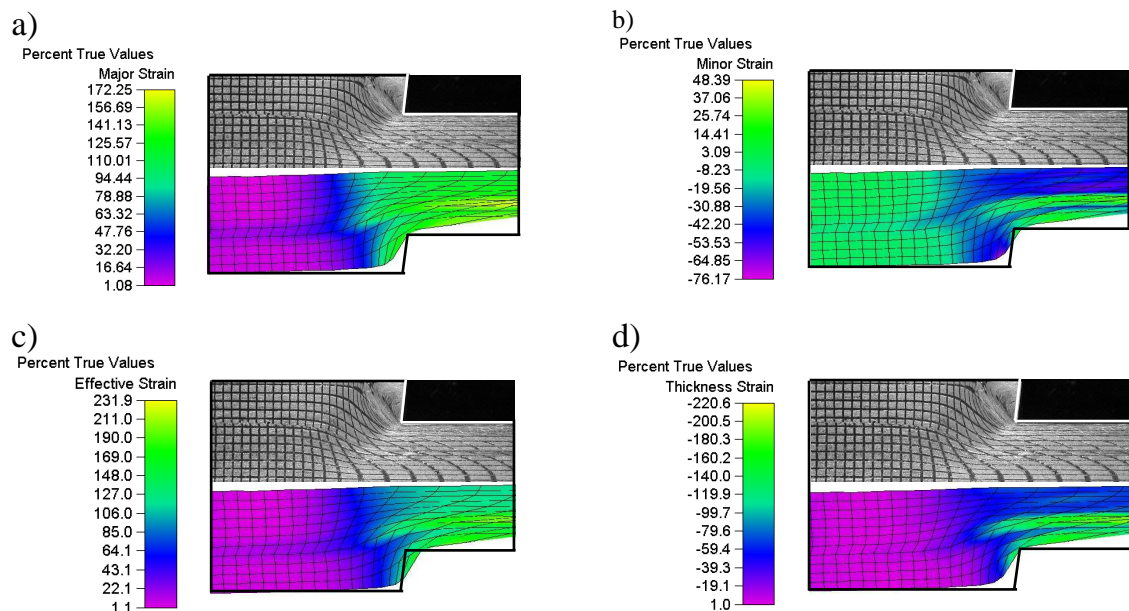


*Fig. 8. Strain distribution in composite sample extruded through convex die ($\alpha = 95^o$), hard core-soft sleeve type system, $\lambda = 3$, $V_{core}/V_{composite} = 0.31$: a) major strain, b) minor strain c) effective strain, d) thickness strain*

Obtained results show a difference between effective strain distribution for flat die and convex die. Basing on the images can be observe area changes from small effective strain through some minimum until achieve again higher values.

Based on analysis it is possible to note that obtained results aren't definite in some areas. It is especially apparent for the area of sample contact with die. The program algorithm recognized the grid incorrectly, omitting significant part of its details. Effort calculations made based on displacement field can be incorrect. The ASAME program treated the whole displacement field as uniform, without diversifying material properties, and did not perform detection of displacement faults at the composite material contact, making the results less reliable. Moreover program require retouching of grid in purpose remove of defect, which can disturb correct course of a numerical analysis.

## CONCLUSIONS

Used in research commercial program give possibility determine of strain distribution in layered composite during extrusion. Determined strain distribution using numerical image analysis method have been shown their diversification in depend on choose die. Obtained results indicated on some limitations of used program. In the case of very grid distortion in area of die occurrences disturbances made impossible correct course of numerical analysis.

## REFERENCES

1. Kocańda A., Świłło S.: *Modelowanie fizyczne z zastosowaniem numerycznej obróbki obrazu.* Przegląd Mechaniczny nr 23-24, 1998, s. 9-14.
2. Orłoś Z. (red.).: *Doświadczalna analiza odkształceń i naprężeń.* PWN, Warszawa, 1972.
3. Świłło S.: *Automatyzacja pomiarów odkształceń plastycznych z zastosowaniem numerycznej analizy obrazu.* Praca doktorska, Warszawa 1999.
4. Świłło S, Kocańda A.: *Techniki numerycznej analizy obrazu w metodach doświadczalnych pomiaru odkształceń i badaniu kształtu.* Przegląd Mechaniczny 3/2000.

**Pavol PAPCUN**
**Daniel JANKURA**

Technical University in Kosice, Slovakia

# STRUCTURE AND ADHESIVE PROPERTIES OF CERAMIC AND COMPOSITE COATINGS ON AL$_2$O$_3$ BASE

*Paper deals with application of new composite powder materials, which are prepared by heating sprayed with plasma with water stabilized arc. Investigated coating powder material is on ceramics (Al$_2$O$_3$) - metal (Ni) base. Ceramic sand composite coatings were deposited on substrate of steel 11 373 (ISO 630 - 80). Adhesive - cohesive of properties was used norm STN EN 582 – Determination of tensile adhesive strength. The adhesive test showed, that composite coatings with nickel, reach better adhesion.*

## INTRODUCTION

Nowadays, thermal spraying has become a well-accepted technology as a coating method for metallic, ceramic and composite materials and has been used in variety industrial fields. Ceramic and other coatings on the metal substrate of structural elements which, in this way, gain some specific properties, such as corrosion resistance, wear resistance, resistance against thermal stresses, etc.

For spraying powder materials are used wide range of various types of equipment. Plasma spraying equipment consists of a set of individual apparatuses and devices. A plasma torch is a powerful spraying unit. In dependence on the method of plasma formation in the torch, plasma torches can be divided into non-transferred arc torches, transferred-arc plasma torches and combined torches.

The majority of applied ceramic based added materials consist of ceramic materials with a dominant portion of Al$_2$O$_3$, followed by the other oxides (Cr$_2$O$_3$, ZrSiO$_4$, ZrO$_2$, MgO, CaO, HfO$_3$, MoO$_2$), applied either in the pure condition or with various doping agents, and other chemical compounds (nitrides, borides, etc.) [1, 2].

This paper deals with the influence of metal component (K30 on base of nickel) on the adhesion of coatings and the structure of ceramic (Al$_2$O$_3$) and composite coatings prepared by plasma spraying.

## MATERIAL AND TREATMENT

Ceramic and composite coatings were prepared using a plasma torch of the AC – 160 type with water stabilization of plasma and with the electric input of 160 kVA. As

added material, non-sieved $Al_2O_3$ powder with the particle size of 40-100 µm was used [6]. Composite powders were prepared with following volume percentage: $Al_2O_3$ + 5% K 30, $Al_2O_3$ + 12 % K30 and $Al_2O_3$ + 20 % K30.  K 30 powder contains: Ni – min. 90 %, Cr – max. 2,5 %, Si – max. 3,5 %, Cu – max. 0,3%, Fe – max. 0,3%. Particle size of 45 - 90 µm was used. For research of adhesion, powders were sprayed on front surface of steel samples with diameter 25 mm.  For research of the structure, coatings were sprayed onto samples with the dimensions of 20 x 10 x 6 mm, which were cut of steel 11 373.  Prior to spraying, the surface of samples was pre-treated by blasting with corundum grains with the grain size $d_{zk} = 0.9$ mm [3]. The spraying distance was 300 mm. The thickness of sprayed coatings ranged from 150 to 200 µm.

The coating microstructures were examined by scanning electron microscopy (JEOL JSM – 7000 F). Test of adhesion was realized by shredder ZD – 10. Fig. 1 presents principle of adhesion test.
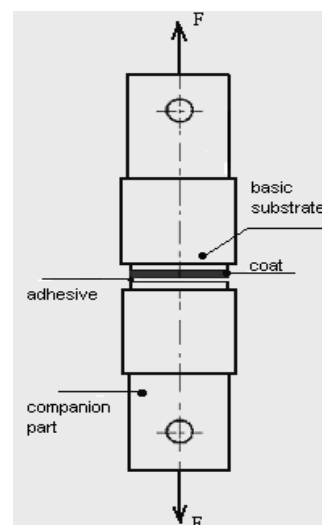


*Fig. 1. Test of adhesion*

**EXPERIMENTAL RESULTS AND DISCUSSION**

Fig. 2 shows the structure of surface $Al_2O_3$ coating. This surface is characterized by a very heterogeneous structure. Individual particles are separated from each other by wide-angled boundaries and a great number of balls appear on the surface. Large flat particles are cracked due to dilatation stresses during solidification.
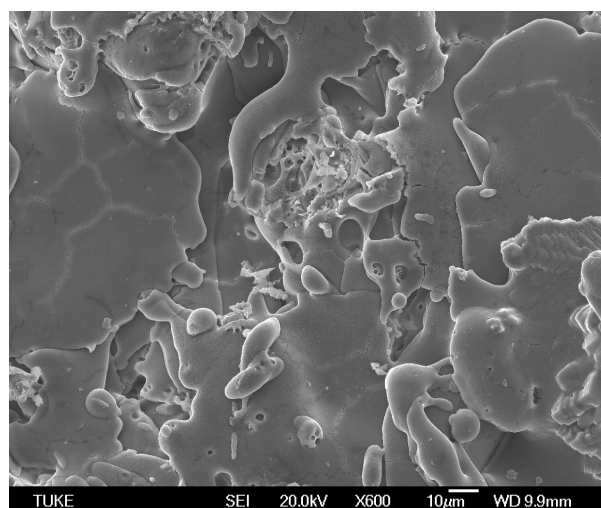


*Fig. 2. Structure of surface $Al_2O_3$ coating*

Fig. 3 shows the structure of surface of composite coating and detail of structure is in the Fig. 4.  Mold of structure of composite coating is similar in compare with $Al_2O_3$ coating. The composite coating contains less mistakes, cracks, pores and other structural defects.
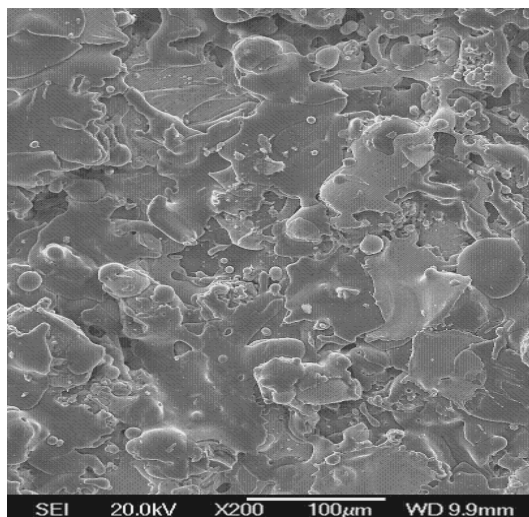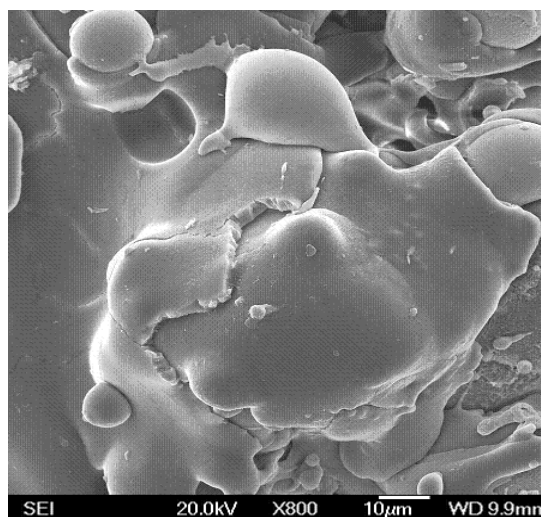
Fig. 3. Structure of composite coating      Fig. 4. Detail of structure of composite coating

Adhesion of particular ceramic and composite coatings was measured on four samples. Fig. 5 shows the average values of adhesion particular coatings. Lowest values of adhesion was measured on the ceramic coating ($Al_2O_3$) without intermediate layer. Intermediate layer was increased of adhesive power approximately doubly. The addition metal component K30 to $Al_2O_3$ powder increases adhesion power of composite coatings. Already, five percentuage addition K30 in composite coating achievings value of adhesion abreast of ceramic coating with intermediate layer. Adhesion value of composite coatings with 12 percentuage K30 achievings just 25 MPa.
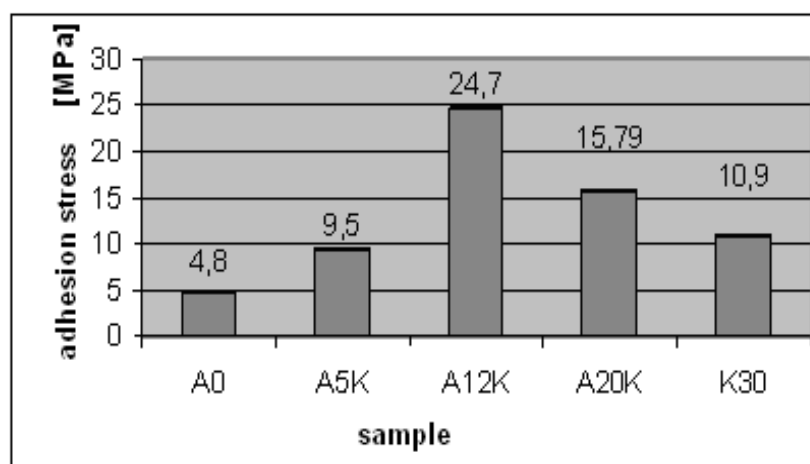


Fig. 5. Average values of adhesion coatings: A0 - $Al_2O_3$, A5K- $Al_2O_3$+5%K30, A12K-
$Al_2O_3$+12%K30, A20K- $Al_2O_3$+20%K30, K30 - $Al_2O_3$+ intermediate layer

## CONCLUSIONS

Contribution was oriented for research of ceramic and composite coatings on ceramic ($Al_2O_3$) – metal (Ni) base. Coatings were sprayed with water plasma torch with extremely high temperature ($30\,000^{\circ}C$) [4]. Results of experiments was

confirmed that addition of metal components on base of nickel increases adhesive power of composite coatings. Lowest adhesion was measured in the course of ceramic coating $Al_2O_3$ without intermediate layer (4,8 MPa). Composite coating $Al_2O_3$ +12% K30 has achieved adhesion power 24,7 MPa. Composite coatings were applied without intermediate layer too.

## REFERENCES

1. Matejka D., Benko B.: *Plazmové striekanie kovových a keramických práškov*. 1. vyd. Bratislava 1988.

2. Sololenko O.P.: *Thermal plasma torches and technologies*. Cambridge international science publishing, Cambridge, 2000.

3. Poľak J.: *Štúdium tvorby a vlastností nových kompozitných žiarovo striekaných materiálov*. (Doktorandská dizertačná práca). SjF TU, Košice, 2006.

4. http://en.wikipedia.org/wiki/Plasma_Spray (20.03.2008)

5. STN EN 582 : *Žiarové striekanie, stanovenie priľnavosti v ťahu*. November 2000

6. Jankura D., Papcun P.: *Adhézne vlastnosti kompozitných plazmovo striekaných povlakov na báze keramika - kov*. In: Acta Mechanica Slovaca. roč. 11, 2007, č. 4, Povrchové inžinierstvo 2007, s. 108-111.

7. Bačová, V., Jankura D., Draganovska D.: *Influence of cyclic heat stress on the properties of plasma – sprayed ceramic coatings*. In.: Metalurgija, Zagreb, 2008, s. 125-128.

**Masud M. PARVEZ**
**Mojahidul HQUE**
**Tamas SZECSI**

Dublin City University, Ireland

# A STUDY OF DIFFERENT MANUFACTURING FEATURE RECOGNITION METHODS

*To represent 3-D objects properly, several types of techniques have been developed in the field of solid modeling. Solid modeling techniques describe 3-D products and in recent year we have seen a growth by the rapid multiplication of solid modelers and 3-D CAD systems. The geometric elements of the solid model will be analyzed and features those are recognized as manufacturing entities will be extracted and organized according to topological manner. To detect manufacturing information from solid models produced by computer-aided design (CAD), feature recognition technique is used that focuses on the design and implementation of algorithms. Automatic feature recognition (AFR) technique is an important tool for achieving a true integration of design and manufacturing stages during the product development, and considered to be a critical component for integration of CAD and CAM. This paper is concerned with the overview of different feature recognition research focusing on four of the major feature recognition algorithmic approaches. Detailed description of algorithm for each approach will be presented along with some examples.*

## INTRODUCTION

Depending upon the manufacturing process, feature information is considered to be about volumes of material to be removed or to be added. The necessity of feature recognition is more important to report the existence of a feature in the part including its attributes and relationships. However, feature recognition can be described as the finding of features within a geometric model after its creation. A geometric model accurately represents the shape of a whole engineering component by which we can easily acknowledge where the slots, holes and their projecting slugs are. Different ideas presented from different backgrounds. Two of them are:
"A feature is a region of interest on the surface of a part"[1].
"Features are defined as geometric and topological patterns of interest in a part model and which represent high level entities useful in part analysis" [2].
Feature recognition is typically thought of as a process that is performed on a geometric model of a finished part but is not commonly employed in a design process. This paper focuses on the five currently active approaches.

## DIFFERENT FEATURE RECOGNITION METHODS

The literature on feature recognition is large in volume. Various approaches and algorithms are proposed by different researchers. Different feature recognition

methods have been shown in Figure. 1. In this section every approaches and algorithms have been described.
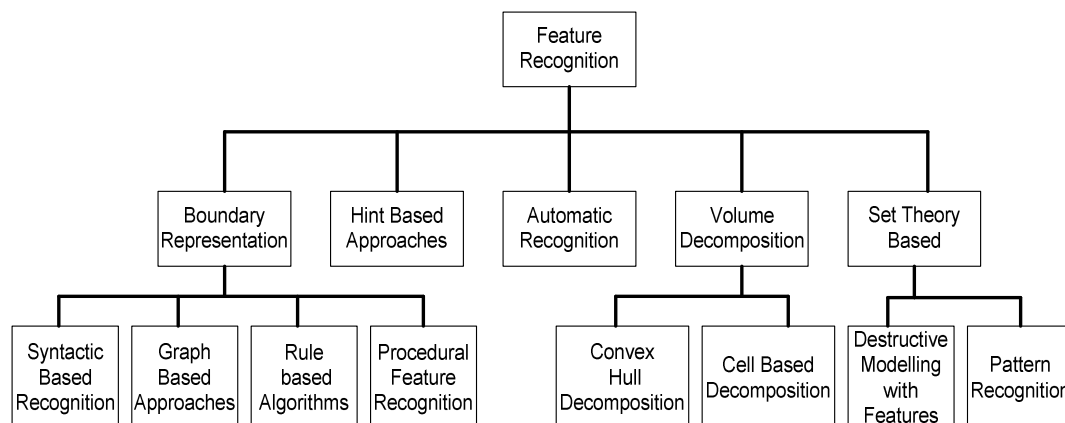


*Fig. 1. Different feature recognition methods*

## BOUNDARY REPRESENTATION APPROACHES

### Graph Based Approach

The graph pattern matching approach was first formalized by Joshi and Chang [3]. A graph pattern easily viewed the boundary representation of a part where, faces are considered nodes of the graph and face-face relationships from the arcs of the graph. To understand the graph notation, let us study the example of slot given in Figure 2-(a). Additional information may be incorporated into the graph, e.g. edge-convexity, face-orientation, etc. The neighborhoods relationships of the faces can be modeled by means of a face adjacency graph (FAG) in Figure 2-(a). Nodes of the graph represent the faces, and arcs between the nodes, the neighborhood relationships between the faces. In Figure 2-(a), (f7, f8, f9) will be matched with the slot template in Figure 2-(b).



(a): A solid part



(b): A part and its graph representation



(c): Slot temple: W1, W2: wall face, B: bottom face



(d): Missing pattern (2D)



(e) Invalid Invalid slot
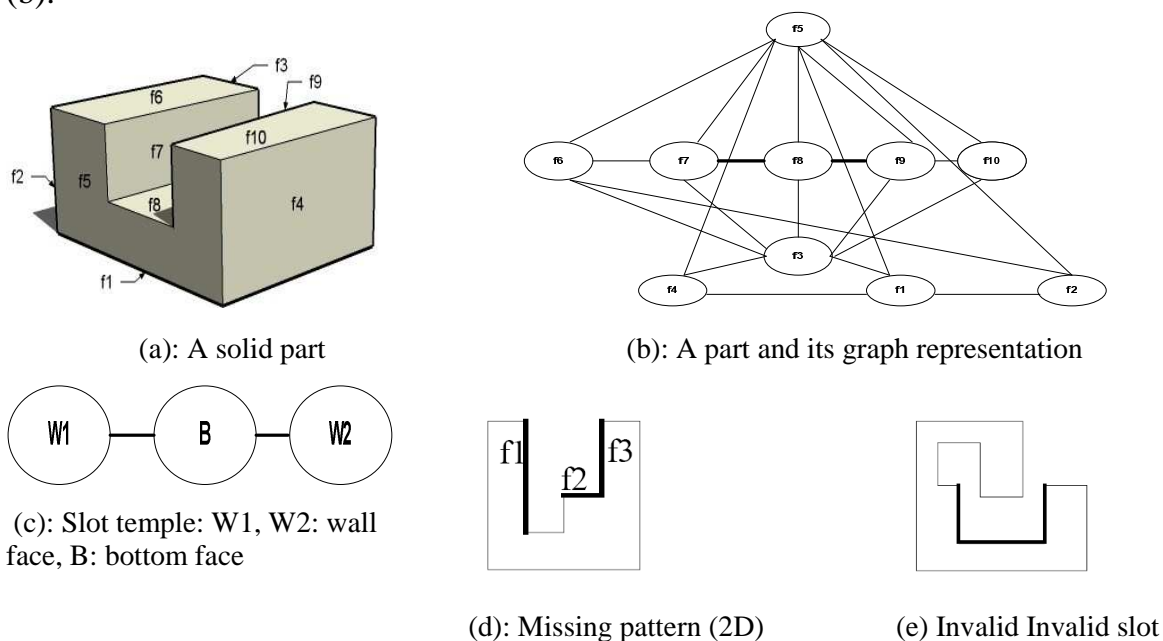
*Fig. 2: Graph Pattern Matching*

## Syntactic Based Recognition

Syntactic pattern recognition is a classical method for recognizing shapes from raster images. Three surfaces such as start surfaces, some element surfaces, and a bottom surfaces are required for a valid feature. Fig. 3 establishes an example of a valid feature using this system. A hole can have a number of bottom surfaces: for example a flat bottom, a cone bottom or a through hole; each of these are distinguished by slight variations in the syntactic patterns [4]. Valid syntactic pattern at any point, the surface type or edge type are important during the recognition phase otherwise feature recognizer drops out from the search.
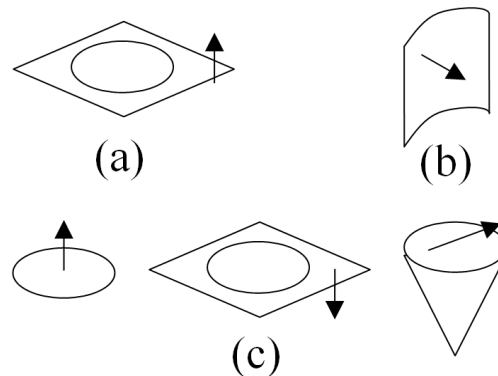


*Fig. 3. (a) Hole Start Surface HSS, (b) Hole Element Surface HES, (c) Hole Bottom Surfaces HBS*

## Rule-Based Algorithms

In this approach, features are formalized by templates, are defined for both general features (like holes) and specific features (e.g., flat bottomed, constant diameter hole) that consist of pattern rule." The hole begins with an entrance face. All subsequent faces of the hole share a common axis. All faces of the hole are sequentially adjacent. The hole terminates with a valid hole bottom [5]". General features (depression, protrusion, passage), and classification of general features into specific features (T-slot, round hole, rectangular pocket, etc.) is recognized in this procedure, create and subtract the volume corresponding to each feature from the cavity and repeat the procedure until there are no residual entities

## Procedural Feature Recognition

Formalism of feature definition is not only way for feature recognition; purely procedural representations can be used. In this approach, the recognition is performed by a specialized procedure that can recognize features of a particular type. The boundary model, references to relevant model entities can be scanned during the traversal and after all entities forming a feature have been found, feature attributes are computed.

## VOLUME DECOMPOSITION APPROACHES

In the previous section several important issues in feature recognition have been discussed. The most critical issue is how to recognize intersecting features. Two algorithms of intersecting features have been discussed which shows similar characteris-

tics. In this algorithms input object decomposed into a set of intermediate volumes and then influence the volumes to produce features.

*Convex Hull Decomposition*

In 1980 Kyprianou in his work on seminal feature recognition originally developed the convex hull decomposition method [6]. The example below Figure 4, a solid rectangular work piece is considered to be machined. The interpretation and mapping of the design features into machining feature is done using volume decomposition methods by identifying the removal volumes from the initial work piece and attribute them to manufacturing features.
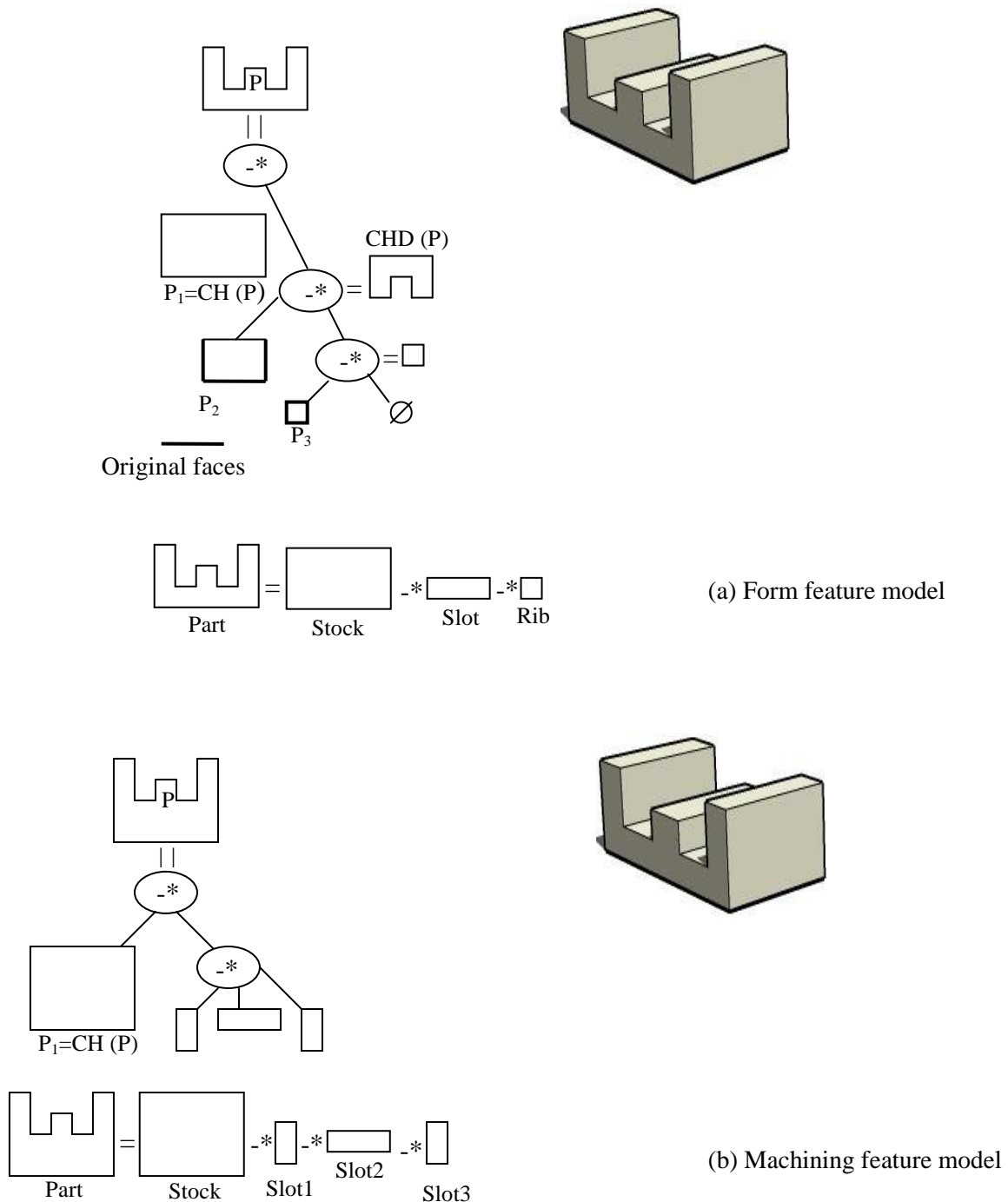


*Fig. 4. Convex hull decomposition*

**Cell Based Decomposition**

In 1983 a research group from Allied Signal Aerospace in Kansas City explored the cell decomposition approach [7]. In 1994 Sakurai and Chin described cell decomposition method who aim at generating all possible machinable feature accompanying a given part and stock. In Figure 5. Assuming that the top left part is manufactured off a rectangular block of material. In the first step, cross-shape delta volumes recognized as feature. The top right figure shows that the delta volume has been portioned in five convex cells. The partitioning is performed by splitting the delta volume with the extended surfaces contained in it; in this case the volume is split with the "side" surfaces of the cells. In the cell based decomposition approach, the differences of the proposed algorithms mostly lie in the methods for combining cells into feature. In the figure the bottom part shown the various features have been generated by combining the cells; these include an open pocket, two long slots, and four smaller slots.
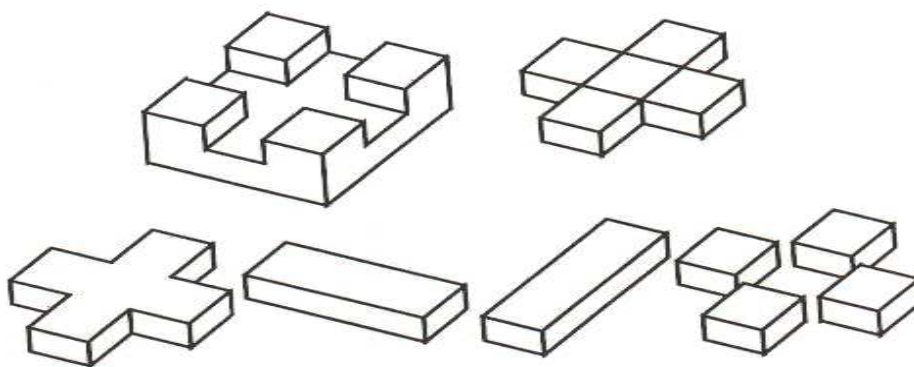


*Fig. 5. Feature recognition by cell decomposition*

**SET THEORY-BASED APPROACHES**

A set- theoretic modeller needs little modification to encompass design-by-features technology, as the feature primitives along with their associated operators are stored explicitly within the modeller's data structure. By using the full characteristics of a set-theoretic geometric modeller Requicha [8] created a design-by-features interface.

**Destructive Modeling with Features (Destructive Solid Geometry-DSG)**

In 1982 Arbab [9] first developed the technique follows the manufacturing process of a 21/2 D component closely. Although the name of this is the same as destructive solid geometry (Fig. 6) in design-by-features, the actual process is quite different and Li et al. developed the process [10, 11]. In design-by-features the model was created by removing feature primitives by hand from a blank with the set difference operator but in the case of destructive modeling with features three set operators (Union, Intersection & Difference) and feature primitives are used to build the model. When the model is complete by entirely subtracted volumes the CSG is automatically traversed and modified to produce the DSG.
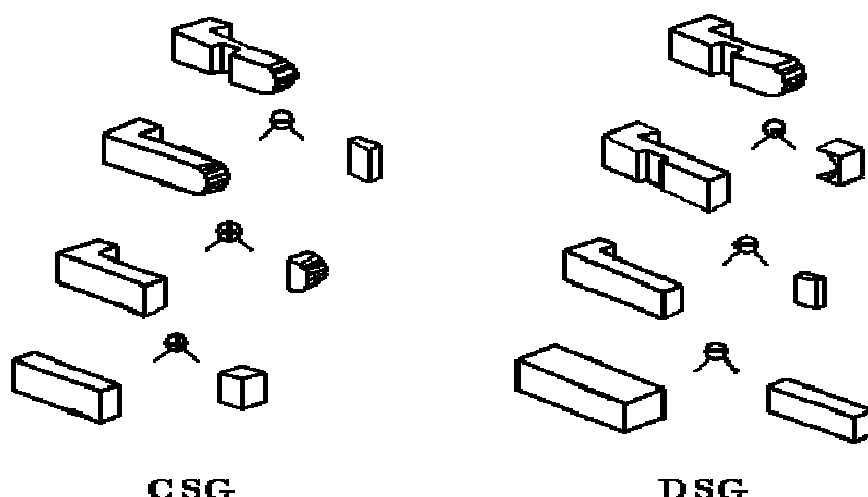
*Fig. 6. Destructive solid geometry (CSG to DSG )*

## HINT-BASED APPROACHES

To avoid the intersecting features problem in faces, edges, vertices Vandenbrande and Requicha [12, 13] proposed hint based reasoning. This section discusses the hint-based reasoning algorithms with IF² example. Holes, slots and pocket are recognized by IF² method. In this example slot features have been discussed. Slot hint is generated from nominal geometry when a parallel opposing planar faces is encountered and which is defined to be the wall faces of a slot. In Fig. 7a slot feature represent by shaded faces. More traces are being in hint-based approaches which are a problem to recognized good features. A trace or hint is nothing but an implication for the possible existence of a feature, and therefore a significant number of traces may not lead to valid features.
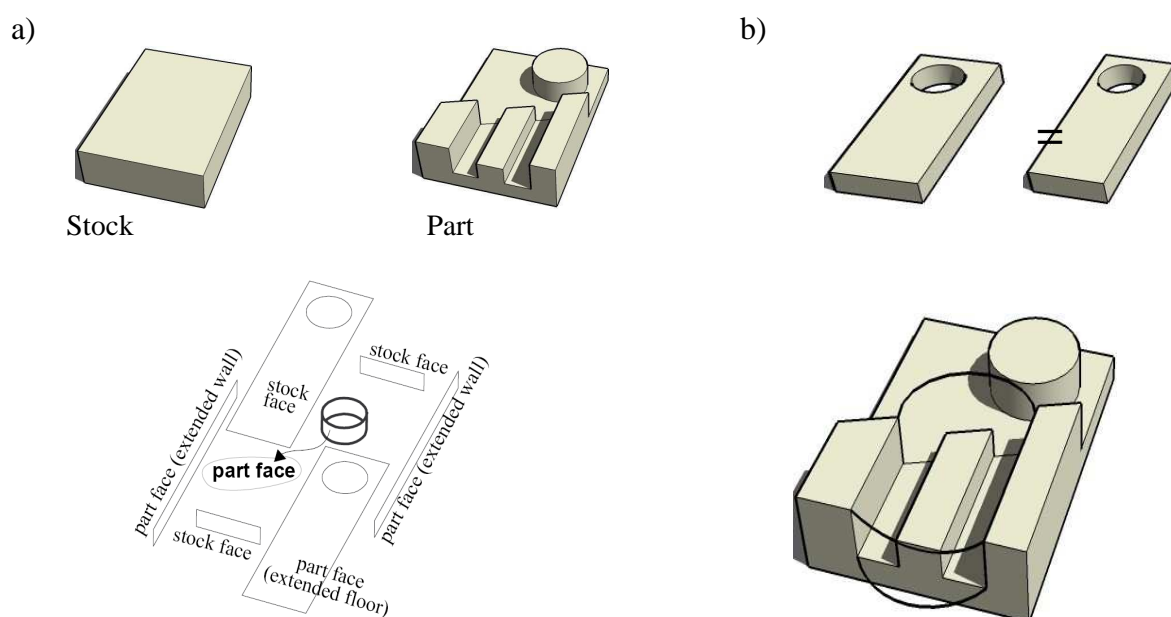


*Fig. 7. Slot recognition in IF$^2$: a) input stock and part, b) proposed removal volume, c) boundary analysis, recognized slot*

## AUTOMATIC FEATURE RECOGNITION (AFR)

AFR method applies knowledge acquisition techniques for generating feature recognition rules and feature hints automatically which is a major advantage in comparison with other rule-based and hint-based AFR methods. To construct valid features from the geometrical and topological information which is stored in B-Rep part models, a set of rules and two geometric reasoning algorithms are employed by feature recognition process.

## SOME MACHINING SLOT FEATURE EXTRACTED BY FEATURE RECOGNITION PROCESSES (Figs 8 & 9)

Rectangular slot          Round slot          V-Shaped slot

Dovetail slot          T-Slot          Free form slot
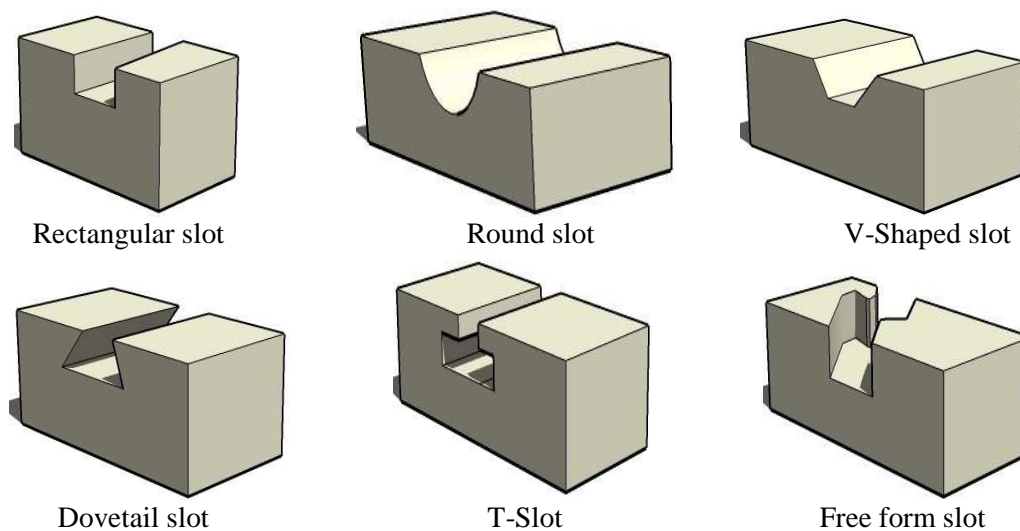
Fig. 8. Different through slot features

Rectangular slot          Free form slot
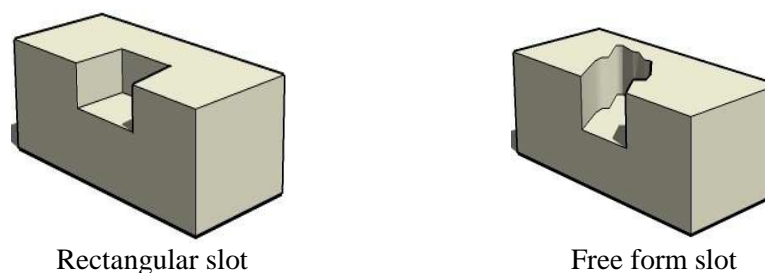
*Fig. 9. Two blind slot features*

## CONCLUSIONS

In this paper, briefly, we have tried to present an overview of the different classified feature recognition methods. Features play a key rule in integrating CAD and process planning, but feature recognition research has not been guided by the requirements of process planning. For example, much of the manufacturing knowledge, which is typically used in process planning, is rarely incorporated into feature recognition. Feature needs to be validated either at design phase or at recognition to prevent false

features being represented. Examples of such features are pockets being contained totally within larger pockets. Such things need to be highlighted to prevent time being wasted unnecessarily during machining processes.

The machining domain is just one of many mechanical engineering application areas now being addressed in terms of features. In order to apply design-for-manufacture rules (guidelines), in the manufacturing features they have to be systematized and organized into a hierarchical rule system. Rules at the higher level of the hierarchical system will be applied to more generic manufacturing features, and more specific rules are applied to more detailed features. The hierarchical structure enables to minimize the number of rules used and to avoid repetition when applying the rules.

## REFERENCES

1. Pratt M. J., Wilson P. R: *Requirements for support of form features in a solid modelling system'*. CAM-I, R-85-ASPP-01, 1985.

2. Henderson M. R., Chuang S. N., Ganu P., Gavankar P: *Graph-based feature extraction*. Arizona State University, 1990.

3. Joshi S., Chang T. C: *Graph based Heuristics for Recognition of Machined Features from a 3-D Solid Model*. Computer Aided Design, 20:58{66, 1988.

4. Barwick S. P., Bowyer A: *Feature technology technical report*. University of Bath, 001/1993.

5. Henderson M. R., Anderson D. C: *Computer recognition and extraction of form features*. A CAD/CAM link, Computers in Industry 5, pp329-339, 1984.

6. Kyprianou L. K: *Shape classification in computer-aided design*. PhD thesis, Christ College, University of Cambridge, Cambridge, United Kingdom, July 1980.

7. Christensen N. C., Emory J. D., Smith M. L: *Phoenix method for automatic conversion between geometric models*. Allied Signal Incorporated, Kansas City, MO. US Patent 728367, 1983.

8. Requicha A. A., Vandenbrande J. H: *Form features for mechanical design and manufacturing*. ASME Computers in Engineering Conference, Anaheim, CA, USA, Book number G0502A-1989, eds. Riley. D et al., pp47-52, Aug 1988.

9. Arab M: *Requirements and architecture of CAM oriented CAD systems for design and manufacture of mechanical parts*. PhD Dissertation, University of California, Los Angles, USA, 1982.

10. Li R. and Yu M.: *A framework for prismatic part-data generation-unit-machined loop concept*. In International Journal Computer Integrated Manufacturing, Vol. 3, No. 2, pp. 96-111, 1990.

11. Perng D., Chen Z., Li R.: *Automatic 3D machining feature extraction from 3D CSG solid input*. Computer Aided Design, Vol. 22, No. 5, pp. 285-295, June 1990.

12. Vandenbrande J. H., Requicha A. A. G.: *Special resoning for the automatic recognition of machinable features in solid models*. IEEE Trans. Pattern Analysis and Machine Intelligence, Vol.15, pp. 1-17, Dec 1993.

13. Vandenbrande J. H., Requicha A. A. G.: *Geometric computation for the recognition of spatially interacting machinable features*. In Shah J. J., Mantyla M. and Nau D. S. Advances in Feature Based Manufacturing, pp. 83-106, Elsevier Science, B. V., Amsterdam, The Netherlands, 1994.

**Paweł PAWLUS**
**Andrzej DZIERWA**

Rzeszów University of Technology, Poland

# FUNCTIONAL IMPORTANCE OF SURFACE TOPOGRAPHY PARAMETERS

*The paper presents the review of research investigations concerning functional importance of different surface topography parameters. The results of own investigations are also taken into consideration. Four groups of parameters were analysed: amplitude, spatial, hybrid and connected with material ratio curve.*

## INTRODUCTION

The manufacturing industry is moving towards higher degree of production acumen. Many of the demands concern to the surface of component. The surface topography is generated in the last stages of machining processes. Some properties, such as materials contact, sealing, friction, lubricant retention and wear resistance are related to surface topography. The designer should decide on the number of surface topography parameters that will meet the functional demands on the product with regard to some functional properties. The surface topography is the fingerprint of the manufacturing processes. The knowledge about the relationship between surface topography and surface function is still incomplete.

## THE ROLE OF SURFACE TOPOGRAPHY

We measure surface topography for 2 reasons. The first is the quality control. The second is understanding and prediction of surface functional properties. The surface is a link between manufacturing processes and function of machine parts. It is fingerprint of manufacturing process.

The roughness is essentially a second order effect in physical systems, and would therefore never assume an important place in engineering science. However in some cases the effect of surface topography on functional properties can be big.
The surface topography influences the functional properties in the following order: contact (stiffness, conductivity, adhesive properties) friction, lubrication, wear and fatigue. Whitehouse [1] introduced the so-called functional maps. It is possible to obtain information based on them, what parameters are the most important in some fields.

The change of surface topography during wear process is very important. When loss of material occurs on a relatively small area, the surface morphology is changed, wear particles are generated and some energy is dissipated at the interface. The wear process has been intensively studied from the wear particles point of view or using dissipated energy approach, however not much studies have been dedicated to link wear kinetics to topographical changes of the surface. Single geometrical variables, like wear depth, volume or scar radius are usually recorded [2].

## AMPLITUDE PARAMETERS

In 18 and 19 centuries people believed that optimum surface topography should be smooth. Only height parameters were considered. However during the progress in industry during 20-th century it was found that not only height parameters were important. However a majority of industrial firms use Ra parameter. The surface height influences the kind of deformation. From the point of view of minimisation of deformation the smooth surface is better than rough surface.

The plasticity index, introduced by Greenwood and Williamson [3] was frequently used, because of the opinion that if it was greater (plastic deformation) the intensity of surface wear was also larger. This is proportional to surface height determined by Rq parameter or standard deviation of peak height. It depends also on spacing parameters. The stiffness of joints is better when surfaces are smooth [4]. From the point of lubrication view smooth surface is not always desirable. Too smooth surfaces are not good for lubricant capacity, but wear of too rough surfaces is very big, so initial surface should be similar to worn surface (see Figure 1).
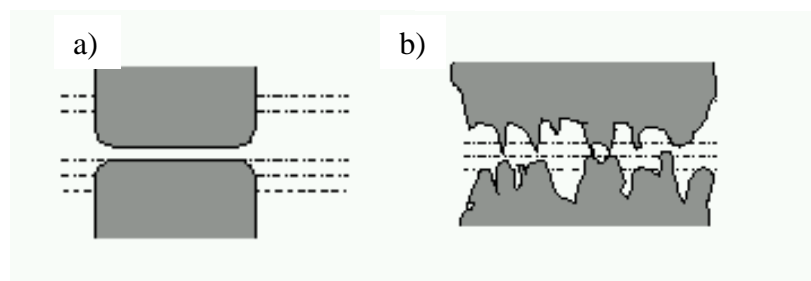


*Fig. 1. The co-action between  too smooth (a) and too rough surfaces (b)*

The roughness height affects the kind of lubrication. The ratio of the oil film thickness to the sum of roughness height (determined usually as Ra and Rq parameters of collaborating surfaces) is  called the relative thickness of lubricant ($\lambda$ ratio). When the oil film thickness is bigger than roughness height, the influence of surface topography on lubrication is not substantial. However in order to achieve HD lubrication the smooth surface is needed (see Figure 2).

The high peaks may cause contact between surfaces during hydrodynamic oil film formation, as the effect of it the oil film can be broken.

Not always fluid friction is needed. The smooth pavement surface as well as the smooth tyres are not good, in this case the braking force is small [5]. The surfaces of marines shoes should be rough. The rough skies are good when snow is wet, but smooth, when snow is frozen.

The roughness height affects also the possibility of failure. The smooth polishing cylinder surface is very dangerous from the failure point of view. On that surface, the honing valleys are not visible.

The surface tendency to pitting depends on relative height of contacting surfaces, $D_w=(R_{z1}+R_{z2})/h$; where h – the EHD oil film thickness (see Figure 3). It was also found that the roughness amplitude decrease caused bigger fretting distortion [6]. The increase of roughness height caused increase of cavitation wear.
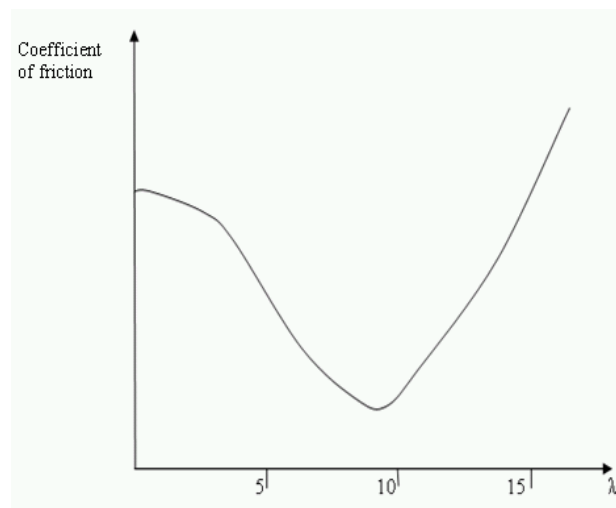


*Fig. 2. The coefficient of friction as function of λ parameter*
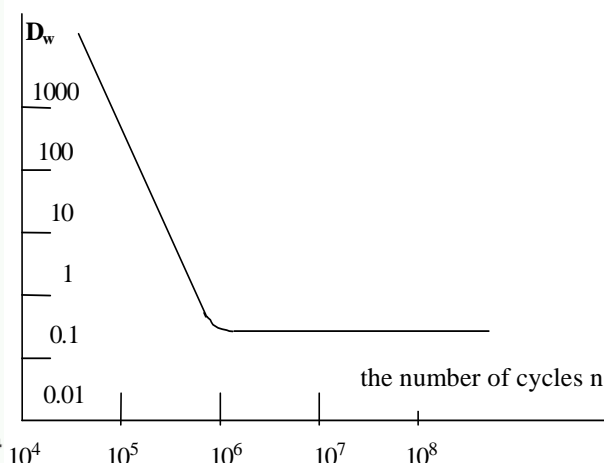
*Fig. 3. The effect of $D_w$ parameter on pitting existence*

The effect of surface topography is especially important during running-in or wear values smaller than initial surface height ('zero-wear'). However this effect on stabilized wear can be also important [7].

The wear intensity is often proportional to initial surface height. It was found that wear of the assembly: cam-follower decreased when roughness height decreased [8]. The wear of piston skirts during 'zero-wear' is proportional to initial surface topography height [9]. The similar effect of surface roughness on cylinder wear was found [7].

Usually the amplitude parameters decreased during wear. During 'zero-wear' the profilometric method can be only one possible method to assess the local linear wear. It is possible to use the changes of amplitude parameters. For example, the authors of publication [10] used Ra, but of Reference [11] Rtm. Decrease of roughness height causes increase of corrosion resistance.

The roughness height affects the fatigue strength. The smooth surfaces are better from that point of view. However the effects of microhardness and residual stresses are also important. It is believed that the effect of surface topography is the biggest.

## SPATIAL PARAMETERS

The spatial parameters can be obtained based on autocorrelation or power spectral density functions. Whitehouse presented possibilities of monitoring manufacturing processes based on these curves [6]. The majority of methods of modelling random surfaces are based on autocorrelation or power spectral density functions.

The mentioned above plasticity index depends also on correlation length (distance in which autocorrelation function decays to 0.1 value). Three-dimensional version of plasticity index depends on anisotropy level of surfaces. The conditions of contact depend on anisotropy level.

During hydrodynamic (HD) lubrication the position of surface with regard to the movement direction is important. In Figure 4 the roughness opposes the movement, thereby increasing the friction and improving the load-carrying capacity of the bearing. In the case (b) the surface direction is the same direction as the flow, thereby helping it. This implies a lower coefficient of friction but conversely a poorer load-carrying capacity [6].
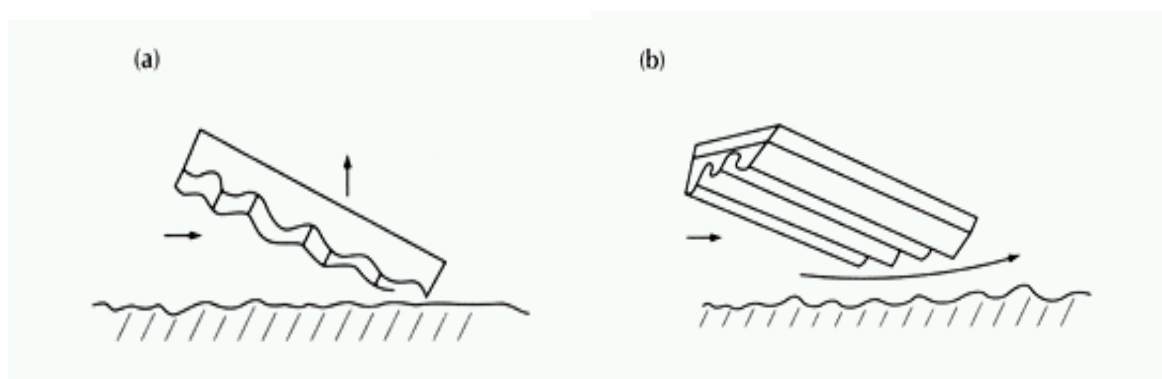


*Fig. 4. The effect of surface lay on hydrodynamic lubrication*

The authors of paper [12] studied the effect of surface anisotropy on oil flow in partial HD conditions. The surfaces transversely oriented don't cause flow resistance, the side flow is small. For isotropic surfaces main and side flow had similar values. For surfaces longitudinally oriented the side flow increased and main flow resistance, too.

The crosses on plain bearing surface can cause increase of the oil film thickness distribution. The waviness longitudinal to movement direction can improve conditions of elastohydrodynamic (EHD) lubrication [13].

Hirst and Hollander [14] found that the load-carrying surface capability under boundary friction conditions was bigger for bigger values of spacing parameters (it depends also on roughness height).

There is dependence between scuffing resistance and spacing parameters, like correlation distance [5] (see Figure 5).

The authors of publication [15] stated that surfaces characterized by bigger correlation length in sliding direction had smaller wear intensity during lubrication.

Whitehouse and Archard [16] found that the short-wavelength structure was removed from surface profile during initial part of wear, but structure of bigger wavelength still existed on surface.

One of the present author found that under increased dustiness conditions the distance between deep valleys was very important from functional point of view.

The summits geometry in contact between non-conforming surfaces is very important. It is well known that the contact between rough surfaces occurs at asperities and results in high pressure in the contacting asperities and small real contact area which is only a fraction of the nominal contact area. Relations between the real contact area and

the load, and between separation and load, are two basic characteristics necessary for understanding many tribological situations such as friction, adhesion, wear thermal and electrical conductance, and sealing. The analysis of the contact process shows that it is extremely complicated to predict the nature of contact owing to the random diversity of the shape and height of contacting asperities, the elastoplastic type of deformation, material hardening and asperity deformation. However, several attempts have been made in this field. According to the deformation laws which were applied, the models could in most cases be easily divided into two opposite vision: purely plastic and purely elastic models [17].

The comfort of travelers depends on wavelengths existed on surfaces (see Figure 6) [4].
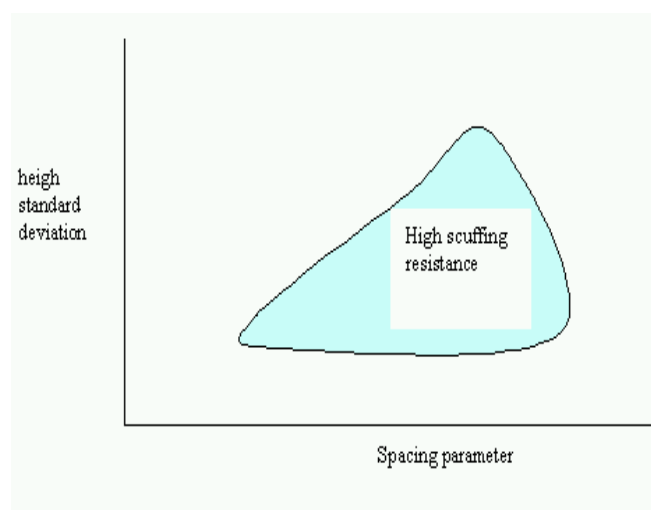


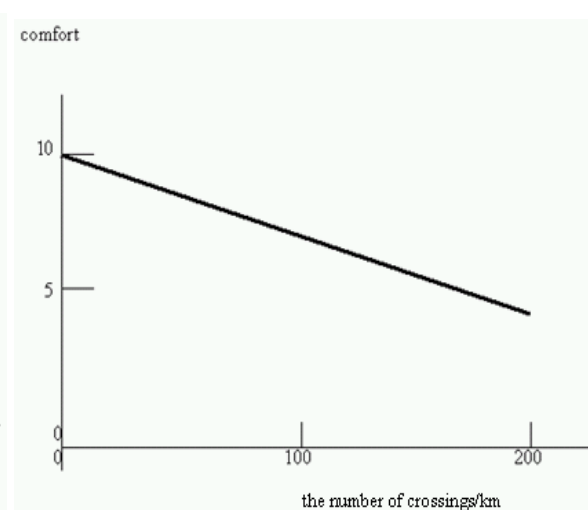Fig. 5. The effect of surface topography on scuffing existence

Fig. 6. The comfort of travelers as a function of number of crossing

## HYBRID PARAMETERS

The radius of curvature is very substantial parameter in contact problems of rough surfaces. It is also connected with heat or electricity conductance. The friction, elastic or plastic contact, light reflection, HD and spalling are sensitive on surface slope [4].

The plasticity index is proportional to root square of ratio of standard deviation of peak height to mean radius of peak curvature. However the authors of papers [19, 20] think that plasticity index is proportional to surface slope. The big slopes are not good from the point of stresses and lubrication view.

The adhesion capability is bigger for smooth surface of bigger radius of peak curvature [6].

In most publications the frictional force is proportional to surface slope [6, 20]. Generally the surface slope decreased during operating. It can be useful to monitor changes of surface topography during wear. The developed surface ratio can define surface capability to be sticky.

## PARAMETERS CONNECTED WITH MATERIAL RATIO CURVE

The multi-process surface cannot be characterized by only one height parameter. Therefore the engine producers use parameter connected with material ratio curve for

the assessment of cylinder surface topography. In Europe the parameters from Rk family are commonly used. In the opinion of Nielsen [21] the honing process of cylinder liners can be monitor by change of these parameters. However in USA the probability parameters originated from Cummins standard are used. The authors of paper [22] think that they are more connected with parameters of plateau honing than the Rk parameters.

From the tribological point of view, the most interesting parameter that can be extracted from the bearing curve is core roughness depth Rk, as it indicates working plane of a component, which after initial running-in period carries the load. Adequately, reduced peak height Rpk, is related to the top portion of the surface which will be worn away in the running-in period and reduced valley depth Rvk, is the lowest part of the surface which has the function of retaining the lubricant.

During modeling and simulation of surface topography parameters Rsk and Rku are used [23]. The authors of Reference [24] analysed the contact of rough surfaces. They found that skewness affects the contact properties like the real surface area, load and number of areas of contact.

Jeng analysed the effect of surfaces of Gaussian ordinate distribution and plateaued structure on friction and lubrication (when Rq parameter was the same). He found out that under HD condition the friction of 2 surfaces was similar but during mixed lubrication condition the friction force of plateaued surface was smaller, because Rpq parameter of this surface was smaller than Rq parameter of surface of normal ordinate distribution [25].

The existence of oil pockets on surface causes increase of load-carrying capability in plain bearings and as a consequence the friction can be minimized. The so-called oil capacity obtained basing on the material ratio curve can be important.  It was found that it has positive influence on some engine operating parameters [26].

The change of surface topography during wear can be monitored by the analysis of changes of parameters characterizing the material ratio curve or the shape of the ordinate distribution [27, 28, 29, 30, 31].

During 'zero-wear' parameter Rsk usually decreased, but Rku increased. One of the present authors found that the wear of cylinder liners is proportional to Rp/Rt parameter.

It is possible to obtain information of local 'zero-wear' value basing on measurement of surface topography only during wear process [10]. The idea of this method depends on the fact that the ordinate distribution of worn and machined surface should be the same to the truncation level (plastic deformation is excluded). However similar information can be obtained based on the analysis of worn (initially deterministic) surface. The material ratio curve should be used (see Figure 7). The local linear wear will be between A and B.

The authors of References [32, 33, 34, 35, 36] use the material ratio curve in order to obtain information about 'zero-wear' value.

Figure 3a presents the material ratio curve of a machined piston skirt profile, while Figure 8b of axial profile during 'zero-wear'

King et all [37] developed model of surface topography changes during wear. However the model parameters can be obtained basing on probability description of two-process surface [38].
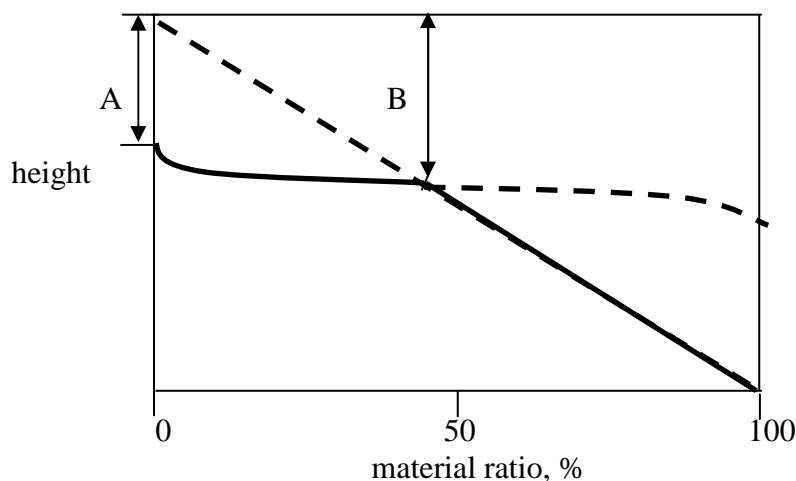
*Fig. 7. The method of obtaining the local wear value of piston skirt surface*
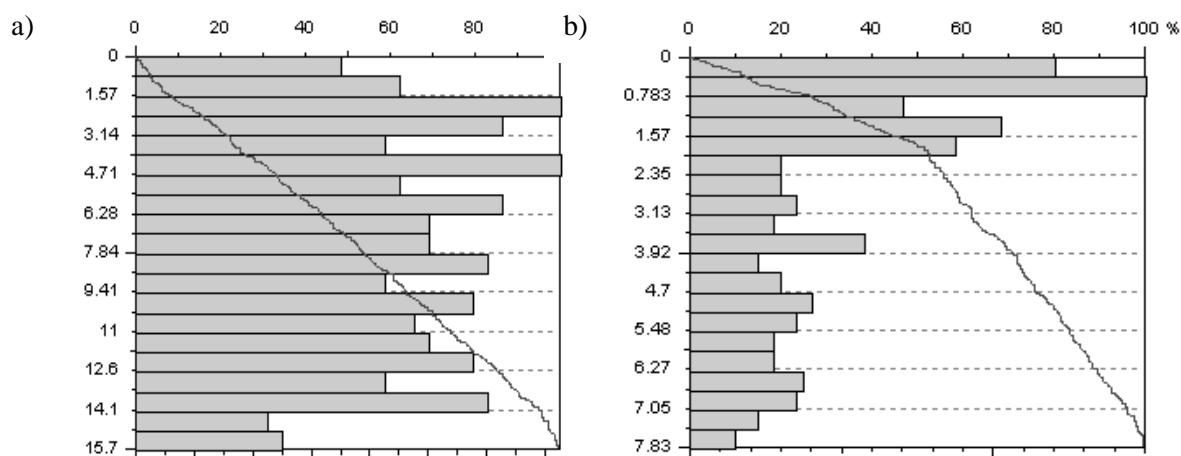


*Fig. 8. Graphs showing (a) a material ratio curve of a machined piston skirt profile, (b) a material ratio curve of a worn piston skirt profile*

## CONCLUSIONS

The amplitude parameters are most often used in industry. The surface height influences the kind of deformation. The roughness height affects the kind of lubrication and the possibility of failure. The wear intensity is often proportional to initial surface height. Decrease of roughness height causes increase of corrosion resistance.

The surface deformation is dependent on the spatial properties. During lubrication the position of surface with regard to the movement direction is important. The dependence between scuffing resistance and spacing parameters was found.
The radius of curvature is very substantial parameter in contact problems of rough surfaces. In the majority of publications the frictional force is proportional to surface slope.

The machining or wear process can be monitored by change of parameters connected with material ratio curve. These parameters can be used during modeling and

simulation of surface topography. It is possible to obtain information about wear value basing on the material ratio curve.

## REFERENCES

1. Whitehouse D.J: *Function maps and the role of surfaces*. International Journal of Machine Tools and Manufacture, 41/2001, 1847-1861.

2. Liskiewicz T., T. Mathia, S. Fouvry, A. Neville: *Systematic approach for morphological analysis of worn surfaces*. Tribotest 2007, 13, 139-150.

3. Greenwood J.A., J.B.P. Wiliamson: *Contact of nominally flat surfaces*. Proc. Roy. Soc., 295 A, 1966, 300-316.

4. Thomas T.R.: *Rough Surfaces*. Imperial College Press, London 1999.

5. Ludema K.C.: *Friction, wear, lubrication*. A textbook in tribology. CRC Press, 1996.

6. Whitehouse D.J.: *Handbook of surface metrology*. Institute of Physics Publishing. Bristol and Philadelphia, 1994.

7. Pawlus P.: *The effect of cylinder surface topography on the selected functional properties of multi-cylinder internal combustion engine*. PhD thesis, Rzeszow University of Technology, Rzeszow 1993 (in Polish).

8. Roylance B.J., C.H. Bovington, G. Wang, A. Hubbard: *Running-in wear behaviours of valve train system*. W: Vehicle Tribology, (Editors) D. Dowson, C.M. Taylor, M. Godet, Tribology series 18, 1991, 143-147.

9. Krzyzak Z., Pawlus P.: *Zero-wear' of piston skirt surface topography*. Elsevier, Wear 260, 2006, 554-561.

10. Jeng Y.-R., Z.-W. Lin, S.-H. Shyu: *A microscopic wear measurement method for general surfaces*. ASME J. of Tribology, 124, 2002, 829-833.

11. Pawlus P.: *A method of measuring "zero-wear" of the cylinder liner*. Tribotest Journal, 5/1, 1998, 53-70.

12. Patir N., H.S. Cheng: *An average flow model for determining effects of threedimensional roughness on partial hydrodynamic lubrication*. Trans. ASME 100, 1978, 12-17.

13. Tonder K.: *Effects of skew unidirectional straight roughness on hydrodynamic lubrication*. ASME J. of Tribology, 109, 1987, 671-678.

14. Hirst W., A.E. Hollander: *Surface finish and damage in sliding*. Proc. R. Soc. Lond., A 337, 1974, 379-394.

15. Wu C., L. Zheng: *Effect of waviness and roughness on lubricated wear related to running-in*. Wear 147, 1991, 323-334.

16. Whitehouse D.J., J.F. Archard: *The properties of random surface of significance in their contact*. Proc. R. Soc. A 316, 1970, 97-121.

17. Zahouani H., M. Assoul, R. Vargiolu, T. Mathia: *The morphological tree transform of surface motifs. Incidence in Tribology*. Transactions of 8th International Conference on Metrology and Properties of Engineering Surfaces, Huddersfield, United Kingdom, 2000, 95-108.

18. Greenwood J.A.: *Contact pressure fluctuations*. Proc. Instn Mech. Engrs, 210, 1996, 210, 281-283.

19. Tabor D.: *A simplified account of surface topography and the contact between solids*. Wear 32, 1975, 269-271.

20. Childs T.H.: *Dry and boundary lubricated sliding friction and wear for engine component materials*. In: Engine Tribology (C.M.Taylor – Editor), 1993, 51-74.

21. Nielsen H.S.: *New approaches to surface roughness evaluation of special surfaces*. Precision Engineering 10, 1988, 209-213.

22. Malburg M.C., M.B. Grant: *The characterization of two-process surface texture using the cumulative Gaussian probability distribution*. ISO Paper, 1992.

23. Mathia T.G, H. Zahouani, W. Rakowski, J.M. Schissle: *Analysis of cylinder bores-relationship between metallurgical structure, manufacture and wear characterisation*. Proceedings of Congress "EUROTRIB'93", 1993, 311-316.

24. Yu A., A.S. Polycarpou: *Contact of rough surfaces with asymmetric distribution of asperity heights*. ASME Journal of Tribology, 124, 2002, 367-376.

25. Jeng Y.: *Impact of plateaued surfaces on tribological performance*. Tribology Transactions, 39/2, 1996, 354-361.

26. Santochi M., M. Vignale: *A study on the functional properties of a honed surface*. CIRP Annals, 31, 1982, 431-434.

27. Bigerelle M, A. Iost: *A numerical method to calculation the Abbott parameters: a wear application*. Tribology International, available online.

28. Codgel J.D: *A convolved multi-Gaussian probability distribution for surface topography application*. Precision Engineering available online.

29. Johansson S, R. Ohlsson, Z. Dimkovski, B.-G. Rosen: *Manufacturing mechanisms of cylinder liner surface roughness*. 11th International Conference on Metrology and Properties of Engineering Surfaces. Huddersfield, UK, 2007, 376.

30. Pawlus P.: *A study of the dependence of the functional properties of the cylinder liner surface layer on the operating conditions*. Proceedings of the Institution of Mechanical Engineers, 210, part J, 1996, 17-27.

31. Pawlus P.: *Characterization of low wear of engine parts*. Finnish Journal of Tribology "Tribologia", 26/2, 2007, 10-23.

32. Brinkman S., H. Bodschwinna: *Characterisation of automotive bore performance using 3D surface metrology*. In L.Blunt, X. Jiang (eds): Assessment surface topography. Kogan Page Science, London and Sterling 2003, 307-347.

33. Daskivich R.A.: *Bearing length ratio applied to the measurement of engine cylinder-bore wear*. Precision Engineering, 6, 1984, 31-33.

34. Kumar R., S. Kumar, B. Prakash, A. Sethuramiah: *Assessment of engine line wear from bearing area curves*. Wear 239, 2000, 282-286.

35. Rosen B.-G., R. Ohlsson, T.R. Thomas: *Tribological implications of AFM measurements of cylinder bore microtopography*. Proceedings of the Conference on Atomic Scale Control of Surfaces and Interfaces, Brighton, 1994.

36. Gałda L., Pawlus P., Dzierwa A.: *Wear proces of textured ring examined by measurement of surface topography*. Materiały XII International Colloquium on Surfaces. Chemnitz (Niemcy) 2008, pp. 78-87.

37. King T.G., W. Watson, K.J. Stout: *Modelling the micro-geometry of lubricated wear*. In: Proceedings of the 4th Leeds-Lyon Symposium on Tribology. London, MEP, 1978, 333-343.

38. Pawlus P., W. Graboń: *Truncation parameters and local linear wear estimation from worn surface profile*. "Proceeding of 11th International Conference "Metrology and Properties of Engineering Surfaces" Huddersfield, 2007, 329-334.

**Alexandre POLOZINE**
**Lírio SCHAEFFER**

Federal University of Rio Grande do Sul, Brazil

# TESTING OF THERMOCOUPLES IN THE HIGH GRADIENT TEMPERATURE FIELD

*Two identical thermocouples were placed in the fields of different temperature gradients. The comparison of thermocouple readings revealed that the traditional method of temperature measurement is unfit for high gradient temperature fields.*

## INTRODUCTION

A thermocouple is a simple device for measuring temperatures. The working principle of a thermocouple is based on the Thomas Seebeck effect discovered by him in 1821. A schematic drawing of a thermocouple is shown in Fig.1.
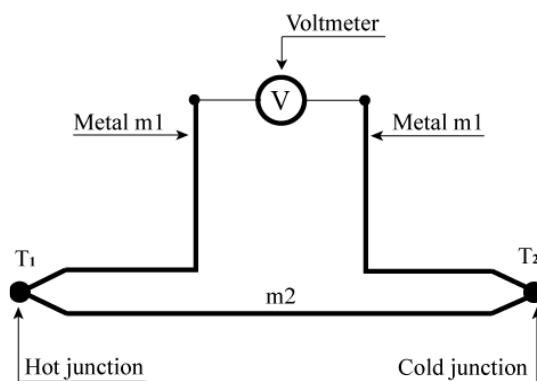


*Fig. 1. Scheme of a thermocouple*

The essence of the Seebeck effect consists in the following: if the electrical circuit of a thermocouple is closed, the thermoelectric current arises; if the circuit is open, the thermal electromotive force is observed between the points 1 and 2. A value of $dV$ depends on materials of the thermocouple arms and also on the temperatures $T_1$ and $T_2$ of each junction. If the temperature difference between the points 1 and 2 is insignificant, the thermal electromotive force is determined by using the empirical equation (1):

$$dV = \alpha \cdot dT ,\tag{1}$$

where

$$dT = T_1 - T_2 .$$

(Symbols and abbreviations, used in this paper, are listed in Table 1).

In the simplest case, $\alpha = const$, the equation (1) has a shape

$$dV = \alpha \cdot (T_1 - T_2)\tag{2}$$

*Table 1. Symbols and abbreviations*

| Symbols | |
|---|---|
| $\alpha$ | Seebeck coefficient |
| $G$ | temperature gradient |
| $dV$ | thermal electromotive force of a thermocouple electromotive force |
| $T_\infty$ | temperature of the environment (air) |
| Abbreviations | |
| HGTF | high gradient temperature field |
| LGTF | low gradient temperature field |
| HHMJ | homogeneously Heated Measuring Junction |
| IHMJ | inhomogeneously Heated Measuring Junction |

Modern thermocouples are more perfect than the first thermocouple from XIX century, what is due to the optimal selection of metals $m_1$ and $m_2$ (materials of arms). As to the nameless empirical equation (1), it continues to remain the same since the time of Seebeck. This equation is used widely in temperature measuring devices for the recalculation of the registered thermal electromotive force into the temperature.

It is important to note that researchers always considered the junction temperature field as homogeneous, and the equation (1) has been developed exactly for this case [1, 3]. In practice, the junction temperature field of the thermocouple usually is not homogeneous. In this case, a temperature measuring device calculates the conventional (averaged) temperature of the IHMJ.

It is obvious that the application of the equation (1) to the IHMJ thermocouples is not justified.

## INFLUENCE OF THE IHMJ ON READINGS OF A TEMPERATURE MEASURING DEVICE

Influence of the IHMJ on readings of a temperature measuring device can be evaluated by comparing the temperatures of the same object, obtained by using the HHMJ and IHMJ thermocouples. Data for such evaluation have been obtained in the experiment described below.

### Experimental set-up

Experimental set-up (Fig.2) for the evaluation of the influence of the IHMJ consists of the following components:

- Two metal-sheathed thermocouples type K (exposed junction; 1.0 mm in external diameter);
- Steel ABNT 1045 cylindrical test piece, $\varnothing54\text{x}54$mm;
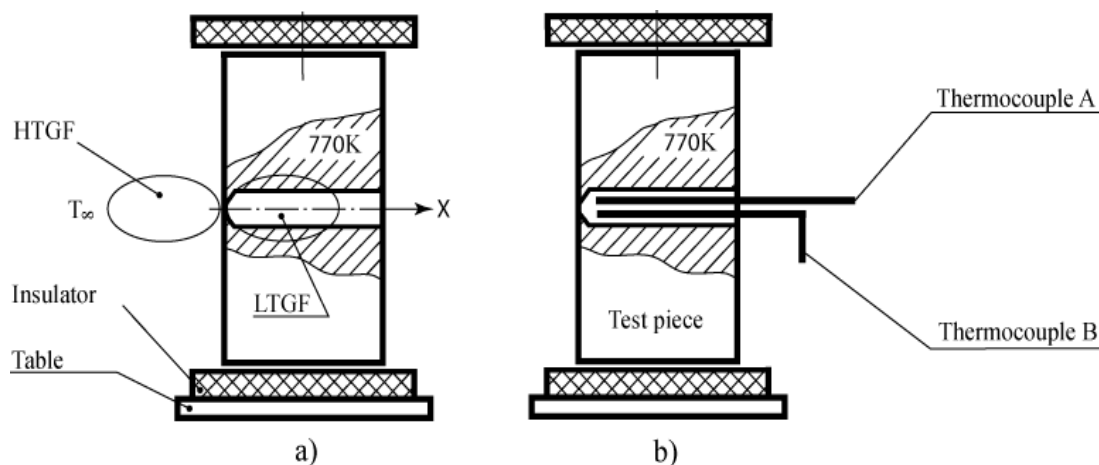- Temperature measuring device "USB-TC" for the record of the junction temperatures.



*Fig. 2. Experimental set-up*

### Test procedure

Test procedure consisted of three steps. A goal of the first step was the simultaneous generation of LGTF and HGTF by the same object.

The second step was the verification of the thermocouple A and B identity under the same conditions.

The third step was aimed at the simultaneous recording of the thermocouples A and B readings, by placing them in the LGTF and HGTF of the same object.

Step 1. The steel test piece with a deep horizontal hole was heated into the muffle oven to 800K. Then, the test piece was placed between two heated asbestos plates. While in this position, it was cooled by natural convection, conduction and radiation. Two different temperature fields generated by the test piece are shown in Fig. 2a.

Step 2. Two identical thermocouples A and B were placed in the hole at the lateral surface of the test piece and were pressed to the bottom of the hole, as it shown in Fig. 2b. The contact of the thermocouples with the test piece was maintained manually. Temperature gradient along the horizontal axis of the LGTF (axis X in Fig. 2) was determined experimentally, and it turned out to be to 1000K/m. Temperature gradient along the vertical axis of this field has been evaluated as negligible (<<1000K/m).

Step 3. Thirty seconds later, the thermocouple A was removed from the hole and was pressed to the test piece surface fragment CDEF, as it shown in Fig. 3. Temperature gradient along the axis X of the HGTF has been evaluated as high [2]:

$$G = \frac{770K - T_\infty}{L} \gg 1000\frac{K}{m}, \tag{3}$$

where $L$ is the thickness of the hot air layer which provides the conventional cooling of the cylindrical lateral surface of the test piece; $T_\infty = 300K$.

Like to the previous step, the contact of the thermocouples with the test piece was maintained manually.
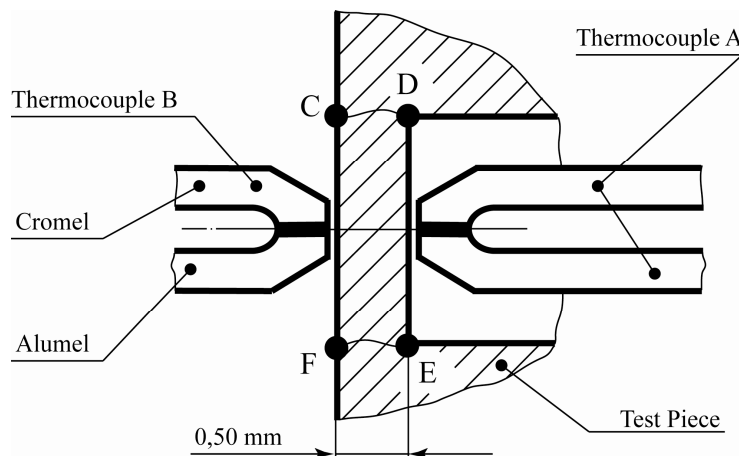


*Fig. 3. Scheme of the set-up for measuring of the temperature of the test piece surface fragment CDEF*

Readings of the thermocouples A and B were recorded by temperature measuring device "USB-TC".

**Experimental results**

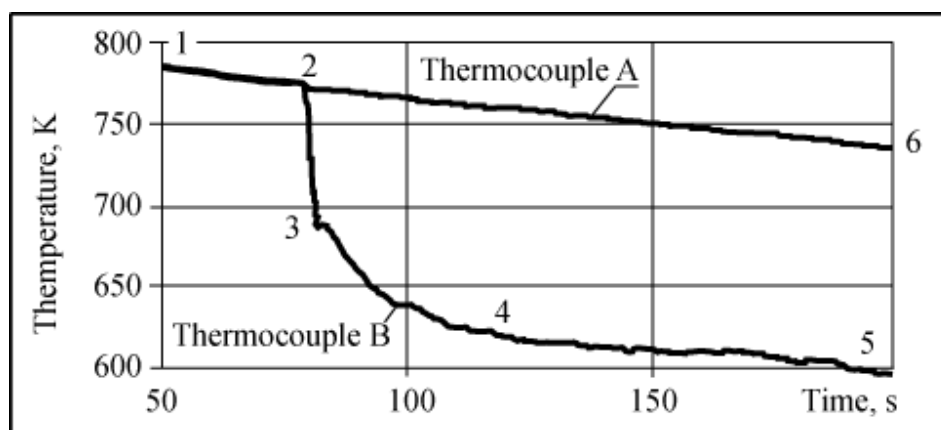The results of the experiment are presented in Fig. 4.



*Fig. 4. Cooling curves of the thermocouple A and B junctions*

Explanations to Fig. 4 are as follows:
- "1-2" – cooling curves of the thermocouple A and B junctions, obtained for the LGTF in the bottom of the hole. This part of the cooling curves shows certain non-identity of the thermocouples A and B;

- "2-3-4" – a part of the cooling curve of the thermocouple B junction, obtained while replacing this thermocouple from the hole to the external test piece surface;
- "2-6" – a part of the cooling curve of the thermocouple A junction, obtained for the LGTF in the bottom of the hole.
- "4-5" – a part of the cooling curve of the thermocouple B junction, obtained in the HGTF during the contact of this thermocouple with the external cylindrical lateral surface of the test piece.

Irregularities in the shape of the cooling curve "4-5" and "2-6" have been provoked by manual maintenance of contacts between the thermocouples and the test piece. These irregularities correspond to variations of the "thermocouple junction - test piece" interface pressure as well as to variations of geometric parameters of this interface.

## Analysis of the experimental results

Measured *dV* values generated by the IHMJ thermocouple A and HHMJ thermocouple B were used by the "USB-TC" device for the calculation of the CDEF fragment temperatures. The calculation was performed according to the equation (1). The difference between the calculated temperatures was about 140K, as one can see in Fig. 4.

Such great difference between the cooling curves of the thermocouple A and B junctions can not be provoked by variations of the "thermocouple junction - test piece" interface characteristics, what follows from the insignificant variations of cooling curve shapes. Therefore, this difference was resulted by inhomogeneous heating of the thermocouple B measuring junction in the HGTF.

## CONCLUSION AND FUTURE WORK

Obtained results show that in case of using the IHMJ thermocouples, the equation (1) is inapplicable to the recalculation of the measured *dV* values to temperatures.

Unfortunately, the insufficient development of the thermoelectricity theory [1, 3] also does not allow to predict (calculate) the value of the thermal electromotive force, generated by IHMJ thermocouples. Therefore, the study of IHMJ properties is useful both for the development of the thermoelectricity theory and practical purposes, for example, for the study of high gradient temperature fields, including the temperature fields of micro-objects.

This kind of investigations was performed at the Laboratory for Mechanical Conformation, Federal University of Rio Grande do Sul (Brazil), within the framework of the project on the experimental determination of the thermal contact resistance in metal forging.

Some of the obtained experimental data allow to conclude that an IHMJ thermocouple is equivalent in thermoelectric properties in thermoelectric properties to a beam of micro-thermocouples connected in parallel which have the same physical characteristics (material, length, integral cross section) as the initial IHMJ thermocouple. The empirical formula of the relation between the thermal electromotive force of a thermocouple and temperatures of its IHMJ has been developed and is under verification.

## REFERENCES

1. ASTM:    *Manual on the Use of Thermocouples in Temperature Measurement*. ASTM, Philadelphia, 1981.
2. Kreith F., Bohnt M.S.: *Princípios de transferência de calor*. Pioneira Thomson  Learning,    São Paulo, 2003 (in Portuguese).
3. Pollock D.D.: *Thermocouples: Theory and Properties*. CRC Press, 1991.

**Agáta RADVANSKÁ**
**Sergej HLOCH**

Technical university of Košice with a seat in Prešov, Slovak Republic

# EXPERIMENTAL ANALYSIS OF THE DUST AT PLASMA CUTTING

*The paper deals with the elimination of negative aspects of plasma cutting by means of emission exhausting and filtration. The point of the technology application is to minimize the worker exposure as well as the environmental pollution. Plasma cutting technology is characterized by high operation costs, mainly high energy consumption, gases consumption, as well as device wear. In addition, it has negative impact on the working environment by its noisiness, UV radiation emissions and last but not least by harmful substances emissions. These last consist of metallic oxides and toxic gases. It is necessary to exhaust them right after they are generated and filter them from the exhausted air to avoid the environment impairment. One of the noxious dusts elimination methods is the application of the proper type of patron filter that would be able to separate the dusts.*

## INTRODUCTION

The subject of environmental science and management is vast and interdisciplinary, ranging from highly technical matters such as the design of emission control equipment to socioeconomic matters such as the valuation of the impacts of pollution. The goal is to prevent or mitigate undesirable impacts of human activities on the environment. Within this endeavour there are several different areas where mechanical engineers can make important contributions. One of the approaches concerns the design of equipment in particular for the control of emissions; an example is an electrostatic precipitator or patron filter to reduce emissions of particulates from the cutting process. The matter of such technology implementation is to achieve the maximum separation effectiveness.

Plasma cutting is nowadays one of the technologies which are preferred especially due to its high efficiency mainly at detail cutting for the further processing by welding. High-speed and accurate operation is incomparable with flame cutting. Tooling is not delimited by material mechanical properties and is not exposed to cutting force and deformation due to mechanical load. Cutting profile depends on plasma arc cutting speed, material type and thickness and can vary from very fine surface to sharp kerfs. Fine profile is obtained by cutting zone cooling. Surface layer oxidation can be eliminated by application of proper protecting atmosphere. Disadvantage of plasma arc machining is the taper, high operating costs, and last but not least, the negative impact on the working environment and the workplace operation. Plasma cutting, as well as the

next thermal process – laser cutting technology, influences significantly the working environment by the gaseous emission production. Melt and evaporated material is the source of dangerous and risk substances with different quantitative and qualitative composition in form of finely diffused particles or gases that can penetrate into respiratory tract and thus threaten a human health.

## EXPERIMENTAL ANALYSIS

The size of the plasma cutting centre ADVANCED HD 3070 is 5 to 2 meters, while the cutting area is 4 to 2 meters. Support carries the plasma arc torch concurrently with the underneath bath movement in the y-axis direction. The bath absorbs the metal dust. Through the gap in the bath side dirt is sucked out and exhausted to the duct due to cleft. The contact has to be isolated to avoid the pressure loss. Ducts are directed through the wall out of the hall. Behind the wall, there are fans that force the air mixture up to stack into the atmosphere. Each duct exhausts independently what is inefficient for increased demands on exhausting and energy consumption.

Although particulate material varies in both size and composition, certain particle types are usually associated with a range of particle sizes. Particulate material produced at plasma cutting crushing or grinding or re-suspended from settled dusts is generally made up of particles with diameters larger than 1 mm. On the other hand, particulate material produced by condensation or gas-phase chemical reactions is comprised of many small particles, all much smaller than 1 mm in diameter. At plasma cutting process, two dust patterns were observed – particle size 1.25 - 20 µm and 3 - 50 µm. Particle shape is characterized as a ball without agglomeration (99%) and as a crystal (1%). Dust colour is black to rusty red, what indicates the presence of metallic oxides (Fig.1, Table 1).
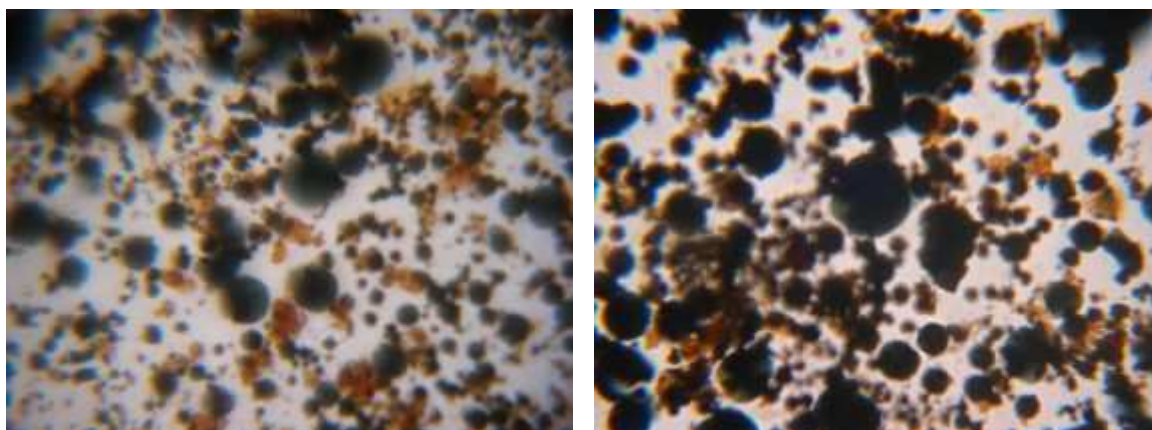


*Fig. 1. Photographs of the samples from the plasma cutting (by HD 3070) exhaust*
*Sample 1 – fine dust (1.25-20 µm)   Sample 2 – coarse dust (3-50 µm)*

*Table. 1. Dust samples characteristics*

| Particle size | Sample 1 | Sample 2 |
|---|---|---|
| Coarse particles | 0.02 mm = 20 µm | 0.0475 mm = 47,5 µm |
| Medium-size particles | 0.0075 mm = 7,5 µm | 0.015 mm = 15 µm |
| Fine particles | 1.25 µm ÷ 2 µm | 0.003 mm = 3 µm |

Filters are designed for both vacuum and gauge pressure air-conditioning system. Device can be installed in the rooms with explosion danger and without chemical activity. Filters are not applicable for hygroscopic dusts, for adhesive dusts, for moist air dusts (particularly below the saturation point) and for dusts that become malleable by filtration. The filter application in certain conditions, their performance and fabric type convenience has to be discussed with the producer. Jet pulse regeneration system of the filter patrons is preferable mainly when filtering agglomerating dust, cohesive dust and dust with specific mass. Oils, solid particles and moisture have to be removed from compressed air. Baghouses separate particles from outlets in separate compartments containing tube-shaped or pocket-shaped bags or fabric filters fig 2. Baghouses are effective in controlling both total and fine particulate matter. They can filter air-mixtures at collection efficiencies of 99.9%. The main parameters in baghouse design are the pressure drop and air-to-cloth ratio. Pressure drop is important because higher pressure drops imply that more energy is required to pull gas through the system. The air-to-cloth ratio determines the unit size and thus, capital cost. This ratio is the result of dividing the volume flow of gas received by a baghouse by the total area of the filtering cloth fig. 2. This ratio is also referred to as the face velocity. Higher air-to-cloth ratios mean less fabric, therefore less capital cost.
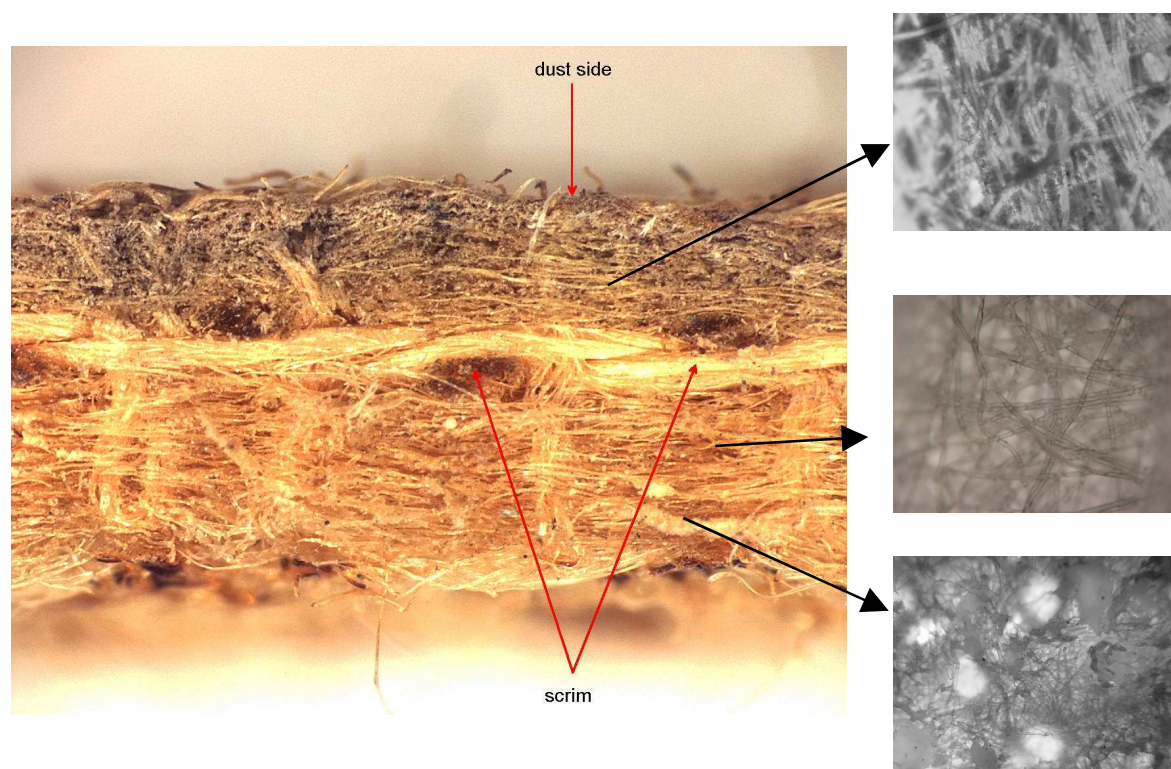


*Fig. 2. Photographs of the filtration fabric*

## PROPOSAL OF THE EQUIPMENT FOR ELIMINATION THE HAZARDOUS PARTICLES

However, higher ratios can lead to high pressure drops forcing energy costs up. Also, more frequent bag cleanings may be required, increasing downtime. Fabric filters are classified by their cleaning method or the direction of gas flow and hence the

location of the dust deposit. Filtering station consists of outlet chamber under control lid and compressed air distribution, filtering box, collector box with motion equipment, support (stand).
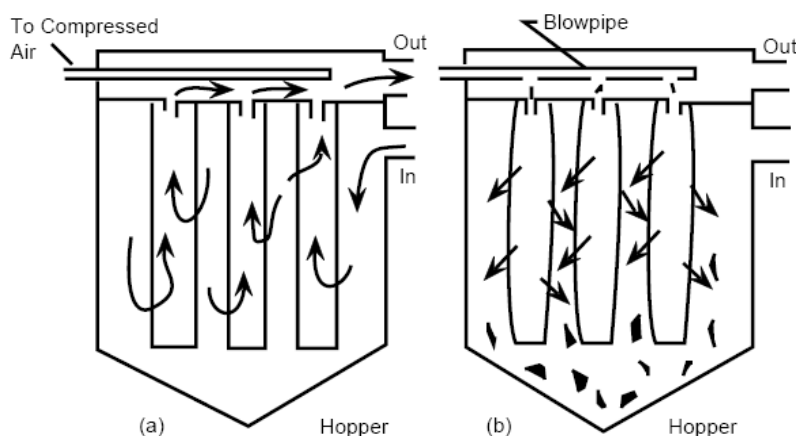


*Fig. 4. Reverse-gas flow cleaning in inside collectors*

Dusty air mixture is supplied through inlet into the filter. Heavier solid particles are segregated by the velocity loss and drop into the collector box. Light-weight particles are segregated on the external surface of the filtering patrons. Purified air passes through filtering medium into patron interior, whence is lead into outlet chamber and fan. Dust stack on the filter surface is released by jet-pulse regeneration. This is performed through electromagnetic valves. Amidst, over each patron outlet gauge are impulse valves. In regeneration process, the compressed air impulse passes through the throat orifice into the patron interior.
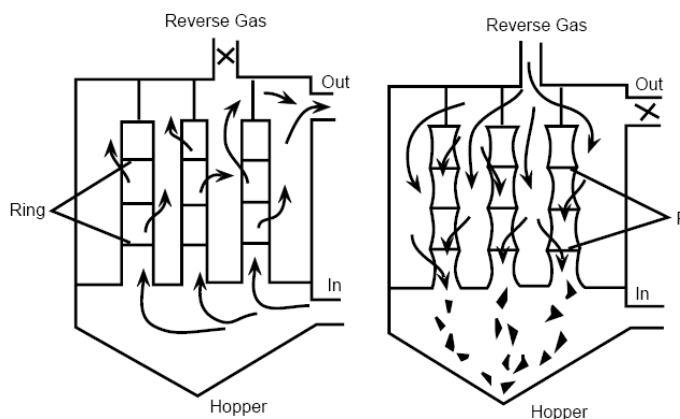


*Fig. 4. Pulse-jet cleaning in outside collectors*

Following the expansion as the effect of the high velocity of the airflow, the suction of the secondary air from the outlet chamber succeeds. This air together with the compressed air expands inside the patron. Pulse-jet regeneration system (fig 5) is integrated on the back of the filter housing. Compressed air is supplied to the auxiliary reserve cartridges placed on the filter backside. Exhausting is provided by two ducts of ø160 mm, these are merged into one outlet duct of ø225 mm and pass across the wall out of the room. Behind the wall, these are connected to the filter FPAT 66 (Fig. 6).

Further, filtered air is lined up to a fan type RVE 400 5N, which forces it through stack into the outdoor air. It is necessary to supply the adapter (400 V) for the fan engine and regeneration control as well as the compressed air distribution (0.4-0.5 MPa). During filtration, dusty gas passes upward into tube-shaped or pocket-shaped bags that are closed at the top. Tube-shaped bags are typically 10 meters tall and 300 mm in diameter. A dust cake builds-up on the inside bag surface during filtration. Clean gas passes out through the filter housing. Filtration velocities are about 10 mm.s$^{-1}$. Many bags in a bag-house act in parallel, and a fabric filter usually comprise several compartments.
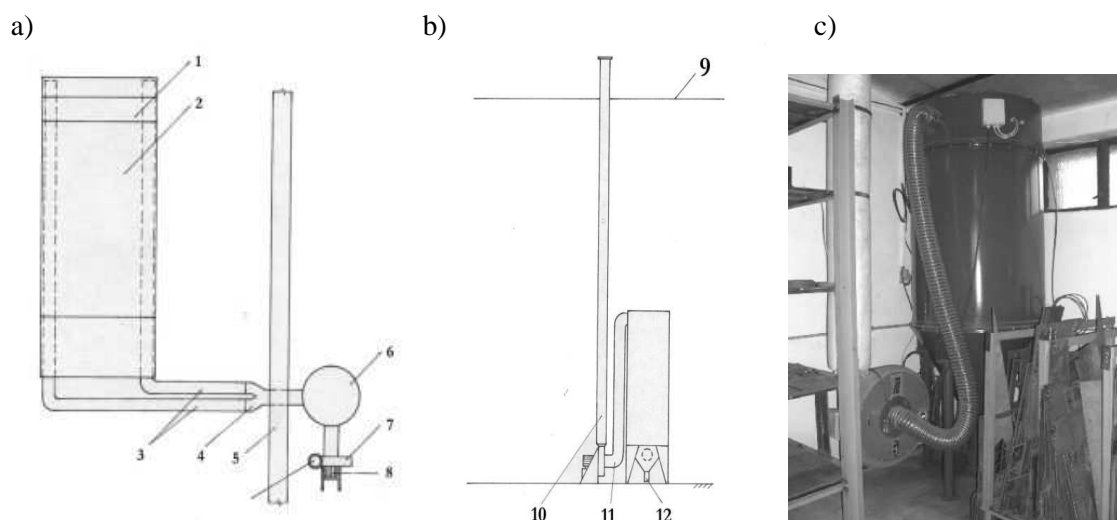


*Fig. 5. Air-mixture exhausting and filtration: a) cross-section, b) longitudinal section, c) projection (1 – support with plasma torch, 2 – plasma cutting center ADVANCED HD 3070, 3 – exhausting ducts ⌀160 mm, 4 – joining piece, 5 – wall, 6 – filter FPAT 66, 7 - fan RVE 400 5N, 8 – electromotor, 9 – building roof, 10 – stack, 11 – filer and fan interconnection, 12 – collector box)*

Filter problems are caused by improper bag specifications, installation, or tensioning. Other problems are related to bag blinding, a gradual, irreversible increase in pressure drop. In outside collectors, dusty gas flows radially inward through cylindrical bags held open by a metal frame inside them. Dust is collected on the outside bag surfaces. Clean gas passes out of the top of each bag to a plenum. Cleaning outside collectors usually involves injecting a pulse of compressed air at the outlet of each bag. This pulse snaps the bag open and drives the collected dust away from the bag surface into the hopper. Because pulse-jet cleaning takes a fraction of a second, it can be done online without interrupting the gas flow to a compartment. Pulse-jet filters generally use thick felt fabrics to reduce dust penetration even when the dust cake is not thick. Filtration velocities through a pulse-jet filter are several times higher than through a reverse gas filter; therefore, pulse-jet filters can be smaller and less expensive. Operating at high filtration velocities can lead to an excessive pressure drop, dust penetration, and fabric wear. Pulse-jet cleaning can be ineffective when the dust is fine. The particles are driven beneath the fabric surface and are not easily removed. As fine dust accumulates below the surface, the pressure drop across the filter gradually increases. If the pressure drop becomes too high, the blinded bags must be replaced. With online cleaning of pulse-jet filters, as little as 1% of the dust on a bag can fall to the hopper after each cleaning pulse.

## CONCLUSION

Plasma cutting technology is characterized by high operation costs, mainly high energy consumption, gases consumption, as well as device wear. In addition, it has negative impact on the working environment by its noisiness, UV radiation emissions and last but not least by harmful substances emissions. These last consist of metallic oxides and toxic gases. It is necessary to exhaust them properly after they are generated and filter them from the exhausted air to avoid the environment impairment. One of the noxious dusts elimination methods is the application of the proper type of patron filter that would be able to separate the majority of the emitted dusts.

## REFERENCES

1. Boháčik Ľ., Hloch S.: *Mechanika tekutín a aerodynamika - základné teórie a cvičenia*. Fakulta výrobných technológií TU Košice s o sídlom v Prešove, 2003, ISBN 80-8073-069-5.

2. David M.L., Cornwell D.A.: Introduction to environmental engineering. New York, N.Y.: McGraw-Hill, Inc., 1991.

3. Hačunda P.: *Technické zariadenia na ochranu ovzdušia*. Alfa Bratislava 1984,

4. Harris M.: *Inhouse solvent reclamation efforts in air force maintenance operations, of hazardous waste minimization within the department of defense*, edited by J.A. Kaminsky. Office of the Deputy Assistant Secretary of Defense (Environment) Washington, D.C., 1988.

5. Maňková I.: *Progresívne technológie*. Vienala Košice, 2000.

6. McGeough J.A.: *Advanced Methods of Machining*. Chapman and Hall, London, 1988.

7. Radvanská A., Hloch S.: *Ekotechnológie a ekotechnika*. Fakulta výrobných technológií TU Košice so sídlom v Prešove, 2002, ISBN 80-7099-928-4.

8. Urbánek T.: *Odstraňovanie prašnosti filtračnými odlučovačmi prachu*. Ekologický radca 1999-2000, ALLDATA Prešov 1999.

**Ján SLOTA**
**Ivan GAJDOŠ**

Technical University of Košice, Slovakia

# THE APPLICATION OF RAPID PROTOTYPING, CAE AND CAM METHODS IN PRODUCT DEVELOPMENT PROCESSES

*In order to shorten manufacturing time for new products and their moulds, the use and the development of modern techniques are critical. One of such technologies is the rapid prototyping method, which enables to designers and customers to see the physical presentation of a new product. Application of the CAE methods is accentuated in the development phase of the product, which redounds to cost reducing on tools and moulds development. The paper deals with several steps in prototype development, the application of computer simulation by means of CAE system Moldflow MPI in mould development for mold plastic part and utilization of CAM system for NC programming of the mould manufacturing.*

## INTRODUCTION

A present–day rapid growth in diverse industries put the demanding requirements on rapid innovations of products. In order to reduction of manufacturing time for new products and their moulds, the use and the development of modern techniques are critical. One of such technologies is the Rapid Prototyping method, which enables to both, designer and customer to see the physical presentation of a new product.

The design of molded plastic parts as well as design of moulds for plastic injection processes is comparatively complicated process. It is needs takes into the account costs, production time, part design, ergonomic and aesthetic requirements. The part development process includes conceptual design – CAD model, engineering analysis, process simulation, manufacturing of prototype and testing. The utilization of CAE methods allows through simulation to speed up the mould design process and the injection molding process optimization. Research in plastic injection molding area has brought a many scientific papers with the aim to improving optimalization algorithms of mold design [1-3]. Many other authors utilize CAE tools for optimization of variable parameters in plastic injection processes, as are minimal pressure [4], elimination of distortion and uniform of hot-melt flow in mold cavity [5], determination and evaluation of weld/melt lines [6] and shrinkage prediction [7].

The integration of product development processes like Rapid Prototyping, CAE and CAM methods has been presented in the paper. The procedure in prototype manu-

facturing by FDM method and subsequent plastic injection simulation by means of Moldflow MPI software was presented.  In this analysis was analyzed injection molding parameters as are the fill time, injection pressure, distortion, shape precision as well as the influence of gate location.

## THE RAPID PROTOTYPING

The Dimension 3D printers utilize for build model the FDM technology also known as Fused Deposition Modeling is layered manufacturing process.. Dimension SST machine offers functional prototypes with ABS. The required geometry is produced in thin layers by a small CNC-controlled extruder A thin bead of molten plastic is extruded through the computer controlled nozzle, which is deposited on a layer-by-layer basis to construct a prototype directly from 3D CAD data. The technology is commonly applied to form, fit and function analysis and concept visualization. In addition, parts can be used for form fit and light testing purpose.

In order to reduction of manufacturing time and increasing of design reliability is needs to utilize the Rapid Prototyping methods in product development phase.  After this it is possible to check if the product is adequately aesthetic, or if the part meets to specifications for requirement function. The Rapid Prototyping contributes to early mold development for given part.
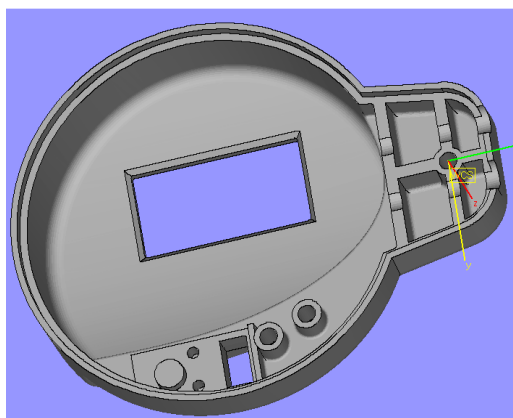


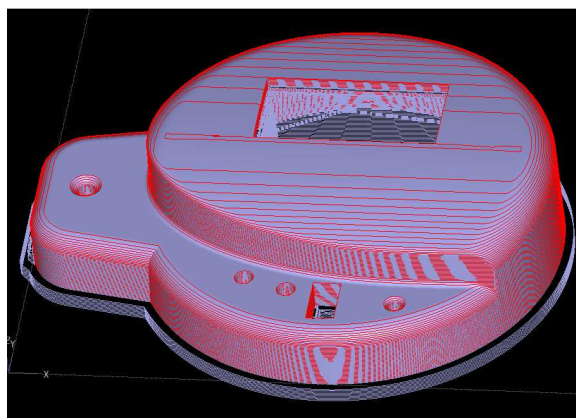Fig. 1. *3D model of the product*         Fig. 2. Model with supports

A 3D computer model of the product presents the basis for the prototype manufacturing is shown in Fig. 1. The prototype was oriented in machine's working area in consideration of functional, stiffness, and other product requirements. For the quality of manufacturing of the prototype, so-called supports that are attached to the model have to be determined, these supports being presented in Fig. 3. After that the manufactured parameters must be prepared. When the prototype is finished, the supports must be removed, and the prototype must be cleaned, hardened and completed. For rapid removing the supports from the prototype, it is suitable to apply device making use of sinuous flow of special solution.

Protolypes can be used for manufacluring of a silicon mould and for the first production (up to 100 parts), for easier design of the real mould, as an aid in visualizalion and as an aid in sales aclivilies.

## EXPERIMENTAL RESULTS

### Injection molding simulation

The simulation was performed in three variants of gate location. The gate selection was performed on the basis of part geometry, surface quality of part and analysis performed for optimal gate location (MPI) (see Fig. 3). The simulation was done with equal terms in all three cases, listed in Table 1.
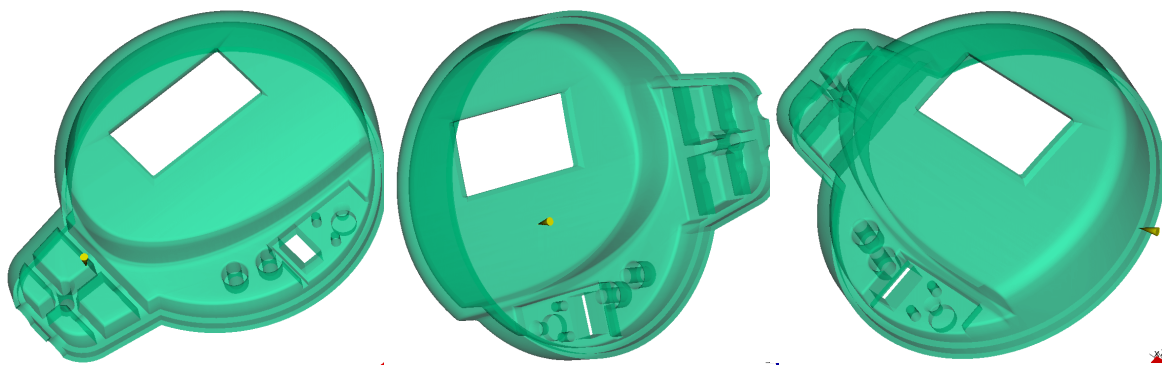


*Fig. 3. Gate location for variant A, B and C (from left to right)*

*Table1 Settings of simulation process*

| Material | Enduran 7065 PBT |
|---|---|
| Melt temperature | $280^{\circ}$ C |
| Mold temperature | $60^{\circ}$ C |
| Cooling time | 20 s |
| Fill control | automatická |
| No. of nodes | 17579 |
| No. of tetraeder elements | 97916 |

Manufacturability was checked from severe different point of view, among which the optimal one had to found: the lowest fill time, the lowest injection pressure and minimal shrinkage and warpage of part. The results of simulation for concrete examined parameters and all variants are mentioned below.
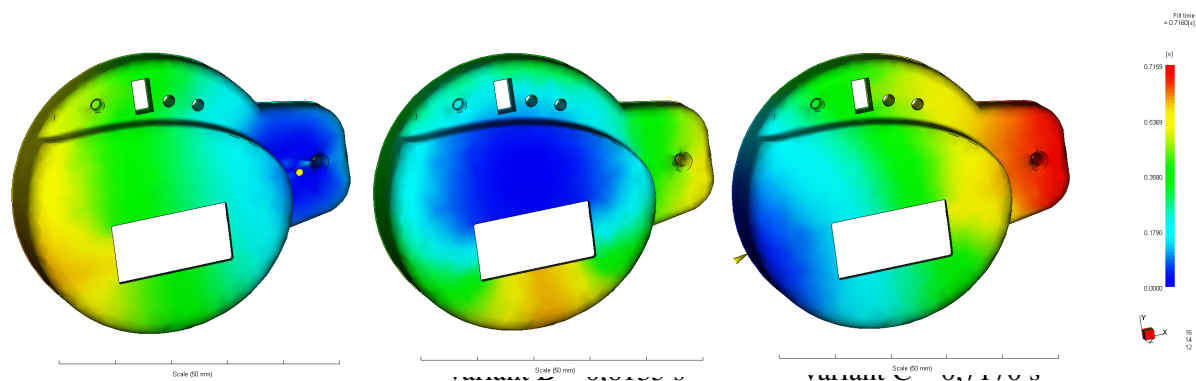


*Fig. 4. Results of analysis – fill time*

From results (Fig. 4) it is possible to see, the fill time is shortest for variant A, however, the difference among all variants is within the range 0,1 s. Considering this small difference, the fill time will have low importance in selection of final variant.

Injection pressure was analyzed for selection of injection molding machine, especially, at which tendency is to minimize it. Fig. 5 shows minimal injection pressure for variant B and maximum injection pressure for variant C.
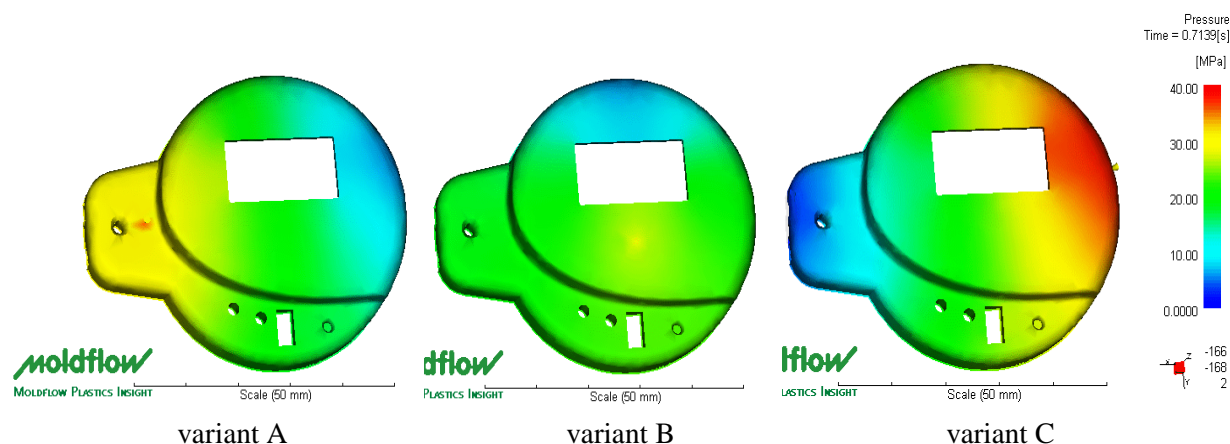


variant A        variant B        variant C

*Fig. 5. Injection pressure at end of fill*

From Fig. 6, it is possible to see shrinkage and warpage of part as well as geometrical precision of molded parts. For better illustration, the results were enlarged 20 times. The precision of molded pieces is very important due to fact, that part is component of thermometer who measures the fluid flow exactly. An emphasis will be focused just on this criterion.
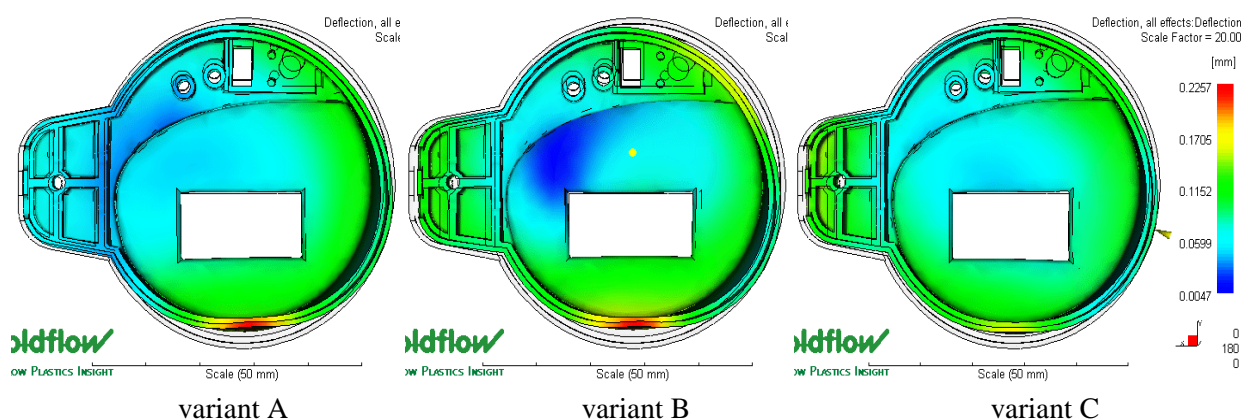


variant A        variant B        variant C

*Fig. 6. Shrinkage and warpage of part*

## Manufacturing of the mould

In the mould making industry there are even higher demands for the reduction of manufacturing time. In order to achieve the most optimal manufacturing as regards reduction of manufacturing time and surface quality, some different milling strategies were carried out. A detailed description of milling operations will be done only for the

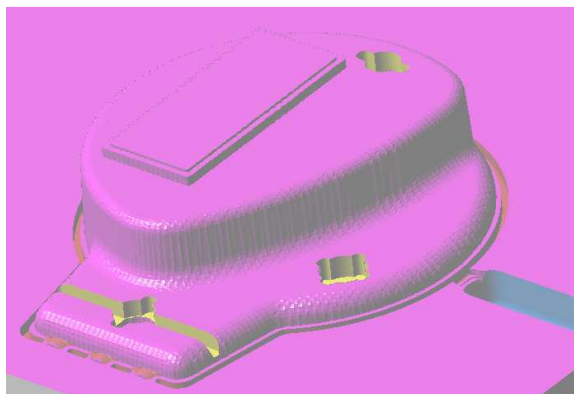core side of the mould – Fig.8. Manufacturing for the core side of the mould was simulated in system Catia V5.
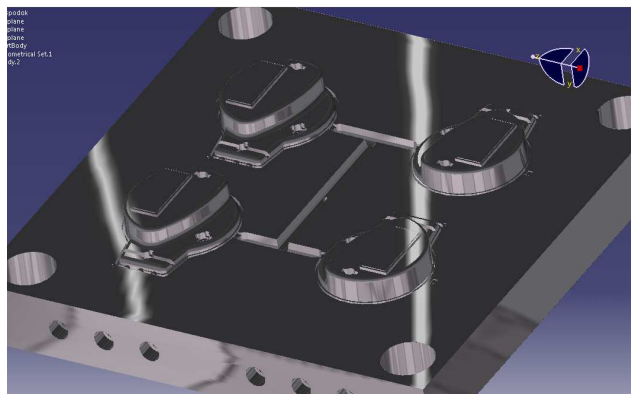


*Fig. 7. Rough manufacturing*



*Fig. 8. The detail of core side of the mould (bottom part)*

The machining was developed as described: rough milling by sweeping strategy (also runner system) – Fig.7, finish milling by pocketing strategy, drilling of tempering system and finish milling by sweep roughing strategy applied on runner system too. The material of the mould forming system is Alumec 89 with hardness 199 HV30. All milling operations were made on the Emco Mill 155 machine tool. The forming system of the mould was assembled by standard parts form catalogue HASCO.



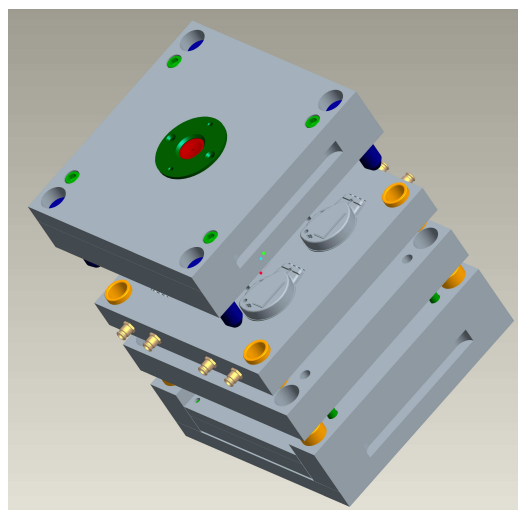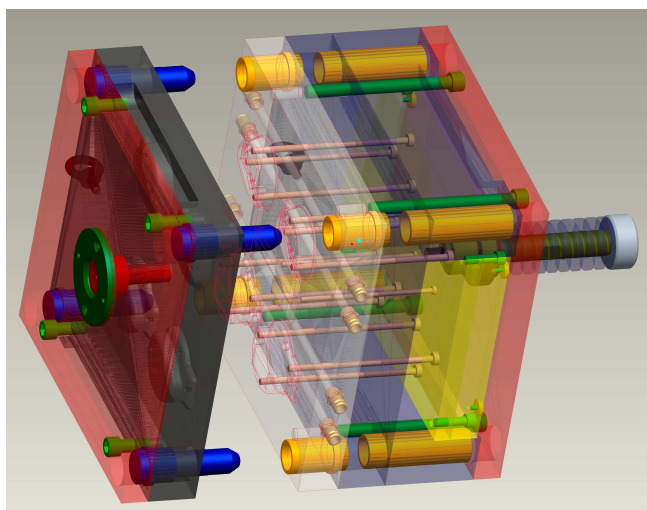*Fig. 9. Complete forming system of the mould*

**CONCLUSIONS**

In this paper, all key points in modem product like Rapid Prototyping, CAD/CAM/CAE tools and mould development are presented. This kind of knowledge enables the possibility to develop a completely new product in a period of 6 months, from the idea to the start of the production. This paper does not deal with the preparation of production in the plant.

CAE tools enables, except the design of moulds and optimization process conditions, respectively, determination some injection molding process limits like minimal thickness of thinnest area of the product to achieve required quality of molded part. In simulation of injection molding process, it is possible to assess some critical parameters some variables.

At the moment the ability to manufacture the prototype of the product in the period of 3-4 days, injection molding simulation in 4-5 days and the manufacturing of the mould in 2-2,5 months is given. If these processes are conducted simultaneously, the decrease of the development time of the mould down to less than 3 months is possible.

## REFERENCES

1. Lee B.H., Kim B.H.: Polym-Plast Technol. Eng. 34(1995), 793-811.

2. Pandelidis I., Zou Q.: Polym. Eng. Sci. 30 (1990), 873-882.

3. Pandelidis I., Zou Q.: Polym. Eng. Sci. 30 (1990), 883-892.

4. Tumg L.S., Chiang H.H., Stevenson J.F.: SPE Tech. Pap., 1 (1995), 668-672.

5. Seow L.W., Lam Y.C.: J. Mat. Proc. Tech., 72 (1997), 333-341

6. Lautenbach S., Wang K.X., Chiang H.H., Jonh W.R.: In: Proceedings of the SPE Annual Technical Conference, ANTEC ´91, 1991, pp. 372-376

7. Jansen K.M.B., Van Dijk D.L., Burgers E.V.: Int. Polym. Process 13 (1) (1998), pp. 99-104.

8. Kuzman K., Nardin B., Kovač M., Jurkošek B.: *The integration of rapid prototyping and CAE in mould manufacturing*. Journal of Material Processing Technology 111 (2001) 279-285.

9. http://www.moldflow.com  (15.3.2006)

10. Manual Moldflow MPI.

**Victor SPUSKANYUK**
**Alexander DAVIDENKO**
**Alexander GANGALO**

Donetsk Institute for Physics and Engineering named after O.O.Galkin
of the National Academy of Sciences of Ukraine

# NEW METHOD OF CALCULATING THE EQUAL CHANNEL ANGULAR EXTRUSION PRESSURE

*New method of calculating the equal channel angular extrusion (ECAE) pressure is introduced. Calculation of the pressure is produced by using friction factor of Siebel. This method of pressure calculation is proposed for ECAE of short billets and for the equal-channel angular hydroextrusion.*

## INTRODUCTION

ECAE is a process where an elongated billet is forced to pass through two channels of equal cross-section intersecting at an angle, usually between 90° and 135°. The deformation is produced by simple shear as the specimen crosses the shear plane. The subject material can thus undergo repeated processes of ECAE without reducing the billet cross-section. Severe strains and simple shear deformation mode contribute to strong, sometimes unusual effects of ECAE on material structure and properties [1].

Among the known methods of severe plastic deformation, ECAE is considered the most prospective candidate for many practical applications. The process optimization presents significant practical interest and, sometimes, it is the key factor for successful commercialization. Optimization of ECAE is provided by control over contact friction, channel geometry, strain/strain rate, billet shape, punch/tool pressure [2].

This report describes the new method of calculating the ECAE pressure. The punch pressure is calculated by using the friction factor of Siebel.

## METHOD OF CALCULATING THE ECAE PRESSURE

Segal et al. considered the billet stress-strain state during ECAE [1]. Calculation of punch pressure was realized with assuming Coulomb friction ($\tau_f = \mu\sigma_\theta$) as the axial pressure distribution in the line of billet is nonuniform. The proposed method assumes Siebel friction in the form of $\tau_f = mk$, where $k$ is the maximum shear stress. The new method of pressure calculation is proposed for ECAE of short billets. It is proposed also for the equal-channel angular hydroextrusion (ECAH) as the relative area of billet and die contact is small [3]. Such approach is convenient for ECAE pressure calculation in view of material hardening.

ECAH is a new version of ECAE [3]. A schematic of the ECAH facility is shown in Fig.1. The characteristic property of ECAH process is extruding a billet through the

die channel by the fluid pressure. Using a fluid during the extrusion of lengthy billets diminishes the friction effect on the total deformation load, thus providing substantial advantage compared to the other known processing methods.

Under ECAH conditions the relative area of billet and die contact must be optimal. It is desirable to ensure the minimal contact area but it is necessary to provide the simple shear mode of deformation. The output channel segment length must be long enough to make sure that the billet main part is linear after the deformation. The conical die takes up position in front of the angular die in order to seal fluid. Indicated requirements determine the rational relative area of billet and die contact. At that condition the rational relative length of contact area for billet, conical die and input channel of angular die L/d is not in excess of 3.

The punch pressure is calculated as

$$p_z = p_{z0} + p_{f1} + p_0, \qquad (1)$$



Fig. 1. A schematic of the ECAH facility: 1 - plunger, 2 - fluid, 3 - roll cage, 4 - cartridge, 5 - billet, 6 – conical die, 7 - angular die

where $p_{zo}$ is the pressure in lower part of the input channel; $p_{f1}$ is the component of pressure necessary for overcoming the friction force in the input channel; $p_0$ is the backpressure.

Normal stress $F_N$ and frictional stress $\mu F_N$ that affect the lower wall of the output channel were described (Fig. 2) in [1].

Then the friction force of billet in the output channel is

$$Q = \mu F_N S, \qquad (2)$$
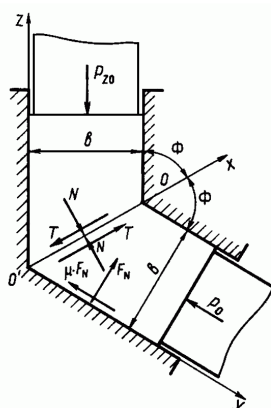


Fig. 2. Scheme for the action of forces on billet and tool under ECAE [1]

where $S$ is the cross-section area of the channel.

This friction force is given also as

$$Q = m_2 k S_c, \qquad (3)$$

where $m_2$ is the friction factor in the output channel; $S_c$ is the area of billet and output channel contact. From (2) and (3) follows

$$\mu = m_2 \frac{k S_c}{F_N S}. \qquad (4)$$

Contact area of billet and output channel is given by

$$S_c = Sn = G\Delta z, \qquad (5)$$
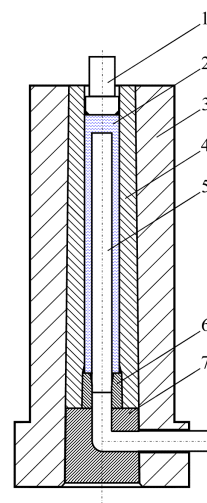
where $n$ is the index of areas $S_c$ and $S$ relationship; $G$ is the perimeter of the channel cross-section; $\Delta z$ is the magnitude of billet top displacement. Then from (4) and (5) follows

$$\mu = m_2 \frac{kn}{F_N} \tag{6}$$

where $n = 4\Delta\bar{z}$; $\Delta\bar{z}$ is the relative value of billet top displacement ($\Delta\bar{z} = \Delta z / D$ for circular cross-section of channel and $\Delta\bar{z} = \Delta z / B$ - for square cross-section of channel, $D$ - diameter, $B$ - side of channel square).

   Taking into account that [1]

$$F_N = k + pctg\Phi,$$

where $p$ is the hydrostatic pressure at shear line, the Coulomb friction factor is

$$\mu = m_2 \frac{kn}{k + pctg\Phi} \tag{7}$$

   From equation for hydrostatic pressure at shear line [1]

$$p = \frac{p_0 + k(\mu + ctg\Phi)}{1 - \mu ctg\Phi} \tag{8}$$

we have

$$\mu = \frac{p - p_0 - kctg\Phi}{k + pctg\Phi} \tag{9}$$

   Then from (7), (9) and equation for the axial pressure in lower part of the input channel [1]

$$p_{Z0} = p + kctg\Phi \tag{10}$$

follows

$$p_{Z0} = p_0 + 2kctg\Phi + m_2 kn \tag{11}$$

   Using (11), the value of Siebel friction factor in the output channel can be calculated as

$$m_2 = \frac{1}{kn}(p_{Z0} - p_0 - 2kctg\Phi) \tag{12}$$

   It is expedient to use the mean value of maximum shear stress for the purpose of calculating the material hardening. Therefore equation $k_m = \sqrt{k_0 k_d}$ is proposed, where values of the maximum shear stress before and after the deformation are $k_0$ and $k_d$ accordingly. Then

$$p_{Z0} = p_0 + 2k_m ctg\Phi + m_2 k_d n \tag{13}$$

Component of pressure necessary for overcoming the friction force in the input channel is estimated as

$$p_{f1} = 4m_1 k_0 \bar{z} \tag{14}$$

Here $m_1$ is the friction factor in the input channel, $\bar{z}$ is the billet relative length in the input channel of the ECAE die ($\bar{z} = z/D$ or $\bar{z} = z/B$). In the case of ECAH the relative length of contact area for billet and conical die is also taken into account. Then from (13) - (14) taken the punch pressure is

$$p_Z = 2k_m ctg\Phi + 4m_1 k_0 \bar{z} + m_2 k_d n + p_0 \tag{15}$$

As $n = 4\Delta\bar{z}$ pressure is

$$p_Z = 2k_m ctg\Phi + 4m_1 k_0 \bar{z} + 4m_2 k_d \Delta\bar{z} + p_0 \tag{16}$$

For $\Delta\bar{z} << 1$, the friction in the output channel is not taken into account. Then

$$p_Z = 2k_m ctg\Phi + 4m_1 k_0 \bar{z_0} + p_0 \tag{17}$$

where $\bar{z_0}$ is the relative length of initial billet.

ECAE load is the product of pressure $p_z$ and billet cross-section area. ECAH load is the product of pressure $p_z$ and cross-section area of cartridge channel, and it is necessary to add about 10% of load for taking into account the plunger seal friction forces in the cartridge channel.

## CONCLUSION

Simple equations of pressure were proposed for ECAE of short billets and for ECAH. The components of pressure necessary for overcoming the friction forces in the input and output channels were calculated. The proposed equations are suitable for the purpose of calculating the material hardening.

## REFERENCES

1. Segal V., et al.: *Processy Plasticheskogo Structuroobrazovania Metallov*. Sci. Eng, Minsk 1994.
2. Segal V.: *Engineering and commercialization of equal channel angular extrusion (ECAE)*. Mater.Sci.Eng., A 386, 2004.
3. Spuskanyuk V., et al.: *Development of the equal-channel angular hydroextrusion*. J. Mater. Process. Tech. 203/1-3, 2008.

**Wiktor SHABAJKOWITCH**

Rzeszow University of Technology, Poland

# A NEW APPROACH IN DEVELOPMENT
# OF TECHNOLOGICAL PROCESSES

*It is necessary to bring in additional stages in the method for development of the techno-logical processes in manufacture and assembling of details, which are linked with the use of technological heredity and the use of effect self-organization and the purpose of di-rected forming of the rise indexes of quality products.*

The planning of technological processes for making of the details or their assem-bling is indicating enough all range of complex and multiple problems, the implemen-tation of which requires thorough knowledge, a good practice and trade. At the imple-mentation stage of technological process during realizations of the technological trans-formations, the phases of all actions of the material, power and informative types above the billet, details or product, which would have the entrances, outputs and the management issues. The technological transformations have a feedback with providing the objects of the system used to receive information on quantitative and high-quality parameters of these transformations [1].

Taking into consideration the basic lack of traditional methods for planning of the technological processes, it is possible to deliver the following resolution. Initially, as a part of decision on the securing process of quality products, some of the index of un-dertaken quality, like level of precision or accuracy is more frequent than all and a me-thod of treatment provided, would get out from the reference data. If it was needed to promote a wear resistance of the detail, a question to decide will be fairly simple: more resistance material would get out or some of the covering that were used etc. The in-dexes of quality did not associate between themselves, obviously a technological prime price should be poorly analyzed. Secondly, the properties of the details, which are based on the providing level of quality, were not fully used. Thirdly, a clear feed-back from the operating properties of the details and technology of their recipient or rather providing of quality, was not practically used. Fourthly, the technological possi-bilities of all known methods and the methods of the treatment for the details and their assembling process were not fully used, also worth to mention about new, recently de-veloped. If to talk of any possibilities for the self attuned technological systems, many of us heard by hearsay that they could not be used. Excepting the known requirements to the traditional technological processes, like high quality, low price, some new para-digms came: flexibility, intelligence, virtualization, enterprise, being now as the main index of the strategy [2]. All of they could not be used in the traditional method of planning of the technological processes.

The basic signs of the progressive technological processes of a new generation appear to be high quality by a new aggregate of the detail properties, products and high quality by a new measure of their utility as a consequence. The features of progressive technologies can be highlighted: its science capacity, high informative level and computerising, high level of energy supply, optimum of the technological processes, new ways and methods for the treatment of details and their assembling, high level of automation, stability and reliability of processes, safety, flexibility for the development, ecological sustainability.

In spite of the known peculiarities in the method of planning of the modern technological processes, it is possible to stop on some not being in use or not used enough properties. One of them is the directed forming of indexes quality and proper operating properties of products. A study of fundamental conformities to the rules of cooperation and mutual influence of the formed detail properties considerably diminishes the level of influence of the accidental factors, fields of dispersion of the values indexes of quality that is instrumental in the upgrading process for the products. The set of the properties are determined, depending on construction-technological parameters of the products, to take into the account of the external environment of the details and the assembling of the units. A processed approach to the transformation of the detail properties is able to allow building of some models for the transformation of quality indexes. Such models should be simple, representing provision of the automated reflection of the forming process for the detail properties, providing full calculations of all values for the set containing the quality indexes and being in the position to determinate of the necessary descriptions for the elements of the technological mediums depending on a set direction of property changes and quality indexes.

The following was input into mathematical model: quality of detail formed to the technological interference and the most of his indexes are result of this period (previous phases); technological influence on the blank changes of all properties and quality indexes; any quality index, change, changes of the rest of the properties and quality indexes (mutual influence between the quality indexes). It is necessary and generally accepted and also known suggestion in the technology, based on every of the detail properties, products are formed regardless of others. On the basis of such models for the transformation process of properties, it's presumed that their quantitative integral descriptions and desired levels of all values on every separate operation can be certain.

Change in index values of the detail quality as a consequence of any action, different factors has been found

$$
\left[\Delta K\right]_i = \begin{vmatrix} k_{11} & k_{12} & ... & k_{1n} \\ k_{21} & k_{22} & ... & k_{2n} \\ . & . & ... & . \\ k_{m1} & k_{m2} & ... & k_{mn} \end{vmatrix}_j \begin{vmatrix} K_1 \\ K_2 \\ ... \\ K_n \end{vmatrix}_{j-1}
$$

(1)

where $K_1, K_2,..., K_n$ - the index values for the quality received after $j\text{-}1$ operation; $k_{11}, k_{22},...,k_{mn}$ - coefficients of change index values of the quality at the end of $j$ technological method of the treatment (coefficients of the correlation).

All difficulties of the subsequent consideration will be brought up to the determination of the coefficients correlation.

If inherited change of index quality, it is possible to indicate by the following

$$\pm \Delta K_i = k_{i1}(K_1)_{j-m} + k_{i2}(K_2)_{j-m} + ... + k_{in}(K_n)_{j-m}$$

(2)

where $k_{in}$ - coefficients of influencing of the properties on a property $j$; $K_n$ - the values of index quality, attained to the operation $j$; ($j$-$m$) - index of the property influence formed to operation $j$ on the result of its implementation.

This approach requires many calculations of all values of index influence of the quality, special coefficients of correlation, and application of methods generation of the primary structures of route technological processes, and closely associated with the automation of technological calculations and synthesis of the structures of the technological objects. Therefore a technological process, which would be able to provide the forming of necessary operating properties, should be worked up at the automated rate, both on the basis of general technological grounds and taking into consideration their fundamental conformities of the rule for technological inheritance. By creating of the technological mediums with necessary descriptions of the property transformation and managing cooperation of separate elements between themselves and through the processed detail, it is possible to direct the forming of the desired quality indexes and operating properties.

In the technological systems at the production level and assembling of the details, products of the inherited communications are expressly traced and so a change of technological influence can be examined as bifurcation, that causes some new and on the turn results in the appearance of new physic - mechanical properties [3]. With justification of the limits of the action negative properties, can be considerably decreased and even removed. Though along with the appearance of whole row of positive properties from such processes and chance of process not being studied, could get worse of quality indexes by the incomprehensible development.

It is necessary to analyses phenomenon of self-organization in close relation to the inherited properties of liquid metal in the blank structure, so a size of corn of the pressed blank will depend on the temperature of recrystallisation, its degree and speed of deformation. With the critical speed of deformation it is sharply multiplied all sizes of corns at falling of durability blank material. If the blanks turn out the methods of pressing from powder for different materials, inherited properties of separate particles and between them show up clear enough. Thus in blank preparation production is subject to research of the phenomenon of bifurcation in do- and post-evolutional development of the system, limitation and its firmness with the purpose of the use of self organization of different technological blank preparation systems.

At tooling of blanks details the processes of self-organization behave to their sizes, form, mutual placing of surfaces and especially blanket. Blank material is a continuous environment with a geometrical form; on the way of transmission of the inherited properties thermal operations settling their alteration, passes after structure and tensions and basic barrier. There is phenomenon of bifurcation resulting in the appearance of a new self getting organized structure with new properties. There are enough

examples of this: special change of the rates of treatment and assembling, nursing, assembling in the self set systems, adapted treatment and assembling etc.

A lot of attention is forwarded to the quality management, however the mechanisms of this type of management are not quite specified, which actually deprives this type of developments of its practical value. The flow diagram of mechanism forming of indexes quality of the products is developed on the basis of the theoretical and experimental developments on the problem of quality, influence of four groups of determining entrance variables (designer, technological, organizational and operational) on output variables were taken into consideration, i.e. indexes of quality. Every entrance is variable through the coefficients of the level of influencing and actually forms the correlations of all quality indexes. The offered mechanism forming of quality indexes is fully adequate to the technological process, like quality of the products is formed and can be considered as a type. Complication of such type model can be looked over only in the correct exposure of basic entrance variables and special coefficients of the correlation [4].

The technological ensuring of the operating detail properties and their products has the above all value. Apart that, all operating detail properties and their products contact harshness, wear resistance, durability of fits, corrosive firmness and dynamic contact durability, fretting - resistance, heat conductivity is understood. The technological ensuring of the contact harshness is based on equalizations of the communication between concrete surfaces of the details in terms of their treatment. Increase of the contact harshness is possible to attain due to optimization of the rates of cutting and account of technological heredity. It is proved that the technological provision and increase of the wear resistance of the details by the technological determination of their parameters in quality blanket in accordance with external environment. Combination of thermal and power influence on the blanket of the processed detail is based on the consolidating of the surface. Causing of the special covering will be the next methods to increase of wear resistance. The technological ensuring and increase of corrosive firmness of the details are provided by setting of required parameters of contact surfaces as a necessary containment and then development of the technological process that will allow getting the indicated parameters. The technological provision and increase of corrosive firmness of the details is provided due to creation of a proper quality of blankets at mechanical heat treatment and with use of inhibitor corrosion and different metallic and non-metal sheeting.

Technological insurance and increase of fatigue strength of the details are related to the plastic deformation, which is different co-operations of dislocations of accumulation vacancies and also the origin of fatigue crack flow that consists in application of cold-hardening of blankets promoting tireless firmness on 25...30%, by creation of hindrances to the increase of the existing origins of new fatigue cracks [5]. By the technological insurance and increase of durability connections with interference, it is possible to manage due to the change of coefficient friction in fit and geometrical parameters of the attended surfaces of details. It is achieved by increase of durability connections in a number of different ways and methods.

It is possible to draw a conclusion that at working stage of the technological processes receiving blanks, treatment of the details and assembling, especially in the automatic rate, it is necessary to use a new method of directed increase of quality in-

dexes. A method consists of highlighting of the constructional, technological, operating factors and communications between, which form all indexes of quality products. The use of whole range of the technological influence, especially technological heredity and self-organization of the processes is an obligatory.

The mechanism of the directed increase in the quality products as a system of the organic influence of the constructional and technological factors through the coefficients of influence (correlations) create all indexes of quality that have been examined. It is obvious that every factor influences at any level on all indexes of quality through keeping communicating with others.

## REFERENCES

1. Manuylov V.F.: *Machine-building. Encyclopedia. Technology of casting productions*. P IIIM.: Machine-building, 1996 (in Russian).

2. Suslov A.G., et al: *Technological providing and increase of operating properties of details and their connections*. M.: Machine-building. 2006 (in Russian).

3. Suslov A.G., et al.: *Quality of machines: Reference book in 2 p.*Under general red. A.G. Suslov. M.: Machine-building, 1995 (in Russian).

4. Bozydarnic V., Grigorieva N., Shabaycovitch V.: *Technology of production details articles.* Lutsk, „Nadstyr'ya", 2006 (in Ukrainian).

5. Vasyliev A.C., et al.: *Directed forming of properties articles of machine-building*. M.: Machine-building, 2005 (in Russian).

**Slawomir SWIRAD**

Rzeszow University of Technology, Poland

# THE EFFECT OF BURNISHING PARAMETERS ON STEEL FATIGUE STRENGTH

*The possibilities of sliding burnishing with cylindrical elements made of diamond composite with ceramic bonding phase are presented in this paper. The influence of some parameters of sliding burnishing on fatigue strength of 401Cr4 steel is also included.*

## INTRODUCTION

All various types of machining, but now more frequently superficial plastic working by burnishing are applied in the technology of machines and devices [3]. Burnishing is superficial plastic working which can be performed at machining centre as finishing. In this process created chips, sparks or dusts, redundant cooling liquids which are necessary in the case of application of machining, e.g. during abrasive machining are not presented. Burnishing is then ecological machining having considerable prospects of development as a method of shaping defined and operation-useful properties of surface layer of machine elements. [4].

This process is applied in machine-building and aircraft industries  in machining of various sorts of materials – from hardened steel through mild steel to nonferrous alloys – of such machine elements as e.g.  shafts of compressors of turbines, rings of rolling bearings. It is also used as operation preparing elements for galvanic- and heat-chemical treatment and for machining of galvanic coats [2].
Burnishing of machine elements can be applied for the following purposes:
- possibility of obtaining surface of very small roughness and big radii of roundings of vertexes and cuts,
- creation of durable internal compressive stresses in surface layer of cold work, and the increase of hardness,
- the increase of resistance to operation results such as abrasion, superficial fatigue, corrosion,
- the decrease of costs of production of machines,
- making the product more ecological.

 In practice all mentioned purposes can be achieved at the same time, but in a different degree.

   The following kinds of burnishing were developed:
- rolling burnishing (with rollers, balls, steel rolls made of steel or of ceramics and sintered carbides),
- oscillatory burnishing (sliding or rolling),
- electromechanical burnishing (with current of low voltage and high intensity flowing through the system 'object - tool'),

- dynamic burnishing (centrifugal and stream ball peening ),
- sliding burnishing (with spherical elements made of natural and artificial diamonds) [5].

Parts of spherical shape are the most often applied (described in literature) elements for sliding burnishing. There are the following their disadvantages:

- difficulty in setting the vertex precisely in the axis of the burnished element,
- necessity to replace the working element of the tool after losing the required shape (radius of rounding),
- lower durability in comparison to other types of burnishing elements.

Cylindrical elements sliding burnishing with a cylindrical is presented in Fig.1 do not have these defects, and their merits are:

- the area of their contact with the object can be changed with wear of working surface,
- they do not require precise setting at the machine tool,
- they enable more precise machining, because they show lesser susceptibility to vibrations during burnishing.
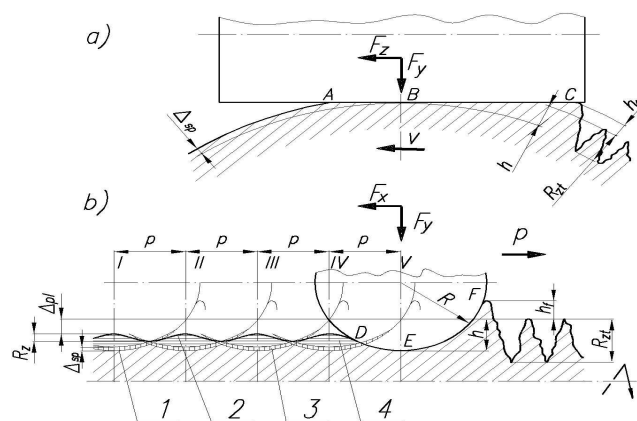


*Fig. 1. Diagram of distortions of roughness during sliding burnishing with a cylindrical element: a) cross-section; b) longitudinal section of burnishing zone*

## DIAMOND COMPOSITE WITH CERAMIC BONDING PHASE

Tools materials for burnishing have to be characterized by series of properties ensuring their long operation.

There are the following most important properties of the tools:

- hardness – tool should not require frequent regeneration or replacement,
- shock-resistance,
- preservation of constant properties in wide range of temperatures,
- high thermal conductivity,
- chemical resistance excluding the possibility of chemical reaction with the machined material,
- low coefficient of sliding friction.

Working ends of burnishing tools can be made from natural single-crystal diamonds or synthetic diamonds in the form of composite containing diamond dust and binder. Tools made from single-crystal diamonds are not much comfortable in use – due to strong anisotropy of crystals of the diamond they require precise setting of the

tool during machining. They wear not only by abrasion but also by chipping, which unfavorably influences the quality of the machined surface. The diamond composite tools have the similar properties, are more comfortable in use and  cheaper. These tools wear only by abrasion (abrasion occurs in working area).

At present, materials of the following trade names are the diamond composites applied for SB (sliding burnishing)

- ballas (ABS).
- carbonado (ASPK),
- AKTM,
- Syndax-3.

Quite high (2,5 – 4 higher), in comparison to natural diamond coefficient of sliding friction (important for SB) and relatively big quantity (about 10% of weight) of metallic (Ni and Cr), which causes high porosity of surface and worse frictional properties are the main defect of these materials (especially ballas and carbonado).  Materials AKTM and Syndax-3 contain matrix of diamond particles (85 – 90% of weight) between which there are particles of filler – silicon carbide. Stresses in material arising during hardening of silicon (increase of silicon's volume by about 10%), which leads to growth of cracks after sintering and causes brittleness of such type of shaping elements are the serious disadvantages of these materials [6].

The use of composite material which properties will comprise features of phases creating grains of diamond constituting the phase of high hardness, and the bonding phase ensuring fracture toughness and shock-resistance is the way leading to the possibility of using the full properties of diamond and simultaneously reducing its features unfavorable for properties of the tool's operation. The following  types of bonding phases are applied for manufacturing diamond composites:

- metallic bonding phase,
- non-metallic bonding phase,
- phase bonding carbide-making metal – metal.

The method of high-pressure sintering in the conditions of static loads is one of the ways of manufacturing diamond composites. For the purposes of industrial production presses which enable sintering at the pressure in the range 5-9 GPa and temperature 1500 – 2300 K are applied. High-pressure devices consist of hydraulic press and special chambers making sintering possible (Figs 2 & 3) [1].

For realization of the process of burnishing with cylindrical composite elements shaping elements of diamond composite with ceramic bonding phase containing  Ti and Si in the form of $Ti_3SiC_2$ were manufactured. Shaping elements were made in IOS in Cracow in the chamber of high-pressure sintering with spherical anvils of Bridgman's type.

The process of sintering is characterized by the following parameters:

- pressure of sintering – 8GPa $\pm$ 0,2 GPa,
- sintering point - 2073  K $\pm$ 50 K,
- time of sintering – 25 seconds.

Selected physical and mechanical properties of diamond composite of $Ti_3SiC_2$ are: density 3,06 g/cm$^3$, hardness HV1 = 38 GPa, Young's modulus 487 MPa, Ra = 0,05 $\mu$m , Rz = 0,69 $\mu$m .
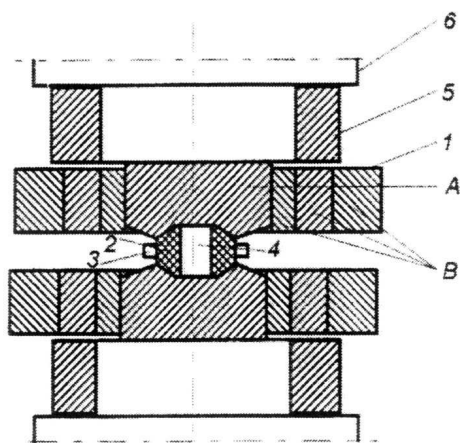
*Fig. 2. Chamber for high-pressure sintering with spherical anvils of Bridgman's type: 1- die (A – carbide anvil, B – binding rings), 2 – pyrophyllite shield , 3 – packing ring of pyrophyllite, 4 - reactionary insert, 5 - punch, 6 – plates of the press [1]*

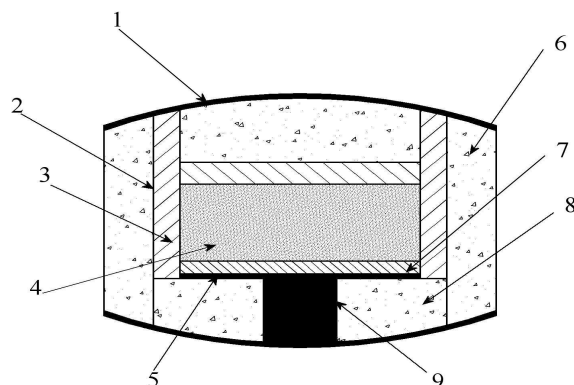*Fig. 3. Reactionary insert for sintering in the chamber of Bridgman's type: 1 – contact plate of molybdenum, 2 – foil of Ta or Zr,3 – graphite heater, 4 – sintered material, 5 – separator of Mo, 6 - pyrophyllite shield, 7 – graphite separator, 8 – pyrophyllite roller, 9 – molybdenic element improving distribution of temperatures [1]*

Application of titanic-siliceous carbide allowed to obtain composite of very good parameters, i.e. resistance to high temperature, chemical resistance, high rigidity at simultaneous plasticity, very high abrasion and low coefficient of friction at metals. This composite does not contain graphite, which favorably influences its mechanical properties.
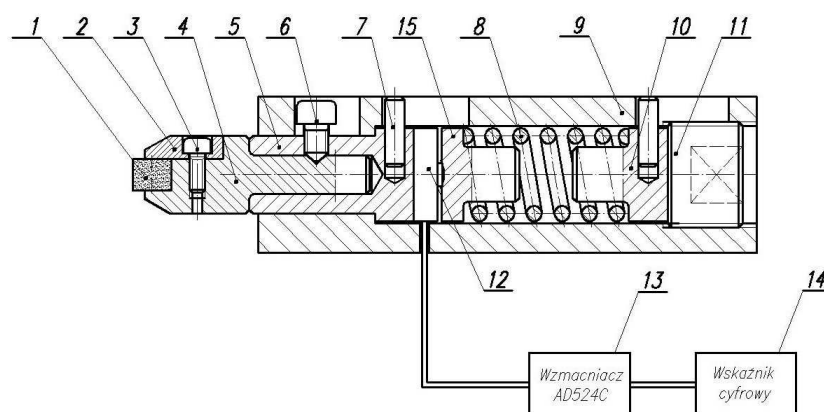


*Fig. 4. Chuck for sliding burnishing with cylindrical elements: 1 – burnishing element, 2 – clamp plate, 3 – screw, 4 – replaceable end , 5 – fastening sleeve, 6 – screw , 7 – base pin, 8 – spring, 9 – body, 10 – stop, 11 – adjusting screw, 12 – extensometer bridge*

Practical realization of the tool consisted on making the holder in which one can mount sinters made previously (Fig. 4). The tool has simple structure and can be fastened at engine lathes, it also allows regulation of clamp force of the device to the machined object in the range from 5 to 500 N.

## EXPERIMENTAL

The main target of the performed investigations was to evaluate the effect of various burnishing parameters on the steel fatigue strength (Zgw).

The studies were conducted on steel 41Cr4 of hardness 32 HRC – Ø 27 mm. The base pretreatment included turning and grinding.

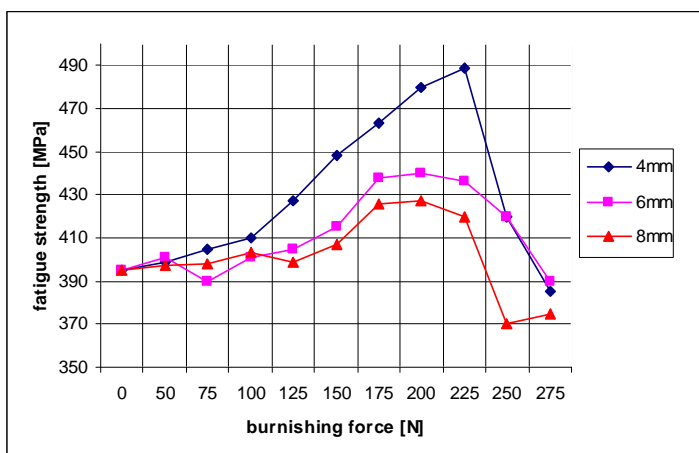| Force [N] | r = 4mm Zgw [MPa] | r = 6mm Zgw [MPa] | r = 8mm Zgw [MPa] |
|---|---|---|---|
| 0 | 395 | 395 | 395 |
| 50 | 399 | 401 | 397 |
| 75 | 405 | 390 | 398 |
| 100 | 410 | 401 | 403 |
| 125 | 427 | 405 | 399 |
| 150 | 448 | 415 | 407 |
| 175 | 463 | 438 | 426 |
| 200 | 480 | 440 | 427 |
| 225 | 495 | 436 | 420 |
| 250 | 420 | 420 | 370 |
| 275 | 385 | 390 | 375 |



*Fig. 5. Influence of burnishing force on the value of Zgw, feed  p = 0,066 mm/r, velocity v = 500 rpm*

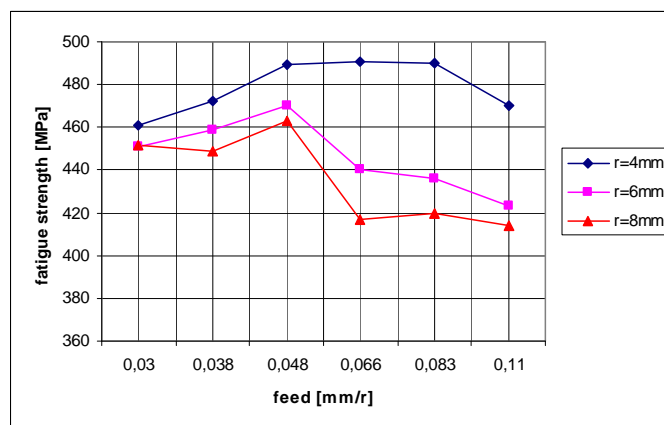| Feed mm/r | r = 4 mm Zgw [MPa] | r = 6 mm Zgw [MPa] | r = 8 mm Zgw [MPa] |
|---|---|---|---|
| 0,03 | 461 | 451 | 452 |
| 0,038 | 472 | 459 | 449 |
| 0,048 | 489 | 470 | 463 |
| 0,066 | 491 | 440 | 417 |
| 0,083 | 490 | 436 | 420 |
| 0,11 | 470 | 423 | 414 |



*Fig. 6. Influence of feed on the value of Zgw, burnishing force F = 225[N], velocity v = 500 rpm*

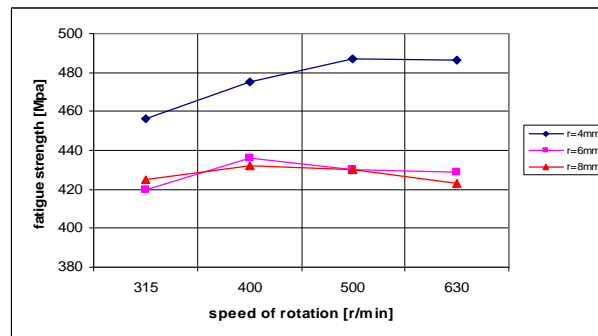| Velocity r/min | r = 4mm Zgw [MPa] | r = 6mm Zgw [MPa] | r = 8mm Zgw [MPa] |
|---|---|---|---|
| 315 | 456 | 420 | 425 |
| 400 | 475 | 436 | 432 |
| 500 | 487 | 430 | 430 |
| 630 | 486 | 429 | 423 |



*Fig. 7. Influence of velocity on the value of Zgw, burnishing force F = 225[N],  feed p = 0,066 mm/r*

Roughness before burnishing was Ra = 0,80 μm. The process of burnishing was performed with three cylindrical elements of diameters r=4,6,8 mm. The hasten pendu-

lar bending fatigue tests were carried out using an electrodynamics vibrator with resonance frequency of the samples adopting the boundary number of cycles of $2 \cdot 10^6$. The used technique, that consisted in cutting samples out of special shaped cylinders, was described in [7] in details. The fatigue strength was calculated using stepped method on the basis of results of experiments on 16-sampled batches [8]. The fatigue experiments results are shown in Figs 5, 6 & 7.

## CONCLUSION

The technology of sliding burnishing with cylindrical elements of diamond composite can be used in very simple and uncomplicated way for smoothing machining of various types of materials. Application of the new diamond sinter with ceramic binding phase in the form of titanic-siliceous carbide as the tool material for sliding burnishing will allow eliminating hitherto existing defects of the applied composites. Application of a cylindrical element as the tool in the place of applied spherical elements has several merits. A cylindrical element is easier to manufacture and easier to grind, which reduces the costs of its production, when the contact zone 'tool-machined object' will wear, we can easily change its position through turn of the tool or change of its height in relation to the machined object. After exhausting the possibilities of turn of the tool we can easily grind it – in this way we will extend its life several or several dozen times.

After carried out machining we can draw the following conclusions. The highest fatigue strength we managed to obtain was Zgw = 495 [MPa] for parameters p = 0,066 mm/rotation, v = 500 rotations/min, force F = 225[N] and radius of the cylinder was 4mm. For the rest of cylindrical elements (6 and 8 mm) Zgw was from range 385 [MPa] to 440 [MPa], for the highest force 275 [N] we can observe decrease (to 375 MPa) the fatigue strength below value before burnishing (395 MPa). For the feed and burnishing speed parameters difference are not so visible except for 4 mm element.

The results of the realized fatigue experiments showed the distinctly advantageous effect of diamond burnishing with cylindrical elements on the improvement of the fatigue strength of the steel 41Cr4.

## REFERENCES

1. Jaworska L.: *High-Pressure Sintering of Diamond Powders*. Zeszty Naukowy IOS w Krakowie. 2002.

2. Korzyński M.: *Nagniatanie powłok chromowych*. Mechanika z.41, 1994.

3. Przybylski W.: *Perspektywy rozwoju obrabiarek i narzędzi nagniatających*. Inżynieria Maszyn, R. 6, z. 2, 2001, s. 71-87.

4. Przybylski W.: *Technologia powierchnostnoj plasticzeskoj obrabotki*. Metalurgia, Moskwa 1991.

5. Przybylski W.: *Technologia obróbki nagniataniem*. Wydawnictwo Naukowo Techniczne, Warszawa 1987.

6. Rozenberg. A.O., Swirad S. i in.: *Problemy poprawy właściwości kompozytów diamentowych*. Zeszyty Naukowe PRz, Rzeszów 2000.

7. Lunarski J.: *Porównawcza ocena własności zmęczeniowych w badaniach technologicznych*. Technika Lotnicza i Astronautyczna, 3, 1981 r.

8. Dylag Z., Orłos Z.: *Wytrzymałość zmęczeniowa materiałów*. WNT, Warszawa 1962 r.

**Jana TKACOVA**
**Monika MADEJ***
**Eva LUKCOVA**

Technical University of Kosice, Slovakia
*Technical University of Kielce, Poland

# ANALYSIS OF SELECTED PROPERTIES OF DLC FILMS

*This paper is oriented to the study of advanced materials on the base of - DLC (diamond like carbon) coatings – namely a: C (amorphous carbon films). The type and thickness of deposited coatings by PVD method can influence their quality and adhesion to the substrate. PVD process parameters are strongly affecting the coatings and substrate interface as well as the adhesion and tribological properties. Experimental samples were made of commercial CrMoCo alloy-substrate system used for artificial joints. Amorphous carbon layers were deposited by equipment UVNIPA-1-001. The wear resistance of the coatings was evaluated by microtribotest and DSI curves measured by the NanoTest NT 600 apparatus at different maximal loads from 5, 10, 20, 50, and 100 mN with diamond Berkovich tip using the analysis developed.*

## INTRODUCTION

Diamond-like carbon (DLC) coatings cover a wide range of different types of carbon-based coatings, which generally have properties such as low friction and high wear resistance [1].

The low friction coefficient and good wear resistance of diamond-like carbon coatings make them suitable for many tribological applications such as wear-resistant coatings e.g. cutting tools and magnetic storage systems, etc. In order to use DLC coatings reliably in different applications, it is important to understand the tribological behaviour of the coatings under different operating conditions. This has been studied intensively by more scientists e.g. [2, 3, 4] during the last few years. The friction and wear performance of amorphous carbon (a-C) coatings greatly depends on the deposition method and the deposition parameters used as well as the test environment.

Diamond-like carbon (DLC) is an umbrella term that refers to 7 forms of amorphous carbon materials that display some of the unique properties of natural diamond. In 2006 the Association of German Engineers, VDI, has provide a classification and nomenclature for diamond-like-carbon (DLC) and diamond films in order to clarity the existing multiplicity of confusing terms and trade names - Tab. 1.

To identify which of the forms is on a particular sample, the fraction of hydrogen and the fraction of sp3 bonded carbon atoms (not graphite) must be measured. Knowing those two numbers enables a user to plot the "location" of the sample on the VDI-map. The closer to the upper left corner that a material plots, the better (and more) pure is the DLC. Dilutions with hydrogen and graphitic carbon degrade the DLC - Fig. 1.

The hardest, strongest, and slickest DLC is known as tetrahedral amorphous carbon, or *ta-C*. Such *ta-C* can be considered to be the "pure" form of DLC, since it consists only of $sp^3$ bonded carbon atoms.

*Tab. 1. Classification of Amorphous carbon thin films (diamond-like-carbon films / DLC)*

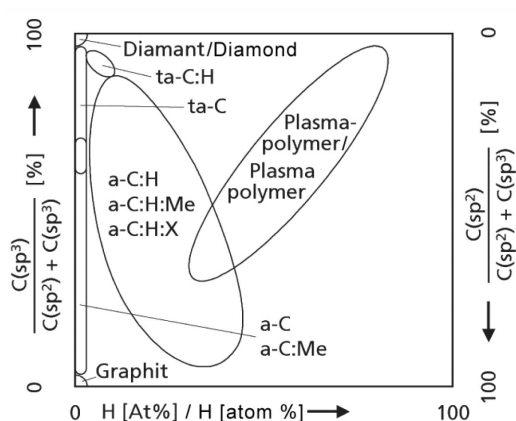| Designation | Amorphous carbon thin films (diamond-like-carbon films / DLC) | | | | | | |
|---|---|---|---|---|---|---|---|
| Doping, additional elements | hydrogen-free | | modified | hydrogenated | | modified | |
| | | | with metal | | | with metal | with non-metal |
| Crystal size on the growth side | (amorphous) | | | | | | |
| Predomina-ting C-C-bond type | $sp^2$ | $sp^3$ | $sp^2$ | $sp^2$ or $sp^3$ | $sp^3$ | $sp^2$ | $sp^2$ |
| Designation | Hydrogen-free amorphous carbon film | Tetrahedral hydrogen-free amorphous carbon film | Metal-containing hydrogen-free amorphous carbon film | Hydrogenated amorphous carbon film | Tetrahedral hydrogenated amorphous carbon film | Metal-containing hydrogenated amorphous carbon film | Modified hydrogenated amorphous carbon film |
| Recom-mended abbreviation | a-C | ta-C | a-C:Me | a-C:H | ta-C:H | a-C:H:Me (Me = W, Ti, ...) | a-C:H:X (X = Si, O, N, F, B, ...) |

© 2007    Fraunhofer-Gesellschaft



*Fig. 1. DLC composition_map (according to The German Fraunhofer - IST institute [5]*

Fillers such as hydrogen, graphitic $sp^2$ carbon, and metals are used in the other 6 forms to reduce production expenses, but at the cost of decreasing the service lifetimes of the articles being coated. The bond types have a considerable influence on the material properties of amorphous carbon films. If the $sp^2$ type is predominant the film will be softer, if the $sp^3$ type is predominant the film will be harder. These [sp3] bonds can occur not only with crystals - in other words, in solids with long-range order - but also in amorphous solids where the atoms are in a random arrangement. In this case there will be bonding only between a few individual atoms, and not in a long-range order extending over a large number of atoms. There are several methods available to deposit **DLC** or other coatings at the outer surface of components; such as chemical vapor deposition (CVD), physical vapor deposition (PVD), electroplating, flame spray and sol-gel.

DLC films can be deposited on various materials that can be put in a vacuum, they reduce friction and wear, and may be harder than natural diamond.

## EXPERIMENTAL SETUP

The films were deposited by low arc discharge UVNIPA-1-001 vacuum system with three sources (gas ion source for cleaning, electric arc source for non-magnetic metal sputtering and pulse arc carbon source for DLC deposition). The pulse sputtering of graphite target is a possible setup in wide range. Entered samples were sputtered in one vacuum cycle. All substrates were cleaned for 10 min with Ar ions. DLC layer was deposited at temperature down to 150°C. Nitrogen and Ar gasses were added dur-

ing the DLC deposition into working chamber - Tab. 2. The substrates were planetary rotating through all the deposition steps to achieve homogeneity.

The coatings were produced on a highly polished flat CrCoMo substrate material with $R_a = 0.05 \mu m$. One fine polished face of each CrCoMo substrate was coated by DLC film. The hardness and another mechanical characteristics were determined from depth sensing indentations (DSI) curves measured with Nano TEST NT 600.

*Tab. 2. Deposition parameters*

| No. | | Ar [sccm] | N[sccm] |
|---|---|---|---|
| II | a-C | 70 | 60 |
| III | a-C | 80 | 60 |
| IIII | a-C | 80 | 50 |

## EVALUATION OF NANOINDENTATION

Coating hardness was tested using a nanoindenter [6, 9]. The hardness $H_{IT}$ was determined from depth sensiting indentations (DSI curves measured by the NanoTest NT600 apparatus at different maximal loads from 5 to 100 mN with diamond Berkovich tip [6]. The indentation cycle was repeated five times in slightly different places for each maxima load. The samples were indented at the different maximal load 5, 10, 20, 50 and 100 mN. Records DSI curves served to determination of maximal penetration depth $h_{max}$, at maximal loading force $F_{max.}$

Hardness was evaluated according to:

$$H_{IT} = P_{max} / A(h_c),$$

where $A(h_c)$ - projected contact area, for Berkovich indenter $\beta \sim 1.034$.

The dependence $H_{iT}$ versus load is shown in Fig. 2.



*Fig. 2. Dependence $H_{iT}$ versus load*

Values of $H_{iT}$ for coatings of type III and IIII deposited under conditions given in Tab. 2 – are compared, the lowest value was observed for coating II, what can be connected with lower content of N.
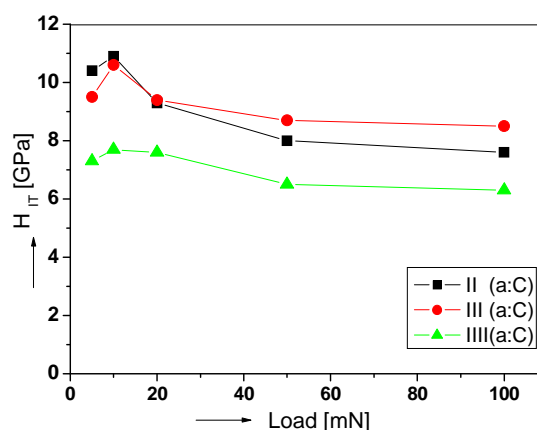
## FRICTION TESTS

Friction tests were performed on the same samples as used for indentations by applying a microtribometer with dry sliding line contact between corundum ball ($\alpha$-$Al_2O_3$) and coatings. The coefficient of friction COF was recorded during testing by increasing normal force $F_n$ from 30 to 90 mN, temperature T= 23°C, relative humidity 50%, normal force $F_n$ continuously increased from 30 mN to 90 mN, friction couple: a-C coatings $Al_2O_3$ and ball d = 5.5 mm. Material of ball was $Al_2O_3$. Speed of ball movement v = 0.4 mm/s. Graphical output of friction coefficients COF for different load during sliding line contact are drawn in Fig. 3.

From point of view of COF, coating marked as II (DLC) was the best. The resistance to plastic deformation – the quantity which can more distinctly divide film materials.

## DISCUSSION

The friction coefficient of DLC coatings was more stable over the wide range of normal loads from 30 to 90 mN against corundum ball used at microtribotests. Its lowest values was recorded for coatings with highest h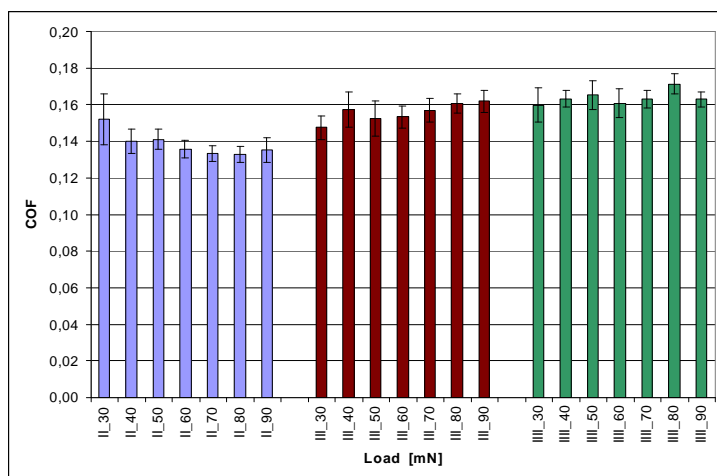ardness and content of sp3 bonds for II coating (Ar: 70 sccm / N2: 60 sccm) and the highest values of friction coefficient were recorded for IIII coating (Ar: 80 sccm / N2: 50 sccm) with lowest sp3/sp2 ratio and hardness. [7, 8]



*Fig. 3. Dependence of friction coefficient COF versus load*

For DLC coatings deposited by UVNIPA-1-001 equipment the lowest value of hardness HIT was observed for IIII coating with highest content of sp2 bonds (Ar: 80 sccm / N2: 50 sccm). II and IIII coatings have almost the same values of HIT and content of N2 (60 sccm)

## CONCLUSIONS

Development and applications of thin hard DLC films are open to further research and they represent always very attractive and challenging theme.

Experimental tests shown that average value of friction coefficients about COF 0,1 was obtained for a: C coatings. Application of a-C coatings decreases wear during transfer of load in friction systems.

Nowadays, the applications of thin hard layers are very broad and manysided.

## REFERENCES

1. Robertson J.: Surf. Coat. Technol. 50, 1992, 185.

2. Kim D.H. et. al.: *A Study on Diamond-like-Carbon Films for Medical Applications*. Materials Science and Engineering: C, Volume 22, Issue 1, 1 October 2002, pp. 9-14

3. Rickerby D.S, Matthews A.: *Advanced surface coatings*. A handbook of surface engineering.Glasgow.1991

4. Hauert R., Müller U.: Diam. Relat. Mater. 12, 2003, 171.

5. Index of Carbon Coatings. Fraunhofer-Gesellschaft 2007. http://www.ist.fraunhofer.de

6. Boháč P., Zdravecká,E., Kulikovský V., Strayánek M., Ctvrtlik R.: *Mechanical properties of amorphous carbon based films for artificial joints*. Beijing. 3-5. 9. 2007. Elsevier UK. 2007. P 2.37

7. Vojs, M. et al..: Diamond & Related Materials 14, 2005; 613–616.

8. Vojs, M., E. at al.: *Properties of amorphous carbon layers for bio-tribologicla aplications*. Workshop on Recent advances of low dimension structure and devices. 7.-8.4.2008, Nothingen

9. Zdravecká E., et al: *Study of DLC coatings on flat and Shaped CoCrMo Substatres*. In: Materials for Improved Wear Resistance of Total Artificial Joints. Eibar 10, 2007

**Pavel TOPALĂ** *
**Laurenţiu SLĂTINEANU** **
**Oana DODUN** **
**Natalia PÎNZARU***

* State University "Alecu Russo" of Bălţi, Republic of Moldova
** Technical University „Gh. Asachi" of Iaşi, Romania

# INFLUENCE OF SOME FACTORS
# ON THE POWDER DEPOSITION PROCESS
# BY ELECTRICAL DISCHARGES

*The paper presents the results of some experimental researches concerning the electrical discharges deposition of the metallic powders on the workpieces cylindrical surfaces. The process could be included in the group of the manufacturing processes based on the physical effects of the electric current. The powder is introduced in the electrical discharge channel developed between the workpiece and the electrode. As consequence of the high temperature developed within the discharge channel, the powder and the superficial layer of the workpiece are melted and they constitute the new metallic layer, presenting more convenient properties from the point of view of the part behavior in service. Adequate mechanical and electric equipment was used to ensure the work conditions for the electrical discharge deposition. The experimental researches were developed to study the influence exerted by certain work conditions on the mass of the deposited material.*

## INTRODUCTION

The manufacturing processes that use the electrical discharges or other physical effects of the electric current could be classified in the following manner:

*a)* Manufacturing processes based on the workpiece material removal; thus, there are manufacturing processes with the discharges initiation by the dielectric medium breakdown and manufacturing processes with discharges initiation by breaking the electrical contact between electrodes;

*b)* Manufacturing methods based on the material addition; these processes use the physical effects of the electrical discharges or of other physical effects of the electric current;

*c)* Classical manufacturing processes assisted by the preheating of the workpiece material, based on certain physical effects of the electric current (cutting or superficial plastic deformation; in such a case, the superficial layer to be removed or deformed is softened as consequence of the preheating by electric resistance or by induction.

In the second group of machining methods, the deposition by electrical discharges could be included. The main objectives followed by the using of the material deposition by pulse electrical discharges are:

- Increasing of the hardness, of the corrosion resistance, of the wear resistance, of the heat-resistance;

- Changing of the electrical, magnetic and emission properties of the metallic superficial layers.

The electrical discharges deposition processes are based on phenomena initial studied by B. R. Lazarenko and N. I. Lazarenko; they established the work conditions which permit the deposition on the cathode surface and they built the first equipments able to materialize the above mentioned process.

Physical phenomena specific to the electrical discharge deposition process were studied and interpreted by B.N. Zolotykh, I. G. Nekrashevich, I.A. Bakuto, K.K. Namitokov etc. Within the Institute of the Applied Physics belonging to the Academy of Sciences of Republic of Moldova, researches concerning the electrical discharges deposition by the using of metallic powders were made by A.E. Gitlevich, I. I. Fursov, V. V. Mykhaylov, N. I. Parcanski etc. [1, 3, 4, 5, 6].

Different electrical discharges deposition method were also proposed and studied within the techniques and technology department from the State University "Alecu Russo" of Bălți (Republic of Moldova) [1, 5, 6].

## PHYSICAL PHENOMEANA

The electrical discharges were applied to obtain deposition layers on the workpiece surfaces when special properties are needed. Generally, such layers have the properties of the electrode-tool material. If the deposition powders are used, there is the possibility to obtain layers with improved properties. In this last case, some conditions must be fulfilled:
- On the workpiece surface, the liquid phase must be created;
- The particles of powder must be melted before their impact with the workpiece surface;
- The joining of the melted particles with the liquid phase of the workpiece material must occur during the pulse electrical discharge.

The liquid phase appears on the workpiece surface when the following relation is fulfilled:

$$Q = \frac{4W}{\pi d^2 S} \geq Q_m,$$  (1)

where $W$ is the pulse energy, $d$ - the diameter of the liquid phase crater on the cathode surface, S – the mean size of the gap and $Q_m$ – the melting heat of the workpiece material, which can be determined as:

$$Q_m = q_m \rho,$$  (2)

$\rho$ being the workpiece material density and $q_m$ – the specific melting heat of the workpiece material density.

If the voltage $U$ applied to the gap and the discharge circuit capacity $C$ are known, the energy $W$ can be written as:

$$W = \eta \frac{CU^2}{2}$$  (3)
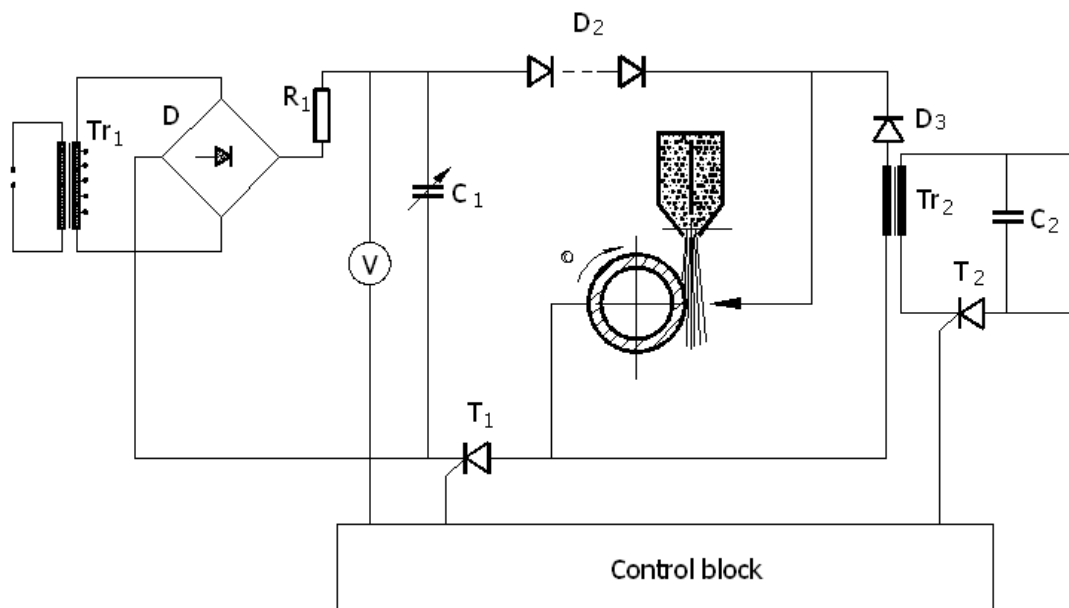
where $\eta$ is the equipment efficiency.



*Fig. 1. Schematical representation of the equipment used for layers deposition by the using of metallic powders*

## EQUIPMENT USED FOR ELECTRICAL DISCHARGES DEPOSITION

To study the physical and technological aspects of the deposition process by the using of the pulse electrical discharges, the equipment schematically presented in figure 1 was used. The experimental equipment includes some components belonging to the installation Razriad – M [5, 6]. The equipment permits the deposition of metallic layers on workpieces having lengths up to 250 mm and diameters up to 50 mm. A control block ensures the changing of the rotation speed of the workpiece clamped in a chuck. The power pulses are obtained by means of the capacitors battery $C_1$, including six capacitors ($U = 1000$ V, $C = 100$ μF). The transformer $Tr_1$ permits to obtain the adequate work voltage. The direct current is transmitted by the rectifier $D$ to the capacitors battery $C_1$. The resistance $R_1$ limits the size of the electric current for the capacitors charging. The diodes $D_2$ protect the power block of the pulse generator.

The initiation pulses are generated when the capacitor $C_2$ discharges on the primary coil $T_{r2}$. The priming pulse obtained from the secondary coil of the transformer $Tr_2$ is transmitted to the electrodes by the diodes $D_3$ ($I = 0.2$ mA, $U = 10$-24 kV). The thyristors $T_1$ and $T_2$ and the control block materialize a multivibrator. The both discharges circuits are simultaneously opened; the fact ensures the synchronization of the pulses and the process stability.

The gradually control of the voltage applied to the capacitors $C_1$ is possible due to the existence of the control block. The metallic powder placed in hopper feeds to the work gap, as consequence of the gravitation. An adequate dosage device permits the control of the powder feeding in the work gap.

**EXPERIMENTAL RESEARCH**

A first series of experimental researches has the objective to establish an empirical model able to emphasize the influence exerted by some input factors (the gap size, the powder debit, the pulse energy and the energy density on the quantity (mass) of the deposited material.

As material for deposition, the boron carbide was used. The sizes of the input factors and of the output parameter are presented in the Table 1.

*Table 1. Experimental results*

| Exp. No. | Sizes of the input factors | | | | Mean size of the deposited material mass, $m$, g |
|---|---|---|---|---|---|
| | Gap size, $s$, mm | Powder debit, $Q$, mg/min | Energy W, J | Energy density, $\delta$, J/mm | |
| 1 | 1.5 | 3.1 | 4.3 | 9.25 | 0.408 |
| 2 | 1.5 | 0.3 | 4.3 | 9.25 | 0.438 |
| 3 | 0.3 | 3.1 | 4.3 | 9.25 | 0.410 |
| 4 | 0.3 | 0.3 | 4.3 | 9.25 | 0.440 |
| 5 | 0.9 | 1.7 | 7.8 | 2 | 0.683 |
| 6 | 0.9 | 1.7 | 0.8 | 16.5 | 0.415 |
| 7 | 0.9 | 1.7 | 0.8 | 2 | 0.320 |
| 8 | 0.9 | 1.7 | 4.3 | 9.25 | 0.532 |
| 9 | 1.5 | 1.7 | 4.3 | 16.5 | 0.508 |
| 10 | 1.5 | 1.7 | 4.3 | 2 | 0.413 |
| 11 | 0.3 | 1.7 | 4.3 | 16.5 | 0.510 |
| 12 | 0.3 | 1.7 | 4.3 | 2 | 0.415 |
| 13 | 0.9 | 3.1 | 7.8 | 9.25 | 0.678 |
| 14 | 0.9 | 3.1 | 0.8 | 9.25 | 0.315 |
| 15 | 0.9 | 0.3 | 7.8 | 9.25 | 0.708 |
| 16 | 0.9 | 0.3 | 0.8 | 9.25 | 0.345 |
| 17 | 0.9 | 1.7 | 4.3 | 9.25 | 0.532 |
| 18 | 1.5 | 1.7 | 7.8 | 9.25 | 0.663 |
| 19 | 1.5 | 1.7 | 0.8 | 9.25 | 0.300 |
| 20 | 0.3 | 1.7 | 7.8 | 9.25 | 0.665 |
| 21 | 0.3 | 1.7 | 0.8 | 9.25 | 0.615 |
| 22 | 0.9 | 3.1 | 4.3 | 16.5 | 0.522 |
| 23 | 0.9 | 3.1 | 4.3 | 2 | 0.428 |
| 24 | 0.9 | 0.3 | 4.3 | 16.5 | 0.553 |
| 25 | 0.9 | 0.3 | 4.3 | 2 | 0.458 |
| 26 | 0.9 | 1.7 | 4.3 | 9.25 | 0.532 |

The experimental results were processed by means of software based on the method of the smallest squares [2]. Thus, the following relation was determined:

$$m = 0.212 + 0.162s - 0.115s^2 + 0.0790Q - 0.0264Q^2 +$$
$$+ 0.0134W - 0.00354W^2 + 0.0122\delta - 0.000319\delta^2 \tag{4}$$

To obtain a more direct image concerning the influence exerted by the input factors on the output parameter, the power type function was determined by the using of the same experimental results:

$$m = 0.314 s^{-0.0530} Q^{-0.00386} W^{0.216} \delta^{0.0579} \tag{5}$$

By analyzing the relation (5), one can conclude that for the investigated experimental field, the mass $m$ of the deposited material diminishes at the increasing of the gap size $s$ and increases at the increasing of the energy $W$ and of the energy density $\delta$. The biggest influence is exerted by energy $W$, because the exponent attached to this factor (0.216) has the biggest absolute size.

Some graphical representations elaborated by taking into consideration the relation (4) are presented in figures 2 and 3.
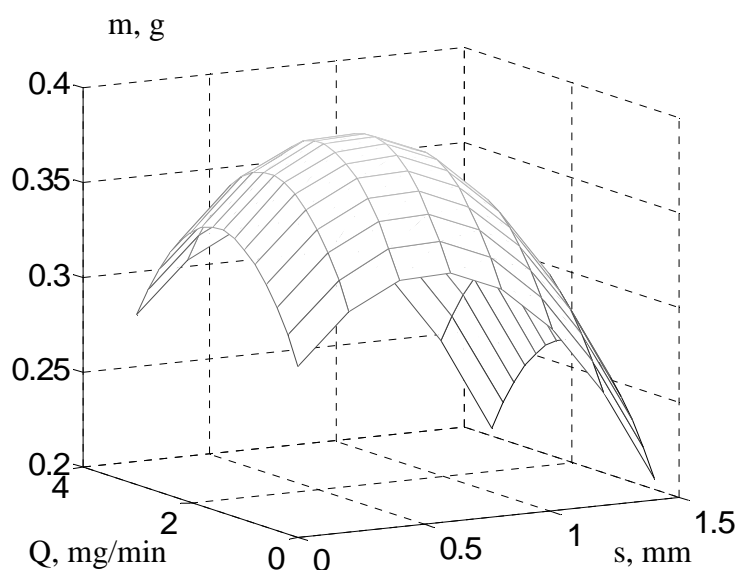


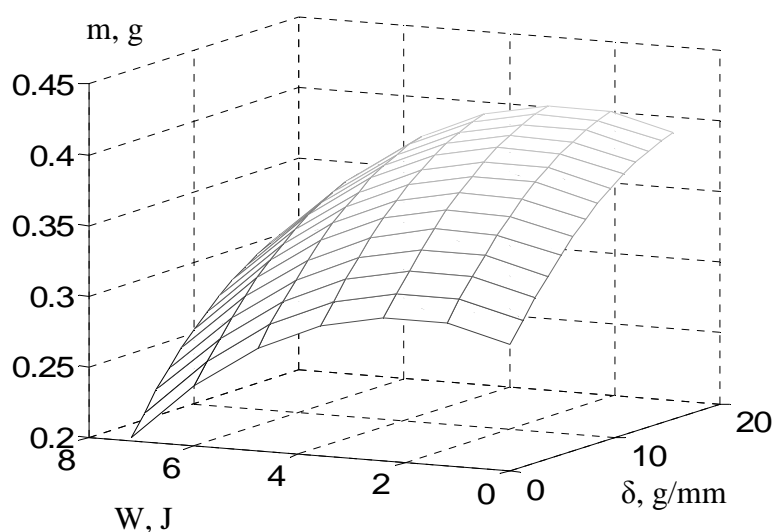*Fig. 2. Influence exerted by the gap size s and by the powder debit Q on the mass of deposited layer (W = 4.3 J , = J/mm)*



*Fig. 3. Influence exerted by the pulse discharge energy W and by the energy density δ on the mass of the deposited layer (s = 0.9 mm, Q = 1.7 J/mm)*

## CONCLUSIONS

One of the ways used at present to improve the usage properties of the mechanical parts is the layers deposition of metallic powders by pulse electrical discharges.

The study of the physical phenomena occurring in the work gap emphasized the important role exerted by the discharge pulse energy.

To investigate the influence exerted by different work factors on the mass of the deposited layer, adequate equipment was used. The experimental researches permitted the establishing of some empirical models able to show the influence exerted by the gap size, the powder debit, the discharge pulse energy and by the energy density on the mass of deposited layers.

## REFERENCES

1. Abramciuc Al.: *Alierea prin scântei electrice cu pulberi*. Tehnomus IX, III, Suceava (Romania): Universitatea  Ştefan cel Mare, 30-31 May 1997, 192-199.

2. Creţu G.: *Bazele cercetării experimentale*. Îndrumar de laborator, Iaşi (Romania): Universitatea Tehnică "Gh. Asachi", 1992.

3. Gitlevich A.I., Mickhaylov V.V., Parkanskiy N.I, Revutskiy V.M.: *Elektroiskroveo legirovanie metallicheskikh poverkhnostey*. Kishinev: Shtiintsa, 1985.

4. Slătineanu L., Nagîţ G., Dodun O., Coteaţă M., Chinesta F.,  Gonçalves-Coelho A.,  Pamies Teixeira A.J., San Juan M.,   Santo S., Santos S.: *Non-traditional manufacturing processes.* Kishinew (Republic of Moldova): Editura Tehnica Info, 2004.

5. Topala P.: *Studiul fundamental şi aplicativ al efectelor electroerozive în tehnologiile neconvenţionale*. Teză de doctor habilitat în tehnică. Bălţi (Republic of Moldova): Unversitatea de Stat "Alecu Russo", 2008.

6. Topala P., Stoicev P.: *Tehnologii de prelucrare a materialelor conductibile cu aplicarea descărcărilor electrice în impuls*. Chişinău (Republic of Moldova): Editura Tehnica-Info, 2008.

**Jan VALÍČEK\***
**Sergej HLOCH**
**Katarína MONKOVÁ**

\*Institute of physics, VŠB TU – Ostrava, Czech Republic
Technical university of Košice with a seat in Prešov, Slovak Republic

# IDENTIFICATION OF SURFACE TEXTURE CREATED BY THE ABRASIVE WATERJET AND A PROPOSAL FOR CRITERIA FOR ITS EVALUATION

*The submitted contribution deals with the identification of texture of metal surfaces produced by the abrasive waterjet with the aim to increase surface quality. To the measurement of surface irregularities, a developed contactless shadow method was applied. A dimensionless statistical parameter $C_{Ra}$ for experimentally tested metal materials has been derived the discrete value of which will contribute, in the automated on-line system of feedback, to the optimization of traverse speed of the cutting head, i.e. that technological factor which influences the quality of machined surfaces most.*

## INTRODUCTION

The economic effectiveness of operation of production systems for waterjet cutting and subsequently the economic competitiveness of them are mainly conditioned by the cutting performance and the quality of cutting surface. For accurate measuring the quality of cutting surface, an objective method and a parameter of cutting surface quality must be available. The contribution presents a new progressive contactless shadow method and a proposed statistical parameter of roughness of cutting surface with emphasis put on the examination of functional dependence of the roughness of surface generated on the depth of cut.

## RELATED AND PREVIOUS WORKS

To parameters used most, *Ra* [µm] – the arithmetical mean deviation of the profile and *Rq* [µm] – the root mean square deviation of the profile belong. According to the norms CSN EN ISO 4287 and CSN EN ISO 4288, the basic profile, the waviness profile and the roughness profile are defined (see Fig. 1a) [1]. As a criterion, e.g. the criterion of spatial frequency $f$ [mm$^{-1}$] is used most frequently when irregularities of $f$ = (0-2.5) mm$^{-1}$ are taken as waviness and irregularities of $f$ = (20-25) mm$^{-1}$ are regarded as roughness for surfaces generated by the abrasive waterjet. The frequency from $f$ = (2.5-20) mm$^{-1}$ can be designated as surface striation and grooving.
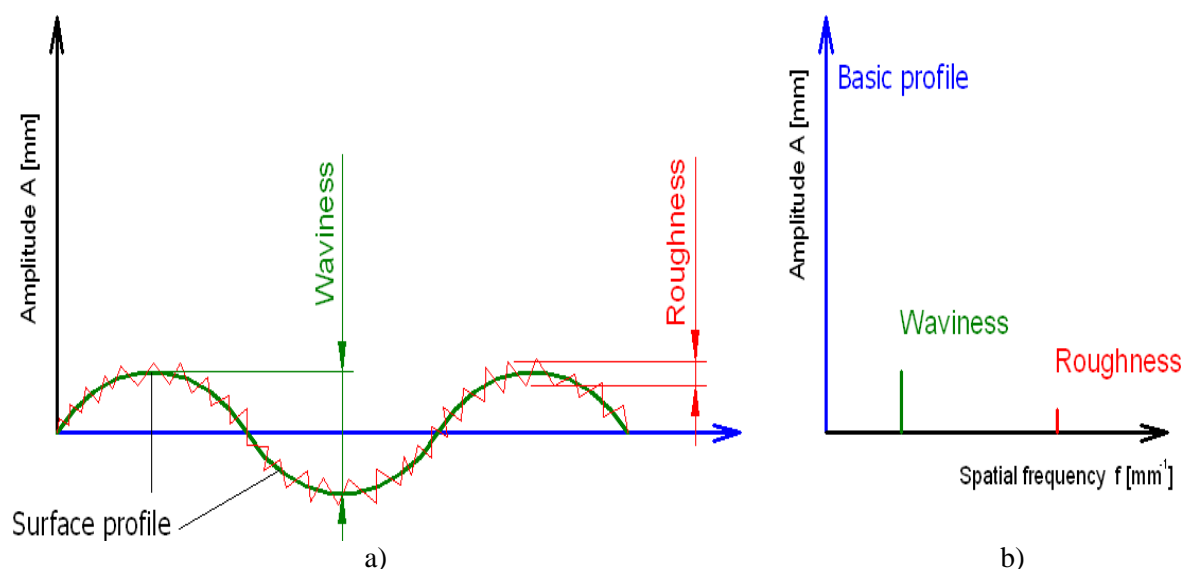
*Fig. 1. Height fluctuations of surface profile ad a) and its amplitude-frequency spectrum ad b)*

It can be said that the basic profile is an ideal smooth surface [2]. The waviness profile is characterised by low frequencies and high amplitudes of surface irregularities $A$ [mm]. The roughness profile is characterised by high frequencies and low amplitudes of surface irregularities [3 - 12]. On the waviness, surface roughness is superposed (Fig. 1). For this surface profile, the amplitude-frequency characteristic is presented here (Fig. 1b), where we can see that the basic profile of surface is identical with the $A$ axis; waviness appears in the region of low spatial frequencies and roughness of the surface is there in the region of high spatial frequencies.

However, this is only a model situation; the real surfaces have far more complicated amplitude-frequency spectra. That is why amplitude-frequency decomposition into individual spectral levels (Fig. 2c) is often carried out at the evaluation of the surface (Figs. 2a, 2b). As main parameters of cut-wall geometry we have proposed the roughness of surface $Ra$, the retardation of cutting trace $Y_{ret}$ [mm], the angle of deviation $\delta$ [º] and the depth of cut $h$ [mm] (Fig. 2a). According to Hashish [9], on every surface a so-called critical depth $h_c$ [mm] can be identified, where an area above this critical depth is a so-called cutting zone and below it, a so-called deformation zone $h_d$ [mm] is there (Fig. 2a); it holds true that $h = h_c + h_d$ [mm]. The critical depth depends on technological factors, above all on the traverse speed of cutting head $v$ [mm.min$^{-1}$].

**EXPERIMENTAL PROCEDURE AND ANALYSIS**

On each material and each wall of sample we took measurements along 22 horizontal lines (Fig. 2a); the size of the samples being (20 x 20 x 8) mm. The method is presented below by means of an example of steel AISI 309. From each measuring line we obtained a signal which was then processed by means of Fast Fourier Transform (FFT). By this transform, we got amplitude-frequency spectra. As already mentioned in the model case (Fig. 1), we shall search for both the zone where waviness is concentrated and that where roughness is concentrated in the given spectra.
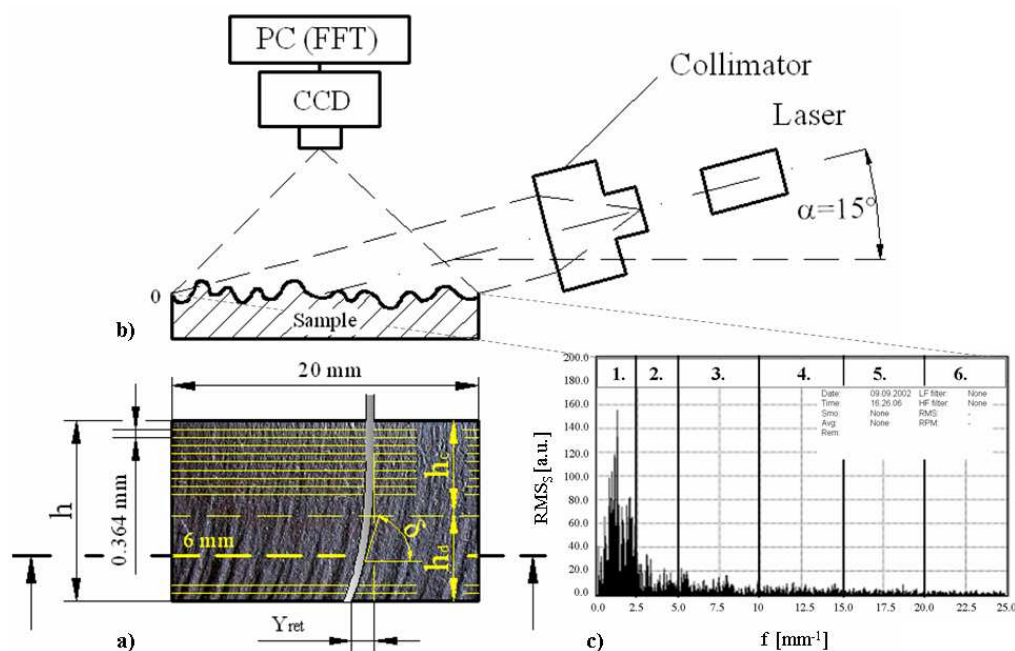
*Fig. 2. A photograph of the surface of cut wall **a**) (magnified 12 x)**,** and proposed main parameters of surface profile ad **b**) and ad **c**) amplitude-frequency spectrum of surface studied (material: steel AISI 309, traverse speed of cutting head of 200 mm.min$^{-1}$) obtained from one horizontal measuring line of the length of 20 mm at the depth of 6 mm below the surface topography*

As already stated, the spectrum of waviness will appear in the region of low frequencies to which high amplitudes of surface irregularities will correspond; on the contrary, roughness will appear in the region of high frequencies with low amplitudes of surface irregularities. From performed experiments it follows that with the increasing depth of cut *h*, the kinetic energy of jet diminishes, and thus surface irregularities grow, i.e. their height amplitudes grow and simultaneously their spatial frequencies decrease. This is a result of a change in the mechanism of material removal from the prevailing tensile stress and shear stress to the pressure stress. In the case of samples generated by the abrasive waterjet (AWJ) it is possible to say that with the increasing depth *h*, the low spatial frequencies of surface irregularities dominate (i.e. waviness) over the high spatial frequencies (i.e. surface roughness). We have verified this fact in 22 equidistant measuring horizontal lines of the length of 20 mm (Fig. 2a), where we measured the $RMS_s$ amplitude of surface irregularities in six various frequency bands, namely 0-2.5 mm$^{-1}$ ($RMS_s$(1.)), 2.5-5 mm$^{-1}$ ($RMS_s$(2.)), 5-10 mm$^{-1}$ ($RMS_s$(3.)), 10-15 mm$^{-1}$ ($RMS_s$(4.)), 15-20 mm$^{-1}$ ($RMS_s$(5.)), 20-25 mm$^{-1}$ ($RMS_s$(6.)) (see Fig. 2c). Frequency intervals selected like that simulated the "cut-off" of contact profilometer for the decomposition of surface topography into its specific subcomponents.

## RESULST AND DISCUSSION

Results obtained from the horizontal equidistant lines are given in the graph of behaviour of $RMS_s$ of irregularities depending upon the depth *h* (Fig. 3). From the performed 22 measuring lines, 22 signals were received, and by means of FFT then 22 amplitude-frequency spectra were obtained from these signals. Each spectrum is represented by the parameter $RMS_s$, which is the output signal which is assessed by means

of shadow method. The parameter is linearly related to the parameter $Ra$ (relation (1)) and is expressed in a.u. (auxiliary unit). The relation between $RMS_s$ and $Ra$ is given by the following empirical relation (1):

$$Ra = \frac{RMS_S}{k} \tag{1}$$

where k – is the constant dependent on materials (e.g. for steel, $k = 20$).

It is possible to say that the total value of $Ra$ represents one signal which is processed by FFT, and is defined by one point. The number of these spectra is 22, and thus 22 points are plotted in the graph as function related to the depth $h$ according to Fig. 3. The amplitude-frequency spectrum, see Fig. 2c, is for metal materials further empirically divided into representative frequency bands to obtain information on a proportion of waviness to the proportion of roughness. Thus, for the amplitude-frequency spectrum, which we divided into 6 frequency bands, we also obtain the same number of values from the horizontal lines (Fig. 3) for the total depth of cut of 8 mm with 22 height horizons. For high spatial frequencies of surface irregularities, this quantity is practically independent of the depth $h$. For low spatial frequencies of surface irregularities, the parameter $Ra$ grows with the depth.
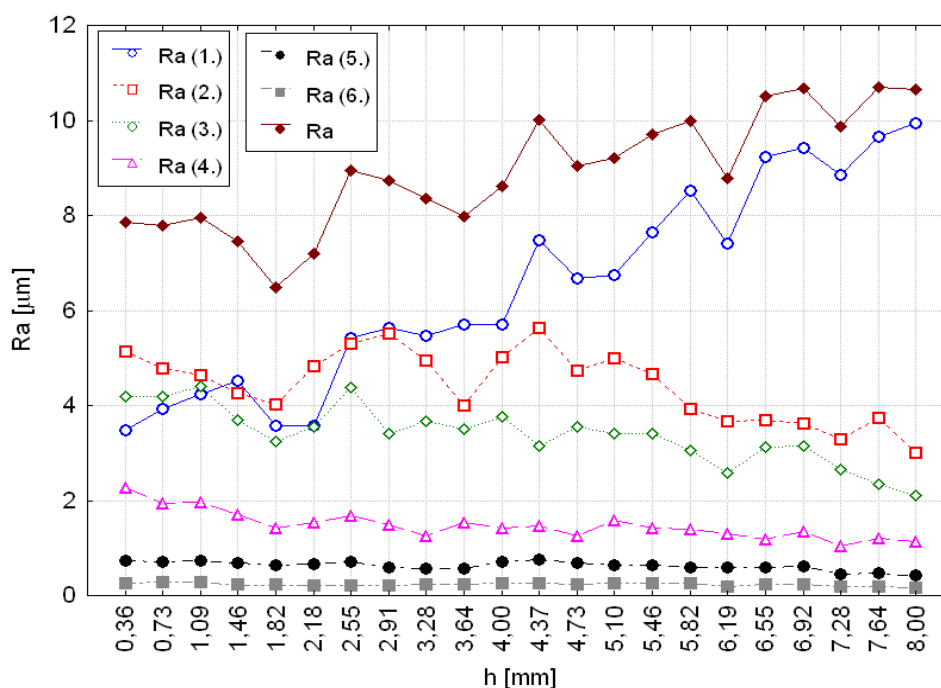


*Fig. 3. The behaviour of Ra of surface irregularities in individual frequency bands (material: steel AISI 309, traverse speed of cutting head of 200 mm.min$^{-1}$)*

The total value of $Ra$ of surface irregularities in the horizontal measuring line can be found according to the relation (2):

$$Ra = \sqrt{\left[Ra(1.)\right]^2 + \left[Ra(2.)\right]^2 + \left[Ra(3.)\right]^2 + \left[Ra(4.)\right]^2 + \left[Ra(5.)\right]^2 + \left[Ra(6.)\right]^2} \tag{2}$$

where $Ra(1.)$ - $Ra(6.)$

(Fig. 3) are $Ra's$ of irregularities determined according to (Fig. 2c). From the point of view of description of AWJ spread and degradation towards the depth of cut $h$ and according to the measured values of $Ra$, it is possible to observe the existence of initiation zone, which is the zone formed in the material by the first contact with AWJ. This initiation zone is characterised by a steep increase in $Ra$ values; after overcoming the total resistance of material in the initiation zone, a sharp drop in $Ra$ values will take place. In the next phases, an increase in the values of $Ra$ occurs with regard to the increasing resistance of material to the penetration of destruction tool into the depth of the cut. The behaviour of function $Ra$ ($h$) is then equivalent to the physical-mechanical conditions of cut at individual depth levels and to the mechanism of disintegration dependent on the selection of technological factors and the material [4], [6], [7], [8]. In Fig. 4, it is possible to observe how $C_{Ra}$ changes depending upon the depth $h$ for individual materials (AISI 309, DIN GS – 20 Mn 5, EN S355J2G3, EN S235JRG2 and CSN EN 13 116) at the traverse speed of cutting head of 200 mm.min$^{-1}$. In Fig. 5 these dependences can be seen for the same materials at the traverse speed of cutting head of 50 mm.min$^{-1}$. According to Fig. 5, it can be seen that for the hardest material, i.e. steel CSN EN 13 116, the parameter $C_{Ra}$ grows most quickly; for the softest material, i.e. steel EN S235JR62, it grows most slowly. From Figs. 4 and 5 it is evident that the statistical parameter $C_{Ra}$ reacts well to the properties of material and also changes in the mechanism of loading the material on the surface of cut wall. From the technological point of view, it is possible to say that at the traverse speed of 50 mm.min$^{-1}$, the material behaves likes more plastic than in the case of speed of 200 mm.min$^{-1}$.
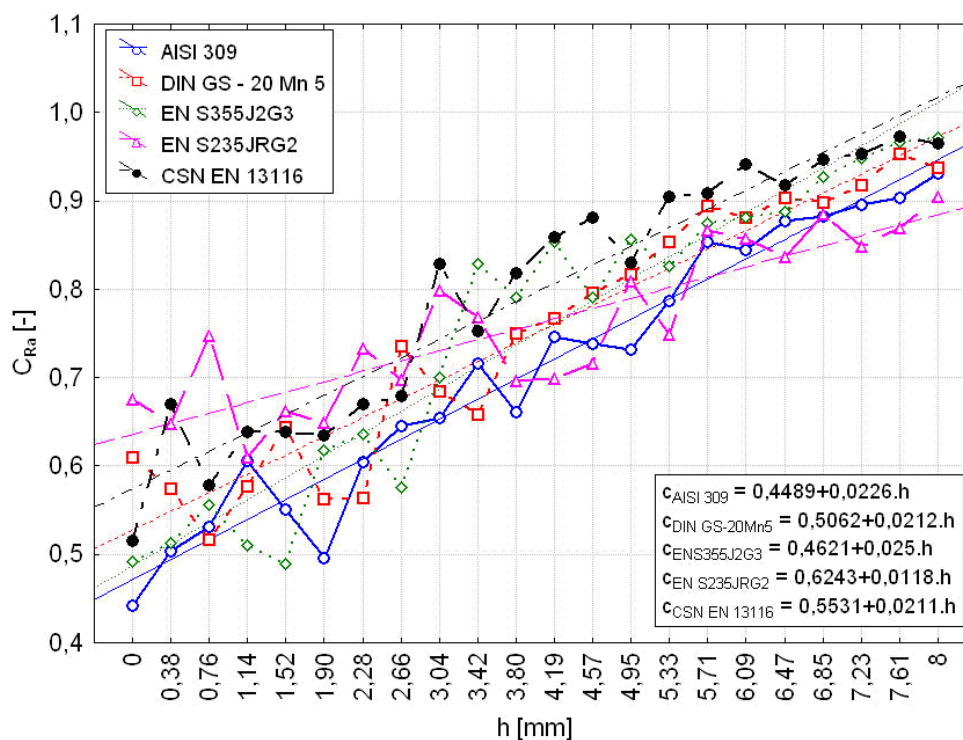


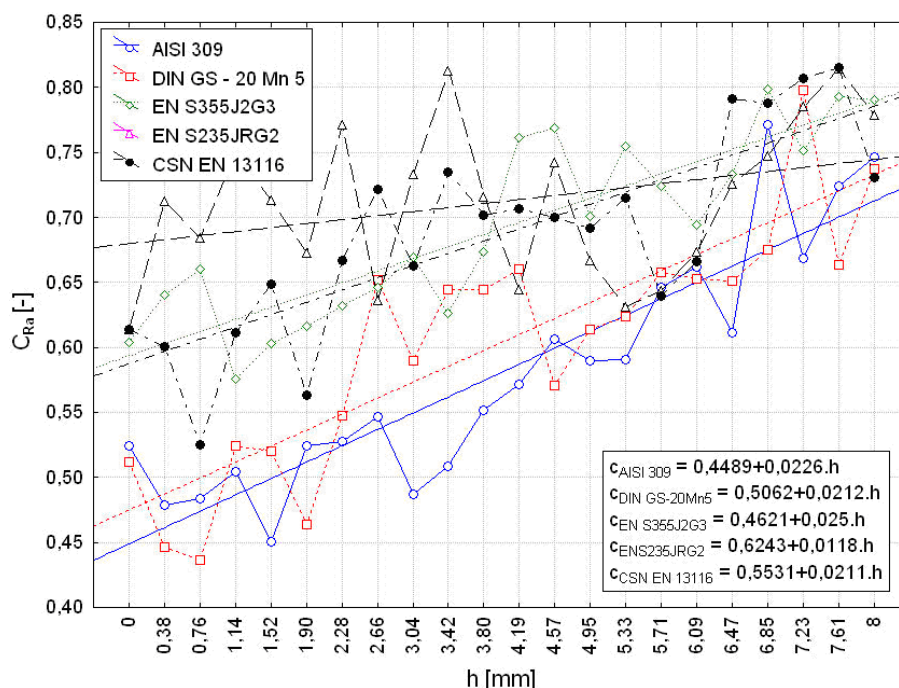**Fig. 4. Th**e dependence of $C_{Ra}$ on the depth h for various steels at the traverse speed of cutting head of 200 mm.min$^{-1}$

*Fig. 5. The dependence of $C_{Ra}$ on the depth h for various steels at the traverse speed of cutting head of 50 mm.min$^{-1}$*

A lot of statistical and analytical studies of results of measuring various materials carried out by us [11], [12] lead to the conclusion that the distribution of characteristic height and longitudinal parameters of roughness, or waviness into individual zones in the direction of growing depth of cut shows certain regularities. Because the majority of important topographic and mechanical parameters are directly functionally related to these sizes of cut wall surface, the same regularities in their distribution are also valid for these next parameters. They are especially the roughness of surface *Ra*, retardation (lag of jet trace from the perpendicular direction at material cutting) and the deviation of cutting trace (angle of trace bend), and also the values of oscillation and stress-deformation parameters of disintegration of the material of surface layer of cut wall and the development of these parameters into the depth of cut. The quantitative criterion for the division of the cut into zones of various surface qualities is the proposed parameter $C_{Ra}$, which is defined as follows (3):

$$C_{Ra} = \frac{Ra(1.)}{Ra} \tag{3}$$

This parameter $C_{Ra}$ is the constant for the given horizontal measuring line. The value of $C_{Ra}$ is then the ratio of *Ra* (1) to total *Ra* measured in each measuring line (see Fig. 6a and relation (3)). It is necessary to distinguish the parameter $C_{Ra}$, which is the constant for the given measuring line, from the function *c*, which is the distribution function of values ($C_{Ra1} - C_{Ra22}$) in relation to the depth *h* (4):

$$c_{Ra} = f(C_{Ra1} - C_{Ra22}, h) \tag{4}$$

The dependence of parameter $C_{Ra}$ upon the depth $h$ is illustrated in Fig. 6b. As for this ratio, two extremes can be considered. If $C_{Ra}$ approximates to zero, it is a case of surface, with which roughness dominates over waviness. If $C_{Ra}$ approximates to 1, it is a case of surface, with which waviness dominates over roughness. With real surfaces, it moves in the range of $0.3 \div 0.95$.
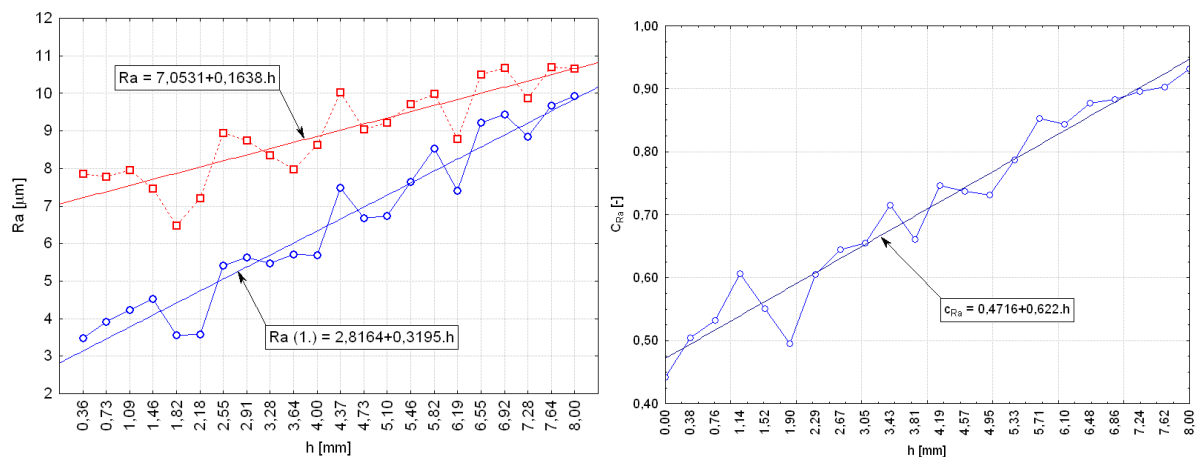


*Fig. 6. a) The dependence of Ra on the depth h and b) The dependence of $C_{Ra}$ value on the depth h, (material: steel AISI 309, traverse speed of cutting head of 200 mm.min$^{-1}$)*

## CONCLUSIONS

For the evaluation of surface generated by the abrasive waterjet technology (AWJ) we have proposed to use the parameter $C_{Ra}$, which is the statistical parameter obtained by the decomposition of values of *Ra* according to the bands of spatial frequencies of surface, with the aim to increase the effectiveness of this technology. This parameter expresses the relative proportion of waviness in all irregularities in individual profiles of surface measured at various depths of cut perpendicularly to the original cutting plane (see relation (1)). The use of this parameter will make it possible to distinguish good-quality cutting zones from poor-quality deformation zones, which is of impor-tance to the satisfaction of qualitative requirements of consumers of cut products. This is a discrete parameter, by which the traverse speed of cutting head can be checked and controlled depending upon the required quality of cut wall. It follows from analyses performed on the basis of evaluation of extensive experimental measurements [11], [12] that the parameter $C_{Ra}$ reacts well to a change in the traverse speed of cutting head *v* and also to a change in the material parameters. Thus the parameter $C_{Ra}$ can be used well for the check of producing the cut wall and increasing its quality, and thus also for achieving greater depths of cut, improving the performance and overall economics of machining process done by the AWJ technology. It will be possible to use the pa-rameter $C_{Ra}$ for a feedback in the automated cutting process, i.e. also in the on-line control of cutting various materials by the AWJ technology.

**REFERENCES**

1. ISO 4287: 1997 Geometrical product specifications (GPS) – Surface texture: Profile method – Terms, definitions and surface texture parameters.
2. Bátora, B., Vasilko, K. Machined surfaces: technological heredity, functionality. Trenčín : 2000. pp. 183.
3. Guo, N. S. *Schneidprozess und Schnittqualität beim Wasserabrasiusstrahl – schneiden*, VDI Verlag, pp. 1-174, 1994.
4. Hloch, S., Gombár, M., Fabian, S., Straka, L. Factor analysis of abrasive waterjet process factors influencing the cast aluminum surface roughness, *In: Manufacturing science and technology*. Malaysia, 2006, pp. 145–149.
5. Lebar, A., Junkar, M. Simulation of abrasive water jet cutting process - Part 1 : unit event approach. *In. Model. simul. mater. sci. eng.*, 2004, 12, pp. 1159-1170.
6. Lebar, A., Junkar, M. Surface evaluation methods for advanced AWJ cutting techniques. *In. Manufacturing systems* (Aachen), 2001, vol. 31, no. 2, pp. 101-103.
7. Orbanic, H., Junkar, M. Simulation of abrasive water jet cutting process - Part 2 : cellular automata approach. *In. Model. simul. mater. sci. eng.*, 2004, letn. 12, pp. 1171-1184.
8. Raja, J., Muralikrishnan, B., Fu, S., Recent advances in separation of roughness, waviness and form, *Precision Engineering: Journal of the International Societies for Precision Engineering and Nanotechnology*, 26 pp. 222–235 (2002).
9. Hashish, M.: Modeling Study of Metal Cutting with Abrasive Waterjets. Trans. of the ASME, *Journal of Engineering Material & Technology*, vol. 106, no. 1, 1984
10. Kušnerová, M., Hlaváč, L. M. Self vibrating chambers with continuous passage of liquid. Sborník vědeckých prací VŠB - TUO. Řada strojní č. 1/2006, roč. LII. VŠB-TUO, Ostrava, 2006, s. 127- 134. ISSN 1210-0471.
11. Valíček, J., Držík, M., Ohlídal, M., Mádr, V., Hlaváč, L., M., Optical method for surface analyses and their utilization for abrasive liquid jet automation. *In: Proc. of the 2001 WJTA American Waterjet Conference, M. Hashish (ed.)*, WJTA, Minneapolis, Minnesota, pp. 1–11, 2001.
12. Valíček, J., Hloch, S. Surface topography optical identification generated by abrasive waterjet. *In: Fine Mechanics and Optics.* vol. 51, no. 11-12 (2006), pp. 320-322.

**Alexandr VASILIEV\***
**Michail KHEIFETZ**
**Sergey KOUKHTA**
**Gennady PREMENT**

*Moscow State Technical University it N. Bauman[1], Russia
Polotsk State University, Belarus

# FORMATION OF QUALITY INDEXES OF MACHINE DETAILS ON THE BASIS OF TECHNOLOGICAL INHERITANCE

*From positions of technological inheritance of operational parameters actions on quality management of products of mechanical engineering are offered. The mathematical model of inheritance of quality indexes in life cycle of the product, describing various modes of behavior is developed by manufacture and application of technical systems. Use of mathematical model at computer designing gives ample opportunities for reduction of expenses at manufacturing and operation of constructive - complex products of mechanical engineering.*

## INTRODUCTION

The use of a principle of superposition is a distinctive feature of existing approaches in definition and forecasting of quality indexes of machine-building production. According to this principle, each of technology contributors operates irrespective of others, and the result of joint action is defined as their partial sum represented in this or that form [1, 2].

Technological systems are multiply connected, objects of manufacture are characterized by nonlinearity, irreversibility and non-equilibriallity. However application of a principle of superposition reduces the multiply connected interactions which are carried out in technological systems, to one-coherent, ignoring mutual influence of technology contributors [3].

Growth of requirements to quality of manufacturing of machine elements make the methods of definition and forecasting the qualities based on a principle of superposition, practically useless as the effect of mutual influence of factors is commensurable with the results of their direct influence. Process of property change of products should be considered as a set of cooperating processes, changes and preservations of properties [4, 5].

Plurality of product properties, each of which is characterized by corresponding set of quality indexes, is also display of multicoupling of technology factors in the process of formation of product quality. Product properties are interdependently formed in the process of manufacturing. However in work practice of mechanical engineering this fact is insufficiently taken into account. Such isolated consideration of process of formation of the allocated quality indexes can lead to serious mistakes at designing and realization of technological processes [1, 2].

The technical difficulties connected to the description of multiply connected interactions, at formation of set of quality indexes at product manufacturing can be got over on the basis of application of modern information technologies and methodology of acceptance of technological solutions [4, 5].

## 1. THE CONCEPTUAL APPROACH

The mathematical device of methodology is based on substantive provisions [3]:

- Quality of a detail is formed during all its technological background and the set of quality indexes is a result of backgrounds;

-Each technological or connected to it influence lead to changes of all quality indexes of material blank;

- Change of any quality index results in change of all other quality indexes of material blank.

Characteristics of technological mediums and laws of their change have permitted to generate the primary goal of the directed formation quality indexes of a product: at knowing initial and final properties of a manufacture subject to define the optimal technological medium from the point of view of property transformation.

The major feature of the approach is formation for each technological repartition of through process of manufacturing of a product of the optimum technological medium providing the most rational distribution of levels of quality indexes on repartitions and giving to process of formation of product quality a necessary orientation. While changing medium or its characteristics, it is possible to operate forming product properties.

**1.1. Model of multiply connected interactions of a medium.** Necessary adjusting influences on structure change, structure and conditions of interaction of technological medium elements and of the element with a manufacture subject can be determined on the basis of comparison of characteristics of medium of a technological process and desirable processes.

On the basis of the conceptual approach it is offered to define the following factors [3]:

- Operative change quality index $i$ while using technological method $j - (mi)_j$;

- Changes of quality index $i$ of the product connected to conditions of realization of technological method $j - (ui)_j$;

- Changes of quality index $i$ in interaction with medium of an operation level, realizing a technological method $j - (Si)_j$.

Operatively forming component $(Ki)_{jon}$ values of parameter $K_i$ is:

$$(K_i)_j^{on} = (m_i)_j (K_i)_{j-1} + (u_i)_j (K_i)_{j-1},$$

where $(K_i)_j$ – a set of levels of product quality indexes after performance of operation of its manufacturing in view of laws of a technological heredity; $(K_i)_{j-1}$ – a set of levels of the quality indexes describing a product condition after performance of the previous operation.

If the method is not realized $(m_i)_j = 1$, $(u_i)_j = 0$, otherwise $0 < (m_i)_j \leq 1$. Change of a sign and value of a quality index occurs as a result of cumulative change of factors $(m_i)_j$ and $(u_i)_j$. For each technological method the regular conditions of realization determining values $(m_i)_j$ are found. The factor $(m_i)_j$ takes into account regular conditions of realization of a method (in particular, the regular economically justified conditions of processing), and $(u_i)_j$ - distinguished from regular, and also other conditions in addition describing the medium (basing and fastening of preparation, elastic characteristics of elements of technological system, etc.).

Analytical definition of factors $(mi)_j$, $(u_i)_j$, $(S_i)_j$ is impossible, therefore they are defined by statistical processing of an experimental material.

For a concrete method with an index of realization $r$ composed $(u_i)_j (K_i)_{j-1}$ it is allocated in a regular component $(C)$:

$$[(Ki)^{on}_j]_r = (m_i)_j [(K_i)^{on}_{j-1}]_r + C.$$

**1.2 Techniques of definition of factors of transfer.** At definition of values of factors of operative change of quality indexes $(m_i)_j$ techniques of the maximal crossing of set of entrance and target values of quality indexes, and also averaging of borders of ranges (fig. 1) are used.

At known $(m_i)_j$ values $(u_i)_j$ are defined according to

$$\left[(u_i)_j\right]_\gamma = \left[(K_i)^{on}_j\right]_\gamma \Big/ \left[(K_i)^{on}_{j-1}\right]_\gamma - (m_i)_j.$$
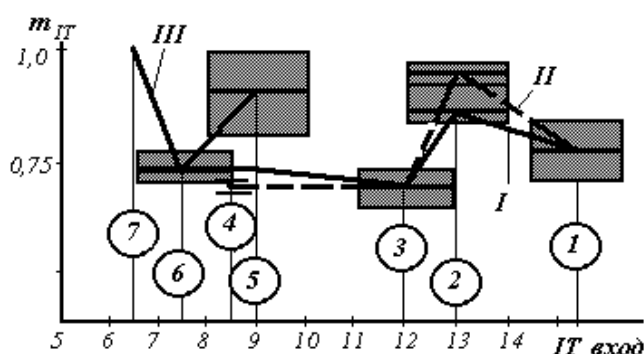


*Fig. 1. Comparison of factors of operative change of accuracy of the size ($m_{IT}$) for methods of processing of external cylindrical surfaces: 1, 2, 3, 4 - accordingly точение draft, получистовое, fair, thin; 5, 6, 7 - accordingly grinding preliminary, final, thin; I, III - a technique of the maximal crossing of sets; II - a technique of averaging of borders*

At knowing $(m_i)_j$, $(u_i)_j$

$$(S_i)_j = \frac{(K_i)^{on}_j}{(K_i)^{on}_{j-1}}$$

Tables of the average values of factors of operative change of properties *(mi)*$_j$ for the basic technological methods of processing of external and internal cylindrical surfaces, and also planes are used.

It is established, that the optimum error of definition of factors of operative change of quality indexes of processable material blanks for methods of abrasive machining on the average is in 3 times higher, than for edge cutting machining, that testifies to the greater sensitivity of corresponding technological mediums to condition change of realization and a condition of objects forming them.

Average value of a relative error of definition of size $m_{IT}$ factor of operative change of accuracy of the sizes for group of methods of detail sharpening and grindings from constructional carbonaceous steels has made 2,5 %, and roughnesses $m_{Ra}$ - 11,0 %. Dependences of characteristics of technological medium of an operation level on a condition of objects forming them are adequately represented with the help of linear regression models or are piecewise -linear approximated at the relative error which are not exceeding 10 %

It is established, that preservation and mutual influence of properties are especially shown while flat-topped diamond-abrasive machining, polishing and super finishing when the removed allowance is within the limits of initial height of rough edges asperity.

**1.3. Definition of factors of preservation and interference.** Multicoupling of technological mediums, distinction of the physical processes accompanying interaction of mediums with a subject of work, is a principal cause of absence of the uniform methodical approach to definition of elements of factors of preservation and mutual influence of formed properties $k_{ij}$ matrixes *[k$_{ij}$]*. Factors are defined at realization of through technological process of product manufacturing at continuous research of quality condition of a subject of manufacture.

Primary value $k_{ij}$ for an initial phase of process:

$$k_{ij} \approx \frac{(K_i)_1 - S_{ij}(K_i)_0}{(K_i)_0},$$

where *(K$_i$)*$_1$ - value of parameter $K_i$ after operation performance; *(K$_i$)*$_0$ - value of parameter $K_i$ prior to the beginning of operation performance; $S_{ij}$ - factor of change of a quality index at interaction of a subject of manufacture with the technological medium of an operation level.

In contrast to $m_i, u_i$, factors $k_{ij}$ have physical dimension.

The offered device of the description of transformation of quality indexes in view of their interaction and mutual influence in multiply connected technological mediums is adequate to real processes of property formation of mechanical engineering products and can be used for forecasting technological decisions. Application of the offered approach allows from 2 up to 5 times to reduce a relative error of preliminary definition of level of quality index in comparison with the value received on the basis of known laws of mechanical engineering technology [3].

## 2. CALCULATING AND ANALYTICAL METHOD

Consideration of mutual influence of technology factors at interaction of technological mediums with a subject of manufacture allows to bring in corresponding specifications to a settlement - analytical method of definition of a total error of machining. Preparations of an error arising at processing are interconnected and influence against each other and a total error of processing. Making errors are formed as a result of interaction of preparation with the technological medium of a level of operation, and with the technological medium of a level of process.

**2.1. Definition of an error of processing.** In result the mathematical device of definition of values of components and a total error of processing is developed. For the first it is fair that

$$
\begin{bmatrix} \Delta Y \\ \varepsilon \\ \Delta H \\ \Delta u \\ \Delta T \end{bmatrix}_j = \begin{bmatrix} 1 & a_{\Delta Y,\varepsilon} & a_{\Delta Y,\Delta H} & a_{\Delta Y,\Delta u} & a_{\Delta Y,\Delta T} \\ a_{\varepsilon,\Delta Y} & 1 & a_{\varepsilon,\Delta H} & a_{\varepsilon,\Delta u} & a_{\varepsilon,\Delta T} \\ a_{\Delta H,\Delta Y} & a_{\Delta H,\varepsilon} & 1 & a_{\Delta H,\Delta u} & a_{\Delta H,\Delta T} \\ a_{\Delta u,\Delta Y} & a_{\Delta u,\varepsilon} & a_{\Delta u,\Delta H} & 1 & a_{\Delta u,\Delta T} \\ a_{\Delta T,\Delta Y} & a_{\Delta T,\varepsilon} & a_{\Delta T,\Delta H} & a_{\Delta T,\Delta u} & 1 \end{bmatrix}_j \begin{bmatrix} \Delta Y \\ \varepsilon \\ \Delta H \\ \Delta u \\ \Delta T \end{bmatrix}_{\partial j} ,
$$

where $(\Delta Y, \varepsilon, \Delta H, \Delta u, \Delta T)^T_j$ – a vector - column of values of making errors (an error caused by elastic deformations; an error of installation; an error of adjustment; an error caused by dimensional deterioration; an error caused by thermal deformations), determined in view of mutual influence; $a$- factors of transformation of the errors, taking into account mutual influence of errors; $(\Delta Y, \varepsilon, \Delta H, \Delta u, \Delta T)^T_{\partial j}$ – a vector - column of the determined values, the making errors determined on the basis of a traditional settlement - analytical method.

The square of final value of total error $\Delta$ is defined in the form

$$
\Delta^2 = [\lambda_i P_i]^T [P_i],
$$

where $\lambda_i$ – The factors determining the form of a curve of distribution of the making error $P_i$; $T$ – Symbol of transposing.

The account of multiconnectivity of technological mediums at definition of a total error of processing allows more than in 2 times to raise accuracy of existing methods of calculation [3].

**2.2. Model of formation of quality indexes.** The developed device of the description of transformation of properties of products allows to distribute in the desirable image levels of properties of a product on stages of technological process of its manufacturing. For any part of through technological process of manufacturing of a product and for any of properties of the last on the basis of the developed technique can be determined and the desirable level of values of corresponding quality indexes is if necessary optimized.

So, for example, after end of procuring repartition the achieved levels of quasi-stable $K_c^3$ and changing $K_v^3$ quality indexes are defined as following:

$$\begin{cases} K_c^3 = S_c^3 \cdot K^M + k_c^{3,M} K^M; \\ K_v^3 = S_v^3 \cdot K^M + k_v^{3,M} K^M, \end{cases}$$

where $S_c^3$, $S_v^3$ – factors of property change of a subject of manufacture as a result of its interaction with the technological medium of a level of procuring repartition; $K^M$ – levels of quality indexes of an initial material;

$k_c^{3,M}$, $k_v^{3,M}$ – factors of preservation and mutual influence of properties of the initial material, shown at a procuring stage of through process of manufacturing of a product.

Similar parities can be determined for repartitions of manufacturing of details and assembly of a product. These parities can be considered as model of formation of properties of a product in through technological process of his manufacturing. Practically for any stage $N$ of group of operations parities of a kind can be received:

$$K_N = H_N \cdot K^M,$$

where $K_N$ – value of the quality index generated after stage $N$; $H_N$ – factor of transformation of properties of a product in relation to initial ($K^M$).

Introduction of set of criteria of optimization it is possible to proceed to the decision of problems of optimization of values of quality indexes for each stage (operation) of technological process. As not all quality indexes are equivalent from a position of technological maintenance of their values expediently to define desirable levels not for everything, and only for hard-to-achieve quality indexes, considering thus "by default", that other indexes will be provided. Use of "passport" of a subject of the manufacture including, for example, for a detail the data about most hard-to achieve levels of quality indexes and the general number of its surfaces, allows to lower dimension of technological problems solved in a correct way.

## 3. TECHNOLOGICAL ALGORITHM

Distribution of levels of properties in a combination to definition of quantitative characteristics of possible property transformation allows to change essentially existing approaches to construction of technological processes [6].

For successful performance of the set of functions the technological medium should be provided with necessary reserves. A reserve of the technological medium sets of its characteristics and values form the last which are not used at performance by the medium of set functions and conditions of their realization. The estimation of medium on each of its parameters can be carried out on the basis of the offered quantitative characteristics. The medium of any level should possess necessarily a reserve on parameters (opportunities) which size should correspond optimum to set of carried out functions and a range of possible changes of conditions of their realization. The choice of technological mediums and any of the technological objects possessing rational reserves, can effectively be carried out on the basis of the suggested device of an estimation of quality of corresponding technological decisions. Formation of a reserve of medium can be carried out on each of its separately taken parameters and should take into account both stochastic character of the last, and their interaction.

In view of influence of all cycle of manufacturing of a detail on its operational properties the algorithm according to which on required operational properties values of parameters of a condition of a superficial layer of a ready detail are recommended is developed and the technological process of its manufacturing providing the specified parameters is formed, modes of cutting, the characteristic of the tool and the equipment, mark lubricant-cooling agent (the lubricant-cooling technological medium), providing necessary parameters of a condition of a superficial layer of preparation and a semifinished item at each stage of processing are appointed.

The technological algorithm includes the following stages:

- Proceeding from operational properties and conditions of operation of elementary surfaces of  detail requirements to condition of a surface of a detail are established;

- On the basis of mathematical models or in a database on a required condition of a superficial layer modes of processing, the tool, the equipment, lubricant-cooling agent, necessary for realization of final processing the set of details are defined;

- On parameters of a condition of a superficial layer modes of processing, the tool, the equipment, lubricant-cooling agent, necessary for realization of the previous operation (transition) of processing are defined.

Designing of technological processes of product manufacturing in view of mutual influence of formed quality indexes is ineffective outside of his automation on the basis of modern computer facilities. Designing of individual routing technological processes (RTP) of detail manufacturing is desirable for carrying out in a mode of the automated synthesis at the minimal dialogue of the user with system [7, 8].

Strategy of the sanction of a problem of automated synthesis of RTP in view of laws of change, preservation and mutual influence of formed quality indexes, provides:

- Performance of synthesis of RTP in the automated mode on a basis general technological principles and reception of the basic characteristics of a route;

- Forecasting change of quality indexes in view of laws of property transformation on the basis of structure generated by RTP;

- Performance of necessary updating RTP in case a desirable level of values of quality indexes does not achieve.

## CONCLUSION

The automated generation of technological mediums of the set level concerning the allocated object is possible on the basis of their functional models created with application of CALS-technologies. Functional models of multiply connected technological mediums allow to carry out depending on statement of a decided problem decrease in its dimension by allocation of set of essential communications and suppression insignificant at preservation of a correctness and adequacy.

Reduction in sensitivity of technological and operational mediums to change of conditions of realization of modes of manufacture and application of products allows to carry out with the least expenses the directed formation of quality indexes in life cycle of products of mechanical engineering.

## REFERENCES

1. Kolesnickov K., Balandin G., Dalsckiy A. et al.: *Technological Basis of Machine Quality Control.* Moscow: Mechanical Engineering, 1990, 256 p.

2. Kuznetzov N., Tzeitlin V., Volkov V.: *Technological Methods of Machine's Details Reliability Growth*. Moscow: Mechanical Engineering, 1993, 304 p.

3. Vasilyev A. Dalsckiy A., Klimencko S. et al.: *Technological Basis of Machine Quality Control.* Moscow, Mechanical Engineering, 2003, 256 p.

4. Yaschericyn P., Averchenckov V., Kheifetz M., Koukhta S.: *Analysis of Property Relations of Technological Solutions at Designing of Combined Methods of Materials Processing.* Report of National Academy of Sciences of Belarus, 4, 2001, v. 45, pp. 106 – 109.

5. Vityaz P., Kozhuro L., Filonov I., Kheifetz M.: *Property Control of Technological Medium at Electrophysical Processing.* Heavy Engineering Construction. 7, 2004, pp. 18 – 23.

6. Kheifetz M., Chenisov B. (red): *Intelligent Production: State and Future* Prospects. Novopolotsk: PSU 2002, 268 p.

7. Ryzhov A., Averchenckov V.: *Technological Process Optimization of Machine Working*. Kiyiv: Navukovaia dumka, 1989, 192 p.

8. Rakovich A. (red): *Automatization of Technological Processes and Equipment Aids Designing.* Minsk: ITC of National Academy of Sciences of Belarus, 1997, 276 p.

**Ján VIŇÁŠ**
**Ľuboš KAŠČÁK**
**Dagmar DRAGANOVSKÁ**
**Milan ÁBEL**

Technical University of Košice, Slovakia

# THE CHOICE FACTORS ANALYSIS INFLUENCING QUALITY OF MIG BRAZED JOINTS OF GALVANIZED STEEL SHEETS

*In the paper results of metallographic analyses of joints made by MIG brazing on deep-drawn galvanized steel sheets of DC 05 EN 10152 are presented. The quality of brazed joints made by SG CuSi3 and SG CuAl8 braze with fluctuating welding rectifier CLOOS 303 MC4 was evaluated. Argon 4,80 was used as gaseous shield.*

## INTRODUCTION

Even though surface modified construction steels don't belong to the new materials, its consumption is still growing. Automobile industry shows the most dynamic growth of deep-drawing sheets with surface treatment because its consumption is more than double for last twenty years. At the same time the consumption of "black" sheets during the car-body production decreased. Surface treatment by galvanizing guarantees good corrosive resistance of car-body sheets and enables more than 10 years guaranty of car-body lifetime. Practically several methods of coating application are used, most frequently Zn coating. The most used method is hot-dip zinc galvanizing where thickness of coating is from 10 to 30 μm. At capacity of production this method is followed by electrogalvanizing with thickness of coating from 2 to 10 μm. Above mentioned methods are most widely used at car-body production. Besides of them Zn metal spraying and coating system on the basis of Zn are used too but those methods are practically not used at automobile production [1, 8, 9].

Zn coating at steel sheets causes some problems during the all welding process. The biggest one is relatively low melting temperature of Zn (419ºC), however the huge problem is Zn vaporization at the temperature over 908 ºC. When steel melting temperature is higher and also the melting temperature of brazes applied at car-body production, there are some destruction of coatings and subsequently corrosive resistance decreases at the joints.

The effort of automobile producers is safety reliable automobile with low fuel consumption. Therefore in order to decrease car-body mass combinations of deep-drawing surface modified sheets, high-strength sheets for reinforcement, aluminum alloys, sandwich sheets, compounds and plastics are used in automobile production. Possibilities of these materials utilization require applying wide range of knowledge and precise parameters optimalization in technologies of its joining. One increasingly used method of car-body joining is MIG brazing (GMAB – Gas Metal Arc Brazing).

This technology has already been applied at car-body production in early seventies, but its participation to the car-body production still grows.

## METODOLOGY OF EXPERIMENTS

For experiment deep-drawing sheets of DC 05 EN 10152 were used. The used material is the deep-drawing steel with ferritic structure. Surface treatment of sheet was realized by dip-zinc galvanizing. Zinc coating thickness, stated by producer, is 13µm. Chemical composition of observed sheet is presented in the Table 1.

Chemical composition of used types of brazes and its strength characteristics are presented in Table 2. Used A 384 brazes were made by UTP company.

*Table 1. Chemical composition and mechanical characteristics of DC 05 EN 10152 steel [3]*

| Material | C [%] | Mn [%] | P [%] | S [%] | $R_m$ [MPa] | $R_{p0,2}$ [MPa] | $A_{80}$ [%] |
|----------|-------|--------|-------|-------|-------------|------------------|--------------|
| DC 05 | 0,05 | 0,33 | ≤ 0,0025 | ≤ 0,0025 | 270 - 330 | ≤180 | ≥ 40 |

*Table 2. Standard chemical composition and mechanical characteristics of brazes [4]*

| Material DIN 1733 | Cu [%] | Mn [%] | Si [%] | Sn [%] | Al [%] | $R_m$ [MPa] | $R_{p0,2}$ [MPa] | $A_5$ [%] | KU [J] | Melting temperature [ºC] |
|-------------------|--------|--------|--------|--------|--------|-------------|------------------|-----------|--------|--------------------------|
| SG CuSi3 | 96,0 | 1,0 | 3,0 | - | - | 300 | 160 | 23 | 25 | 910 - 1025 |
| SG CuAl8 | 92,0 | 0,2 | - | 7,8 | - | 380 | 180 | 40 | 70 | 950 - 1080 |



*Fig. 1. Welding rectifier CLOOS 303 MC*

Samples of 200 mm x 150 mm dimension were cut from sheets of 1mm thickness of 1000 mm x 2000 mm dimension on the table shear. Upsets after shearing were removed from the samples which would negatively affect the pureness of brazing metal near the shear edge. Brazing surfaces were cleaned out of shearing emulsion by acetone.

Brazing of car-body sheets were realized on CLOOS 303 MC4 equipment which is illustrated at Fig. 1.

Joint formed by brazing technology was formed in shielding gas of argon 4,80 at lapped sheets. Method of joint making is illustrated schematically at Fig. 2. The angle of torch sloping during brazing was 45º.

*Table 3. Used parameter of brazing*

| Thickness of Brazing Sheets | Type of Braze | Wire Diameter of Braze | Impulse | Brazing Current [A] | Voltage [V] | Inert Gas |
|-----------------------------|---------------|------------------------|---------|---------------------|-------------|-----------|
| 1,0  + 1,0 | CuSi3 | 1,0 mm | Yes | 76 | 14 - 15 | Argon 4,80 |
| 1,0  + 1,0 | CuAl8 | 1,0 mm | Yes | 80 | 13 - 14 | Argon 4,80 |

Macrostructure and microstructure analyses of brazing joints quality were realized due to STN EN 1321 standard with the metallographic scratch patterns on optical light microscope Olympus CX-31. For visualization of basic material microstructure, following etching was used: Nital in 3% concentration. Microstructure of braze CuSi3 a CuAl8 was etched by solution of ammonium persulphate (10g of ammonium persulphate + 100 cm$^3$ of distilled water).
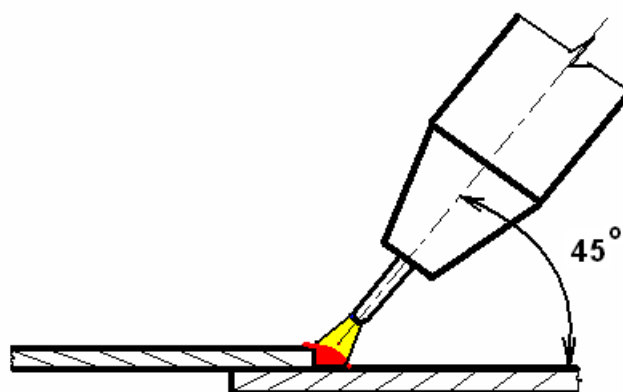


*Fig. 2. Kind of weld making*

## ANALYSIS OF ACHIEVED RESULTS

Material DC 05 EN 10152 was analyzed by microstructural analysis. At Fig. 3, a ferritic structure of tested material is presented.
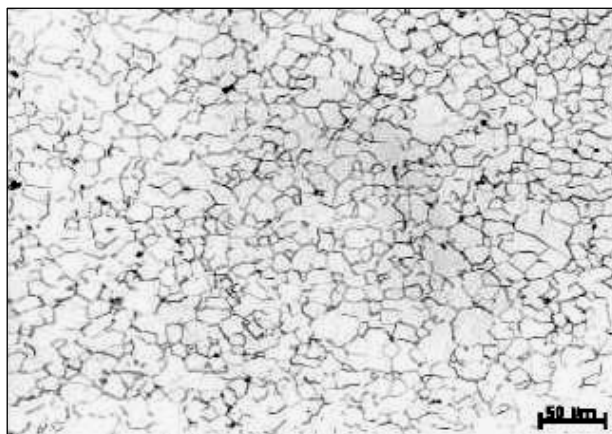


*Fig. 3.  Microstructure of DC 05 EN 10152 steel*

At chosen angle of torch sloping 45° according to the place of brazing, the process of more intense metal melting from the upper edge of the sheet starts – see the Fig. 4. This is in compliance with observed Fe particles diffused in brazing metal during the higher distinction near the edge of top brazing material.

On macrostructure of joint it is possible to see relatively small thermal impact of joining sheets in the process of MIG brazing. The detail shows good wettability and fluidity of braze. The pores were observed in the brazing metal. With increasing amount of pores in brazing metal the strength characteristics of joint significantly decrease.

During the brazing by CuSi3 wire it is suitable to use blended gases, namely: Ar + 1% $O_2$, or Ar + 2,5% $CO_2$. By addition of these active components it is possible to achieve lower porosity, more stable arcing and minimum splash. Blended gases bring into the brazing process more heat compared to the using pure argon what could result

in negative impact during the thin sheets brazing [6, 7]. At Fig.5 you can see the metal microstructure of the CuSi3 braze.

In comparison with CuSi3 solder, CuAl8 solder has double electrical conductivity and higher toughness. It is suitable for brazing of two-phase galvanized steel. CuAl8 has lower predisposition on porosity [2] what is visible from macrostructure at Fig. 6.

By influence of big amount of preheating, it is possible to see wide range of heat influence on basic (brazing) materials compared with the macrostructure of lapped sheets joined by SG CuSi3 solder (Fig. 4).
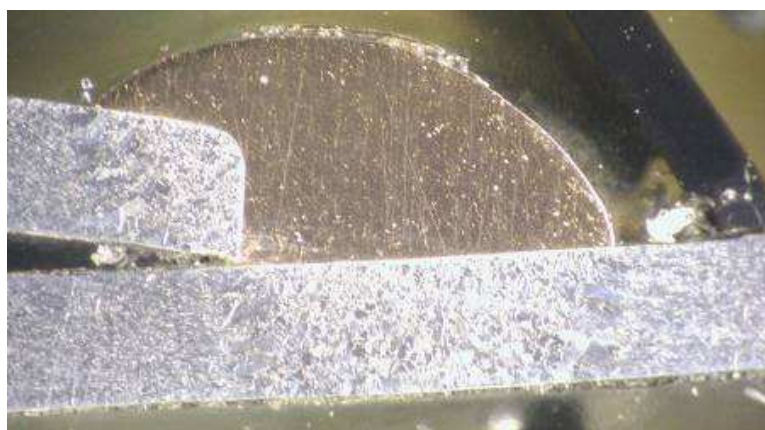


*Fig. 4. Macrostructure of lap-joining sheets jointed by SG CuSi3 braze*
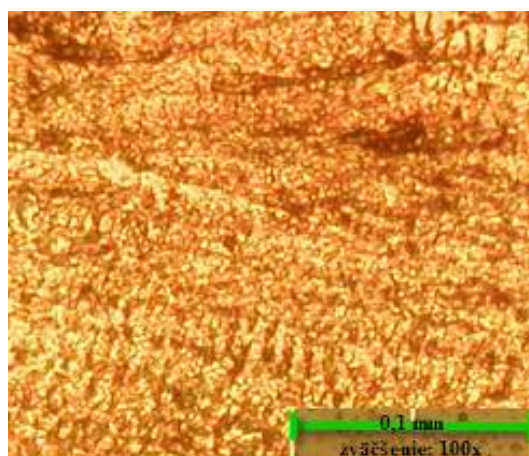


*Fig. 5. Microstructure of CuSi3 brazing metal*



*Fig. 6. Macrostructure of lap-joining sheet jointed with SG CuAl8 braze*

Microstructure of pure brazing metal CuAl8 is presented at Fig. 7. In the microstructure there were identified a small amount of Al fine-grained needle formations.
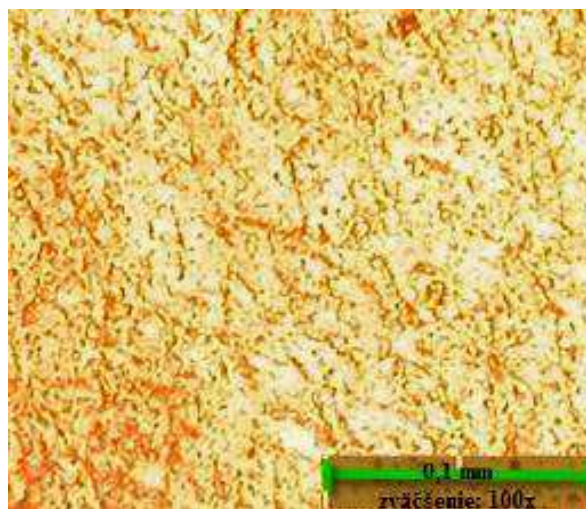


*Fig. 7. Microstructure of CuAl8brazing metal*

CuAl8 solders have a good stability of arcing. Pure argon is recommended as a gaseous shield. The additions of active gases in following volumes - 1% $O_2$ or 2,5% $CO_2$ haven't essential impact on the brazing process and final quality of joint [2].

One of the possibilities how to compensate negative influence of zinc evaporation on the lapped joint is position modification of brazing sheets (Fig. 8). Modification of the parallelness of brazing sheets contact areas with angle α (1-5°) enables better Zn evaporation from the place of brazing, thereby decrease their possibility to influence of melting metal transfer into the joint.

The flow of inert gas also influences the splash of brazing metal (Fig. 9). Concerning a necessity of short arcing (2 - 3 mm) at the brazing process, the sooting of metal from splash could appear while insufficient lining of wire from the torch outlet that is leading to the change of gas flow and then to the insufficient protection of fusing bath.



*Fig. 8. Possibility of improving the Zn vapors from the place of brazing [2]*



*Fig. 9. Detail of the brazed joint with the splash on the car body*

During the MIG brazing it is necessary to monitor the outlet regularly and applying the preparations based on silicone oils that avoid the melting metal particles to be bonded.

## CONCLUSION

Surface treatment by Zn, Al, Sn metals and their alloys negatively influence on all conventional and unconventional welding processes. Main part of negative impact on the welding process has mostly low melting temperature of these metals as well as its low evaporation temperature. Because of Zn evaporation during the arc methods of welding there is instability of weld arcing. Evaporated zinc from sheet surface causes the moving of arc from the place of joint to the area with lower electric resistance. It is suitable to use arc about length of 2-3 mm in brazing process.

Influence of zinc vapours on the quality of joint could be also decreased by the choice of direction of torch motion (bead storing). Left-hand burner operation decreases the influence of Zn vapours on the welding arc, because the evaporation comes before the transfer of additional melting material. But this method is very sensitive to the speed optimalization of torch motion during the brazing. Decreasing of speed could cause burnouts in thin sheets in the reason of more intense preheating of joined materials in the place of joint in comparison with right-hand torch operation. Right-hand torch operation provides only short time for zinc evaporation from the metal which has negative influence on electric arc. Dynamic effect of zinc vapours could affect the splash of additional melting metal which was confirmed by metallographic analysis of tested materials.

## REFERENCES

1. Ondrejček P.: *Zváranie ocelí v ochrane plynov taviacou sa elektródou*, Eterna press s.r.o. Bratislava, 2003
2. Sejč P.: *Špecifikácia oblúkového zvárania a spájkovania pozinkovaných plechov*. Bratislava, 2005.
3. Čambál E.: *Kvalita zvárania*, Strojárstvo 3/2001, s.21.
4. Bohler Thyssen Welding, UTP Schweiβmaterial FmbH, Bad Krozingen, 2004, 435 s.
5. Chovet C., Guiheux S.: *Possibilities offered by MIG and TIG brazing of galvanized ultra high strength steels for automotive applications*. In: La Metallurgia Italiana, 7-8 2006, s 47- 54.
6. Kersche A., Trube S.: *Schutzgase zum MSG-Loten*, Linde Technische Gase GmbH, Hollriegelskreuth, 1998
7. Roubíček M.: *Příspěvek do problematiky spojování pozinkovaných plechu*. Air Liquide CZ, s.r.o 2003,
8. Roubíček M.: *Problematika spojování pozinkovaných ocelí*. Seminář nové materiály, technológie a zařízení pro svařování, Ostravice, 2003.
9. Sejč P.: *Optimalizácia vybraných parametrov oblúkového MIG/MAG spájkovania pozinkovaných plechov*. Zváranie- Svařování 53, 2004, č.3, str. 57-62.

**Eva ZDRAVECKÁ**
**\*Jaroslav BRIANČIN**
**ŠtefanFECSU**

Technical University of Kosice, Slovakia
\*Slovak Academy of Sciences,Kosice, Slovakia

# ANALYSIS OF SELECTED PROPERTIES OF PVD FILMS

*Thin ceramic coatings deposited on the surface of tools and machine parts by PVD methods improve considerably their tribological properties. These hard brittle coatings can be damaged rapidly if a plastic deformation initiates in the substrate near the coating-substrate interface when subject to a relatively high intensity loading. The load bearing capacity of the coating-substrate system increases with improved substrate properties. The typical duplex processinvolves thermochemical treatment and the PVD coating treatment of steels. Tested duplex treated low-alloy steels were pulse plasma nitrided and then coated by CrN. The fretting tests showed the high wear resistance of duplex treated steel.*

## INTRODUCTION

Fretting is a wear phenomenon occurring when two contacting solids are subjected to a relative oscillatory tangentional motion of small displacement amplitude. This small oscillatory displacement along the contact interface can result in the renewal of material by wear or in the initiation of cracks by cyclic contact stresses. Fretting conditions are found in virtually any technical system where contact vibrations are induced by cyclic accelerations, fatigue stresses, acoustical noise or temperature variations. It is known that even displacement amplitudes in the sub-micron range can result in wear damage. Fretting becomes an important aspect to designers when the functionality of a component deteriorates or its lifetime is reduced by the induced material damage. In severe cases, the material damage initiates or promotes other failure mechanisms. Fretting fatigue, fretting corrosion, or stress-corrosion cracking are typical examples.

The damage features being developed on materials surfaces in vibrating contact are determined by the variables of the fretting process. Most important are the contact conditions (displacement stroke, vibration frequency, contact pressure), the environmental conditions (temperature, relative humidity, lubricants), and the material properties (hardness, yield strength, fracture toughness, chemical inertness). A real vibrating contact is often characterized by an extremely complex interaction of these variables making fretting a true system property [1]. In the presented paper, the simulation of fretting tests is described.

Investigated coatings were duplex treated low-alloy steels by pulse plasma nitrided and then coated by CrN– PVD with different thickness. These coatings belong to the thin ceramic coatings deposited on the surface of tools and machine parts by PVD methods improve considerably their tribological properties. These hard brittle coatings can be damaged rapidly if a plastic deformation initiates in the substrate near the coating-substrate interface when subject to a relatively high intensity loading. The load bearing capacity of the coating-substrate system increases with improved substrate properties. The logical solution of such problems is the improvement of mechanical characteristics of subsurface layers by a heat treatment or a thermochemical treatment like plasma nitriding. The duplex surface treatment involves the sequential application of two (or more) surface technologies to produce a surface composite with combined properties.

There are three main aspects for an optimisation of the duplex surface treatment technology:

- the structure of the coating,
- the structure of the strengthened subsurface layers
- the properties of their interface.

The critical point of duplex surfaces treatment is a state of interface that depends on quality of surface treatment and on their purity before of PVD process. Interface isimportant factor for coating adhesion, decides about adhesion of coating to substrate [4].

In this contribution the properties of duplex treated low-alloy steels nitrided by pulse plasma and then coated by CrN are analysed by fretting test.


## EXPERIMENTAL SETUP

For tests the steel 31CrMoV9 was selected. Chemical composition of steel is shown in Fig. 1. All the specimens from the low-alloyed steels (31CrMoV9 were heat treated (hardening 865-870°C/$N_2$ + tempering 600°C/2hours) and they were prepared for plasma nitridation and PVD coatings. All the samples were prepared by grinding (Ra ~ 0,1 μm) before nitridation.

*Tab. 1. Chemical compositions of 31CrMoV9*

| Steel | Volume elements(%) | | | | | | | |
|---|---|---|---|---|---|---|---|---|
| | C | Mn | Si | Cr | Ni | Mo | V | Al |
| 31CrMoV 9 | 0,3 | 0,59 | 0,28 | 2,39 | -- | 0,16 | 0,12 | -- |

Influence of pulse plasma nitridation parameters (temperatures – 500, 520, 550, 570⁰C, time – 5, 10, 20 40 hours, concentration $H_2$:$N_2$ = 3.1 and 6:1) on the phase composition of steel 31CrMoV9 by X-ray diffraction – Tab. 2.
Practically for all nitridation processes the layer of nitrides on the surface was recorded which according to some authors [2, 3] during of deposition processes of PVD coatings degrades and induces deterioration of coating adhesion to nitrided substrate. Therefore all sample functional surfaces from nitrided steel 31CrMoV9 were grinding.

*Tab. 2.X-ray diffraction analysis results*

| Ratio H/N | Temperature of nitridation [$^0$C] | Time [hours] | | | |
|---|---|---|---|---|---|
| | | 5 | 10 | 20 | 40 |
| 3:1 | 500 | strong Fe$_4$N, weak Fe$_3$N, weak Fe | 72% Fe$_4$N, 15% Fe, 13% Fe$_3$N | main Fe$_4$N, medium Fe$_3$N, weak Fe | 75% Fe$_4$N, 3% Fe, 22% Fe$_3$N |
| | 520 | main Fe$_4$N, weak Fe, trace Fe$_3$N | 76% Fe$_4$N, 7% Fe, 17% Fe$_3$N | 82% Fe$_4$N, 3% Fe, 15% Fe$_3$N | 81% Fe$_4$N, 2% Fe, 17% Fe$_3$N |
| | 550 | main Fe$_4$N, weak Fe, trace Fe$_3$N | 88% Fe$_4$N, 12% Fe | 95% Fe$_4$N, 5% Fe | main Fe$_4$N, trace Fe, trace Fe$_3$N |
| | 570 | 55% Fe, 45% Fe$_4$N | 73% Fe, 27% Fe$_4$N | 96% Fe$_4$N, 4% Fe | 95% Fe$_4$N, 2% Fe, 3% CrN |
| 6:1 | 500 | 58% Fe$_4$N, 42% Fe | 87% Fe, 13% Fe$_4$N | strong Fe, medium Fe$_4$N, trace Fe$_3$N | 77% Fe, 23% Fe$_4$N |
| | 520 | 87% Fe, 13% Fe$_4$N | 80% Fe$_4$N, 20% Fe | 69% Fe$_4$N, 31% Fe | 50% Fe$_4$N, 50% Fe |
| | 550 | 95% Fe, 5% Fe$_4$N | 72% Fe, 28% Fe$_4$N | 65% Fe, 35% Fe$_4$N | 63% Fe$_4$N, 37% Fe |
| | 570 | 97% Fe, 3% Fe$_4$N | 94% Fe, 6% Fe$_4$N | 84% Fe$_4$N, 16% Fe | very strong Fe, weak Fe$_4$N, trace Fe$_3$N |

## Adhesion of CrN coatings

The characteristics of surface coatings were analyzed by methods of the micro-hardness measurement. Microstructure of coatings CrN and subsurface layers were studied by optical microscopy, REM. Adhesion was tested by scratch tests (Tab. 3).

*Tab. 3. Results scratch tests of duplex coatings*

| Coating | Thickness of coating [µm] | Critical load [N] |
|---|---|---|
| CrN | 1 | 42,05 |
| CrN | 2,5 - 3 | 49,63 |

The values for critical loading are relative great and indicate about good adhesioun coatings on the substrate. The results are in Tab. 3.

Measurement of depth profile for plasma nitriding surface and also selected duplex coating by GDOES - optical emission spectrometry with using glow-discharge lamp was provided in Institute Terotechnologia in Radomi (Poland).

Measurements were made on the reference samples for steel 31CrMoV9. Vertical depth profile of Cr, N and Fe shows uniform change between coating and substrate (Fig.2)
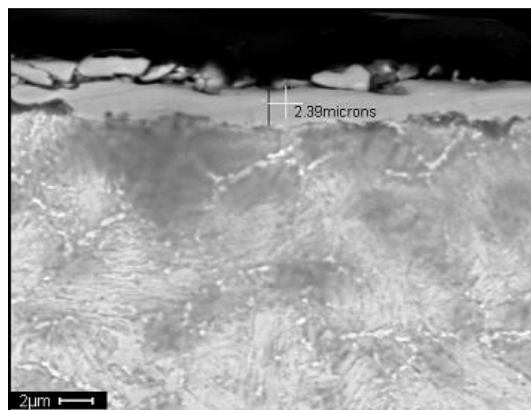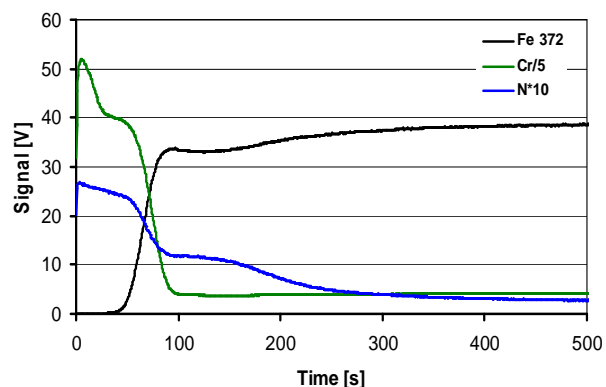
Fig. 1. REM of duplex coating



Fig. 2. Depth profile of duplex coating PPN + CrN (3μm)

**Fretting test:**

Fretting wear tests were carried out in the laboratory conditions for understanding the fretting wear behavior of tested materials. PPN+CrN coatings to unlubricated sliding against corundum ball ($\alpha$-$Al_2O_3$) were investigated.

Parameters of tests:

| | |
|---|---|
| Temperature | $T = 23^{o}C$ |
| The relative humidity of | 50% |
| The diameter of ($\alpha$-$Al_2O_3$) contrebodies | d = 10 mm. |
| Linear displacement strokes | 100 μm |
| The vibration frequency | 10 Hz |
| Normal force | F = 5N. |
| Number of cycles | 10 000 |



Fig. 3. View on the apparatus for fretting test
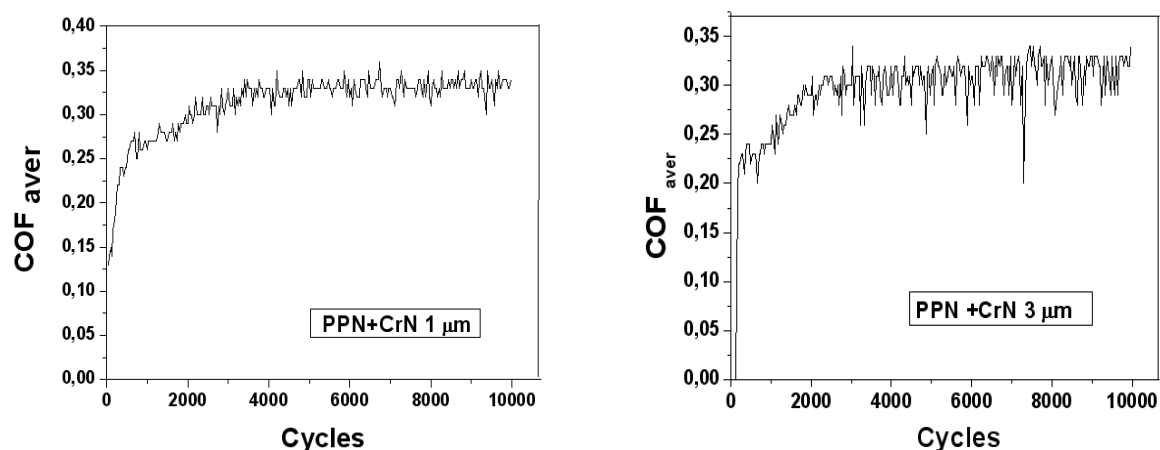
*Fig. 5. Graphical output of COF$_{aver}$ for duplex coating PPN + CrN*

Graphical output of COFs at duplex treated low-alloy steels pulse plasma nitrided and then coated by CrN– PVD with thickness CrN 1 µm and CrN 3 µm during dry sliding are shownin Fig. 5.

The best value of coefficient friction was observed for coating PPN+3 CrN 1 µm, what can be connected with thickness. From the results of experimental tests the mean value of friction coefficient obtained for PPN + CrN 1 µm was COF$_{aver}$ = 0.311667 and for PPN + CrN 3 µm was COF$_{aver}$ = 0.2334.

Typical morphology of duplex treated low-alloy steels pulse plasma nitrided and then coated by CrN 3 µm is in Fig. 6
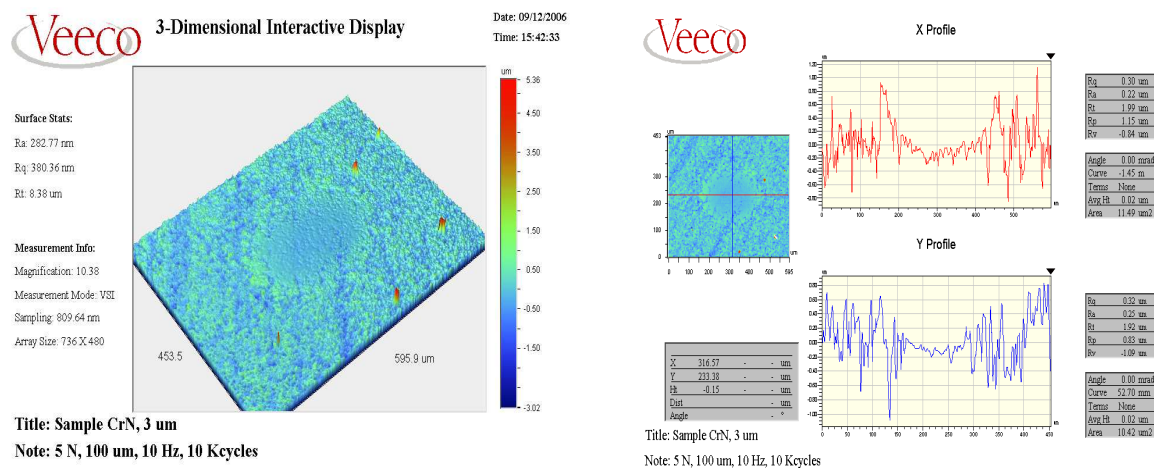


*Fig. 6. Morphology of PPN + CrN 3 µm*

From point of view of COF, coating CrN 3µm was the best. The resistance to plastic deformation – the quantity which can more distinctly divide film materials.

## DISCUSSION

The results of experimental works showed the duplex surface treatments that combine the both plasma nitridation and PVD coating processes may enhance the adhesive wear resistance at dry friction.

Thin PVD coatings (≈1 μm) deposited on nitrided surface can not favourably to influence the adhesive wear resistance because they are damaged in early phase of wear process what is connected with higher friction coefficient.

Coatings PVD with thickness 2,5-3 μm showed lower friction coefficient, and more resistant to vibrating contact characterized by the variables of the fretting process. These results from fretting testes are in correlation to scratch test**.**

## CONCLUSIONS

Tribological properties of thin and hard layers are influenced by structure, chemical composition and deposition parameters. Adhesion of thin and hard layers is dependent on character of coupling forces between layer and substrate. Tribological properties of thin and hard layers are influenced by structure, chemical composition and parameters of deposition. Adhesion of thin and hard layers is dependent on character of coupling forces between layer and substrate.

## REFERENCES

1. Mohrbacher H., Celis J.P., Roos J.R.: *Laboratory testing of displacement and load induced fretting*. Tribology International. Vol. 28. 269-278, 1995.

2. Bell T.: *Realising the potential of duplex surface engineering*. New directions in Tribology, MEP, London, 1997, pp. 121-133

3. Cho S.J., a kol.: *Wear mechanism in TiN-coated HSS during sliding*. Proc.EUROTRIB´93, Budapest,1993,vol.3, str.231-237

4. Suchanek J., Jurči P., Zdravecká E.: Adhesive wear of duplex-treated low-alloyed steels. Tribotechnika v teorii a praxi. Praha.2007,str. 118-122

**Nikola ŽIVKOVIĆ**
**Predrag STEFANOVIĆ**
**Dejan CVETINOVIĆ**

Institute of Nuclear Sciences „Vinča", Belgrade, Serbia

# COAL POWDER FRACTIONS DISTRIBUTION IN THERMAL POWER PLANT MIXTURE CHANNEL PRESENTED BY NUMERICAL CALCULATIONS

*One of the problems during exploatation period of thermal power plant is to determine and optimize distribution of various coal powder fractions in the mixture channel. Regulation of distribution with shutters, positioned after the mills, is proposed solution. The paper present distribution of coal powder fractions, obtained by numerical calculations, using numerical software for modelling of two-phase flow problems. The problem is two-dimensional, considering that, transversal dimension of the domain is relatively big compared with the other two dimensions, and volume occupied by solid phase is much less than volume occupied by continual phase. Continual phase is treated by an Eulerian approach, and solid phase is modeled by Lagrangian approach. The model takes in consideration coupling of phases by PSI-CELL method. Turbulence was modeled with standard k-ε model. The model treats particles as an ideal sphere. In order to determine particle movement, all relevant forces, (with continual affect and impulse affect), are incorporated in the model. The results obtained, include velocity field and profiles of continual phase, concentration field and profiles of coal particles and mass flow distribution at the outlet cross section of mixture channel for various coal particle diameters and various angular positions of shutters.*

## INTRODUCTION

Plasma system for black mineral oil free fire stabilization of pulverized coal combustion on thermal power plant boilers was implemented throughout the world, [6]. In Serbia, this kind of plasma technology is in implementation phase on thermal power plant „Nikola Tesla"–A, 210 MW, Obrenovac, [4].

In order to implement plasma system for fire stabilization of pulverized coal combustion on thermal power plant there were a few requirements to be fulfilled. The most important of them are:

- optimal air−coal mixture flow rate in the sections where plasma generators are introduced and
- uniform distribution of coal particles in those sections.

The mixture channel is divided in eight sections-channels. Four sections on the right side of the channel direct the mixture to plasma generators. The mixture channel is equipped with groups of movable shutters whose aim is to direct the air–coal mixture towards four sections on the right side of the channel. Three movable shutter groups conducts air–coal mixture stream in order to achieve proper concentration of coal particles. It is necessary to achieve uniform profiles: velocity profile of continual phase and mass flow distribution of coal particles (concentration profile of disperse phase), in four sections on the right side of the channel, which conduct the mixture to the plasma generators.

This paper take into account distribution of various coal particle fractions along the width of the channel. In order to obtain and present the results numerical software for modelling two-phase flow problems, developed in Laboratory for Thermal Engineering and Energy was used.

## THE MIXTURE CHANNEL AND THE SHUTTER SYSTEM

The shutter system consists of three groups of shutters (A), (B) and (C), as shown on Figure 1. Group (A) is a non-adjustable group of four shutters. Shutters of this group may have only two positions (open (90°), close (0°)). Group (B) is a group of adjustable shutters, and they may have angle positions in the range 0° to 135°. Shutter group (C) was introduced to obtain more uniform velocity and concentration profiles, and may have angle positions in the range 0° to 90°. Fictitious shutter-obstacle (D) was introduced in computation only, with the intention to find out is it possible to meet the requirements already mentioned. This shutter was positioned in the right side of the channel, Figure 1.

Channel sections are numbered from 1 - 8 from right to left. The first section is always the first near to the boiler furnace.
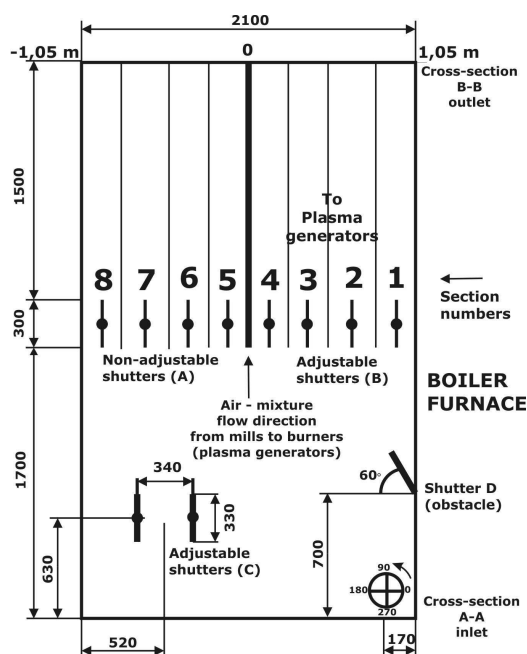


*Figure 1. Mixture channel with shutters*

## TWO PHASE FLOW MODEL

In order to determine velocity profiles and solid particle concentration profiles an Euler-Lagrange multiphase model was developed. Continual phase (fluid - gas) is treated by an Eulerian approach. Disperse phase is modeled by Lagrangian approach, which means that all parameters are the function of time only, as introduced by Durst et. all [2]. Despite the fact that the time appears explicitly in the particle movement equations, averaged disperse phase characteristics for a long period of time do not change, so it can be treated as stationary. That approach is compatible with the basic intention modelling stationary regimes of plasma generators.

Transversal dimension of the straight section of the channel is relatively big compared with the other two dimensions of the channel, so the problem can be treated as two-dimensional neglecting the influence of side walls.

The model takes in consideration coupling of phases by PSI-CELL method developed by Crowe et. all [1]. In accordance with the method, the influence of disperse phase on continual phase is reduced to an existing additional article in the continual phase equations. That can be done in such cases when a volume occupied by disperse phase is much less than the one occupied by continual phase. Continual phase can be treated completely as Newtonian fluid. Turbulence was modeled with standard two-equation $k$-$\varepsilon$ model, which with the two Navier-Stokes equations for velocity components and continuity equation compose system of five partial differential equations describing continual phase flow.

The model treats particle as an ideal sphere. Although it is a rough idealization that is the standard method, even for the particles of small size (about 100 μm) considered in this paper. It is based on the experience of many authors. In order to accurately determine particle movement it is necessary to incorporate all relevant forces in the model that determine the movement. There are two groups of the forces: forces with continual affect and the forces with the impulse affect. The source of the forces with continual affect is presence of continual phase and gravity. The source of the forces with impulse affect is interaction of particles with boundaries-walls. The presented models in [3, 5, 7] were developed in order to determine forces mentioned above.

## RESULTS

Input parameters in numerical calculations are velocity profile of continual phase, concentration profile of disperse phase at the inlet cross-section A-A, and angular positions of shutter groups are presented in Table 1.

Particle size distribution in numerical calculations was: fraction 1 (30 μm – 60 μm, 25%), fraction 2 (60 μm – 90 μm, 15%), fraction 3 (90 μm – 200 μm, 32%), fraction 4 (200 μm – 500 μm, 18%), fraction 5 (500 μm – 1000 μm, 6%) and fraction 6 (1000 μm ,5%). Particle diameter distribution was considered as uniform. Figure 2 presents velocity profile of continual phase at the inlet cross section. As can be seen, velocity profile have a "parabolic" shape. Velocity profile have a peak around the center of the channel (29 m/s) and reduces to 24 m/s on the left and the right side of the channel, beside the walls. Figure 3 represents particle concentration profile. It is evident that the concentration values on the right side of the channel are much higher than the values on the left side. It would be necessary to obtain more uniform profiles in the right side

of the channel than those obtained by the experiments, since the concentration profile in the right side of the channel, is of great importance for the proper work of plasma system.
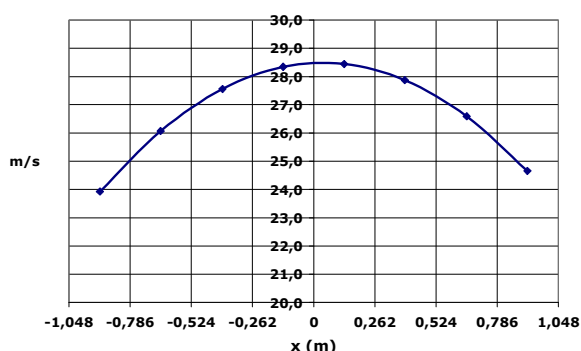


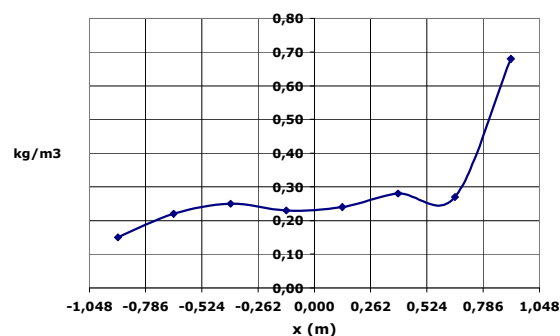*Figure 2. Velocity profile of continual phase in inlet cross section A−A*



*Figure 3. Concentration profile of particles in continual phase, in inlet cross section A−A*

The position of groups of shutters, shown in Figure 1, has a great influence on mass flow distribution along the channel sections and concentration field, so it is important to vary shutter inclination angles, and find the optimal solution.

*Table 1: Regimes considered in numerical calculations*

| | Angular positin of shutters | | | | |
|---|---|---|---|---|---|
| Regime | A | B | C | D | Fractions |
| 1 | 90° | 90° | 60° | - | All |
| 2 | 90° | 90° | 60° | - | 30-60 μm |
| 3 | 90° | 90° | 60° | - | 60-90 μm |
| 4 | 90° | 90° | 60° | - | 90-200 μm |
| 5 | 90° | 90° | 60° | - | 200-500 μm |
| 6 | 90° | 90° | 60° | - | 500-1000 μm |
| 7 | 90° | 90° | 60° | - | 1000- μm |
| 8 | 90° | 90° | 60° | + | All |

In this paper, eight regimes were considered in numerical calculations. The regimes are grouped in two main groups. The first group includes the regimes with numbers 1 and 8. These two regimes are different from the others because they involve all fractions of coal particles in numerical calculations. The second group are the regimes with the numbers 2 – 7 (Table 1). Each of these regimes involve only one fraction of coal particles. Presenting the results in that way gives us a possibility to track the particles of various diameter ranges, their mass flow distribution in the channel sections, etc.

Regimes 1 and 8 include all of the coal powder fractions in calculations. Shutter groups A and B are in opened positions. Shutter group C is placed at the angular

position of 60°, and it is the only shutter group that strongly affects the fluid flow and particle distribution. In that position the shutters direct mixture towards the four sections on the right side of the channel and forward to the plasma zone. Figures 4 and 5 present velocity fields and Figures 6 and 7 present concentration fields of solid particles for the two regimes.
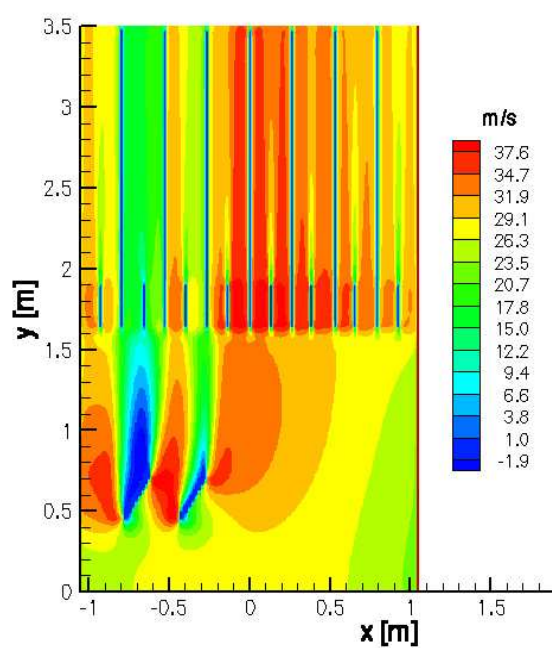


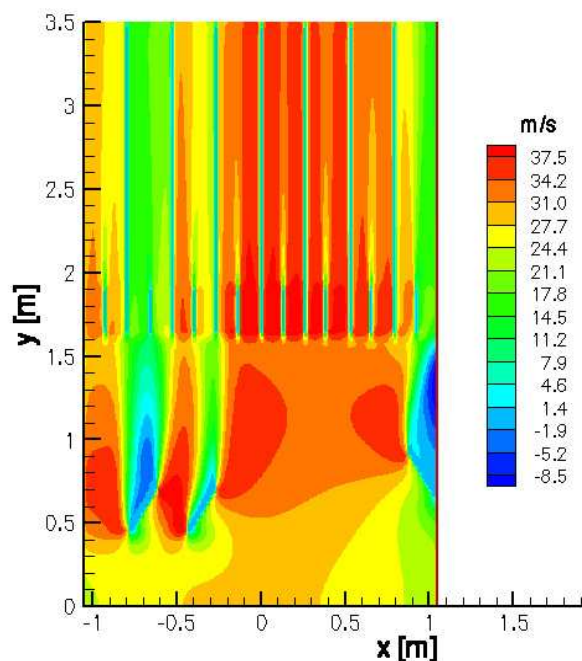*Figure 4. Velocity field, Regime 1, without D obstacle*
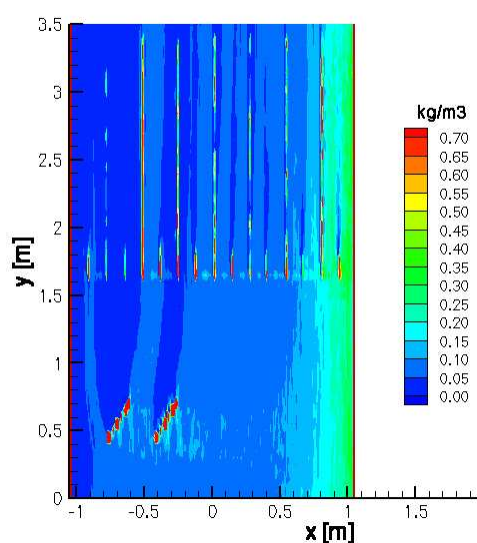


*Figure 5. Velocity field, Regime 8, with D obstacle*



*Figure 6. Concentration field, Regime 1, without D obstacle*
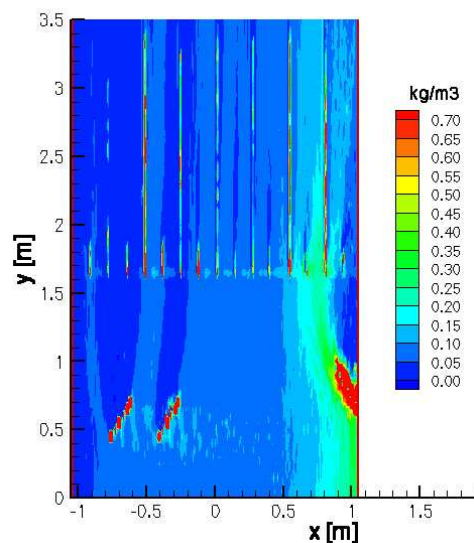


*Figure 7. Concentration field, Regime 8, with D obstacle*

315

The problem that occurs for the regime1, is non-uniform mass flow distribution of powder coal particles in sections 1 – 4 (Figure 9). About 35% of coal mass flow is directed in section 1, and about 50% is directed in the first two sections of the channel (sections 1 and 2). With the fictitious shutter (D) – obstacle (regime 8), positioned on the right side, beside the wall, it is possible to obtain a moderate uniform distribution in the sections on the right side (Figure 9).

Figure 8 presents side-by-side, velocity profiles for the regimes 1 and 8 (with and without the obstacle D). The difference between the profiles is minimal, except in the section 1, where velocity intensities are significantly reduced because of the presence of the obstacle D.
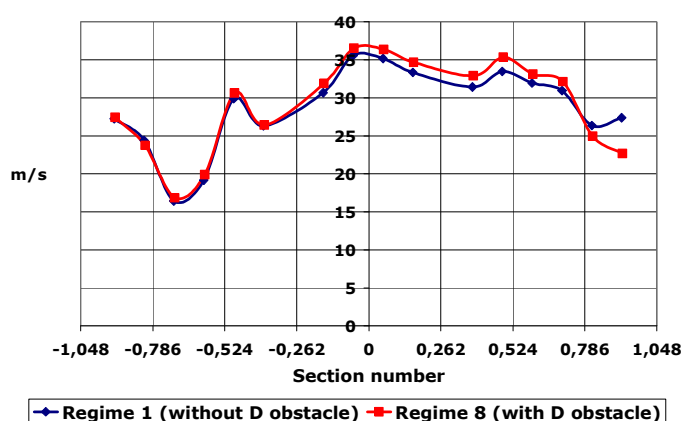


*Figure 8. Velocity profiles at outlet cross-section B-B, Regimes 1 and 8*

Figure 10 presents side-by-side mass flow rates in the sections 1 – 8 of the mixture channel, for the fractions 1 (30 µm – 60 µm) and fraction 2 (60 µm – 90 µm). Distribution of mass flow for the two fractions is fairly similar. These fractions differ a little by mean particle diameter, and the fluid flow have similar influence on their trajectories and distribution. Analyzing the results presented in the Figure 10, distribution of the fractions 30 µm – 60 µm and 60 µm – 90 µm is non-uniform across the channel.
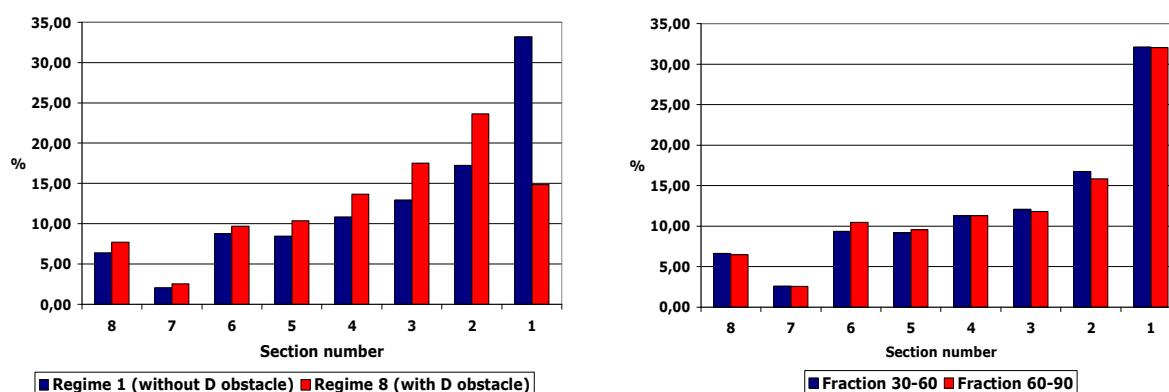


*Figure 9. Coal particles mass flow rates in various mixture channel sections, Regimes 1 and 8*



*Figure 10. Mass flow rates in channel sections, fractions 30-60 µm and 60-90 µm, (Regimes 2 and 3)*

Figure 11 presents results of numerical calculations for the fractions 3 (90 µm – 200 µm) and fraction 4 (200 µm – 500 µm), and their distribution. It can be concluded that the particles of fraction 3 (90 µm – 200 µm) have a much anisotropic distribution in the sections of the channel, in comparation with distribution of particles of fraction 4 (200 µm – 500 µm).



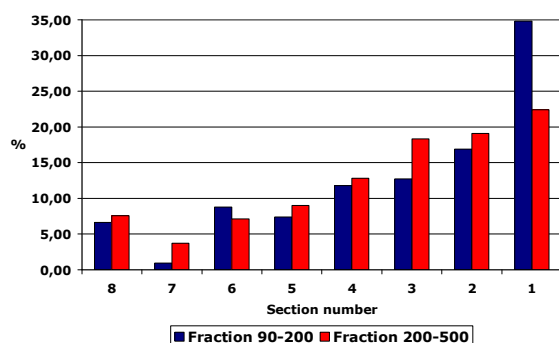*Figure 11. Mass flow rates in channel sections, fractions 90-200 µm and 200-500 µm, (Regimes 4 and 5)*

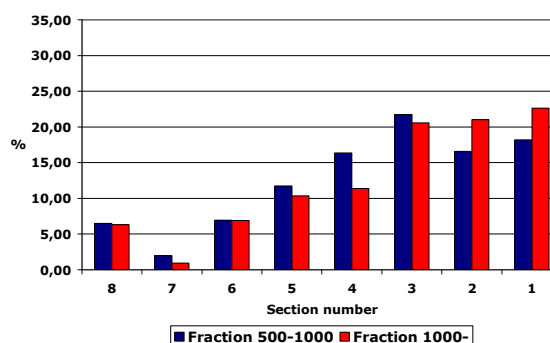*Figure 12. Mass flow rates in channel sections, fractions 500-1000 µm and 1000 µm, (Regimes 6 and 7)*

Summarizing results presented on the Figures 11 and 12 it is obvious that the distribution of the particles with bigger diameter (200 µm – 500 µm, 500 µm – 1000 µm and 1000 µm – ) is moderately uniform (about 16%-22% of total mass flow of particles in the sections 1, 2 and 3 and 10%-15% of total mass flow in the fourth section). Distribution of these fractions is less influenced by fluid flow, because of its inertia, directing them towards the sections that conduct the mixture to the plasma zone.

## CONCLUSION

The results in the paper present the influence of groups of shutters on distribution of coal particles in the mixture channel.

According to the results presented, conclusions are:

- Distribution of small coal particles is non-uniform across the sections of the channel,
- Distribution of bigger coal particles is moderately uniform in the four sections on the right side of the channel,
- Some changes on shutter system have to be made in order to improve regulation,
- The shutter system is an adequate solution for regulation of distribution of coal particles in mixture channel.

## REFERENCES

1. Crowe C.T., Sharma M.P., Stock D.E.: *The Particle−Source−in−Cell (PSI−CELL) model for gas−droplet flows.* J. Fluids Eng. 99, 325–332, 1977.

2. Lee S.L., Durst F.: *On the motion of particles in turbulent duct flows.* Int. J. Multiphase Flow 8, 125–146, 1982.

3. Matsumoto S., Saito S.: *Monte Carlo simulation of horizontal pneumatic conveying based on the rough wall model.* J. Chem. Engng. Japan 3, 223–230, 1970.

4. *Pavlović P., Stefanović P., et al.:* Application of plasma generators for black mineral oil free boiler kindling on the power plant 210 MW „Nikola Tesla". *Technical solution, NIV−ITE−155, Belgrade−Vinča, 1999. (In Serbian).*

5. Sommerfeld M., Živković G.: *Recent advances in the numerical simulation of pneumatic conveying through pipe systems, Computational Methods in Applied Science.* Invited Lectures and Special Technological Sessions of the First European Computational Fluid Dynamics Conference, Brussels, 201−212, 1992.

6. Stefanović P., Pavlović P., Cvetinović D., Živković N., Pavlović Z., Marković Z.: *Plasma systems for start−up and flame support on power plant boilers fired with coal powder – review of implemented industrial plants in the world.* Processing Technology, Vol 1, Year 19, March 2003, Belgrade, (In Serbian).

7. Živković G.: *Mathematical Modelling of Two−Phase Gas−Particle Flow in Horizontal Tubes and Channels.* PhD Dissertation, University of Belgrade, 1996.